Efficient Algorithms for the Computation of Optimal Quadrature Points on Riemannian Manifolds

Inaugural–Dissertation

zur Erlangung des Akademischen Grades
Doktor eines Wissenschaftszweiges
doctor rerum naturalium

vorgelegt der
Fakultät für Mathematik
der
Technischen Universität Chemnitz

von
Dipl.–Math. Manuel Gräf
geboren am 19. Oktober 1983
in Eisenach

Chemnitz, den 04. Februar 2013

Vorsitzender:	Prof. Dr. Roland Herzog, Technische Universität Chemnitz
1. Gutachter:	Prof. Dr. Daniel Potts, Technische Universität Chemnitz
2. Gutachter:	Prof. Dr. Volker Michel, Universität Siegen

Tag der öffentlichen Prüfung: 30.05.2013

Contents

1 Introduction

In various fields of applied mathematics one is confronted with the problem of distributing points over a prescribed subset of the Euclidean space. Depending on the specific application one can impose several optimality criteria.

We consider the problem of numerical integration, where one aims to approximate an integral of a given continuous function from the function values at given sampling points, also known as quadrature points. A useful framework for such an approximation process is provided by the theory of reproducing kernel Hilbert spaces and the concept of the worst case quadrature error. However, the computation of optimal quadrature points, which minimize the worst case quadrature error, is in general a challenging task and requires efficient algorithms, in particular for large numbers of points.

The focus of this thesis is on the efficient computation of optimal quadrature points on the torus $\mathbb{T}^d$, the sphere $\mathbb{S}^d$, and the rotation group $\mathrm{SO}(3)$, since these manifolds are of particular importance in science and engineering applications, cf. [48, 17, 23]. Especially, the problem of constructing quadrature points which integrate exactly all polynomials up to a prescribed degree on the sphere $\mathbb{S}^d$ has released an overwhelming amount of literature, since the seminal papers of Sobolev [122] and McLaren [89]. We like to mention the recent papers of Lebedev and Laikov [84], Popov [105], Ahrens and Beylkin [2], Hardin and Sloane [62], Chen, Frommer and Lang [22], and Sloan and Womersley [117, 118], which concern constructions on the sphere $\mathbb{S}^2$. For constructions on higher dimensional spheres $\mathbb{S}^d$, and projective spaces, such as the rotation group $\mathrm{SO}(3)$, we refer to the papers of Goethals and Seidel [52] and de la Harpe, Pache, and Venkov [63].

We contribute to these recent developments by presenting a general framework for the minimization of the worst case quadrature error on Riemannian manifolds, in order to construct numerically such quadrature points. Therefore, we consider, for M quadrature points on a manifold $\mathcal{M}$, the worst case quadrature error as a function defined on the product manifold $\mathcal{M}^M$. For the optimization on such high dimensional manifolds we consider the method of steepest descent, the Newton method, and the conjugate gradient method, which have been originally adapted to Riemannian manifolds by Udrişte [131], and Smith [121]. Depending on the optimization method we need to evaluate the worst case quadrature error, its gradient, its Hessian, and matrix-vector multiplications with its Hessian. Therefore, we propose two efficient evaluation approaches. The first evaluation approach follows ideas from computational physics, cf. [68], where we interpret the quadrature error as a pairwise potential energy. These ideas allow us to reduce for certain instances the complexity of the evaluations from $\mathcal{O}(M^2)$ to $\mathcal{O}(M \log(M))$. For the second evaluation approach we express the worst case quadrature error in Fourier domain. This enables us

to utilize the nonequispaced fast Fourier transforms developed by Keiner, Kunis, Potts, Prestin, and Vollrath [72, 106] for the torus $\mathbb{T}^d$, the sphere $\mathbb{S}^2$, and the rotation group SO(3), which reduce the computational complexity of the worst case quadrature error for polynomial spaces with degree N from $\mathcal{O}(N^k M)$ to $\mathcal{O}(N^k \log^2(N) + M)$, where k is the dimension of the corresponding manifold. For the usual choice $N^k \sim M$ we achieve the complexity $\mathcal{O}(M \log^2(M))$ instead of $\mathcal{O}(M^2)$. Moreover, we will see that the evaluation of the gradients, and matrix-vector multiplications with the Hessian matrix can be realized with the same computational complexity. In conjunction with the proposed conjugate gradient method on Riemannian manifolds, where we incorporate one-dimensional Newton steps into the line search procedure, we arrive at a particular efficient optimization approach for the computation of optimal quadrature points on the manifolds $\mathcal{M} \in \{\mathbb{T}^d, \mathbb{S}^2, \mathrm{SO}(3)\}$.

We like to mention that the nonequispaced fast Fourier transforms have been already successfully applied for solving efficiently large systems of linear equations arising in problems of approximation theory, cf. [79, 81, 71, 54], and that we establish in this thesis for the first time the use of the nonequispaced fast Fourier transforms for high dimensional nonlinear optimization problems.

With the proposed optimization methods we are able to provide new lists with quadrature formulas for high polynomial degrees N on the sphere $\mathbb{S}^2$, and the rotation group SO(3). More precisely, we construct numerically quadrature points up to degree $N = 124$ and $N = 23$ on the sphere $\mathbb{S}^2$ and the rotation group SO(3), respectively, which have apparently the minimal number of quadrature points. Moreover, we compute a distribution of about half a million quadrature points which integrates highly accurately all polynomials on the sphere $\mathbb{S}^2$ up to degree $N = 1000$. Surprisingly, the numerically found quadrature points on the rotation group SO(3) for degree $N = 7$ lead to an explicit construction of an apparently new spherical 15-design on the sphere $\mathbb{S}^3$ with 336 quadrature points, cf. [119].

Further applications of the proposed optimization framework are found due to the interesting connections between worst case quadrature errors, discrepancies and potential energies, see the monographs of Drmota and Tichy [35], and Novak and Woźniakowski [97], and the paper of Damelin [30]. Especially, discrepancies provide us with an intuitive notion for describing the uniformity of point distributions and we note that the construction of points with low discrepancy is of particular importance for high dimensional integration in quasi-Monte Carlo methods. For instance, Brauchart and Dick [18] proposed an explicit construction, based on digital nets, to generate such low-discrepancy points on the sphere $\mathbb{S}^2$. In contrast to their approach, we are able to compute almost optimally distributed points even for higher dimensional spheres $\mathbb{S}^d$, and show by numerical examples that the discrepancies of these points follow the well-know asymptotics established by Beck [12]. A generalized form of uniform point distributions arises in applications of image processing and computer graphics, where one is concerned with the problem of distributing points in an optimal way accordingly to a prescribed density function. We will show that such problems can be naturally described by the notion of discrepancy, and thus fit perfectly into our framework. A typical application is halftoning of images, where nonuniform distributions of black dots create the illusion of gray toned images, see the monograph of Ulichney [132]. We showed in [58] that the proposed optimization methods compete with state-of-the-art halftoning methods, cf. [129].

Finally, we would like to point out that partial results of this thesis have been published in [56, 57, 53, 59, 58]. Moreover, the computed quadrature formulas on the sphere $\mathbb{S}^2$ and the rotation group SO(3) together with a C++ subroutine library are publicly available at http://www.tu-chemnitz.de/~potts/workgroup/graef/quadrature/.

Outline of the Thesis

Chapter 2. We describe for compact subsets $X \subset \mathbb{R}^n$ the quadrature problem in reproducing kernel Hilbert spaces $H_K(X)$ with reproducing kernel $K : X \times X \to \mathbb{R}$, where we aim to approximate an integral functional I_ν, which is induced by a complex measure ν, by a quadrature functional $Q(\boldsymbol{P}, \boldsymbol{w})$, which is determined by its quadrature points $\boldsymbol{P} := (\boldsymbol{p}_1, \dots, \boldsymbol{p}_M) \in X^M$ and quadrature weights $\boldsymbol{w} := (w_1, \dots, w_M) \in \mathbb{C}^M$. More precisely, we aim to minimize the worst case quadrature error

$$\operatorname{err}_{K,\nu}(\boldsymbol{P}, \boldsymbol{w}) := \sup_{\substack{f \in H_K(X), \\ \|f\|_{H_K(X)} \leq 1}} |I_\nu f - Q(\boldsymbol{P}, \boldsymbol{w}) f|, \tag{1.1}$$

which is defined as the operator norm of the difference between the integral functional I_ν and the quadrature functional $Q(\boldsymbol{P}, \boldsymbol{w})$. In Theorem 2.7 we present two expressions of the quadrature error $\operatorname{err}_{K,\nu}$, one in terms of the given kernel K and the Riesz representative of the functional I_ν and one in terms of the eigenfunctions and eigenvalues associated to the kernel K together with the corresponding Fourier coefficients of the measure ν.

Relations between the worst case quadrature error and potential energies are given in Section 2.3.

In Section 2.4 we introduce the L^2-discrepancy $D^2_{\mathcal{B}}(\nu, \boldsymbol{P}, \boldsymbol{w})$ between the measure ν and the point measure $\delta_{\boldsymbol{P},\boldsymbol{w}} = \sum_{i=1}^M w_i \delta_{\boldsymbol{p}_i}$, and we show in Theorem 2.10 that we can associate to the L^2-discrepancy $D^2_{\mathcal{B}}$, under certain assumptions, a positive definite kernel $K_{\mathcal{B}}$ such that $D^2_{\mathcal{B}}(\nu, \boldsymbol{P}, \boldsymbol{w}) = \operatorname{err}_{K_{\mathcal{B}},\nu}(\boldsymbol{P}, \boldsymbol{w})$. Afterward, we present in Section 2.4.1–2.4.3 some explicit constructions of L^2-discrepancies $D^2_{\mathcal{B}}$ and compute the corresponding kernels $K_{\mathcal{B}}$. In particular, in Section 2.4.2 we recapitulate an idea of Alexander [4], which leads to a geometrically motivated construction of the positive definite Euclidean distance kernel

$$K_{\mathrm{E}}(\boldsymbol{x}, \boldsymbol{y}) = C_X - \|\boldsymbol{x} - \boldsymbol{y}\|_2, \qquad \boldsymbol{x}, \boldsymbol{y} \in X. \tag{1.2}$$

We adopt this idea in Section 2.4.3 for the construction of positive definite kernels with arbitrarily small support.

We close the chapter with selected examples. In Section 2.5.1 we compute optimal quadrature points on the interval $[-1, 1]$ for the Lebesgue measure, the point measure concentrated at the interval endpoints, and the measure induced by the arcsine-distribution. In Section 2.5.2 we discuss quadrature problems in the Euclidean plane for the canonical measures of the unit circle and the disc.

Chapter 3. We develop the theory for optimization methods on Riemannian manifolds. Based on considerations of geodesic curves we arrive in a concise and simple manner at the description of the method of steepest descent, the Newton method, and the conjugate gradient (CG) method on Riemannian manifolds. Moreover, we propose a CG method which incorporates second order derivative information by matrix-vector multiplication with the Hessian matrix representation, as suggested similarly by Daniel [31], so that we do not rely on the concept of parallel transport, which simplifies the description of the CG method in comparison to the abstract derivation of Smith [121].

For the torus $\mathbb{T}^d$, the sphere $\mathbb{S}^d$, and the rotation groups $\mathrm{SO}(n)$, we provide in Section 3.2 explicit formulas of geodesic curves and related differential geometric objects. These formulas enable us to apply the proposed optimization methods also on the product manifolds $\mathcal{M} := X^M \times \mathbb{R}^M$, for $X = \{\mathbb{T}^d, \mathbb{S}^d, \mathrm{SO}(n)\}$, which is essential in our approach for the minimization of the worst case quadrature error $\operatorname{err}_{K,\nu} : \mathcal{M} \to \mathbb{R}$, cf. (1.1), on these manifolds.

Since the generic Newton and CG methods are only locally convergent we propose with Algorithm 3.2 and Algorithm 3.3 globally convergent adaptions, cf. Corollary 3.26. The local convergence rates summarized in Theorem 3.27 are mainly due to the work of Smith [121], where

we additionally incorporate, for the proposed CG method, a result of Cohen [24]. Finally, we give in Section 3.3.3 a detailed motivation for the optimization methods on Riemannian manifolds.

Chapter 4. We introduce the usual Fourier bases on the torus $\mathbb{T}^d$, the sphere $\mathbb{S}^d$, and the rotation group SO(3) and provide the corresponding Fourier expansions of selected positive definite kernels. For the torus $\mathbb{T}^d$ and the sphere $\mathbb{S}^d$ we present in Theorem 4.1 and Theorem 4.5, respectively, formulas for the Fourier coefficients of kernels associated to a special type of L^2-discrepancy. In particular, Theorem 4.5 enables us to state in Theorem 4.6 the Fourier expansion of the Euclidean distance kernel K_{E}, cf. (1.2), on the sphere $\mathbb{S}^d$.

For the rotation group SO(3) we recapitulate in Section 4.3.2 well-known connections to the sphere $\mathbb{S}^3$, which are based on our investigations in [53] and summarized in Theorem 4.7. Moreover, we present in Theorem 4.8 the Fourier expansion of the Euclidean distance kernel K_{E}, cf. (1.2), on the rotation group SO(3).

Chapter 5. We propose two approaches for the efficient evaluation of the worst case quadrature error, its gradient, and its Hessian.

In Section 5.1 we describe an algorithm which reduces the computational complexity for kernels with small support, by following ideas from computational physics, cf. [68]. We show in Corollary 5.9 that for well distributed quadrature points and suitably chosen kernels the complexity is reduced from $\mathcal{O}(M^2)$ to $\mathcal{O}(M \log(M))$ in the number of quadrature points M.

The second approach described in Section 5.2 utilizes the nonequispaced fast Fourier transforms, which are available on the torus $\mathbb{T}^d$, the sphere $\mathbb{S}^2$, and the rotation group SO(3) and implemented in the NFFT-library [72]. The main ingredient of this approach is that we can represent for these manifolds the gradient and the Hessian matrix of polynomial kernels K_N with degree $N \in \mathbb{N}_0$ in terms of nonequispaced Fourier matrices, cf. Theorem 5.13, 5.19, and 5.23. Using these relations we are able to compute for such polynomial kernels K_N the worst case quadrature error $\mathrm{err}_{K_N,\nu}$, its gradient, and matrix-vector multiplications with its Hessian matrix in $\mathcal{O}(N^k \log^2(N) + M)$ instead of $\mathcal{O}(N^k M)$ arithmetic operations, where $k \in \mathbb{N}_0$ is the dimension of the corresponding manifold, cf. Corollary 5.18, 5.22, and 5.26.

Chapter 6. We apply the proposed framework of optimal quadrature functionals in reproducing kernel Hilbert spaces to concrete applications.

In Section 6.1 we introduce the notion of classical quadrature problems, where we aim to construct quadrature functionals which coincide with a prescribed integral functional on a finite dimensional function space. We show in Theorem 6.1 that in general such quadrature functionals do exist. Related problems are constructions of interpolatory quadrature functionals such as Gauß- or Chebyshev-type quadrature rules on the interval [0,1].

In Section 6.2 and 6.3 we mainly contribute to classical quadrature problems on the sphere $\mathbb{S}^2$ and the rotation group SO(3), where we propose to minimize the associated worst case quadrature error via the CG method in conjunction with the corresponding nonequispaced fast Fourier transforms. Moreover, we utilize the theory of quadrature functionals invariant under orthogonal groups, which has been originally developed by Sobolev [122] and McLaren [89]. The incorporation of group symmetry into quadrature functionals is naturally motivated and reduces the complexity of the problem. In that respect, we show in Corollary 6.9 that the additionally imposed symmetry constraints are naturally respected by the CG method on Riemannian manifolds, cf. Corollary 6.9. The suitability of our optimization approach is shown by the numerical results presented in Table 6.1, 6.2, 6.5, and 6.6, where we present new lists of quadrature functionals for the sphere $\mathbb{S}^2$ and the rotation group SO(3), which integrate exactly all polynomial of a prescribed degree and which are putatively optimal with respect to the number of quadrature points. Moreover, we are able to compute quadrature functionals for very high polynomial degrees of exactness on the sphere $\mathbb{S}^2$, cf. Table 6.3. On the sphere $\mathbb{S}^3$ we discover an apparently new spherical 15-design with 336 points, and prove by an explicit construction its existence in Theorem 6.26.

In Section 6.4 we compute uniformly distributed points on the unit sphere $\mathbb{S}^d$ for $d \leq 5$. In

order to show the suitability of the evaluation approaches presented in Chapter 5, we recall in Theorem 6.29 the asymptotics of low-discrepancy points and compare it with the corresponding L^2-discrepancy of our numerically computed point distributions. In Figure 6.3 and 6.5 we observe that the numerical results are in perfect accordance with the theoretic predictions.

Finally, we consider in Section 6.5 the problem of halftoning, which arises in image processing. We show that this problem fits perfectly into our general framework such that our proposed optimization methods lead to efficient halftoning algorithms, which can compete with the recently suggested optimization approach of Schmaltz et al. [114]. Moreover, we generalize the ideas to halftoning on the sphere $\mathbb{S}^2$.

Acknowledgments

This thesis would not have been possible without the constant encouragement and support of my doctoral adviser Prof. Daniel Potts, who had the patience and confidence in my working methods. I highly appreciate his valuable advises and ideas throughout the years.

Special thanks go to Prof. Gabriele Steidl for pointing my attention to the theory of reproducing kernel Hilbert spaces, which becomes a substantial part of this thesis.

Moreover, in the countless coffee breaks I have learned a lot from the fruitful discussions with my colleagues Ralf Hielscher, Lutz Kämmerer, Franziska Nestler, Michael Pippig, and Toni Volkmer and I appreciate their valuable comments and suggestions that helped to improve my work.

Financial support by Deutsche Forschungsgemeinschaft Grant PO 711/9-2 is gratefully acknowledged.

2

Quadratures and their Relations to Discrepancies and Potential Energies

In this chapter we introduce for compact sets X of the Euclidean space $\mathbb{R}^n$ the general concept of the worst case quadrature error in a reproducing kernel Hilbert space $H_K(X)$ with reproducing kernel $K : X \times X \to \mathbb{R}$, and develop the relations to discrepancies and potential energies. These fundamental relations are similarly presented in an article of Damelin [30] and the book of Novak and Woźniakowski [97], where the focus in [30] is on the potential theoretic point of view, and that in [97] is on discrepancies. Furthermore, our emphasis is on the numerical optimization rather than asymptotic estimates of minimal energies or discrepancies.

We introduce in Section 2.1 the notion of an integral functional I_ν, induced by a Borel measure ν, and a quadrature functional $Q(\boldsymbol{P}, \boldsymbol{w})$, associated to quadrature points $\boldsymbol{P} \in X^M$ and weights $\boldsymbol{w} \in \mathbb{C}^M$, $M \in \mathbb{N}$, on the space of continuous functions $C(X)$. Afterward, we describe the general quadrature problem, where we aim to approximate a given integral functional by quadrature functionals. The concept of strong convergence in the dual space $C^*(X)$ leads us to the 'quadrature problem in the strong sense', which provides us with an optimality criterion for quadrature functionals.

It turns out that the space $C(X)$ is in general to big for a meaningful approximation, so that we consider in Section 2.2 the quadrature problem in the strong sense for reproducing kernel Hilbert spaces $H_K(X) \subset C(X)$. After presenting in Section 2.2.1 the necessary parts of the theory of reproducing kernel Hilbert spaces, we are able to define in Section 2.2.2 the worst case quadrature error $\mathrm{err}_K(\nu, \boldsymbol{P}, \boldsymbol{w})$ between an integral functional I_ν and a quadrature functional $Q(\boldsymbol{P}, \boldsymbol{w})$. With help of the Riesz Representation Theorem for Hilbert spaces we arrive at the central Theorem 2.7, which provides us with explicit formulas, and thus forms the foundation for the computation of optimal quadrature points. Moreover, Theorem 2.7 establishes the relations between worst case quadrature errors err_K, the potential energies E_K, and certain L^2-discrepancies $D^2_{\mathcal{B}}$.

In Section 2.3 we recall the notion of the electrostatic energy and present a brief outlook for further generalizations of potential energies, which include the well studied Riesz, and logarithmic energies $E_{K_{\alpha,n}}$. However, these generalized energies are beyond the scope of worst case quadrature errors in reproducing kernel Hilbert spaces, so that we refer to the literature of potential theory.

In Section 2.4 we introduce the concept of discrepancy from a rather abstract point of view, where the discrepancy is intended to describe the similarity of the two Borel measures ν and $\delta_{\boldsymbol{P},\boldsymbol{w}}$ associated to the integral I_ν and quadrature functional $Q(\boldsymbol{P}, \boldsymbol{w})$, respectively. Under suitable assumptions we can define the L^2-discrepancy $D^2_{\mathcal{B}}$, which can be regarded as a weighted L^2-norm

in the space of Borel measures over a prescribed basis set $\mathcal{B}$ consisting of measurable subsets of $\mathbb{R}^n$. It turns out that we can associate to some L^2-discrepancy $D_{\mathcal{B}}^2$ a discrepancy kernel $K_{\mathcal{B}}$, which gives rise to a reproducing kernel Hilbert space $H_{K_{\mathcal{B}}}(X)$, such that the worst case quadrature error $\mathrm{err}_{K_{\mathcal{B}}}$ coincides with the L^2-discrepancy $D_{\mathcal{B}}^2$, i.e, $\mathrm{err}_{K_{\mathcal{B}}}(\nu, \boldsymbol{P}, \boldsymbol{w}) = D_{\mathcal{B}}^2(\nu, \boldsymbol{P}, \boldsymbol{w})$ for any choices of the Borel measure ν, points $\boldsymbol{P} \in X^M$, and weights $\boldsymbol{w} \in \mathbb{C}^M$, cf. Theorem 2.10. In the Section 2.4.1– 2.4.3 we present constructions of basis sets $\mathcal{B}$, which lead to a variety of positive definite kernels $K_{\mathcal{B}}$, for which the worst case quadrature error $\mathrm{err}_{K_{\mathcal{B}}}$ has a geometric meaning. We note, that applications for the use of such particular constructed kernels are given later in the Sections 6.4 and 6.5.

We close this chapter by providing illustrative examples in Section 2.5, where we describe some possible issues concerning the determination of optimal quadrature functionals. The examples are self-explanatory in the sense that we do not need the whole machinery of optimization on Riemannian manifolds and the harmonic analysis presented in Chapter 3 and 4, respectively, nor do we care about the efficient evaluation methods, as proposed in Chapters 5. Moreover, we are able to compute analytically the optimal quadrature functionals for some prescribed integral functionals. The results provided by these examples are interesting and help us to get used to the notation.

2.1 The General Quadrature Problem

Throughout this thesis we consider the Euclidean space $\mathbb{R}^n$, $n \in \mathbb{N}$, equipped with the *Euclidean norm*

$$\|\boldsymbol{x}\|_2 := \sqrt{\sum_{i=1}^{n} x_i^2}, \qquad \boldsymbol{x} := (x_1, \dots, x_n)^\top \in \mathbb{R}^n,$$

such that the standard topology of open sets is induced by the *Euclidean distance* $\|\boldsymbol{x} - \boldsymbol{y}\|_2$, $\boldsymbol{x}, \boldsymbol{y} \in \mathbb{R}^n$. Thus, the Borel sets are determined by the standard topology, i.e., open or closed sets are measurable, and we consider only Borel measures on $\mathbb{R}^n$ with respect to the sigma algebra of Borel sets. For recapitulating the basics in measure and integration theory we refer to the literature [25]. We recall that a *Borel measure* μ is called *finite* if $\mu(\mathbb{R}^n) < \infty$. For our further considerations we define *complex Borel measures* ν which are of the form

$$\nu := \nu_{(1)} - \nu_{(2)} + \mathrm{i}\nu_{(3)} - \mathrm{i}\nu_{(4)} \tag{2.1}$$

where $\nu_{(1)}$, $\nu_{(2)}$, $\nu_{(3)}$, and $\nu_{(4)}$ are finite Borel measures. The space of complex Borel measures in $\mathbb{R}^n$ is denoted by $M_{\mathbb{C}}(\mathbb{R}^n)$. Using this convention, a finite Borel measure μ is a complex Borel measure with $\mu_{(2)} = \mu_{(3)} = \mu_{(4)} = 0$. Similarly, we call a complex Borel measure ν a *signed Borel measure* if $\nu_{(3)} = \nu_{(4)} = 0$. Furthermore, we call a measurable set $N \subset \mathbb{R}^n$ a *μ-null set* if $\mu(N) = 0$, and we say that a certain property is satisfied *μ-almost everywhere* if it is satisfied for all points $\boldsymbol{x} \in \mathbb{R}^n$ except for a μ-null set. The *support* of a Borel measure μ is defined by

$$\mathrm{supp}(\mu) := \mathbb{R}^n \setminus \{\boldsymbol{x} \in U \ : \ U \subset \mathbb{R}^n \text{ open}, \ \mu(U) = 0\}. \tag{2.2}$$

In words, the support of the measure μ is the complement of the largest open μ-null set. We recall, a measure μ is called *discrete* if the support of μ is at most a countable set, and it is called *continuous* if for any point $\boldsymbol{x} \in \mathbb{R}^n$ the set $\{\boldsymbol{x}\}$ is a μ-null set.

An example of a discrete measure is given by the *Dirac measure* $\delta_{\boldsymbol{x}}$, concentrated at $\boldsymbol{x} \in \mathbb{R}^n$,

which is defined for measurable sets $\Omega \subset \mathbb{R}^n$ by

$$\delta_{\boldsymbol{x}}(\Omega) := \begin{cases} 1, & \boldsymbol{x} \in \Omega, \\ 0, & \text{else}, \end{cases} \qquad \boldsymbol{x} \in \mathbb{R}^n. \tag{2.3}$$

A continuous measure is given by the *Lebesgue measure* $\mu_{\mathbb{R}^n}$, which is normalized by $\mu_{\mathbb{R}^n}([0,1]^n) = 1$, $n \in \mathbb{N}$.

In what follows we consider compact sets $X \subset \mathbb{R}^n$ with a fixed and finite Borel measure μ_X which has support $\operatorname{supp}(\mu_X) = X$. Examples of particular interest to us are given if X is a compact Riemannian manifold, cf. Section 3.1, with canonical measure μ_X defined by (3.51). In that case the measure μ_X is continuous.

The space of continuous complex-valued functions on X is denoted by $C(X)$ and equipped with the supremum norm

$$\|f\|_\infty := \sup_{\boldsymbol{x} \in X} |f(\boldsymbol{x})|, \qquad f \in C(X).$$

In this function space the general quadrature problem takes place. In order to formulate the quadrature problem we recall that any (complex) Borel measure ν induces a bounded linear functional $I_\nu : C(X) \to \mathbb{C}$ given by

$$I_\nu f := \int_X f(\boldsymbol{x}) \mathrm{d}\nu(\boldsymbol{x}), \qquad f \in C(X), \tag{2.4}$$

with operator norm, cf. (2.1),

$$\|I_\nu\|_{C(X)\to\mathbb{C}} := \sup_{\substack{f \in C(X), \\ \|f\|_\infty \leq 1}} |I_\nu f| \leq \nu_{(1)}(X) + \nu_{(2)}(X) + \nu_{(3)}(X) + \nu_{(4)}(X) < \infty.$$

We call the functional I_ν the induced *integral functional* of $\nu \in M_{\mathbb{C}}(\mathbb{R}^n)$. We remark that the dual space $C^*(X)$, the space of bounded linear functionals on $C(X)$, is actually spanned by the integral functionals I_ν, $\nu \in M_{\mathbb{C}}(\mathbb{R}^n)$, cf. [25, Theorem 7.3.5]. A particular important class of linear functionals is given by point evaluation functionals of the form

$$Q(\boldsymbol{P}, \boldsymbol{w}) f := \sum_{i=1}^{M} w_i f(\boldsymbol{p}_i), \qquad f \in C(X), \tag{2.5}$$

where $\boldsymbol{P} := (\boldsymbol{p}_1, \ldots, \boldsymbol{p}_M) \in X^M$ and $\boldsymbol{w} := (w_1, \ldots, w_M) \in \mathbb{C}^M$, $M \in \mathbb{N}$. We call $Q(\boldsymbol{P}, \boldsymbol{w})$ a *quadrature functional* of *size* M with *quadrature points* $\boldsymbol{P}$ and *quadrature weights* $\boldsymbol{w}$. Via the connection between functionals in $C^*(X)$ and complex Borel measures we may interpret the quadrature functional $Q(\boldsymbol{P}, \boldsymbol{w})$ also as a complex measure $\delta_{\boldsymbol{P},\boldsymbol{w}}$ concentrated at the points $\boldsymbol{p}_i \in X$, $i = 1, \ldots, M$, i.e.,

$$Q(\boldsymbol{P}, \boldsymbol{w}) = I_{\delta_{\boldsymbol{P},\boldsymbol{w}}} \in C^*(X), \qquad \delta_{\boldsymbol{P},\boldsymbol{w}} := \sum_{i=1}^{M} w_i \delta_{\boldsymbol{p}_i} \in M_{\mathbb{C}}(\mathbb{R}^n). \tag{2.6}$$

We refer to the *general quadrature problem* as the problem of approximating a given integral functional I_ν, $\nu \in M_{\mathbb{C}}(\mathbb{R}^n)$, by quadrature functionals $Q(\boldsymbol{P}, \boldsymbol{w})$, $\boldsymbol{P} \in X^M$, $\boldsymbol{w} \in \mathbb{C}^M$, $M \in \mathbb{N}$. There are two naturally concepts for the mean of such approximations, namely, one could ask for a sequence of quadrature functionals $\{Q(\boldsymbol{P}_n, \boldsymbol{w}_n)\}_{n\in\mathbb{N}}$ such that for any $f \in C(X)$ it satisfies

$$\left| I_\nu f - Q(\boldsymbol{P}_n, \boldsymbol{w}_n) f \right| \to 0, \qquad n \to \infty, \tag{2.7}$$

or that, independently of f, it satisfies

$$\|I_\nu - Q(\boldsymbol{P}_n, \boldsymbol{w}_n)\|_{C(X)\to\mathbb{C}} = \sup_{\substack{f\in C(X),\\ \|f\|_\infty\le 1}} \left|I_\nu f - Q(\boldsymbol{P}_n, \boldsymbol{w}_n) f\right| \to 0, \qquad n\to\infty. \tag{2.8}$$

The first condition (2.7) is related to the weak (or pointwise) convergence of linear functionals in $C^*(X)$ and the second relation (2.8) corresponds to the strong (or uniform) convergence of linear functionals in $C^*(X)$. We recall that strong convergence in $C^*(X)$ implies weak convergence in $C^*(X)$. However, there is no canonical optimality criterion for the weak convergence in $C^*(X)$, which can be used to prefer a sequence over another. On the other hand, the strong convergence in $C^*(X)$ leads for quadrature functionals $Q(\boldsymbol{P}, \boldsymbol{w})$ of fixed size $M \in \mathbb{N}$ to an optimality criterion induced by the operator norm. Unfortunately, the space $C(X)$ is in general too big, so that the set of quadrature functionals is not dense in the set of integral functionals with respect to the operator norm, cf. Example 2.1. For that reason we restrict our attention to subspaces $H(X) \subset C(X)$ which are *continuously embedded*, i.e., there exists a constant $c > 0$ such that

$$\|f\|_\infty \le c\|f\|_{H(X)}, \qquad f \in H(X), \tag{2.9}$$

where $\|\cdot\|_{H(X)}$ is the norm in $H(X)$. For continuously embedded subspaces $H(X) \subset C(X)$ we write $H(X) \hookrightarrow C(X)$. Particularly important subspaces $H(X)$ are given by what is known as reproducing kernel Hilbert spaces. We will see that reproducing kernel Hilbert spaces offer a very rich and interesting theory, where the quadrature functionals are dense in the dual space $H^*(X)$ of integral functionals, cf. Theorem 2.4 and 2.6.

In this thesis we refer to the *quadrature problem in the strong sense* as the strong convergence in the dual space $H^*(X)$ similar to (2.8), i.e., we ask for a sequence of quadrature functionals $\{Q(\boldsymbol{P}_n, \boldsymbol{w}_n)\}_{n\in\mathbb{N}}$ which satisfies

$$\|I_\nu - Q(\boldsymbol{P}_n, \boldsymbol{w}_n)\|_{H(X)\to\mathbb{C}} = \sup_{\substack{f\in H(X),\\ \|f\|_{H(X)}\le 1}} \left|I_\nu f - Q(\boldsymbol{P}_n, \boldsymbol{w}_n) f\right| \to 0, \qquad n\to\infty. \tag{2.10}$$

We refer to the *quadrature problem in the weak sense* as the weak convergence in $C^*(X)$ given by (2.7).

Example 2.1. We briefly illustrate that the strong convergence (2.8) in $C(X)$ is in general unachievable. Therefore, we consider the interval $X := [0,1]$ and the Lebesgue measure $\nu := \mu_{[0,1]}$ with support $\operatorname{supp}(\mu_{[0,1]}) = [0,1]$. Then we can construct for any given quadrature functional $Q(\boldsymbol{P}, \boldsymbol{w})$, $\boldsymbol{P} := (p_1, \dots, p_M)^\top \in [0,1]^M$, $\boldsymbol{w} := (w_1, \dots, w_M)^\top \in \mathbb{C}^M$, a sequence of functions $f_k \in C([0,1])$, $\|f_k\|_\infty = 1$ with

$$f_k(p_i) = \begin{cases} \overline{w}_i/|w_i|, & w_i \neq 0, \\ 0, & \text{else}, \end{cases}, \qquad i = 1, \dots, M, \qquad k \in \mathbb{N},$$

and $\lim_{k\to\infty} I_\nu f_k = 0$. For such a sequence we have

$$\lim_{k\to\infty} |Q(\boldsymbol{P}, \boldsymbol{w}) f_k - I(w) f_k| = \sum_{i=1}^{M} |w_i| = \|Q(\boldsymbol{P}, \boldsymbol{w})\|_{C([0,1])\to\mathbb{C}},$$

and we infer that $\|Q(\boldsymbol{P}, \boldsymbol{w}) - I(w)\|_{C(X)\to\mathbb{C}} > 0$ whenever $\boldsymbol{w} \neq \boldsymbol{0} \in \mathbb{C}^M$. Hence, there can be no sequence of quadrature functionals $Q(\boldsymbol{P}, \boldsymbol{w})$ converging to the integral functional I_ν in the strong sense (2.8). □

2.2 Quadrature Errors in Reproducing Kernel Hilbert Spaces

Since the appearance of the seminal work of Aronszajn [5], the theory of reproducing kernel Hilbert spaces has been found useful in several fields of mathematics, and it might be no surprise that it also plays a fundamental role for our further consideration. Due to some subtle details, we will thoroughly develop in Section 2.2.1 the parts of that theory which suit our purposes. In particular, we present a suitable and concise version of Mercer's Theorem, cf. Theorem 2.2, which is central for the Fourier-based characterization of reproducing kernel Hilbert spaces. Later we will arrive at the well-know characterization of reproducing kernel Hilbert spaces $H_K(X) \subset C(X)$ with positive definite kernels K, which is attributed to Moore and Aronszajn, cf. Theorem 2.4. This result shows us together with Theorem 2.6 that the quadrature problem in the strong sense, cf. (2.10), is meaningful for such function spaces. Thus, we are able to define in Section 2.2.2 the worst case quadrature error err_K for reproducing kernel Hilbert spaces $H_K(X)$, for which we establish explicit formulas in Theorem 2.7. For further investigations of the worst case quadrature error, especially in the abstract setting of tractability of multivariate problems, we refer to [97, Ch. 10], and we remark that the results of Section 2.2.2 are slight generalizations of those for the multivariate integration problem given in [97, Sec. 10.7].

2.2.1 Reproducing Kernel Hilbert Spaces

For compact sets $X \subset \mathbb{R}^n$ we denote the space of complex-valued square-integrable functions on X by

$$L^2(X) := \left\{ f : X \to \mathbb{C} \ : \ \int_X |f(\boldsymbol{x})|^2 \mathrm{d}\mu_X(\boldsymbol{x}) < \infty \right\}, \tag{2.11}$$

and remark that the definition of the space $L^2(X)$ depends on the chosen Borel measure μ_X. Therefore, we use the convention, whenever we refer to the space $L^2(X)$ we associate to X a fixed and finite Borel measure μ_X which has support $\mathrm{supp}(\mu_X) = X$, cf. (2.2). We recall that the L^2-product defined by

$$(f,g)_{L^2(X)} := \int_X f(\boldsymbol{x})\overline{g}(\boldsymbol{x})\mathrm{d}\mu_X(\boldsymbol{x}), \qquad f,g \in L^2(X), \tag{2.12}$$

induces the seminorm

$$\|f\|_{L^2(X)} := \sqrt{(f,f)_{L^2(X)}}, \qquad f \in L^2(X), \tag{2.13}$$

and note that in the presence of μ_X-null sets the seminorm (2.13) is not a norm. Hence, in order to obtain a Hilbert space we need to pass in such a case to the set of equivalence classes of functions $f, g \in L^2(X)$ defined by, cf. [25, Theorem 3.4.1],

$$f \sim g \quad :\Leftrightarrow \quad f(\boldsymbol{x}) = g(\boldsymbol{x}), \quad \boldsymbol{x} \in X, \quad \mu_X\text{-almost everywhere.} \tag{2.14}$$

We remark, that an equivalence class with more than one element is hardly identified with a function. Hence, the so constructed Hilbert space, which by abuse of notation, we denote also as $L^2(X)$ is in general no function space, and point evaluation functionals may not be well defined. Nevertheless, we consider the elements of the Hilbert space $L^2(X)$, accordingly to the original definition (2.11), as functions and keep in mind the equivalence relation (2.14). Thus, we can construct an orthonormal basis of functions $\psi_l \in L^2(X)$, $l \in \mathbb{N}_0$, i.e.,

$$L^2(X) := \mathrm{cl}\,\mathrm{span}\{\psi_l \ : \ l \in \mathbb{N}_0\}, \qquad (\psi_l, \psi_k)_{L^2(X)} = \delta_{l,k}, \qquad l,k \in \mathbb{N}_0,$$

where 'cl span' is the closure of the linear span with respect to the L^2-norm, and where the *Kronecker delta* is defined by

$$\delta_{l,k} := \begin{cases} 1, & l = k, \\ 0, & \text{else.} \end{cases} \tag{2.15}$$

It is well known that up to the equivalence (2.14), any function $f \in L^2(X)$ admits a uniquely determined *Fourier series*

$$f = \sum_{l=0}^{\infty} \hat{f}_l \psi_l, \qquad \hat{f}_l := (f, \psi_l)_{L^2(X)} = \int_X f(\boldsymbol{x}) \overline{\psi}_l(\boldsymbol{x}) \mathrm{d}\mu_X(\boldsymbol{x}). \tag{2.16}$$

The quantities $\hat{f}_l$, $l \in \mathbb{N}_0$, in (2.16) are the *Fourier coefficients* of $f \in L^2(X)$, and we recall that Parseval's identity states

$$(f, g)_{L^2(X)} = \sum_{l=0}^{\infty} \hat{f}_l \overline{\hat{g}_l}, \qquad f, g \in L^2(X). \tag{2.17}$$

A function $K : X \times X \to \mathbb{R}$ is called *symmetric* if $K(\boldsymbol{x}, \boldsymbol{y}) = K(\boldsymbol{y}, \boldsymbol{x})$, $\boldsymbol{x}, \boldsymbol{y} \in X$. A symmetric function $K : X \times X \to \mathbb{R}$ is called *positive definite* if for any finite number $M \in \mathbb{N}$ of points $\boldsymbol{x}_1, \ldots, \boldsymbol{x}_M \in X$, it satisfies

$$\sum_{i,j=1}^{M} K(\boldsymbol{x}_i, \boldsymbol{x}_j) a_i a_j \geq 0, \qquad (a_1, \ldots, a_M) \in \mathbb{R}^M \setminus \{\mathbf{0}\}. \tag{2.18}$$

If additionally there is strict inequality in (2.18) we say that the function K is *strictly positive definite*. The function $K : X \times X \to \mathbb{R}$ is called a *(strictly) positive definite kernel* if it is (strictly) positive definite and continuous.[1]

The theory of reproducing kernel Hilbert spaces is build upon positive definite kernels $K : X \times X \to \mathbb{R}$, where it is convenient to associate to K the bounded linear integral operator $T_K : L^2(X) \to L^2(X)$ defined by the integral transformation

$$T_K f(\boldsymbol{x}) := \int_X K(\boldsymbol{x}, \boldsymbol{y}) f(\boldsymbol{y}) \mathrm{d}\mu_X(\boldsymbol{y}), \qquad f \in L^2(X), \quad \boldsymbol{x} \in X. \tag{2.19}$$

The following Theorem 2.2, which originally is due to Mercer [90], states that the integral operator T_K has very appealing properties. We note that there are various versions of Mercer's Theorem found in the literature. For our purposes we rely on the results given in [28] and refer for a nice survey of Mercer's Theorem and further generalizations to [125].

Theorem 2.2. *Let $X \subset \mathbb{R}^n$ be compact with finite Borel measure μ_X and let $K : X \times X \to \mathbb{R}$ be a positive definite kernel, cf.* (2.18)*. Then the integral transformation* (2.19) *defines a compact operator $T_K : L^2(X) \to C(X)$ which is* self-adjoint*, i.e.,*

$$(T_K f, g)_{L^2(X)} = (f, T_K g)_{L^2(X)}, \qquad f, g \in L^2(X), \tag{2.20}$$

and positive*, i.e.,*

$$(T_K f, f)_{L^2(X)} \geq 0, \qquad f \not\equiv 0 \in L^2(X). \tag{2.21}$$

Furthermore, there exists an orthonormal basis of eigenfunctions $\psi_l \in L^2(X)$, $l \in \mathbb{N}_0$, of T_K

[1] Recall that the product space $X \times X$ is equipped with the canonical product topology and product measure $\mu_{X \times X}$, cf. [25, Ch. 5].

with corresponding eigenvalues $\lambda_l \geq 0$*, i.e.,*

$$T_K \psi_l = \lambda_l \psi_l, \qquad l \in \mathbb{N}_0, \tag{2.22}$$

where for any $f \in L^2(X)$ *the Fourier series, cf.* (2.16)*,*

$$T_K f = \sum_{l=0}^{\infty} (f, \psi_l)_{L^2(X)} \lambda_l \psi_l = \sum_{l=0}^{\infty} \hat{f}_l \lambda_l \psi_l \tag{2.23}$$

converges absolutely and uniformly on X*.*

For every $l \in \mathbb{N}_0$ *with eigenvalue* $\lambda_l > 0$*, the corresponding eigenfunctions* ψ_l *are continuous. Moreover, the Fourier expansion*

$$K(\boldsymbol{x}, \boldsymbol{y}) = \sum_{l=0}^{\infty} \lambda_l \psi_l(\boldsymbol{x}) \overline{\psi}_l(\boldsymbol{y}), \qquad \boldsymbol{x}, \boldsymbol{y} \in X, \tag{2.24}$$

converges absolutely and uniformly on $X \times X$*, and the eigenvalues are absolutely summable, i.e.,* $\sum_{l=0}^{\infty} \lambda_l < \infty$*.*

Proof. We briefly follow the lines given in [28, Ch. III]. It is shown in [28, Proposition 1 (Ch. III)] that $T_K : L^2(X) \to C(X)$ is a well-defined, bounded, and compact operator. The continuity of the function $T_K f$ follows for $f \in L^2(X)$ from Cauchy–Schwartz's inequality due to

$$\begin{aligned} \left| T_K f(\boldsymbol{x}_1) - T_K f(\boldsymbol{x}_2) \right| &= \left| \int_X (K(\boldsymbol{x}_1, \boldsymbol{y}) - K(\boldsymbol{x}_2, \boldsymbol{y})) f(\boldsymbol{y}) \mathrm{d}\mu_X(\boldsymbol{y}) \right| \\ &\leq \|K(\boldsymbol{x}_1, \cdot) - K(\boldsymbol{x}_2, \cdot)\|_2 \|f\|_2 \\ &\leq \sqrt{\mu_X(X)} \max_{\boldsymbol{y} \in X} |K(\boldsymbol{x}_1, \boldsymbol{y}) - K(\boldsymbol{x}_2, \boldsymbol{y})| \|f\|_2, \quad \boldsymbol{x}_1, \boldsymbol{x}_2 \in X, \end{aligned}$$

since K is continuous and X is compact. The boundedness follows from the relation

$$|T_K f(\boldsymbol{x})| \leq \sqrt{\nu(X)} \max_{\boldsymbol{y} \in X} |K(\boldsymbol{x}, \boldsymbol{y})| \|f\|_2, \qquad \boldsymbol{x} \in X, \quad f \in L^2(X),$$

which is proved as above. For the compactness of the integral operator $T_K : L^2(X) \to C(X)$ we refer to the proof of [28, Proposition 1 (Ch. III)], which involves the theorem of Arzelà-Ascoli.

The self-adjointness (2.20) of the integral operator $T_K : L^2(X) \to L^2(X)$ is a simple consequence of Fubini's Theorem and the symmetry of the kernel $K : X \times X \to \mathbb{R}$. For the positiveness, cf. (2.21), we refer to the proof of [28, Proposition 2 (Ch. III)], where it is indicated to approximate the positive definite kernel K by elementary functions.

Hence, we can apply the spectral theorem for self-adjoint operators to T_K and arrive at the Fourier series (2.23) of $T_K f$. From the continuity of $T_K f$ we infer for any eigenvalue $\lambda_l > 0$ that the eigenfunction $\psi_l = \lambda_l^{-1} T_K \psi_l$ is continuous.

The absolute and uniform convergence of the Fourier expansion (2.24) is stated in [28, Theorem 1 (Ch. III)]. Hence, the summability of the sequence of eigenvalues λ_l, $l \in \mathbb{N}_0$, follows from the uniform convergent series $K(\boldsymbol{x}, \boldsymbol{x}) = \sum_{l=0}^{\infty} \lambda_l |\psi_l(\boldsymbol{x})|^2$, $\boldsymbol{x} \in X$, and integration of both sides

$$\int_X K(\boldsymbol{x}, \boldsymbol{x}) \mathrm{d}\mu_X(\boldsymbol{x}) = \sum_{l=0}^{\infty} \lambda_l \int_X |\psi_l(\boldsymbol{x})|^2 \mathrm{d}\mu_X(\boldsymbol{x}) = \sum_{l=0}^{\infty} \lambda_l,$$

which finishes the proof. ∎

Remark 2.3. Conversely to Theorem 2.2 we can construct a positive definite kernel $K : X \times X \to \mathbb{C}$ using the series expansion (2.24) as definition, such that the function K is continuous for a given orthonormal system of continuous functions $\psi_l \in L^2(X)$ and a sequence of Fourier coefficients $\lambda_l \geq 0$, $l \in \mathbb{N}_0$. In general the constructed function K might be complex-valued, but if it is symmetric, i.e., $K(\boldsymbol{x}, \boldsymbol{y}) = K(\boldsymbol{y}, \boldsymbol{x})$, $\boldsymbol{x}, \boldsymbol{y} \in X$, it is real valued. Then the positive definiteness follows from

$$\sum_{i,j=1}^{M} K(\boldsymbol{x}_i, \boldsymbol{x}_j) a_i a_j = \sum_{l=0}^{\infty} \lambda_l \Big| \sum_{i=1}^{M} a_i \psi_l(\boldsymbol{x}_i) \Big|^2 \geq 0, \qquad (a_1, \ldots, a_M)^\top \in \mathbb{R}^M. \qquad \square$$

We use Theorem 2.2 to define reproducing Kernel Hilbert spaces. For that reason, we restrict the domain of the integral operator $T_K : L^2(X) \to L^2(X)$, cf. (2.19), to the space

$$L^2_+(X) := \operatorname{cl} \operatorname{span}\{\psi_l \ : \ \lambda_l > 0, \ l \in \mathbb{N}_0\} \subset L^2(X), \tag{2.25}$$

where $\psi_l \in L^2(X)$, $l \in \mathbb{N}_0$, are the orthonormal eigenfunctions of T_K, cf. (2.22), and the closure is taken with respect to the standard L^2-product. Thus, we can define the square root $S_K : L^2_+(X) \to L^2_+(X)$ of the integral operator $T_K : L^2_+(X) \to L^2_+(X)$ by

$$S_K f := \sum_{l=0}^{\infty} \lambda_l^{\frac{1}{2}} \hat{f}_l \psi_l, \qquad f := \sum_{l=0}^{\infty} \hat{f}_l \psi_l \in L^2_+(X).$$

We note that indeed $T_K f = S_K \circ S_K f$, $f \in L^2_+(X)$. Now, the range of the operator S_K defines the Hilbert space

$$H_K(X) := \big\{ S_K f \ : \ f \in L^2_+ \big\} = \big\{ f \in L^2_+(X) \ : \ \|f\|_{H_K(X)} < \infty \big\} \tag{2.26}$$

equipped with the inner product[2]

$$(f, g)_{H_K(X)} := \sum_{l=0}^{\infty} \lambda_l^{-1} \hat{f}_l \overline{\hat{g}_l}, \qquad f, g \in H_K(X) \tag{2.27}$$

and induced norm

$$\|f\|_{H_K(X)} := \sqrt{(f, f)}_{H_K(X)}, \qquad f, g \in H_K(X).$$

The right identity in (2.26) follows from Parseval's identity (2.17) due to

$$\|S_K f\|^2_{H_K(X)} = \sum_{l=0}^{\infty} \lambda_l^{-1} |\lambda_l^{\frac{1}{2}} \hat{f}_l|^2 = \sum_{l=0}^{\infty} |\hat{f}_l|^2 = \|f\|^2_{L^2(X)} < \infty, \qquad f \in L^2_+(X),$$

which shows that the operator $S_K : L^2_+(X) \to H_K(X)$ is an isometry, and thus, $H_K(X)$ is indeed a Hilbert space.

We note that the definition (2.26) of the Hilbert space $H_K(X)$ depends, by construction of the operator S_K, on the chosen orthonormal basis $\psi_l \in L^2(X)$, $l \in \mathbb{N}_0$, and in particular on the finite Borel measure μ_X, cf. (2.19). However, by the Moore–Aronszajn Theorem, presented as Theorem 2.4, we see that the space $H_K(X)$ is a function space and depends only on the positive definite kernel K.

[2]Throughout this thesis, we will use the formal convention $0/0 := 0$ in the definition (2.27) and related series.

Theorem 2.4. *Let $X \subset \mathbb{R}^n$ be compact with finite Borel measure μ_X and $K : X \times X \to \mathbb{R}$ be a positive definite kernel which is given accordingly to Theorem 2.2 by the Fourier expansion* (2.24) *with a system of orthonormal basis functions $\psi_l \in L^2(X)$, and an associated summable sequence $\lambda_l \geq 0$, $l \in \mathbb{N}_0$. Then the Hilbert space $H_K(X)$ defined by* (2.26) *is a function space with the following properties:*

(i) *$H_K(X) \hookrightarrow C(X)$, cf.* (2.9)*, and for $f \in H_K(X)$ the Fourier series*

$$f(\boldsymbol{x}) = \sum_{l=0}^{\infty} \hat{f}_l \psi_l(\boldsymbol{x}), \qquad \boldsymbol{x} \in X, \tag{2.28}$$

converges absolutely and uniformly on X,

(ii) $K(\boldsymbol{x}, \cdot) \in H_K(X), \qquad \boldsymbol{x} \in X,$

(iii) $f(\boldsymbol{x}) = (f, K(\boldsymbol{x}, \cdot))_{H_K(X)}, \qquad f \in H_K(X), \quad \boldsymbol{x} \in X,$

(iv) *the space*

$$H_K^0(X) := \left\{ \sum_{i=1}^{M} a_i K(\boldsymbol{x}_i, \cdot) \ : \ \boldsymbol{x}_i \in X,\ a_i \in \mathbb{C},\ i = 1, \ldots, M,\ M \in \mathbb{N} \right\}$$

is dense in $H_K(X)$ with respect to $\| \cdot \|_{H_K(X)}$.

Moreover, the Hilbert space $H_K(X)$ is characterized alone by the properties (ii)-(iv). In particular, it does not depend on the functions ψ_l, $l \in \mathbb{N}_0$, nor the measure μ_X on X.

Proof. We follow the lines given in [28, Theorem 3 (Ch. III)]. Let $f \in H_K(X)$ be given by its Fourier series $f = \sum_{l=0}^{\infty} \hat{f}_l \psi_l \in L^2_+(X)$, cf. (2.25). We conclude for $\boldsymbol{x} \in X$ by the Cauchy–Schwarz inequality that

$$\Big| \sum_{l=0}^{\infty} \hat{f}_l \psi_l(\boldsymbol{x}) \Big| \leq \Big| \sum_{l=0}^{\infty} \big(\lambda_l^{-\frac{1}{2}} \hat{f}_l\big) \big(\lambda_l^{\frac{1}{2}} \psi_l(\boldsymbol{x})\big) \Big| \leq \Big(\sum_{l=0}^{\infty} \lambda_l^{-1} |\hat{f}_l|^2 \sum_{l=0}^{\infty} \lambda_l |\psi_l(\boldsymbol{x})|^2 \Big)^{\frac{1}{2}} \leq \|f\|_{H_K(X)} \sqrt{K(\boldsymbol{x}, \boldsymbol{x})}, \tag{2.29}$$

where we used the Fourier expansion (2.24) in Theorem 2.2. Since the kernel K is continuous and X is compact we infer $\|f\|_\infty \leq C \|f\|_{H_K(X)}$ for some constant $C > 0$. Hence, convergence in $H_K(X)$ implies convergence in $C(X)$ and thus the uniform convergence of the partial sums $f_N := \sum_{l=0}^{N} \hat{f}_l \psi_l$, $N \in \mathbb{N}_0$, to f, so that f is continuous by the continuity of ψ_l. Moreover, for fixed $\boldsymbol{x} \in X$ the series $\sum_{l=0}^{\infty} |\hat{f}_l \psi_l(\boldsymbol{x})|$, converges by inequality (2.29) applied to $\tilde{f}_{\boldsymbol{x}} := \sum_{l=0}^{\infty} (\hat{f}_{\boldsymbol{x}})_l \psi_l \in H_K(X)$, with Fourier coefficients satisfying $(\hat{f}_{\boldsymbol{x}})_l \psi_l(\boldsymbol{x}) = |\hat{f}_l \psi_l(\boldsymbol{x})|$. This implies absolute convergence of the series (2.28) and part (i) is proved.

For the further proof we observe for fixed $\boldsymbol{x} \in X$ that

$$K(\boldsymbol{x}, \cdot) = \sum_{l=0}^{\infty} \lambda_l \psi_l(\boldsymbol{x}) \overline{\psi}_l = \sum_{l=0}^{\infty} \lambda_l \overline{\psi}_l(\boldsymbol{x}) \psi_l \in L^2_+(X),$$

where we used the estimate $\sum_{l=0}^{\infty} |\lambda_l \overline{\psi}_l(\boldsymbol{x})|^2 \leq \lambda_{\max} \sum_{l=0}^{\infty} \lambda_l |\psi_l(\boldsymbol{x})|^2 = \lambda_{\max} K(\boldsymbol{x}, \boldsymbol{x}) < \infty$ with $\lambda_{\max} = \max_{l \in \mathbb{N}_0} \lambda_l$. Similarly, we find $\|K(\boldsymbol{x}, \cdot)\|_{H_K(X)} \leq K(\boldsymbol{x}, \boldsymbol{x}) < \infty$ which leads to the assertion (ii).

The property (iii) follows by the relations

$$(f, K(\boldsymbol{x}, \cdot))_{H_K(X)} = \sum_{l=0}^{\infty} \lambda_l^{-1} \hat{f}_l \overline{\lambda_l \overline{\psi}_l(\boldsymbol{x})} = \sum_{l=0}^{\infty} \hat{f}_l \psi_l(\boldsymbol{x}) = f(\boldsymbol{x}), \qquad \boldsymbol{x} \in X,$$

where the last equation follows from (i).

For proving the statement (iv) we observe at first that cl $H_K^0(X) \subset H_K(X)$ since $H_K(X)$ is complete. On the other hand let $f \in H_K(X)$ be in the orthogonal complement of $H_K^0(X)$, i.e., $(f,g) = 0$, $g \in H_K^0$. Then for $g = K(\boldsymbol{x},\cdot)$, $\boldsymbol{x} \in X$, we find by property (iii) that $f(\boldsymbol{x}) = (f, K(\boldsymbol{x},\cdot)) = 0$, $\boldsymbol{x} \in X$, which shows $H_K(X) = \text{cl } H_K^0(X) \oplus \{0\} = \text{cl } H_K^0(X)$.

For proving the uniqueness of H_K we assume that another Hilbert space H with inner product $(\cdot,\cdot)_H$ satisfies the conditions (ii)-(iv). By (ii) and (iii) we find

$$(K(\boldsymbol{x},\cdot), K(\boldsymbol{y},\cdot))_H = K(\boldsymbol{x},\boldsymbol{y}) = (K(\boldsymbol{x},\cdot), K(\boldsymbol{y},\cdot))_{H_K(X)}, \qquad \boldsymbol{x},\boldsymbol{y} \in X.$$

Moreover, with $H_K^0(X) \subset H$ we conclude by linearity of the inner product, that $(f,g)_H = (f,g)_{H_K(X)}$, $f,g \in H_K^0(X)$. Hence, the inner products are identically on $H_K^0(X)$ and since the completion cl $H_K^{(0)} = H$ is uniquely determined we have finished the proof. ■

A Hilbert space $H_K(X)$ which satisfies the properties (ii)-(iv) of Theorem 2.4 is called *reproducing Kernel Hilbert space* with *reproducing kernel* $K : X \times X \to \mathbb{R}$.

The most remarkable feature of a reproducing kernel Hilbert space $H_K(X)$ is the reproducing property (iii), which states that for any $\boldsymbol{x} \in X$ the point evaluation functional $I_{\delta_{\boldsymbol{x}}} : H_K(X) \to \mathbb{C}$, cf. (2.4) and (2.3), may be written as

$$I_{\delta_{\boldsymbol{x}}} f = f(\boldsymbol{x}) = (f, K(\boldsymbol{x},\cdot))_{H_K(X)}, \qquad f \in H_K(X). \tag{2.30}$$

In other words, the function $K(\boldsymbol{x},\cdot)$ is the Riesz representative of the point evaluation functional $I_{\delta_{\boldsymbol{x}}}$, $\boldsymbol{x} \in X$. We note further that for any Hilbert space of functions where point evaluation is defined and bounded for all points, there is by the Riesz Representation Theorem a uniquely defined kernel, which turns out to be positive definite.

Remark 2.5. Additionally to Theorem 2.4, any finite dimensional function space $H(X) \subset C(X)$, $X \subset \mathbb{R}^n$, which is spanned by real-valued functions, can be considered as a reproducing kernel Hilbert space. More precisely, we might equip $H(X)$ with an arbitrary inner product $(\cdot,\cdot)_{H(X)}$, e.g., the L^2-product defined by (2.12). Then via Gram–Schmidt orthonormalization we can construct an orthonormal basis of continuous real-valued functions $\psi_l \in H(X)$, $l = 0,\dots,L-1$, and find that the kernel

$$K_L(\boldsymbol{x},\boldsymbol{y}) := \sum_{l=0}^{L-1} \psi_l(\boldsymbol{x})\overline{\psi}_l(\boldsymbol{y}), \qquad \boldsymbol{x},\boldsymbol{y} \in X, \tag{2.31}$$

is a reproducing kernel, cf. (2.30), of the Hilbert space $H(X)$ with inner product $(\cdot,\cdot)_{H(X)}$. For polynomial spaces, the kernel K_L is also know as the *Christoffel–Darboux kernel.* □

2.2.2 The Worst Case Quadrature Error

With the theory of reproducing kernel Hilbert spaces at hand, we return to the quadrature problem in the strong sense, cf. (2.10). By Theorem 2.4 we see that we can associate to compact sets $X \subset \mathbb{R}^n$ and positive definite kernels $K : X \times X \to \mathbb{R}$ a reproducing kernel Hilbert space $H_K(X)$, which is continuously embedded in the space $C(X)$ of continuous functions on X, cf. (2.9). Hence, the integral functional I_ν, $\nu \in M_{\mathbb{C}}(\mathbb{R}^n)$, cf. (2.4), and the quadrature functional $Q(\boldsymbol{P},\boldsymbol{w})$, $\boldsymbol{P} = (\boldsymbol{p}_1,\dots,\boldsymbol{p}_M) \in X^M$, $\boldsymbol{w} = (w_1,\dots,w_M) \in \mathbb{C}^M$, $M \in \mathbb{N}$, cf. (2.5), are bounded linear functionals on $H_K(X) \hookrightarrow C(X)$. Thus, we can define the *worst case quadrature error*

between I_ν and $Q(\boldsymbol{P},\boldsymbol{w})$ in the reproducing kernel Hilbert space $H_K(X)$ as the function

$$\mathrm{err}_K(\nu,\boldsymbol{P},\boldsymbol{w}) := \sup_{\substack{f\in H_K(X),\\ \|f\|_{H_K(X)}\le 1}} |I_\nu f - Q(\boldsymbol{P},\boldsymbol{w})f| = \|I_\nu - Q(\boldsymbol{P},\boldsymbol{w})\|_{H_K(X)\to\mathbb{C}}, \tag{2.32}$$

which depends on the measure $\nu \in M_{\mathbb{C}}(\mathbb{R}^n)$, the quadrature points $\boldsymbol{P} \in X^M$, and the quadrature weights $\boldsymbol{w} \in \mathbb{C}^M$. Moreover, for a fixed finite Borel measure ν we will mostly consider the worst case quadrature error for *equal weights quadrature functionals*

$$Q_\nu(\boldsymbol{P}) := Q(\boldsymbol{P},\boldsymbol{w}), \quad \boldsymbol{P}\in X^M, \tag{2.33}$$

where the quadrature weights $\boldsymbol{w} := (w_1,\dots,w_M) \in \mathbb{R}^M$ are given by $w_i := \nu(X)/M$, $i = 1,\dots,M$. In that case the worst case quadrature error $\mathrm{err}_K(\nu,\boldsymbol{P},\boldsymbol{w})$ depends only on $\boldsymbol{P}\in X^M$ and we write $\mathrm{err}_K(\nu,\boldsymbol{P})$.

The most remarkable feature of the worst case quadrature error err_K of a reproducing kernel Hilbert space $H_K(X)$ is that it allows for an explicit evaluation formula, which is essentially based on the Riesz Representation Theorem for Hilbert spaces. Therefore, we start by presenting the Riesz representations of the integral and quadrature functionals.

Theorem 2.6. *Let $X\subset\mathbb{R}^n$ be compact and $H_K(X)$ be a reproducing kernel Hilbert space with reproducing kernel $K : X\times X\to\mathbb{R}$. Then the quadrature functional $Q(\boldsymbol{P},\boldsymbol{w}) : H_K(X)\to\mathbb{C}$, $\boldsymbol{P} := (\boldsymbol{p}_1,\dots,\boldsymbol{p}_M)\in X^M$, $\boldsymbol{w} = (w_1,\dots,w_M)^\top\in\mathbb{C}^M$, $M\in\mathbb{N}$, cf. (2.5), and the integral functional $I_\nu : H_K(X)\to\mathbb{C}$, $\nu\in M_{\mathbb{C}}(\mathbb{R}^n)$, cf. (2.4), are bounded and have the following Riesz representations*

$$Q(\boldsymbol{P},\boldsymbol{w})f = \sum_{i=1}^M w_i f(\boldsymbol{p}_i) = (f,h_Q)_{H_K(X)}, \quad f\in H_K(X), \qquad h_Q := \sum_{i=1}^M \overline{w}_i K(\boldsymbol{p}_i,\cdot), \tag{2.34}$$

$$I_\nu f = \int_X f(x)\mathrm{d}\nu(\boldsymbol{x}) = (f,h_{K,\nu})_{H_K(X)}, \quad f\in H_K(X), \qquad h_{K,\nu} := \int_X K(\boldsymbol{x},\cdot)\mathrm{d}\overline{\nu}(\boldsymbol{x}). \tag{2.35}$$

In particular, the operator norms are given by

$$\|Q(\boldsymbol{P},\boldsymbol{w})\|_{H_K(X)\to\mathbb{C}} = \sqrt{(h_Q,h_Q)}_{H_K(X)} = \Big(\sum_{i,j=1}^M w_i\overline{w}_j K(\boldsymbol{p}_i,\boldsymbol{p}_j)\Big)^{\frac{1}{2}}, \tag{2.36}$$

$$\|I_\nu\|_{H_K(X)\to\mathbb{C}} = \sqrt{(h_{K,\nu},h_{K,\nu})}_{H_K(X)} = \Big(\int_{X\times X} K(\boldsymbol{x},\boldsymbol{y})\mathrm{d}\overline{\nu}(\boldsymbol{x})\mathrm{d}\nu(\boldsymbol{y})\Big)^{\frac{1}{2}}. \tag{2.37}$$

Proof. We recall the observation that the integral functional $I_\nu : C(X)\to\mathbb{C}$ and the quadrature functional $Q(\boldsymbol{P},\boldsymbol{w}) : C(X)\to\mathbb{C}$ are bounded linear functionals in $C^*(X)$. Hence, by the property (i) of Theorem 2.4 we have $H_K(X)\hookrightarrow C(X)$, and the continuity of $I_\nu : H_K(X)\to\mathbb{C}$ and $Q(\boldsymbol{P},\boldsymbol{w}) : H_K(X)\to\mathbb{C}$ follows. Thus, for both functionals the Riesz Representation Theorem applies.

The representation (2.34) of the quadrature functional $Q(\boldsymbol{P},\boldsymbol{w})$ is obtained by using the representation of the point evaluation functional $I_{\delta_{\boldsymbol{x}}}$, $\boldsymbol{x}\in X$, cf. (2.30).

For the rest of the proof we need to show that the function $h_{K,\nu}$ defined by (2.35) induces the integral functional I_ν. Therefore, we let μ_X be an arbitrary Borel measure and choose for the kernel K the orthonormal basis functions $\psi_l\in L^2(X)$, $l\in\mathbb{N}_0$, with corresponding eigenvalues λ_l, accordingly to Theorem 2.2, and consider the original definition of $H_K(X)$, cf. (2.26). Thus, the

Fourier coefficients of the function $h_{K,\nu}$ are given by

$$(\hat{h}_{K,\nu})_l = \int_X h_{K,\nu}(\boldsymbol{y})\overline{\psi}_l(\boldsymbol{y})\mathrm{d}\mu_X(\boldsymbol{y}) = \int_X \int_X K(\boldsymbol{x},\boldsymbol{y})\overline{\psi}_l(\boldsymbol{y})\mathrm{d}\mu_X(\boldsymbol{y})\mathrm{d}\overline{\nu}(\boldsymbol{x}) = \lambda_l \int_X \overline{\psi}_l(\boldsymbol{x})\mathrm{d}\overline{\nu}(\boldsymbol{x}), \tag{2.38}$$

where we apply Fubini's Theorem and use the fact that the functions ψ_l, $l \in \mathbb{N}_0$ are eigenfunctions of the integral operator T_K, cf. (2.19). By definition of the inner product of $H_K(X)$, cf. (2.27), we conclude that the function $h_{K,\nu}$ is indeed a function of the reproducing kernel, since we have by Cauchy–Schwarz, cf. (2.1),

$$(h_{K,\nu}, h_{K,\nu})_{H_K(X)} = \sum_{l=0}^{\infty} \lambda_l^{-1} |(\hat{h}_{K,\nu})_l|^2 \leq \big(\nu_{(1)}(X) + \nu_{(2)}(X) + \nu_{(3)}(X) + \nu_{(4)}(X)\big)^2 \sum_{l=0}^{\infty} \lambda_l < \infty. \tag{2.39}$$

It follows that the functionals I_ν and $f \mapsto (f, h_{K,\nu})_{H_K(X)}$, $f \in H_K(X)$, are continuous in $H_K(X)$. Thus, it is sufficient to prove the relation (2.35) for the functions ψ_l, with $\lambda_l > 0$, which, by using (2.38), follows from

$$I_\nu \psi_l = \int_X \psi_l(\boldsymbol{x})\mathrm{d}\nu(\boldsymbol{x}) = \lambda_l^{-1}\overline{(\hat{h}_{K,\nu})_l} = \sum_{k=0}^{\infty} \lambda_k^{-1} \delta_{k,l} \overline{(\hat{h}_{K,\nu})_k} = (\psi_l, h_{K,\nu})_{H_K(X)}.$$

The statements (2.36), (2.37) for the operator norms follow from the Cauchy–Schwarz inequality, by applying the corresponding formulas for the Riesz representatives. ∎

By Theorem 2.6, we can rewrite the worst case quadrature error, by using the Riesz representation $h_{K,\nu}$, cf. (2.35), and h_Q, cf. (2.34), of the integral functional I_ν, $\nu \in M_{\mathbb{C}}(\mathbb{R}^n)$, and the quadrature functional $Q(\boldsymbol{P}, \boldsymbol{w})$, $\boldsymbol{P} \in X^M$, $\boldsymbol{w} \in \mathbb{C}^M$, respectively, and find

$$\mathrm{err}_K(\nu, \boldsymbol{P}, \boldsymbol{w}) = \|h_{K,\nu} - h_Q\|_{H_K(X)} = \Big\| \int_X K(\boldsymbol{x}, \cdot)\mathrm{d}\overline{\nu}(\boldsymbol{x}) - \sum_{i=1}^{M} \overline{w}_i K(\boldsymbol{p}_i, \cdot) \Big\|_{H_K(X)}. \tag{2.40}$$

Hence, from the fact $h_Q \in H_K^0(X)$, cf. property (iv) of Theorem 2.4, we conclude that the quadrature functionals are dense in the dual space $H_K^*(X)$. That is, the quadrature problem in the strong sense, cf. (2.10), makes sense in the reproducing kernel Hilbert space $H_K(X)$. More precisely, for a fixed measure ν we define the *minimal worst case quadrature error* on $H_K(X)$ by

$$\mathrm{err}_{K,\nu}^*(M) := \inf_{(\boldsymbol{P},\boldsymbol{w}) \in X^M \times \mathbb{C}^M} \mathrm{err}_K(\nu, \boldsymbol{P}, \boldsymbol{w}), \qquad \nu \in M_{\mathbb{C}}(\mathbb{R}^n), \quad M \in \mathbb{N}, \tag{2.41}$$

and infer monotonic convergence

$$\lim_{M\to\infty} \mathrm{err}_{K,\nu}^*(M) = 0, \qquad \mathrm{err}_{K,\nu}^*(M) \geq \mathrm{err}_{K,\nu}^*(M+1), \qquad M \in \mathbb{N}, \quad \nu \in M_{\mathbb{C}}(\mathbb{R}^n).$$

If additionally ν is a finite Borel measure, it is remarkable that we obtain even convergence results for equal weights quadrature functionals $Q_\nu(\boldsymbol{P})$, cf. Corollary 2.8. Therefore, we define the *minimal equal weights worst case quadrature error* on $H_K(X)$ by, cf. (2.1),

$$\mathrm{err}_{K,\nu}^{**}(M) := \min_{\boldsymbol{P} \in X^M} \mathrm{err}_K(\nu, \boldsymbol{P}), \qquad \nu \in M_{\mathbb{C}}(\mathbb{R}^n), \quad \nu_{(2)} = \nu_{(3)} = \nu_{(4)} = 0, \quad M \in \mathbb{N}. \tag{2.42}$$

However, in contrast to the quadrature error $\mathrm{err}_{K,\nu}^*(M)$ the quadrature error $\mathrm{err}_{K,\nu}^{**}(M)$ does not need to converge monotonically, see the last example in Section 2.5.1.

Throughout this thesis we make the following conventions. A quadrature functional $Q(\boldsymbol{P}^*, \boldsymbol{w}^*)$

of size M is called *optimal* for a complex Borel measure ν if it attains the minimal worst case quadrature error $\mathrm{err}^*_{K,\nu}(M)$. Similarly, we call an equal weights quadrature functional $Q_\nu(\boldsymbol{P}^*)$ of size M optimal for a finite Borel measure ν if it attains the minimal worst case quadrature error $\mathrm{err}^{**}_{K,\nu}(M)$. In the latter case the quadrature points $\boldsymbol{P}^* \in X^M$ are also called optimal.

The computation of optimal quadrature functionals or points, is based on the following central Theorem 2.7, which provides us with explicit formulas for the worst case quadrature error err_K in reproducing Hilbert spaces $H_K(X)$ with reproducing kernel K.

Theorem 2.7. *Let $X \subset \mathbb{R}^n$ be compact and $H_K(X)$ be a reproducing kernel Hilbert space with reproducing kernel $K : X \times X \to \mathbb{R}$. Then for $M \in \mathbb{N}$, the worst case quadrature error, cf.* (2.32)*, between the integral functional I_ν, $\nu \in M_{\mathbb{C}}(\mathbb{R}^n)$, and the quadrature functional $Q(\boldsymbol{P}, \boldsymbol{w})$ with quadrature points $\boldsymbol{P} = (\boldsymbol{p}_1, \ldots, \boldsymbol{p}_M) \in X^M$ and weights $\boldsymbol{w} = (w_1, \ldots, w_M) \in \mathbb{C}^M$ is given by*

$$\mathrm{err}_K(\nu, \boldsymbol{P}, \boldsymbol{w})^2 = \sum_{i,j=1}^{M} w_i \overline{w}_j K(\boldsymbol{p}_i, \boldsymbol{p}_j) - 2\mathrm{Re}\Big(\sum_{i=1}^{M} w_i h_{K,\nu}(\boldsymbol{p}_i) \Big) + \int_X h_{K,\nu}(\boldsymbol{y}) \mathrm{d}\nu(\boldsymbol{y}), \tag{2.43}$$

where $h_{K,\nu}$ is the Riesz representative of the integral functional I_ν defined by

$$h_{K,\nu}(\boldsymbol{y}) := \int_X K(\boldsymbol{x}, \boldsymbol{y}) \mathrm{d}\overline{\nu}(\boldsymbol{x}), \qquad \boldsymbol{y} \in X.$$

If additionally μ_X is a finite Borel measure and the orthonormal functions $\psi_l \in L^2(X)$ with eigenvalues $\lambda_l \geq 0$, $l \in \mathbb{N}_0$, are given as in Theorem 2.2, then the above relations have the series representations

$$\mathrm{err}_K(\nu, \boldsymbol{P}, \boldsymbol{w})^2 = \sum_{l=0}^{\infty} \lambda_l \Big| \hat{\overline{\nu}}_l - \sum_{i=1}^{M} \overline{w_i \psi_l(\boldsymbol{p}_i)} \Big|^2 \tag{2.44}$$

and

$$h_{K,\nu} = \sum_{l=0}^{\infty} \lambda_l \hat{\overline{\nu}}_l \psi_l, \qquad \hat{\overline{\nu}}_l := \int_X \overline{\psi}_l(\boldsymbol{x}) \mathrm{d}\overline{\nu}(\boldsymbol{x}), \tag{2.45}$$

where the convergence for is absolutely and uniformly on compact sets of $X^M \times \mathbb{C}^M$ and X, respectively.

Proof. The Fourier expansion (2.45) of the function $h_{K,\nu}$ follows from the relation (2.38) in the proof of Theorem 2.6. By relation (2.40) and Theorem 2.6 we conclude

$$\begin{aligned}
\mathrm{err}_K(\nu, \boldsymbol{P}, \boldsymbol{w})^2 &= \|h_{K,\nu}\|^2_{H_K(X)} + \|h_Q\|^2_{H_K(X)} - 2\mathrm{Re}\big((h_{K,\nu}, h_Q)_{H_K(X)} \big) \\
&= \|h_{K,\nu}\|^2_{H_K(X)} + \sum_{i,j=1}^{M} w_i \overline{w}_j K(\boldsymbol{p}_i, \boldsymbol{p}_j) - 2\mathrm{Re}\Big(\sum_{i=1}^{M} w_i (h_{K,\nu}, K(\boldsymbol{p}_i, \cdot))_{H_K(X)} \Big),
\end{aligned}$$

which proves together with (2.37) the equation (2.43). In order to show the equation (2.44) we interchange the summation and arrive at

$$\begin{aligned}
&\sum_{l=0}^{\infty} \lambda_l \Big| \hat{\overline{\nu}}_l - \sum_{i=1}^{M} \overline{w_i \psi_l(\boldsymbol{p}_i)} \Big|^2 = \sum_{l=0}^{\infty} \lambda_l \Big(|\hat{\overline{\nu}}_l|^2 + \Big| \sum_{i=1}^{M} w_i \psi_l(\boldsymbol{p}_i) \Big|^2 - 2\mathrm{Re}\Big(\sum_{i=1}^{M} \hat{\overline{\nu}}_l w_i \psi_l(\boldsymbol{p}_i) \Big) \Big) \\
&= \sum_{l=0}^{\infty} \lambda_l |\hat{\overline{\nu}}_l|^2 + \sum_{i,j=1}^{M} w_i \overline{w}_j \sum_{l=0}^{\infty} \lambda_l \psi_l(\boldsymbol{p}_i) \overline{\psi}_l(\boldsymbol{p}_j) - 2\mathrm{Re}\Big(\sum_{i=1}^{M} w_i \sum_{l=0}^{\infty} \hat{\overline{\nu}}_l \lambda_l \psi_l(\boldsymbol{p}_i) \Big),
\end{aligned}$$

Together with the Fourier expansions of the kernel K and the Riesz representative $h_{K,\nu}$, cf.

(2.24) and (2.45), we arrive at the assertion (2.44). The occurring series converge absolutely and uniformly on compact sets by the uniform and absolute convergence of the Fourier expansion of K, cf. (2.24), and the Riesz representative $h_{K,\nu} \in H_K(X)$, cf. (2.39). ■

The identity (2.43) in Theorem 2.7 provides the fundamental relation for the interpretation of the worst case quadrature error err_K, as an potential energy E_K, cf. (2.48) in Section 2.3, or an L^2-discrepancy $D_{\mathcal{B}}^2$, cf. Theorem 2.10 in Section 2.4. Moreover, by a probabilistic argument we are able to deduce from Theorem 2.7 a general asymptotic estimate for the minimal worst case quadrature errors $\mathrm{err}_{K,\nu}^*, \mathrm{er}_{K,\nu}^{**}$, given by Corollary 2.8. However, we note that substantially better bounds can be achieved for certain special cases of the compact set $X \subset \mathbb{R}^n$, the Borel measure ν, and the kernel K, e.g., see Theorem 6.29 in Section 6.4.

Corollary 2.8. *Let $X \subset \mathbb{R}^n$ be compact, $H_K(X)$ be a reproducing kernel Hilbert space with reproducing kernel $K : X \times X \to \mathbb{R}$, and ν be a finite Borel measure. Then the minimal worst case quadrature errors given by* (2.41) *and* (2.42) *satisfy*

$$\mathrm{err}_{K,\nu}^*(M) \leq \mathrm{err}_{K,\nu}^{**}(M) \leq \frac{C_{K,\nu}}{\sqrt{M}}, \qquad M \in \mathbb{N}, \tag{2.46}$$

where

$$C_{K,\nu} := \left(\int_{X \times X} \big(K(\boldsymbol{x},\boldsymbol{x}) - K(\boldsymbol{x},\boldsymbol{y})\big) \mathrm{d}\nu(\boldsymbol{x}) \mathrm{d}\nu(\boldsymbol{y}) \right)^{\frac{1}{2}} \geq 0.$$

Proof. The first inequality in (2.46) is trivial by the definitions (2.41) and (2.42). For the proof of the second inequality we use a probabilistic argument and consider the normalized measure $\tilde{\nu} := (1/\nu(X))\nu$ as an probability density of a randomly chosen quadrature point. The expectation value of the squared worst case quadrature error (2.32) with constant weights is then given by

$$\mathbb{E}_\nu(M) := \int_{X^M} \mathrm{err}_K\big(\nu, (\boldsymbol{p}_1, \ldots, \boldsymbol{p}_M)\big)^2 \mathrm{d}\tilde{\nu}(\boldsymbol{p}_1) \cdots \mathrm{d}\tilde{\nu}(\boldsymbol{p}_M), \qquad M \in \mathbb{N}.$$

For computing the expectation value we make use of the first equation in (2.43) of Theorem 2.7 and we arrive with $h_{K,\nu}(\boldsymbol{y}) := \int_X K(\boldsymbol{x},\boldsymbol{y}) \mathrm{d}\overline{\nu}(\boldsymbol{x})$, $\boldsymbol{y} \in X$, at

$$\begin{aligned}
\mathbb{E}_\nu(M) =& \|h_{K,\nu}\|_{H_K(X)}^2 + \frac{\nu(X)^2}{M^2} \sum_{\substack{i,j=1,\\ i \neq j}}^{M} \int_X \int_X K(\boldsymbol{p}_i,\boldsymbol{p}_j) \mathrm{d}\tilde{\nu}(\boldsymbol{p}_i) \mathrm{d}\tilde{\nu}(\boldsymbol{p}_j) \\
&+ \frac{\nu(X)^2}{M^2} \sum_{i=1}^{M} \int_X K(\boldsymbol{p}_i,\boldsymbol{p}_i) \mathrm{d}\tilde{\nu}(\boldsymbol{p}_i) \\
&- \frac{2\nu(X)}{M} \sum_{i=1}^{M} \int_X \int_X K(\boldsymbol{p}_i,\boldsymbol{x}) \mathrm{d}\nu(\boldsymbol{x}) \mathrm{d}\tilde{\nu}(\boldsymbol{p}_i).
\end{aligned}$$

The above equation simplifies by using the expression (2.37) of Theorem 2.6 for $\|h_{K,\nu}\|_{H_K(X)}^2$ and we arrive by Fubini's Theorem at

$$\begin{aligned}
\mathbb{E}_\nu(M) =& \|h_{K,\nu}\|_{H_K(X)}^2 \left(1 - 2 + (M^2 - M)/(M)^2\right) + \frac{\nu(X)}{M} \int_X K(\boldsymbol{x},\boldsymbol{x}) \mathrm{d}\nu(\boldsymbol{x}) \\
=& \frac{1}{M} \left(\nu(X) \int_X K(\boldsymbol{x},\boldsymbol{x}) \mathrm{d}\nu(\boldsymbol{x}) - \int_X \int_X K(\boldsymbol{x},\boldsymbol{y}) \mathrm{d}\nu(\boldsymbol{x}) \mathrm{d}\nu(\boldsymbol{y}) \right).
\end{aligned}$$

Since $\mathrm{err}^{**}_{K,\nu}(M) \leq \mathrm{err}_K(\nu, \boldsymbol{P})$ for $\boldsymbol{P} \in X^M$ we conclude after integration with respect to $\tilde{\nu}^M$ that $\mathrm{err}^{**}_{K,\nu}(M)^2 \leq \mathbb{E}_\nu(M)$, which finishes the proof. ■

Remark 2.9. For compact sets $X \subset \mathbb{R}^n$ with positive definite kernel $K : X \times X \to \mathbb{R}$ it is sometimes more convenient to consider for fixed $C \in \mathbb{R}$ a kernel of the form

$$\tilde{K}(\boldsymbol{x}, \boldsymbol{y}) := K(\boldsymbol{x}, \boldsymbol{y}) + C, \qquad \boldsymbol{x}, \boldsymbol{y} \in X.$$

The kernel $\tilde{K}$ does not need to be positive definite. However, for an equal weights quadrature formula $Q_\nu(\boldsymbol{P})$, $\boldsymbol{P} := (\boldsymbol{p}_1, \ldots, \boldsymbol{p}_M) \in X^M$, of some finite Borel measure ν, the worst case quadrature error err_K can be computed by replacing K with $\tilde{K}$ in the formula (2.43), i.e.,

$$\mathrm{err}_K(\nu, \boldsymbol{P})^2 = \left(\frac{\nu(X)}{M}\right)^2 \sum_{i,j=1}^{M} \tilde{K}(\boldsymbol{p}_i, \boldsymbol{p}_j) - 2\frac{\nu(X)}{M} \sum_{i=1}^{M} h_{\tilde{K},\nu}(\boldsymbol{p}_i) + \int_X h_{\tilde{K},\nu}(\boldsymbol{y}) \mathrm{d}\nu(\boldsymbol{y}),$$

where $h_{\tilde{K},\nu}(\boldsymbol{y}) := \int_X \tilde{K}(\boldsymbol{x}, \boldsymbol{y}) \mathrm{d}\nu(\boldsymbol{x})$, $\boldsymbol{y} \in X$. Moreover, minimizing the worst case quadrature error $\mathrm{err}_K(\nu, \boldsymbol{P})$ is equivalent to minimize the energy

$$E_K(\nu, \boldsymbol{P}) := \frac{\nu(X)}{M} \sum_{i=1}^{M-1} \sum_{j=i+1}^{M} \tilde{K}(\boldsymbol{p}_i, \boldsymbol{p}_j) + \sum_{i=1}^{M} \left[\frac{\nu(X)}{2M} K(\boldsymbol{p}_i, \boldsymbol{p}_i) - h_{\tilde{K},\nu}(\boldsymbol{p}_i)\right], \qquad \boldsymbol{P} \in X^M. \quad \square$$

2.3 Potential Energies

In this section we give a physical interpretation of the worst case quadrature error in reproducing kernel Hilbert spaces. Furthermore, we briefly present some possible generalizations in terms of generalized potential energies of signed Borel measures, used in potential theory, cf. [82, 113].

Electrostatic Energy

For a physical point of view, we assume that M pairwise distinct particles $\boldsymbol{p}_i \in \mathbb{R}^3$ of negative charge $q_i < 0$, $i = 1, \ldots, M$, are interacting accordingly to Coulomb's Law. Moreover, we assume that a certain measurable domain $X \subset \mathbb{R}^3$ corresponds to a positively charged external electric field given by a density distribution $\mathrm{d}\nu$ of some finite Borel measure ν. Then the electrostatic energy of the particle system is given by

$$E_\nu(\boldsymbol{P}, \boldsymbol{q}) = \frac{1}{2} \sum_{\substack{i,j=1,\\ i \neq j}}^{M} \frac{q_i q_j}{\|\boldsymbol{p}_i - \boldsymbol{p}_j\|_2} + \sum_{i=1}^{M} \int_X \frac{q_i}{\|\boldsymbol{p}_i - \boldsymbol{x}\|_2} \mathrm{d}\nu(\boldsymbol{x}) + C, \tag{2.47}$$

where $\boldsymbol{P} := (\boldsymbol{p}_1, \ldots, \boldsymbol{p}_M) \in \mathbb{R}^{3M}$, $\boldsymbol{q} := (q_1, \ldots, q_M) \in \mathbb{R}^M$, and $C \in \mathbb{R}$ is some fixed constant. For a fixed external field described by ν and fixed charges $\boldsymbol{q}$ with $\sum_{i=1}^{M} q_i = -\nu(X)$ we allow the particles $\boldsymbol{p}_i$, $i = 1, \ldots, M$, to move freely in $\mathbb{R}^3$. By physical principles the particles $\boldsymbol{P}$ tend to minimize the electrostatic energy and arrange in some stationary state. Visually speaking, the first term of the electrostatic energy E_ν, cf. (2.47), enforces the particles to repulse each other, whereas the second term leads to an attraction force of the negatively charged particles towards the positively charged domain X. In regions where the density of ν is high one might expect more particles than in regions where the density of ν is low. Hence, in some sense the distribution of the particles in stationary state should mimic the density distribution of ν. We remark that this interpretation has been recently used in [114] for halftoning of images, see Section 6.5.

A particular important problem arises if the particles $\boldsymbol{p}_i$ are restricted to the unit sphere $\mathbb{S}^2 := \{\boldsymbol{x} \in \mathbb{R}^3 \ : \ \|\boldsymbol{x}\|_2 = 1\}$ and have charge $q_i = 1$, $i = 1, \dots, M$, and where the Borel measure $\nu = \mu_{\mathbb{S}^2}$ is the canonical surface measure, cf. (3.72). For given $M \in \mathbb{N}$ the determination of the optimal distribution of particles $\boldsymbol{P} \in (\mathbb{S}^2)^M$, i.e., with minimal electrostatic energy $E_{\mu_{\mathbb{S}^2}}(\boldsymbol{P}, \boldsymbol{q})$, is known as the Thomson Problem, cf. [130], and has attracted a lot of attention in several fields of mathematics. For recent results and a list of putatively optimal point distributions we refer to [138, 137] and the online database [16]. We like also to mention that in our paper [7] we applied a PDE approach to tackle that problem. We remark further that the Thomson Problem is strongly related to the 7th problem of Smale's list of 'Mathematical Problems for the next century', cf. [120], where the electrostatic energy (2.47) is replaced by the logarithmic potential energy

$$E(\boldsymbol{P}) := -\frac{1}{2} \sum_{\substack{i,j=1,\\ i \neq j}}^{M} \log(\|\boldsymbol{p}_i - \boldsymbol{p}_j\|_2), \qquad \boldsymbol{P} := (\boldsymbol{p}_1, \dots, \boldsymbol{p}_M) \in (\mathbb{S}^2)^M.$$

Potentials and Potential Energies

In potential theory one generalizes the above electrostatic energy by certain potential energies of measures. In what follows we let $X \subset \mathbb{R}^n$ be a measurable set, which is not necessarily bounded, and $K : X \times X \to \mathbb{R}$ be some measurable function. We note that the function K should possess some further properties, similar to the properties of positive definite kernels. For brevity we will not go further in to this and refer to the literature [82, 113]. Of particular interest in potential theory are the Riesz kernels, and the Green kernels associated to the Dirichlet problem of the Laplace equation. The Riesz kernels for dimension $n \in \mathbb{N}$ are defined by

$$K_{\alpha,n}(\boldsymbol{x}, \boldsymbol{y}) = \begin{cases} \|\boldsymbol{x} - \boldsymbol{y}\|_2^{\alpha - n}, & \boldsymbol{x} \neq \boldsymbol{y}, \\ 0, & \boldsymbol{x} = \boldsymbol{y}, \end{cases} \qquad \boldsymbol{x}, \boldsymbol{y} \in \mathbb{R}^n, \quad 0 < \alpha < n,$$

and the logarithmic kernel, as a certain limit of Riesz kernels $K_{\alpha,n}$ for $\alpha \to n$, is given by[3]

$$K_{n,n}(\boldsymbol{x}, \boldsymbol{y}) = \begin{cases} -\ln\left(\|\boldsymbol{x} - \boldsymbol{y}\|_2\right), & \boldsymbol{x} \neq \boldsymbol{y}, \\ 0, & \boldsymbol{x} = \boldsymbol{y}, \end{cases}, \qquad \boldsymbol{x}, \boldsymbol{y} \in \mathbb{R}^n.$$

We remark that the kernel $K_{2,n}$ is, if suitably normalized, the fundamental solution of the Laplace equation in Euclidean space $\mathbb{R}^n$, respectively, cf. [82].

In what follows we allow $K : X \times X \to \mathbb{R}$ to be a positive definite kernel or a kernel of the form $K_{\alpha,n}$, $0 < \alpha \leq n$, restricted to X. Then for a signed Borel measure μ, cf. Section 2.1, with compact support $\operatorname{supp}(\mu) \subset X$ the *K-potential* of μ is defined by

$$U_{K,\mu}(\boldsymbol{x}) := \int_X K(\boldsymbol{x}, \boldsymbol{y}) \mathrm{d}\mu(\boldsymbol{y}), \qquad \boldsymbol{x} \in X,$$

and the *K-potential energy* of μ is defined by

$$E_K(\mu) := \int_X \int_X K(\boldsymbol{x}, \boldsymbol{y}) \mathrm{d}\mu(\boldsymbol{y}) \mathrm{d}\mu(\boldsymbol{x}) = \int_X U_{K,\mu}(\boldsymbol{x}) \mathrm{d}\mu(\boldsymbol{x}).$$

In particular, if we set $\mu := \nu - \delta_{\boldsymbol{P},\boldsymbol{w}}$, cf. (2.6), for some fixed finite Borel measure ν, points $\boldsymbol{P} := (\boldsymbol{p}_1, \dots, \boldsymbol{p}_M) \in X^M$ and weights $\boldsymbol{w} := (w_1, \dots, w_M) \in \mathbb{R}^M$, we find that the K-potential

[3] For convenience we use these definitions of the kernels $K_{\alpha,n}$, $0 < \alpha \leq n$, which differ from the usual ones where the value ∞ is allowed at the point $(\boldsymbol{x}, \boldsymbol{x}) \in \mathbb{R}^n \times \mathbb{R}^n$.

energy reads as

$$E_{K,\nu}(\boldsymbol{P},\boldsymbol{w}) := E_K(\nu - \delta_{\boldsymbol{P},\boldsymbol{w}}) = \int_X \int_X K(\boldsymbol{x},\boldsymbol{y})\mathrm{d}\nu(\boldsymbol{y})\mathrm{d}\nu(\boldsymbol{x}) + \sum_{i,j=1}^{\infty} w_i w_j K(\boldsymbol{p}_i,\boldsymbol{p}_j) - 2\sum_{i=1}^{M} w_i \int_X K(\boldsymbol{x},\boldsymbol{p}_i)\mathrm{d}\nu(\boldsymbol{x}). \tag{2.48}$$

Hence, for $X \subset \mathbb{R}^3$ and kernel $K := \frac{1}{2}K_{2,3}$ we recover the electrostatic energy E_ν of pairwise distinct particles $\boldsymbol{p}_i$ of charge $q_i := -w_i$, $i = 1,\ldots,M$, in an external field described by the measure ν, cf. (2.47). Moreover, by comparing the relation (2.48) with the worst case quadrature error given by the formula (2.43) in Theorem 2.7 we observe a remarkable concordance, where the function $h_{K,\nu}$ takes the role of the K-potential $U_{K,\nu}$. Thus, the worst case quadrature error in reproducing kernel Hilbert spaces $H_K(X)$, $X \subset \mathbb{R}^n$, might be considered as a special case of K-potential energies.

By relation (2.48), the K-potential energy can also be considered as a quantity which describes the similarity between the measure ν and $\delta_{\boldsymbol{P},\boldsymbol{w}}$, $\boldsymbol{P} \in X^M$, $\boldsymbol{w} \in \mathbb{R}^M$. In Section 2.4 we discuss a more natural and geometric notion of similarity between measures which leads us back to quadrature errors in reproducing kernel Hilbert spaces.

2.4 Discrepancies

In this section we consider the general quadrature problem described in Section 2.1 from a slightly different point of view, which leads us to geometric interpretations of quadrature errors in certain reproducing kernel Hilbert spaces. Therefore, we take a look into the theory of discrepancies. We remark, that the notion of discrepancy was originally introduced in the field of number theory for quantifying the uniformity of point sequences, cf. [78]. Later on, the discrepancy theory, also known as the theory of irregularities of distributions, becomes a broad and versatile field, with strong connection to multivariate integration problems. For recent developments we refer to the monographs [13, 35, 88, 97].

The notion of discrepancy can be considered as a quantity which describes the similarity between two different complex Borel measures $\nu_1, \nu_2 \in M_{\mathbb{C}}(\mathbb{R}^n)$. However, of most interest, for say numerical integration, is the comparison of a prescribed measure $\nu \in M_{\mathbb{C}}(\mathbb{R}^n)$, supported on a compact set $X \subset \mathbb{R}^n$, and a discrete measure $\delta_{\boldsymbol{P},\boldsymbol{w}}$, cf. (2.6), concentrated at the points $\boldsymbol{P} := (\boldsymbol{p}_1,\ldots,\boldsymbol{p}_M) \in X^M$ with weights $\boldsymbol{w} := (w_1,\ldots,w_M)^\top \in \mathbb{C}^M$, cf. (2.6). Then a natural quantity for measuring the similarity between the measure ν and $\delta_{\boldsymbol{P},\boldsymbol{w}}$ is the L^∞-discrepancy defined by

$$D^\infty_{\mathcal{B}}(\nu,\boldsymbol{P},\boldsymbol{w}) := \sup_{B\in\mathcal{B}} \Big|\nu(B) - \delta_{\boldsymbol{P},\boldsymbol{w}}(B)\Big|, \qquad \nu,\ \delta_{\boldsymbol{P},\boldsymbol{w}} \in M_{\mathbb{C}}(\mathbb{R}^n), \quad \boldsymbol{P} \in X^M, \quad \boldsymbol{w} \in \mathbb{C}^M, \tag{2.49}$$

where the supremum is taken over some prescribed *basis set* $\mathcal{B}$, which is a family of measurable sets of X.

For practical questions, the measure ν is in general a finite, continuous Borel measure so that the discrete measure $\delta_{\boldsymbol{P},\boldsymbol{w}}$ has weights $\boldsymbol{w} \in \mathbb{R}^M$. For example, if ν is a probability measure and the weights are all equal with $w_i = 1/M$, $i = 1,\ldots,M$, then the L^∞-discrepancy $D^\infty_{\mathcal{B}}(\nu,\boldsymbol{P},\boldsymbol{w})$ represents the maximal error over all sets $B \in \mathcal{B}$ between the measure $\nu(B)$ and the relative number of points $\boldsymbol{p}_i \in X$, $i = 1,\ldots,M$, contained in B.

Obviously, the choice of the basis set $\mathcal{B}$ is crucial for obtaining a meaningful notion of similarity by the L^∞-discrepancy $D^\infty_{\mathcal{B}}(\nu,\boldsymbol{P},\boldsymbol{w})$. The basis set $\mathcal{B}$ should be not to big, as the set of all measurable sets of X, since in this the case L^∞-discrepancy $D^\infty_{\mathcal{B}}(\nu,\boldsymbol{P},\boldsymbol{w})$ cannot be made small even if the normalized counting measures $\delta_{\boldsymbol{P},\boldsymbol{w}}$ converge to the measure ν in the weak sense (2.7).

On the other hand the basis set $\mathcal{B}$ should be not to small in order to distinguish between different measures. A more thorough treatment of the requisite properties of reasonable basis sets $\mathcal{B}$ can be found in [35, Sec. 2.1]. Nevertheless, there is a lot of freedom for the choice of a meaningful basis set $\mathcal{B}$, as seen by the geometric constructions presented in the Sections 2.4.1–2.4.3.

For example, on the interval $X = [1, 0]$, a well-studied type of discrepancy, cf. [78, Ch. 2], is determined by the basis set $\mathcal{B}$, which consists of all subintervals of X, i.e., $\mathcal{B} := \{B(\boldsymbol{t}) := [t_1, t_2) \subset X \ : \ \boldsymbol{t} \in D\}$, $D := \{\boldsymbol{t} := (t_1, t_2) \in \mathbb{R}^2 \ : \ 0 \leq t_1 < t_2 \leq 1\}$.

The L^∞-discrepancy (2.49) can be considered as the L^∞-error between the (complex) measures ν and $\delta_{\boldsymbol{P},\boldsymbol{w}}$, $\boldsymbol{P} \in X^M$, $\boldsymbol{w} \in \mathbb{C}^M$, with respect to the basis set $\mathcal{B}$. In a similar fashion, we aim to introduce the L^2-discrepancy as the L^2-error between these two measures, which turns out to be strongly related to quadrature errors in certain reproducing kernel Hilbert spaces.

For that reason we assume that the basis set $\mathcal{B}$ can be parameterized by a parameter $\boldsymbol{t}$ over a certain domain $D \subset \mathbb{R}^d$, $d \in \mathbb{N}$, equipped with some finite Borel measure μ_D, where the function $(\boldsymbol{t}, \boldsymbol{x}) \mapsto 1_{B(\boldsymbol{t})}(\boldsymbol{x})$ is measurable on $D \times X$. In particular, the functions $1_{B(\cdot)}(\boldsymbol{x})$, $\boldsymbol{x} \in X$, and $\mu_X(B(\cdot))$ are measurable, cf. [25, Lemma 5.1.1 and Proposition 5.2.1]. Then the *L^2-discrepancy* given by

$$D_{\mathcal{B}}^2(\nu, \boldsymbol{P}, \boldsymbol{w}) := \left(\int_D \left| \nu(B(\boldsymbol{t})) - \delta_{\boldsymbol{P},\boldsymbol{w}}(B(\boldsymbol{t})) \right|^2 \mathrm{d}\mu_D(\boldsymbol{t}) \right)^{\frac{1}{2}}, \qquad \nu \in M_{\mathbb{C}}(\mathbb{R}^n),\ \boldsymbol{P} \in X^M,\ \boldsymbol{w} \in \mathbb{C}^M, \tag{2.50}$$

is well defined. One can think of the L^2-discrepancy $D_{\mathcal{B}}^2(\nu, \boldsymbol{P}, \boldsymbol{w})$ as a root mean square error of the differences between $\nu(B)$ and $\delta_{\boldsymbol{P},\boldsymbol{w}}(B)$ taken over all possible sets $B \in \mathcal{B}$, where loosely speaking every set $B(\boldsymbol{t}) \in \mathcal{B}$ is weighted by the density $\mathrm{d}\mu_D(\boldsymbol{t})$, $\boldsymbol{t} \in D$. An evident relation to the L^∞-discrepancy $D_{\mathcal{B}}^\infty(\nu, \boldsymbol{P}, \boldsymbol{w})$ is given by

$$D_{\mathcal{B}}^2(\nu, \boldsymbol{P}, \boldsymbol{w}) \leq \sqrt{\mu_D(D)}\, D_{\mathcal{B}}^\infty(\nu, \boldsymbol{P}, \boldsymbol{w}), \qquad \nu \in M_{\mathbb{C}}(\mathbb{R}^n), \quad \boldsymbol{P} \in X^M, \quad \boldsymbol{w} \in \mathbb{C}^M.$$

Hence, the L^2-discrepancy $D_{\mathcal{B}}^2(\nu, \boldsymbol{P}, \boldsymbol{w})$ is a weaker notion of similarity between the (complex) measures ν and $\delta_{\boldsymbol{P},\boldsymbol{w}}$, such that in the theory of discrepancy, one usually considers the L^∞-discrepancy $D_{\mathcal{B}}^\infty(\nu, \boldsymbol{P}, \boldsymbol{w})$. However, the striking argument for considering the L^2-discrepancy $D_{\mathcal{B}}^2$ is that it coincides for certain instances with the worst case quadrature error $\mathrm{err}_{K_{\mathcal{B}}}$ of a reproducing kernel Hilbert space $H_{K_{\mathcal{B}}}(X)$.

Theorem 2.10. *Let $X \subset \mathbb{R}^n$ be compact and the basis set*

$$\mathcal{B} := \{B(\boldsymbol{t}) \subset X \ : \ \boldsymbol{t} \in D\}, \qquad D \subset \mathbb{R}^d,$$

with finite Borel measure μ_D accordingly to definition (2.50) *be given, such that $(\boldsymbol{t}, \boldsymbol{x}) \mapsto 1_{B(\boldsymbol{t})}(\boldsymbol{x})$ is measurable on $D \times X$. Then the function*

$$K_{\mathcal{B}}(\boldsymbol{x}, \boldsymbol{y}) := \int_D 1_{B(\boldsymbol{t})}(\boldsymbol{x}) 1_{B(\boldsymbol{t})}(\boldsymbol{y}) \mathrm{d}\mu_D(\boldsymbol{t}), \qquad \boldsymbol{x}, \boldsymbol{y} \in X, \tag{2.51}$$

is symmetric and positive definite.

If additionally the function $K_{\mathcal{B}}$ is continuous then the worst case quadrature error $\mathrm{err}_{K_{\mathcal{B}}}$, *cf.* (2.32), *of the corresponding reproducing kernel Hilbert space $H_{K_{\mathcal{B}}}(X)$ coincides with the L^2-discrepancy $D_{\mathcal{B}}^2$, cf.* (2.50), *i.e.,*

$$\mathrm{err}_{K_{\mathcal{B}}}(\nu, \boldsymbol{P}, \boldsymbol{w}) = D_{\mathcal{B}}^2(\nu, \boldsymbol{P}, \boldsymbol{w}), \qquad \nu \in M_{\mathbb{C}}(\mathbb{R}^n), \quad \boldsymbol{P} \in X^M, \quad \boldsymbol{w} \in \mathbb{C}^M. \tag{2.52}$$

Proof. At first, we observe that the function $K_{\mathcal{B}}$ is well defined since, for every fixed $\boldsymbol{x} \in X$, the function $1_{B(\cdot)}(\boldsymbol{x})$, and so the product in definition (2.51) is measurable. Obviously, the

function $K_{\mathcal{B}}$ is symmetric and bounded by $\mu_D(D)$. The positive definiteness, cf. (2.18), follows for $\boldsymbol{a} = (a_1, \ldots, a_M) \in \mathbb{R}^M$ by

$$\sum_{i,j=1}^{M} K_{\mathcal{B}}(\boldsymbol{x}_i, \boldsymbol{x}_j) a_i a_j = \int_D \Big(\sum_{i=1}^{M} a_i 1_{B(\boldsymbol{t})}(\boldsymbol{x}_i) \Big)^2 \mathrm{d}\mu_D(\boldsymbol{t}) \geq 0.$$

Hence, the reproducing kernel Hilbert space $H_{K_{\mathcal{B}}}(X)$ is well defined if $K_{\mathcal{B}}$ is continuous.

From the definition of the L^2-discrepancy (2.50) we obtain

$$\big(D^2_{\mathcal{B}}(\nu, \boldsymbol{P}, \boldsymbol{w})\big)^2 = \int_D \Big(\big|\nu(B(\boldsymbol{t}))\big|^2 - 2\mathrm{Re}\big(\nu(B(\boldsymbol{t}))\overline{\delta_{\boldsymbol{P},\boldsymbol{w}}(B(\boldsymbol{t}))}\big) + \big|\delta_{\boldsymbol{P},\boldsymbol{w}}(B(\boldsymbol{t}))\big|^2 \Big) \mathrm{d}\mu_D(\boldsymbol{t}). \tag{2.53}$$

We define $h_{K,\nu}(\boldsymbol{y}) := \int_X K(\boldsymbol{x}, \boldsymbol{y}) \mathrm{d}\overline{\nu}(\boldsymbol{x})$, $\boldsymbol{y} \in X$. Thus, the first term on the right hand side of equation (2.53) simplifies by Fubini's Theorem to

$$\begin{aligned} \int_D \big|\nu(B(\boldsymbol{t}))\big|^2 \mathrm{d}\mu_D(\boldsymbol{t}) &= \int_X \int_X \Big(\int_D 1_{B(\boldsymbol{t})}(\boldsymbol{x}) 1_{B(\boldsymbol{t})}(\boldsymbol{y}) \mathrm{d}\mu_D(\boldsymbol{t}) \Big) \mathrm{d}\overline{\nu}(\boldsymbol{x}) \mathrm{d}\nu(\boldsymbol{y}) \\ &= \int_X \int_X K_{\mathcal{B}}(\boldsymbol{x}, \boldsymbol{y}) \mathrm{d}\overline{\nu}(\boldsymbol{x}) \mathrm{d}\nu(\boldsymbol{y}) = \|h_{K,\nu}\|^2_{H_{K_{\mathcal{B}}}(X)}, \end{aligned}$$

where we used the relation (2.37) in Theorem 2.6. In the same manner we simplify the second and third term in equation (2.53) to

$$2 \int_D \mathrm{Re}\big(\nu(B(\boldsymbol{t}))\overline{\delta_{\boldsymbol{P},\boldsymbol{w}}(B(\boldsymbol{t}))}\big) \mathrm{d}\mu_D(\boldsymbol{t}) = 2\mathrm{Re}\Big(\sum_{i=1}^{M} w_i \int_X K_{\mathcal{B}}(\boldsymbol{x}, \boldsymbol{p}_i) \mathrm{d}\overline{\nu}(\boldsymbol{x}) \Big)$$

and

$$\int_D \big|\delta_{\boldsymbol{P},\boldsymbol{w}}(B(\boldsymbol{t}))\big|^2 \mathrm{d}\mu_D(\boldsymbol{t}) = \sum_{i,j=1}^{M} w_i \overline{w}_j K_{\mathcal{B}}(\boldsymbol{p}_i, \boldsymbol{p}_j),$$

respectively. Comparing the above findings with the evaluation formula (2.43) of the worst case quadrature error $\mathrm{err}_{K_{\mathcal{B}}}$ in Theorem 2.7 we arrive at the assertion (2.52). ∎

By Theorem 2.10 it is appropriate to denote the kernel $K_{\mathcal{B}}$ defined by (2.51) as the *discrepancy kernel* corresponding to the L^2-discrepancy $D^2_{\mathcal{B}}(\nu, \boldsymbol{P}, \boldsymbol{w})$ with respect to the basis set $\mathcal{B}$.

As already mentioned, the choice of the basis set $\mathcal{B}$, as well as the corresponding measure μ_D, for defining L^2-discrepancies $D^2_{\mathcal{B}}$, cf. (2.50), can be quite arbitrary. However, we present in Section 2.4.1–2.4.3 some interesting constructions, which lead by Theorem 2.10 to a geometric meaning for the worst case quadrature errors $\mathrm{err}_{K_{\mathcal{B}}}$ in the corresponding reproducing kernel Hilbert spaces $H_{K_{\mathcal{B}}}(X)$.

We briefly motivate our particular interest in the three constructions of Section 2.4.1–2.4.3 as follows. Provided that the set $X \subset \mathbb{R}^n$ is equipped with a metric d_X we define in Section 2.4.1 the weighted ball discrepancy $D^2_{\mathcal{B}_{\mathrm{d}_X}}$. With the formula given in Theorem 2.11 we are able to compute explicitly, for certain special cases, the Fourier expansions of the corresponding discrepancy kernel $K_{\mathcal{B}_{\mathrm{d}_X}}$ on the torus $X = \mathbb{T}^d$ and the sphere $X = \mathbb{S}^d$, see Theorem 4.1 and Theorem 4.5 in Chapter 4, respectively. These Fourier expansions are particular useful for the efficient computation of low-discrepancy points on the sphere $\mathbb{S}^2$, cf. Section 6.4.1, and for efficient halftoning of images, cf. Section 6.5. Another important type of discrepancy is considered in Section 2.4.2 and called the L^2-discrepancy over halfspaces $D^2_{\mathcal{H}_+}$, where in a special case the corresponding discrepancy kernel has the particular simple form $K_{\mathcal{H}_+}(\boldsymbol{x}, \boldsymbol{y}) = C_X - c_n \|\boldsymbol{x} - \boldsymbol{y}\|_2$, $\boldsymbol{x}, \boldsymbol{y} \in X$, for some constants $C_X, c_n > 0$, cf. Theorem 2.14. We note that the kernel $K_{\mathcal{H}_+}$ plays, due to its simplicity, a special

role in the theory of low-discrepancy points, see Section 6.4. For the efficient computation of low-discrepancy points on the sphere $\mathbb{S}^d$, cf. Section 6.4.2, we introduce the L^2-discrepancy over Euclidean balls $D^2_{\mathcal{B}_{\mathbb{R}^n,R}}$ in Section 2.4.3, which leads to a family of compactly supported, positive definite kernels $K_{\mathcal{B}_{\mathbb{R}^n},R}$, $R > 0$, cf. Theorem 2.16. This type of L^2-discrepancy seems to be new, and we note that further types of L^2-discrepancies are investigated in the book of Novak and Woźniakowski, cf. [97, Ch. 9].

2.4.1 Weighted Ball Discrepancies

In this section, we let the compact set $X \subset \mathbb{R}^n$ with finite Borel measure μ_X be given and equip it additionally with a metric d_X which induces the same topology on X as the Euclidean space $\mathbb{R}^n$, i.e., for every $\boldsymbol{x} \in X$ there exists constants $c, C > 0$ such that

$$c\mathrm{d}_X(\boldsymbol{x},\boldsymbol{y}) \leq \|\boldsymbol{x}-\boldsymbol{y}\|_2 \leq C\mathrm{d}_X(\boldsymbol{x},\boldsymbol{y}), \qquad \boldsymbol{y} \in X. \tag{2.54}$$

In particular, the metric d_X is continuous on $X \subset \mathbb{R}^n$. Hence, the (closed) *balls*

$$B_X(\boldsymbol{c},r) := \{\boldsymbol{x} \in X \ : \ \mathrm{d}_X(\boldsymbol{c},\boldsymbol{x}) \leq r\} \subset X$$

with *center* $\boldsymbol{c} \in X$ and *radius* $r \geq 0$ are measurable sets. The corresponding basis set of all balls is then simply defined by

$$\mathcal{B}_{\mathrm{d}_X} := \{B_X(\boldsymbol{c},r) \subset X \ : \ (\boldsymbol{c},r) \in D\}, \qquad D := X \times \mathbb{R}_+, \tag{2.55}$$

where $\mathbb{R}_+ := [0,\infty)$ is the set of the nonnegative real numbers. If for a fixed maximal radius $R > 0$ the parameterization

$$\Phi : X \times [0,R] \to \mathcal{B}_{\mathrm{d}_X}, \qquad \Phi(\boldsymbol{c},r) := B_X(\boldsymbol{c},r), \qquad (\boldsymbol{c},r) \in X \times [0,R],$$

is injective, it might be naturally to equip the domain D with the product measure $\mu_D := \mu_X \times \mu_{\mathbb{R}_+}$ where $\mu_{\mathbb{R}_+}$ is a finite Borel measure on the set $\mathbb{R}_+$ with $\mathrm{supp}(\mu_{\mathbb{R}_+}) \subset [0,R]$. Thus, we define, via the definition (2.50) of the L^2-discrepancy $D^2_{\mathcal{B}}$, the *weighted ball discrepancy*

$$D^2_{\mathcal{B}_{\mathrm{d}_X}}(\nu,\boldsymbol{P},\boldsymbol{w}) := \left(\int_{\mathbb{R}_+}\int_X \left|\nu(B_X(\boldsymbol{c},r)) - \delta_{\boldsymbol{P},\boldsymbol{w}}(B(\boldsymbol{c},r))\right|^2 \mathrm{d}\mu_X(\boldsymbol{c})\mathrm{d}\mu_{\mathbb{R}_+}(r)\right)^2 \tag{2.56}$$

for a complex measure $\nu \in M_{\mathbb{C}}(\mathbb{R}^n)$, points $\boldsymbol{P} \in X^M$, and weights $\boldsymbol{w} \in \mathbb{C}^M$. The weighted ball discrepancy $D^2_{\mathcal{B}_{\mathrm{d}_X}}$ is indeed well defined and leads to another formula of the cooresponding discrepancy kernel $K_{\mathcal{B}_{\mathrm{d}_X}}$.

Theorem 2.11. *Let $X \subset \mathbb{R}^n$ be compact and equipped with a metric d_X satisfying* (2.54)*, and a finite Borel measure μ_X. Then, for any finite Borel measure $\mu_{\mathbb{R}_+}$, the L^2-discrepancy $D^2_{\mathcal{B}_{\mathrm{d}_X}}$, cf.* (2.56)*, is well defined, and the corresponding discrepancy kernel is given by*

$$K_{\mathcal{B}_{\mathrm{d}_X}}(\boldsymbol{x},\boldsymbol{y}) = \int_{\mathbb{R}_+} A_{\boldsymbol{x},\boldsymbol{y}}(r)\mathrm{d}\mu_{\mathbb{R}_+}(r), \qquad \boldsymbol{x},\boldsymbol{y} \in X, \tag{2.57}$$

where the quantity, cf. (2.55)*,*

$$A_{\boldsymbol{x},\boldsymbol{y}}(r) := \mu_X\big(B_X(\boldsymbol{x},r) \cap B_X(\boldsymbol{y},r)\big), \qquad r \geq 0, \tag{2.58}$$

is the measure of two intersecting balls of radius r centered at $\boldsymbol{x}$ and $\boldsymbol{y}$.

Proof. The L^2-discrepancy $D^2_{\mathcal{B}_{\mathrm{d}_X}}$ is well defined since the set $\Omega := \{(\boldsymbol{c}, r, \boldsymbol{x}) \in D \times X \ : \ \mathrm{d}_X(\boldsymbol{c}, \boldsymbol{x}) \leq r\} \subset \mathbb{R}^{2n+1}$ is closed and thus a measurable set on $D \times X$. Hence, the characteristic function $1_{B_X(\boldsymbol{c},r)}(\boldsymbol{x}) = 1_\Omega(\boldsymbol{c}, r, \boldsymbol{x})$ is measurable on $D \times X$. Moreover, by the symmetry of the metric d_X we obtain $1_{B_X(\boldsymbol{c},r)}(\boldsymbol{x}) = 1_{B_X(\boldsymbol{x},r)}(\boldsymbol{c})$, $\boldsymbol{c}, \boldsymbol{x} \in X$, $r \in \mathbb{R}_+$. Thus, the discrepancy kernel, cf. (2.51), can be written as

$$K_{\mathcal{B}_{\mathrm{d}_X}}(\boldsymbol{x}, \boldsymbol{y}) := \int_{\mathbb{R}_+} \int_X 1_{B_X(\boldsymbol{x},r)}(\boldsymbol{c}) 1_{B_X(\boldsymbol{y},r)}(\boldsymbol{c}) \mathrm{d}\mu_X(\boldsymbol{c}) \mathrm{d}\mu_{\mathbb{R}_+}(r), \qquad \boldsymbol{x}, \boldsymbol{y} \in X,$$

which leads to the relation (2.57). ■

We remark that for certain instances the function $A_{\boldsymbol{x},\boldsymbol{y}}(r)$, $r \in \mathbb{R}_+$, cf. (2.58), of the volume of intersection of the two balls $B_X(\boldsymbol{x}, r)$ and $B_X(\boldsymbol{y}, r)$ can be computed explicitly and simplifies the computation of the discrepancy kernel $K_{\mathcal{B}_{\mathrm{d}_X}}$ of the weighted ball discrepancy $D^2_{\mathcal{B}_{\mathrm{d}_X}}$. We note further that the choice of the finite measure $\mu_{\mathbb{R}_+}$ is somehow arbitrary. Usually, we use the Lebesgue measure $\mu_{\mathbb{R}}$ restricted to the interval $[0, R]$ for some fixed $R > 0$. But the Dirac measure δ_R is also possible, which leads to the L^2-discrepancy over all balls in X with constant radius R.

2.4.2 L^2-Discrepancies over Halfspaces

In this section we present an integral geometric idea of Alexander [4]. The interesting result [4, Proposition 2.1] shows that certain Borel measures on the set of hyperplanes can be related to certain metrics d_X on the compact set $X \subset \mathbb{R}^n$. In [4] such metrics where used in a slightly different context, but the presented results provide us with an idea to relate these metrics with L^2-discrepancies over halfspaces, cf. [4, Proposition 3.1 and 3.3]. In particular, we will see that the Euclidean distance $\|\boldsymbol{x} - \boldsymbol{y}\|_2$, $\boldsymbol{x}, \boldsymbol{y} \in X$, allows for such an interesting relation.

We start with considering the set $\mathcal{H}_+$ which consists of all halfspaces

$$h_+(\boldsymbol{n}, d) := \{\boldsymbol{x} \in \mathbb{R}^n \ : \ \boldsymbol{n}^\top \boldsymbol{x} \geq d\} \subset \mathbb{R}^n \tag{2.59}$$

where $\boldsymbol{n} \in \mathbb{R}^n$ is a unit normal vector and $d \in \mathbb{R}$ is the distance of the *halfspace* $h_+(\boldsymbol{n}, d)$ from the origin. Thus, the space $\mathcal{H}_+$ is parameterized by

$$\Phi_+ : D \to \mathcal{H}_+, \qquad \Phi_+(\boldsymbol{n}, d) := h_+(\boldsymbol{n}, d), \qquad (\boldsymbol{n}, d) \in D := \mathbb{S}^{n-1} \times \mathbb{R},$$

where the set

$$\mathbb{S}^{n-1} := \{\boldsymbol{x} \in \mathbb{R}^n \ : \ \|\boldsymbol{x}\|_2 = 1\} \subset \mathbb{R}^n$$

denotes the $(n-1)$-dimensional unit sphere. We note that the parameterization Φ_+ is actually an isomorphisms. Thus, it is naturally to identify the measurable sets on $\mathcal{H}_+$ with Borel sets on $D = \mathbb{S}^{n-1} \times \mathbb{R}$ induced by $\mathbb{R}^{n+1}$, so that the measures on $\mathcal{H}_+$ are given by

$$\mu_{\mathcal{H}_+} := \mu_D \circ \Phi_+^{-1}$$

where μ_D is a Borel measure on D. We call the measure $\mu_{\mathcal{H}_+}$ *symmetric* if the measure μ_D is symmetric, i.e., for every measurable set $\Omega \subset D$ it satisfies

$$\mu_D(\Omega) = \mu_D(-\Omega) \tag{2.60}$$

where $-\Omega := \{(-\boldsymbol{n}, -d) \in \Omega\}$. By $\mathcal{H}$ we denote the set of all hyperplanes

$$h(\boldsymbol{n}, d) := \{\boldsymbol{x} \in \mathbb{R}^n \ : \ \boldsymbol{n}^\top \boldsymbol{x} = d\} \subset \mathbb{R}^n, \qquad (\boldsymbol{n}, d) \in D,$$

which is parameterized by

$$\Phi : D \to \mathcal{H}, \qquad \Phi(\boldsymbol{n}, d) := h(\boldsymbol{n}, d), \qquad (\boldsymbol{n}, d) \in D. \tag{2.61}$$

Using the relation

$$h(\boldsymbol{n}, d) = h_+(\boldsymbol{n}, d) \cap h_+(-\boldsymbol{n}, -d) = h(-\boldsymbol{n}, -d), \qquad (\boldsymbol{n}, d) \in D,$$

we see that the set $\mathcal{H}$ of hyperplanes can be identified with the quotient space $D/\{-1, 1\}$. More precisely, any hyperplane $h \in \mathcal{H}$ corresponds to the two-element set $\Phi^{-1}(h) = \{(\boldsymbol{n}, d) \in D \,:\, h = h(\boldsymbol{n}, d)\}$. Thus, we define a set $U \subset \mathcal{H}$ to be open if and only if the set $\Phi^{-1}(U) = \{(\boldsymbol{n}, d) \in D \,:\, h(\boldsymbol{n}, d) \in U\}$ is open in D. Hence, the notion of the Borel sets on the set of hyperplanes $\mathcal{H}$ is clarified when we speak about a Borel measure $\mu_{\mathcal{H}}$ on $\mathcal{H}$. Moreover, any measure $\mu_{\mathcal{H}}$ on $\mathcal{H}$ is induced by some measure $\mu_{\mathcal{H}_+}$ on $\mathcal{H}_+$ by averaging over the equivalence classes, i.e.,

$$\mu_{\mathcal{H}} := \frac{1}{2}\mu_{\mathcal{H}_+} \circ \Phi_+ \circ \Phi^{-1} = \frac{1}{2}\mu_D \circ \Phi^{-1}. \tag{2.62}$$

We note that the corresponding measure $\mu_{\mathcal{H}_+}$ is unique whenever it is assumed to be symmetric, cf. (2.60). Measurable sets on $\mathcal{H}$ are given for example by

$$H_\Omega := \{h \in \mathcal{H} \,:\, h \cap \Omega \neq \emptyset\} = \{h(\boldsymbol{n}, d) \,:\, \boldsymbol{n} \in \mathbb{S}^{n-1},\ \boldsymbol{y} \in \Omega,\ d := \boldsymbol{n}^\top \boldsymbol{y}\} \subset \mathcal{H}, \tag{2.63}$$

whenever $\Omega \subset \mathbb{R}^n$ is measurable. The set H_Ω consists of all hyperplanes in $\mathbb{R}^n$ which have points in Ω. Before we state the relation of Borel measures on $\mathcal{H}$ with metrics on X we introduce the set

$$\overline{\boldsymbol{x}\boldsymbol{y}} := \{t\boldsymbol{x} + (1-t)\boldsymbol{y} \in \mathbb{R}^n \,:\, t \in [0,1]\} \subset \mathbb{R}^n, \qquad \boldsymbol{x}, \boldsymbol{y} \in \mathbb{R}^n,$$

which is the set of points of the straight line segment connecting $\boldsymbol{x}$ and $\boldsymbol{y}$. Furthermore, the convex hull of a set $\Omega \subset \mathbb{R}^n$ is defined by

$$\operatorname{conv}(\Omega) := \left\{ \sum_{i=1}^{M} a_i \boldsymbol{x}_i \in \mathbb{R}^n \,:\, \boldsymbol{x}_i \in \Omega,\ a_i \geq 0,\ \sum_{i=1}^{M} a_i = 1,\ M \in \mathbb{N} \right\} \subset \mathbb{R}^n. \tag{2.64}$$

Theorem 2.12. *Let $X \subset \mathbb{R}^n$ be compact and $\mu_{\mathcal{H}}$ be a Borel measure on the set $\mathcal{H}$ of hyperplanes in $\mathbb{R}^n$ satisfying, cf.* (2.63),

(i) $\mu_{\mathcal{H}}(H_{\operatorname{conv}(X)}) < \infty$,

(ii) $\mu_{\mathcal{H}}(H_{\{\boldsymbol{x}\}}) = 0, \qquad \boldsymbol{x} \in X$,

(iii) $\mu_{\mathcal{H}}(H_{\overline{\boldsymbol{x}\boldsymbol{y}}}) > 0, \qquad \boldsymbol{x}, \boldsymbol{y} \in X$.

Then the function $d_{X,\mathcal{H}} : X \times X \to [0, \infty)$ defined by

$$d_{X,\mathcal{H}}(\boldsymbol{x}, \boldsymbol{y}) := \mu_{\mathcal{H}}(H_{\overline{\boldsymbol{x}\boldsymbol{y}}}), \qquad \boldsymbol{x}, \boldsymbol{y} \in X, \tag{2.65}$$

is a continuous metric on X.

Proof. For $\boldsymbol{x}, \boldsymbol{y} \in X$ we find by the properties (i) - (iii) that the number $\mathrm{d}_{X,\mathcal{H}}(\boldsymbol{x}, \boldsymbol{y})$ is positive if $\boldsymbol{x} \neq \boldsymbol{y}$ and zero otherwise. The triangle inequality and continuity of $d_{X,\mathcal{H}}$ follows from general properties of measures. For details, we refer to the proof of [4, Proposition 2.1]. ∎

Theorem 2.12 states literally, that a certain continuous measure $\mu_{\mathcal{H}}$ on the set of hyperplanes induces by (2.65) on a compact set $X \subset \mathbb{R}^n$ a continuous metric $\mathrm{d}_{X,\mathcal{H}}$, which is defined by the

measure of all hyperplanes which intersect the straight line segment $\overline{\boldsymbol{xy}} \subset \mathbb{R}^n$, $\boldsymbol{x}, \boldsymbol{y} \in \mathbb{R}^n$. We emphasize that the metric $\mu_{X,\mathcal{H}}$ on X does not depend on X rather than the line segment $\overline{\boldsymbol{xy}}$ joining $\boldsymbol{x}, \boldsymbol{y} \in X$. It follows that a measure $\mu_{\mathcal{H}}$ induces a metric on $\mathbb{R}^n$ if for any compact set $X \subset \mathbb{R}^n$ the conditions in Theorem 2.12 are satisfied.

The following example shows that such metrics $d_{X,\mathcal{H}}$ respectively measures $\mu_{\mathcal{H}}$ exist. For that reason, we recall that the measure $\mu_{\mathcal{H}}$ can be expressed in terms of the mapping $\Phi : D \to \mathcal{H}$ and a measure μ_D on $D = \mathbb{S}^{n-1} \times \mathbb{R}$, cf. (2.61) and (2.62).

Example 2.13. We consider on D the product measure

$$\mu_D := \mu_{\mathbb{S}^{n-1}} \times \mu_{\mathbb{R}}, \tag{2.66}$$

where $\mu_{\mathbb{S}^{n-1}}$ is the canonical measure on the sphere $\mathbb{S}^{n-1}$, cf. (3.72), and $\mu_{\mathbb{R}}$ is the Lebesgue measure on $\mathbb{R}$. It is seen readily that the pre-image of Φ over the set $H_{\overline{\boldsymbol{xy}}}$, $\boldsymbol{x}, \boldsymbol{y} \in \mathbb{R}^n$, is given by

$$\Phi^{-1}(H_{\overline{\boldsymbol{xy}}}) = \{(\boldsymbol{n}, d) \in D \,:\, \boldsymbol{n}^\top \boldsymbol{x} \leq d \leq \boldsymbol{n}^\top \boldsymbol{y}\} \cup \{(\boldsymbol{n}, d) \in D \,:\, \boldsymbol{n}^\top \boldsymbol{y} \leq d \leq \boldsymbol{n}^\top \boldsymbol{x}\} \subset D. \tag{2.67}$$

For fixed $\boldsymbol{n} \in \mathbb{S}^{n-1}$, the intersection of the sets on the right hand side is a $\mu_{\mathbb{R}}$-null set since it consists of one point d satisfying $d = \boldsymbol{n}^\top \boldsymbol{x}$ or $d = \boldsymbol{n}^\top \boldsymbol{y}$. Hence, we obtain

$$\mu_{\mathcal{H}}(H_{\overline{\boldsymbol{xy}}}) = \frac{1}{2}\mu_D \circ \Phi^{-1}(H_{\overline{\boldsymbol{xy}}}) = \frac{1}{2}\int_{\mathbb{S}^{n-1}} |\boldsymbol{n}^\top \boldsymbol{x} - \boldsymbol{n}^\top \boldsymbol{y}| \mathrm{d}\mu_{\mathbb{S}^{n-1}}(\boldsymbol{n}), \qquad \boldsymbol{x}, \boldsymbol{y} \in \mathbb{R}^n.$$

Moreover, using the rotational invariance of the canonical measure on the sphere $\mathbb{S}^{n-1}$, cf. (3.73), we arrive for $\boldsymbol{x}, \boldsymbol{y} \in \mathbb{R}^n$ at the remarkable relation

$$\mu_{\mathcal{H}}(H_{\overline{\boldsymbol{xy}}}) = \frac{1}{2}\|\boldsymbol{x} - \boldsymbol{y}\|_2 \int_{\mathbb{S}^{n-1}} \left|\boldsymbol{n}^\top \frac{\boldsymbol{x} - \boldsymbol{y}}{\|\boldsymbol{x} - \boldsymbol{y}\|_2}\right| \mathrm{d}\mu_{\mathbb{S}^{n-1}}(\boldsymbol{n}) = C_{n-1}\|\boldsymbol{x} - \boldsymbol{y}\|_2, \tag{2.68}$$

for some $C_{n-1} > 0$, depending only on the dimension $n \in \mathbb{N}$. Thus, the properties (ii),(iii) in Theorem 2.12 follow immediately. For a given compact set $X \subset \mathbb{R}^n$ we find similarly that property (i) is satisfied by observing

$$\mu_{\mathcal{H}}(H_{\mathrm{conv}(X)}) \leq \mu_{\mathbb{S}^{n-1}}(\mathbb{S}^{n-1}) \sup_{\boldsymbol{x},\boldsymbol{y} \in X} \|\boldsymbol{x} - \boldsymbol{y}\|_2.$$

Thus, we conclude that the metric $\mathrm{d}_{X,\mathcal{H}}$ obtained by the natural measure μ_H is in fact, up to a constant, the Euclidean distance. We remark further that the measure μ_D is actually symmetric and thus corresponds to a symmetric measure $\mu_{\mathcal{H}_+}$ on the set of halfspaces $\mathcal{H}_+$. □

The *L^2-discrepancy over halfspaces* $D^2_{\mathcal{H}_+}$ is defined as the L^2-discrepancy $D^2_{\mathcal{B}}$ over the basis set $\mathcal{B}$ consisting of all intersections $h_+(\boldsymbol{n}, d) \cap X$, $(\boldsymbol{n}, d) \in D_X := \Phi^{-1}(H_{\mathrm{conv}(X)}) \subset D$. By definition (2.50) we find that the L^2-discrepancy over halfspaces reads for complex measures $\nu \in M_{\mathbb{C}}(\mathbb{R})$, points $\boldsymbol{P} \in X^M$, and weights $\boldsymbol{w} \in \mathbb{C}^M$ as

$$D^2_{\mathcal{H}_+}(\nu, \boldsymbol{P}, \boldsymbol{w}) := \left(\int_{D_X} \left|\nu(h_+(\boldsymbol{n}, d) \cap X) - \delta_{\boldsymbol{P},\boldsymbol{w}}(h_+(\boldsymbol{n}, d) \cap X)\right|^2 \mathrm{d}\mu_D(\boldsymbol{n}, d)\right)^{\frac{1}{2}}. \tag{2.69}$$

We note that, as in the case of the weighted ball discrepancy $D^2_{\mathcal{B}_{\mathrm{d}_X}}$, cf. (2.56), the integrals are well defined. Moreover, if the measure μ_D is symmetric then the discrepancy kernel $K_{\mathcal{H}_+}$, cf. (2.51), which corresponds to the L^2-discrepancy over halfspaces $D^2_{\mathcal{H}_+}$, can be expressed by the metric $d_{X,\mathcal{H}}$ defined in Theorem 2.12.

Theorem 2.14. *Let $X \subset \mathbb{R}^n$ be compact and $\mu_{\mathcal{H}}$ be a Borel measure on the set $\mathcal{H}$ of hyperplanes in $\mathbb{R}^n$ which is induces by the corresponding symmetric measure $\mu_{\mathcal{H}_+}$ on the set of halfspaces $\mathcal{H}_+$, cf.* (2.62)*, and which satisfies the properties (i) - (iii) in Theorem 2.12. Then the metric $d_{X,\mathcal{H}}$ defined by* (2.65) *gives rise to the discrepancy kernel, cf.* (2.51)*,*

$$\begin{aligned} K_{\mathcal{H}_+}(\boldsymbol{x},\boldsymbol{y}) :=& \int_{D_X} 1_{h_+(\boldsymbol{n},d)}(\boldsymbol{x}) 1_{h_+(\boldsymbol{n},d)}(\boldsymbol{y}) \mathrm{d}\mu_D(\boldsymbol{n},d) \\ =& \mu_{\mathcal{H}}(H_{\mathrm{conv}(X)}) - \mathrm{d}_{X,\mathcal{H}}(\boldsymbol{x},\boldsymbol{y}), \qquad\qquad \boldsymbol{x},\boldsymbol{y} \in X, \end{aligned} \tag{2.70}$$

where $D_X := \Phi^{-1}(H_{\mathrm{conv}(X)})$.

Proof. In what follows we let $\boldsymbol{x},\boldsymbol{y} \in X$ be fixed. In Example 2.13 we already observed that $h(\boldsymbol{n},d) \cap \overline{\boldsymbol{xy}} \neq \emptyset$ if and only if $\boldsymbol{n}^\top \boldsymbol{x} \leq d \leq \boldsymbol{n}^\top \boldsymbol{y}$ or $\boldsymbol{n}^\top \boldsymbol{y} \leq d \leq \boldsymbol{n}^\top \boldsymbol{x}$ for $\boldsymbol{n} \in \mathbb{S}^{n-1}$, $d \in \mathbb{R}$, cf. (2.67). Hence, we infer that

$$\Phi^{-1}(H_{\overline{\boldsymbol{xy}}}) = \Big(\{-\boldsymbol{n}^\top \boldsymbol{x} \geq -d\} \cap \{\boldsymbol{n}^\top \boldsymbol{y} \geq d\}\Big) \cup \Big(\{-\boldsymbol{n}^\top \boldsymbol{y} \geq -d\} \cap \{\boldsymbol{n}^\top \boldsymbol{x} \geq d\}\Big) \subset D.$$

The above relation can be written in the form of characteristic functions as

$$\begin{aligned} 1_{H_{\overline{\boldsymbol{xy}}}}(h(\boldsymbol{n},d)) =& 1_{h_+(-\boldsymbol{n},-d)}(\boldsymbol{x}) 1_{h_+(\boldsymbol{n},d)}(\boldsymbol{y}) + 1_{h_+(\boldsymbol{n},d)}(\boldsymbol{x}) 1_{h_+(-\boldsymbol{n},-d)}(\boldsymbol{y}) \\ & - 1_{h_+(-\boldsymbol{n},-d)}(\boldsymbol{x}) 1_{h_+(\boldsymbol{n},d)}(\boldsymbol{y}) 1_{h_+(\boldsymbol{n},d)}(\boldsymbol{x}) 1_{h_+(-\boldsymbol{n},-d)}(\boldsymbol{y}). \end{aligned}$$

Using the property (ii) of $\mu_{\mathcal{H}}$ in Theorem 2.12 we observe

$$\frac{1}{2} \int_D 1_{h_+(-\boldsymbol{n},-d)}(\boldsymbol{x}) 1_{h_+(\boldsymbol{n},d)}(\boldsymbol{x}) \mathrm{d}\mu_D(\boldsymbol{n},d) = \frac{1}{2} \mu_D \circ \Phi^{-1}(H_{\{\boldsymbol{x}\}}) = \mu_{\mathcal{H}}(H_{\{\boldsymbol{x}\}}) = 0,$$

and we conclude that μ_D-almost everywhere it holds

$$1_{H_{\overline{\boldsymbol{xy}}}}(h(\boldsymbol{n},d)) = 1_{h_+(-\boldsymbol{n},-d)}(\boldsymbol{x}) 1_{h_+(\boldsymbol{n},d)}(\boldsymbol{y}) + 1_{h_+(\boldsymbol{n},d)}(\boldsymbol{x}) 1_{h_+(-\boldsymbol{n},-d)}(\boldsymbol{y}). \tag{2.71}$$

Similarly, we have μ_D-almost everywhere the relation

$$1 = 1 \cdot 1 = \left(1_{h_+(\boldsymbol{n},d)}(\boldsymbol{x}) + 1_{h_+(-\boldsymbol{n},-d)}(\boldsymbol{x})\right) \left(1_{h_+(\boldsymbol{n},d)}(\boldsymbol{y}) + 1_{h_+(-\boldsymbol{n},-d)}(\boldsymbol{y})\right).$$

Expanding the terms in the above expression we find together with (2.71) that μ_D-almost everywhere it holds

$$1 - 1_{H_{\overline{\boldsymbol{xy}}}}(h(\boldsymbol{n},d)) = 1_{h_+(\boldsymbol{n},d)}(\boldsymbol{x}) 1_{h_+(\boldsymbol{n},d)}(\boldsymbol{y}) + 1_{h_+(-\boldsymbol{n},-d)}(\boldsymbol{x}) 1_{h_+(-\boldsymbol{n},-d)}(\boldsymbol{y}). \tag{2.72}$$

Using that the set $D_X = \Phi^{-1}(H_{\mathrm{conv}(X)})$ is symmetric, i.e., $D_X = -D_X$, we finished the proof by integrating the equation (2.72) over D_X, which yields

$$\mu_D(D_X) - \mu_D \circ \Phi^{-1}(H_{\overline{\boldsymbol{xy}}}) = 2 \int_{D_X} 1_{h_+(\boldsymbol{n},d)}(\boldsymbol{x}) 1_{h_+(\boldsymbol{n},d)}(\boldsymbol{y}) \mathrm{d}\mu_D(\boldsymbol{n},d)$$

and thus the assertion (2.70). ∎

Corollary 2.15. *For every compact set $X \subset \mathbb{R}^n$ there exists a constant $C_X > 0$ such that the function*

$$K_{\mathrm{E}}(\boldsymbol{x},\boldsymbol{y}) := C_X - \|\boldsymbol{x} - \boldsymbol{y}\|_2, \qquad \boldsymbol{x},\boldsymbol{y} \in X, \tag{2.73}$$

is a positive definite kernel on X.

Proof. The assertion (2.73) follows from Theorem 2.14 by using that discrepancy kernels are positive definite, cf. Theorem 2.10, and the fact that the Euclidean distance is induced by a measure on halfspaces, cf. Example 2.13. ∎

We refer to the kernel K_{E} given by (2.73) in Corollary 2.15 to as the *Euclidean distance kernel*, and we remark that this kernel does not essentially depend on the given set $X \subset \mathbb{R}^n$, cf. Remark 2.9.

2.4.3 L^2-Discrepancies over Euclidean Balls

In order to obtain explicit formulas of local discrepancy kernels on compact sets $X \subset \mathbb{R}^n$ we consider another special case of the L^2-discrepancy $D^2_{\mathcal{B}}$ defined by (2.50). Therefore, we make use of the idea presented in the previous paragraph, where we have constructed basis sets $\mathcal{B}$ by the intersection of X with halfspaces, cf. (2.69). This time we obtain basis sets $\mathcal{B}$ by intersecting the set X with *Euclidean balls*

$$B_{\mathbb{R}^n}(\boldsymbol{c}, r) := \{\boldsymbol{x} \in \mathbb{R}^n \ : \ \|\boldsymbol{c} - \boldsymbol{x}\|_2 \leq r\} \subset \mathbb{R}^n, \qquad \boldsymbol{c} \in \mathbb{R}^n, \qquad r > 0. \tag{2.74}$$

More precisely, the basis set $\mathcal{B}$ of the L^2-discrepancy $D^2_{\mathcal{B}}$ defined by (2.50) consists of all non-empty intersections

$$B(\boldsymbol{t}) := B_{\mathbb{R}^n}(\boldsymbol{c}, r) \cap X, \qquad \boldsymbol{t} := (\boldsymbol{c}, r) \in D := \{(\boldsymbol{c}, r) \in \mathbb{R}^n \times \mathbb{R}_+ \ : \ B_{\mathbb{R}^n}(\boldsymbol{c}, r) \cap X \neq \emptyset\}. \tag{2.75}$$

In what follows we restrict our attention to L^2-discrepancies $D^2_{\mathcal{B}}$ with respect to the measure μ_D on $D \subset \mathbb{R}^{n+1}$ given by the product measure

$$\mu_D := \mu_{\mathbb{R}^n} \times \delta_R,$$

where $\mu_{\mathbb{R}^n}$ is the Lebesgue measure on $\mathbb{R}^n$ and δ_R is the Dirac measure concentrated at some prescribed $R > 0$. Thus, the *L^2-discrepancy over Euclidean balls* $D^2_{\mathcal{B}_{\mathbb{R}^n},R}$ with radius $R > 0$ is defined for complex measures $\nu \in M_{\mathbb{C}}(\mathbb{R}^n)$, points $\boldsymbol{P} \in X^M$, and weights $\boldsymbol{w} \in \mathbb{C}^M$ by

$$D^2_{\mathcal{B}_{\mathbb{R}^n},R}(\nu, \boldsymbol{P}, \boldsymbol{w}) := \left(\int_{\mathbb{R}^n} \left| \nu(B_{\mathbb{R}^n}(\boldsymbol{c}, R) \cap X) - \delta_{\boldsymbol{P},\boldsymbol{w}}(B_{\mathbb{R}^n}(\boldsymbol{c}, R) \cap X) \right|^2 \mathrm{d}\boldsymbol{c} \right)^{\frac{1}{2}}. \tag{2.76}$$

The following Theorem 2.16 states that this definition makes sense and leads to explicit formulas for the corresponding discrepancy kernels.[4] Before we are able to state the results, we need the following special functions. The *gamma function* Γ is defined by

$$\Gamma(x) := \int_0^\infty t^{x-1} \mathrm{e}^{-t} \mathrm{d}t, \qquad x > 0, \tag{2.77}$$

and the *hypergeometric functions* ${}_pF_q$, $p, q \in \mathbb{N}$, are defined for $p \leq q + 1$ and $z \in \mathbb{C}$, $|z| < 1$, by

$$\begin{aligned} {}_pF_q(a_1, \ldots, a_p; b_1, \ldots, b_q; z) &:= \sum_{k=0}^{\infty} \frac{(a_1)_k \cdots (a_p)_k}{(b_1)_k \cdots (b_q)_k} \frac{z^k}{k!}, \\ (x)_k &:= \begin{cases} 1, & k = 0, \\ x(x+1)\cdots(x+k-1), & k > 0. \end{cases} \end{aligned} \tag{2.78}$$

[4] Interestingly, for general measures μ_D a complete characterization of the corresponding discrepancy kernels is given by Gneiting [51].

Theorem 2.16. *For $n \in \mathbb{N}$ let $X \subset \mathbb{R}^n$ be compact and $R > 0$ be given. Then the L^2-discrepancy over Euclidean balls $D^2_{\mathcal{B}_{\mathbb{R}^n},R}$, cf. (2.76), is well-defined and the corresponding discrepancy kernel is given by*

$$K_{\mathcal{B}_{\mathbb{R}^n},R}(\boldsymbol{x},\boldsymbol{y}) := \mu_{\mathbb{R}^n}(B_{\mathbb{R}^n}(\boldsymbol{x},R) \cap B_{\mathbb{R}^n}(\boldsymbol{y},R)) = a_n(s,R), \qquad \boldsymbol{x},\boldsymbol{y} \in X, \tag{2.79}$$

where $s := \|\boldsymbol{x}-\boldsymbol{y}\|_2$ and

$$a_n(s,R) := \begin{cases} \pi^{n/2}R^n \left(\frac{1}{\Gamma\left(\frac{n}{2}+1\right)} - \frac{s\,{}_2F_1\left(\frac{1-n}{2},\frac{1}{2};\frac{3}{2};\frac{s^2}{4R^2}\right)}{\sqrt{\pi}R\Gamma\left(\frac{n+1}{2}\right)} \right), & 0 \le s \le 2R \\ 0, & s \ge 2R. \end{cases} \tag{2.80}$$

Proof. We observe, that the set D defined by (2.75) reads for a fixed radius $R > 0$ as

$$D := \{(\boldsymbol{c},r) \in \mathbb{R}^n \times \{R\} \ : \ \boldsymbol{x} \in X,\ \|\boldsymbol{c}-\boldsymbol{x}\|_2 \le R\} \subset \mathbb{R}^{n+1}.$$

Hence, the set D is compact for any compact set $X \subset \mathbb{R}^n$ and thus measurable with $\mu_D(D) < \infty$. As in the proof of Theorem 2.11 it is seen that the characteristic functions $1_{B_{\mathbb{R}^n}(\boldsymbol{c},r)}(\boldsymbol{x})$ are measurable on $D \times X$ and that the discrepancy kernel $K_{\mathcal{B}_{\mathbb{R}^n},R}$ is given by the first equation of (2.79). We recall that the volume of an n-dimensional Euclidean ball of radius $r \ge 0$ calculates from

$$V_n(r) := \mu_{\mathbb{R}^n}(B_{\mathbb{R}^n}(\boldsymbol{c},r)) = \frac{\pi^{n/2}}{\Gamma\left(\frac{n}{2}+1\right)} r^n, \qquad \boldsymbol{c} \in \mathbb{R}^n, \quad n \in \mathbb{N}. \tag{2.81}$$

Thus, the measure of two intersecting Euclidean balls $B_{\mathbb{R}^n}(\boldsymbol{x},R)$ and $B_{\mathbb{R}^n}(\boldsymbol{y},R)$ of radius $R \ge 0$ and centers $\boldsymbol{x},\boldsymbol{y} \in \mathbb{R}^n$ is given by the integral

$$2\int_{\frac{s}{2}}^{R} V_{n-1}\left(\sqrt{R^2-t^2}\right) \mathrm{d}t = 2\frac{\pi^{(n-1)/2}}{\Gamma\left(\frac{n+1}{2}\right)} \int_{\frac{s}{2}}^{R} (R^2-t^2)^{\frac{n-1}{2}} \mathrm{d}t, \qquad s = \|\boldsymbol{x}-\boldsymbol{y}\|_2. \tag{2.82}$$

For abbreviation, we define the function

$$\tilde{a}_n(x,R) := \int_0^x (R^2-t^2)^{\frac{n-1}{2}} \mathrm{d}t, \qquad 0 \le x \le R,$$

and obtain after a change of variable $t = x\sqrt{\tilde{t}}$ and Euler's integral representation of the hypergeometric function ${}_2F_1$, cf. [1, Eq. 15.3.1], the relation

$$\begin{aligned} \tilde{a}_n(x,R) &= \frac{1}{2}R^{n-1}x \int_0^1 \tilde{t}^{\frac{1}{2}-1}(1-\tilde{t})^{\frac{3}{2}-\frac{1}{2}-1} \left(1-\frac{x^2}{R^2}\tilde{t}\right)^{\frac{n-1}{2}} \mathrm{d}\tilde{t} \\ &= \frac{\Gamma\left(\frac{1}{2}\right)\Gamma\left(\frac{3}{2}-\frac{1}{2}\right)}{2\Gamma\left(\frac{3}{2}\right)} R^{n-1}x\,{}_2F_1\left(-\frac{n-1}{2},\frac{1}{2};\frac{3}{2};\frac{x^2}{R^2}\right), \qquad 0 < x < R. \end{aligned}$$

Using furthermore that $\Gamma(x+1) = x\Gamma(x)$ and $\Gamma(1) = 1$, cf. [1, Eq. 6.1.15], we arrive by continuity at

$$\tilde{a}_n(x,R) = R^{n-1}x\,{}_2F_1\left(\frac{1-n}{2},\frac{1}{2};\frac{3}{2};\frac{x^2}{R^2}\right), \qquad 0 \le x \le R.$$

This leads with equation (2.82) to the closed form expression

$$\mu_{\mathbb{R}^n}(B_{\mathbb{R}^n}(\boldsymbol{x},R) \cap B_{\mathbb{R}^n}(\boldsymbol{y},R)) = 2\frac{\pi^{(n-1)/2}}{\Gamma\left(\frac{n+1}{2}\right)} \left(\tilde{a}_n(R,R) - \tilde{a}_n\left(\frac{s}{2},R\right)\right), \qquad s = \|\boldsymbol{x}-\boldsymbol{y}\|_2.$$

We finish the proof by applying the Gauß formula for evaluating hypergeometric functions at $z = 1$, cf. [1, Eq. 5.1.20],

$$\tilde{a}_n(R,R) = R^n \, {}_2F_1\left(\frac{1-n}{2}, \frac{1}{2}; \frac{3}{2}; 1\right) = R^n \frac{\Gamma\left(\frac{3}{2}\right)\Gamma\left(\frac{3}{2} - \frac{1-n}{2} - \frac{1}{2}\right)}{\Gamma\left(\frac{3}{2} - \frac{1-n}{2}\right)\Gamma\left(\frac{3}{2} - \frac{1}{2}\right)} = R^n \frac{\sqrt{\pi}\Gamma\left(\frac{n+1}{2}\right)}{2\Gamma\left(1 + \frac{n}{2}\right)}. \qquad \blacksquare$$

Theorem 2.16 states that discrepancy kernels $K_{\mathcal{B}_{\mathbb{R}^n},R}$ which correspond to L^2-discrepancies over Euclidean balls $D^2_{\mathcal{B}_{\mathbb{R}^n},R}$ depend only on the Euclidean distance between two points in $X \subset \mathbb{R}^n$. We observed a similar behavior for the L^2-discrepancies over halfspaces $D^2_{\mathcal{H}_+}$. The reason for introducing the discrepancy over balls is that, independently of X, cf. Theorem 2.16, we have closed form expressions for discrepancy kernels which are additionally local kernels, i.e., for any given $R > 0$ the discrepancy kernels satisfy, cf. (5.11),

$$K_{\mathcal{B}_{\mathbb{R}^n},R}(\boldsymbol{x}, \boldsymbol{y}) = 0, \qquad \|\boldsymbol{x} - \boldsymbol{y}\|_2 \geq 2R, \qquad \boldsymbol{x}, \boldsymbol{y} \in X. \tag{2.83}$$

We finally remark that the discrepancy over half spaces $D^2_{\mathcal{B}_{\mathbb{R}^n},R}$ may be considered as a limiting cases of the discrepancy over Euclidean balls, as the radius R tends to infinity.

2.5 Illustrative Examples

In this section we present some interesting examples, where we try to illustrate some issues concerning optimal quadrature functionals in reproducing kernel Hilbert spaces $H_K(X)$. In particular, the uniqueness of optimal equal weights quadratures $Q_\nu(\boldsymbol{P}^*)$ for a prescribed number $M \in \mathbb{N}$ of quadrature points $\boldsymbol{P} \in X^M$, cf. (2.33), is not necessarily assured. Furthermore, we will see that several local extrema (value at a stationary point) may occur for the worst case quadrature error err_K, even for these seemingly easy cases.

In Section 2.5.1 we consider quadrature functionals I_ν with respect to two different discrepancy kernels K on the interval $X = [-1, 1]$, where we are able to determine analytically the optimal quadrature points for three choices of finite Borel measures ν. The obtained results are particular interesting and should help us to get used to the notation.

In Section 2.5.2 we consider for two different Borel measures the corresponding quadrature problems in the Euclidean plan $\mathbb{R}^2$ with respect to the Euclidean distance kernel K_{E}, cf. Corollary 2.15. The Borel measures ν_1 and ν_2 are supported on the circle $\mathbb{S}^1$ and the unit disc D, respectively. It turns out that the determination of optimal quadrature functionals becomes much harder. Even the computation of explicit formulas for the worst case quadrature error involves non-elementary functions, cf. Theorem 2.17. Surprisingly, the associated potential energies E_{K_{E},ν_1}, E_{K_{E},ν_2}, cf. (2.48) in Section 2.3, which we aim to minimize, are almost indistinguishable, cf. Figure 2.2, and lead to very different optimal point distributions, cf. Figure 2.3. Moreover, we observe that optimal quadrature points with respect to the measure ν_1 are not contained in its support $\mathrm{supp}(\nu_1) = \mathbb{S}^1$. Finally, the example for the measure ν_2 shows the need of more sophisticated optimization and evaluation methods.

2.5.1 Optimal Quadrature Points for the Interval $[-1, 1]$

In what follows we are interested in optimal equal weights quadrature rules on the interval $X := [-1, 1]$ for three different Borel measures and two different reproducing kernel Hilbert spaces $H_K(X)$ with reproducing kernels $K : X \times X \to \mathbb{R}$. The Hilbert spaces of consideration are associated to the following positive definite kernels. The first kernel is given by the Euclidean

distance kernel

$$K_{\mathrm{E}}(x,y) := \int_{-1}^{1} 1_{[-1,h]}(x)1_{[-1,h]}(y) + 1_{[h,1]}(x)1_{[h,1]}(y)\mathrm{d}h$$
$$= 1 - \max(x,y) + \min(x,y) + 1 = 2 - |x-y|, \quad x,y \in [-1,1].$$

We recall that the kernel K_{E} corresponds to an L^2-discrepancy $D^2_{\mathcal{H}_+}$ over halfspaces, cf. Example 2.13 and Theorem 2.14. More precisely, the associated basis set $\mathcal{B}$ consists of all intervals of the form $[-1,h]$ and $[h,1]$, $h \in D = [-1,1]$, and the measure μ_D is the Lebesgue measure $\mu_{\mathbb{R}}$ restricted to the interval $[-1,1]$, cf. (2.50). The second kernel is defined by

$$K_{\mathrm{B}}(x,y) := \int_{-1}^{1}\int_{a}^{1} 1_{[a,b]}(x)1_{[a,b]}(y)\mathrm{d}b\mathrm{d}a$$
$$= (\min(x,y)+1)(1-\max(x,y)) = 1 - |x-y| - xy, \qquad x,y \in [-1,1],$$

which corresponds to, what is called in [97, Sec. 9.5.5], the extreme or unanchored discrepancy. In our terminology the basis set $\mathcal{B}$ of the corresponding L^2-discrepancy $D^2_{\mathcal{B}}$, cf. (2.50), is given by all intervals of the form $[a,b]$ with $(a,b) \in D = \{(a,b) \in \mathbb{R}^2 \ : \ -1 \le a \le b \le 1\}$ where the associated measure μ_D is the Lebesgue measure $\mu_{\mathbb{R}^2}$ restricted to the set D. We remark that the intervals $[a,b]$ may also considered as balls $B_X(c,r)$ with center $c := (a+b)/2$ and radius $r := (b-a)/2$ with respect to the metric $\mathrm{d}_X(x,y) := |x-y|$, $x,y \in [-1,1]$. Thus, the discrepancy kernel K_{B} might be associated to a certain type of weighted ball discrepancy, cf. (2.56).

A characterization of the associated reproducing kernel Hilbert spaces $H_K(X)$, $K = K_{\mathrm{E}}, K_{\mathrm{B}}$, is given in terms of absolutely continuous functions. We recall, an *absolutely continuous function* $f \in C([a,b])$, $a < b \in \mathbb{R}$, can be represented by a Lebesgue integrable function $f' : [a,b] \to \mathbb{C}$, called the derivative of f, such that

$$f(x) = f(a) + \int_a^x f'(t)\mathrm{d}t, \quad x \in [a,b].$$

For absolutely continuous functions $f, g \in C([-1,1])$ it is easy to check the reproducing property of the kernel K_{E} for the inner product

$$(f,g)_{H_{K_{\mathrm{E}}}(X)} = \frac{1}{4}(f(-1)+f(1))(g(-1)+g(1)) + \frac{1}{2}\int_{-1}^{1} f'(t)g'(t)\mathrm{d}t$$

and, if additionally $f(-1) = f(1) = g(-1) = g(1) = 0$, of the kernel K_{B} for the inner product

$$(f,g)_{H_{K_{\mathrm{B}}}(X)} = \frac{1}{2}\int_{-1}^{1} f'(t)g'(t)\mathrm{d}t.$$

Hence, by the uniqueness of reproducing kernel Hilbert spaces, cf. Theorem 2.4, we have that

$$H_{K_{\mathrm{E}}}(X) = \{f : [-1,1] \to \mathbb{C} \text{ absolutely continuous } : \ \|f\|_{H_{K_{\mathrm{E}}}} < \infty\},$$
$$H_{K_{\mathrm{B}}}(X) = \{f : [-1,1] \to \mathbb{C} \text{ absolutely continuous } : \ f(-1) = f(1) = 0, \quad \|f\|_{H_{K_{\mathrm{B}}}} < \infty\}.$$

From the above relations we find that functions in the Hilbert space $H_{K_{\mathrm{B}}}(X)$ vanish at the endpoints of the interval $[-1,1]$. This observation leads to interesting behaviors when considering optimal quadratures in $H_{K_{\mathrm{B}}}(X)$, since quadrature points at ± 1 have effectively zero weights and may be omitted. We remark further that the constant function $f \equiv 1$ does not belong to $H_{K_{\mathrm{B}}}(X)$, and thus there is a priori no need for the weights to equal $\nu(X)/M$, as it does by definition in an equal weights quadrature Q_ν, cf. (2.33).

The three different Borel measures $\nu_1, \nu_2, \nu_3 \in M_{\mathbb{C}}(\mathbb{R})$ are defined for measurable subsets $\Omega \subset \mathbb{R}$ by

$$\nu_1(\Omega) := \int_{X\cap\Omega} 1\mathrm{d}x, \qquad \nu_2(\Omega) := \int_{X\cap\Omega} \frac{1}{\sqrt{1-x^2}}\mathrm{d}x, \qquad \nu_3(\Omega) := \delta_{-1}(\Omega) + \delta_1(\Omega).$$

In words, ν_1 is the Lebesgue measure $\mu_{\mathbb{R}}$ restricted to $[-1,1]$, ν_2 is the measure which corresponds to the arcsine-distribution, and ν_3 is a measure concentrated at the endpoints of the interval $[-1,1]$. We consider the measure ν_1 since it is the standard measure for uniformly distributed points. The measure ν_2 is chosen since it is associated with the limit distribution of the zeros of orthogonal polynomials on the interval $[-1,1]$ for a large class of weight functions, this fact is known as the Arcsine Law, cf. [40, 133]. For an illustration of the measures ν_1, ν_2 see Figure 2.1. The measure ν_3 is an example of a discrete measure which should be easily approximated by quadrature functionals, since it is itself a quadrature functional, however if we restrict to equal weights quadratures the worst case quadrature error for the measure ν_3 does not need not to vanish for more than two quadrature points.

We recall that the equal weights worst case quadrature $\mathrm{err}_K(\nu, \boldsymbol{P})$ between an integral functional I_ν, $\nu \in M_{\mathbb{C}}(\mathbb{R})$, and an equal weights quadrature functional $Q_\nu(\boldsymbol{P})$, $\boldsymbol{P} := (p_1, \ldots, p_M) \in X^M$, in a reproducing kernel Hilbert space $H_K(X)$ can be computed by, cf. Theorem 2.7,

$$\mathrm{err}_K(\nu, \boldsymbol{P})^2 = \left(\frac{\nu(X)}{M}\right)^2 \sum_{i,j=1}^{M} K(p_i, p_j) - 2\frac{\nu(X)}{M}\sum_{i=1}^{M} h_{K,\nu}(p_i) + C_{K,\nu},$$

where

$$h_{K,\nu}(y) := \int_X K(x,y)\mathrm{d}\nu(x), \quad y \in X, \quad C_{K,\nu} := \int_X\int_X K(x,y)\mathrm{d}\nu(x)\mathrm{d}\nu(y) = \int_X h_{K,\nu}(y)\mathrm{d}\nu(y).$$

Before we start with the explicit computation of optimal quadrature points $\boldsymbol{P} \in [-1,1]^M$, we assume with out loss of generality that the quadrature points are given in ascending order, i.e., $-1 \le p_1 \le p_2 \le \cdots \le p_M \le 1$, and we consider the more convenient functions

$$\begin{aligned} E_{K_{\mathrm{E}},\nu}(\boldsymbol{P}) :=& \frac{\nu(X)}{M}\sum_{i=1}^{M-1}\sum_{j=i+1}^{M}(p_i - p_j) - \sum_{i=1}^{M} h_{K_{\mathrm{E}},\nu}(p_i) \\ =& \sum_{i=1}^{M}\left[\nu(X)\left(1 - \frac{2i-1}{M}\right)p_i - h_{K_{\mathrm{E}},\nu}(p_i)\right], \\ E_{K_{\mathrm{B}},\nu}(\boldsymbol{P}) :=& \sum_{i=1}^{M}\left[\nu(X)\left(1 - \frac{2i-1}{M}\right)p_i - h_{K_{\mathrm{B}},\nu}(p_i)\right] - \frac{\nu(X)}{2M}\left(\sum_{i=1}^{M} p_i\right)^2 \end{aligned} \tag{2.84}$$

for the kernels K_{E}, K_{B}, respectively. As in Remark 2.9, it is readily seen that minimizing the worst case quadrature error $\mathrm{err}_{\mathrm{K},\nu}$ for equal weights quadrature functionals $Q_\nu(\boldsymbol{P})$ in the Hilbert spaces $H_K(X)$, $K = K_{\mathrm{E}}, K_{\mathrm{B}}$, is equivalent to minimizing the functions $E_{K,\nu}$ for ordered points. Note the relation to the potential energies given in Section 2.3.

For optimization purposes we recall that the gradient and Hessian of the functions $E_{K,\nu}$ are given for $K = K_{\mathrm{E}}, K_{\mathrm{B}}$ by

$$\begin{aligned} \nabla E_{K,\nu}(\boldsymbol{P}) &:= \left(\frac{\partial}{\partial p_1}E_{K,\nu}(\boldsymbol{P}), \ldots, \frac{\partial}{\partial p_M}E_{K,\nu}(\boldsymbol{P})\right)^\top \in \mathbb{R}^M, \qquad \boldsymbol{P} \in [-1,1]^M, \\ \mathbf{H}E_{K,\nu}(\boldsymbol{P}) &:= \left(\frac{\partial^2}{\partial p_i \partial p_j}E_{K,\nu}\right)_{i,j=1}^{M} \in \mathbb{R}^{M\times M}, \qquad \boldsymbol{P} \in [-1,1]^M, \end{aligned} \tag{2.85}$$

where the partial derivatives read as

$$\begin{aligned}
\frac{\partial}{\partial p_i} E_{K_{\mathrm{E}},\nu}(\boldsymbol{P}) &= \nu(X)\left(1 - \frac{2i-1}{M}\right) - h'_{K_{\mathrm{E}},\nu}(p_i), \\
\frac{\partial}{\partial p_i} E_{K_{\mathrm{B}},\nu}(\boldsymbol{P}) &= \nu(X)\left(1 - \frac{2i-1}{M}\right) - h'_{K_{\mathrm{B}},\nu}(p_i) - \frac{\nu(X)}{M}\sum_{j=1}^{M} p_j, \\
\frac{\partial^2}{\partial p_i \partial p_j} E_{K_{\mathrm{E}},\nu}(\boldsymbol{P}) &= -\delta_{i,j} h''_{K_{\mathrm{E}},\nu}(p_i), \qquad \frac{\partial^2}{\partial p_i \partial p_j} E_{K_{\mathrm{B}},\nu}(\boldsymbol{P}) = -\delta_{i,j} h''_{K_{\mathrm{B}},\nu}(p_i) - \frac{\nu(X)}{M},
\end{aligned} \tag{2.86}$$

for $i, j = 1, \ldots, M$. We remark that we will consider later generalizations of the gradient and Hessian on Riemannian manifolds, for which the above definitions (in Euclidean space) are special cases, cf. (3.34) and (3.35). Furthermore, if $E_{K,\nu}$ is (twice) continuously differentiable it is reasonable to look at first for stationary points $\boldsymbol{P}^* \in [-1,1]^M$, i.e., $\nabla E_{K,\nu}(\boldsymbol{P}^*) = \boldsymbol{0} \in \mathbb{R}^M$, cf. Theorem 3.18. Then it is well known, if additionally $E_{K,\nu}$ is convex, the stationary point $\boldsymbol{P}^*$ is a global minimizer, which is unique if $E_{K,\nu}$ is strictly convex, cf. [99, Theorem 1.1.9]. We will see that all energies $E_{K,\nu}$ of consideration are convex, except for E_{K_{B},ν_2}, and that E_{K_{E},ν_1}, E_{K_{E},ν_2}, are strictly convex.

The Lebesgue Measure. For the measure ν_1 we have the normalization $\nu_1(X) = 2$ and the potential functions (Riesz representatives)

$$\begin{aligned}
h_{K_{\mathrm{E}},\nu_1}(y) &= \int_{-1}^{1} 2 - |x-y| \mathrm{d}x = 3 - y^2, \qquad y \in [-1,1], \\
h_{K_{\mathrm{B}},\nu_1}(y) &= \int_{-1}^{1} 1 - |x-y| - xy \mathrm{d}x = 1 - y^2, \qquad y \in [-1,1].
\end{aligned}$$

Since the derivatives are simply $h'_{K,\nu_1}(y) = -2y$ and $h''_{K,\nu_1}(y) = -2$, for $y \in [-1,1]$, $K = K_{\mathrm{E}}, K_{\mathrm{B}}$, we find that the Hessians are given by, cf. (2.85) and (2.86),

$$\mathbf{H} E_{K_{\mathrm{E}},\nu_1}(\boldsymbol{P}) = 2\boldsymbol{I}, \quad \mathbf{H} E_{K_{\mathrm{B}},\nu_1}(\boldsymbol{P}) = 2\boldsymbol{I} - \frac{2}{M}\boldsymbol{E}, \qquad \boldsymbol{P} \in [-1,1]^M,$$

where $\boldsymbol{I} := (\delta_{i,j})_{i,j=1}^M \in \mathbb{R}^{M\times M}$ is the identity matrix and $\boldsymbol{E} := (1)_{i,j=1}^M \in \mathbb{R}^{M\times M}$ is the matrix where all entries are one. Hence, for all points $\boldsymbol{P} \in [-1,1]^M$, the Hessian of E_{K_{E},ν_1} is positive definite, and the Hessian of E_{K_{B},ν_1} is positive semidefinite with rank $M-1$. We conclude by well known facts about convex functions that the energies E_{K_{E},ν_1} and E_{K_{B},ν_1} are convex, cf. [99, Theorem 5.2.14]. Moreover, since E_{K_{E},ν_1} is strictly convex there is exactly one global minimizer. The corresponding equation systems $\nabla E_{K,\nu_1}(\boldsymbol{P}^*) = \boldsymbol{0}$, $K = K_{\mathrm{E}}, K_{\mathrm{B}}$, are linear and given by

$$2\boldsymbol{I}\boldsymbol{P}^* = 2\left(\frac{2i-1}{M} - 1\right)_{i=1}^{M}, \quad \left(2\boldsymbol{I} - \frac{2}{M}\boldsymbol{E}\right)\boldsymbol{P}^* = 2\left(\frac{2i-1}{M} - 1\right)_{i=1}^{M}, \qquad \boldsymbol{P}^* \in [-1,1]^M,$$

respectively. It follows, that the optimal quadrature points for the Lebesgue measure ν_1 in the reproducing kernel Hilbert spaces $H_K(X)$, $K = K_{\mathrm{E}}, K_{\mathrm{B}}$, are given by the equidistributed points

$$\boldsymbol{P}^*_{K_{\mathrm{E}},\nu_1} := \left(\frac{2i-1}{M} - 1\right)_{i=1}^{M}, \ \boldsymbol{P}^*_{K_{\mathrm{B}},\nu_1} := \left(\frac{2i-1}{M} - 1 + c_M\right)_{i=1}^{M} \in [-1,1]^M, \ -\frac{1}{M} \le c_M \le \frac{1}{M},$$

respectively. We remark, for $c_M = \pm\frac{1}{M}$ the optimal quadrature functional $Q_{\nu_1}(\boldsymbol{P}^*_{K_{\mathrm{B}}})$ in $H_{K_{\mathrm{B}}}(X)$ consists effectively only of $M-1$ quadrature points, since the quadrature point points ± 1 may be omitted. An illustration of these points is given on the left in Figure 2.1. We infer that the

minimal equal weights worst case quadrature errors are, cf. (2.42),

$$\mathrm{err}^{**}_{K_{\mathrm{E}},\nu_1}(M) = \mathrm{err}^{**}_{K_{\mathrm{B}},\nu_1}(M) = \frac{2}{\sqrt{3}} M^{-1}, \qquad M \in \mathbb{N}, \tag{2.87}$$

and that the optimal quadrature points may but need not to be unique.

The Arcsine Distribution. For the measure ν_2 we have the normalization $\nu_2(X) = \pi$ and the potential functions

$$h_{K_{\mathrm{E}},\nu_2}(y) = \int_1^1 \frac{2 - |x-y|}{\sqrt{1-x^2}} \mathrm{d}x = 2\pi - 2\sqrt{1-y^2} - 2y \arcsin(y), \qquad y \in [-1,1],$$
$$h_{K_{\mathrm{B}},\nu_2}(y) = \int_1^1 \frac{1 - |x-y| - xy}{\sqrt{1-x^2}} \mathrm{d}x = \pi - 2\sqrt{1-y^2} - 2y \arcsin(y), \qquad y \in [-1,1],$$

with derivatives, for $K = K_{\mathrm{E}}, K_{\mathrm{B}}$, given by

$$h'_{K,\nu_2}(y) = -2 \arcsin(y), \quad y \in [-1,1], \qquad h''_{K,\nu_2}(y) = -\frac{2}{\sqrt{1-y^2}}, \quad y \in (-1,1).$$

We conclude, as in the former example that the Hessian of $E_{K_{\mathrm{E}},\nu_2}(\boldsymbol{P})$ is positive definite with smallest eigenvalue $\lambda_1 \geq 2$, for all $\boldsymbol{P} \in (-1,1)^M$. Hence by continuity, E_{K_{E},ν_2} is strictly convex on $[-1,1]^M$ and admits exactly one global minimizer $\boldsymbol{P}^*_{K_{\mathrm{E}},\nu_2} \in [-1,1]^M$. After solving $\nabla E_{K_{\mathrm{E}},\nu_2}(\boldsymbol{P}^*) = \boldsymbol{0}$, i.e.,

$$\frac{2i-1}{M} - 1 = \frac{2}{\pi} \arcsin(p_i^*) = 1 - \frac{2}{\pi} \arccos(p_i^*), \qquad i = 1, \ldots, M,$$

we find that the unique global minimizer of E_{K_{E},ν_2} is

$$\boldsymbol{P}^*_{K_{\mathrm{E}},\nu_2} = \left(\cos\left(\pi \frac{2M-2i+1}{2M} \right) \right)_{i=1}^M \in [-1,1]^M,$$

which is given by the zeros of the Chebyshev polynomials of the first kind $T_M : [-1,1] \to \mathbb{R}$, cf. [1, Eq. 22.16.4]. We observe, that the point $\boldsymbol{P}^*_{K_{\mathrm{E}},\nu_2}$ solves also the equation system $\nabla E_{K_{\mathrm{B}},\nu_2}(\boldsymbol{P}^*) = \boldsymbol{0}$, cf. (2.86), since

$$\sum_{i=1}^M \cos\left(\pi \frac{2M-2i+1}{2M} \right) = 0, \qquad M \in \mathbb{N}.$$

However, numerical tests indicate that the Hessian $\mathbf{H}E_{\mathrm{B},\nu_2}(\boldsymbol{P}^*_{K_{\mathrm{E}},\nu_2})$ is indefinite with one negative eigenvalue, so that the point $\boldsymbol{P}^*_{K_{\mathrm{E}},\nu_2}$ seems to be just a saddle point of the worst case quadrature error in the reproducing kernel Hilbert space $H_{K_{\mathrm{B}}}(X)$. Indeed, we find slightly better quadrature points by setting

$$\boldsymbol{P}^*_{K_{\mathrm{B}},\nu_2} := \left(\cos\left(\pi \frac{M-i+1}{M} \right) \right)_{i=1}^M \text{ or } \boldsymbol{P}^*_{K_{\mathrm{B}},\nu_2} := \left(\cos\left(\pi \frac{M-i}{M} \right) \right)_{i=1}^M \in [-1,1]^M,$$

which consist of the zeros of the Chebyshev polynomials of the second kind $U_{M-1} : [-1,1] \to \mathbb{R}$, cf. [1, Eq. 22.16.4], together with one point at ± 1. These points are stationary points since, cf. (2.86),

$$\frac{2i-1}{M} - 1 + \frac{1}{M} \sum_{i=1}^M p_i^* = 1 - \frac{2}{\pi} \arccos(p_i^*), \qquad p_i^* := \cos\left(\pi \frac{M-i}{M} \right), \quad i = 1, \ldots, M,$$

and it is likely that they are global minimizers of the worst case quadrature error $\mathrm{err}_{K_\mathrm{B},\nu_2}$ for equal weights quadrature rules. As remarked previously, the quadrature points at ± 1 may be omitted in the quadrature rule $Q_{\nu_2}(\boldsymbol{P}^*_{K_\mathrm{B}})$. An illustration of these points is given on the right hand side in Figure 2.1. Using the above quadrature points $\boldsymbol{P}_{K_\mathrm{E},\nu_2}$, $\boldsymbol{P}_{K_\mathrm{B},\nu_2}$ we can estimate the minimal equal weights worst case quadrature errors by

$$\begin{aligned}
\mathrm{err}^{**}_{K_\mathrm{E},\nu_2}(M) &= \sqrt{\frac{4\pi}{\sin\left(\frac{\pi}{2M}\right) M} - 8} = \frac{\pi}{\sqrt{3}} M^{-1} + o\left(M^{-1}\right), \qquad \lim_{M\to\infty} o(M^{-1})M = 0, \quad M \in \mathbb{N},\\
\mathrm{err}^{**}_{K_\mathrm{B},\nu_2}(M) &\le \sqrt{\frac{4\pi}{\tan\left(\frac{\pi}{2M}\right) M} + \frac{\pi^2}{M^2} - 8} \le \frac{\pi}{\sqrt{3}} M^{-1}, \qquad M \in \mathbb{N}.
\end{aligned} \tag{2.88}$$

In this example we were confronted with the problem of solving the non-linear equation system $\nabla E_{K_\mathrm{B},\nu_2}(\boldsymbol{P}^*) = \boldsymbol{0}$, $\boldsymbol{P}^* \in [-1,1]^M$, which turned out to be a delicate problem. Moreover, we have observed that several stationary points may occur, and that finding the global optimum can be a very hard problem.

The Dirac Measure at the Points ± 1. For the measure ν_3 we have the normalization $\nu(X) = 2$ and the potential functions

$$\begin{aligned}
h_{K_\mathrm{E},\nu_3}(y) &= (2 - |-1-y|) + (2 - |1-y|) = 2, \qquad y \in [-1,1],\\
h_{K_\mathrm{B},\nu_3}(y) &= (1 - |-1-y| + y) + (1 - |1-y| - y) = 0, \qquad y \in [-1,1].
\end{aligned}$$

Hence, for the kernel K_E we have to minimize the sum, cf. (2.84),

$$\tilde{E}_{K_\mathrm{E},\nu_3}(\boldsymbol{P}) := \sum_{i,j=1}^{M} (M - 2i + 1)\, p_i, \qquad -1 \le p_1 \le p_2 \le \cdots \le p_M \le 1,$$

which is simply done by minimizing every summand separately. This leads to the optimal quadrature points

$$\boldsymbol{P}^*_{K_\mathrm{E},\nu_3} := \begin{cases} p_i = -1, i = 1,\dots,m,\ p_i = 1, i = m+1,\dots,M, & M = 2m,\\ p_i = -1, i = 1,\dots,m,\ p_{m+1} \in [-1,1],\ p_i = 1, i = m+2,\dots,M, & M = 2m+1, \end{cases}$$

with minimal equal weights worst case quadrature error

$$\mathrm{err}^{**}_{K_\mathrm{E},\nu_3}(M) = \begin{cases} 0, & M = 2m,\\ 2M^{-1}, & M = 2m+1. \end{cases} \tag{2.89}$$

This shows that the minimal equal weights worst case quadrature error does not need not to converge monotonically. In contrast, it is obvious that the minimal worst case quadrature for arbitrary quadrature functionals satisfies $\mathrm{err}^*_{K_\mathrm{E},\nu_3}(M) = 0$ for $M \ge 2$.

Another interesting behavior is observed by considering the kernel K_E, where the minimal quadrature error is achieved by putting all quadrature points at the endpoints of the interval $[-1,1]$, i.e.,

$$\mathrm{err}^{**}_{K_\mathrm{B},\nu_3}(M) = \mathrm{err}_{K_\mathrm{B},\nu_3}(\boldsymbol{P}^*_{K_\mathrm{B},\nu_3}) = 0, \qquad \boldsymbol{P}^*_{K_\mathrm{B},\nu_3} \in \{-1,1\}^M, \qquad M \in \mathbb{N}. \tag{2.90}$$

This is explained by the previous observation that the integral functional I_{ν_3} is effectively zero, as are all quadrature functionals $Q(\boldsymbol{P}^*_{K_\mathrm{B},\nu_3}, \boldsymbol{w})$, $\boldsymbol{w} \in \mathbb{C}^M$. Moreover, we observe that strong convergence in $H^*_{K_\mathrm{B}}(X)$, cf. (2.10), does not necessarily imply weak convergence in $C^*(X)$, cf.

(2.7), since there are functions $f \in C(X)$ with

$$Q_{\nu_3}(\boldsymbol{e})f = 2f(1) \neq f(-1) + f(1) = I_{\nu_3}f, \qquad \boldsymbol{e} := (1, \dots, 1) \in \mathbb{R}^M.$$

The main motivation for considering the last example is to show that in contrast to the minimal worst case quadrature error $\mathrm{err}^*_{K,\nu}$ the minimal equal weights worst case quadrature error $\mathrm{err}^{**}_{K,\nu}$ does not necessarily converge monotonically to zero. Moreover, we have seen that the L^2-discrepancy $D^2_{\mathcal{B}_{\mathrm{d}_X}}$ which corresponds to the kernel K_{B} cannot distinguish between measures $\nu \in M_{\mathbb{C}}(\mathbb{R})$ with support $\mathrm{supp}(\nu) \subset \{-1, 1\}$.

Finally, we note that the minimal equal weights worst case quadrature errors $\mathrm{err}^{**}_{K,\nu}(M)$ decay with order M^{-1} for increasing size $M \in \mathbb{N}$, cf. (2.87), (2.88), (2.89), (2.90), which is much faster than the estimate provided by Corollary 2.8.

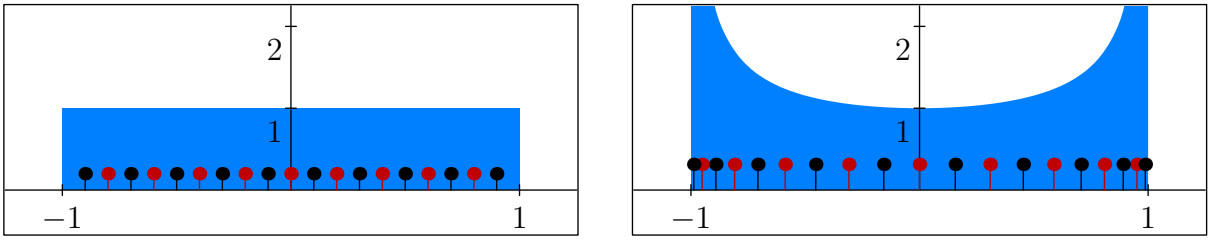

Figure 2.1: Schematic illustrations of the densities of the Lebesgues measure ν_1 (left) and the arcsine distribution ν_2 (right). For $M = 10$ the optimal equal weights quadrature rules $Q_\nu(\boldsymbol{P}^*_{K,\nu})$, $\nu = \nu_1, \nu_2$, are illustrated by black ($K = K_{\mathrm{E}}$) and red ($K = K_{\mathrm{B}}$) dots, respectively. We remark that for $K = K_{\mathrm{B}}$ the quadrature points at ± 1 are omitted.

2.5.2 Optimal Quadrature Points in the Plane $\mathbb{R}^2$ for the Circle $\mathbb{S}^1$ and the Disc D

In this section we present some numerical results for equal weights quadrature functionals $Q_\nu(\boldsymbol{P})$, $\boldsymbol{P} \in (\mathbb{R}^2)^M$, $M \in \mathbb{N}$, and finite Borel measures $\nu = \nu_1, \nu_2$ supported on the unit circle

$$\mathbb{S}^1 := \{\boldsymbol{x} \in \mathbb{R}^2 \ : \ \|\boldsymbol{x}\|_2 = 1\} \subset \mathbb{R}^2$$

and the unit disc

$$D := B_{\mathbb{R}^2}(\boldsymbol{0}, 1) = \{\boldsymbol{x} \in \mathbb{R}^2 \ : \ \|\boldsymbol{x}\|_2 \leq 1\} \subset \mathbb{R}^2,$$

respectively. Using polar coordinates

$$\boldsymbol{x}(r, \alpha) := (r\cos(\alpha), r\sin(\alpha))^\top \in \mathbb{R}^2, \qquad (r, \alpha) \in \mathbb{R}_+ \times [0, 2\pi),$$

we define for measurable sets $\Omega \subset \mathbb{R}^2$ the measures

$$\begin{aligned} \nu_1(\Omega) &:= \int_{\mathbb{S}^1} 1_\Omega(\boldsymbol{x}) \mathrm{d}\nu_1(\boldsymbol{x}) := \int_0^{2\pi} 1_\Omega(\boldsymbol{x}(1, \alpha)) \mathrm{d}\alpha, \\ \nu_2(\Omega) &:= \int_D 1_\Omega(\boldsymbol{x}) \mathrm{d}\nu_2(\boldsymbol{x}) := \int_0^{2\pi} \int_0^1 1_\Omega(\boldsymbol{x}(r, \alpha)) r \mathrm{d}r \mathrm{d}\alpha. \end{aligned} \tag{2.91}$$

In words, ν_1 corresponds to the canonical measure $\mu_{\mathbb{S}^1}$ of the manifold $\mathbb{S}^1$ and ν_2 is the restriction of the Lebesgue measure $\mu_{\mathbb{R}^2}$ to the unit disc D. The normalizations are $\nu_1(\mathbb{S}^1) = 2\pi$ and $\nu_2(D) = \pi$.

In what follows we allow $X \subset \mathbb{R}^2$ to be any compact set which contains the unit disc D. We remark that the unit disc D is the convex hull of the unit circle $\mathbb{S}^1$, cf. (2.64). For such sets X

we consider the reproducing kernel Hilbert space $H_{K_{\mathrm{E}}}(X)$ with the positive definite Euclidean distance kernel

$$K_{\mathrm{E}}(\boldsymbol{x},\boldsymbol{y}) := C_X - \|\boldsymbol{x}-\boldsymbol{y}\|_2, \qquad \boldsymbol{x},\boldsymbol{y} \in X,$$

where $C_X > 0$ is some suitable constant, cf. Corollary 2.15. As pointed out in the proof of Corollary 2.15 this kernel can be considered as a discrepancy kernel over halfspaces, cf. Example 2.13 and Theorem 2.14. By Remark 2.9 the worst case quadrature error $\mathrm{err}_{K_{\mathrm{E}}}$ between the equal weights quadrature functional $Q_\nu(\boldsymbol{P})$, $\boldsymbol{P} := (\boldsymbol{p}_1,\ldots,\boldsymbol{p}_M) \in X^M$, and the integral functional I_ν, $\nu = \nu_1, \nu_2$, can be computed by omitting the constant C_X, i.e.,

$$\mathrm{err}_{K_{\mathrm{E}}}(\nu,\boldsymbol{P}) = -\left(\frac{\nu(X)}{M}\right)^2 \sum_{i,j=1}^{M} \|\boldsymbol{p}_i-\boldsymbol{p}_j\|_2 + 2\frac{\nu(X)}{M}\sum_{i=1}^{M} \tilde{h}_{K_{\mathrm{E}},\nu}(\boldsymbol{p}_i) - \int_X \tilde{h}_{K_{\mathrm{E}},\nu}(\boldsymbol{y})\mathrm{d}\nu(\boldsymbol{y}),$$

where

$$\tilde{h}_{K_{\mathrm{E}},\nu_1}(\boldsymbol{y}) := \int_{\mathbb{S}^1} \|\boldsymbol{x}-\boldsymbol{y}\|_2 \mathrm{d}\nu_1(\boldsymbol{x}), \quad \tilde{h}_{K_{\mathrm{E}},\nu_2}(\boldsymbol{y}) := \int_D \|\boldsymbol{x}-\boldsymbol{y}\|_2 \mathrm{d}\nu_2(\boldsymbol{x}), \qquad \boldsymbol{y} \in X. \tag{2.92}$$

We observe that the worst case quadrature error $\mathrm{err}_{K_{\mathrm{E}}}$ does not essentially depend on X, and that the energy functions, cf. Remark 2.9,

$$E_{K_{\mathrm{E}},\nu}(\boldsymbol{P}) = -\frac{\nu(D)}{M}\sum_{i=1}^{M-1}\sum_{j=i+1}^{M} \|\boldsymbol{p}_i-\boldsymbol{p}_j\|_2 + \sum_{i=1}^{M} \tilde{h}_{K_{\mathrm{E}},\nu}(\boldsymbol{p}_i) \tag{2.93}$$

can be simply extended to any point $\boldsymbol{P} \in (\mathbb{R}^2)^M$. Therefore, we are left to consider an unrestricted optimization problem on $\mathbb{R}^{2M}$, which is in general easier to solve than the restricted optimization problem on X^M. In fact, we will see, at least numerically, that the (locally) optimal points $\boldsymbol{P}_i^* \in \mathbb{R}^{2M}$ of $E_{K_{\mathrm{E}},\nu_i}(\boldsymbol{P}_i^*)$, $i = 1,2$, lie in the unit disc D. It follows, that for all compact sets $X \subset \mathbb{R}^2$ with $D \subset X$ the worst case quadrature error $\mathrm{err}_{K_{\mathrm{E}}}$, is minimized for the measures ν_1, ν_2 by some points $\boldsymbol{P}_i^* \in X^M$, $i = 1,2$, independently of X. For the evaluation and optimization of the energies $E_{K_{\mathrm{E}},\nu}$ we present a closed form expression of the potential functions $\tilde{h}_{K_{\mathrm{E}},\nu}$ defined by (2.92) in terms of the *complete elliptic integral of the first kind*, cf. [1, Eq. 17.3.1],

$$K(m) := \int_0^1 [(1-mt^2)(1-t^2)]^{-\frac{1}{2}}\mathrm{d}t, \qquad m \in [0,1], \tag{2.94}$$

and the *complete elliptic integral of the second kind*, cf.[1, Eq. 17.3.3] ,

$$E(m) := \int_0^1 (1-mt^2)^{\frac{1}{2}}(1-t^2)^{-\frac{1}{2}}\mathrm{d}t, \qquad m \in [0,1]. \tag{2.95}$$

Theorem 2.17. *Let the measures ν_1 and ν_2 be defined by (2.91). Then, for $s := \|\boldsymbol{y}\|_2$, $\boldsymbol{y} \in \mathbb{R}^2$, the functions h_{K_{E},ν_i}, $i = 1,2$, given by (2.92) can be computed by*

$$\begin{aligned}
\tilde{h}_{K_{\mathrm{E}},\nu_1}(\boldsymbol{y}) &= 4(s+1)E\left(\frac{4s}{(s+1)^2}\right) =: \bar{h}_{K_{\mathrm{E}},\nu_1}(s),\\
\tilde{h}_{K_{\mathrm{E}},\nu_2}(\boldsymbol{y}) &= \frac{2}{9}(s+1)\left[(s^2+7)E\left(\frac{4s}{(s+1)^2}\right) - (s-1)^2K\left(\frac{4s}{(s+1)^2}\right)\right] =: \bar{h}_{K_{\mathrm{E}},\nu_2}(s),
\end{aligned} \tag{2.96}$$

where K, cf. (2.94), and E, cf. (2.95), are the complete elliptic integrals of the first and second kind, respectively.

Proof. We consider the slightly more general problem by computing the integral over the circle $r\mathbb{S}^1$ of radius $r > 0$ given by

$$h(\boldsymbol{y}, r) := r \int_0^{2\pi} \|\boldsymbol{x}(r,\alpha) - \boldsymbol{y}\|_2 \mathrm{d}\alpha = r \int_0^{2\pi} (r^2 + \|\boldsymbol{y}\|_2^2 - 2\boldsymbol{x}(r,\alpha)^\top \boldsymbol{y})^{\frac{1}{2}}, \qquad \boldsymbol{y} \in \mathbb{R}^2.$$

For $\boldsymbol{y}_s := (s, 0)^\top \in \mathbb{R}^2$, $s > 0$, we find

$$h(\boldsymbol{y}_s, r) = r \int_0^{2\pi} (r^2 + s^2 - 2rs\cos(\alpha))^{\frac{1}{2}} \mathrm{d}\alpha = 2r \int_{-1}^{1} (r^2 + s^2 + 2rsa)^{\frac{1}{2}} (1 - a^2)^{-\frac{1}{2}} \mathrm{d}a.$$

Together with the rotational invariance of the measure ν_1 we arrive after a change of variable $a := 1 - 2t^2$, $t \in [0, 1]$, at

$$h(\boldsymbol{y}, r) = 4r(s + r) \int_0^1 \left(1 - \frac{4sr}{(s+r)^2} t^2\right)^{\frac{1}{2}} (1 - t^2)^{-\frac{1}{2}} \mathrm{d}t = 4r(s + r) E\left(\frac{4sr}{(s+r)^2}\right), \quad \boldsymbol{y} \in \mathbb{R}^2,$$

where $s := \|\boldsymbol{y}\|_2$. With $r = 1$ we find the first equation in (2.96). For the second equation in (2.96) we use the relation

$$\int_D \|\boldsymbol{x} - \boldsymbol{y}\|_2 \mathrm{d}\nu_2(\boldsymbol{x}) = \int_0^1 h(\boldsymbol{y}, r) \mathrm{d}r, \qquad \boldsymbol{y} \in \mathbb{R}^2,$$

where we integrate the function $h(\boldsymbol{y}, \cdot)$ over the interval $[0, 1]$. Hence, for proving the assertion (2.96) it is sufficient to show the relations

$$\frac{\mathrm{d}}{\mathrm{d}r} H(\boldsymbol{y}, r) = h(\boldsymbol{y}, r), \quad r > 0, \qquad H(\boldsymbol{y}, 0) = 0, \qquad \boldsymbol{y} \in \mathbb{R}^2, \tag{2.97}$$

for

$$H(\boldsymbol{y}, r) := \frac{2}{9}(s + r) \left[(s^2 + 7r^2) E\left(\frac{4sr}{(s+r)^2}\right) - (s - r)^2 K\left(\frac{4sr}{(s+r)^2}\right)\right], \qquad \boldsymbol{y} \in \mathbb{R}^2.$$

The first relation in (2.97) is established by the representations of the derivatives

$$\frac{\mathrm{d}}{\mathrm{d}m} K(m) = \frac{1}{2}\left(\frac{E(m)}{m - m^2} - \frac{K(m)}{m}\right), \qquad \frac{\mathrm{d}}{\mathrm{d}m} E(m) = \frac{E(m) - K(m)}{2m}, \qquad m \in [0, 1],$$

and the second relation in (2.97) by using $E(0) = K(0)$, which finishes the proof. ∎

By Theorem 2.17 it follows that the potential functions $\tilde{h}_{K_{\mathrm{E}},\nu}$, $\nu = \nu_1, \nu_2$, cf. (2.92), in the energy $E_{K_{\mathrm{E}},\nu}$, cf. (2.93), are radially symmetric. The radial parts $\bar{h}_{K_{\mathrm{E}},\nu}$, $\nu = \nu_1, \nu_2$, are plotted in Figure 2.2 . We observe that the first notable difference in the shape of these functions occurs for the second order derivatives, where $\bar{h}''_{K_{\mathrm{E}},\nu_1}(1)$ does not exist. Therefore, it is surprising that even due to such slightly differences in the potential functions numerical optimization leads to very different patterns of the computed local minimizers, cf. Figure 2.3.

One can check that stationary points of the energies E_{K_{E},ν_i}, $i = 1, 2$, are given by equidistributed points

$$\boldsymbol{P}_i^* := \left(r_i^* \cos\left(\frac{2\pi j}{M}\right), r_i^* \sin\left(\frac{2\pi j}{M}\right)\right)_{j=1}^{M} \in \mathbb{R}^{2M}, \qquad M \in \mathbb{N}, \tag{2.98}$$

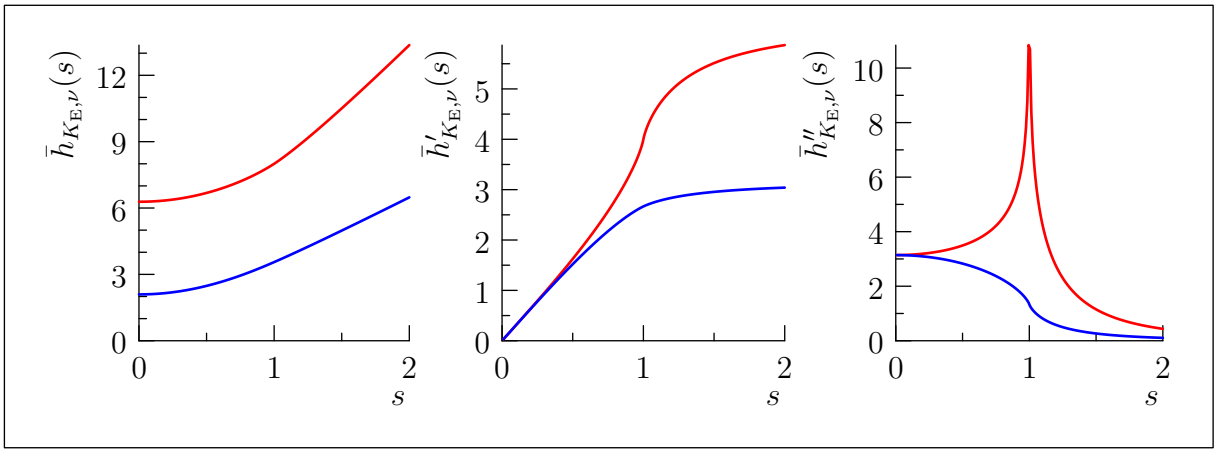

Figure 2.2: Illustrations of the radial parts of the potential functions $\tilde{h}_{K_E,\nu_i}$, $i = 1, 2$, and their first two derivatives for the measures ν_1 (red) and ν_2 (blue).

on a circle of radius $r_i^* < 1$, where r_i^* is the unique solution of the equation

$$\frac{\nu_i(D)}{M} \cot\left(\frac{\pi}{M}\right) = \bar{h}'_{K_E,\nu_i}(r), \qquad r \geq 0, \qquad i = 1, 2.$$

An illustration of the points $\boldsymbol{P}_i^*$, $i = 1, 2$, is given in Figure 2.4. For the measure ν_1, supported on the unit circle $\mathbb{S}^1$, the points $\boldsymbol{P}_1^* \in X^M$ seem to be the optimal quadrature points, which minimize the worst case quadrature error err_{K_E} for any compact set $X \subset \mathbb{R}^2$ containing the unit disc D. In contrast, for the measure ν_2, supported on the unit disc D, the points $\boldsymbol{P}_2^* \in X^M$ seem to minimize the worst case quadrature error err_{K_E}, only for $1 \leq M \leq 6$, whereas the picture changes if we consider more than six points, cf. Figure 2.3.

Finally, we conclude from these examples that optimal quadrature points $\boldsymbol{P}^* \in X^M$ do not necessarily lie in the support of a measure ν which is aimed to be approximate. Moreover, we have seen that standard optimization methods on Euclidean space $\mathbb{R}^n$ can be applied to compute optimal quadrature points $\boldsymbol{P}^* \in X^M$, and that even little differences in the potential functions may lead to very different point distributions. However, if one asks for the computation of optimal quadrature points lying on Riemannian manifolds, e.g., the unit circle $\mathbb{S}^1$, it is more natural and convenient to consider optimization methods on Riemannian manifolds as presented in Chapter 3.

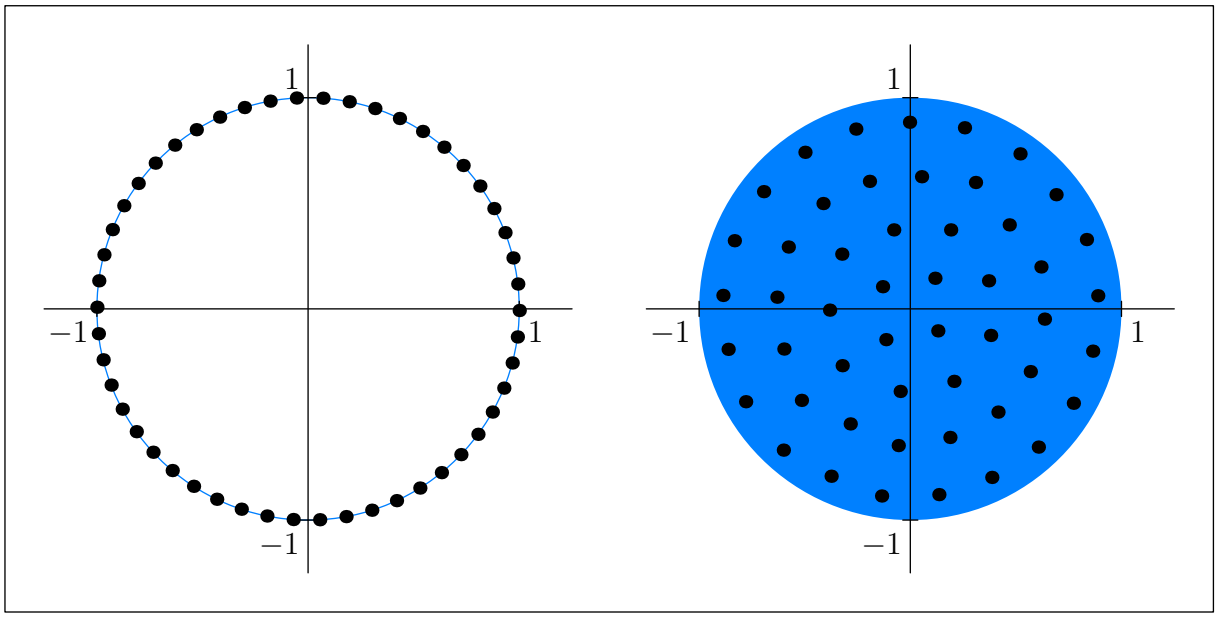

Figure 2.3: Local minimizers of the worst case quadrature error $\mathrm{err}_{K_{\mathrm{E}},\nu_i}$, $i = 1, 2$, with $M = 50$ points in $\mathbb{R}^2$ for the measure ν_1 on the unit circle $\mathbb{S}^1$ (left) and the measure ν_2 on the disc D (right), respectively. The computations were performed by using the 'NMinimize'-function in Mathematica, which tries to find numerically a global minimum.

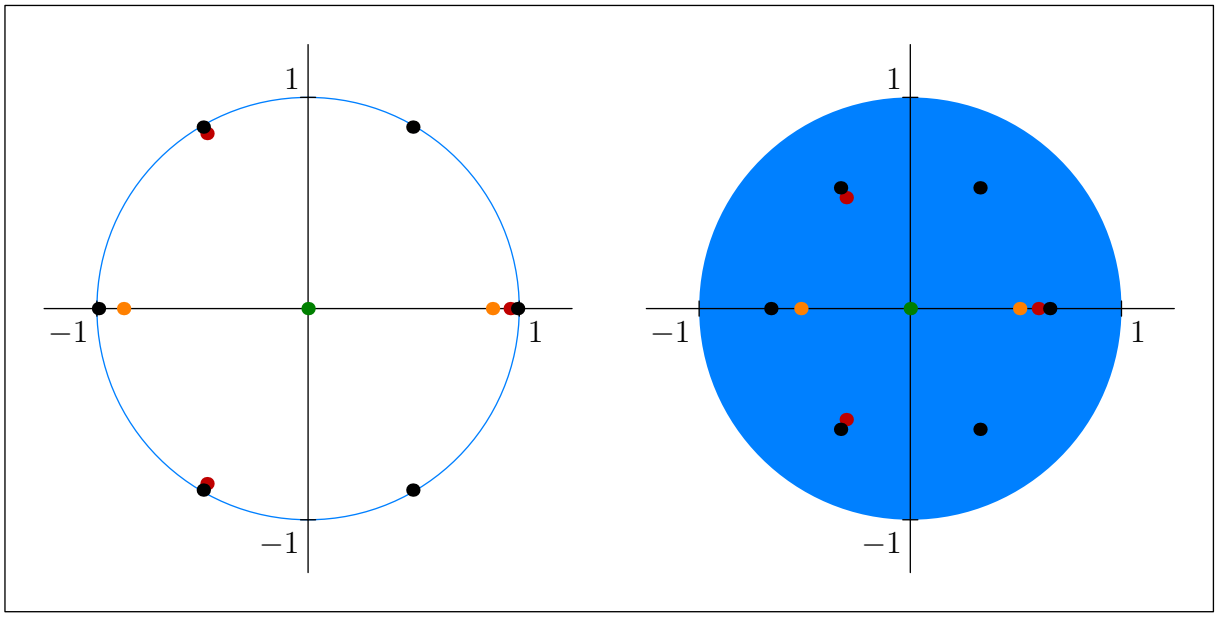

Figure 2.4: The stationary points $\boldsymbol{P}_i^* \in \mathbb{R}^{2M}$ defined by (2.98) of the worst case quadrature error $\mathrm{err}_{K_{\mathrm{E}},\nu_i}$, $i = 1, 2$, for the measure ν_1 on the unit circle $\mathbb{S}^1$ (left) and the measure ν_2 on the disc D (right), respectively. Color coding: M=1 (green), M=2 (orange), M=3 (red), M=6 (black)

3

Optimization on Riemannian Manifolds

In this Chapter we present a general framework for the optimization on Riemannian manifolds, where the standard optimization methods for Euclidean space have been recently adapted to Riemannian manifolds, see for example the seminal work of Udrişte [131] and Smith [121]. In this thesis it is sufficient to restrict our attention to smooth manifolds $\mathcal{M}$ which are subsets of some Euclidean space $\mathbb{R}^n$, and we refer for the more general theory of Riemannian manifolds to the monographs [66, 124, 49, 70].

In Section 3.1 we develop thoroughly the basic notations and relations of differential geometry on Riemannian manifolds, in order to get a concise description of the optimization methods of Riemannian manifolds given in Section 3.3. Afterward, we recapitulate in Section 3.2 explicit formulas of the differential geometric objects on the torus $\mathbb{T}^d$, the sphere $\mathbb{S}^d$, and the rotation group $\mathrm{SO}(n)$, which we need for the numerical computations. Finally, we introduce in Section 3.3 adaptions of the method of steepest descent, Newton's method, and the method of conjugate gradients to Riemannian manifold. Furthermore, we analyze the convergence properties of proposed optimization methods by adapting the ideas of the corresponding, well-studied optimization methods of Euclidean space. A detailed motivation for the use of optimization on Riemannian manifolds is given in Section 3.3.3.

3.1 Riemannian Geometry

This section is to be understood as an introduction to Riemannian manifolds, where we follow the classical approach to manifolds. We start in Section 3.1.1 with basic definitions concerning smooth curves in Euclidean space, on which the classical theory of manifolds is based. Afterward, we give in Section 3.1.2–3.1.4 the usual definitions and characterizations of a manifold, the tangent space, the induced Riemannian structure, and geodesics. Based on these notations we define in Section 3.1.5 for smooth functions on Riemannian manifolds the gradient and the Hessian, which are of essential importance for the derivation of optimization methods on Riemannian manifolds in Section 3.3. Furthermore, the central Theorem 3.5 shows that the gradient and the Hessian encode the first and second order derivatives of geodesic curves, respectively, so that the most convergence results for optimization methods on Riemannian manifolds, cf. Section 3.3.1, are obtained by imitating the proofs of the corresponding results in Euclidean space. For the optimization of the worst case quadrature error in reproducing kernel Hilbert spaces on Riemannian manifolds we briefly summarize the notations for product manifolds in Section 3.1.7. Finally, we define the

canonical measure of a Riemannian manifold in Section 3.1.6, since it is essential for the harmonic analysis on the torus $\mathbb{T}^d$, sphere $\mathbb{S}^d$, and rotation group SO(3) presented in Chapter 4.

3.1.1 Curves in Euclidean Space

A *curve* γ is a continuous map from an interval $I \subset \mathbb{R}$ into the Euclidean space $\mathbb{R}^n$, i.e.,

$$\gamma : I \to \mathbb{R}^n, \qquad \gamma(t) := (\gamma_1(t), \ldots, \gamma_n(t)), \quad t \in I,$$

where the *coordinate functions* $\gamma_i : I \to \mathbb{R}^n$, $i = 1, \ldots, n$, are continuous. A curve γ is called *smooth* if all coordinate functions γ_i, $i = 1, \ldots, n$ are indefinitely often differentiable. A smooth curve γ is called *regular* if its *velocity vector*[1]

$$\dot{\gamma}(s) := \frac{\mathrm{d}}{\mathrm{d}t}\gamma(t)\Big|_{t=s} := \lim_{t \to 0} \frac{1}{t}(\gamma(t) - \gamma(0)) = (\dot{\gamma}_1(s), \ldots, \dot{\gamma}_n(s)) \in \mathbb{R}^n$$

does not vanish for any $s \in I$. Loosely speaking, a regular curve has no cusps. Throughout this thesis we assume, if not stated otherwise, that all curves are regular or constant.

We remark that the term curve is sometimes also used for the image $\gamma(I) \subset \mathbb{R}^n$ of γ, which may lead to some confusion, since different curves may have the same image. In that respect, we call two curves $\gamma_1 : I_1 \to \mathbb{R}^n$ and $\gamma_2 : I_2 \to \mathbb{R}^n$ equivalent, if there is a smooth function $\tau : I_1 \to I_2$ with smooth inverse τ^{-1} such that

$$\gamma_1(t) = \gamma_2 \circ \tau(t), \qquad t \in I_1.$$

The above relation of reparameterization is an equivalence relation and the equivalence class $[\gamma]$ is called an *arc*. Obviously, for two equivalent curves γ_1, γ_2 we have $\gamma_1(I_1) = \gamma_2(I_2)$, but the inverse statement need not to be true.

The *arc length* of a curve $\gamma : [a, b] \to \mathbb{R}^n$, $a < b$, is defined by

$$L(\gamma) := \sup \left\{ \sum_{i=1}^{M} \|\gamma(t_{i-1}) - \gamma(t_i)\|_2 \ : \ M \in \mathbb{N},\ a = t_0 < t_1 < \cdots < t_{n-1} < t_n = b \right\} \tag{3.1}$$

and it is well-known that it can be calculated by

$$L(\gamma) = \int_a^b \|\dot{\gamma}(t)\|_2 \,\mathrm{d}t = \int_a^b \sqrt{\dot{\gamma}(t)^\top \dot{\gamma}(t)} \,\mathrm{d}t. \tag{3.2}$$

By definition (3.1), one can imagine that the arc length $L(\gamma)$ of a curve γ should be equal for curves representing the same arc $[\gamma]$, and indeed it is. Thus, the arc length of a curve does not depend on its parameterization. Particular nice representatives of an arc $[\gamma]$ are curves γ which are parameterized proportional to the arc length, i.e., there exists a constant $c \geq 0$ such that

$$L\left(\gamma\big|_{[t_0,t_1]}\right) = \int_{t_0}^{t_1} \|\dot{\gamma}(t)\|_2 \,\mathrm{d}t = c(t_1 - t_0), \qquad t_0 < t_1 \in I, \tag{3.3}$$

or equivalently $\|\dot{\gamma}(t)\|_2 = c$, $t \in I$.

[1] We use the convention that the dot reflects the derivative with respect to the 'time' variable t.

3.1.2 Submanifolds of Euclidean Space and Local Parameterizations

For open sets $U \subset \mathbb{R}^n$, $V \subset \mathbb{R}^m$ the map $F : U \to \mathbb{R}^m$, $F(\boldsymbol{x}) = (F_1(\boldsymbol{x}), \dots, F_m(\boldsymbol{x}))$, is called *smooth* if every *coordinate function* $F_i : U \to \mathbb{R}$, $i = 1, \dots, m$, is indefinitely often differentiable. A *diffeomorphism* is a smooth map F with smooth inverse F^{-1}. We recall, that for a diffeomorphism $F : U \to V$ the inverse function theorem implies $n = m$. The *differential* of F at a fixed point $\boldsymbol{x} \in \mathbb{R}^n$ is the unique linear map $\mathrm{D}F(\boldsymbol{x}) : \mathbb{R}^n \to \mathbb{R}^m$, if it exists, with the approximation property

$$F(\boldsymbol{x} + \boldsymbol{v}) = F(\boldsymbol{x}) + \mathrm{D}F(\boldsymbol{x})\boldsymbol{v} + o(\boldsymbol{v}), \qquad \lim_{\boldsymbol{v} \to \boldsymbol{0}} \frac{o(\boldsymbol{v})}{\|\boldsymbol{v}\|_2} = 0, \qquad \boldsymbol{v} \in \mathbb{R}^n,\ \boldsymbol{x} + \boldsymbol{v} \in U.$$

The matrix representation of the differential $\mathrm{D}F(\boldsymbol{x})$, $\boldsymbol{x} \in \mathbb{R}^n$, with respect to the standard basis is given by the *Jacobian matrix*

$$\mathrm{D}F(\boldsymbol{x}) = \begin{pmatrix} \frac{\partial}{\partial x_1} F_1(\boldsymbol{x}) & \cdots & \frac{\partial}{\partial x_n} F_1(\boldsymbol{x}) \\ \vdots & \ddots & \vdots \\ \frac{\partial}{\partial x_1} F_m(\boldsymbol{x}) & \cdots & \frac{\partial}{\partial x_n} F_m(\boldsymbol{x}) \end{pmatrix} \in \mathbb{R}^{m \times n},$$

where $\frac{\partial}{\partial x_i}$, $i = 1, \dots, n$, are the partial derivatives.

In this thesis a manifold is a subset $\mathcal{M}$ of the Euclidean space $\mathbb{R}^n$ with a certain regularity assumption. Informally speaking, one can bend smoothly the ambient space $\mathbb{R}^n$ of the manifold $\mathcal{M}$ such that locally the manifold deforms to a Euclidean subspace of dimension d. More precisely, for $d \leq n$ we call a subset $\mathcal{M} \subset \mathbb{R}^n$ a *d-dimensional manifold* if for any $\boldsymbol{x} \in \mathcal{M}$ there exists a diffeomorphism $\Phi : U \to V$ between open subsets $U, V \subset \mathbb{R}^n$ with $\boldsymbol{x} \in U$ such that

$$\Phi(U \cap \mathcal{M}) = V \cap \mathbb{R}^d \times \{0\}^{n-d} = \{\boldsymbol{y} \in V \ : \ y_{d+1} = \cdots = y_n = 0\}. \tag{3.4}$$

A useful criterion for a set $\mathcal{M} \subset \mathbb{R}^n$ being a manifold is given as follows.

Theorem 3.1. *Let $U \subset \mathbb{R}^n$ be open and $F : U \to \mathbb{R}^{n-d}$ be a smooth map with surjective differential $\mathrm{D}F(\boldsymbol{x}) : \mathbb{R}^n \to \mathbb{R}^{n-d}$ whenever $F(\boldsymbol{x}) = \boldsymbol{0} \in \mathbb{R}^{n-d}$. Then $\mathcal{M} = F^{-1}(\boldsymbol{0})$ is a d-dimensional manifold.*

Proof. This follows from the implicit function theorem and definition (3.4), cf. [123, Theorem 5.1]. ∎

Another important characterization of a manifold $\mathcal{M} \subset \mathbb{R}^n$ is that it can be parameterized in a precise sense.

Theorem 3.2. *A set $\mathcal{M} \subset \mathbb{R}^n$ is a d-dimensional manifold if and only if, for any $\boldsymbol{x} \in \mathcal{M}$, there exists an open neighborhood U of $\boldsymbol{x}$ in $\mathbb{R}^n$, an open subset $\Omega \subset \mathbb{R}^d$, and a smooth map $h : \Omega \to \mathcal{M} \subset \mathbb{R}^n$ such that*

(i) $h(\Omega) = \mathcal{M} \cap U$,

(ii) $\mathrm{D}h(\boldsymbol{y}) : \mathbb{R}^d \to \mathbb{R}^n$ *is injective for all* $\boldsymbol{y} \in \Omega$,

(iii) $h^{-1} : h(\Omega) \to \Omega$ *is continuous.*

Proof. Since $\mathcal{M}$ is a d-dimensional manifold we find for every $\boldsymbol{x} \in \mathcal{M}$ a diffeomorphism $\Phi : U \to V$ satisfying (3.4). We set

$$h(y_1, \dots, y_d) := \Phi^{-1}(y_1, \dots, y_d, 0, \dots, 0)$$

for all $\boldsymbol{y} \in \Omega := \mathrm{pr}_{n,d}\left(V \cap \mathbb{R}^d \times \{0\}^{n-d}\right) \subset \mathbb{R}^d$, where $\mathrm{pr}_{n,d} : \mathbb{R}^n \to \mathbb{R}^d$ is the canonical projection onto the first d components. Hence, we have $h(\Omega) = \mathcal{M} \cap U$, and with $\Phi \circ h(\boldsymbol{y}) = (y_1, \ldots, y_d, 0, \ldots, 0)$ we conclude that the inverse is given by

$$h^{-1} = \mathrm{pr}_{n,d} \circ \Phi\big|_{U\cap M} = (\Phi_1, \ldots, \Phi_d)\big|_{U\cap M}. \tag{3.5}$$

Hence h is smooth and h^{-1} is continuous, which proves (i) and (iii). For proving (ii), we set $\tilde{\Phi} := \mathrm{pr}_{n,d} \circ \Phi$ and infer from the chain rule together with $\tilde{\Phi} \circ h(\boldsymbol{y}) = \boldsymbol{y}$, cf. (3.5), the relation

$$\mathrm{D}(\tilde{\Phi} \circ h)(\boldsymbol{y}) = \mathrm{D}\tilde{\Phi}(h(\boldsymbol{y}))\mathrm{D}h(\boldsymbol{y}) = \boldsymbol{I} \in \mathbb{R}^{d\times d}, \qquad \boldsymbol{y} \in \Omega,$$

where $\boldsymbol{I}$ is the identity matrix. Thus, using $d \leq n$ we conclude that $\mathrm{D}h(\boldsymbol{y})$ must be injective.

Conversely, if $h : \Omega \to \mathcal{M}$ is a map satisfying (i)-(iii) we can construct by the inverse function theorem for every $\boldsymbol{x} = h(\boldsymbol{y})$, $\boldsymbol{y} \in \Omega$, a diffeomorphism $\Phi : U \to V$ between open subsets $U, V \subset \mathbb{R}^n$ satisfying

$$h \circ \mathrm{pr}_{n,d}\left(V \cap \Omega \times \{0\}^{n-d}\right) = \Phi^{-1}\left(V \cap \mathbb{R}^d \times \{0\}^{n-d}\right) = \mathcal{M} \cap U.$$

For details see the proof of [123, Theorem 5.2]. ∎

For a d-dimensional manifold $\mathcal{M} \subset \mathbb{R}^n$ we call a map $h : \Omega \to \mathcal{M}$ which satisfies the properties (i)-(iii) in Theorem 3.2 a *local parameterization of $\mathcal{M}$ around $\boldsymbol{x}$*, and we refer to $\boldsymbol{y} \in \Omega$ as the *local coordinates* of $\boldsymbol{x} = h(\boldsymbol{y}) \in \mathcal{M}$. We remark that there might be no single local parameterization which parameterizes the manifold $\mathcal{M}$ at once, i.e., $h(\Omega) = \mathcal{M}$. The proof of Theorem 3.2 leads to the following notable observation.

Theorem 3.3. *Let $\mathcal{M} \subset \mathbb{R}^n$ be a d-dimensional manifold. For any two local parameterizations $h_1 : \Omega_1 \to U_1 \cap \mathcal{M}$, $h_2 : \Omega_2 \to U_2 \cap \mathcal{M}$ of $\mathcal{M}$ with open subsets $\Omega_1, \Omega_2 \subset \mathbb{R}^d$ and neighborhoods $U_1, U_2 \subset \mathbb{R}^n$ of $\boldsymbol{x} = h_1(\boldsymbol{y}) = h_2(\boldsymbol{z})$ there exists a diffeomorphism $\varphi : \tilde{\Omega}_1 \to \tilde{\Omega}_2$, with*

$$h_1(\tilde{\boldsymbol{y}}) = h_2 \circ \varphi(\tilde{\boldsymbol{y}}), \qquad \tilde{\boldsymbol{y}} \in \tilde{\Omega}_1, \tag{3.6}$$

where $\tilde{\Omega}_1 := h_1^{-1}(U_1 \cap U_2 \cap M)$ and $\tilde{\Omega}_2 := h_2^{-1}(U_1 \cap U_2 \cap M)$. In particular the differentials obey

$$\mathrm{D}h_1(\tilde{\boldsymbol{y}}) = \mathrm{D}h_2(\varphi(\tilde{\boldsymbol{y}}))\mathrm{D}\varphi(\tilde{\boldsymbol{y}}), \quad \tilde{\boldsymbol{y}} \in \tilde{\Omega}_1. \tag{3.7}$$

Proof. We explicitly set

$$\varphi = h_2^{-1} \circ h_1\Big|_{\tilde{\Omega}_1}, \qquad \varphi^{-1} = h_1^{-1} \circ h_2\Big|_{\tilde{\Omega}_2},$$

so φ and φ^{-1} are continuous and φ fulfills (3.6). From the proof of Theorem 3.2 we infer that the inverse maps h_1^{-1} and h_2^{-1} are given locally by the first d components of some diffeomorphism $\Phi : U \to V$ for a neighborhood U of $\boldsymbol{x} \in \mathcal{M}$, cf. (3.5). Hence by the chain rule we obtain that φ and φ^{-1} is indefinitely differentiable at any point of $\tilde{\boldsymbol{y}} \in \tilde{\Omega}_1$ and $\tilde{\boldsymbol{z}} \in \tilde{\Omega}_2$, respectively, so that φ is a diffeomorphism. The relation (3.7) follows from the chain rule and the assertion (3.6). ∎

3.1.3 Tangent Spaces and the Induced Riemannian Structure

From Theorem 3.3 we observe that the range of the differentials of local parameterizations of a d-dimensional manifold $\mathcal{M}$ around $\boldsymbol{x} \in \mathcal{M}$ is independent of the particular parameterization, cf. (3.7). This enables us to define, independently of the choice of the local parameterization $h : \Omega \to \mathcal{M}$, $\Omega \subset \mathbb{R}^d$, the *tangent space of $\mathcal{M}$ at $\boldsymbol{x} \in \mathcal{M}$* as the subspace of $\mathbb{R}^n$ given by

$$\mathrm{T}_{\boldsymbol{x}}\mathcal{M} := \mathrm{range}\,\mathrm{D}h(\boldsymbol{y}) := \{\mathrm{D}h(\boldsymbol{y})\boldsymbol{w} \ : \ \boldsymbol{w} \in \mathbb{R}^d\} \subset \mathbb{R}^n, \qquad \boldsymbol{x} = h(\boldsymbol{y}), \quad \boldsymbol{y} \in \Omega, \tag{3.8}$$

Elements of the tangent space $\mathrm{T}_{\boldsymbol{x}}\mathcal{M}$ are referred to as *tangent vectors*. Since the differential $\mathrm{D}h(\boldsymbol{y}) : \mathbb{R}^d \to \mathrm{T}_{\boldsymbol{x}}\mathcal{M} \subset \mathbb{R}^n$ is injective, we conclude that it is an isomorphism between the Euclidean space $\mathbb{R}^d$ and the tangent space $\mathrm{T}_{\boldsymbol{x}}\mathcal{M}$. To be more precise, a basis on $\mathrm{T}_{\boldsymbol{x}}\mathcal{M} \subset \mathbb{R}^n$, is given by the *canonical basis*

$$\boldsymbol{h}_i(\boldsymbol{y}) := \mathrm{D}h(\boldsymbol{y})\boldsymbol{e}_i = \left(\frac{\partial h_1}{\partial y_i}(\boldsymbol{y}), \ldots, \frac{\partial h_n}{\partial y_i}(\boldsymbol{y})\right)^\top \in \mathrm{T}_{\boldsymbol{x}}\mathcal{M}, \quad \boldsymbol{x} = h(\boldsymbol{y}), \quad \boldsymbol{y} \in \Omega, \quad i = 1, \ldots, d, \tag{3.9}$$

where $\boldsymbol{e}_1, \ldots, \boldsymbol{e}_d$ is the standard basis in $\mathbb{R}^d$. In other words, any tangent vector $\boldsymbol{v} \in \mathrm{T}_{\boldsymbol{x}}\mathcal{M}$ is represented by a unique *coordinate vector* $\boldsymbol{w} = (w_1, \ldots, w_d) \in \mathbb{R}^d$ due to

$$\boldsymbol{v} = w_1\boldsymbol{h}_1(\boldsymbol{y}) + \cdots + w_n\boldsymbol{h}_n(\boldsymbol{y}) = \mathrm{D}h(\boldsymbol{y})\boldsymbol{w}.$$

We emphasize that the canonical basis $\boldsymbol{h}_i(\boldsymbol{y})$ defined by (3.9) depends on the chosen local parameterization h, as does the coordinate vector $\boldsymbol{w} \in \mathbb{R}^d$. Furthermore, it is convenient to introduce the orthogonal complemt of the tangent space $\mathrm{T}_{\boldsymbol{x}}\mathcal{M}$ given by

$$\mathrm{T}_{\boldsymbol{x}}\mathcal{M}^\perp := \{\boldsymbol{n} \in \mathbb{R}^n \ : \ \boldsymbol{n}^\top\boldsymbol{v} = 0, \quad \boldsymbol{v} \in \mathrm{T}_{\boldsymbol{x}}\mathcal{M}\}, \qquad \boldsymbol{x} \in \mathcal{M}. \tag{3.10}$$

Since any tangent space $\mathrm{T}_{\boldsymbol{x}}\mathcal{M}$ is a subspace of the Euclidean space $\mathbb{R}^n$ it admits a canonical inner product $g_{\mathcal{M}}(\boldsymbol{x}) : \mathrm{T}_{\boldsymbol{x}}\mathcal{M} \times \mathrm{T}_{\boldsymbol{x}}\mathcal{M} \to \mathbb{R}$ induce by the standard inner product of the Euclidean ambient space $\mathbb{R}^n$, i.e.,

$$g_{\mathcal{M}}(\boldsymbol{x})(\boldsymbol{v}_1, \boldsymbol{v}_2) := \boldsymbol{v}_1^\top\boldsymbol{v}_2, \qquad \boldsymbol{v}_1, \boldsymbol{v}_2 \in \mathrm{T}_{\boldsymbol{x}}\mathcal{M}, \qquad \boldsymbol{x} \in \mathcal{M}, \tag{3.11}$$

and we denote $g_{\mathcal{M}}$ as the *induced Riemannian structure* $g_{\mathcal{M}}$ of the manifold $\mathcal{M}$.[2] Together with the Riemannian structure $g_{\mathcal{M}}$ we denote $\mathcal{M}$ a *Riemannian manifold*.[3] For any local parameterization $h : \Omega \to \mathcal{M}$ the canonical basis $\boldsymbol{h}_1(\boldsymbol{y}), \ldots, \boldsymbol{h}_d(\boldsymbol{y}) \in \mathrm{T}_{\boldsymbol{x}}\mathcal{M}$, cf. (3.9), leads to the matrix representation

$$g_{\mathcal{M}}(\boldsymbol{x})(\boldsymbol{v}_1, \boldsymbol{v}_2) = \boldsymbol{w}_1^\top\boldsymbol{G}_h(\boldsymbol{y})\boldsymbol{w}_2, \qquad \boldsymbol{v}_i = \mathrm{D}h(\boldsymbol{y})\boldsymbol{w}_i \in \mathrm{T}_{\boldsymbol{x}}\mathcal{M}, \quad \boldsymbol{w}_i \in \mathbb{R}^d, \quad i = 1, 2, \tag{3.12}$$

where the matrix $\boldsymbol{G}_h(\boldsymbol{y}) \in \mathbb{R}^{d\times d}$ is given by the matrix entries

$$(\boldsymbol{G}_h(\boldsymbol{y}))_{i,j} := g_{\mathcal{M}}(\boldsymbol{x})(\boldsymbol{h}_i(\boldsymbol{y}), \boldsymbol{h}_j(\boldsymbol{y})) = \sum_{l=1}^{n} \frac{\partial h_l}{\partial y_i}(\boldsymbol{y})\frac{\partial h_l}{\partial y_j}(\boldsymbol{y}) = \big(\mathrm{D}h(\boldsymbol{y})^\top \mathrm{D}h(\boldsymbol{y})\big)_{i,j} \tag{3.13}$$

for $i, j = 1, \ldots, d$.

The use of the tangent space $\mathrm{T}_{\boldsymbol{x}}\mathcal{M}$, cf. (3.8), and the induced inner product $g_{\mathcal{M}}$, cf. (3.8), might become more enlightening if one considers curves in $\mathcal{M}$. Therefore, we let $h : \Omega \to \mathcal{M} \cap U$, $U \subset \mathbb{R}^d$ open, be a local parameterization of $\mathcal{M}$ around $\boldsymbol{x} = h(\boldsymbol{y}) \in \mathcal{M} \cap U$, cf. Theorem 3.2. Then any curve $\gamma : I \to \mathcal{M} \cap U$, $I := [a, b] \subset \mathbb{R}$, $a \leq 0 \leq b$, can be parameterized by a unique *coordinate curve* $\gamma_h := h^{-1} \circ \gamma$, i.e.,

$$\gamma(t) = h \circ \gamma_h(t), \quad t \in I.$$

If $\gamma(0) = \boldsymbol{x}$ then it is $\gamma_h(0) = \boldsymbol{y}$, and we infer from the chain rule that the velocity vector is a

[2] In the general theory of Riemannian manifolds the Riemannian structure can be any "smooth" symmetric positive definite bilinear form $g_{\mathcal{M}}(\boldsymbol{x}) : \mathrm{T}_{\boldsymbol{x}}\mathcal{M} \times \mathrm{T}_{\boldsymbol{x}}\mathcal{M} \to \mathbb{R}$. However, since we are only interested in submanifolds of the Euclidean space we consider only manifolds with the induced Riemannian structure.

[3] We will use equivalently the term *Riemannian manifold* and *manifold* since every manifold $\mathcal{M}$ has a unique induced Riemannian structure $g_{\mathcal{M}}$.

tangent vector of $\mathrm{T}_{\boldsymbol{x}}\mathcal{M}$, i.e.,

$$\dot{\gamma}(0) = \mathrm{D}(h \circ \gamma_h)(t)\big|_{t=0} = \mathrm{D}h(\gamma_h(t))\dot{\gamma}_h(t)\big|_{t=0} = \mathrm{D}h(\boldsymbol{y})\dot{\gamma}_h(0) \in \mathrm{T}_{\boldsymbol{x}}\mathcal{M}. \tag{3.14}$$

Moreover, every tangent vector $\boldsymbol{v} = \mathrm{D}h(\boldsymbol{y})\boldsymbol{w} \in \mathrm{T}_{\boldsymbol{x}}\mathcal{M}$, $\boldsymbol{w} \in \mathbb{R}^d$, can be expressed by a curve $\gamma : (-\varepsilon, \varepsilon) \to \mathcal{M} \cap U$, $\varepsilon > 0$ sufficiently small depending on $\boldsymbol{v}$, which is given for example by

$$\gamma := h \circ \gamma_h, \quad \text{with} \quad \gamma_h(t) := \boldsymbol{y} + t\boldsymbol{w} \in \Omega,\ t \in (-\varepsilon, \varepsilon). \tag{3.15}$$

Let us recall that the arc length $L(\gamma)$ of a curve γ in $\mathbb{R}^n$, cf. (3.1), is defined by means of the Euclidean distance in $\mathbb{R}^n$, and that the arc length computes by an integral over the norm of velocity vectors of γ, cf. (3.2).[4] Using the induced Riemannian structure $g_{\mathcal{M}}$, cf. (3.11), and its matrix representation $\boldsymbol{G}_h$, cf. (3.13), we may write the arc length of the curve $\gamma : I \to \mathcal{M}$ as, cf. (3.2),

$$L(\gamma) = \int_a^b \|\dot{\gamma}(t)\|_2 \mathrm{d}t = \int_a^b \sqrt{g_{\mathcal{M}}(\gamma(t))(\dot{\gamma}(t), \dot{\gamma}(t))}\mathrm{d}t = \int_a^b \sqrt{\dot{\gamma}_h(t)^\top \boldsymbol{G}_h(\gamma_h(t))\dot{\gamma}_h(t))}\mathrm{d}t \tag{3.16}$$

since $\dot{\gamma}(t) \in \mathrm{T}_{\gamma(t)}\mathcal{M}$, $t \in I$, cf. (3.14). This relation shows that, even though the tangent spaces are just defined locally by parameterizations, one can compute global properties as for example the length of curves. In a certain sense we have related the different tangent spaces along the curve γ by the integrals on the right hand side in (3.16).

3.1.4 Geodesics and Exponential Maps

Our further analysis on manifolds $\mathcal{M} \subset \mathbb{R}^n$ is carried out by the use of curves in $\mathcal{M}$. A manifold $\mathcal{M}$ is called *connected* if for any pairs of points $\boldsymbol{x}_1, \boldsymbol{x}_2 \in \mathcal{M}$ there is a *joining curve* $\gamma : [0, 1] \to \mathcal{M}$, i.e., it satisfies $\gamma(0) = \boldsymbol{x}_1$, $\gamma(1) = \boldsymbol{x}_2$. Hence, curves induce on connected manifolds $\mathcal{M}$ a metric $\mathrm{d}_{\mathcal{M}}$ by setting

$$\mathrm{d}_{\mathcal{M}}(\boldsymbol{x}_1, \boldsymbol{x}_2) := \inf\{L(\gamma)\ :\ \gamma : [a, b] \to \mathcal{M},\ \gamma(a) = \boldsymbol{x}_1,\ \gamma(b) = \boldsymbol{x}_2,\ a < b \in \mathbb{R}\}. \tag{3.17}$$

Indeed, one can show that this definition yields a metric, which induces the same topology as the Euclidean ambient space $\mathbb{R}^n$, cf. [66, Sec. I.9]. Thus for complete manifolds $\mathcal{M}$ (with respect to $\mathbb{R}^n$) the infimum in (3.17) is attained by particular curves, called geodesics, cf. Theorem 3.4. In that respect the term *geodesic distance of* $\mathcal{M}$ for the metric $\mathrm{d}_{\mathcal{M}}$ is appropriate. Before we arrive at these well-known results, we define geodesic curves in another way. A *geodesic of* $\mathcal{M}$ is a curve $\gamma : I \to \mathcal{M}$ such that the *acceleration vector*

$$\ddot{\gamma}(t) := \frac{\mathrm{d}^2}{\mathrm{d}t^2}\gamma(t) = (\ddot{\gamma}_1(t), \ldots, \ddot{\gamma}_n(t))^\top \in \mathbb{R}^n, \qquad t \in I,$$

is orthogonal to the tangent spaces $\mathrm{T}_{\gamma(t)}\mathcal{M}$, i.e., it satisfies, cf. (3.10),

$$\ddot{\gamma}(t) \in \mathrm{T}_{\gamma(t)}\mathcal{M}^\perp, \quad t \in I. \tag{3.18}$$

For example, we take the Euclidean space as manifold $\mathcal{M} = \mathbb{R}^d$. Then, the only geodesics in $\mathcal{M}$ are curves with acceleration vector $\ddot{\gamma}(t) = \boldsymbol{0} \in \mathbb{R}^d$. Thus, geodesics in Euclidean space $\mathbb{R}^d$ are

[4] This is a fundamental property of the Euclidean space, since one has to keep in mind that the definition of the arc length $L(\gamma)$ involves only sums of distances between points in $\mathbb{R}^n$, but computes by a formula involving norms of tangent vectors $\dot{\gamma}(t) \in \mathbb{R}^n = \mathrm{T}_{\gamma(t)}\mathbb{R}^n$.

straight line segments

$$\gamma(t) = \boldsymbol{x} + t \cdot \boldsymbol{v}, \qquad \boldsymbol{x} \in \mathcal{M} = \mathbb{R}^d, \quad \boldsymbol{v} \in \mathrm{T}_{\boldsymbol{x}}\mathcal{M} = \mathbb{R}^d, \quad t \in \mathbb{R},$$

which are parameterized proportional to arc length, cf. (3.3).

Let $\mathcal{M} \subset \mathbb{R}^n$ be again an arbitrary manifold. From the definition (3.18) of geodesics it follows immediately that geodesics are always parameterized proportional to arc length, since from

$$\frac{\mathrm{d}}{\mathrm{d}t}\|\dot\gamma(t)\|_2^2 = \frac{\mathrm{d}}{\mathrm{d}t}\sum_{l=1}^{n}\dot\gamma_l(t)\dot\gamma_l(t) = 2\sum_{l=1}^{n}\ddot\gamma_l(t)\dot\gamma_l(t) = 2(\ddot\gamma(t)^\top\dot\gamma(t)) = 0, \qquad t \in I,$$

we infer $\|\dot\gamma(t)\|_2 = c$, $t \in I$. Hence, the norm of the tangent vectors $\dot\gamma(t) \in \mathrm{T}_{\gamma(t)}\mathcal{M}$ remains constant for $t \in I$. We call a geodesic γ *maximal* if it is not a proper restriction of any geodesic. The existence and uniqueness of maximal geodesics in $\mathcal{M}$ is assured by Theorem 3.4. Before we state these results, we introduce for a local parameterization $h : \Omega \to \mathcal{M}$ of $\mathcal{M}$ around $\boldsymbol{x} = h(\boldsymbol{y}) \in \mathcal{M}$ the *Christoffel symbols of the first* and *the second kind*, which are defined in local coordinates by

$$\begin{aligned}\Gamma_h(\boldsymbol{y})_{i,j;l} &:= \frac{1}{2}\left(\frac{\partial}{\partial y_i}\left(\boldsymbol{G}_h(\boldsymbol{y})\right)_{j,l} + \frac{\partial}{\partial y_j}\left(\boldsymbol{G}_h(\boldsymbol{y})\right)_{i,l} - \frac{\partial}{\partial y_l}\left(\boldsymbol{G}_h(\boldsymbol{y})\right)_{i,j}\right),\\ \Gamma_h(\boldsymbol{y})^m_{i,j} &:= \sum_{l=1}^{d}\Gamma_h(\boldsymbol{y})_{i,j;l}\left(\boldsymbol{G}_h^{-1}(\boldsymbol{y})\right)_{l,m}, \qquad i,j,l,m = 1,\ldots,d,\end{aligned} \tag{3.19}$$

respectively, where the matrix representation $\boldsymbol{G}_h(\boldsymbol{y})$ and its inverse $\boldsymbol{G}_h^{-1}(\boldsymbol{y})$ of the induced Riemannian structure $g_{\mathcal{M}}$ are used, cf. (3.13).[5] We remark that the Christoffel symbols of the first and the second kind have the symmetry properties

$$\Gamma_h(\boldsymbol{y})_{i,j;l} = \Gamma_h(\boldsymbol{y})_{j,i;l}, \quad \Gamma_h(\boldsymbol{y})^m_{i,j} = \Gamma_h(\boldsymbol{y})^m_{j,i}, \quad \boldsymbol{y} \in \Omega, \qquad i,j,l,m = 1,\ldots,d,$$

respectively, since the matrix $\boldsymbol{G}_h(\boldsymbol{y}) \in \mathbb{R}^{d\times d}$ of the Riemannian structure $g_{\mathcal{M}}$ is symmetric. Sometimes it will be convenient to write the Christoffel symbols of the second kind as matrices

$$\boldsymbol{\Gamma}^m_h(\boldsymbol{y}) := \left(\Gamma_h(\boldsymbol{y})^m_{i,j}\right)_{i,j=1}^{d}, \quad \boldsymbol{y} \in \Omega, \qquad m = 1,\ldots,d. \tag{3.20}$$

Furthermore, for the Euclidean space $\mathcal{M} = \mathbb{R}^d$ the Christoffel symbols vanish at every point $\boldsymbol{x} \in \mathbb{R}^d$ for the canonical local parameterization $h(\boldsymbol{x}) = \boldsymbol{x} \in \mathbb{R}^d$, i.e.,

$$\Gamma_h(\boldsymbol{x})_{i,j;l} = 0, \quad \Gamma_h(\boldsymbol{x})^m_{i,j} = 0, \qquad i,j,l,m = 1,\ldots,d, \tag{3.21}$$

since $\left(\boldsymbol{G}_h(\boldsymbol{x})\right)_{i,j} = \delta_{i,j}$, $i,j = 1,\ldots,n$.

The following Theorem 3.4 may be referred to as the famous Hopf-Rinow Theorem.

Theorem 3.4. *Let $\mathcal{M} \subset \mathbb{R}^n$ be a d-dimensional Riemannian manifold. Then there exists for every $\boldsymbol{x} \in \mathcal{M}$ and $\boldsymbol{v} \in \mathrm{T}_{\boldsymbol{x}}\mathcal{M}$ a unique maximal geodesic $\gamma_{\boldsymbol{x},\boldsymbol{v}}$ in $\mathcal{M}$, cf.* (3.18)*, such that*

$$\gamma_{\boldsymbol{x},\boldsymbol{v}}(0) = \boldsymbol{x}, \qquad \dot\gamma_{\boldsymbol{x},\boldsymbol{v}}(0) = \boldsymbol{v}. \tag{3.22}$$

In local coordinates, geodesics γ satisfy the system of ordinary differential equations, cf. (3.19)

[5] The inverse matrix $\boldsymbol{G}_h^{-1}(\boldsymbol{y})$ exists since $\boldsymbol{G}_h(\boldsymbol{y})$ is by definition (3.13) positive definite.

and (3.20),

$$\begin{aligned} 0 &= (\ddot{\gamma}_h)_m(t) + \sum_{i,j=1}^{d} \Gamma_h(\gamma_h(t))_{i,j}^m (\dot{\gamma}_h)_i(t)(\dot{\gamma}_h)_j(t) \\ &= (\ddot{\gamma}_h)_m(t) + \dot{\gamma}_h(t)^\top \boldsymbol{\Gamma}_h^m(\gamma_h(t))\dot{\gamma}_h(t), \qquad m = 1, \ldots, d, \end{aligned} \tag{3.23}$$

where $h : \Omega \to \mathcal{M}$, $\Omega \subset \mathbb{R}^d$ *open, is a local parameterization around* $\gamma(t) = h \circ \gamma_h(t)$, $|t|$ *sufficiently small, cf. Theorem 3.2.*

Moreover, if $\mathcal{M}$ *is complete then each maximal geodesic is defined for every* $t \in \mathbb{R}$, *and each pair of points* $\boldsymbol{x}_1, \boldsymbol{x}_2 \in \mathcal{M}$ *can be joined by a geodesic* $\gamma_{\boldsymbol{x}_1\widehat{\boldsymbol{x}_2}} : [0, T] \to \mathcal{M}$, $T > 0$, *of arc length* $L(\gamma_{\boldsymbol{x}_1\widehat{\boldsymbol{x}_2}}) = \mathrm{d}_{\mathcal{M}}(\boldsymbol{x}_1, \boldsymbol{x}_2)$, *cf.* (3.17), *i.e.,*

$$\boldsymbol{x}_1 = \gamma_{\boldsymbol{x}_1,\boldsymbol{x}_2}(0), \quad \boldsymbol{x}_2 = \gamma_{\boldsymbol{x}_1\widehat{\boldsymbol{x}_2}}(T), \quad \|\dot{\gamma}_{\boldsymbol{x}_1\widehat{\boldsymbol{x}_2}}(t)\|_2 = L(\gamma_{\boldsymbol{x}_1\widehat{\boldsymbol{x}_2}})/T, \ t \in [0, T]. \tag{3.24}$$

Proof. We consider local coordinates $\gamma_h : (-\varepsilon, \varepsilon) \to \Omega$ whit $\varepsilon > 0$, $\Omega \subset \mathbb{R}^d$ open, i.e., $\gamma = h \circ \gamma_h$, where $h : \Omega \to \mathcal{M}$ is a local parameterization of $\mathcal{M}$ around $\boldsymbol{x} = h(\boldsymbol{y})$. Thus, the geodesic equation (3.18) is equivalent to the system of ordinary differential equations

$$\ddot{\gamma}(t)^\top \boldsymbol{h}_l(\gamma_h(t)) = \sum_{l'=1}^{n} \frac{\partial h_{l'}}{\partial y_l}(\gamma_h(t)) \frac{\mathrm{d}^2}{\mathrm{d}t^2}(h \circ \gamma_h)_{l'}(t) = 0, \qquad l = 1, \ldots, d, \ t \in (-\varepsilon, \varepsilon),$$

where $\boldsymbol{h}_l(\gamma_h(t)) \in \mathrm{T}_{\boldsymbol{\gamma}(t)}\mathcal{M}$ are the canonical basis vectors, cf. (3.9). By using the matrix representation $\boldsymbol{G}_h(\boldsymbol{y})$, cf. (3.13), we write the above equations as

$$\begin{aligned} 0 &= \ddot{\gamma}(t)^\top \boldsymbol{h}_l(\gamma_h(t)) \\ &= \sum_{l'=1}^{n} \sum_{i,j=1}^{d} \frac{\partial h_{l'}}{\partial y_l}(\gamma_h(t)) \frac{\partial^2 h_{l'}}{\partial y_i \partial y_j}(\gamma_h(t))(\dot{\gamma}_h)_i(t)(\dot{\gamma}_h)_j(t) \\ &\quad + \sum_{l'=1}^{n} \sum_{i=1}^{d} \frac{\partial h_{l'}}{\partial y_l}(\gamma_h(t)) \frac{\partial h_{l'}}{\partial y_i}(\gamma_h(t))(\ddot{\gamma}_h)_i(t) \\ &= \sum_{l'=1}^{n} \sum_{i,j=1}^{d} \frac{\partial^2 h_{l'}}{\partial y_i \partial y_j}(\gamma_h(t)) \frac{\partial h_{l'}}{\partial y_l}(\gamma_h(t))(\dot{\gamma}_h)_i(t)(\dot{\gamma}_h)_j(t) + \sum_{i=1}^{d} (\boldsymbol{G}_h(\gamma_h(t)))_{l,i} (\ddot{\gamma}_h)_i(t). \end{aligned}$$

One checks by using (3.13) that the Christoffel symbols of the first kind (3.19) can be written as

$$\Gamma_h(\boldsymbol{y})_{i,j;l} = \sum_{l'=1}^{n} \frac{\partial^2 h_{l'}}{\partial y_i \partial y_j}(\boldsymbol{y}) \frac{\partial h_{l'}}{\partial y_l}(\boldsymbol{y}), \qquad i, j, l = 1, \ldots, d,$$

which together with the inverse matrix $\boldsymbol{G}_h(\boldsymbol{y})^{-1}$ yields

$$\begin{aligned} 0 &= \sum_{l=1}^{d} \left(\ddot{\gamma}(t)^\top \boldsymbol{h}_l(\gamma_h(t)) \right) \left(\boldsymbol{G}_h^{-1}(\gamma_h(t)) \right)_{l,m} \\ &= (\ddot{\gamma}_h)_m(t) + \sum_{i,j,l=1}^{d} \Gamma_h(\gamma_h(t))_{i,j;l} \left(\boldsymbol{G}_h^{-1}(\gamma_h(t)) \right)_{l,m} (\dot{\gamma}_h)_i(t)(\dot{\gamma}_h)_j(t) \\ &= (\ddot{\gamma}_h)_m(t) + \sum_{i,j}^{d} \Gamma_h(\gamma_h(t))_{i,j}^m (\dot{\gamma}_h)_i(t)(\dot{\gamma}_h)_j(t), \qquad m = 1, \ldots, d. \end{aligned}$$

Finally, the Picard-Lindelöf Theorem tells us that the above second order system of ordinary differential equations with initial conditions $\gamma_h(0) = \boldsymbol{y} \in \Omega$ and $\dot{\gamma}_h(0) = \boldsymbol{w} \in \mathbb{R}^d$, $\boldsymbol{v} = \mathrm{D}h(\boldsymbol{y})\boldsymbol{w}$, has a unique solution. For details we refer to [66, Proposition 5.3]. The assertions for geodesics in complete manifolds follow from [66, Theorem 10.3 and Theorem 10.4]. ■

Through out this thesis we will associate to any point $\boldsymbol{x} \in \mathcal{M}$ and tangent vector $\boldsymbol{v} \in \mathrm{T}_{\boldsymbol{x}}\mathcal{M}$ the unique geodesic $\gamma_{\boldsymbol{x},\boldsymbol{v}}$ with the properties (3.22), and the unique *normal vector* defined by

$$\boldsymbol{n}_{\boldsymbol{x},\boldsymbol{v}} := \ddot{\gamma}_{\boldsymbol{x},\boldsymbol{v}}(0) \in \mathrm{T}_{\boldsymbol{x}}\mathcal{M}^{\perp}, \qquad \boldsymbol{v} \in \mathrm{T}_{\boldsymbol{x}}\mathcal{M}, \quad \boldsymbol{x} \in \mathcal{M}. \tag{3.25}$$

We note that by the uniqueness of geodesics we have for maximal geodesics of a complete manifold $\mathcal{M}$ the scaling relation

$$\gamma_{\boldsymbol{x},a\boldsymbol{v}}(t) = \gamma_{\boldsymbol{x},\boldsymbol{v}}(at), \qquad t, a \in \mathbb{R}, \qquad \boldsymbol{x} \in \mathcal{M}, \qquad \boldsymbol{v} \in \mathrm{T}_{\boldsymbol{x}}\mathcal{M}. \tag{3.26}$$

Furthermore, we associate to points $\boldsymbol{x}_1, \boldsymbol{x}_2 \in \mathcal{M}$ some geodesic $\gamma_{\boldsymbol{x}_1\widehat{\boldsymbol{x}}_2}$ which satisfies (3.24). In addition, Theorem 3.4 allows us to define for any fixed point $\boldsymbol{x} \in \mathcal{M}$ the *exponential map*

$$\exp_{\boldsymbol{x}} : \mathrm{T}_{\boldsymbol{x}}\mathcal{M} \to \mathcal{M}, \qquad \exp_{\boldsymbol{x}}(\boldsymbol{v}) := \gamma_{\boldsymbol{x},\boldsymbol{v}}(1), \qquad \boldsymbol{v} \in \mathrm{T}_{\boldsymbol{x}}\mathcal{M}. \tag{3.27}$$

At a first glance it seems that this definition is redundant since by the property

$$\gamma_{\boldsymbol{x},\boldsymbol{v}}(t) = \exp_{\boldsymbol{x}}(t\boldsymbol{v}), \qquad t \in \mathbb{R}, \qquad \boldsymbol{v} \in \mathrm{T}_{\boldsymbol{x}}\mathcal{M}, \tag{3.28}$$

we can express geodesics by the exponential map and vice versa. However, the use of curves restricts us to one-dimensional considerations, whereas the exponential map $\exp_{\boldsymbol{x}}$ leads to a wider point of view, since it maps the whole tangent space $\mathrm{T}_{\boldsymbol{x}}\mathcal{M}$ at $\boldsymbol{x} \in \mathcal{M}$ continuously into $\mathcal{M}$, cf. Corollary 3.8. Moreover, the exponential map $\exp_{\boldsymbol{x}}$ is a local diffeomorphism between the two manifolds $\mathrm{T}_{\boldsymbol{x}}\mathcal{M}$ and $\mathcal{M}$, cf. [66, Theorem 6.1]. To be more precise, given any basis $\boldsymbol{v}_1, \ldots, \boldsymbol{v}_d \in \mathrm{T}_{\boldsymbol{x}}\mathcal{M}$ there is a neighborhood $\Omega \subset \mathbb{R}^d$ of $\mathbf{0} \in \mathbb{R}^d$ such that the map

$$h(\boldsymbol{y}) := \exp_{\boldsymbol{x}}(y_1\boldsymbol{v}_1 + \cdots + y_d\boldsymbol{v}_d), \qquad \boldsymbol{y} = (y_1, \ldots, y_d) \in \Omega, \tag{3.29}$$

is a local parameterization of $\mathcal{M}$ around $\boldsymbol{x} = h(\mathbf{0})$. The coordinates $\boldsymbol{y} = (y_1, \ldots, y_2) \in \mathbb{R}^d$ are referred to as *normal coordinates* around $\boldsymbol{x} \in \mathcal{M}$ with respect to the basis $\boldsymbol{v}_1, \ldots, \boldsymbol{v}_d \in \mathrm{T}_{\boldsymbol{x}}\mathcal{M}$. From the relation, cf. (3.28) and (3.26),

$$\frac{\partial}{\partial y_i} h(\mathbf{0}) = \frac{\mathrm{d}}{\mathrm{d}t} \exp_{\boldsymbol{x}}(t\boldsymbol{v}_i) = \frac{\mathrm{d}}{\mathrm{d}t} \gamma_{\boldsymbol{x},t\boldsymbol{v}_i}(1) = \dot{\gamma}_{\boldsymbol{x},\boldsymbol{v}_i}(t) = \boldsymbol{v}_i, \qquad i = 1, \ldots, d,$$

it follows that at $\boldsymbol{y} = \mathbf{0}$ the differential of the local parameterization $h : \Omega \to \mathcal{M}$, given by (3.29), is represented by the matrix

$$\mathrm{D}h(\mathbf{0}) = (\boldsymbol{v}_1, \ldots, \boldsymbol{v}_d) \in \mathbb{R}^{n \times d}. \tag{3.30}$$

In particular, if $\boldsymbol{v}_1, \ldots, \boldsymbol{v}_d \in \mathrm{T}_{\boldsymbol{x}}\mathcal{M}$ is an orthonormal basis we have, cf. (3.13),

$$\boldsymbol{G}_h(\mathbf{0}) = \boldsymbol{I} \in \mathbb{R}^{d \times d} \tag{3.31}$$

for the matrix representation of the Riemannian structure $g_{\mathcal{M}}$. Moreover, using equation (3.28) we infer that the coordinate curve in normal coordinates of the geodesic $\gamma_{\boldsymbol{x},\boldsymbol{v}}$ with $\boldsymbol{v} = \mathrm{D}h(\mathbf{0})\boldsymbol{w} \in \mathrm{T}_{\boldsymbol{x}}\mathcal{M}$ is given, together with its derivatives, by

$$\gamma_h(t) = t\boldsymbol{w}, \qquad \dot{\gamma}_h(t) = \boldsymbol{w}, \qquad \ddot{\gamma}_h(t) = \mathbf{0},$$

where $\boldsymbol{w} \in \mathbb{R}^d$ and $|t|$ is sufficiently small. That is, geodesics through $\boldsymbol{x} \in \mathcal{M}$ represented in normal coordinates around $\boldsymbol{x}$ are simply straight line segments. Thus, we obtain together with the geodesic equation (3.23) that for normal coordinates the Christoffel symbols fulfill

$$\Gamma_h(\mathbf{0})_{i,j}^m = 0, \qquad i,j,m = 1,\ldots,d. \tag{3.32}$$

It is needless to say that these are very useful properties of normal coordinates.

3.1.5 Smooth Functions and their Gradients, and Hessians

We say that a function $f : \mathcal{M} \to \mathbb{R}$ on the manifold $\mathcal{M} \subset \mathbb{R}^n$ is *k-times differentiable at* $\boldsymbol{x} \in \mathcal{M}$ if there exists a local parameterization $h : \Omega \to \mathcal{M}$, $\Omega \subset \mathbb{R}^d$ of $\mathcal{M}$ around $\boldsymbol{x} = h(\boldsymbol{y})$ such that the *coordinate representation* f_h *of* f given by

$$f_h(\boldsymbol{y}) := f \circ h(\boldsymbol{y}) = f(h_1(\boldsymbol{y}),\ldots,h_n(\boldsymbol{y})), \qquad \boldsymbol{y} \in \Omega, \tag{3.33}$$

is k-times differentiable at $\boldsymbol{y} \in \Omega$. As usual, we call the function f *k-times differentiable* if it is k-times differentiable at every $\boldsymbol{x} \in \mathcal{M}$. It follows by Theorem 3.3 that for any local parameterization h the coordinate representation f_h of a k-times differentiable function f is k-times differentiable.[6] Similarly, the class of smooth functions on $\mathcal{M}$ is defined in the obvious manner.

Let $f : \mathcal{M} \to \mathbb{R}$ be once differentiable, then the *gradient* $\nabla_{\mathcal{M}} f(\boldsymbol{x}) \in \mathrm{T}_{\boldsymbol{x}}\mathcal{M}$ *of* f *at* $\boldsymbol{x} = h(\boldsymbol{y}) \in \mathcal{M}$ is defined in local coordinates by the tangent vector, cf. (3.9),

$$\nabla_{\mathcal{M}} f(\boldsymbol{x}) := (\nabla_h f_h(\boldsymbol{y}))_1 \boldsymbol{h}_1(\boldsymbol{y}) + \cdots + (\nabla_h f_h(\boldsymbol{y}))_d \boldsymbol{h}_d(\boldsymbol{y}) = \mathrm{D}h(\boldsymbol{y}) \nabla_h f_h(\boldsymbol{y}) \in \mathrm{T}_{\boldsymbol{x}}\mathcal{M}, \tag{3.34}$$

where the coordinate vector is given by

$$\nabla_h f_h(\boldsymbol{y}) := \boldsymbol{G}_h^{-1}(\boldsymbol{y}) \nabla f_h(\boldsymbol{y}) \in \mathbb{R}^d, \qquad \boldsymbol{y} \in \Omega,$$

and where

$$\nabla f_h(\boldsymbol{y}) := \left(\frac{\partial f_h}{\partial y_1}(\boldsymbol{y}), \ldots, \frac{\partial f_h}{\partial y_d}(\boldsymbol{y}) \right)^\top \in \mathbb{R}^d, \qquad \boldsymbol{y} \in \Omega, \qquad \boldsymbol{y} \in \Omega,$$

is the usual gradient of f_h at $\boldsymbol{y} \in \Omega$. If f is furthermore twice differentiable, then the *Hessian* $\mathrm{H}_{\mathcal{M}} f(\boldsymbol{x}) : \mathrm{T}_{\boldsymbol{x}}\mathcal{M} \times \mathrm{T}_{\boldsymbol{x}}\mathcal{M} \to \mathbb{R}$ *of* f *at* $\boldsymbol{x} = h(\boldsymbol{y}) \in \mathcal{M}$ is defined as the symmetric bilinear form

$$\mathrm{H}_{\mathcal{M}} f(\boldsymbol{x})(\boldsymbol{v}_1, \boldsymbol{v}_2) := \boldsymbol{w}_1^\top \mathbf{H}_h f_h(\boldsymbol{y}) \boldsymbol{w}_2, \qquad \boldsymbol{v}_i = \mathrm{D}h(\boldsymbol{y}) \boldsymbol{w}_i \in \mathrm{T}_{\boldsymbol{x}}\mathcal{M},\ i = 1,2, \tag{3.35}$$

where the matrix representation $\mathbf{H}_h f_h(\boldsymbol{y}) \in \mathbb{R}^{d \times d}$ in local coordinates is given by, cf. (3.20),

$$\mathbf{H}_h f_h(\boldsymbol{y}) := \mathbf{H} f_h(\boldsymbol{y}) - \mathbf{N}_h f_h(\boldsymbol{y}), \quad \mathbf{N}_h f_h(\boldsymbol{y}) := \sum_{m=1}^{d} \big(\nabla f_h(\boldsymbol{y})\big)_m \boldsymbol{\Gamma}_h^m(\boldsymbol{y}) \in \mathbb{R}^{d \times d}, \qquad \boldsymbol{y} \in \Omega,$$

where

$$\mathbf{H} f_h(\boldsymbol{y}) := \begin{pmatrix} \frac{\partial^2 f}{\partial y_1 \partial y_1}(\boldsymbol{y}) & \cdots & \frac{\partial^2 f}{\partial y_1 \partial y_d}(\boldsymbol{y}) \\ \vdots & \ddots & \vdots \\ \frac{\partial^2 f}{\partial y_d \partial y_1}(\boldsymbol{y}) & \cdots & \frac{\partial^2 f}{\partial y_d \partial y_d}(\boldsymbol{y}) \end{pmatrix} \in \mathbb{R}^{d \times d}, \qquad \boldsymbol{y} \in \Omega,$$

is the usual Hessian matrix of f_h at $\boldsymbol{y} \in \Omega$.

[6] This definition is in concordance with the definition of k-times differentiable functions in $\mathbb{R}^n$ since the restriction of a k-times differentiable function $f : \mathbb{R}^n \to \mathbb{R}$ to $\mathcal{M}$ is k-times differentiable on $\mathcal{M}$. In particular, k-times differentiable functions $f : \mathcal{M} \to \mathbb{R}$ exist.

We remark that in the case of the Euclidean space $\mathcal{M} = \mathbb{R}^d$ the above definitions coincide with the usual notations of the gradient and the Hessian since the Christoffel symbols vanish at every point $\boldsymbol{x} \in \mathbb{R}^d$, cf. (3.21). However, for general manifolds $\mathcal{M} \subset \mathbb{R}^n$ we need proof that these definitions make sense and are independent of the local parameterization h.

Theorem 3.5. *Let a d-dimensional Riemannian manifold $\mathcal{M} \subset \mathbb{R}^n$ and a function $f : \mathcal{M} \to \mathbb{R}$ be given. If f is once differentiable at $\boldsymbol{x} \in \mathcal{M}$, then the gradient satisfies*

$$\nabla_{\mathcal{M}} f(\boldsymbol{x})^\top \boldsymbol{v} = \frac{\mathrm{d}}{\mathrm{d}t} f \circ \gamma(t)\Big|_{t=0} \tag{3.36}$$

for any curve γ with $\gamma(0) = \boldsymbol{x}$ and $\dot\gamma(0) = \boldsymbol{v} \in \mathrm{T}_{\boldsymbol{x}}\mathcal{M}$. If f is twice differentiable at $\boldsymbol{x} \in \mathcal{M}$, then the Hessian satisfies

$$\mathrm{H}_{\mathcal{M}} f(\boldsymbol{x})(\boldsymbol{v}, \boldsymbol{v}) = \frac{\mathrm{d}^2}{\mathrm{d}t^2} f \circ \gamma_{\boldsymbol{x},\boldsymbol{v}}(t)\Big|_{t=0} \tag{3.37}$$

for any geodesic $\gamma_{\boldsymbol{x},\boldsymbol{v}}$ associated to $\boldsymbol{x}$ and $\boldsymbol{v} \in \mathrm{T}_{\boldsymbol{x}}\mathcal{M}$. Moreover, the gradient and Hessian of f at $\boldsymbol{x}$ is uniquely determined by (3.36) *and* (3.37)*, respectively.*

Proof. Let $h : \Omega \to \mathcal{M}$, $\Omega \in \mathbb{R}^d$ open, be a local parameterization of $\mathcal{M}$ around $\boldsymbol{x} = h(\boldsymbol{y})$. The coordinate representation of f and $\gamma_{\boldsymbol{x},\boldsymbol{v}}$ are denoted by $f_h : \Omega \to \mathbb{R}$ and $\gamma_h : (-\varepsilon, \varepsilon) \to \Omega$, $\varepsilon > 0$, respectively. Hence, we have

$$f \circ \gamma_{\boldsymbol{x},\boldsymbol{v}}(t) = f_h \circ \gamma_h(t), \qquad t \in (-\varepsilon, \varepsilon), \quad \dot\gamma_h(0) = \boldsymbol{w} \in \mathbb{R}^d.$$

Together with the definition of the gradient (3.34) and the matrix representation $\boldsymbol{G}_h(\boldsymbol{y})$ of the Riemannian structure $g_{\mathcal{M}}$, cf. (3.12), we arrive by

$$\begin{aligned}
\nabla_{\mathcal{M}} f(\boldsymbol{x})^\top \boldsymbol{v} &= g_{\mathcal{M}}(\boldsymbol{x})(\nabla_{\mathcal{M}} f(\boldsymbol{x}), \boldsymbol{v}) \\
&= \nabla_h f_h(\boldsymbol{y})^\top \boldsymbol{G}_h(\boldsymbol{y}) \boldsymbol{w} \\
&= \nabla f_h(\boldsymbol{y})^\top \boldsymbol{G}_h(\boldsymbol{y})^{-\top} \boldsymbol{G}_h(\boldsymbol{y}) \boldsymbol{w} \\
&= \sum_{i=1}^{d} \frac{\partial f_h}{\partial y_i}(\boldsymbol{y})(\dot\gamma_h)_i(0) = \frac{\mathrm{d}}{\mathrm{d}t} f_h \circ \gamma_h(t)\Big|_{t=0}, \qquad \boldsymbol{v} = \mathrm{D}h(\boldsymbol{y})\boldsymbol{w} \in \mathrm{T}_{\boldsymbol{x}}\mathcal{M},
\end{aligned} \tag{3.38}$$

at the first assertion (3.36). In fact, the relation (3.36) is valid for arbitrary curves γ through $\boldsymbol{x}$. The converse statement follows by considering the linear independent coordinate curves e_i in Ω with $\dot e_i(0) = \boldsymbol{e}_i \in \mathbb{R}^d$, $i = 1, \ldots, d$. These curves determine the gradient uniquely by the linear system

$$\boldsymbol{G}_h(\boldsymbol{y}) \nabla_h f_h(\boldsymbol{y}) = \left(\frac{\mathrm{d}}{\mathrm{d}t} f_h \circ e_1(\boldsymbol{y})(t)\big|_{t=0}, \ldots, \frac{\mathrm{d}}{\mathrm{d}t} f_h \circ e_d(\boldsymbol{y})(t)\big|_{t=0} \right)^\top = \nabla f_h(\boldsymbol{y}).$$

For the Hessian we have

$$\begin{aligned}
\mathrm{H}_{\mathcal{M}} f(\boldsymbol{x})(\boldsymbol{v}, \boldsymbol{v}) &= \boldsymbol{w}^\top \mathbf{H}_h f_h(\boldsymbol{y}) \boldsymbol{w} \\
&= \sum_{i,j=1}^{d} (\dot\gamma_h)_i(0)(\dot\gamma_h)_j(0) \left(\frac{\partial^2 f_h}{\partial y_i \partial y_j}(\boldsymbol{y}) - \sum_{m=1}^{d} \Gamma_h(\boldsymbol{y})_{i,j}^m \frac{\partial f_h}{\partial y_m}(\boldsymbol{y}) \right) \\
&= \sum_{i,j=1}^{d} (\dot\gamma_h)_i(0)(\dot\gamma_h)_j(0) \frac{\partial^2 f_h}{\partial y_i \partial y_j}(\boldsymbol{y}) + \sum_{m=1}^{d} (\ddot\gamma_h)_m(0) \frac{\partial f_h}{\partial y_m}(\boldsymbol{y}) \\
&= \frac{\mathrm{d}^2}{\mathrm{d}t^2} f_h \circ \gamma_h(t)\Big|_{t=0},
\end{aligned} \tag{3.39}$$

where we used the definition (3.35) and that the coordinate curve γ_h of the geodesic $\gamma_{\boldsymbol{x},\boldsymbol{v}}$ satisfies (3.23). Furthermore, using the polarization identity of symmetric bilinear forms

$$\mathrm{H}_{\mathcal{M}} f(\boldsymbol{x})(\boldsymbol{v}_1, \boldsymbol{v}_2) = \frac{1}{4}\big(\mathrm{H}_{\mathcal{M}} f(\boldsymbol{x})(\boldsymbol{v}_1 + \boldsymbol{v}_2, \boldsymbol{v}_1 + \boldsymbol{v}_2) - \mathrm{H}_{\mathcal{M}} f(\boldsymbol{x})(\boldsymbol{v}_1 - \boldsymbol{v}_2, \boldsymbol{v}_1 - \boldsymbol{v}_2)\big)$$

we obtain that the matrix entries of $\mathbf{H}_h f_h(\boldsymbol{y})$ are determined by

$$(\mathbf{H}_h f_h(\boldsymbol{y}))_{i,j} = \frac{1}{4}\left[\frac{\mathrm{d}^2}{\mathrm{d}t^2} f_h \circ e^+_{i,j}(t)\Big|_{t=0} - \frac{\mathrm{d}^2}{\mathrm{d}t^2} f_h \circ e^-_{i,j}(t)\Big|_{t=0}\right], \qquad i,j = 1,\ldots,d,$$

where the coordinate curves $e^+_{i,j}$ and $e^-_{i,j}$ in Ω with $e^\pm_{i,j}(0) = \boldsymbol{y}$, $\dot{e}^\pm_{i,j}(0) = \boldsymbol{e}_i \pm \boldsymbol{e}_j \in \mathbb{R}^d$, $i,j = 1,\ldots,d$, parameterize geodesics of $\mathcal{M}$. ∎

Theorem 3.5 can be stated in a slightly different form if the function f is a restriction of some function $\tilde{f}$ defined on the Euclidean space $\mathbb{R}^n$. Then the gradient and Hessian of f can be simply expressed by the usual gradient and Hessian of $\tilde{f}$, respectively. For convenience we introdue the orthogonal projection operator $\mathrm{P}_{\mathrm{T}_{\boldsymbol{x}}\mathcal{M}} : \mathbb{R}^n \to \mathrm{T}_{\boldsymbol{x}}\mathcal{M}$ of $\mathbb{R}^n$ to the tangent space $\mathrm{T}_{\boldsymbol{x}}\mathcal{M} \subset \mathbb{R}^n$, which is uniquely determined by the relations, cf. (3.8) and (3.10),

$$\mathrm{P}_{\mathrm{T}_{\boldsymbol{x}}\mathcal{M}} \boldsymbol{v} = \boldsymbol{v}, \quad \boldsymbol{v} \in \mathrm{T}_{\boldsymbol{x}}\mathcal{M}, \qquad \mathrm{P}_{\mathrm{T}_{\boldsymbol{x}}\mathcal{M}} \tilde{\boldsymbol{v}} = \boldsymbol{0}, \quad \tilde{\boldsymbol{v}} \in \mathrm{T}_{\boldsymbol{x}}\mathcal{M}^\perp. \tag{3.40}$$

We remark that the matrix representation $\mathbf{P}_{\mathrm{T}_{\boldsymbol{x}}\mathcal{M}} \in \mathbb{R}^{n\times n}$ in standard coordinates of the projection operator $\mathrm{P}_{\mathrm{T}_{\boldsymbol{x}}\mathcal{M}}$ can be obtained by any orthonormal basis $\boldsymbol{v}_1,\ldots,\boldsymbol{v}_d \in \mathrm{T}_{\boldsymbol{x}}\mathcal{M}$ due to

$$\mathbf{P}_{\mathrm{T}_{\boldsymbol{x}}\mathcal{M}} := \boldsymbol{V}\boldsymbol{V}^\top \in \mathbb{R}^{n\times n}, \qquad \boldsymbol{V} := (\boldsymbol{v}_1,\ldots,\boldsymbol{v}_d) \in \mathbb{R}^{n\times d}.$$

Corollary 3.6. *Let $\mathcal{M} \subset U$, $U \subset \mathbb{R}^n$ open, be a d-dimensional Riemannian manifold and $f : \mathcal{M} \to \mathbb{R}$ be the restriction $f := \tilde{f}\big|_{\mathcal{M}}$ of some function $\tilde{f} : U \to \mathbb{R}$. If $\tilde{f}$ is once differentiable at $\boldsymbol{x} \in \mathcal{M}$, then the gradient reads as, cf.* (3.40),

$$\nabla_{\mathcal{M}} f(\boldsymbol{x}) = \mathrm{P}_{\mathrm{T}_{\boldsymbol{x}}\mathcal{M}} \nabla \tilde{f}(\boldsymbol{x}) \in \mathrm{T}_{\boldsymbol{x}}\mathcal{M}. \tag{3.41}$$

In particular it satisfies

$$\nabla_M f(\boldsymbol{x})^\top \boldsymbol{v} = \nabla \tilde{f}(\boldsymbol{x})^\top \boldsymbol{v}, \qquad \boldsymbol{v} \in \mathrm{T}_{\boldsymbol{x}}\mathcal{M}. \tag{3.42}$$

If $\tilde{f}$ is twice differentiable at $\boldsymbol{x} \in \mathcal{M}$, then the Hessian can be written as

$$\mathrm{H}_{\mathcal{M}} f(\boldsymbol{x})(\boldsymbol{v},\boldsymbol{v}) = \boldsymbol{v}^\top\big(\mathbf{H}\tilde{f}(\boldsymbol{x}) + \mathbf{N}\tilde{f}(\boldsymbol{x})\big)\boldsymbol{v}, \qquad \boldsymbol{v} \in \mathrm{T}_{\boldsymbol{x}}\mathcal{M}, \tag{3.43}$$

where $\mathbf{N}\tilde{f}(\boldsymbol{x}) \in \mathbb{R}^{n\times n}$ is a symmetric matrix satisfying

$$\boldsymbol{v}^\top \mathbf{N}\tilde{f}(\boldsymbol{x})\boldsymbol{v} = \nabla \tilde{f}(\boldsymbol{x})^\top \boldsymbol{n}_{\boldsymbol{x},\boldsymbol{v}}, \qquad \boldsymbol{v} \in \mathrm{T}_{\boldsymbol{x}}\mathcal{M},$$

for the normal vector $\boldsymbol{n}_{\boldsymbol{x},\boldsymbol{v}} \in \mathrm{T}_{\boldsymbol{x}}\mathcal{M}^\perp$ associated to $\boldsymbol{x}$ and $\boldsymbol{v}$, cf. (3.25).

Proof. We observe that for any curve γ in $\mathcal{M}$, it holds $f \circ \gamma = \tilde{f} \circ \gamma$. Hence, from Theorem 3.5 we arrive by differentiation at the assertion (3.42) and the relation

$$\mathrm{H}_{\mathcal{M}} f(\boldsymbol{x})(\boldsymbol{v},\boldsymbol{v}) = \boldsymbol{v}^\top \mathbf{H}\tilde{f}(\boldsymbol{x})\boldsymbol{v} + \nabla \tilde{f}(\boldsymbol{x})^\top \boldsymbol{n}_{\boldsymbol{x},\boldsymbol{v}}, \qquad \boldsymbol{v} \in \mathrm{T}_{\boldsymbol{x}}\mathcal{M}, \qquad \boldsymbol{x} \in \mathcal{M}, \tag{3.44}$$

see the equations (3.38) and (3.39). From relation (3.42) the assertion (3.41) follows by orthogonal projection. Since the function $b_{\boldsymbol{x}} : \mathrm{T}_{\boldsymbol{x}}\mathcal{M} \times \mathrm{T}_{\boldsymbol{x}}\mathcal{M} \to \mathbb{R}$ defined by

$$b_{\boldsymbol{x}}(\boldsymbol{v},\boldsymbol{w}) := \mathrm{H}_{\mathcal{M}} f(\boldsymbol{x})(\boldsymbol{v},\boldsymbol{w}) - \boldsymbol{v}^\top \mathbf{H}\tilde{f}(\boldsymbol{x})\boldsymbol{w}, \qquad \boldsymbol{v},\boldsymbol{w} \in \mathrm{T}_{\boldsymbol{x}}\mathcal{M}, \qquad \boldsymbol{x} \in \mathcal{M},$$

is a symmetric bilinear form on the tangent space $\mathrm{T}_{\boldsymbol{x}}\mathcal{M}$, there exists a symmetric matrix $\mathbf{N}\tilde{f}(\boldsymbol{x}) \in \mathbb{R}^{n\times n}$ with

$$\nabla\tilde{f}(\boldsymbol{x})^{\top}\boldsymbol{n}_{\boldsymbol{x},\boldsymbol{v}} = b_{\boldsymbol{x}}(\boldsymbol{v},\boldsymbol{v}) = \boldsymbol{v}^{\top}\mathbf{N}\tilde{f}(\boldsymbol{x})\boldsymbol{v}, \qquad \boldsymbol{v} \in \mathrm{T}_{\boldsymbol{x}}\mathcal{M}, \qquad \boldsymbol{x} \in \mathcal{M},$$

and the assertion (3.43) follows form equation (3.44). ■

The relations (3.36) and (3.37) in Theorem 3.5 are particular useful for deriving optimization procedures on manifolds $\mathcal{M}$ from optimization methods in the standard Euclidean space $\mathbb{R}^n$ by imitating one-dimensional optimization steps. As a first taste for the benefit of the above definitions we state some well-known properties of the particular tangent vector $\nabla_{\mathcal{M}}f(\boldsymbol{x}) \in \mathrm{T}_{\boldsymbol{x}}\mathcal{M}$.

Corollary 3.7. *Let a d-dimensional Riemannian manifold $\mathcal{M} \subset \mathbb{R}^n$ and a function $f : \mathcal{M} \to \mathbb{R}$ be given. If f is once differentiable at $\boldsymbol{x} \in \mathcal{M}$, then the gradient $\nabla_{\mathcal{M}}f(\boldsymbol{x}) \in \mathrm{T}_{\boldsymbol{x}}\mathcal{M}$ is orthogonal to the level surfaces of f, and shows for $\nabla_{\mathcal{M}}f(\boldsymbol{x}) \neq \mathbf{0}$ in the direction of the steepest ascent of f.*

Proof. Let $\gamma : I \to \mathcal{M}$, $I \subset \mathbb{R}$, with $\gamma(0) = \boldsymbol{x}$ be a curve of the level surface with $c := f(\boldsymbol{x})$, i.e., $f \circ \gamma \equiv c$. Hence, differentiation yields the first assertion, cf. (3.36),

$$g_{\mathcal{M}}(\boldsymbol{x})(\nabla_{\mathcal{M}}f(\boldsymbol{x}), \dot{\gamma}(0)) = \frac{\mathrm{d}}{\mathrm{d}t} f \circ \gamma(t)\Big|_{t=0} = 0.$$

The second assertion follows from the Cauchy-Schwarz inequality

$$|g_{\mathcal{M}}(\boldsymbol{x})(\nabla_{\mathcal{M}}f(\boldsymbol{x}), \boldsymbol{v})| \leq \|\nabla_{\mathcal{M}}f(\boldsymbol{x})\|_2\|\boldsymbol{v}\|_2, \qquad \boldsymbol{v} \in \mathrm{T}_{\boldsymbol{x}}\mathcal{M},$$

where equality is only attained if $\boldsymbol{v} = \alpha\, \nabla_{\mathcal{M}}f(\boldsymbol{x})$ for $\alpha \in \mathbb{R}$. Thus the maximal value

$$\|\nabla_{\mathcal{M}}f(\boldsymbol{x})\|_2 = \max_{\substack{\boldsymbol{v}\in\mathrm{T}_{\boldsymbol{x}}\mathcal{M},\\ \|\boldsymbol{v}\|_2=1}} \frac{\mathrm{d}}{\mathrm{d}t} f \circ \gamma_{\boldsymbol{x},\boldsymbol{v}}(t)\Big|_{t=0}$$

is attained for the coordinate vector $\boldsymbol{v} := \nabla_{\mathcal{M}}f(\boldsymbol{x})/\|\nabla_{\mathcal{M}}f(\boldsymbol{x})\|_2$, whenever $\nabla_{\mathcal{M}}f(\boldsymbol{x}) \neq \mathbf{0}$. ■

Another very important property of the gradient and Hessian is that they lead to approximations of $f : \mathcal{M} \to \mathbb{R}$ in the tangent space $\mathrm{T}_{\boldsymbol{x}}\mathcal{M}$ for some fixed $\boldsymbol{x} \in \mathcal{M}$. Therefore, we recall the Theorem of Taylor for one-dimensional functions, which leads with the equations (3.34) and (3.35) to

$$f \circ \gamma_{\boldsymbol{x},\boldsymbol{v}}(t) = f(\boldsymbol{x}) + t\,\nabla_{\mathcal{M}}f(\boldsymbol{x})^{\top}\boldsymbol{v} + o_{\boldsymbol{x},\boldsymbol{v}}(t), \qquad t \in \mathbb{R},\ \boldsymbol{v} \in \mathrm{T}_{\boldsymbol{x}}\mathcal{M}, \tag{3.45}$$

and

$$f \circ \gamma_{\boldsymbol{x},\boldsymbol{v}}(t) = f(\boldsymbol{x}) + t\,\nabla_{\mathcal{M}}f(\boldsymbol{x})^{\top}\boldsymbol{v} + \frac{t^2}{2}\mathrm{H}_{\mathcal{M}}f(\boldsymbol{x})(\boldsymbol{v},\boldsymbol{v}) + o_{\boldsymbol{x},\boldsymbol{v}}(t^2), \qquad t \in \mathbb{R},\ \boldsymbol{v} \in \mathrm{T}_{\boldsymbol{x}}\mathcal{M}, \tag{3.46}$$

where the remainder satisfies $\lim_{t\to 0} o_{\boldsymbol{x},\boldsymbol{v}}(t)/t = 0$ if $f : \mathcal{M} \to \mathbb{R}$ is a once and twice differentiable function at $\boldsymbol{x}$, respectively. We remark that in the above formulas the remainder $o_{\boldsymbol{x},\boldsymbol{v}}$ depends on the tangent vector $\boldsymbol{v} \in \mathrm{T}_{\boldsymbol{x}}\mathcal{M}$. This little flaw is overcome by the use of the exponential map $\exp_{\boldsymbol{x}}$, cf. (3.27). With it, we identify the function f naturally for a fixed point $\boldsymbol{x} \in \mathcal{M}$ with the function $f_{\boldsymbol{x}} : \mathrm{T}_{\boldsymbol{x}}\mathcal{M} \to \mathbb{R}$ on the tangent space, defined by

$$f_{\boldsymbol{x}}(\boldsymbol{v}) := f \circ \exp_{\boldsymbol{x}}(\boldsymbol{v}) = f \circ \gamma_{\boldsymbol{x},\boldsymbol{v}}(1), \qquad \boldsymbol{v} \in \mathrm{T}_{\boldsymbol{x}}\mathcal{M}, \tag{3.47}$$

and we obtain slightly stronger statements than (3.45), (3.46).

Corollary 3.8. *Let a d-dimensional Riemannian manifold $\mathcal{M} \subset \mathbb{R}^n$ and function $f : \mathcal{M} \to \mathbb{R}$ be given. If f is once and twice differentiable at $\boldsymbol{x} \in \mathcal{M}$, then the Taylor expansion of the function $f_{\boldsymbol{x}} : \mathrm{T}_{\boldsymbol{x}}\mathcal{M} \to \mathbb{R}$, cf. (3.47), is*

$$f_{\boldsymbol{x}}(\boldsymbol{v}) = f(\boldsymbol{x}) + \nabla_{\mathcal{M}} f(\boldsymbol{x})^\top \boldsymbol{v} + o_{\boldsymbol{x}}(\boldsymbol{v}), \qquad \lim_{\boldsymbol{v}\to\boldsymbol{0}} \frac{o_{\boldsymbol{x}}(\boldsymbol{v})}{\|\boldsymbol{v}\|_2} = 0, \qquad \boldsymbol{v} \in \mathrm{T}_{\boldsymbol{x}}\mathcal{M}, \tag{3.48}$$

and

$$f_{\boldsymbol{x}}(\boldsymbol{v}) = f(\boldsymbol{x}) + \nabla_{\mathcal{M}} f(\boldsymbol{x})^\top \boldsymbol{v} + \frac{1}{2}\mathrm{H}_{\mathcal{M}} f(\boldsymbol{x})(\boldsymbol{v},\boldsymbol{v}) + o_{\boldsymbol{x}}(\boldsymbol{v}), \qquad \lim_{\boldsymbol{v}\to\boldsymbol{0}} \frac{o_{\boldsymbol{x}}(\boldsymbol{v})}{\|\boldsymbol{v}\|_2^2} = 0, \qquad \boldsymbol{v} \in \mathrm{T}_{\boldsymbol{x}}\mathcal{M}, \tag{3.49}$$

respectively.

Proof. For fixed $\boldsymbol{x} \in \mathcal{M}$ we use a local parameterization in normal coordinates $h : \Omega \to \mathcal{M}$, cf. (3.29), with respect to an orthonormal basis $\boldsymbol{v}_1, \ldots, \boldsymbol{v}_d \in \mathrm{T}_{\boldsymbol{x}}\mathcal{M}$. Thus, for $\boldsymbol{v} := w_1\boldsymbol{v}_1 + \cdots + w_d\boldsymbol{v}_d = \mathrm{D}h(\boldsymbol{0})\boldsymbol{w} \in \mathrm{T}_{\boldsymbol{x}}\mathcal{M}$, cf. (3.30), we obtain that the coordinate representation fulfills

$$f_h(\boldsymbol{w}) = f \circ \exp_{\boldsymbol{x}}(w_1\boldsymbol{v}_1 + \cdots + w_d\boldsymbol{v}_d) = f_{\boldsymbol{x}}(\boldsymbol{v}).$$

Note that we insert in the coordinate representation f_h the variable $\boldsymbol{w} \in \Omega \subset \mathbb{R}^d$ instead of $\boldsymbol{y}$, since we are operating in the tangent space $\mathrm{T}_{\boldsymbol{x}}\mathcal{M}$ with $\boldsymbol{x} = h(\boldsymbol{y} = \boldsymbol{0})$. In what follows we restrict our attention to the second statement (3.49), since the first one (3.48) follows similarly. The multivariate Theorem of Taylor states that

$$f_h(\boldsymbol{w}) = f_h(\boldsymbol{0}) + \nabla f_h(\boldsymbol{0})^\top \boldsymbol{w} + \frac{1}{2}\boldsymbol{w}^\top \mathbf{H} f_h(\boldsymbol{0})\boldsymbol{w} + \tilde{o}_{\boldsymbol{x}}(\boldsymbol{w}), \qquad \lim_{\boldsymbol{w}\to\boldsymbol{0}} \tilde{o}_{\boldsymbol{x}}(\boldsymbol{w})/\|\boldsymbol{w}\|_2^2 = 0. \tag{3.50}$$

From the definition of the gradient (3.34) and relation (3.31) we obtain

$$\nabla f_h(\boldsymbol{0})^\top \boldsymbol{w} = \nabla_{\mathcal{M}} f(\boldsymbol{x})^\top \boldsymbol{v}.$$

Moreover, since the Christoffel symbols $\Gamma_h(\boldsymbol{y})_{ij}^m$ vanish for normal coordinates at $\boldsymbol{y} = \boldsymbol{0} \in \Omega$, cf. (3.32), we find by definition of the Hessian (3.35) that

$$\boldsymbol{w}^\top \mathbf{H} f_h(\boldsymbol{0})\boldsymbol{w} = \boldsymbol{w}^\top \mathbf{H}_h f_h(\boldsymbol{0})\boldsymbol{w} = \mathrm{H}_{\mathcal{M}} f(\boldsymbol{x})(\boldsymbol{v},\boldsymbol{v}).$$

We arrive together with (3.50) at the assertion (3.49), if we use $\|\boldsymbol{v}\|_2 = \|\mathrm{D}h(\boldsymbol{0})\boldsymbol{w}\|_2 = \|\boldsymbol{w}\|_2$ and that the remainder in (3.49) is given by $o_{\boldsymbol{x}}(\boldsymbol{v}) = \tilde{o}_{\boldsymbol{x}}(\boldsymbol{w})$. ∎

3.1.6 The Canonical Measure

The *canonical measure* $\mu_{\mathcal{M}}$ on a d-dimensional Riemannian manifold $\mathcal{M} \subset \mathbb{R}^n$ with induced Riemannian structure $g_{\mathcal{M}}$ is defined in local coordinates by the density, cf. (3.11),

$$\mathrm{d}\mu_{\mathcal{M}}(\boldsymbol{x}) := \sqrt{|\det \boldsymbol{G}_h(\boldsymbol{y})|}\mathrm{d}\boldsymbol{y}, \qquad \boldsymbol{x} = h(\boldsymbol{y}) \in \mathcal{M}, \qquad \boldsymbol{y} \in \Omega, \tag{3.51}$$

where $h : \Omega \to \mathcal{M}$ is a local parameterization of $\mathcal{M}$. One checks that the canonical measure $\mu_{\mathcal{M}}$ is a well defined Borel measure with support $\mathrm{supp}(\mu_{\mathcal{M}}) = \mathcal{M}$ by using the formula for the change of variable in multivariate integration and a partition of unity argument, cf. [49, Sec. 3.H]. In that respect the canonical measure $\mu_{\mathcal{M}}$ might be considered as a generalization of the Lebesgue measure in $\mathbb{R}^d$ to Riemannian manifolds $\mathcal{M}$. We call a function $f : \mathcal{M} \to \mathbb{C}$ *measurable* if the coordinate representation $f_h = f \circ h$ is measurable for any local parameterization h. Note, this definition is in concordance with the definition of measurable functions on compact sets $X \subset \mathbb{R}^n$.

3.1.7 Product Manifolds

The product of d_i-dimensional manifolds $\mathcal{M}_i \subset \mathbb{R}^{n_i}$, $i = 1, \dots, M$, is defined by the Cartesian product

$$\mathcal{M} := \mathcal{M}_1 \times \cdots \times \mathcal{M}_M = \left\{ \boldsymbol{x} := \begin{pmatrix} \boldsymbol{x}_1 \\ \vdots \\ \boldsymbol{x}_M \end{pmatrix} \;:\; \boldsymbol{x}_i \in \mathcal{M}_i,\ i = 1, \dots, M \right\} \subset \mathbb{R}^n, \quad n := \sum_{i=1}^{M} n_i.$$

Accordingly to definition (3.4) it is easily seen that the set $\mathcal{M}$ is a manifold of dimension $d := \sum_{i=1}^{M} d_i$, which we denote as the *product manifold* of the manifolds $\mathcal{M}_i$, $i = 1, \dots, M$. Similarly, for any local parameterizations $h_i : \Omega_i \to \mathcal{M}_i$, $\Omega_i \subset \mathbb{R}^{d_i}$ open, of $\mathcal{M}_i$ around $\boldsymbol{x}_i$, we find that the map

$$h : \Omega \to \mathcal{M}, \qquad h(\boldsymbol{y}) := \begin{pmatrix} h_1(\boldsymbol{y}_1) \\ \vdots \\ h_M(\boldsymbol{y}_M) \end{pmatrix}, \qquad \boldsymbol{y} := \begin{pmatrix} \boldsymbol{y}_1 \\ \vdots \\ \boldsymbol{y}_M \end{pmatrix} \in \Omega := \Omega_i \times \cdots \times \Omega_M, \tag{3.52}$$

is a local parameterization of $\mathcal{M}$ around $\boldsymbol{x} := (\boldsymbol{x}_1, \dots, \boldsymbol{x}_M)$. Hence, the tangent space is given by

$$\mathrm{T}_{\boldsymbol{x}}\mathcal{M} = \mathrm{T}_{\boldsymbol{x}_1}\mathcal{M}_1 \times \cdots \times \mathrm{T}_{\boldsymbol{x}_M}\mathcal{M}_M, \qquad \boldsymbol{x} \in \mathcal{M},$$

where the canonical basis at $\boldsymbol{x} = h(\boldsymbol{y})$ is given by the columns of the differential of h

$$\mathrm{D}h(\boldsymbol{y}) = \begin{pmatrix} \mathrm{D}h_1(\boldsymbol{y}_1) & \mathbf{0} & \cdots & \mathbf{0} \\ \mathbf{0} & \ddots & \ddots & \vdots \\ \vdots & \ddots & \ddots & \mathbf{0} \\ \mathbf{0} & \cdots & \mathbf{0} & \mathrm{D}h_M(\boldsymbol{y}_M) \end{pmatrix} \in \mathbb{R}^{n \times d}, \qquad \boldsymbol{y} \in \Omega.$$

Thus, we arrive for the induced Riemannian structure $g_{\mathcal{M}}$ at the corresponding matrix representation

$$\boldsymbol{G}_h(\boldsymbol{y}) = \begin{pmatrix} \boldsymbol{G}_{h_1}(\boldsymbol{y}_1) & \mathbf{0} & \cdots & \mathbf{0} \\ \mathbf{0} & \ddots & \ddots & \vdots \\ \vdots & \ddots & \ddots & \mathbf{0} \\ \mathbf{0} & \cdots & \mathbf{0} & \boldsymbol{G}_{h_M}(\boldsymbol{y}_M) \end{pmatrix} \in \mathbb{R}^{d \times d}, \qquad \boldsymbol{x} = h(\boldsymbol{y}), \quad \boldsymbol{y} \in \Omega. \tag{3.53}$$

In other words, the induced Riemannian structure $g_{\mathcal{M}}$, cf. (3.11), may be written as

$$g_{\mathcal{M}}(\boldsymbol{x})(\boldsymbol{v}_1, \boldsymbol{v}_2) = \sum_{i=1}^{M} g_{\mathcal{M}_i}(\boldsymbol{x}_i)(\boldsymbol{v}_{1,i}, \boldsymbol{v}_{2,i}), \qquad \boldsymbol{v}_j := \begin{pmatrix} \boldsymbol{v}_{j,1} \\ \vdots \\ \boldsymbol{v}_{j,M} \end{pmatrix} \in \mathrm{T}_{\boldsymbol{x}}\mathcal{M}, \quad j = 1, 2,$$

with $\boldsymbol{v}_{j,i} \in \mathrm{T}_{\boldsymbol{x}_i}\mathcal{M}_i$, $i = 1, \dots, M$.

For the computation of the Christoffel symbols with respect to the parameterization $h : \Omega \to \mathcal{M}$, cf. (3.52), we let the local coordinates $\boldsymbol{y} = (\boldsymbol{y}_1^\top, \dots, \boldsymbol{y}_M^\top)^\top \in \Omega$ be given by

$$\boldsymbol{y}_i := (y_{i,1}, \dots, y_{i,d_i})^\top \in \Omega_i, \qquad i = 1, \dots, M.$$

Then, we identify the coordinates $y_{i,k}$ by the index (i,k), $i=1,\dots,M$, $k=1,\dots,d_i$. With the matrix representation $\boldsymbol{G}_h(\boldsymbol{y})$ given in (3.53) and the observation

$$\frac{\partial}{\partial y_{i,k}}\boldsymbol{G}_{h_j}(\boldsymbol{y}_j)=0, \qquad i\neq j, \quad i,j=1,\dots,M, \quad k=1,\dots,d_i,$$

we can express the Christoffel symbols of the second kind as, cf. (3.19),

$$\Gamma_h(\boldsymbol{y})_{(i,k),(j,l)}^{(m,n)}=\begin{cases}\Gamma_{h_i}(\boldsymbol{y}_i)_{k,l}^n, & i=j=m, \quad k,l,n=1,\dots,d_i\\ 0, & \text{else,}\end{cases}$$

where $i,j,m=1,\dots,M$, $k=1,\dots,d_i$, $l=1,\dots,d_j$, $n=1,\dots,d_m$. In matrix vector notation this relation reads as, cf. (3.20),

$$\boldsymbol{\Gamma}_h^{(m,n)}(\boldsymbol{y})=\begin{pmatrix}\delta_{m,1}\boldsymbol{\Gamma}_{h_1}^n(\boldsymbol{y}_1) & \mathbf{0} & \cdots & \mathbf{0}\\ \mathbf{0} & \ddots & \ddots & \vdots\\ \vdots & \ddots & \ddots & \mathbf{0}\\ \mathbf{0} & \cdots & \mathbf{0} & \delta_{m,M}\boldsymbol{\Gamma}_{h_M}^n(\boldsymbol{y}_M)\end{pmatrix}\in\mathbb{R}^{d\times d}, \qquad \boldsymbol{y}\in\Omega, \tag{3.54}$$

where $m=1,\dots,M$, $\quad n=1,\dots,d_m$ and δ denotes the Kronecker delta, cf. (2.15). Loosely speaking, only the coordinates $y_{i,k}$ and $y_{i,l}$, $i=1,\dots,M$, $k,l=1,\dots,d_i$, are connected.

Thus, it is readily seen that the geodesic curves $\gamma_{\boldsymbol{x},\boldsymbol{v}}: I\to\mathcal{M}$, $I\subset\mathbb{R}$, of $\mathcal{M}$ associated to $\boldsymbol{x}\in\mathcal{M}$ and $\boldsymbol{v}\in\mathrm{T}_{\boldsymbol{x}}\mathcal{M}$, cf. (3.18) and Theorem 3.4, are given by

$$\gamma_{\boldsymbol{x},\boldsymbol{v}}(t):=(\gamma_{\boldsymbol{x}_1,\boldsymbol{v}_1}(t),\dots,\gamma_{\boldsymbol{x}_M,\boldsymbol{v}_M}(t)), \qquad t\in I, \tag{3.55}$$

where the curves $\gamma_{\boldsymbol{x}_i,\boldsymbol{v}_i}: I\to\mathcal{M}_i$ are geodesics in $\mathcal{M}_i$ associated to $\boldsymbol{x}_i\in\mathcal{M}_i$ and $\boldsymbol{v}_i\in\mathrm{T}_{\boldsymbol{x}_i}\mathcal{M}_i$, $i=1,\dots,M$. It follows that the geodesic distance $\mathrm{d}_{\mathcal{M}}$, cf. (3.17), can be calculated using the Pythagorean Theorem, i.e.,

$$\mathrm{d}_{\mathcal{M}}(\boldsymbol{x}_1,\boldsymbol{x}_2)=\left(\sum_{i=1}^M \mathrm{d}_{\mathcal{M}_i}(\boldsymbol{x}_{1,i},\boldsymbol{x}_{2,i})^2\right)^{\frac{1}{2}}, \qquad \boldsymbol{x}_j:=\begin{pmatrix}\boldsymbol{x}_{j,1}\\ \vdots\\ \boldsymbol{x}_{j,M}\end{pmatrix}, \ j=1,2,$$

where $\boldsymbol{x}_{j,i}\in\mathcal{M}_i$, $i=1,\dots,M$, $j=1,2$.

The gradient $\nabla_{\mathcal{M}}f(\boldsymbol{x})$ and the Hessian $\mathrm{H}_{\mathcal{M}}f(\boldsymbol{x})$ at $\boldsymbol{x}\in\mathcal{M}$ of a suitable smooth function $f:\mathcal{M}\to\mathbb{R}$ can be similarly composed from gradients and Hessians on the manifolds $\mathcal{M}_i$, $i=1,\dots,M$. Therefore, let us consider the local coordinate representation $f_h=f\circ h$ and denote by

$$\nabla_{\boldsymbol{y}_m}f_h(\boldsymbol{y}):=\left(\frac{\partial f_h}{\partial y_{m,1}}(\boldsymbol{y}),\dots,\frac{\partial f_h}{\partial y_{m,d_m}}(\boldsymbol{y})\right)^\top\in\mathbb{R}^{d_m}, \qquad \boldsymbol{y}\in\Omega, \quad m=1,\dots,M, \tag{3.56}$$

the usual gradients of f_h at $\boldsymbol{y}$ with respect to the coordinate $\boldsymbol{y}_m\in\Omega_m$. Then together with relation (3.53) the coordinate vector of the gradient $\nabla_{\mathcal{M}}f(\boldsymbol{x})$ is given by, cf. (3.34),

$$\nabla_h f_h(\boldsymbol{y})=\boldsymbol{G}_h^{-1}(\boldsymbol{y})\nabla f_h(\boldsymbol{y})=\begin{pmatrix}\boldsymbol{G}_{h_1}^{-1}(\boldsymbol{y}_1)\nabla_{\boldsymbol{y}_1}f_h(\boldsymbol{y})\\ \vdots\\ \boldsymbol{G}_{h_M}^{-1}(\boldsymbol{y}_M)\nabla_{\boldsymbol{y}_M}f_h(\boldsymbol{y})\end{pmatrix}\in\mathbb{R}^d, \qquad \boldsymbol{y}\in\Omega, \tag{3.57}$$

In other words, the gradient can be written as

$$\nabla_{\mathcal{M}} f(\boldsymbol{x}) = (\nabla_{\mathcal{M}_1} f(\boldsymbol{x})^\top, \dots, \nabla_{\mathcal{M}_M} f(\boldsymbol{x})^\top)^\top \in \mathrm{T}_{\boldsymbol{x}}\mathcal{M}, \qquad \boldsymbol{x} \in \mathcal{M}, \tag{3.58}$$

where $\nabla_{\mathcal{M}_i} f(\boldsymbol{x})$ is the gradient with respect to the variable $\boldsymbol{x}_i \in \mathcal{M}_i$, $i = 1, \dots, M$.

Similarly, the Hessian matrix representation of the Hessian $\mathrm{H}_{\mathcal{M}} f(\boldsymbol{x})$ is in local coordinates given by, cf. (3.35),

$$\mathbf{H}_h f_h(\boldsymbol{y}) = \mathbf{H} f_h(\boldsymbol{y}) - \mathbf{N}_h f_h(\boldsymbol{y}) \in \mathbb{R}^{d\times d}, \qquad \boldsymbol{y} \in \Omega, \tag{3.59}$$

where the matrix

$$\mathbf{N}_h f_h(\boldsymbol{y}) = \sum_{m=1}^{M} \sum_{n=1}^{d_m} \big(\nabla f_h(\boldsymbol{y})\big)_{(m,n)} \boldsymbol{\Gamma}_h^{(m,n)}(\boldsymbol{y}) \in \mathbb{R}^{d\times d}, \qquad \boldsymbol{y} \in \Omega,$$

can be written by (3.54) and (3.56) as

$$\mathbf{N}_h f_h(\boldsymbol{y}) = \begin{pmatrix} \mathbf{N}_{\boldsymbol{y}_1} f_h(\boldsymbol{y}) & \mathbf{0} & \cdots & \mathbf{0} \\ \mathbf{0} & \ddots & \ddots & \vdots \\ \vdots & \ddots & \ddots & \mathbf{0} \\ \mathbf{0} & \cdots & \mathbf{0} & \mathbf{N}_{\boldsymbol{y}_M} f_h(\boldsymbol{y}) \end{pmatrix} \in \mathbb{R}^{d\times d}, \qquad \boldsymbol{y} \in \Omega, \tag{3.60}$$

with

$$\mathbf{N}_{\boldsymbol{y}_m} f_h(\boldsymbol{y}) := \sum_{n=1}^{d_m} \big(\nabla_{\boldsymbol{y}_m} f_h(\boldsymbol{y})\big)_n \boldsymbol{\Gamma}_{h_m}^n(\boldsymbol{y}_m), \qquad \boldsymbol{y} \in \Omega, \qquad m = 1, \dots, M. \tag{3.61}$$

3.2 Specific Riemannian Manifolds

In this section we introduce the torus, sphere, and rotation group as subsets of Euclidean space, and apply the previously introduced theory of Riemannian manifolds, cf. Section 3.1, in order to obtain in Section 3.2.1–3.2.3 explicit representations of the geometric objects on these manifolds as for example the tangent spaces, geodesics, gradients and Hessians.

The *d-dimensional sphere* is defined by

$$\mathbb{S}^d := \{\boldsymbol{x} \in \mathbb{R}^{d+1} \ : \ \|\boldsymbol{x}\|_2 = 1\} \subset \mathbb{R}^{d+1}, \qquad d \in \mathbb{N}. \tag{3.62}$$

The *d-dimensional torus* is given by the product of $d \in \mathbb{N}$ one-dimensional spheres $\mathbb{S}^1 \subset \mathbb{R}^2$, namely

$$\mathbb{T}^d := \underbrace{\mathbb{S}^1 \times \cdots \times \mathbb{S}^1}_{d\text{-times}} \subset \mathbb{R}^{2d}. \tag{3.63}$$

The *orthogonal group* and the *rotation group* of the n-dimensional Euclidean space is denoted by

$$\mathrm{O}(n) := \{\boldsymbol{R} \in \mathbb{R}^{n\times n} \ : \ \boldsymbol{R}^\top = \boldsymbol{R}^{-1}\}, \quad \mathrm{SO}(n) := \{\boldsymbol{R} \in \mathrm{O}(n) \ : \ \det \boldsymbol{R} = 1\}, \qquad n \in \mathbb{N}, \tag{3.64}$$

respectively. For odd $n \in \mathbb{N}$, these sets are related by $\mathrm{O}(n) = \{\pm\boldsymbol{R} \ : \ \boldsymbol{R} \in \mathrm{SO}(n)\}$, where the rotation group $\mathrm{SO}(n)$ is the connected part of $\mathrm{O}(n)$ which contains the identity matrix. We will restrict our attention to the rotation group $\mathrm{SO}(n)$ and consider it by the canonical identification $\mathbb{R}^{n\times n} \cong \mathbb{R}^{n^2}$ as a subset of the Euclidean space $\mathbb{R}^{n^2}$. Thus, the rotation group $\mathrm{SO}(n)$ fits into the setting of Riemannian manifolds defined by (3.4).

Theorem 3.9. *The torus $\mathbb{T}^d$, the sphere $\mathbb{S}^d$, $d \in \mathbb{N}$, and the rotation group $\mathrm{SO}(n)$, $n \geq 2$, are compact and connected d-dimensional respectively $n(n-1)/2$-dimensional manifolds.*

Proof. For proofing the assertion for the sphere $\mathbb{S}^d$ defined by (3.62) we consider the smooth map $F : \mathbb{R}^{d+1} \setminus \{\mathbf{0}\} \to \mathbb{R}$ given by

$$F(\boldsymbol{x}) := \boldsymbol{x}^\top \boldsymbol{x} - 1 = \sum_{i=1}^{d+1} x_i^2 - 1, \qquad \boldsymbol{x} \in \mathbb{R}^{d+1} \setminus \{\mathbf{0}\}.$$

Since the differential $\mathrm{D}F(\boldsymbol{x})$ of F at $\boldsymbol{x}$, given by $\mathrm{D}F(\boldsymbol{x})\boldsymbol{v} = 2\boldsymbol{x}^\top \boldsymbol{v}$, $\boldsymbol{v} \in \mathbb{R}^{d+1}$, is obviously surjective for $\boldsymbol{x} \in F^{-1}(\mathbf{0}) = \mathbb{S}^d$ we conclude after application of Theorem 3.1 that the sphere $\mathbb{S}^d$ is a d-dimensional manifold. Moreover, it is seen that the sphere $\mathbb{S}^d$ is a connected and compact manifold.

By definition (3.63) we have that the torus $\mathbb{T}^d$ is a product manifold of d one-dimensional spheres $\mathbb{S}^1$. Hence, the torus $\mathbb{T}^d$ is a d-dimensional connected and compact manifold.

In order to show that the rotation group $\mathrm{SO}(n)$ is an $n(n-1)/2$-dimensional manifold we consider the smooth map $F : \mathbb{R}^{n \times n} \to \mathbb{R}^{n(n+1)/2}$ given by

$$F(\boldsymbol{A}) := \mathrm{pr}_n \left(\boldsymbol{A}^\top \boldsymbol{A} - \boldsymbol{I} \right) = \left(\boldsymbol{a}_i^\top \boldsymbol{a}_j - \delta_{i,j} \right)_{1 \leq i \leq j \leq n}$$

for the matrix

$$\boldsymbol{A} := (\boldsymbol{a}_1, \ldots, \boldsymbol{a}_n) \in \mathbb{R}^{n \times n}, \qquad \boldsymbol{a}_i \in \mathbb{R}^n, \quad i = 1, \ldots, n,$$

where $\mathrm{pr}_n : \mathbb{R}^{n \times n} \to \mathbb{R}^{n(n+1)/2}$ is the canonical projection onto the upper triangular matrix elements, which are arranged in a vector. The differential $\mathrm{D}F(\boldsymbol{A}) : \mathbb{R}^{n \times n} \to \mathbb{R}^{n(n+1)/2}$ of F at $\boldsymbol{A} \in \mathbb{R}^{n \times n}$ is given by

$$\mathrm{D}F(\boldsymbol{A})\boldsymbol{V} = \mathrm{pr}_n \left(\boldsymbol{V}^\top \boldsymbol{A} + \boldsymbol{A}^\top \boldsymbol{V} \right), \qquad \boldsymbol{V} \in \mathbb{R}^{n \times n}.$$

Now, for any fixed $\boldsymbol{R} \in \mathrm{SO}(n)$ and arbitrary $\boldsymbol{s} \in \mathbb{R}^{n(n+1)/2}$ we let $\boldsymbol{S} \in \mathbb{R}^{n \times n}$ be the unique symmetric matrix satisfying $\boldsymbol{s} = \mathrm{pr}_n(\boldsymbol{S})$. With $\boldsymbol{V} := \frac{1}{2}\boldsymbol{R}\boldsymbol{S}$ we obtain

$$\mathrm{D}F(\boldsymbol{R})\boldsymbol{V} = \mathrm{pr}_n \left(\frac{1}{2}(\boldsymbol{S}^\top + \boldsymbol{S}) \right) = \boldsymbol{s},$$

which shows that the differential $\mathrm{D}F(\boldsymbol{R})$ is surjective for $\boldsymbol{R} \in \mathrm{SO}(n)$. By the continuity of the determinant $\det : \mathbb{R}^{n \times n} \to \mathbb{R}$ it follows that the set of matrices with positive determinant

$$\mathrm{GL}_n^+ := \{\boldsymbol{A} \in \mathbb{R}^{n \times n} \,:\, \det(\boldsymbol{A}) > 0\}$$

is open in $\mathbb{R}^{n \times n} \cong \mathbb{R}^{n^2}$. Together with the observation $F^{-1}(\mathbf{0}) \cap \mathrm{GL}_n^+ = \mathrm{SO}(n)$ and an application of Theorem 3.1 we conclude that the rotation group $\mathrm{SO}(n)$ can be considered as an $n(n-1)/2$-dimensional manifold in $\mathbb{R}^{n^2}$. Moreover, it is seen that it is a connected and complete manifold. ■

3.2.1 The Sphere $\mathbb{S}^d$

In Theorem 3.10 we summarize explicit descriptions of the tangent space $\mathrm{T}_{\boldsymbol{x}}\mathbb{S}^d \subset \mathbb{R}^{d+1}$, $\boldsymbol{x} \in \mathbb{S}^d$, the geodesics $\gamma_{\boldsymbol{x},\boldsymbol{v}}$, normal vector $\boldsymbol{n}_{\boldsymbol{x},\boldsymbol{v}}$, $\boldsymbol{v} \in \mathrm{T}_{\boldsymbol{x}}\mathbb{S}^d$, and the geodesic distance $\mathrm{d}_{\mathbb{S}^d}$, which have been defined in Section 3.1.3 and 3.1.4. In Figure 3.1 we illustrate the tangent space and a geodesic curve for the sphere $\mathbb{S}^2$.

Theorem 3.10. *For $d \in \mathbb{N}$ let the sphere $\mathbb{S}^d$, cf. (3.62), be given. Then the tangent space is*

$$\mathrm{T}_{\boldsymbol{x}}\mathbb{S}^d = \{\boldsymbol{v} \in \mathbb{R}^{d+1} \ : \ \boldsymbol{v}^\top \boldsymbol{x} = 0\}, \qquad \boldsymbol{x} \in \mathbb{S}^d, \tag{3.65}$$

the maximal geodesic $\gamma_{\boldsymbol{x},\boldsymbol{v}} : \mathbb{R} \to \mathbb{S}^d$ associated to $\boldsymbol{x} \in \mathbb{S}^d$ and $\boldsymbol{v} \in \mathrm{T}_{\boldsymbol{x}}\mathbb{S}^d$ is parameterized by

$$\gamma_{\boldsymbol{x},\boldsymbol{v}}(t) = \cos\left(t\|\boldsymbol{v}\|_2\right)\boldsymbol{x} + \sin(t\|\boldsymbol{v}\|_2)\frac{\boldsymbol{v}}{\|\boldsymbol{v}\|_2}, \qquad t \in \mathbb{R}, \tag{3.66}$$

and the normal vector of $\boldsymbol{v}$ at $\boldsymbol{x}$, cf. (3.25), is given by

$$\boldsymbol{n}_{\boldsymbol{x},\boldsymbol{v}} = -\|\boldsymbol{v}\|_2^2 \boldsymbol{x}, \qquad \boldsymbol{v} \in \mathrm{T}_{\boldsymbol{x}}\mathbb{S}^d, \quad \boldsymbol{x} \in \mathbb{S}^d. \tag{3.67}$$

The geodesic distance is

$$\mathrm{d}_{\mathbb{S}^d}(\boldsymbol{x}_1, \boldsymbol{x}_2) = \arccos(\boldsymbol{x}_1^\top \boldsymbol{x}_2), \qquad \boldsymbol{x}_1, \boldsymbol{x}_2 \in \mathbb{S}^d. \tag{3.68}$$

Proof. In order to determine the tangent space $\mathrm{T}_{\boldsymbol{x}}\mathbb{S}^d$ at $\boldsymbol{x} \in \mathbb{S}^d$ we let $\gamma : (-\varepsilon, \varepsilon) \to \mathbb{S}^d$ for some $\varepsilon > 0$ be an arbitrary curve with $\gamma(0) = \boldsymbol{x}$. From $\|\gamma\|_2 \equiv 1$, we infer by relation (3.14) that any tangent vector $\boldsymbol{v} := \dot{\gamma}(0) \in \mathrm{T}_{\boldsymbol{x}}\mathbb{S}^d$ satisfies

$$0 = \frac{\mathrm{d}}{\mathrm{d}t}\|\gamma(t)\|_2^2\Big|_{t=0} = 2\dot{\gamma}(t)^\top \gamma(t)\Big|_{t=0} = 2\boldsymbol{v}^\top \boldsymbol{x}.$$

Since for any tangent vector $\boldsymbol{v} \in \mathrm{T}_{\boldsymbol{x}}\mathbb{S}^d$ there exists a corresponding curve γ, cf. (3.15), we deduce by a simple dimension argument that the tangent space is given by (3.65).

For the curve $\gamma_{\boldsymbol{x},\boldsymbol{v}}$ defined by (3.66) we observe the relations

$$\|\gamma_{\boldsymbol{x},\boldsymbol{v}}(t)\|_2 = 1, \qquad \ddot{\gamma}_{\boldsymbol{x},\boldsymbol{v}}(t) = -\gamma_{\boldsymbol{x},\boldsymbol{v}}(t)\|\boldsymbol{v}\|_2^2, \qquad t \in \mathbb{R}, \quad \boldsymbol{v} \in \mathrm{T}_{\boldsymbol{x}}\mathbb{S}^d, \quad \boldsymbol{x} \in \mathbb{S}^d.$$

Hence, by the definition of geodesic curves, cf. (3.18), and relation (3.65) we find that the maximal geodesic on the sphere $\mathbb{S}^d$ associated to $\boldsymbol{x} \in \mathbb{S}^d$ and $\boldsymbol{v} \in \mathrm{T}_{\boldsymbol{x}}\mathbb{S}^d$ is parameterized by (3.66). Moreover, we conclude that the normal vector of $\boldsymbol{v}$ at $\boldsymbol{x}$ is given by (3.67).

Using the relations (3.24) in Theorem 3.4 and equation (3.66) one checks that the geodesic distance is given by (3.68). ∎

For sufficiently smooth functions f on the sphere $\mathbb{S}^d$, we arrive by Corollary 3.6 at explicit representations of the gradient $\nabla_{\mathbb{S}^d} f$, and the Hessian $\mathrm{H}_{\mathbb{S}^d} f$, cf. Section 3.1.5.

Theorem 3.11. *For $d \in \mathbb{N}$ let the sphere $\mathbb{S}^d$, cf. (3.62), be given and $f : \mathbb{S}^d \to \mathbb{R}$ be the restriction $f := \tilde{f}\big|_{\mathbb{S}^d}$ of some function $\tilde{f} : U \to \mathbb{R}$, $\mathbb{S}^d \subset U$, $U \subset \mathbb{R}^{d+1}$ open. If $\tilde{f}$ is once differentiable, then the gradient of f has the representation*

$$\nabla_{\mathbb{S}^d} f(\boldsymbol{x}) = \nabla \tilde{f}(\boldsymbol{x}) - (\nabla \tilde{f}(\boldsymbol{x})^\top \boldsymbol{x})\boldsymbol{x} \in \mathrm{T}_{\boldsymbol{x}}\mathbb{S}^d, \qquad \boldsymbol{x} \in \mathbb{S}^d. \tag{3.69}$$

If $\tilde{f}$ is twice differentiable, then the Hessian of f has the representation

$$\mathrm{H}_{\mathbb{S}^d} f(\boldsymbol{x})(\boldsymbol{v}, \boldsymbol{v}) = \boldsymbol{v}^\top \left(\mathbf{H}\tilde{f}(\boldsymbol{x}) - (\nabla \tilde{f}(\boldsymbol{x})^\top \boldsymbol{x})\boldsymbol{I}\right)\boldsymbol{v}, \qquad \boldsymbol{v} \in \mathrm{T}_{\boldsymbol{x}}\mathbb{S}^d, \quad \boldsymbol{x} \in \mathbb{S}^d. \tag{3.70}$$

Proof. Together with Theorem 3.10 the relation (3.42) in Corollary 3.6 leads by orthogonal projection onto the tangent space to the representation (3.69). Similarly, we obtain by relation (3.43) in Corollary 3.6 and equation (3.67) the representation (3.70). ∎

The results for the sphere $\mathbb{S}^d$ given in Theorem 3.10 and Theorem 3.11 are independent of any local parameterization. However, for the efficient evaluation of polynomials on the sphere $\mathbb{S}^2$,

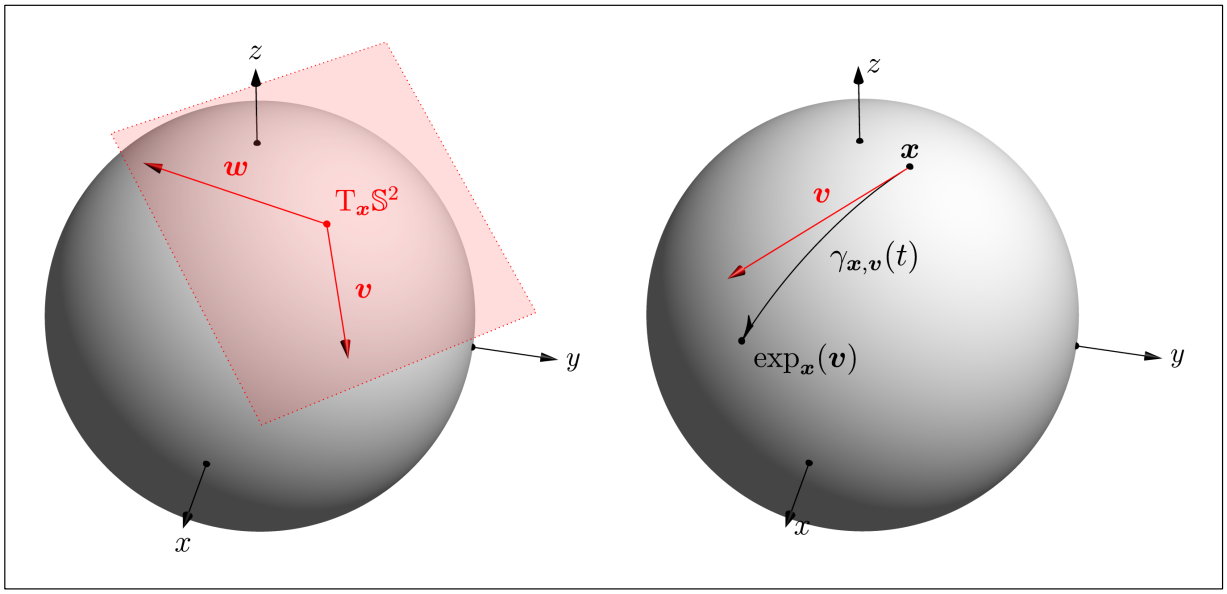

Figure 3.1: Left: Illustration of the tangent space $\mathrm{T}_{\boldsymbol{x}}\mathbb{S}^2$ at a point $\boldsymbol{x} \in \mathbb{S}^2$ spanned by two tangent vectors $\boldsymbol{v}, \boldsymbol{w} \in \mathrm{T}_{\boldsymbol{x}}\mathbb{S}^2$, cf. (3.65). Right: Illustration of the geodesic curve $\gamma_{\boldsymbol{x},\boldsymbol{v}}$ starting at a point $\boldsymbol{x} \in \mathbb{S}^2$ with direction vector $\boldsymbol{v} \in \mathrm{T}_{\boldsymbol{x}}\mathbb{S}^2$, cf. (3.66). Recall the relation $\exp_{\boldsymbol{x}}(\boldsymbol{v}) = \gamma_{\boldsymbol{x},\boldsymbol{v}}(1)$, cf. (3.28).

cf. Section 5.2.2, we need to perform calculations in spherical coordinates corresponding to the parameterization

$$h(\theta,\varphi) := \begin{pmatrix} \sin(\theta)\cos(\varphi) \\ \sin(\theta)\sin(\varphi) \\ \cos(\theta) \end{pmatrix} \in \mathbb{S}^2, \qquad (\theta,\varphi) \in [0,\pi] \times [0,2\pi). \tag{3.71}$$

The following Theorem 3.12 summarizes the well-known properties and differential geometric formulas of the parameterization $h : [0,\pi] \times [0,2\pi) \to \mathbb{S}^2$.

Theorem 3.12. *The restriction $h\big|_\Omega$ of the parameterization $h : [0,\pi] \times [0,2\pi) \to \mathbb{S}^2$ defined by (3.71) to the open set $\Omega := (0,\pi) \times (0,2\pi)$ is a local parameterization, cf. Theorem 3.2, of the sphere $\mathbb{S}^2$ with range*

$$h(\Omega) = \mathbb{S}^2 \setminus \big\{h(\theta,0) \ : \ \theta \in [0,\pi]\big\} = \mathbb{S}^2 \setminus \big\{\boldsymbol{x} := (x_1,x_2,x_3) \in \mathbb{R}^3 \ : \ x_2 = 0 \text{ and } x_1 \geq 0\big\}$$

and inverse

$$h^{-1}(\boldsymbol{x}) = \begin{pmatrix} \arccos(x_3) \\ 2\arctan\left(x_2 / \left(x_1 - \sqrt{x_1^2 + x_2^2}\right)\right) + \pi \end{pmatrix}, \quad \boldsymbol{x} := \begin{pmatrix} x_1 \\ x_2 \\ x_3 \end{pmatrix} \in h(\Omega).$$

Furthermore, for $\boldsymbol{x} := h(\theta,\varphi) \in \mathbb{S}^2 \setminus \{\pm(0,0,1)^\top\}$, $(\theta,\varphi) \in (0,\pi) \times [0,2\pi)$, the canonical basis of the tangent space $\mathrm{T}_{\boldsymbol{x}}\mathbb{S}^2$, cf. (3.9), reads as

$$\boldsymbol{h}_\theta(\theta,\varphi) = \begin{pmatrix} \cos(\theta)\cos(\varphi) \\ \cos(\theta)\sin(\varphi) \\ -\sin(\theta) \end{pmatrix}, \quad \boldsymbol{h}_\varphi(\theta,\varphi) = \begin{pmatrix} -\sin(\theta)\sin(\varphi) \\ \sin(\theta)\cos(\varphi) \\ 0 \end{pmatrix} \in \mathrm{T}_{\boldsymbol{x}}\mathbb{S}^2$$

where the corresponding matrix representation of the induced Riemannian structure $g_{\mathbb{S}^2}$, cf. (3.12)*, is given by*

$$\boldsymbol{G}_h(\theta,\varphi) = \begin{pmatrix} 1 & 0 \\ 0 & \sin(\theta)^2 \end{pmatrix}, \qquad (\theta,\varphi) \in (0,\pi)\times[0,2\pi),$$

and the Christoffel symbols of the second kind, cf. (3.19)*, are given in matrix form, cf.* (3.20)*, by*

$$\boldsymbol{\Gamma}_h^{\theta}(\theta,\varphi) = \begin{pmatrix} \Gamma_h(\theta,\varphi)^{\theta}_{\theta,\theta} & \Gamma_h(\theta,\varphi)^{\theta}_{\theta,\varphi} \\ \Gamma_h(\theta,\varphi)^{\theta}_{\varphi,\theta} & \Gamma_h(\theta,\varphi)^{\theta}_{\varphi,\varphi} \end{pmatrix} = \begin{pmatrix} 0 & 0 \\ 0 & -\sin(\theta)\cos(\theta) \end{pmatrix},$$
$$\boldsymbol{\Gamma}_h^{\varphi}(\theta,\varphi) = \begin{pmatrix} \Gamma_h(\theta,\varphi)^{\varphi}_{\theta,\theta} & \Gamma_h(\theta,\varphi)^{\varphi}_{\theta,\varphi} \\ \Gamma_h(\theta,\varphi)^{\varphi}_{\varphi,\theta} & \Gamma_h(\theta,\varphi)^{\varphi}_{\varphi,\varphi} \end{pmatrix} = \begin{pmatrix} 0 & \cot(\theta) \\ \cot(\theta) & 0 \end{pmatrix}.$$

Proof. The assertions are obtained by straightforward application of the corresponding definitions given in Section 3.1.2– 3.1.4. ■

The parametrization $h : [0,\pi]\times[0,2\pi) \to \mathbb{S}^2$, cf. (3.71), can be generalized to the sphere $\mathbb{S}^d$, so that we arrive in Remark 3.13 at a formula for the canonical measure $\mu_{\mathbb{S}^d}$, cf. Section 3.1.6.

Remark 3.13. For $d \geq 3$ we obtain inductively parameterizations of the sphere $\mathbb{S}^d$ by setting

$$h_d(\boldsymbol{\theta},\varphi) := \sin(\theta_1)\begin{pmatrix} h_{d-1}(\tilde{\boldsymbol{\theta}},\varphi) \\ 0 \end{pmatrix} + \cos(\theta_1)\begin{pmatrix} \mathbf{0} \\ 1 \end{pmatrix} \in \mathbb{S}^d, \qquad (\boldsymbol{\theta},\varphi) \in [0,\pi]^{d-1}\times[0,2\pi),$$

where $h_2 := h$ defined by (3.71) and $\tilde{\boldsymbol{\theta}} := (\theta_2,\dots,\theta_{d-1})$ is the restriction of $\boldsymbol{\theta} := (\theta_1,\dots,\theta_{d-1})$ to the last $d-2$ coordinates. With this inductive definition of the parameterizations h_d it is readily seen that the canonical measure $\mu_{\mathbb{S}^d}$, cf. (3.51), on the sphere $\mathbb{S}^d$ is given by the density

$$\mathrm{d}\mu_{\mathbb{S}^d}(\boldsymbol{x}) := \left(\prod_{k=1}^{d-1}\sin(\theta_k)^{d-k}\mathrm{d}\theta_k\right)\mathrm{d}\varphi, \qquad \boldsymbol{x} := h_d(\boldsymbol{\theta},\varphi), \quad (\boldsymbol{\theta},\varphi) \in [0,\pi]^{d-1}\times[0,2\pi). \tag{3.72}$$

We note further that the canonical measure $\mu_{\mathbb{S}^d}$ is rotational invariant, i.e., for any measurable set $O \subset \mathbb{S}^d$ it satisfies the relation

$$\mu_{\mathbb{S}^d}(O) = \mu_{\mathbb{S}^d}(\boldsymbol{R}\,O), \qquad \boldsymbol{R}\,O := \{\boldsymbol{R}\boldsymbol{x} \;:\; \boldsymbol{x} \in O\}, \quad \boldsymbol{R} \in \mathrm{SO}(d+1). \tag{3.73}$$

□

3.2.2 The Torus $\mathbb{T}^d$

We recall that the torus $\mathbb{T}^d \subset \mathbb{R}^{2d}$, $d \in \mathbb{N}$, is defined as product manifold of spheres $\mathbb{S}^1 \subset \mathbb{R}^2$, cf. (3.63). Hence, we could simply apply Theorem 3.10 and Theorem 3.11 for the sphere $\mathbb{S}^1$ in conjunction with the findings for product manifolds presented in Section 3.1.7 to describe the torus $\mathbb{T}^d$. However, this will lead to cumbersome notations and it is more convenient to consider the parameterization

$$h(\boldsymbol{\alpha}) := (\cos(\alpha_1),\sin(\alpha_1),\dots,\cos(\alpha_d),\sin(\alpha_d))^{\top} \in \mathbb{T}^d, \quad \boldsymbol{\alpha} := (\alpha_1,\dots,\alpha_d)^{\top} \in \mathbb{R}^d. \tag{3.74}$$

Since the parameterization $h : \mathbb{R}^d \to \mathbb{T}^d$ has the identity matrix as matrix representation of the induced Riemannian structure $g_{\mathbb{T}^d}$, i.e., $\boldsymbol{G}_h(\boldsymbol{\alpha}) := \boldsymbol{I}_d \in \mathbb{R}^d$, $\boldsymbol{\alpha} \in \mathbb{R}^d$, we find that all Christoffel symbols Γ_h vanish, as in the case of Euclidean space $\mathbb{R}^d$, cf. (3.21). Thus, the geodesics on the

torus are simply parameterized by straight lines

$$\gamma_{\boldsymbol{x},\boldsymbol{v}}(t) = h \circ \gamma_h(t), \qquad \gamma_h(t) = \boldsymbol{\alpha} + t\boldsymbol{w}, \qquad \boldsymbol{x} = h(\boldsymbol{\alpha}), \quad \boldsymbol{v} = \mathrm{D}h(\boldsymbol{\alpha})\boldsymbol{w}, \quad \boldsymbol{\alpha}, \boldsymbol{w} \in \mathbb{R}^d. \tag{3.75}$$

We note further that the parameterization $h : \mathbb{R}^d \to \mathbb{T}^d$ is not injective since

$$\boldsymbol{x} = h(\boldsymbol{\alpha}) = h(\boldsymbol{\beta}) \in \mathbb{T}^d \qquad \Leftrightarrow \qquad \boldsymbol{\alpha} = \boldsymbol{\beta} + 2\pi\boldsymbol{k}, \quad \boldsymbol{k} \in \mathbb{Z}^d. \tag{3.76}$$

Hence, we have to restrict the parameter space to boxes of the form

$$\Omega_{\boldsymbol{a}} := (a_1, a_1 + 2\pi) \times \cdots \times (a_d, a_d + 2\pi) \subset \mathbb{R}^d, \qquad \boldsymbol{a} := (a_1, \ldots, a_d) \in \mathbb{R}^d, \tag{3.77}$$

such that the restriction $h|_{\Omega_a}$ is a local parameterization, cf. Theorem 3.2. It follows from the relations (3.75), (3.76) that the geodesic distance is given by

$$\mathrm{d}_{\mathbb{T}^d}(\boldsymbol{x}, \boldsymbol{y}) = \min_{\boldsymbol{k} \in \mathbb{Z}^d} \|\boldsymbol{\alpha} - \boldsymbol{\beta} + 2\pi\boldsymbol{k}\|_2, \qquad \boldsymbol{x} = h(\boldsymbol{\alpha}), \quad \boldsymbol{y} = h(\boldsymbol{\beta}), \quad \boldsymbol{\alpha}, \boldsymbol{\beta} \in \mathbb{R}^d. \tag{3.78}$$

Furthermore, the canonical surface measure $\mu_{\mathbb{T}^d}$, cf. (3.51), is given by the density $\mathrm{d}\mu_{\mathbb{T}^d}(\boldsymbol{x}) = \mathrm{d}\boldsymbol{\alpha}$, $\boldsymbol{x} = h(\boldsymbol{\alpha}) \in \Omega_{\boldsymbol{a}}$, which corresponds to the Lebesgue measure restricted to some box $\Omega_{\boldsymbol{a}} \subset \mathbb{R}^d$, $\boldsymbol{a} \in \mathbb{R}^d$, cf. (3.77).

Remark 3.14. With the above observations we can simply use the identification $\mathbb{T}^d \cong \mathbb{R}^2/(2\pi\mathbb{Z}^d)$, where two points $\boldsymbol{\alpha}, \boldsymbol{\beta} \in \mathbb{R}^d$ are identified if the relation (3.76) is satisfied. Therefore, we will simply identify functions f on the torus with 2π-periodic functions on $\mathbb{R}^d$. By abuse of notation we will use for sufficiently smooth and measurable functions $f : \mathbb{T}^d \to \mathbb{C}$ the following conventions

$$f(\boldsymbol{\alpha}) := f \circ h(\boldsymbol{\alpha}) = f(\boldsymbol{x}), \qquad \nabla_{\mathbb{T}^d} f(\boldsymbol{x}) := \nabla f(\boldsymbol{\alpha}) \in \mathbb{R}^d, \qquad \mathbf{H}_{\mathbb{T}^d} f(\boldsymbol{x}) := \mathbf{H} f(\boldsymbol{\alpha}) \in \mathbb{R}^{d \times d},$$

and, cf. (3.77),

$$I_{\mu_{\mathbb{T}^d}} f = \int_{\mathbb{T}^d} f(\boldsymbol{x}) \mathrm{d}\mu_{\mathbb{T}^d}(\boldsymbol{x}) = \int_{\Omega_{\boldsymbol{a}}} f(\boldsymbol{\alpha}) \mathrm{d}\boldsymbol{\alpha}, \quad \boldsymbol{a} \in \mathbb{R}^d, \tag{3.79}$$

respectively, where points on the torus $\mathbb{T}^d$ are always denoted by Roman letters and the corresponding local coordinates in the Euclidean space $\mathbb{R}^d$ by Greek letters, e.g., $\boldsymbol{x} = h(\boldsymbol{\alpha}) \in \mathbb{T}^d$, $\boldsymbol{\alpha} \in \mathbb{R}^d$. □

3.2.3 The Rotation Group $\mathrm{SO}(n)$

We recall that we use the canonical identification $\mathbb{R}^{n \times n} \cong \mathbb{R}^{n^2}$, $n \in \mathbb{N}$. Thus, the standard inner product on $\mathbb{R}^{n \times n}$ is given by

$$\mathrm{tr}(\boldsymbol{A}^\top \boldsymbol{B}) = \sum_{i,j=1}^{n} a_{i,j} b_{i,j} = \mathrm{tr}(\boldsymbol{B}^\top \boldsymbol{A}), \quad \boldsymbol{A} := (a_{i,j})_{i,j=1}^n, \boldsymbol{B} := (b_{i,j})_{i,j=1}^n \in \mathbb{R}^{n \times n},$$

where the *trace* of a matrix is defined by

$$\mathrm{tr}(\boldsymbol{A}) := \sum_{i=1}^{n} a_{i,i}, \qquad \boldsymbol{A} := (a_{i,j})_{i,j=1}^n \in \mathbb{R}^{n \times n}.$$

Moreover, we find that the *Frobenius norm*

$$\|\boldsymbol{A}\|_{\mathrm{F}} := \sqrt{\sum_{i=1}^{n}\sum_{j=1}^{n}|a_{i,j}|^2} = \sqrt{\mathrm{tr}(\boldsymbol{A}^\top\boldsymbol{A})}, \qquad \boldsymbol{A} := (a_{i,j})_{i,j=1}^{n} \in \mathbb{R}^{n\times n}, \tag{3.80}$$

corresponds to the Euclidean norm in $\mathbb{R}^{n^2}$. An important property of that inner product is that a *symmetric* matrix $\boldsymbol{S}$ and a *skew symmetric* matrix $\boldsymbol{T}$, i.e.,

$$\boldsymbol{S}^\top = \boldsymbol{S}, \quad \boldsymbol{T}^\top = -\boldsymbol{T}, \qquad \boldsymbol{S} := (s_{i,j})_{i,j=1}^{n},\ \boldsymbol{T} := (t_{i,j})_{i,j=1}^{n} \in \mathbb{R}^{n\times n},$$

are orthogonal

$$\mathrm{tr}(\boldsymbol{S}^\top\boldsymbol{T}) = \sum_{\substack{i=1\\i<j}}^{n} s_{i,j}t_{i,j} - \sum_{\substack{i=1\\i<j}}^{n} s_{i,j}t_{i,j} = 0. \tag{3.81}$$

In Theorem 3.15, we summarize explicit descriptions of the tangent space $\mathrm{T}_{\boldsymbol{R}}\mathrm{SO}(n) \subset \mathbb{R}^{n\times n}$, $\boldsymbol{R} \in \mathrm{SO}(n)$, the geodesics $\gamma_{\boldsymbol{R},\boldsymbol{V}}$, the normal vector $\boldsymbol{N}_{\boldsymbol{R},\boldsymbol{V}}$, $\boldsymbol{V} \in \mathrm{T}_{\boldsymbol{R}}\mathrm{SO}(n)$, and the geodesic distance $\mathrm{d}_{\mathrm{SO}(n)}$, which have been defined in Section 3.1.3 and 3.1.4. For describing the geodesics in $\mathrm{SO}(n)$ we introduce the *matrix exponential*

$$\exp : \mathbb{R}^{n\times n} \to \mathbb{R}^{n\times n}, \qquad \exp(\boldsymbol{A}) := \boldsymbol{I} + \sum_{k=1}^{\infty}\frac{1}{k!}\boldsymbol{A}^k, \qquad \boldsymbol{A} \in \mathbb{R}^{n\times n}. \tag{3.82}$$

Theorem 3.15. *For $n \in \mathbb{N}$ let the rotation group $\mathrm{SO}(n)$, cf. (3.64), be given. Then the tangent space is given by*

$$\mathrm{T}_{\boldsymbol{R}}\mathrm{SO}(n) = \boldsymbol{R}\,\mathrm{T}_{\boldsymbol{I}}\mathrm{SO}(n) := \{\boldsymbol{R}\boldsymbol{V} \ :\ \boldsymbol{V} \in \mathrm{T}_{\boldsymbol{I}}\mathrm{SO}(n)\} \subset \mathbb{R}^{n\times n}, \qquad \boldsymbol{R} \in \mathrm{SO}(n), \tag{3.83}$$

where

$$\mathrm{T}_{\boldsymbol{I}}\mathrm{SO}(n) = \{\boldsymbol{V} \in \mathbb{R}^{n\times n} \ :\ \boldsymbol{V} = -\boldsymbol{V}^\top\} \tag{3.84}$$

is the tangent space at the identity matrix $\boldsymbol{I} \in \mathrm{SO}(n)$. The maximal geodesic $\gamma_{\boldsymbol{R},\boldsymbol{V}}(t) : \mathbb{R} \to \mathrm{SO}(n)$ associated to $\boldsymbol{R} \in \mathrm{SO}(3)$ and $\boldsymbol{V} \in \mathrm{T}_{\boldsymbol{R}}\mathrm{SO}(n)$ is parameterized by

$$\gamma_{\boldsymbol{R},\boldsymbol{V}}(t) = \boldsymbol{R}\exp(t\,\boldsymbol{R}^\top\boldsymbol{V}), \qquad t \in \mathbb{R}. \tag{3.85}$$

and the normal vector of $\boldsymbol{V}$ at $\boldsymbol{R}$, cf. (3.25), is given by

$$\boldsymbol{N}_{\boldsymbol{R},\boldsymbol{V}} = \boldsymbol{V}\boldsymbol{R}^\top\boldsymbol{V} \in \mathrm{T}_{\boldsymbol{R}}\mathrm{SO}(n), \qquad \boldsymbol{R} \in \mathrm{SO}(n). \tag{3.86}$$

The geodesic distance can be computed by the relation

$$\mathrm{d}_{\mathrm{SO}(n)}(\boldsymbol{R}_1,\boldsymbol{R}_2) = \left(\alpha_1^2 + \cdots + \alpha_n^2\right)^{\frac{1}{2}}, \qquad \boldsymbol{R}_1,\boldsymbol{R}_2 \in \mathrm{SO}(n), \tag{3.87}$$

where $\alpha_i \in [-\pi,\pi]$ are the arguments of the eigenvalues $\lambda_i = \mathrm{e}^{\mathrm{i}\alpha_i}$, $i = 1,\ldots,n$, of $\boldsymbol{R}_1^\top\boldsymbol{R}_2$.

Proof. For the description of the tangent space $\mathrm{T}_{\boldsymbol{R}}\mathrm{SO}(n)$, $\boldsymbol{R} \in \mathrm{SO}(n)$ we use the fact that the rotation group $\mathrm{SO}(n)$ is a matrix group where the group operation is given by matrix multiplication. Thus, it is enough to describe the tangent space $\mathrm{T}_{\boldsymbol{I}}\mathrm{SO}(n) \subset \mathbb{R}^{n\times n}$ of this manifold at the identity element $\boldsymbol{I} \in \mathrm{SO}(n)$. More precisely, let $\gamma : (-\varepsilon,\varepsilon) \to \mathrm{SO}(n)$, $\varepsilon > 0$, be a curve with $\gamma(0) = \boldsymbol{I}$ and $\dot\gamma(0) = \boldsymbol{V} \in \mathrm{T}_{\boldsymbol{I}}\mathrm{SO}(n)$. Then for any given matrix $\boldsymbol{R} \in \mathrm{SO}(n)$ it follows that the curve $\tilde\gamma := \boldsymbol{R}\gamma$ satisfies $\tilde\gamma(0) = \boldsymbol{R}$ with $\dot{\tilde\gamma}(0) = \boldsymbol{R}\boldsymbol{V} \in \mathrm{T}_{\boldsymbol{R}}\mathrm{SO}(n)$ and we infer the relation (3.83).

By the orthogonality of the matrices in the rotation group $\mathrm{SO}(n)$ we have $\gamma(t)^\top\gamma(t) = \boldsymbol{I}$, $t \in (-\varepsilon, \varepsilon)$, which leads to

$$\boldsymbol{0} = \frac{\mathrm{d}}{\mathrm{d}t}\gamma(t)^\top\gamma(t)\Big|_{t=0} = \Big(\dot\gamma(t)^\top\gamma(t) + \gamma(t)^\top\dot\gamma(t)\Big)\Big|_{t=0} = \boldsymbol{V}^\top + \boldsymbol{V} \in \mathbb{R}^{n\times n}.$$

Hence, the tangent vector $\boldsymbol{V}$ is skew symmetric and the tangent space at $\boldsymbol{I} \in \mathrm{SO}(n)$ is given by (3.84).

Since the matrix exponential (3.82) satisfies the relation

$$\frac{\mathrm{d}}{\mathrm{d}t}\exp(t\,\boldsymbol{A}) = \boldsymbol{A}\exp(t\,\boldsymbol{A}), \qquad \boldsymbol{A} \in \mathbb{R}^{n\times n}, \qquad t \in \mathbb{R},$$

we find for the curve $\gamma_{\boldsymbol{R},\boldsymbol{V}}$ defined by (3.85) the relations

$$\dot\gamma_{\boldsymbol{R},\boldsymbol{V}}(t) = \boldsymbol{R}\tilde{\boldsymbol{V}}\boldsymbol{R}^\top\gamma_{\boldsymbol{R},\boldsymbol{V}}(t), \quad \ddot\gamma_{\boldsymbol{R},\boldsymbol{V}}(t) = (\boldsymbol{R}\tilde{\boldsymbol{V}}\boldsymbol{R}^\top)^2\gamma_{\boldsymbol{R},\boldsymbol{V}}(t), \qquad t \in \mathbb{R},$$

where $\tilde{\boldsymbol{V}} := \boldsymbol{R}^\top\boldsymbol{V}$ is a skew symmetric matrix. In order to show that the curve $\gamma_{\boldsymbol{R},\boldsymbol{V}}$ is a geodesic we let for fixed but arbitrary $t \in \mathbb{R}$ a tangent vector $\boldsymbol{W} \in \mathrm{T}_{\gamma_{\boldsymbol{R},\boldsymbol{V}}(t)}\mathrm{SO}(n)$ be given. Hence, the matrix $\tilde{\boldsymbol{W}} := \gamma_{\boldsymbol{R},\boldsymbol{V}}^\top(t)\boldsymbol{W}$ is skew symmetric and we find by the orthogonality of symmetric and skew symmetric matrices, cf. (3.81), that

$$\begin{aligned}\mathrm{tr}\,(\ddot\gamma_{\boldsymbol{R},\boldsymbol{V}}(t), \boldsymbol{W}) &= \mathrm{tr}\left(\Big((\boldsymbol{R}\tilde{\boldsymbol{V}}\boldsymbol{R}^\top)^2\gamma_{\boldsymbol{R},\boldsymbol{V}}(t)\Big)^\top\gamma_{\boldsymbol{R},\boldsymbol{V}}(t)\tilde{\boldsymbol{W}}\right)\\ &= -\mathrm{tr}\left(\Big(\boldsymbol{R}\tilde{\boldsymbol{V}}\boldsymbol{R}^\top\gamma_{\boldsymbol{R},\boldsymbol{V}}(t)\Big)^\top\Big(\boldsymbol{R}\tilde{\boldsymbol{V}}\boldsymbol{R}^\top\gamma_{\boldsymbol{R},\boldsymbol{V}}(t)\Big)\,\tilde{\boldsymbol{W}}\right) = 0.\end{aligned}$$

By definition (3.18) we conclude that the curves $\gamma_{\boldsymbol{R},\boldsymbol{V}}$ defined by (3.85) are maximal geodesics of the rotation group $\mathrm{SO}(n)$ and that the normal vector of $\boldsymbol{V}$ at $\boldsymbol{R}$ is given by (3.86).

In order to compute the geodesic distance between two matrices $\boldsymbol{R}_1, \boldsymbol{R}_2 \in \mathrm{SO}(n)$ we let $\gamma_{\overset{\frown}{\boldsymbol{R}_1,\boldsymbol{R}_2}}$: $[0,1] \to \mathrm{SO}(n)$ be a shortest geodesic joining the matrices $\boldsymbol{R}_1, \boldsymbol{R}_2$, accordingly to Theorem 3.4. Thus, letting $\boldsymbol{V} \in \mathrm{T}_{\boldsymbol{R}_1}\mathrm{SO}(n)$ be the tangent vector defined by $\boldsymbol{V} := \dot\gamma_{\overset{\frown}{\boldsymbol{R}_1,\boldsymbol{R}_2}}(0)$ we find by the uniqueness of geodesics that

$$\gamma_{\overset{\frown}{\boldsymbol{R}_1,\boldsymbol{R}_2}}(t) = \gamma_{\boldsymbol{R}_1,\boldsymbol{V}}(t) = \boldsymbol{R}_1\exp(t\tilde{\boldsymbol{V}}), \qquad t \in \mathbb{R}, \quad \tilde{\boldsymbol{V}} = \boldsymbol{R}_1^\top\boldsymbol{V} \in \mathrm{T}_{\boldsymbol{I}}\mathrm{SO}(n), \tag{3.88}$$

and

$$\mathrm{d}_{\mathrm{SO}(n)}(\boldsymbol{R}_1,\boldsymbol{R}_2) = L(\gamma_{\overset{\frown}{\boldsymbol{R}_1,\boldsymbol{R}_2}}(t)) = \int_0^1\sqrt{\mathrm{tr}\left(\dot\gamma_{\overset{\frown}{\boldsymbol{R}_1,\boldsymbol{R}_2}}^\top(t)\dot\gamma_{\overset{\frown}{\boldsymbol{R}_1,\boldsymbol{R}_2}}(t)\right)}\mathrm{d}t = \sqrt{\mathrm{tr}(\tilde{\boldsymbol{V}}^\top\tilde{\boldsymbol{V}})}. \tag{3.89}$$

Since $\tilde{\boldsymbol{V}}$ is skew symmetric it has only pure imaginary eigenvalues $\lambda_i = \mathrm{i}\alpha_i$, $\alpha_1 \geq \alpha_2 \geq \cdots \geq \alpha_n$, and can be diagonalized by a unitary matrix $\boldsymbol{U} \in \mathbb{C}^{n\times n}$. Moreover, it is seen that the eigenvalues occur in conjugate pairs, i.e., $\alpha_i = -\alpha_{n-i+1}$, $i = 1,\ldots,n$. Hence, we obtain together with equation (3.88) the relation

$$\boldsymbol{R}_1^\top\boldsymbol{R}_2 = \exp(\tilde{\boldsymbol{V}}) = \exp\left(\boldsymbol{U}\begin{pmatrix}\mathrm{i}\alpha_1 & 0 & \boldsymbol{0}\\ 0 & \ddots & 0\\ \boldsymbol{0} & 0 & \mathrm{i}\alpha_n\end{pmatrix}\overline{\boldsymbol{U}}^\top\right) = \boldsymbol{U}\begin{pmatrix}\mathrm{e}^{\mathrm{i}\alpha_1} & 0 & \boldsymbol{0}\\ 0 & \ddots & 0\\ \boldsymbol{0} & 0 & \mathrm{e}^{\mathrm{i}\alpha_n}\end{pmatrix}\overline{\boldsymbol{U}}^\top.$$

That is, the arguments of the complex eigenvalues $\mathrm{e}^{\mathrm{i}\alpha_i}$, $i = 1,\ldots,n$, of the orthogonal matrix

$\boldsymbol{R}_1^\top \boldsymbol{R}_2$ are the eigenvalues of $\tilde{\boldsymbol{V}}$. Since the trace of a matrix is invariant under unitary transformations we conclude that (3.89) simplifies to relation (3.87), and the proof is finished. ■

The three-dimensional rotation group SO(3) is of particular interest to us, so that we present more explicit formulas. The matrix exponential leads to a natural parameterization of the rotation group SO(3) by setting, cf. (3.82),

$$\boldsymbol{R}(\boldsymbol{r},\alpha) := \exp(\alpha \boldsymbol{V}_{\boldsymbol{r}}), \qquad \boldsymbol{V}_{\boldsymbol{r}} := \begin{pmatrix} 0 & -r_3 & r_2 \\ r_3 & 0 & -r_1 \\ -r_2 & r_1 & 0 \end{pmatrix}, \quad \boldsymbol{r} = \begin{pmatrix} r_1 \\ r_2 \\ r_3 \end{pmatrix} \in \mathbb{S}^2, \quad \alpha \in [0,\pi].$$

An explicit representation is given by, cf. [135, Eq. (56), p. 30],

$$\boldsymbol{R}(\boldsymbol{r},\alpha) = (1-\cos(\alpha))\boldsymbol{r}\boldsymbol{r}^\top + \begin{pmatrix} \cos(\alpha) & -r_3\sin(\alpha) & r_2\sin(\alpha) \\ r_3\sin(\alpha) & \cos(\alpha) & -r_1\sin(\alpha) \\ -r_2\sin(\alpha) & r_1\sin(\alpha) & \cos(\alpha) \end{pmatrix}, \tag{3.90}$$

and we observe that the vector $\boldsymbol{r} \in \mathbb{S}^2$ is an eigenvector of $\boldsymbol{R}(\boldsymbol{r},\alpha)$. In that respect, we denote $\boldsymbol{r}$ as the *rotation axis* and α as the *rotation angle* of $\boldsymbol{R}(\boldsymbol{r},\alpha)$. Moreover, we find that the rotation angle α of an arbitrary rotation matrix $\boldsymbol{R} \in \mathrm{SO}(3)$ can be computed by using

$$\mathrm{tr}(\boldsymbol{R}) = 1 + 2\cos(\alpha), \qquad \boldsymbol{R} \in \mathrm{SO}(3), \tag{3.91}$$

which leads to the definition

$$\alpha(\boldsymbol{R}) := \arccos\left(\frac{\mathrm{tr}(\boldsymbol{R})-1}{2}\right) = 2\arccos\left(\frac{\sqrt{\mathrm{tr}(\boldsymbol{R})+1}}{2}\right), \qquad \boldsymbol{R} \in \mathrm{SO}(3). \tag{3.92}$$

Hence, the geodesic distance on the rotation group SO(3) may be computed by, cf. (3.87),

$$\mathrm{d}_{\mathrm{SO}(3)}(\boldsymbol{R}_1,\boldsymbol{R}_2) = \Big(\alpha(\boldsymbol{R}_1^\top\boldsymbol{R}_2) + 0 + \alpha(\boldsymbol{R}_1^\top\boldsymbol{R}_2)\Big)^{\frac{1}{2}} = \sqrt{2}\,\alpha(\boldsymbol{R}_1^\top\boldsymbol{R}_2), \qquad \boldsymbol{R}_1,\boldsymbol{R}_2 \in \mathrm{SO}(3). \tag{3.93}$$

Another convenient way of parameterization the rotation group SO(3) is given by three *Euler angles*[7] $(\varphi_1,\theta,\varphi_2) \in [0,2\pi) \times [0,\pi] \times [0,2\pi)$, cf. [135, p. 21], corresponding to three successive rotations with rotation axes $\boldsymbol{e}_3 := (0,0,1)^\top, \boldsymbol{e}_2 := (0,1,0)^\top \in \mathbb{R}^3$ due to, cf. [135, Eq. (54), p. 30],

$$\begin{aligned} h(\varphi_1,\theta,\varphi_2) :=& \boldsymbol{R}(\boldsymbol{e}_3,\varphi_1)\boldsymbol{R}(\boldsymbol{e}_2,\theta)\boldsymbol{R}(\boldsymbol{e}_3,\varphi_2) \\ =& \begin{pmatrix} \cos(\varphi_1)\cos(\theta)\cos(\varphi_2)-\sin(\varphi_1)\sin(\varphi_2) & -\cos(\varphi_1)\cos(\theta)\sin(\varphi_2)-\sin(\varphi_1)\cos(\varphi_2) & \cos(\varphi_1)\sin(\theta) \\ \sin(\varphi_1)\cos(\theta)\cos(\varphi_2)+\cos(\varphi_1)\sin(\varphi_2) & -\sin(\varphi_1)\cos(\theta)\sin(\varphi_2)+\cos(\varphi_1)\cos(\varphi_2) & \sin(\varphi_1)\sin(\theta) \\ -\sin(\theta)\cos(\varphi_2) & \sin(\theta)\sin(\varphi_2) & \cos(\theta) \end{pmatrix}. \end{aligned} \tag{3.94}$$

We summarize in Theorem 3.16 the well-known properties and differential geometric formulas of the parameterization $h : [0,2\pi) \times [0,\pi] \times [0,2\pi) \to \mathrm{SO}(3)$.

Theorem 3.16. *The restriction $h\big|_\Omega$ of the parameterization $h : [0,2\pi) \times [0,\pi] \times [0,2\pi) \to \mathrm{SO}(3)$ defined by (3.94) to the open set $\Omega := (0,2\pi) \times (0,\pi) \times (0,2\pi)$ is a local parameterization, cf. Theorem 3.2, of the rotation group* SO(3) *with range*

$$h(\Omega) = \mathrm{SO}(3) \setminus \Big\{ \big(R_{i,j}\big)_{i,j=1}^3 \in \mathbb{R}^{3\times 3} \ : \ (R_{2,3} = 0 \text{ and } R_{1,3} \geq 0) \text{ or } (R_{3,2} = 0 \text{ and } R_{3,1} \leq 0) \Big\}$$

[7] There are several definitions of Euler angles found in the literature, depending on the chosen rotation axes.

and inverse

$$h^{-1}(\boldsymbol{R}) = \begin{pmatrix} 2\arctan\left(R_{2,3}/\left(R_{1,3} - \sqrt{R_{1,3}^2 + R_{2,3}^2}\right)\right) + \pi \\ \arccos(R_{3,3}) \\ 2\arctan\left(R_{3,2}/\left(-R_{3,1} - \sqrt{R_{3,1}^2 + R_{3,2}^2}\right)\right) + \pi \end{pmatrix}, \qquad \boldsymbol{R} := \left(R_{i,j}\right)_{i,j=1}^{3} \in h(\Omega).$$

Furthermore, for $\boldsymbol{R} := h(\varphi_1, \theta, \varphi_2) \in \mathrm{SO}(3) \setminus \{(R_{i,j})_{i,j=1}^3 \in \mathbb{R}^{3\times 3} \ : \ R_{3,3} = \pm 1\}$, $(\varphi_1, \theta, \varphi_2) \in [0, 2\pi) \times (0, \pi) \times [0, 2\pi)$, *the canonical basis of the tangent space* $\mathrm{T}_{\boldsymbol{R}}\mathrm{SO}(3)$, *cf.* (3.9), *is given by*

$$\begin{aligned}
\boldsymbol{h}_{\varphi_1}(\varphi_1, \theta, \varphi_2) :=& \frac{\partial}{\partial \varphi_1} h(\varphi_1, \theta, \varphi_2) \\
=& \begin{pmatrix} -\sin(\varphi_1)\cos(\theta)\cos(\varphi_2) - \cos(\varphi_1)\sin(\varphi_2) & \sin(\varphi_1)\cos(\theta)\sin(\varphi_2) - \cos(\varphi_1)\cos(\varphi_2) & -\sin(\varphi_1)\sin(\theta) \\ \cos(\varphi_1)\cos(\theta)\cos(\varphi_2) - \sin(\varphi_1)\sin(\varphi_2) & -\cos(\varphi_1)\cos(\theta)\sin(\varphi_2) - \sin(\varphi_1)\cos(\varphi_2) & \cos(\varphi_1)\sin(\theta) \\ 0 & 0 & 0 \end{pmatrix}, \\
\boldsymbol{h}_{\theta}(\varphi_1, \theta, \varphi_2) :=& \frac{\partial}{\partial \theta} h(\varphi_1, \theta, \varphi_2) \\
=& \begin{pmatrix} -\cos(\varphi_1)\sin(\theta)\cos(\varphi_2) & \cos(\varphi_1)\sin(\theta)\sin(\varphi_2) & \cos(\varphi_1)\cos(\theta) \\ -\sin(\varphi_1)\sin(\theta)\cos(\varphi_2) & \sin(\varphi_1)\sin(\theta)\sin(\varphi_2) & \sin(\varphi_1)\cos(\theta) \\ -\cos(\theta)\cos(\varphi_2) & \cos(\theta)\sin(\varphi_2) & -\sin(\theta) \end{pmatrix}, \\
\boldsymbol{h}_{\varphi_2}(\varphi_1, \theta, \varphi_2) :=& \frac{\partial}{\partial \varphi_2} h(\varphi_1, \theta, \varphi_2) \\
=& \begin{pmatrix} -\cos(\varphi_1)\cos(\theta)\sin(\varphi_2) - \sin(\varphi_1)\cos(\varphi_2) & -\cos(\varphi_1)\cos(\theta)\cos(\varphi_2) + \sin(\varphi_1)\sin(\varphi_2) & 0 \\ -\sin(\varphi_1)\cos(\theta)\sin(\varphi_2) + \cos(\varphi_1)\cos(\varphi_2) & -\sin(\varphi_1)\cos(\theta)\cos(\varphi_2) - \cos(\varphi_1)\sin(\varphi_2) & 0 \\ \sin(\theta)\sin(\varphi_2) & \sin(\theta)\cos(\varphi_2) & 0 \end{pmatrix},
\end{aligned}$$

where the corresponding matrix representation of the induced Riemannian structure $g_{\mathrm{SO}(3)}$, *cf.* (3.13), *reads as*

$$\boldsymbol{G}_h(\varphi_1, \theta, \varphi_2) = \begin{pmatrix} 2 & 0 & 2\cos(\theta) \\ 0 & 2 & 0 \\ 2\cos(\theta) & 0 & 2 \end{pmatrix}, \qquad (\varphi_1, \theta, \varphi_2) \in [0, 2\pi) \times (0, \pi) \times [0, 2\pi),$$

and the Christoffel symbols of the second kind, cf. (3.19), *are given in matrix form, cf.* (3.20), *by*

$$\begin{aligned}
\boldsymbol{\Gamma}_h^{\varphi_1}(\varphi_1, \theta, \varphi_2) &= \begin{pmatrix} \Gamma_h(\varphi_1,\theta,\varphi_2)_{\varphi_1,\varphi_1}^{\varphi_1} & \Gamma_h(\varphi_1,\theta,\varphi_2)_{\varphi_1,\theta}^{\varphi_1} & \Gamma_h(\varphi_1,\theta,\varphi_2)_{\varphi_1,\varphi_2}^{\varphi_1} \\ \Gamma_h(\varphi_1,\theta,\varphi_2)_{\theta,\varphi_1}^{\varphi_1} & \Gamma_h(\varphi_1,\theta,\varphi_2)_{\theta,\theta}^{\varphi_1} & \Gamma_h(\varphi_1,\theta,\varphi_2)_{\theta,\varphi_2}^{\varphi_1} \\ \Gamma_h(\varphi_1,\theta,\varphi_2)_{\varphi_2,\varphi_1}^{\varphi_1} & \Gamma_h(\varphi_1,\theta,\varphi_2)_{\varphi_2,\theta}^{\varphi_1} & \Gamma_h(\varphi_1,\theta,\varphi_2)_{\varphi_2,\varphi_2}^{\varphi_1} \end{pmatrix} = \frac{1}{2}\begin{pmatrix} 0 & \cot(\theta) & 0 \\ \cot(\theta) & 0 & -\sin(\theta)^{-1} \\ 0 & -\sin(\theta)^{-1} & 0 \end{pmatrix}, \\
\boldsymbol{\Gamma}_h^{\theta}(\varphi_1, \theta, \varphi_2) &= \begin{pmatrix} \Gamma_h(\varphi_1,\theta,\varphi_2)_{\varphi_1,\varphi_1}^{\theta} & \Gamma_h(\varphi_1,\theta,\varphi_2)_{\varphi_1,\theta}^{\theta} & \Gamma_h(\varphi_1,\theta,\varphi_2)_{\varphi_1,\varphi_2}^{\theta} \\ \Gamma_h(\varphi_1,\theta,\varphi_2)_{\theta,\varphi_1}^{\theta} & \Gamma_h(\varphi_1,\theta,\varphi_2)_{\theta,\theta}^{\theta} & \Gamma_h(\varphi_1,\theta,\varphi_2)_{\theta,\varphi_2}^{\theta} \\ \Gamma_h(\varphi_1,\theta,\varphi_2)_{\varphi_2,\varphi_1}^{\theta} & \Gamma_h(\varphi_1,\theta,\varphi_2)_{\varphi_2,\theta}^{\theta} & \Gamma_h(\varphi_1,\theta,\varphi_2)_{\varphi_2,\varphi_2}^{\theta} \end{pmatrix} = \frac{1}{2}\begin{pmatrix} 0 & 0 & \sin(\theta) \\ 0 & 0 & 0 \\ \sin(\theta) & 0 & 0 \end{pmatrix}, \\
\boldsymbol{\Gamma}_h^{\varphi_2}(\varphi_1, \theta, \varphi_2) &= \begin{pmatrix} \Gamma_h(\varphi_1,\theta,\varphi_2)_{\varphi_1,\varphi_1}^{\varphi_2} & \Gamma_h(\varphi_1,\theta,\varphi_2)_{\varphi_1,\theta}^{\varphi_2} & \Gamma_h(\varphi_1,\theta,\varphi_2)_{\varphi_1,\varphi_2}^{\varphi_2} \\ \Gamma_h(\varphi_1,\theta,\varphi_2)_{\theta,\varphi_1}^{\varphi_2} & \Gamma_h(\varphi_1,\theta,\varphi_2)_{\theta,\theta}^{\varphi_2} & \Gamma_h(\varphi_1,\theta,\varphi_2)_{\theta,\varphi_2}^{\varphi_2} \\ \Gamma_h(\varphi_1,\theta,\varphi_2)_{\varphi_2,\varphi_1}^{\varphi_2} & \Gamma_h(\varphi_1,\theta,\varphi_2)_{\varphi_2,\theta}^{\varphi_2} & \Gamma_h(\varphi_1,\theta,\varphi_2)_{\varphi_2,\varphi_2}^{\varphi_2} \end{pmatrix} = \frac{1}{2}\begin{pmatrix} 0 & -\sin(\theta)^{-1} & 0 \\ -\sin(\theta)^{-1} & 0 & \cot(\theta) \\ 0 & \cot(\theta) & 0 \end{pmatrix}.
\end{aligned}$$

The canonical measure is given by the density

$$\mathrm{d}\mu_{\mathrm{SO}(3)}(\boldsymbol{R}) = 2\sqrt{2}\sin(\theta)\mathrm{d}\varphi_1\mathrm{d}\theta\mathrm{d}\varphi_2, \qquad \boldsymbol{R} := h(\varphi_1, \theta, \varphi_2), \ (\varphi_1, \theta, \varphi_2) \in \Omega. \tag{3.95}$$

Proof. The assertions are obtained by straightforward application of the corresponding definitions given in Section 3.1.2– 3.1.4. ■

Remark 3.17. On the rotation group SO(3) we will use for convenience normalized versions of the geodesic distance $\mathrm{d}_{\mathrm{SO}(3)}$ and the canonical measure $\mu_{\mathrm{SO}(3)}$, since these are more common in the literature. Therefore, by abuse of notation we will always refer on the rotation group SO(3) to the geodesic distance defined by, cf. (3.93),

$$\mathrm{d}_{\mathrm{SO}(3)}(\boldsymbol{R}_1, \boldsymbol{R}_2) := \alpha(\boldsymbol{R}_1^\top \boldsymbol{R}_2), \qquad \boldsymbol{R}_1, \boldsymbol{R}_2 \in \mathrm{SO}(3), \tag{3.96}$$

and to the canonical measure $\mu_{\mathrm{SO}(3)}$ defined by the density, cf. (3.95),

$$\mathrm{d}\mu_{\mathrm{SO}(3)}(\boldsymbol{R}) := \sin(\theta)\mathrm{d}\varphi_1\mathrm{d}\theta\mathrm{d}\varphi_2, \qquad \boldsymbol{R} := h(\varphi_1, \theta, \varphi_2),\ (\varphi_1, \theta, \varphi_2) \in \Omega. \tag{3.97}$$

These formulas are obtained by defining the Riemannian structure appropriately by a scaling of $1/2$, but this is not the Riemannian structure induced by the Euclidean space $\mathbb{R}^{n^2} \cong \mathbb{R}^{n\times n}$, which we actually use. We note further that the canonical measure $\mu_{\mathrm{SO}(3)}$ is a translational invariant Haar measure, cf. [47, Sec. 2.2], i.e., for any measurable set $O \subset \mathrm{SO}(3)$ it satisfies the relation

$$\mu_{\mathrm{SO}(3)}(O) = \mu_{\mathrm{SO}(3)}(\boldsymbol{R}\,O), \qquad \boldsymbol{R}\,O := \{\boldsymbol{R}\boldsymbol{O} \ :\ \boldsymbol{O} \in O\}, \quad \boldsymbol{R} \in \mathrm{SO}(3). \qquad \square$$

3.3 Optimization

In this Section we let $\mathcal{M} \subset \mathbb{R}^n$ be a complete d-dimensional Riemannian manifold, where we are interested in the computation of optimal points $\boldsymbol{x}_* \in \mathcal{M}$ of a given sufficiently smooth function $f : \mathcal{M} \to \mathbb{R}$, say f is twice continuously differentiable, see Section 3.1.5.

Therefore, we recall the basic definitions. We call $\boldsymbol{x}_* \in \mathcal{M}$ a *global minimizer of* $f : \mathcal{M} \to \mathbb{R}$ if

$$f(\boldsymbol{x}_*) \le f(\boldsymbol{x}), \qquad \boldsymbol{x} \in \mathcal{M}.$$

and say that $\boldsymbol{x}_*$ is a *local minimizer of* f if there exists an open neighborhood of $\boldsymbol{x}_*$, i.e., $\boldsymbol{x} \in \mathcal{M} \cap U$, $U \subset \mathbb{R}^n$ open, such that

$$f(\boldsymbol{x}_*) \le f(\boldsymbol{x}), \qquad \boldsymbol{x} \subset \mathcal{M} \cap U. \tag{3.98}$$

If additionally there is strict inequality in (3.98) we call $\boldsymbol{x}_*$ a *strict local minimizer of* f. Obviously, a global minimizer is a local minimizer. By these definitions we call the function values of a global and local minimizer, a *global* and *local minimum*, respectively.

For compact manifolds $\mathcal{M}$ the existence of a global minimizer of a continuous function $f : \mathcal{M} \to \mathbb{R}$ is assured, and so that of a local minimizer. For local minimizers the usual necessary and sufficient conditions on Riemannian manifolds are given in Theorem 3.18, which follow immediately from the well-known conditions of local minimizers in Euclidean space, cf. [96, Theorem 2.2.–2.4.], and the use of normal coordinates, as in the proof of Corollary 3.8. However, we prove Theorem 3.18 by adapting the ideas of the standard proof in the Euclidean setting to Riemannian manifolds, since the optimization methods are similarly investigated by the use of curves.

Theorem 3.18. *Let a complete d-dimensional Riemannian manifold $\mathcal{M} \subset \mathbb{R}^n$, a function $f : \mathcal{M} \to \mathbb{R}$, and a point $\boldsymbol{x}_* \in \mathcal{M} \cap U$, $U \subset \mathbb{R}^n$ open, be given. If the point $\boldsymbol{x}_*$ is a local minimizer of f, cf.* (3.98)*, then the conditions, cf.* (3.34)*,*

$$\nabla_{\mathcal{M}} f(\boldsymbol{x}_*) = \boldsymbol{0} \in \mathrm{T}_{\boldsymbol{x}}\mathcal{M} \tag{3.99}$$

and, cf. (3.35)*,*

$$\mathrm{H}_{\mathcal{M}} f(\boldsymbol{x}_*)(\boldsymbol{v}, \boldsymbol{v}) \ge 0, \qquad \boldsymbol{v} \in \mathrm{T}_{\boldsymbol{x}_*}\mathcal{M}, \tag{3.100}$$

are necessarily fulfilled whenever f is once and twice continuously differentiable on $\mathcal{M} \cap U$,

respectively. If f is twice continuously differentiable on $\mathcal{M} \cap U$ with

$$\nabla_{\mathcal{M}} f(\boldsymbol{x}_*) = \mathbf{0}, \qquad \mathrm{H}_{\mathcal{M}} f(\boldsymbol{x}_*)(\boldsymbol{v}, \boldsymbol{v}) > 0, \qquad \boldsymbol{v} \in \mathrm{T}_{\boldsymbol{x}_*}\mathcal{M} \setminus \{\mathbf{0}\}, \tag{3.101}$$

then $\boldsymbol{x}_*$ is a strict local minimizer of f.

Proof. Let $\boldsymbol{x}_* \in \mathcal{M}$ be a local minimizer of $f : \mathcal{M} \to \mathbb{R}$. Then by definition (3.98) there exists a neighborhood $\mathcal{M} \cap \tilde{U}$, $\tilde{U} \subset U \subset \mathbb{R}^n$ open, of $\boldsymbol{x}_*$ such that for any curve $\gamma : (-\varepsilon, \varepsilon) \to \mathcal{M} \cap \tilde{U}$ with $\gamma(0) = \boldsymbol{x}_*$ we have for $t \in (0, \varepsilon)$ by the Mean Value Theorem the relation, cf. (3.45),

$$0 \leq f \circ \gamma(t) - f \circ \gamma(0) = t \, \frac{\mathrm{d}}{\mathrm{d}s} f \circ \gamma(s)\Big|_{s=\zeta} = t \, \nabla_{\mathcal{M}} f(\gamma(\zeta))^{\top} \dot{\gamma}(\zeta),$$

for some $\zeta \in (0, t)$, whenever f is once continuously on $\mathcal{M} \cap \tilde{U}$. Since the curve γ and $t \in (0, \varepsilon)$ is arbitrary we conclude by the continuity of $\nabla_{\mathcal{M}} f$ that

$$0 \leq \nabla_{\mathcal{M}} f(\boldsymbol{x}_*)^{\top} \boldsymbol{v}, \qquad \boldsymbol{v} \in \mathrm{T}_{\boldsymbol{x}_*}\mathcal{M},$$

which leads with $\nabla_{\mathcal{M}} f(\boldsymbol{x}_*) \in \mathrm{T}_{\boldsymbol{x}_*}\mathcal{M}$ to the assertion (3.99).

If f is twice continuously differentiable we can use the mean value remainder in the Theorem of Taylor, cf. (3.46), which reads for $t \in (0, \varepsilon)$ together with $\nabla_{\mathcal{M}} f(\boldsymbol{x}_*) = \mathbf{0}$ as

$$0 \leq f \circ \gamma(t) - f \circ \gamma(0) = \frac{t^2}{2} \frac{\mathrm{d}^2}{\mathrm{d}s^2} f \circ \gamma(s)\Big|_{s=\zeta} = \frac{t^2}{2} \mathrm{H}_{\mathcal{M}} f(\gamma(\zeta))(\dot{\gamma}(\zeta), \dot{\gamma}(\zeta)),$$

for some $\zeta \in (0, t)$. Similarly, as in the previous case, we conclude by the continuity of $\mathrm{H}_{\mathcal{M}} f$ the assertion (3.100).

For proving the last statement we find for every point $\boldsymbol{x}_* \in \mathcal{M}$ fulfilling (3.101) by continuity of $\mathrm{H}_{\mathcal{M}} f$ an open ball $\mathring{B}_{\mathcal{M}}(\boldsymbol{x}_*, r) = \{\boldsymbol{x} \in \mathcal{M} \ : \ \mathrm{d}_{\mathcal{M}}(\boldsymbol{x}_*, \boldsymbol{x}) < r\} \subset \mathcal{M} \cap U$ of radius $r > 0$ such that

$$\mathrm{H}_{\mathcal{M}} f(\boldsymbol{x})(\boldsymbol{v}, \boldsymbol{v}) > 0, \qquad \boldsymbol{v} \in \mathrm{T}_{\boldsymbol{x}}\mathcal{M} \setminus \{\mathbf{0}\}, \qquad \boldsymbol{x} \in \mathring{B}_{\mathcal{M}}(\boldsymbol{x}_*, r).$$

Since $\mathcal{M}$ is complete we can join the point $\boldsymbol{x}_*$ with any point $\boldsymbol{x} \in \mathring{B}_{\mathcal{M}}(\boldsymbol{x}_*, r)$ by a geodesic $\gamma_{\overset{\frown}{\boldsymbol{x}_*, \boldsymbol{x}}} : [0, 1] \to \mathcal{M}$ which is seen to run entirely in $\mathring{B}_{\mathcal{M}}(\boldsymbol{x}_*, r)$, cf. (3.24) in Theorem 3.4. Then again with the Mean Value Theorem, we obtain the relation

$$f(\boldsymbol{x}) - f(\boldsymbol{x}_*) = \frac{1}{2} \mathrm{H}_{\mathcal{M}} f(\gamma_{\overset{\frown}{\boldsymbol{x}_*, \boldsymbol{x}}}(\zeta))(\dot{\gamma}_{\overset{\frown}{\boldsymbol{x}_*, \boldsymbol{x}}}(\zeta), \dot{\gamma}_{\overset{\frown}{\boldsymbol{x}_*, \boldsymbol{x}}}(\zeta)) > 0,$$

for some $\zeta \in (0, 1)$, and the proof is finished. ∎

A point $\boldsymbol{x}_* \in \mathcal{M}$ which satisfies the necessary condition (3.99) in Theorem 3.18 is called a *stationary point of f*. We note further that a strict local minimizer need not to satisfy the sufficient condition (3.101), nor is the necessary condition (3.100) sufficient for a local minimizer.

Remark 3.19. In general there are no tests for identifying a global minimizer until all potential points have been checked, which could be indefinitely many. Hence, global optimization is intrinsically a very tough problem and plenty of global optimization strategies have been proposed, cf. [69, 98]. Moreover, even the determination of local minimizers can be very hard, in particular for high dimensions d. Therefore, we are primarily interested in the computation of stationary points, where we may additionally check the conditions given in Theorem 3.18. □

For the numerical computation of a local minimizer, or to be more precise, of a stationary point, we introduce in Section 3.3.1 the method of steepest descent, Newton's method, and the method of conjugate gradients, which are standard optimization algorithms of the class of

descent methods. These methods have been established in various applications and are well-studied. In the case of Euclidean space $\mathbb{R}^n$ we refer to the monographs [33, 99, 96], and for recent generalizations to Riemannian manifolds we refer to [131, 120]. In Section 3.3.2 we present global and local convergence results for these methods, by imitating the proofs of the well-know results in Euclidean space. The central result for global convergence is Theorem 3.25, which is an adapted version of a theorem attributed to Zoutendijk. The local convergence rates presented in Theorem 3.27 are well-know results for the Euclidean space, which have been adapted to Riemannian manifolds essentially by Smith [120]. We illustrate these results by some numerical examples given in Section 3.3.3, which show that the method of conjugate gradient is particular suitable for high dimensional problems if efficient algorithms for the matrix-vector multiplication with the Hessian matrix are available.

3.3.1 Descent Methods

The optimization methods of consideration are straightforward generalizations of the method of steepest descent, Newton's method and the nonlinear conjugate gradient method in Euclidean space $\mathbb{R}^n$. Moreover, they fit into the general class of iterative methods which start from an initial point $\boldsymbol{x}^{(0)} \in \mathcal{M}$ and generate a sequence $\{\boldsymbol{x}^{(k)}\}_{k\in\mathbb{N}_0} \subset \mathcal{M}$ accordingly to the iteration, cf. (3.22),

$$\boldsymbol{x}^{(k+1)} := \gamma_{\boldsymbol{x}^{(k)},\boldsymbol{d}^{(k)}}(\alpha^{(k)}) \in \mathcal{M}, \qquad k = 0, 1, \ldots, \tag{3.102}$$

where $\boldsymbol{d}^{(k)} \in \mathrm{T}_{\boldsymbol{x}^{(k)}}\mathcal{M}$ is called the *search direction* and $\alpha^{(k)} \in \mathbb{R}$ the *step length*.[8] The search direction $\boldsymbol{d}^{(k)}$ and the current iteration point $\boldsymbol{x}^{(k)}$ define the univariate function

$$L^{(k)}(t) := f \circ \gamma_{\boldsymbol{x}^{(k)},\boldsymbol{d}^{(k)}}(t), \qquad t \in \mathbb{R}, \tag{3.103}$$

which is used for the determination of the step length $\alpha^{(k)}$, and so the next iteration point $\boldsymbol{x}^{(k+1)}$. Accordingly to the above definition, the search direction $\boldsymbol{d}^{(k)} \in \mathrm{T}_{\boldsymbol{x}^{(k)}}\mathcal{M}$ is called a *descent direction* at $\boldsymbol{x}^{(k)}$ if

$$L^{(k)\prime}(0) = \frac{\mathrm{d}}{\mathrm{d}t} f \circ \gamma_{\boldsymbol{x}^{(k)},\boldsymbol{d}^{(k)}}(t)\big|_{t=0} = \nabla_{\mathcal{M}} f(\boldsymbol{x}^{(k)})^{\top} \boldsymbol{d}^{(k)} < 0. \tag{3.104}$$

An iterative method of the form (3.102) is called a *descent method* if it generates exclusively descent directions $\boldsymbol{d}^{(k)}$ and step lengths $\alpha^{(k)} > 0$ whenever $\nabla_{\mathcal{M}} f(\boldsymbol{x}^{(k)}) \neq \mathbf{0}$ or sets $\boldsymbol{d}^{(k)} := \nabla_{\mathcal{M}} f(\boldsymbol{x}^{(k)}) = \mathbf{0}$.

The determination of effective search directions $\boldsymbol{d}^{(k)}$ and step lengths $\alpha^{(k)}$ is crucial for the success of such iterative methods and we refer to the convergence results given in Section 3.3.2. The computation of a reasonable step size $\alpha^{(k)} > 0$ is usually referred to as *line search*. Before we go into the details of the line search, we briefly describe the generalizations of the well-known and commonly used descent methods to Riemannian manifolds.

Example 3.20. For describing the conceptional ideas we assume that $f : \mathcal{M} \to [f_0, \infty)$, $f_0 \in \mathbb{R}$, is sufficiently smooth and that the initial point $\boldsymbol{x}^{(0)} \in \mathcal{M}$ is sufficiently close to a local minimizer with positive definite Hessian. If these assumptions are not fulfilled then the Newton method and the method of conjugate gradients given in this example are in general no descent methods and convergence to stationary points is not guaranteed. However, globally convergent modifications are given by Algorithm 3.2 and 3.3.

[8] In the Euclidean space $\mathcal{M} = \mathbb{R}^d$ the iteration becomes the more familiar form $\boldsymbol{x}^{(k+1)} := \boldsymbol{x}^{(k)} + \alpha^{(k)}\boldsymbol{d}^{(k)}$, $k = 0, 1, \ldots$.

The method of steepest descent is obtained by setting

$$\boldsymbol{x}^{(k+1)} := \gamma_{\boldsymbol{x}^{(k)},\boldsymbol{d}^{(k)}}(\alpha^{(k)}), \qquad \boldsymbol{d}^{(k)} := -\nabla_{\mathcal{M}} f(\boldsymbol{x}^{(k)}) \in \mathrm{T}_{\boldsymbol{x}^{(k)}}\mathcal{M}, \qquad k = 0, 1, \ldots, \tag{3.105}$$

where $\alpha^{(k)}$ is determined by a line search. This method is a straight forward generalization of the method of steepest descent in Euclidean space to Riemannian manifolds $\mathcal{M}$, since by Corollary 3.7 the negative gradient shows in the direction of steepest descent.

The Newton method reads as

$$\boldsymbol{x}^{(k+1)} := \gamma_{\boldsymbol{x}^{(k)},\boldsymbol{d}^{(k)}}(1), \qquad k = 0, 1, \ldots, \tag{3.106}$$

where the descent direction $\boldsymbol{d}^{(k)} \in \mathrm{T}_{\boldsymbol{x}^{(k)}}\mathcal{M}$ is determined by the requirement[9]

$$\mathrm{H}_{\mathcal{M}} f(\boldsymbol{x}^{(k)})(\boldsymbol{d}^{(k)}, \boldsymbol{v}) = -\nabla_{\mathcal{M}} f(\boldsymbol{x}^{(k)})^{\top} \boldsymbol{v}, \qquad \boldsymbol{v} \in \mathrm{T}_{\boldsymbol{x}^{(k)}}\mathcal{M}. \tag{3.107}$$

The motivation of this method is that near a local minimizer with positive definite Hessian the function f may admit a good quadratic approximation. To be more precise, at the point $\boldsymbol{x}^{(k)} \in \mathcal{M}$ the quadratic function $Q_{\boldsymbol{x}^{(k)}} : \mathrm{T}_{\boldsymbol{x}^{(k)}}\mathcal{M} \to \mathbb{R}$ given by

$$Q_{\boldsymbol{x}^{(k)}}(\boldsymbol{v}) := f(\boldsymbol{x}^{(k)}) + \nabla_{\mathcal{M}} f(\boldsymbol{x}^{(k)})^{\top} \boldsymbol{v} + \frac{1}{2} \mathrm{H} f(\boldsymbol{x}^{(k)})(\boldsymbol{v}, \boldsymbol{v}), \qquad \boldsymbol{v} \in \mathrm{T}_{\boldsymbol{x}^{(k)}}\mathcal{M},$$

is the best second order approximation to the function $f_{\boldsymbol{x}^{(k)}}(\boldsymbol{v}) = f \circ \exp_{\boldsymbol{x}^{(k)}}(\boldsymbol{v})$, $\boldsymbol{v} \in \mathrm{T}_{\boldsymbol{x}^{(k)}}\mathcal{M}$, cf. Corollary 3.8. If the Hessian $\mathrm{H}_{\mathcal{M}} f(\boldsymbol{x}^{(k)})$ is positive definite it is readily seen that the minimizer of $Q_{\boldsymbol{x}^{(k)}}$ is given by the uniquely determined vector $\boldsymbol{d}^{(k)}$ satisfying (3.107). Hence, by setting $\boldsymbol{x}^{(k+1)} := \exp_{\boldsymbol{x}^{(k)}}(\boldsymbol{d}^{(k)})$ we arrive with relation (3.28) at the iteration (3.106).

The method of conjugate gradients (CG) is given by the iteration

$$\boldsymbol{x}^{(k+1)} := \gamma_{\boldsymbol{x}^{(k)},\boldsymbol{d}^{(k)}}(\alpha^{(k)}), \qquad \boldsymbol{d}^{(k+1)} := -\boldsymbol{g}^{(k+1)} + \beta^{(k)} \tilde{\boldsymbol{d}}^{(k)} \in \mathrm{T}_{\boldsymbol{x}^{(k+1)}}\mathcal{M}, \qquad k = 0, 1, \ldots, \tag{3.108}$$

where $\boldsymbol{g}^{(k)} := \nabla_{\mathcal{M}} f(\boldsymbol{x}^{(k)}) \in \mathrm{T}_{\boldsymbol{x}^{(k)}}\mathcal{M}$ and $\boldsymbol{d}^{(0)} := -\boldsymbol{g}^{(0)} \in \mathrm{T}_{\boldsymbol{x}^{(0)}}\mathcal{M}$ is the initial search direction. In this method we need to introduce the *parallel vector* $\tilde{\boldsymbol{d}}^{(k)}$ of $\boldsymbol{d}^{(k)}$ at $\boldsymbol{x}^{(k+1)}$ defined by

$$\tilde{\boldsymbol{d}}^{(k)} := \dot{\gamma}_{\boldsymbol{x}^{(k)},d^{(k)}}(\alpha^{(k)}) \in \mathrm{T}_{\boldsymbol{x}^{(k+1)}}\mathcal{M}.$$

The choice of the parameter $\beta^{(k)}$ in (3.108) leads to several well-known conjugate gradient methods. In the case of Euclidean space an overview is given in [61]. For instance the CG method proposed by Daniel in [31] adapted to Riemannian manifolds, replaces the scalar $\beta^{(k)}$ by

$$\beta_{\mathrm{D}}^{(k)} := \frac{\mathrm{H}_{\mathcal{M}} f(\boldsymbol{x}^{(k+1)})(\boldsymbol{g}^{(k+1)}, \tilde{\boldsymbol{d}}^{(k)})}{\mathrm{H}_{\mathcal{M}} f(\boldsymbol{x}^{(k+1)})(\tilde{\boldsymbol{d}}^{(k)}, \tilde{\boldsymbol{d}}^{(k)})}. \tag{3.109}$$

Finally, the step size $\alpha^{(k)}$ is given by a line search. For an illustration of the CG method on the sphere $\mathbb{S}^2$ see Figure 3.2. □

Remark 3.21. The method of steepest descent is the simplest descent method, which admits a strong convergence analysis. However, it suffers from a very slow convergence, as seen by Theorem 3.27.

[9] In the Euclidean space $\mathcal{M} = \mathbb{R}^d$ this is equivalent to $\boldsymbol{d}^{(k)} := -\mathbf{H} f(\boldsymbol{x}^{(k)})^{-1} \nabla f(\boldsymbol{x}^{(k)})$.

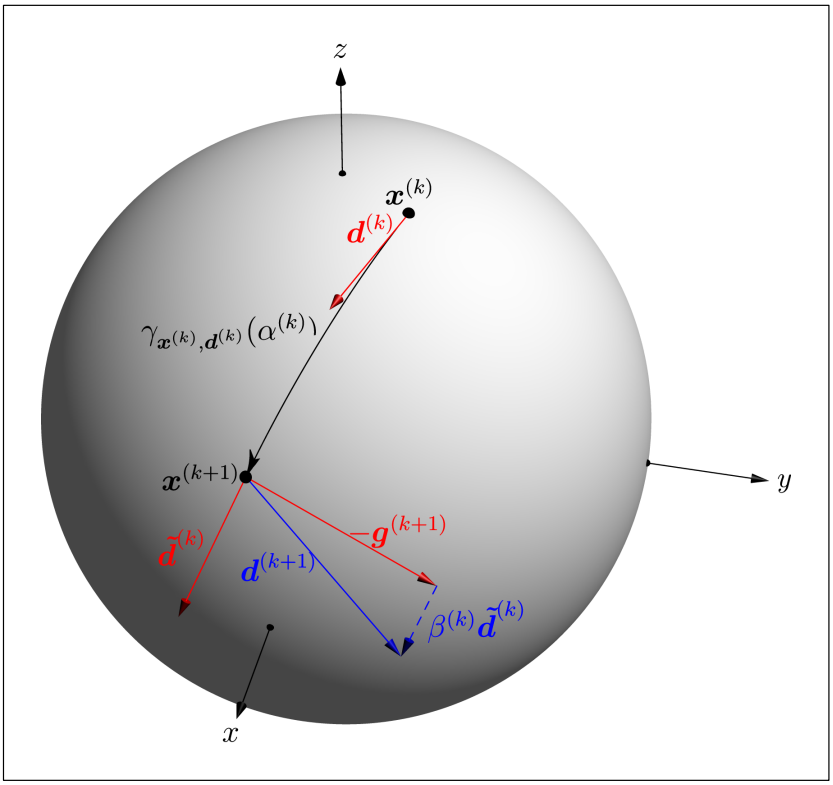

Figure 3.2: Illustration of the kth CG-iteration step on the sphere $\mathbb{S}^2$ at a point $\boldsymbol{x}^{(k)}$ in direction $\boldsymbol{d}^{(k)} \in \mathrm{T}_{\boldsymbol{x}^{(k)}}\mathbb{S}^2$, cf. Algorithm 3.3.

In contrast, the Newton method is more sophisticated and has a rapid convergence nearby a local minimizer with positive definite Hessian, cf. Theorem 3.27. However, it suffers from serious instability problems if the sufficient conditions are not met, and thus needs to be stabilized or globalized, as for example in Algorithm 3.2. Furthermore, the determination of the Newton step, by solving an equation system with the Hessian matrix, cf. (3.107), might be far to expensive for large scale problems, which we are especially interested in.

The method of conjugate gradients turns out to be a reasonable trade of between stability and convergence rate, cf. Theorem 3.27. It was first proposed by Hestenes and Stiefel [67] for solving large systems of linear equations. Subsequently, it was extended for the optimization of twice continuously differentiable functions in Euclidean space by Fletcher and Reeves [44], by using the same idea of quadratic approximation which motivates Newton's method. Generalizations to nonlinear operator equations in Hilbert spaces and Riemannian manifolds seem to be given the first time by Daniel [31] and Smith [121], respectively. Conjugate gradient methods with other update rules than (3.109) try to approximate the Hessian by means of finite differences. However, for the applications given in Chapter 6, we can rely on the assumption that the computation of the matrix-vector product with the Hessian is not very expansive, see Chapter 5, so that we stick to the conjugate gradient method with update rule (3.109).

We like to mention that the presented methods do not need the general notion of parallel transport, as it is demonstrated in [121, 38], which also simplifies the computations to this respect. For the general definiton of parallel transport we refer to the literature [66, 124].

Finally, we present a numerical comparison between slightly modified versions of these methods in Example 3.30 of Section 3.3.3. □

The Line Search

The search of a reasonable step length in an iterative optimization method of the form (3.102) can be considered as a generic one-dimensional optimization problem. Therefore, we let $f : \mathcal{M} \to [f_0, \infty)$, $f_0 \in \mathbb{R}$, be a continuously differentiable function and consider for a point $\boldsymbol{x} \in \mathcal{M}$ and a search direction $\boldsymbol{d} \in \mathrm{T}_{\boldsymbol{x}}\mathcal{M}$ the function $L := f \circ \gamma_{\boldsymbol{x},\boldsymbol{d}} : \mathbb{R} \to \mathbb{R}$, cf. (3.103).

The ideal choice of a step length would be a global minimizer of $f \circ \gamma_{\boldsymbol{x},\boldsymbol{d}}$, provided that such a point exists. By Theorem 3.18, a necessary condition of a global minimum α_* would be

$$L'(\alpha_*) = \frac{\mathrm{d}}{\mathrm{d}t} f \circ \gamma_{\boldsymbol{x},\boldsymbol{d}}(t)\big|_{t=\alpha_*} = 0. \tag{3.110}$$

For descent directions $\boldsymbol{d}$, cf. (3.104), the determination of a step length $\alpha_* > 0$ satisfying (3.110) is referred to as *exact line search*. However, for most instances an exact line search is impractical so that it is only of theoretic interest to us, cf. Theorem 3.27 and Remark 3.28.

More practical conditions for reasonable step lengths $\alpha > 0$ for descent directions $\boldsymbol{d}$ are given by what is known as the *Wolfe conditions*

$$L(\alpha) - L(0) = f \circ \gamma_{\boldsymbol{x},\boldsymbol{d}}(\alpha) - f \circ \gamma_{\boldsymbol{x},\boldsymbol{d}}(0) \quad \leq \quad \mu\alpha \frac{\mathrm{d}}{\mathrm{d}t} f \circ \gamma_{\boldsymbol{x},\boldsymbol{d}}(t)\Big|_{t=0} = \mu\alpha L'(0), \tag{3.111}$$

$$L'(\alpha) = \frac{\mathrm{d}}{\mathrm{d}t} f \circ \gamma_{\boldsymbol{x},\boldsymbol{d}}(t)\big|_{t=\alpha} \quad \geq \quad \eta \frac{\mathrm{d}}{\mathrm{d}t} f \circ \gamma_{\boldsymbol{x},\boldsymbol{d}}(t)\Big|_{t=0} = \eta L'(0), \tag{3.112}$$

where $0 < \mu < \eta < 1$ are fixed constants. The first relation (3.111) ensures a sufficient decrease of the function values, whereas the second relation (3.112) is a useful criterion for keeping $\alpha > 0$ big enough such that convergence results can be obtained, cf. Theorem 3.25. An algorithm witch determines a step length $\alpha > 0$ such that the Wolfe conditions (3.111), (3.112) are satisfied is called an *inexact line search with Wolfe conditions*. Note, since the search direction $\boldsymbol{d} \in \mathrm{T}_{\boldsymbol{x}}\mathcal{M}$ is a descent direction, an exact line search, cf. (3.110), satisfies the second condition (3.112) trivially. Nevertheless, we need proof that the Wolfe conditions can both be satisfied, at least for functions f which are bounded from below.

Theorem 3.22. *Let $\mathcal{M} \subset \mathbb{R}^n$ be a complete d-dimensional Riemannian manifold and $f : \mathcal{M} \to [f_0, \infty)$, $f_0 \in \mathbb{R}$, be a function which is continuously differentiable at $\boldsymbol{x} \in \mathcal{M}$. If $\boldsymbol{d} \in \mathrm{T}_{\boldsymbol{x}}\mathcal{M}$ is a descent direction, cf. (3.104), and the function $L := f \circ \gamma_{\boldsymbol{x},\boldsymbol{d}}$, cf. (3.22), is continuously differentiable, then, for fixed constants $0 < \mu < \eta < 1$, there exists an open interval*

$$I \subset [0, \alpha_{\max}], \qquad \alpha_{\max} := \frac{f_0 - L(0)}{\mu L'(0)},$$

such that the Wolfe conditions (3.111), (3.112) are satisfied for $\alpha \in I$.

Proof. We follow the proof of [96, Lemma 3.1]. Since, the function L is bounded from below by f_0 there exist a value $\tilde{\alpha}$ such that graph of $l(t) := L(0) + \mu t L'(0)$, $t > 0$, intersects the graph of L, i.e.,

$$L(\tilde{\alpha}) = l(\tilde{\alpha}) = L(0) + \mu\tilde{\alpha}L'(0). \tag{3.113}$$

Clearly, $\tilde{\alpha} \leq \alpha_{\max}$ since this is the intersection point of the line l with the constant function defined by the lower bound f_0. Since L is continuously differentiable there exists a smallest step length with property (3.113), which we denote by $\tilde{\alpha}$. It follows that the first Wolfe condition (3.111) is satisfied for every step length $\alpha \in (0, \tilde{\alpha})$.

By the Mean Value Theorem, there exists $\tilde{\alpha}' \in (0, \tilde{\alpha})$ such that

$$L(\tilde{\alpha}) - L(0) = \tilde{\alpha}L'(\tilde{\alpha}'),$$

which leads together with relation (3.113) and the assumptions $\mu < \eta$, $L'(0) < 0$ to

$$L'(\tilde{\alpha}') = \mu L'(0) > \eta L'(0).$$

Hence, $\tilde{\alpha}'$ satisfies the Wolfe conditions with strict inequality in (3.111) and (3.112). Moreover, by the continuity of L and L' we find an interval around $\tilde{\alpha}'$ for which the Wolfe conditions are fulfilled, and the proof is finished. ■

Algorithms which perform an inexact line search with Wolfe conditions can be found in [3, 93, 96]. We will use Algorithm 3.1, which is a particular simple case of the general methods presented in [3]. The corresponding convergence result is due to [3, Theorem 2.1].

Algorithm 3.1 (**Inexact Line Search - Wolfe Conditions**)

Parameters: $0 < \tau_1 < 1 < \tau_2$
Input: differentiable function $f : \mathcal{M} \to [f_0, \infty)$, $f_0 \in \mathbb{R}$, starting point $\boldsymbol{x} \in \mathcal{M}$, descent direction $\boldsymbol{d} \in \mathrm{T}_{\boldsymbol{x}}\mathcal{M}$, cf. (3.104), initial step length $\alpha_0 > 0$, parameters $0 < \mu < \eta < 0$ in the Wolfe conditions; (3.111), (3.112)
Initialization: $L := f \circ \gamma_{\boldsymbol{x},\boldsymbol{d}}$ with geodesic $\gamma_{\boldsymbol{x},\boldsymbol{d}}(0) = \boldsymbol{x}$, $\dot{\gamma}_{\boldsymbol{x},\boldsymbol{d}}(0) = \boldsymbol{d}$, cf. (3.22),
$\alpha_{\max} := (f_0 - L(0))/(\mu L'(0))$, $l_1 := 0$, $u_1 := \infty$, $\alpha_1 := \min(\alpha_0, \alpha_{\max})$, $k := 1$;
while $L(\alpha_k) > f_0$ **do**
  if $L(\alpha_k) > L(0) + \mu\alpha_k L'(0)$ or $L(\alpha_k) \geq L(l_k)$ **then**
    $l_{k+1} := l_k$, $u_{k+1} := \alpha_k$;
    $\alpha_{k+1} := l_{k+1} + \tau_1(u_{k+1} - l_{k+1})$;
  else
    if $L'(\alpha_k) \geq \eta L'(0)$ **then**
      return $\alpha := \alpha_k$;
    else
      $l_{k+1} := \alpha_k$, $u_{k+1} := u_k$;
      if $u_{k+1} = \infty$ **then**
        $\alpha_{k+1} := \min(\tau_2\alpha_{k+1}, \alpha_{\max})$;
      else
        $\alpha_{k+1} := l_{k+1} + \tau_1(u_{k+1} - l_k)$;
      end if
    end if
  end if
  $k := k + 1$;
end while
$\alpha := \alpha_k$;
Output: step length $\alpha > 0$.

Theorem 3.23. *Let $\mathcal{M} \subset \mathbb{R}^n$ be a complete d-dimensional Riemannian manifold and $f : \mathcal{M} \to [f_0, \infty)$, $f_0 \in \mathbb{R}$, be a function which is continuously differentiable at $\boldsymbol{x} \in \mathcal{M}$. If $\boldsymbol{d} \in \mathrm{T}_{\boldsymbol{x}}\mathcal{M}$ is a descent direction, cf.* (3.104)*, and the function $L := f \circ \gamma_{\boldsymbol{x},\boldsymbol{d}}$, cf.* (3.22)*, is continuously differentiable, then Algorithm 3.1 terminates, for fixed constants $0 < \mu < \eta < 1$ and any choice $\alpha_0 > 0$, after a finite number of iterations and provides a step length α which satisfies the Wolfe conditions* (3.111), (3.112) *or fulfills $L(\alpha) = f_0$.*

Proof. We will briefly illustrate the ideas of Algorithm 3.1. For a rigorous discussion we refer to the proof of [3, Theorem 2.1].

Algorithm 3.1 generates a sequence of trial step lengths $\alpha_k \in (0, \alpha_{\max}]$ which will always lie in the intervals (l_k, u_k), $k = 1, 2, \ldots$. Moreover, the lower end point l_k is always the current

best point with smallest function value that satisfies the first Wolfe condition (3.111) but not the second (3.112), and u_k either fails to satisfy the first Wolfe condition (3.111), or $L(u_k) \geq L(l_k)$, or both, whenever $u_k \neq \infty$.

If Algorithm 3.1 generates exclusively $u_k = \infty$ then it must terminate by the choice of $\tau_2 > 1$ after a finite number of iterations with a step length α satisfying $L(\alpha) = f_0$.

In the other cases we find that $(l_k, u_k) \subset (0, \alpha_{\max}]$ for k sufficiently large. Furthermore, the intervals (l_k, u_k) become successively smaller and contain intervals of step lengths satisfying the Wolfe conditions (3.111), (3.112). Using this together with $0 < \tau_1 < 1$ one can show as in the proof of [3, Theorem 2.1] by contradiction that Algorithm 3.1 must terminate after a finite number of iterations with a step length $\alpha > 0$ fulfilling the stated properties. ■

Remark 3.24. The choice of the trial step length α_{k+1} in Algorithm 3.1 is a simple bisection and extrapolation scheme for bounded and unbounded intervals (l_k, u_k), $k = 1, 2, \ldots$, respectively, based on the parameters τ_1, τ_2. More efficient line search algorithms may be obtained by polynomial interpolation schemes, cf. [3, 93, 33, 96]. However, since we usually use a Newton step as a first trial step length α_0, cf. Algorithm 3.2 and 3.3, it is likely that it already satisfies the Wolfe conditions (3.111), (3.112), whenever $\mu < \frac{1}{2}$.[10]

Furthermore, the result of Theorem 3.23 assumes that exact arithmetic is used, and so might be no longer valid for finite precision arithmetic. It can happen that the tests in Algorithm 3.1 lead to wrong results since the two function values $L(\alpha_k) < L(l_k)$ may not be distinguishable, and termination cannot be guaranteed. Therefore, we add in our numerical implementation of Algorithm 3.1 for some prescribe accuracy $\varepsilon > 0$ the termination condition

$$|(\alpha_k - l_k)L'(l_k)| \leq \varepsilon \tag{3.114}$$

in the first if-condition, as suggested in [3]. A deeper discussion of the implementation of stopping criteria in numerical algorithms can be found in [33, Chapter 7]. □

3.3.2 Global and Local Convergence Results

For the convergence of the Newton and CG method given in Example 3.20 by the iterations (3.106) and (3.108), respectively, it is required that the initial point $\boldsymbol{x}^{(0)} \in \mathcal{M}$ is in a sufficiently small neighborhood of a local minimizer with positive definite Hessian. However, in practice such an assumption might be far too restrictive. Therefore, we investigate the convergence behavior of general descent methods given by (3.102) for arbitrary initial points $\boldsymbol{x}^{(0)} \in \mathcal{M}$. Since by Remark 3.19 we are at least interested in the computation of stationary points, we say that an iterative method of the form (3.102) is *globally convergent* for a continuously differentiable function $f : \mathcal{M} \to \mathbb{R}$ if for any initial point $\boldsymbol{x}^{(0)} \in \mathcal{M}$ it generates a sequence $\{\boldsymbol{x}^{(k)}\}_{k \in \mathbb{N}_0} \subset \mathcal{M}$ satisfying

$$\liminf_{k \to \infty} \nabla_{\mathcal{M}} f(\boldsymbol{x}^{(k)}) = 0. \tag{3.115}$$

We remark that this notion of a globally convergent method is very weak since we cannot even conclude the convergence of the sequence $\{\boldsymbol{x}^{(k)}\}_{k \in \mathbb{N}_0}$ from $\lim_{k \to \infty} \nabla_{\mathcal{M}} f(\boldsymbol{x}^{(k)}) = 0$. Nevertheless, it might be the strongest result we can hope for a wide class of optimization algorithms which ensures convergence towards a stationary point.[11] For the analysis of global convergence properties of descent methods in Euclidean space one usually exploits a theorem attributed to Zoutendijk, cf. [96, Theorem 3.2.]. We present a version adapted to Riemannian manifolds.

[10] For conviction, we refer to part (iii) in the proof of Theorem 3.27

[11] The stationary point can 'be at infinity' if one considers for example the function $f(x) := \arctan(x)$, $x \in \mathbb{R}$.

Theorem 3.25. *Let $\mathcal{M} \subset \mathbb{R}^n$ be a complete d-dimensional Riemannian manifold and $f : \mathcal{M} \to [f_0, \infty)$, $f_0 \in \mathbb{R}$, be a function which is twice continuously differentiable on the level set*

$$\mathcal{N}(\boldsymbol{x}^{(0)}) := \{\boldsymbol{x} \in \mathcal{M} \ : \ f(\boldsymbol{x}) \leq f(\boldsymbol{x}^{(0)})\} \tag{3.116}$$

associated to an initial point $\boldsymbol{x}^{(0)} \in \mathcal{M}$ and which satisfies for some constant $C > 0$ the relation, cf. (3.35),

$$\left|\mathrm{H}_{\mathcal{M}} f(\boldsymbol{x})(\boldsymbol{v}, \boldsymbol{v})\right| \leq C\|\boldsymbol{v}\|_2^2, \qquad \boldsymbol{v} \in \mathrm{T}_{\boldsymbol{x}}\mathcal{M}, \qquad \boldsymbol{x} \in \mathcal{N}(\boldsymbol{x}^{(0)}). \tag{3.117}$$

If, for fixed constants $0 < \mu < \eta < 1$, the sequence $\{\boldsymbol{x}^{(k)}\}_{k\in\mathbb{N}_0} \subset \mathcal{N}(\boldsymbol{x}_0)$ is generated by a descent method with descent directions $\boldsymbol{d}^{(k)} \in \mathrm{T}_{\boldsymbol{x}^{(k)}}\mathcal{M}$, cf. (3.102)*, where the step lengths $\alpha^{(k)} > 0$ fulfill the Wolfe conditions* (3.111), (3.112) *for $L^{(k)} := f \circ \gamma_{\boldsymbol{x}^{(k)},\boldsymbol{d}^{(k)}}$, cf.* (3.22)*, then the corresponding gradients $\boldsymbol{g}^{(k)} := \nabla_{\mathcal{M}} f(\boldsymbol{x}^{(k)})$, $k \in \mathbb{N}_0$, cf.* (3.34)*, satisfy*

$$\sum_{k=0}^{\infty} \cos(\theta^{(k)})^2 \|\boldsymbol{g}^{(k)}\|_2^2 < \infty \tag{3.118}$$

where $\theta^{(k)} \in [0, \pi/2]$ is the angle between the descent directions $\boldsymbol{d}^{(k)} \in \mathrm{T}_{\boldsymbol{x}^{(k)}}\mathcal{M}$ and the direction of steepest descent $-\boldsymbol{g}^{(k)} \in \mathrm{T}_{\boldsymbol{x}^{(k)}}\mathcal{M}$, $k \in \mathbb{N}_0$, defined by

$$\cos(\theta^{(k)}) = \begin{cases} \frac{-\boldsymbol{g}^{(k)\top}\boldsymbol{d}^{(k)}}{\|\boldsymbol{g}^{(k)}\|_2\|\boldsymbol{d}^{(k)}\|_2}, & d^{(k)} \neq \boldsymbol{0},\ g^{(k)} \neq \boldsymbol{0}, \\ 0, & \text{else.} \end{cases} \tag{3.119}$$

If additionally there exists a subsequence of $\{\boldsymbol{x}^{(k)}\}_{k\in\mathbb{N}_0}$, denoted by $\{\boldsymbol{x}^{(k_l)}\}_{l\in\mathbb{N}_0}$, and a constant $c > 0$ such that

$$\cos(\theta^{(k_l)}) > c, \qquad l \in \mathbb{N}_0, \tag{3.120}$$

then the sequence $\{\boldsymbol{x}^{(k)}\}_{k\in\mathbb{N}_0}$ is convergent in the sense $\liminf_{k\to\infty} \nabla_{\mathcal{M}} f(\boldsymbol{x}^{(k)}) = 0$.

Proof. By the definition of descent methods we can assume that $\nabla_{\mathcal{M}} f(\boldsymbol{x}^{(k)}) \neq \boldsymbol{0}$, since in the other cases we have $\boldsymbol{g}^{(k)} = \nabla_{\mathcal{M}} f(\boldsymbol{x}^{(k)}) = \boldsymbol{0}$, $k \geq k_0$, for some $k_0 \in \mathbb{N}_0$, where the relation (3.118) is trivially fulfilled.

By assumption (3.117) and $f(\boldsymbol{x}^{(k)}) \in \mathcal{N}(\boldsymbol{x}^{(0)})$, $k \in \mathbb{N}_0$, we can apply the mean value remainder in the Theorem of Taylor, cf. (3.46), for sufficiently small $t > 0$ and find together with $\|\dot{\gamma}_{\boldsymbol{x}^{(k)},\boldsymbol{d}^{(k)}}(s)\|_2 = \boldsymbol{d}^{(k)\top}\boldsymbol{d}^{(k)}$, $s \in \mathbb{R}$, that

$$\begin{aligned} f \circ \gamma_{\boldsymbol{x}^{(k)},\boldsymbol{d}^{(k)}}(t) - f(\boldsymbol{x}^{(k)}) &= t\nabla_{\mathcal{M}} f(\boldsymbol{x}^{(k)})^\top \boldsymbol{d}^{(k)} + \frac{t^2}{2}\mathrm{H}_{\mathcal{M}} f \circ \gamma_{\boldsymbol{x}^{(k)},\boldsymbol{d}^{(k)}}(\zeta)(\dot{\gamma}_{\boldsymbol{x}^{(k)},\boldsymbol{d}^{(k)}}(\zeta), \dot{\gamma}_{\boldsymbol{x}^{(k)},\boldsymbol{d}^{(k)}}(\zeta)) \\ &\leq t\boldsymbol{g}^{(k)\top}\boldsymbol{d}^{(k)} + \frac{t^2}{2}C\boldsymbol{d}^{(k)\top}\boldsymbol{d}^{(k)}, \end{aligned}$$

for some $\zeta \in (0, t)$. Using $\boldsymbol{g}^{(k)\top}\boldsymbol{d}^{(k)} < 0$ we conclude from the above relation that

$$f \circ \gamma_{\boldsymbol{x}^{(k)},\boldsymbol{d}^{(k)}}(t) \in \mathcal{N}(\boldsymbol{x}_0), \qquad t \in \left[0, t_{\max}^{(k)}\right], \qquad t_{\max}^{(k)} := -\frac{2}{C}\frac{\boldsymbol{g}^{(k)\top}\boldsymbol{d}^{(k)}}{\boldsymbol{d}^{(k)\top}\boldsymbol{d}^{(k)}}, \qquad k \in \mathbb{N}_0.$$

Hence, for $\alpha^{(k)} \leq t_{\max}^{(k)}$, $k \in \mathbb{N}_0$, we find with the Mean Value Theorem and assumption (3.117) the bound

$$\alpha^{(k)} C\boldsymbol{d}^{(k)\top}\boldsymbol{d}^{(k)} \geq \frac{\mathrm{d}}{\mathrm{d}t} f \circ \gamma_{\boldsymbol{x}^{(k)},\boldsymbol{d}^{(k)}}(t)\big|_{t=\alpha^{(k)}} - \frac{\mathrm{d}}{\mathrm{d}t} f \circ \gamma_{\boldsymbol{x}^{(k)},\boldsymbol{d}^{(k)}}(t)\Big|_{t=0},$$

which yields together with the second Wolfe condition (3.112) the relation

$$\alpha^{(k)} \geq \frac{\eta - 1}{C} \frac{{\boldsymbol{g}^{(k)}}^\top \boldsymbol{d}^{(k)}}{{\boldsymbol{d}^{(k)}}^\top \boldsymbol{d}^{(k)}}, \qquad k \in \mathbb{N}_0.$$

Since for $\alpha^{(k)} \geq t_{\max}^{(k)}$ the last relation is trivially fulfilled we can insert it into the first Wolf condition (3.111) and get

$$f(\boldsymbol{x}^{(k+1)}) - f(\boldsymbol{x}^{(k)}) \leq -\mu \frac{1 - \eta}{C} \frac{({\boldsymbol{g}^{(k)}}^\top \boldsymbol{d}^{(k)})^2}{\|\boldsymbol{d}^{(k)}\|_2^2}, \qquad k \in \mathbb{N}_0.$$

This leads with definition (3.119) and the boundedness of the function f to

$$f_0 - f(\boldsymbol{x}^{(0)}) \leq f(\boldsymbol{x}^{(k+1)}) - f(\boldsymbol{x}^{(0)}) \leq -\mu \frac{1 - \eta}{C} \sum_{k'=0}^{\infty} \cos(\theta^{(k')})^2 \|\boldsymbol{g}^{(k')}\|_2^2, \qquad k \in \mathbb{N}_0,$$

which implies the assertion (3.118).

The last statement follows immediately from relation (3.118) and assumption (3.120) by the estimate

$$\sum_{l=0}^{\infty} \|\nabla_{\mathcal{M}} f(\boldsymbol{x}^{(k_l)})\|_2^2 \leq \frac{1}{c^2} \sum_{k=0}^{\infty} \cos(\theta^{(k)})^2 \|\nabla_{\mathcal{M}} f(\boldsymbol{x}^{(k)})\|_2^2 < \infty. \qquad \blacksquare$$

Theorem 3.25 can be used to design globally convergent descent methods, or to prove global convergence of certain descent methods, cf. [96]. As seen by the last statement, cf. (3.120), the idea is to bound the angel between the descent direction and the direction of steepest descent away from 90 degree, at least for a subsequence. Using this idea we can modify any iterative optimization method given by (3.102) to obtain a globally convergent method, cf. (3.115), simply by forcing descent directions and at certain iterations a direction of steepest descent. For the Newton method and the method of conjugate gradients given in Example 3.20 we obtain in this way the Algorithms 3.2 and 3.3, respectively, which are globally convergent for a large class of functions.

Corollary 3.26. *Let $\mathcal{M} \subset \mathbb{R}^n$ be a complete d-dimensional Riemannian manifold, $f : \mathcal{M} \to [f_0, \infty)$, $f_0 \in \mathbb{R}$, be a function which satisfies for every $\boldsymbol{x}_0 \in \mathcal{M}$ the assumptions of Theorem 3.25. Then the method of steepest descent with the inexact line search Algorithm 3.1, cf.* (3.105)*, and the Algorithms 3.2 and 3.3 are globally convergent for f, cf.* (3.115)*.*

Proof. The assertions follow from the last statement of Theorem 3.25 by showing (3.120). Without loss of generality we consider only sequences $\{\boldsymbol{x}^{(k)}\}_{k \in \mathbb{N}_0}$ with $\nabla_{\mathcal{M}} f(\boldsymbol{x}^{(k)}) \neq \boldsymbol{0}$, $k \in \mathbb{N}_0$.

If the sequence $\{\boldsymbol{x}^{(k)}\}_{k \in \mathbb{N}_0}$ is generated by the method of steepest descent we have $\cos(\theta^{(k)}) = 1$, $k \in \mathbb{N}_0$, and the assertion follows.

In the CG method with restarts given by Algorithm 3.3 we always enforce a descent direction, and at least after every dth iteration a direction of steepest descent. Hence, the assertion follows, since for every sequence $\{\boldsymbol{x}^{(k)}\}_{k \in \mathbb{N}_0}$ generated by Algorithm 3.3 there is a subsequence $\{\boldsymbol{x}^{(k_l)}\}_{l \in \mathbb{N}_0}$ for which $\cos(\theta^{(k_l)}) = 1$, $l \in \mathbb{N}_0$.

For the globalized Newton method given by Algorithm 3.2 we also enforce descent directions. Note, for a positive definite Hessian $\mathrm{H}_{\mathcal{M}} f(\boldsymbol{x}^{(k)})$ at iteration $k \in \mathbb{N}_0$ we have by definition of $\boldsymbol{d}^{(k)}$ that

$${\boldsymbol{g}^{(k)}}^\top \boldsymbol{d}^{(k)} = -\mathrm{H}_{\mathcal{M}} f(\boldsymbol{x}^{(k)})(\boldsymbol{d}^{(k)}, \boldsymbol{d}^{(k)}) < 0.$$

Moreover, by using matrix representations of the positive definite Hessian $\mathrm{H}_{\mathcal{M}} f(\boldsymbol{x}^{(k)})$ we arrive

Algorithm 3.2 (**Globalized Newton Method**)

Parameters: $0 < \mu < \frac{1}{2}$, $\mu < \eta < 1$ in the Wolfe conditions (3.111), (3.112), bound $\kappa > 0$ on the condition number of the Hessian;
Input: twice differentiable function $f : \mathcal{M} \to [f_0, \infty)$, $f_0 \in \mathbb{R}$, initial point $\boldsymbol{x}^{(0)} \in \mathcal{M}$;
for $k := 0, 1, \ldots$ **do**
compute the smallest and largest eigenvalues $\lambda_{\min}^{(k)}, \lambda_{\max}^{(k)} \in \mathbb{R}$ of the Hessian $\mathrm{H}_{\mathcal{M}} f(\boldsymbol{x}^{(k)})$, i.e.,

$$\lambda_{\min}^{(k)} \|\boldsymbol{v}\|_2^2 \leq \mathrm{H}_{\mathcal{M}} f(\boldsymbol{x}^{(k)})(\boldsymbol{v}, \boldsymbol{v}) \leq \lambda_{\max}^{(k)} \|\boldsymbol{v}\|_2^2, \qquad \boldsymbol{v} \in \mathrm{T}_{\boldsymbol{x}^{(k)}} \mathcal{M};$$

$\boldsymbol{g}^{(k)} := \nabla_{\mathcal{M}} f(\boldsymbol{x}^{(k)})^\top$;
if $\lambda_{\min}^{(k)} > 0$ and $\lambda_{\max}^{(k)} / \lambda_{\min}^{(k)} \leq \kappa$ **then**
compute $\boldsymbol{d}^{(k)} \in \mathrm{T}_{\boldsymbol{x}^{(k)}} \mathcal{M}$ by solving

$$\mathrm{H}_{\mathcal{M}} f(\boldsymbol{x}^{(k)})(\boldsymbol{d}^{(k)}, \boldsymbol{v}) = -{\boldsymbol{g}^{(k)}}^\top \boldsymbol{v}, \qquad \boldsymbol{v} \in \mathrm{T}_{\boldsymbol{x}^{(k)}} \mathcal{M};$$

$\alpha_0^{(k)} := 1$;
else
$\boldsymbol{d}^{(k)} := -\boldsymbol{g}^{(k)}$;
$\alpha_0^{(k)} := \begin{cases} \left| \frac{{\boldsymbol{g}^{(k)}}^\top \boldsymbol{d}^{(k)}}{\mathrm{H}_{\mathcal{M}} f(\boldsymbol{x}^{(k)})(\boldsymbol{d}^{(k)}, \boldsymbol{d}^{(k)})} \right|, & \mathrm{H}_{\mathcal{M}} f(\boldsymbol{x}^{(k)})(\boldsymbol{d}^{(k)}, \boldsymbol{d}^{(k)}) \neq 0, \\ 1, & \text{else;} \end{cases}$
end if
compute $\alpha^{(k)}$ by Algorithm 3.1 with starting point $\boldsymbol{x}^{(k)}$, descent direction $\boldsymbol{d}^{(k)}$, initial step length $\alpha_0^{(k)}$, and parameters μ, η;
$\boldsymbol{x}^{(k+1)} := \gamma_{\boldsymbol{x}^{(k)}, \boldsymbol{d}^{(k)}}(\alpha^{(k)})$, cf. (3.22);
end for
Output: iteration sequence $\boldsymbol{x}^{(0)}, \boldsymbol{x}^{(1)}, \cdots \in \mathcal{M}$.

at the relations[12]

$$\lambda_{\min}^{(k)} \|\boldsymbol{d}^{(k)}\|_2 \leq \|\boldsymbol{g}^{(k)}\|_2 \leq \lambda_{\max}^{(k)} \|\boldsymbol{d}^{(k)}\|_2, \tag{3.121}$$

which imply

$$\cos(\theta^{(k)}) = -\frac{{\boldsymbol{g}^{(k)}}^\top \boldsymbol{d}^{(k)}}{\|\boldsymbol{g}^{(k)}\|_2 \|\boldsymbol{d}^{(k)}\|_2} = \frac{\mathrm{H}_{\mathcal{M}} f(\boldsymbol{x}^{(k)})(\boldsymbol{d}^{(k)}, \boldsymbol{d}^{(k)})}{\|\boldsymbol{g}^{(k)}\|_2 \|\boldsymbol{d}^{(k)}\|_2} \geq \frac{\lambda_{\min}^{(k)}}{\lambda_{\max}^{(k)}} = \kappa^{-1} > 0,$$

and the proof is finished. ∎

Of course, by construction, the Algorithms 3.2 and 3.3 may perform as worse as the method of steepest descent. However, under suitable conditions the local convergence is much faster.

Theorem 3.27. *Let $\mathcal{M} \subset \mathbb{R}^n$ be a complete d-dimensional Riemannian manifold and $f : \mathcal{M} \to [f_0, \infty)$, $f_0 \in \mathbb{R}$, be a function which is twice continuously differentiable on the level set $\mathcal{N}(\boldsymbol{x}^{(0)}) \subset \mathcal{M}$ associated to an initial point $\boldsymbol{x}^{(0)} \in \mathcal{M}$, cf.* (3.116)*, and which satisfies for some constants*

[12] In the Euclidean space $\mathcal{M} = \mathbb{R}^d$ these relations are simply obtained by using $\boldsymbol{d}^{(k)} = -\mathbf{H} f(\boldsymbol{x}^{(k)})^{-1} \boldsymbol{g}^{(k)}$ and ${\boldsymbol{g}^{(k)}}^\top \boldsymbol{g}^{(k)} / \lambda_{\max}^{(k)} \leq {\boldsymbol{g}^{(k)}}^\top \mathbf{H} f(\boldsymbol{x}^{(k)})^{-1} \boldsymbol{g}^{(k)} \leq {\boldsymbol{g}^{(k)}}^\top \boldsymbol{g}^{(k)} / \lambda_{\min}^{(k)}$.

Algorithm 3.3 (**CG Method with Restarts**)

Parameters: $0 < \mu < \frac{1}{2}$, $\mu < \eta < 0$ in the Wolfe conditions (3.111), (3.112);
Input: twice differentiable function $f : \mathcal{M} \to [f_0, \infty)$, $f_0 \in \mathbb{R}$, initial point $\boldsymbol{x}^{(0)} \in \mathcal{M}$;
Initialization: $\boldsymbol{g}^{(0)} := \nabla_{\mathcal{M}} f(\boldsymbol{x}^{(0)})$, $\boldsymbol{d}^{(0)} := -\boldsymbol{g}^{(0)}$, $r := 0$;
for $k := 0, 1, \ldots$ **do**

$$\alpha_0^{(k)} := \begin{cases} \left| \frac{{\boldsymbol{g}^{(k)}}^\top \boldsymbol{d}^{(k)}}{\mathrm{H}_{\mathcal{M}} f(\boldsymbol{x}^{(k)})(\boldsymbol{d}^{(k)}, \boldsymbol{d}^{(k)})} \right|, & \mathrm{H}_{\mathcal{M}} f(\boldsymbol{x}^{(k)})(\boldsymbol{d}^{(k)}, \boldsymbol{d}^{(k)}) \neq 0, \\ 1, & \text{else;} \end{cases}$$

compute $\alpha^{(k)}$ by Algorithm 3.1 with starting point $\boldsymbol{x}^{(k)}$, descent direction $\boldsymbol{d}^{(k)}$, initial step length $\alpha_0^{(k)}$, and parameters μ, η;
$\boldsymbol{x}^{(k+1)} := \gamma_{\boldsymbol{x}^{(k)}, \boldsymbol{d}^{(k)}}(\alpha^{(k)})$, cf. (3.22);
$\boldsymbol{g}^{(k+1)} := \nabla_{\mathcal{M}} f(\boldsymbol{x}^{(k+1)})$;
$\tilde{\boldsymbol{d}}^{(k)} := \dot{\gamma}_{\boldsymbol{x}^{(k)}, d^{(k)}}(\alpha^{(k)})$;

$$\beta^{(k)} := \begin{cases} \frac{\mathrm{H}_{\mathcal{M}} f(\boldsymbol{x}^{(k+1)})(\boldsymbol{g}^{(k+1)}, \tilde{\boldsymbol{d}}^{(k)})}{\mathrm{H}_{\mathcal{M}} f(\boldsymbol{x}^{(k+1)})(\tilde{\boldsymbol{d}}^{(k)}, \tilde{\boldsymbol{d}}^{(k)})}, & \mathrm{H}_{\mathcal{M}} f(\boldsymbol{x}^{(k+1)})(\tilde{\boldsymbol{d}}^{(k)}, \tilde{\boldsymbol{d}}^{(k)}) \neq 0, \\ 0, & \text{else;} \end{cases}$$

$\boldsymbol{d}^{(k+1)} := -\boldsymbol{g}^{(k+1)} + \beta^{(k)} \tilde{\boldsymbol{d}}^{(k)}$;
if ${\boldsymbol{g}^{(k+1)}}^\top \boldsymbol{d}^{(k+1)} > 0$ or $(k+1) \equiv r \mod d$ **then**
$\boldsymbol{d}^{(k+1)} := -\boldsymbol{g}^{(k+1)}$;
$r := k + 1$;
end if
end for
Output: iteration sequence $\boldsymbol{x}^{(0)}, \boldsymbol{x}^{(1)}, \cdots \in \mathcal{M}$.

$0 < c < C$ *the relation, cf.* (3.35),

$$c\|\boldsymbol{v}\|_2^2 \leq \mathrm{H}_{\mathcal{M}} f(\boldsymbol{x})(\boldsymbol{v}, \boldsymbol{v}) \leq C\|\boldsymbol{v}\|_2^2, \qquad \boldsymbol{v} \in \mathrm{T}_{\boldsymbol{x}}\mathcal{M}, \qquad \boldsymbol{x} \in \mathcal{N}(\boldsymbol{x}^{(0)}). \tag{3.122}$$

Furthermore, we assume that the level set $\mathcal{N}(\boldsymbol{x}^{(0)}) \subset \mathcal{M}$ *is compact and that* $\boldsymbol{x}_* \in \mathcal{M}$ *is the unique local minimizer in* $\mathcal{N}(\boldsymbol{x}^{(0)}) \subset \mathcal{M}$.

(i) *If the sequence* $\{\boldsymbol{x}^{(k)}\}_{k \in \mathbb{N}_0}$ *is generated by the method of steepest descent, cf.* (3.105), *with an exact line search, where the corresponding step lengths* $\alpha^{(k)}$, $k \in \mathbb{N}_0$, *are the smallest satisfying* (3.110), *then* it converges linearly to $\boldsymbol{x}_*$, *i.e., there exists constants* $E > 0$, $\theta \in (0, 1)$ *such that, cf.* (3.17),

$$\mathrm{d}_{\mathcal{M}}(\boldsymbol{x}^{(k)}, \boldsymbol{x}_*) \leq E\theta^k, \qquad k \in \mathbb{N}_0. \tag{3.123}$$

(ii) *If the sequence* $\{\boldsymbol{x}^{(k)}\}_{k \in \mathbb{N}_0}$ *is generated by Algorithm 3.2, where* $\kappa \geq C/c$ *and* f *is three-times continuously differentiable on* $\mathcal{N}(\boldsymbol{x}^{(0)})$, *then* it converges quadratically to $\boldsymbol{x}_*$, *i.e., there exists constants* $E > 0$, $k_0 \in \mathbb{N}$ *such that*

$$\mathrm{d}_{\mathcal{M}}(\boldsymbol{x}^{(k+1)}, \boldsymbol{x}_*) \leq E\mathrm{d}_{\mathcal{M}}(\boldsymbol{x}^{(k)}, \boldsymbol{x}_*)^2, \qquad k \in \mathbb{N}_0, \quad k \geq k_0. \tag{3.124}$$

(iii) *If the sequence* $\{\boldsymbol{x}^{(k)}\}_{k \in \mathbb{N}_0}$ *is generated by Algorithm 3.3 with an exact line search, where the corresponding step lengths* $\alpha^{(k)}$, $k \in \mathbb{N}_0$, *are the smallest satisfying* (3.110), *and* f *is three-times continuously differentiable on* $\mathcal{N}(\boldsymbol{x}^{(0)})$, *then* it converges d-step quadratically

to $\boldsymbol{x}_*$, *i.e., there exists constants* $E > 0$, $k_0 \in \mathbb{N}$ *such that*

$$\mathrm{d}_{\mathcal{M}}(\boldsymbol{x}^{(dk+d)}, \boldsymbol{x}_*) \leq E \mathrm{d}_{\mathcal{M}}(\boldsymbol{x}^{(dk)}, \boldsymbol{x}_*)^2, \qquad k \in \mathbb{N}_0, \quad k \geq k_0. \tag{3.125}$$

Proof. We start by proving that the sequences in (i)–(iii) converge towards the unique minimizer $\boldsymbol{x}_*$ of f in the level set $\mathcal{N}(\boldsymbol{x}^{(0)}) \subset \mathcal{M}$. Afterward, we consider the convergence rates (3.123)–(3.125) separately by applying the results of [121].

For the application of Corollary 3.26 we need to prove that an exact line search will satisfy the Wolfe conditions (3.111), (3.112) for $0 < \mu \leq c/(2C)$, $\mu < \eta < 1$ under the above assumptions on the Hessian, cf. (3.122). Therefore, we consider the function $L := f \circ \gamma_{\boldsymbol{x},\boldsymbol{d}}$, cf. (3.22), for arbitrary starting points $\boldsymbol{x} \in \mathcal{N}(\boldsymbol{x}^{(0)})$ and descent directions $\boldsymbol{d} \in \mathrm{T}_{\boldsymbol{x}}\mathcal{M}$. Then the smallest local minimizer $\alpha_* > 0$ of L satisfies by the mean value remainder Theorem of Taylor and assumption (3.122) the relation, see the proof of Theorem 3.25,

$$L(\alpha_*) - L(0) \leq \min_{\alpha > 0} \left\{ \alpha L'(0) + \frac{1}{2} C \alpha^2 \right\} = -\frac{L'(0)^2}{2C}.$$

Similarly, we can bound the step length by $0 < \alpha_* \leq -L'(0)/c$ and obtain

$$L(\alpha_*) - L(0) \leq \frac{c}{2C} \alpha_* L'(0) \leq \mu \alpha_* L'(0).$$

This shows that the Wolfe conditions (3.111), (3.112) with $0 < \mu \leq c/(2C)$, $\mu < \eta < 1$ are satisfied for the smallest step length α_* obtained by an exact line search.

Hence, we can apply Corollary 3.26 and conclude that any sequence $\{\boldsymbol{x}^{(k)}\}_{k \in \mathbb{N}_0}$ generate by the method of steepest descent, Algorithm 3.2, and Algorithm 3.3, converges in the sense $\liminf_{k \to \infty} \nabla_{\mathcal{M}} f(\boldsymbol{x}^{(k)}) = \boldsymbol{0}$. Since the level set $\mathcal{N}(\boldsymbol{x}^{(0)})$ is compact there exits a subsequence $\{\boldsymbol{x}^{(k_l)}\}_{l \in \mathbb{N}_0}$ satisfying $\lim_{l \to \infty} \boldsymbol{x}^{(k_l)} = \tilde{\boldsymbol{x}}$ with $\nabla_{\mathcal{M}} f(\tilde{\boldsymbol{x}}) = \boldsymbol{0}$. Using the assumption (3.122) and the sufficient condition (3.101) of Theorem 3.18 we find by the uniqueness of the local minimizer $\boldsymbol{x}_*$ that $\tilde{\boldsymbol{x}} = \boldsymbol{x}_*$ is in fact the unique global minimizer of the level set $\mathcal{N}(\boldsymbol{x}^{(0)})$. Moreover, by the monotonicity $f(\boldsymbol{x}_*) \leq f(\boldsymbol{x}^{(k)}) \leq f(\boldsymbol{x}^{(k_l)})$, $k \geq k_l$, $l \in \mathbb{N}_0$, and the continuity of f we arrive at $\lim_{k \to \infty} f(\boldsymbol{x}^{(k)}) = f(\boldsymbol{x}_*)$. Hence, the point $\boldsymbol{x}_*$ is the unique accumulation point of the bounded sequence $\{\boldsymbol{x}^{(k)}\}_{k \in \mathbb{N}_0}$, which proves with the theorem of Bolzano–Weierstraß the convergence $\lim_{k \to \infty} \boldsymbol{x}^{(k)} = \boldsymbol{x}_*$. What remains is to show the convergence rates (3.123)–(3.125).

(i) The local convergence rate (3.123) of the method of steepest descent with exact line search follows from [121, Theorem 3.3], where we remark that the cited theorem is also valid for twice continuously differentiable functions.

(ii) Similarly, for the globalized Newton method given by Algorithm 3.2 we aim to apply [121, Corollary 4.5], which states the local convergence result (3.124) for the unmodified Newton method, cf. (3.107). Therefore, we need to show the existence of an index $k_1 \in \mathbb{N}_0$ such that every initial step length $\alpha_0^{(k)} = 1$, $k \geq k_1$, satisfies the Wolfe conditions (3.111), (3.112) for fixed constants $0 < \mu < \frac{1}{2}$, $\mu < \eta < 1$.

Since the function f is three-times continuously differentiable and the level set $\mathcal{N}(\boldsymbol{x}^{(0)})$ is compact we find by the scaling relation (3.26) that

$$\begin{aligned} \left| \frac{\mathrm{d}^3}{\mathrm{d}t^3} f \circ \gamma_{\boldsymbol{x},\boldsymbol{v}}(t) \Big|_{t=0} \right| &= \left| \frac{\mathrm{d}^3}{\mathrm{d}t^3} f \circ \gamma_{\boldsymbol{x}, \frac{\boldsymbol{v}}{\|\boldsymbol{v}\|_2}}(\|\boldsymbol{v}\|_2 t) \Big|_{t=0} \right| \\ &= \|\boldsymbol{v}\|_2^3 \left| \frac{\mathrm{d}^3}{\mathrm{d}s^3} f \circ \gamma_{\boldsymbol{x}, \frac{\boldsymbol{v}}{\|\boldsymbol{v}\|_2}}(s) \Big|_{s=0} \right| \leq \tilde{C} \|\boldsymbol{v}\|_2^3, \qquad \boldsymbol{x} \in \mathcal{N}(\boldsymbol{x}^{(0)}), \qquad \boldsymbol{v} \in \mathrm{T}_{\boldsymbol{x}}\mathcal{M}, \end{aligned} \tag{3.126}$$

where

$$\tilde{C} := \max\left\{ \left| \frac{\mathrm{d}^3}{\mathrm{d}t^3} f \circ \gamma_{\boldsymbol{x},\boldsymbol{v}}(t) \Big|_{t=0} \right| \,:\, \boldsymbol{x} \in \mathcal{N}(\boldsymbol{x}^{(0)}), \quad \boldsymbol{v} \in \mathrm{T}_{\boldsymbol{x}}\mathcal{M}, \quad \|\boldsymbol{v}\|_2 = 1 \right\}.$$

We consider again univariate functions of the form $L^{(k)} := f \circ \gamma_{\boldsymbol{x}^{(k)},\boldsymbol{d}^{(k)}}$, $k \in \mathbb{N}_0$, where $\boldsymbol{d}^{(k)}$ are the search directions determined by (3.107). For k sufficiently large, we can apply the third order mean value remainder in Taylor's theorem and find with relation (3.126) that

$$L^{(k)}(1) - L^{(k)}(0) = L^{(k)\prime}(0) + \frac{1}{2}L^{(k)\prime\prime}(0) + \frac{1}{6}L^{(k)\prime\prime\prime}(\zeta) \leq L^{(k)\prime}(0) + \frac{1}{2}L^{(k)\prime\prime}(0) + \frac{\tilde{C}}{6}\|\boldsymbol{d}^{(k)}\|_2^3$$

for some $\zeta \in (0,1)$. Hence, by definition of the search direction $\boldsymbol{d}^{(k)}$, cf. (3.107), and assumption (3.122) we conclude

$$\begin{aligned} L^{(k)}(1) - L^{(k)}(0) &\leq \boldsymbol{g}^{(k)\top}\boldsymbol{d}^{(k)} + \left(\frac{1}{2} + \frac{\tilde{C}}{6c}\|\boldsymbol{d}^{(k)}\|_2\right) \mathrm{H}_{\mathcal{M}} f(\boldsymbol{x}^{(k)})(\boldsymbol{d}^{(k)}, \boldsymbol{d}^{(k)}) \\ &\leq \left(\frac{1}{2} - \frac{\tilde{C}}{6c}\|\boldsymbol{d}^{(k)}\|_2\right) \boldsymbol{g}^{(k)\top}\boldsymbol{d}^{(k)} = \left(\frac{1}{2} - \frac{\tilde{C}}{6c}\|\boldsymbol{d}^{(k)}\|_2\right) L^{(k)\prime}(0). \end{aligned} \tag{3.127}$$

Similarly, for k sufficiently large, we obtain

$$\begin{aligned} -L^{(k)\prime}(1) \leq \left|L^{(k)\prime}(1)\right| &= \left|L^{(k)\prime}(0) + L^{(k)\prime\prime}(0) + \frac{1}{2}L^{(k)\prime\prime\prime}(\zeta)\right| \\ &\leq \frac{\tilde{C}}{2c}\|\boldsymbol{d}^{(k)}\|_2 \left|L^{(k)\prime}(0)\right| = -\frac{\tilde{C}}{2c}\|\boldsymbol{d}^{(k)}\|_2 L^{(k)\prime}(0) \end{aligned} \tag{3.128}$$

for some $\zeta \in (0,1)$. Using relation $\|\boldsymbol{d}^{(k)}\|_2 \leq \|\boldsymbol{g}^{(k)}\|_2/c$, cf. (3.121), together with $\lim_{k\to\infty} \boldsymbol{g}^{(k)} = \boldsymbol{0}$ we infer that the step length $\alpha_0^{(k)} := 1$ fulfills for fixed $\mu \in (0, \frac{1}{2})$ the first Wolfe condition (3.111) by (3.127) and for fixed $\eta \in (\mu, 1)$ the second Wolfe condition (3.112) by (3.128), whenever $k \geq k_1$ for some $k_1 \in \mathbb{N}_0$. Thus, the globalized Newton method becomes for $k \geq k_1$ the usual Newton method (3.106) introduced in Example 3.20, and we can apply the local convergence result given in [121, Corollary 4.5] to prove (3.124).

(iii) For the local convergence result (3.125) of the conjugate gradient method we refer to [24, Theorem (6)], which states the result for the Euclidean space $\mathcal{M} = \mathbb{R}^d$. By the same reasoning as in the proof of [121, Theorem 5.3], where the convergence result (3.125) is obtained for a CG method on Riemannian manifolds with another update parameter $\beta^{(k)}$, $k \in \mathbb{N}_0$, as in Algorithm 3.3, we can transfer the result from Euclidean space to arbitrary Riemannian manifolds. This finishes the proof. ■

Remark 3.28. The proof of the convergence rates (3.123)–(3.125) given in Theorem 3.27 relies essentially on an exact line search for the step sizes. Nevertheless, the numerical results in Section 3.3.3 and Chapter 6, indicate that the presented descent methods usually show similar convergence behavior if an inexact line search Algorithm 3.1 with Newton step as a first trial step length is used. □

3.3.3 Numerical Comparisons and Concluding Remarks

In this section we begin with an illustrative example, where we apply the proposed optimization methods on Riemannian manifolds for the computation of points on the sphere which minimize the electrostatic energy, cf. Section 2.3. More precisely, we compare in Example 3.30 the method

of steepest descent, the Newton method, and the conjugate gradient method, where the numerical results confirm the corresponding convergence rates given in Theorem 3.27. Afterward, we conclude with some further remarks and motivations for the use of optimization methods on Riemannian manifolds.

Before we proceed, we give the default parameters of the implemented optimization algorithms in Remark 3.29. Moreover, we note that the method of steepest descent, the Newton method, and the conjugate gradient method, cf. Example 3.20 and Algorithm 3.1–3.3, are implemented in C++, where the Eigen template library [39] is utilized for matrix-vector computations, which includes reliable methods for various matrix decompositions.

Remark 3.29. If not stated otherwise we will use in our implementation of Algorithm 3.1, which performs the line search, the default parameters $\tau_1 = 0.8$, $\tau_2 = 10$, and the accuracy $\varepsilon = 10^{-16}$ for the additional termination condition (3.114) given in Remark 3.24. Moreover, the first step for the line search is always a one-dimensional Newton step. Similarly, we use the default parameters $\mu = 0.25$ and $\eta = 0.5$ for the Wolfe conditions (3.111), (3.112) in the globalized Newton and CG method, cf. Algorithm 3.2 and 3.3, respectively. Finally, the Algorithms are always terminated if the line search needs more than 50 iterations. □

Example 3.30. We consider the Thomson problem, cf. Section 2.3, i.e., we aim to minimize the electrostatic energy

$$E(\boldsymbol{P}) := \frac{1}{2} \sum_{\substack{i,j=1,\\ i\neq j}}^{M} \frac{1}{\|\boldsymbol{p}_i - \boldsymbol{p}_j\|_2}, \qquad \boldsymbol{P} := (\boldsymbol{p}_1, \dots, \boldsymbol{p}_M) \in (\mathbb{S}^2)^M. \tag{3.129}$$

From the extensive numerical studies of the Thomson problem, it is believed that for $M = 100$ points the energy of a (global) minimizer $\boldsymbol{P}^* \in (\mathbb{S}^2)^M$ is $E(\boldsymbol{P}^*) = 4448.350634331...$, see the online database [16]. Moreover, the corresponding point distribution is invariant under the tetrahedral group $\mathrm{T} \subset \mathrm{SO}(3)$, i.e., cf. (6.26) in Section 6.2.1,

$$\{\boldsymbol{p}_1, \dots, \boldsymbol{p}_M\} = \{\boldsymbol{G}\boldsymbol{p}_1, \dots, \boldsymbol{G}\boldsymbol{p}_M\} \subset \mathbb{S}^2, \qquad \boldsymbol{G} \in \mathrm{T}. \tag{3.130}$$

We will see that the optimization methods on Riemannian manifolds are able to take advantage of such symmetries, cf. Corollary 6.9, which is reflected by the faster convergence illustrated in Figure 3.3.

In what follows, we aim to compare the method of steepest descent, the Newton method, and the conjugate gradient method, cf. Example 3.20, for the computation of the global minimizer $\boldsymbol{P}^* \in \mathcal{M}$ on the product manifold, $\mathcal{M} := (\mathbb{S}^2)^M$, cf. Section 3.1.7. We recall that all methods use the line search method given by Algorithm 3.1, and that the nonlinear conjugate gradient method is implemented by Algorithm 3.3.

For the computation of the gradient $\nabla_{\mathcal{M}} E(\boldsymbol{P})$ and the Hessian matrix $\mathbf{H}_{\mathcal{M}} E(\boldsymbol{P}) \in \mathbb{R}^{3M\times 3M}$ of the Hessian $\mathrm{H}_{\mathcal{M}} E(\boldsymbol{P})$, $\boldsymbol{P} \in \mathcal{M}$, we refer to Theorem 5.3 and Remark 5.4 and 5.5 in Section 5.1. Furthermore, we recall that explicit formulas for the geodesics $\gamma_{\boldsymbol{P},\boldsymbol{v}} : \mathbb{R} \to \mathcal{M}$, $\boldsymbol{P} \in \mathcal{M}$, $\boldsymbol{v} \in \mathrm{T}_{\boldsymbol{P}}\mathcal{M}$, are provided by the formulas on the sphere $\mathbb{S}^2$, cf. Theorem 3.10, and the relation (3.55) for product manifolds of Section 3.1.7.

Unfortunately, it turns out that the Hessian $\mathrm{H}_{\mathcal{M}} E(\boldsymbol{P})$ has in general negative eigenvalues. That is, there exists an eigenvector $\boldsymbol{v} \in \mathrm{T}_{\boldsymbol{P}}\mathcal{M}$ with an eigenvalue λ such that

$$\lambda \|\boldsymbol{v}\|_2 = \mathrm{H}_{\mathcal{M}} E(\boldsymbol{P})(\boldsymbol{v}, \boldsymbol{v}) < 0.$$

Moreover, it appears that for any sequences $\{\boldsymbol{P}^{(k)}\}_{k\in\mathbb{N}_0} \subset \mathcal{M}$ approaching a local minimizer $\boldsymbol{P}^* \in \mathcal{M}$ of the energy $E : \mathcal{M} \to \mathbb{R}$, cf. (3.129), the minimal eigenvalues λ_k of the corresponding

Hessian $\mathrm{H}_{\mathcal{M}}E(\boldsymbol{P}^{(k)})$, $k \in \mathbb{N}_0$, are less or equal to zero with $\lim_{k\to\infty} \lambda_k = 0$. Hence, the globalized Newton method described by Algorithm 3.2 would degenerate to the method of steepest descent. Therefore, we use a modified Newton method, where we replace the usual Newton step, cf. line 10 in Algorithm 3.2, by the solution $\boldsymbol{d}^{(k)} \in \mathrm{T}_{\boldsymbol{P}^{(k)}}\mathcal{M}$ of the equation system

$$(\mathbf{H}_{\mathcal{M}}E(\boldsymbol{P}^{(k)}) - 2\lambda_k \boldsymbol{I})\boldsymbol{d}^{(k)} = -\boldsymbol{g}^{(k)}, \qquad \boldsymbol{g}^{(k)} := \nabla_{\mathcal{M}}E(\boldsymbol{P}^{(k)}) \in \mathrm{T}_{\boldsymbol{P}^{(k)}}\mathcal{M}, \tag{3.131}$$

whenever the minimal eigenvalue λ_k of the Hessian matrix representation $\mathbf{H}_{\mathcal{M}}E(\boldsymbol{P}^{(k)}) \in \mathbb{R}^{3M\times 3M}$ is negative.

For comparison reasons, we will initialize the method of steepest descent, the modified Newton method, and the conjugate gradient method with the same initial points $\boldsymbol{P}^{(0)} \in \mathcal{M}$ around the global minimizer $\boldsymbol{P}^* \in \mathcal{M}$. In the top row of Figure 3.3, we illustrate two different initial points. The initial points on the right are invariant under the tetrahedral group, cf. (3.130), whereas the initial points on the left are not. The corresponding convergence results are given in the middle row and the bottom row of Figure 3.3, where we plot the norm of the gradient $\|\nabla_{\mathcal{M}}E(\boldsymbol{P}^{(k)})\|_2$, and the geodesic distance $\mathrm{d}_{\mathcal{M}}(\boldsymbol{P}^*, \boldsymbol{P}^{(k)})$ of the iteration points $\boldsymbol{P}^{(k)}$ to the minimizer $\boldsymbol{P}^*$, respectively. Surprisingly, these results are in concordance with the predictions of the convergence rates given in Theorem 3.27, even if the assumptions of the positive definiteness, cf. (3.122), are not fulfilled, i.e., we observe quadratic convergence for the modified Newton method, superlinear convergence for the CG method, and linear convergence of the method of steepest descent. Moreover, we observe a faster convergence for the initial point distribution $\boldsymbol{P}^{(0)}$ which possess the same symmetry as the minimizer $\boldsymbol{P}^*$, cf. right column in Figure 3.3. This might be explained by the fact that the proposed optimization methods on Riemannian manifolds respect these symmetry constraints, cf. Corollary 6.9. Heuristically, for initial point distributions with such constraints there are less degrees of freedom for the search directions, which results in a faster convergence. This feature will be exploited in Section 6.2 and 6.3 for the computation of optimal quadrature functionals on the sphere $\mathbb{S}^2$ and the rotation group $\mathrm{SO}(3)$, respectively.

Finally, we like to mention as in Remark 3.21 that the CG method is a reasonable tradeoff between the poor convergence of the method of steepest descent, and the superior but expansive convergence of the (modified) Newton method. We note, that the computation of the Newton step requires the solution of the equation system (3.131) and the determination of the smallest eigenvalue, which has in general a complexity of $\mathcal{O}(M^3)$, and thus is far too much for large numbers of points M. □

We recall that the optimization methods on Riemannian manifolds are naturally motivated if the objective function, which is aimed to be minimized, is defined on a manifold. Moreover, there are certain advantages of the proposed methods compared to the standard approach by optimizing simply over a function which uses a parameterization of the underlying manifold. For example, the presented optimization methods are independent of the chosen local parameterizations. That means, after a change of the coordinate system the method of steepest descent, the Newton method, and the conjugate gradient method described in Example 3.20 lead always to the same iteration sequences, since the geodesic curves are independent of the local parameterization. In particular, there is no need of parametrization by local coordinates, so that all computations can be taken in Cartesian coordinates, as we do in Example 3.30 and for the computation of low-discrepancy points on the sphere $\mathbb{S}^d$, $d \in \mathbb{N}$, cf. Section 6.4. Furthermore, there are no boundary issues caused by local parametrizations, as for example in the case of spherical coordinates, where the north and south pole are singular points, cf. (3.71). Finally, we like to mention that for example on the sphere $\mathbb{S}^d$ the optimization methods respect naturally symmetry constraints caused by group actions, cf. Corollary 6.9 in Section 6.2.1, which may lead to faster convergence, cf. Figure 3.3. However, on general manifolds the presented methods might be hard to apply since for the computation of geodesics we need to solve a system of differential equations. Moreover, in

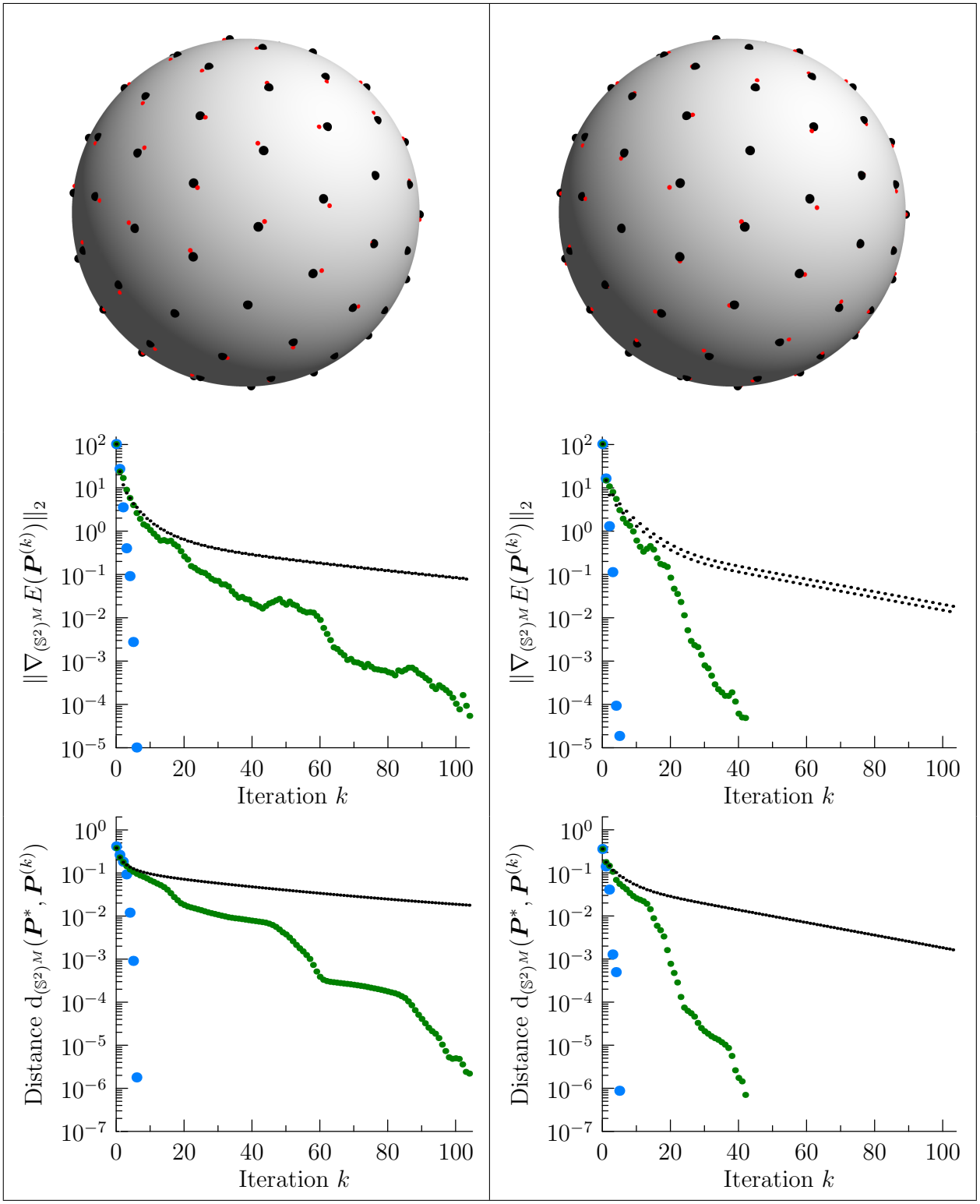

Figure 3.3: Convergence of the method of steepest descent (black), the modified Newton method (blue), and the CG method (green) on the product manifold $(\mathbb{S}^2)^M$ for minimizing the electrostatic energy $E(\boldsymbol{P})$ of $M = 100$ points $\boldsymbol{P} \in (\mathbb{S}^2)^M$, cf. (3.129), starting from a pure random perturbation (left) and a symmetric perturbation (right) of the minimizer $\boldsymbol{P}^*$. Top row: Illustrations of the minimizer (black dots) and the initial points (red dots). Middle row: Plot of the norm of the gradients $\nabla_{(\mathbb{S}^2)^M} E(\boldsymbol{P}^{(k)})$. Bottom row: Plot of the distance $\mathrm{d}_{(\mathbb{S}^2)^M}(\boldsymbol{P}^*, \boldsymbol{P}^{(k)})$ to the minimizer $\boldsymbol{P}^*$. For details see Example 3.30.

general it might be hard to provide closed form expression for the computation of point coordinates on a prescribed manifold. Nevertheless, for computations on the torus $\mathbb{T}^d$, the sphere $\mathbb{S}^d$, and the rotation group SO(3), which are of particular interest to us, we have already presented explicit and quite simple formulas in Section 3.2. For further applications of optimization methods on Riemannian manifolds, especially on matrix manifolds, we refer to the seminal paper of Edelman, Arias, and Smith [38].

4

Analysis and Reproducing Kernels on Specific Riemannian Manifolds

In this chapter we briefly recapitulate some usefull tools provided by harmonic analysis and introduce in Section 4.1–4.3 the standard L^2-basis systems on the torus $\mathbb{T}^d$, the sphere $\mathbb{S}^d$, $d \in \mathbb{N}$ and the rotation group $\mathrm{SO}(3)$. Furthermore, we present for these L^2-basis systems, accordingly to Theorem 2.2, closed form expressions of the Fourier expansions of certain discrepancy kernels, cf. Section 2.4. In particular, for the torus $\mathbb{T}^2$ and the sphere $\mathbb{S}^2$, these Fourier expansions find application for the efficient computation of low-discrepancy points on the sphere $\mathbb{S}^2$, cf. Section 6.4, and for efficient halftoning of images, cf. Section 6.5.

4.1 The Torus $\mathbb{T}^d$

The basics of harmonic analysis on the torus $\mathbb{T}^d$ are recapitulated in Section 4.1.1. Afterward, in Section 4.1.2, we are able to utilize the convolution theorem, cf. (4.5), for the explicit computation of the Fourier expansions of discrepancy kernels $K_{\mathcal{B}_{\mathrm{d}_{\mathbb{T}^d}}}$ which correspond to the weighted ball discrepancy $D^2_{\mathcal{B}_{\mathrm{d}_{\mathbb{T}^d}}}$, cf. Theorem 4.1. For the torus $\mathbb{T}^2$ we will use such a Fourier expansion for the efficient halftoning of images in Section 6.5.

4.1.1 Harmonic Analysis

For the analysis on the torus $\mathbb{T}^d$, $d \in \mathbb{N}$, cf. (3.63), we use the conventions given in Remark 3.14, where we keep in mind the simple identification $\mathbb{T}^d \cong \mathbb{R}^d/(2\pi\mathbb{Z}^d)$ by the parameterization $h : \mathbb{R}^d \to \mathbb{T}^d$, cf. (3.74) and (3.76). That is, by abuse of notation we will omit the subscript h for local coordinate representations $f_h = f \circ h$ of functions $f : \mathbb{T}^d \to \mathbb{C}$. In other words, we will write equivalently $f(\boldsymbol{x})$ or $f(\boldsymbol{\alpha})$ for the evaluation of f at the point $\boldsymbol{x} = h(\boldsymbol{\alpha}) \in \mathbb{T}^d$, $\boldsymbol{\alpha} \in \mathbb{R}^d$.

Using that convention, we will consider the space $L^2(\mathbb{T}^d)$ also as the space of 2π-periodic functions with the inner product, cf. (3.79),

$$(f,g)_{L^2(\mathbb{T}^d)} := \int_{a_1}^{a_1+2\pi} \dots \int_{a_d}^{a_d+2\pi} f(\boldsymbol{\alpha})\overline{g}(\boldsymbol{\alpha})\mathrm{d}\alpha_1 \dots \mathrm{d}\alpha_d, \quad f,g \in L^2(\mathbb{T}^d),$$

where $\boldsymbol{\alpha} := (\alpha_1, \dots, \alpha_d) \in \mathbb{R}^d$, $a_1, \dots, a_d \in \mathbb{R}$. Then the standard basis $\psi_{\boldsymbol{n}} \in L^2(\mathbb{T}^d)$, $\boldsymbol{n} \in \mathbb{Z}^d$, is

given by tensor products of exponentials

$$\psi_{\boldsymbol{n}}(\boldsymbol{x}) := \prod_{i=0}^{d} \mathrm{e}^{\mathrm{i}n_i\alpha_i} = \mathrm{e}^{\mathrm{i}\boldsymbol{n}^\top\boldsymbol{\alpha}}, \qquad \boldsymbol{x} = h(\boldsymbol{\alpha}), \quad \boldsymbol{\alpha} \in \mathbb{R}^d, \qquad \boldsymbol{n} := (n_1, \ldots, n_d)^\top \in \mathbb{Z}^d, \tag{4.1}$$

which obey the orthogonality relation $(\psi_{\boldsymbol{n}}, \psi_{\boldsymbol{m}})_{L^2(\mathbb{T}^d)} = (2\pi)^d \delta_{\boldsymbol{n},\boldsymbol{m}}$, $\boldsymbol{n}, \boldsymbol{m} \in \mathbb{Z}^d$. For later reference, we denote the space of trigonometric polynomials with degree at most $N \in \mathbb{N}_0$ by

$$\Pi^N(\mathbb{T}^d) := \operatorname{span}\{\psi_{\boldsymbol{n}} \,:\, \boldsymbol{n} \in I_N\}, \qquad I_N := \mathbb{Z}^d \cap [-N, N]^d, \tag{4.2}$$

which has dimension $d_N := (2N+1)^d$.

In what follows, we consider *translation invariant* kernels $K : \mathbb{T}^d \times \mathbb{T}^d \to \mathbb{R}$, which obey the relation

$$K(\boldsymbol{x}, \boldsymbol{y}) = k(\boldsymbol{x} - \boldsymbol{y}), \qquad \boldsymbol{x}, \boldsymbol{y} \in \mathbb{T}^d, \qquad k : \mathbb{T}^d \to \mathbb{R}. \tag{4.3}$$

In other words, a 2π-periodic function k on the Euclidean space $\mathbb{R}^d$ induces a translation invariant kernel K on the torus $\mathbb{T}^d$. By the property of the exponentials

$$\psi_{\boldsymbol{n}}(\boldsymbol{\alpha})\overline{\psi}_{\boldsymbol{n}}(\boldsymbol{\beta}) = \mathrm{e}^{\mathrm{i}\boldsymbol{n}^\top\boldsymbol{\alpha}}\mathrm{e}^{-\mathrm{i}\boldsymbol{n}^\top\boldsymbol{\beta}} = \mathrm{e}^{\boldsymbol{n}^\top(\boldsymbol{\alpha}-\boldsymbol{\beta})} = \psi_{\boldsymbol{n}}(\boldsymbol{\alpha} - \boldsymbol{\beta}), \qquad \boldsymbol{\alpha}, \boldsymbol{\beta} \in \mathbb{R}^d, \qquad \boldsymbol{n} \in \mathbb{Z}^d,$$

we have a simple relation between the Fourier coefficients of translation invariant kernels $K \in L^2(\mathbb{T}^d \times \mathbb{T}^d)$ and 2π-periodic functions $k \in L^2(\mathbb{T}^d)$, namely

$$K(\boldsymbol{x}, \boldsymbol{y}) = \sum_{\boldsymbol{n} \in \mathbb{Z}^d} \lambda_{\boldsymbol{n}} \psi_{\boldsymbol{n}}(\boldsymbol{x})\psi_{\boldsymbol{n}}(\boldsymbol{y}), \qquad k(\boldsymbol{x}) = \sum_{\boldsymbol{n} \in \mathbb{Z}^d} \lambda_{\boldsymbol{n}} \psi_{\boldsymbol{n}}(\boldsymbol{x}), \qquad \boldsymbol{x}, \boldsymbol{y} \in \mathbb{T}^d. \tag{4.4}$$

In particular, we have uniform convergence of the Fourier expansion for K if and only if the Fourier expansion of k converges uniformly.

We recall further the convolution theorem on the torus $\mathbb{T}^d$, which states that the convolution of two 2π-periodic functions $f, g \in L^2(\mathbb{T}^d)$ defined by

$$(f * g)(\boldsymbol{\alpha}) := \int_{-\pi+\alpha_1}^{\pi+\alpha_1} \cdots \int_{-\pi+\alpha_d}^{\pi+\alpha_d} f(\boldsymbol{\beta}) g(\boldsymbol{\alpha} - \boldsymbol{\beta}) \mathrm{d}\boldsymbol{\beta}, \qquad \boldsymbol{\alpha} := (\alpha_1, \ldots, \alpha_d) \in \mathbb{R}^d,$$

belongs to $L^2(\mathbb{T}^d)$ and admits the Fourier expansion

$$f * g = (2\pi)^d \sum_{\boldsymbol{n} \in \mathbb{Z}^d} \hat{f}_{\boldsymbol{n}} \hat{g}_{\boldsymbol{n}} \psi_{\boldsymbol{n}}, \qquad f := \sum_{\boldsymbol{n} \in \mathbb{Z}^d} \hat{f}_{\boldsymbol{n}} \psi_{\boldsymbol{n}}, \quad g := \sum_{\boldsymbol{n} \in \mathbb{Z}^d} \hat{g}_{\boldsymbol{n}} \psi_{\boldsymbol{n}}. \tag{4.5}$$

4.1.2 Reproducing Kernels

By Remark 2.3 we find that any translation invariant kernel of the form, cf. (4.3) and (4.4),

$$K(\boldsymbol{x}, \boldsymbol{y}) = \sum_{\boldsymbol{n} \in \mathbb{Z}^d} \lambda_{\boldsymbol{n}} \psi_{\boldsymbol{n}}(\boldsymbol{x})\psi_{\boldsymbol{n}}(\boldsymbol{y}), \qquad \boldsymbol{x}, \boldsymbol{y} \in \mathbb{T}^d. \tag{4.6}$$

with basis function $\psi_{\boldsymbol{n}} \in L^2(\mathbb{T}^d)$, cf. (4.1), and summable Fourier coefficients $\lambda_{\boldsymbol{n}} \geq 0$, $\boldsymbol{n} \in \mathbb{Z}^d$, is continuous and positive definite. Thus, K gives rise to a reproducing kernel Hilbert space $H_K(\mathbb{T}^d)$, cf. (2.4). In what follows we investigate the Fourier expansions (4.6) of certain disrepancy kernels, cf. Section 2.4.

The simplest discrepancy kernel which might come into mind is the Euclidean distance kernel K_{E}, cf. Corollary 2.15, which is induced by the Euclidean distance of the Euclidean space $\mathbb{R}^{2d}$.

With the parameterization $h : \mathbb{R}^d \to \mathbb{T}^d$, cf. (3.74), we obtain for points $\boldsymbol{x} = h(\boldsymbol{\alpha}), \boldsymbol{y} = h(\boldsymbol{\beta}) \in \mathbb{T}^d$, and coordinates $\boldsymbol{\alpha} := (\alpha_1, \ldots, \alpha_d), \boldsymbol{\beta} := (\beta_1, \ldots, \beta_d) \in \mathbb{R}^d$ the formula

$$K_{\mathrm{E}}(\boldsymbol{x}, \boldsymbol{y}) = C - \|\boldsymbol{x} - \boldsymbol{y}\|_2 = C - \sqrt{2d - 2\sum_{i=1}^{d} \cos(\alpha_i - \beta_i)}.$$

For the case $d = 1$ we can use the simple trigonometric relation

$$\|\boldsymbol{x} - \boldsymbol{y}\|_2 = 2 \sin\left(\frac{\mathrm{d}_{\mathbb{S}^1}(\boldsymbol{x}, \boldsymbol{y})}{2}\right), \qquad \boldsymbol{x}, \boldsymbol{y} \in \mathbb{T}^1 = \mathbb{S}^1 \subset \mathbb{R}^2.$$

Together with the uniformly convergent Fourier series

$$2 \sin\left(\frac{|s|}{2}\right) = \frac{4}{\pi} - \frac{8}{\pi} \sum_{n=1}^{\infty} \frac{\cos(ns)}{(2n-1)(2n+1)}, \qquad s \in [-\pi, \pi], \tag{4.7}$$

and the addition theorem of the cosine we arrive at the Fourier expansion

$$K_{\mathrm{E}}(\boldsymbol{x}, \boldsymbol{y}) = C + \frac{4}{\pi} \sum_{n \in \mathbb{Z}} \frac{\psi_n(\boldsymbol{x}) \overline{\psi}_n(\boldsymbol{y})}{(2n-1)(2n+1)}, \qquad \boldsymbol{x}, \boldsymbol{y} \in \mathbb{T}^1, \tag{4.8}$$

which is positive definite for $C \geq 4/\pi$. Unfortunately, for $d > 1$ we are not aware of an explicit formula of the Fourier coefficients $\lambda_{\boldsymbol{n}}$, $\boldsymbol{n} \in \mathbb{Z}^d$, cf. (4.6). Similarly difficult is the situation for other kernels induced by the Euclidean distance, as for example the discrepancy kernels which correspond to the L^2-discrepancy over Euclidean balls $K_{\mathcal{B}_{R^n},R}$, cf. Theorem 2.16.

However, for weighted ball discrepancy kernels $K_{\mathcal{B}_{\mathrm{d}_{\mathbb{T}^d}}}$, cf. Theorem 2.11, we can compute the Fourier coefficients by using the convolution theorem on the torus $\mathbb{T}^d$. We remark that in contrast to the sphere $\mathbb{S}^d$, cf. (4.32), the balls

$$B_{\mathbb{T}^d}(\boldsymbol{c}, r) = \{\boldsymbol{x} \in \mathbb{T}^d \ : \ \mathrm{d}_{\mathbb{T}^d}(\boldsymbol{x}, \boldsymbol{c}) < r\}, \qquad \boldsymbol{c} \in \mathbb{T}^d, \quad r > 0,$$

with respect to the geodesic distance $\mathrm{d}_{\mathbb{T}^d}$, cf. (3.78), cannot be characterized for $d > 1$ as intersections of the torus $\mathbb{T}^d$ with halfspaces. Hence, the Euclidean distance kernel K_{E} is not a special case of the weighted ball discrepancy kernel $K_{\mathcal{B}_{\mathrm{d}_{\mathbb{T}^d}}}$. Before we are able to present explicitly the Fourier expansions of the weighted ball discrepancy kernels $K_{\mathcal{B}_{\mathrm{d}_{\mathbb{T}^d}}}$ in Theorem 4.1, we need to introduce the *Bessel functions of first kind* J_ν, $\nu > -\frac{1}{2}$, which is defined via the gamma function Γ, cf. (2.77), by

$$J_\nu(z) := \sum_{k=0}^{\infty} \frac{(-1)^k}{k! \Gamma(k + \nu + 1)} \left(\frac{z}{2}\right)^{2k+\nu}, \qquad z \in \mathbb{C}. \tag{4.9}$$

Theorem 4.1. *Let the torus $\mathbb{T}^d$, $d \in \mathbb{N}$, with canonical measure $\mu_{\mathbb{T}^d}$, cf.* (3.79)*, and geodesic distance $\mathrm{d}_{\mathbb{T}^d}$, cf.* (3.78)*, be given. Then the discrepancy kernel $K_{\mathcal{B}_{\mathrm{d}_{\mathbb{T}^d}}}$, which corresponds to the weighted ball discrepancy $D^2_{\mathcal{B}_{\mathrm{d}_{\mathbb{T}^d}}}$, cf. Theorem 2.11, with respect to some finite Borel measure $\mu_{\mathbb{R}_+}$ supported on the interval $[0, R]$, $0 \leq R \leq \pi$, is given for $\boldsymbol{x}, \boldsymbol{y} \in \mathbb{T}^d$ by*

$$K_{\mathcal{B}_{\mathrm{d}_{\mathbb{T}^d}}}(\boldsymbol{x}, \boldsymbol{y}) = \int_{\mathbb{R}_+} \mu_{\mathbb{T}^d}(B_{\mathbb{T}^d}(\boldsymbol{x}, r) \cap B_{\mathbb{T}^d}(\boldsymbol{y}, r)) \mathrm{d}\mu_{\mathbb{R}_+}(r) = \sum_{\substack{\boldsymbol{k} \in \mathbb{Z}^d, \\ \boldsymbol{k} \in [0,1]^d}} \int_{\frac{s_{\boldsymbol{k}}}{2}}^{R} a_d(s_{\boldsymbol{k}}, r) \mathrm{d}\mu_{\mathbb{R}_+}(r) \tag{4.10}$$

where the function $a_d : [0, 2R] \times [0, R] \to \mathbb{R}$ *is defined by* (2.80) *in Theorem 2.16 and where* $s_{\boldsymbol{k}} := \|\boldsymbol{d}(\boldsymbol{x}, \boldsymbol{y}) + 2\pi\boldsymbol{k}\|_2$, $\boldsymbol{k} \in \mathbb{Z}^d \cap [0, 1]^d$, *is given by the minimal distant vector* $\boldsymbol{d}(\boldsymbol{x}, \boldsymbol{y}) \in \mathbb{R}^d$ *determined by, cf.* (3.74),

$$\|\boldsymbol{d}(\boldsymbol{x}, \boldsymbol{y})\|_2 = \min_{\substack{\boldsymbol{\alpha} \in h^{-1}(\boldsymbol{x}),\\ \boldsymbol{\beta} \in h^{-1}(\boldsymbol{y})}} \|\boldsymbol{\alpha} - \boldsymbol{\beta}\|_2. \tag{4.11}$$

In particular, for the Dirac measure $\mu_{\mathbb{R}_+} := \delta_R$ *the Fourier expansion is, cf.* (4.9),

$$K_{\mathcal{B}_{\mathrm{d}_{\mathbb{T}^d}},\delta_R}(\boldsymbol{x}, \boldsymbol{y}) = \frac{R^{2d}}{2^d \Gamma\left(\frac{d}{2} + 1\right)^2} + \sum_{\boldsymbol{n} \in \mathbb{Z}^d \setminus \{\boldsymbol{0}\}} \left(\frac{R}{\|\boldsymbol{n}\|_2}\right)^d J_{\frac{d}{2}}(R\|\boldsymbol{n}\|_2)^2 \psi_{\boldsymbol{n}}(\boldsymbol{x}) \overline{\psi}_{\boldsymbol{n}}(\boldsymbol{y}), \qquad \boldsymbol{x}, \boldsymbol{y} \in \mathbb{T}^d \tag{4.12}$$

and for the Lebesgue measure $\mu_{\mathbb{R}_+} := \mu_{[0,R]}$ *restricted to the interval* $[0, R]$ *the Fourier expansion is, cf.* (2.78),

$$\begin{aligned} &K_{\mathcal{B}_{\mathrm{d}_{\mathbb{T}^d}},\mu_{[0,R]}}(\boldsymbol{x}, \boldsymbol{y}) \\ &= \sum_{\boldsymbol{n} \in \mathbb{Z}^d} {}_2F_3\left(\frac{d+1}{2}, \frac{2d+1}{2}; \frac{d+2}{2}, d+1, \frac{2d+3}{2}; -R^2\|\boldsymbol{n}\|_2^2\right) \frac{R^{2d+1} \psi_{\boldsymbol{n}}(\boldsymbol{x}) \overline{\psi}_{\boldsymbol{n}}(\boldsymbol{y})}{2^d(2d+1)\Gamma\left(\frac{d+2}{2}\right)^2}, \quad \boldsymbol{x}, \boldsymbol{y} \in \mathbb{T}^d. \end{aligned} \tag{4.13}$$

Moreover, the Fourier expansions (4.12), (4.13) *are uniformly convergent.*

Proof. We begin with proofing the formula (4.10). From the representation (3.78) of the geodesic distance $\mathrm{d}_{\mathbb{T}^d}$ we infer that for the parameterization $h : \mathbb{R}^d \to \mathbb{T}^d$, cf. (3.74), the pre-image of the ball $B_{\mathbb{T}^d}(\boldsymbol{x}, r)$ with radius $0 \le r \le \pi$ is a disjoint union of d-dimensional Euclidean balls

$$B_{\mathbb{R}^d}(\boldsymbol{\alpha}, r) = \{\boldsymbol{\beta} \in \mathbb{R}^d \ : \ \|\boldsymbol{\alpha} - \boldsymbol{\beta}\|_2 \le r\}.$$

More precisely, we have

$$h^{-1}(B_{\mathbb{T}^d}(\boldsymbol{x}, r)) = \bigcup_{\boldsymbol{k} \in \mathbb{Z}^d} B_{\mathbb{R}^d}(\boldsymbol{\alpha} + 2\pi\boldsymbol{k}, r), \quad \boldsymbol{x} = h(\boldsymbol{\alpha}), \quad \boldsymbol{\alpha} \in \mathbb{R}^d, \quad 0 \le r \le \pi.$$

We recall, that in the proof of Theorem 2.16 we have already shown that the measure of two intersecting Euclidean balls $B_{\mathbb{R}^d}(\boldsymbol{\alpha}, r)$, $B_{\mathbb{R}^d}(\boldsymbol{\beta}, r)$ of radius $r \ge \|\boldsymbol{\alpha} - \boldsymbol{\beta}\|_2/2$ computes by

$$\mu_{\mathbb{R}^d}(B_{\mathbb{R}^d}(\boldsymbol{\alpha}, r) \cap B_{\mathbb{R}^d}(\boldsymbol{\beta}, r)) = a_d(\|\boldsymbol{\alpha} - \boldsymbol{\beta}\|_2, r).$$

Hence, we arrive by relation (3.78) and the relation (3.79) between the canonical measure $\mu_{\mathbb{T}^d}$ and the Lebesgue measure $\mu_{\mathbb{R}^d}$ for $0 \le r \le \pi$ at a formula for the intersections between two balls on the torus $\mathbb{T}^d$ given by

$$\begin{aligned} A_r(\boldsymbol{x}, \boldsymbol{y}) :=& \mu_{\mathbb{T}^d}\big(B_{\mathbb{T}^d}(\boldsymbol{x}, r) \cap B_{\mathbb{T}^d}(\boldsymbol{y}, r)\big) \\ =& \mu_{\mathbb{R}^d}\Big(\bigcup_{\boldsymbol{k} \in \mathbb{Z}^d} \big(B_{\mathbb{R}^d}(\boldsymbol{\beta}, r) \cap B_{\mathbb{R}^d}(\boldsymbol{\alpha} + 2\pi\boldsymbol{k}, r)\big)\Big) \\ =& \sum_{\boldsymbol{k} \in \mathbb{Z}^d} \mu_{\mathbb{R}^d}\big(B_{\mathbb{R}^d}(\boldsymbol{\beta}, r) \cap B_{\mathbb{R}^d}(\boldsymbol{\alpha} + 2\pi\boldsymbol{k}, r)\big) \\ =& \sum_{\boldsymbol{k} \in \mathbb{Z}^d} a_d(\|\boldsymbol{\alpha} - \boldsymbol{\beta} + 2\pi\boldsymbol{k}\|_2, r) \\ =& \sum_{\substack{\boldsymbol{k} \in \mathbb{Z}^d,\\ \boldsymbol{k} \cap [0,1]^d}} a_d(\|\boldsymbol{d}(\boldsymbol{x}, \boldsymbol{y}) + 2\pi\boldsymbol{k}\|_2, r), \qquad \boldsymbol{x} = h(\boldsymbol{\alpha}), \boldsymbol{y} = h(\boldsymbol{\beta}) \in \mathbb{T}^d, \quad \boldsymbol{\alpha}, \boldsymbol{\beta} \in \mathbb{R}^d, \end{aligned}$$

where $\boldsymbol{d}(\boldsymbol{x},\boldsymbol{y})$ is the minimal distance vector defined by (4.11). Thus, we obtain by Theorem 2.11 the expression (4.10) for kernels of the weighted ball discrepancy $D^2_{\mathcal{B}_{\mathrm{d}_{\mathbb{T}^d}}}$ on the torus $\mathbb{T}^d$.

For the computation of the Fourier coefficients $\lambda_{\boldsymbol{n}}$, $\boldsymbol{n}\in\mathbb{Z}^d$, cf. (4.6), in the expansions (4.12) and (4.13) we will use the convolution theorem, cf. (4.5). Therefore, we recall the original definition (2.51) of the discrepancy kernel in Theorem 2.10 and obtain for $0\le R<\pi$ and $\boldsymbol{x}=h(\boldsymbol{\alpha})$, $\boldsymbol{y}=h(\boldsymbol{\beta})\in\mathbb{T}^d$ the relation

$$K_{\mathcal{B}_{\mathrm{d}_{\mathbb{T}^d}}}(\boldsymbol{x},\boldsymbol{y})=\sum_{\boldsymbol{k},\boldsymbol{l}\in\mathbb{Z}^d}\int_0^R\int_{[-\pi,\pi]^d}1_{B_{\mathbb{R}^d}(\boldsymbol{\alpha}+2\pi\boldsymbol{k},r)}(\boldsymbol{\gamma})1_{B_{\mathbb{R}^d}(\boldsymbol{\beta}+2\pi\boldsymbol{l},r)}(\boldsymbol{\gamma})\mathrm{d}\boldsymbol{\gamma}\mathrm{d}\mu_{\mathbb{R}_+}(r).$$

Hence, using the translation invariance of the the Lebesgue measure $\mu_{\mathbb{R}^d}$ and the Euclidean distance in $\mathbb{R}^d$ we can write the above formula as

$$K_{\mathcal{B}_{\mathrm{d}_{\mathbb{T}^d}}}(\boldsymbol{x},\boldsymbol{y})=\sum_{\boldsymbol{k},\boldsymbol{l}\in\mathbb{Z}^d}\int_0^R\int_{[-\pi,\pi]^d}1_{B_{\mathbb{R}^d}(\boldsymbol{0},r)}(\boldsymbol{\gamma}+2\pi\boldsymbol{k})1_{B_{\mathbb{R}^d}(\boldsymbol{0},r)}(\boldsymbol{\alpha}-\boldsymbol{\beta}-\boldsymbol{\gamma}+2\pi\boldsymbol{l})\mathrm{d}\boldsymbol{\gamma}\mathrm{d}\mu_{\mathbb{R}_+}(r)$$

which further simplifies to

$$K_{\mathcal{B}_{\mathrm{d}_{\mathbb{T}^d}}}(\boldsymbol{x},\boldsymbol{y})=\int_0^R(b_r*b_r)(\boldsymbol{\alpha}-\boldsymbol{\beta})\mathrm{d}\mu_{\mathbb{R}_+}(r),\qquad \boldsymbol{x}=h(\boldsymbol{\alpha}),\boldsymbol{y}=h(\boldsymbol{\beta})\in\mathbb{T}^d,\tag{4.14}$$

where we define for $0\le r<\pi$ the 2π-periodic characteristic function

$$b_r(\boldsymbol{\alpha}):=\sum_{\boldsymbol{k}\in\mathbb{Z}^d}1_{B_{\mathbb{R}^d}(\boldsymbol{0},r)}(\boldsymbol{\alpha}+2\pi\boldsymbol{k}),\qquad \boldsymbol{\alpha}\in\mathbb{R}^d.$$

It is well known, cf. [60, Appendix B.5], that the characteristic function b_r has the following Fourier expansion

$$b_r(\boldsymbol{\alpha})=\sum_{\boldsymbol{n}\in\mathbb{Z}^d}\hat{b}_r(\|\boldsymbol{n}\|_2)\mathrm{e}^{\mathrm{i}\boldsymbol{n}^\top\boldsymbol{\alpha}},\qquad \boldsymbol{\alpha}\in\mathbb{R}^d,\quad 0\le r<\pi,$$

where the Fourier coefficients $\hat{b}_r(\|\boldsymbol{n}\|_2)$, $\boldsymbol{n}\in\mathbb{Z}^d$, are expressed via the Bessel functions of first kind J_ν, cf. (4.9), and the volume $V_d(r)$ of a d-dimensional Euclidean ball $B_{\mathbb{R}^d}$ of radius $r\ge 0$, cf. (2.81), by

$$\hat{b}_r(t):=\frac{1}{(2\pi)^d}\begin{cases}V_d(r), & t=0,\\ \left(\frac{2\pi r}{t}\right)^{\frac{d}{2}}J_{\frac{d}{2}}(rt), & t>0.\end{cases}$$

Thus, we infer from the convolution theorem on the torus $\mathbb{T}^d$, cf. (4.5), that, after interchanging integration and summation, the equation (4.14) leads for $0\le R\le\pi$ to the Fourier expansion

$$K_{\mathcal{B}_{\mathrm{d}_{\mathbb{T}^d}}}(\boldsymbol{x},\boldsymbol{y})=\sum_{\boldsymbol{n}\in\mathbb{Z}^d}\lambda_n\psi_{\boldsymbol{n}}(\boldsymbol{x})\overline{\psi}_{\boldsymbol{n}}(\boldsymbol{y}),\qquad \lambda_{\boldsymbol{n}}:=(2\pi)^d\int_0^R\hat{b}_r(\|\boldsymbol{n}\|_2)^2\mathrm{d}\mu_{\mathbb{R}_+}(r),$$

and the assertions (4.12) and (4.13) follow by integration with respect to the Dirac measure δ_R and the Lebesgue measure $\mu_{[0,R]}$. ■

4.2 The Sphere $\mathbb{S}^d$

We briefly recapitulate in Section 4.2.1 the basics of harmonic analysis on the sphere $\mathbb{S}^d$, where we present in Theorem 4.2 the relation between the Fourier expansion of zonal kernels and Gegenbauer polynomials, which we need to describe the convolution theorem on the sphere by Theorem 4.3. In Section 4.2.2 we recall in Theorem 4.4 the interesting relation between the Euclidean distance kernel K_{E}, cf. Section 2.4.2, and a certain weighted ball discrepancy kernel $K_{\mathcal{B}_{\mathrm{d}_{\mathbb{T}^d}}}$, cf. Section 2.4.1. This enables us to compute explicitly the Fourier expansions for the Euclidean distance kernel K_{E} in Theorem 4.6, after presenting the Fourier expansion of general weighted ball discrepancy kernels $K_{\mathcal{B}_{\mathrm{d}_{\mathbb{T}^d}}}$ by means of convolution, cf. Theorem 4.5. For the sphere $\mathbb{S}^2$ we will use this Fourier expansion for the efficient computation of low-discrepancy points and for efficient halftoning, cf. Section 6.4 and 6.5.

4.2.1 Harmonic Analysis

For the analysis on the sphere $\mathbb{S}^d$, $d \in \mathbb{N}$, cf. (3.62), we recall that a polynomial $p : \mathbb{R}^{d+1} \to \mathbb{C}$ in $(d+1)$ variables with complex coefficients is called *homogeneous of degree* $n \in \mathbb{N}_0$ and *harmonic* if it satisfies

$$p(\lambda \boldsymbol{x}) = |\lambda|^n p(\boldsymbol{x}),\ \lambda > 0, \quad \text{and} \quad \sum_{i=1}^{d+1} \frac{\partial^2}{\partial x_i^2} p(\boldsymbol{x}) = 0,\ \boldsymbol{x} := (x_1, \ldots, x_{d+1})^\top \in \mathbb{R}^{d+1},$$

respectively. The restriction of a harmonic homogeneous polynomial p to the sphere $\mathbb{S}^d$ is called a *spherical harmonic*. The space of all spherical harmonics of exact degree n is denote by $\Pi_n(\mathbb{S}^d)$, and the space

$$\Pi^N(\mathbb{S}^d) := \operatorname{span}\{f \in \Pi_n(\mathbb{S}^d), n = 1, \ldots, N\}, \qquad N \in \mathbb{N}_0, \tag{4.15}$$

consists of all spherical harmonics with degree at most N. It is well known, cf. [94], that the spaces $\Pi_n(\mathbb{S}^d)$, $n \in \mathbb{N}_0$, are mutually orthogonal with respect to the L^2-product on the sphere $\mathbb{S}^d$ with canonical measure $\mu_{\mathbb{S}^d}$, cf. (3.51), and that

$$L^2(\mathbb{S}^d) = \text{cl}\ \operatorname{span}\{p \in \Pi_n(\mathbb{S}^d),\ n \in \mathbb{N}_0\}.$$

Moreover, the dimension of the spaces $\Pi_n(\mathbb{S}^d)$ is given by

$$D_{d,n} := \begin{cases} 1, & n = 0, \\ \frac{(2n+d-1)\Gamma(n+d-1)}{\Gamma(n+1)\Gamma(d)}, & n \geq 1, \end{cases} \tag{4.16}$$

where the gamma function Γ is defined in (2.77). Hence, any orthonormal basis consisting of spherical harmonics $Y_{n,k} \in \Pi_n(\mathbb{S}^d)$ of *degree* $n \in \mathbb{N}_0$ and *order* $k \in \mathbb{N}$, $1 \leq k \leq D_{d,n}$, leads to an orthonormal basis of the space $L^2(\mathbb{S}^2)$. We recall that the canonical measure $\mu_{\mathbb{S}^d}$, cf. (3.72), is normalized by

$$\omega_d := \mu_{\mathbb{S}^d}(\mathbb{S}^d) = \int_0^{2\pi} \mathrm{d}\theta_1 \int_0^{\pi} \sin(\theta_2)\mathrm{d}\theta_2 \cdots \int_0^{\pi} \sin(\theta_d)^{d-1}\mathrm{d}\theta_d = \frac{2\pi^{\frac{d+1}{2}}}{\Gamma\left(\frac{d+1}{2}\right)}, \qquad d \in \mathbb{N}. \tag{4.17}$$

Accordingly to the last relation in (4.17) we define $\omega_0 := 2$, which reflects the fact that the 0-dimensional sphere $\mathbb{S}^0 := \{\pm 1\} \subset \mathbb{R}$ is equipped with the counting measure $\mu_{\mathbb{S}^0} := \delta_{-1} + \delta_{+1}$.

We restrict our attention to *zonal* kernels $K : \mathbb{S}^d \times \mathbb{S}^d \to \mathbb{R}$, i.e., kernels of the form

$$K(\boldsymbol{x}, \boldsymbol{y}) = k(\boldsymbol{x}^\top \boldsymbol{y}), \qquad \boldsymbol{x}, \boldsymbol{y} \in \mathbb{S}^d, \qquad k : [-1, 1] \to \mathbb{R}. \tag{4.18}$$

Hence, a zonal kernel K on the sphere $\mathbb{S}^d$ is induced by a function k on the interval $[-1,1]$. Obviously, zonal kernels are *rotational invariant* in the sense that, cf. (3.64),

$$K(\boldsymbol{R}\boldsymbol{x},\boldsymbol{R}\boldsymbol{y}) = K(\boldsymbol{x},\boldsymbol{y}), \qquad \boldsymbol{x},\boldsymbol{y}\in\mathbb{S}^d, \quad \boldsymbol{R}\in\mathrm{SO}(d+1). \tag{4.19}$$

Conversely, any rotational invariant kernel is zonal, cf. [41, Lemma 9.5.2]. In that respect, we recapitulate the famous addition theorem of orthonormal spherical harmonics $Y_{n,k}$, cf. [94, Theorem 2], given by the formula

$$\sum_{k=1}^{D_{d,n}} Y_{n,k}(\boldsymbol{x})\overline{Y}_{n,k}(\boldsymbol{y}) = \frac{D_{d,n}}{\omega_d} P_n^{(d)}(\boldsymbol{x}^\top\boldsymbol{y}), \qquad \boldsymbol{x},\boldsymbol{y}\in\mathbb{S}^d, \quad n\in\mathbb{N}_0, \tag{4.20}$$

where $P_n^{(d)}:[-1,1]\to\mathbb{R}$ are the uniquely determined polynomials of degree n which are normalized by $P_n^{(d)}(1)=1$ and satisfy the orthogonality relations

$$\int_{-1}^{1} P_n^{(d)}(t)P_m^{(d)}(t)(1-t^2)^{\frac{d}{2}-1}\mathrm{d}t = 0, \qquad n\neq m. \tag{4.21}$$

For $d=1$ the polynomials $P_n^{(d)}$ are exactly the *Chebyshev polynomials of the first kind* T_n, $n\in\mathbb{N}_0$, cf. [1, Eq. 22.3.15], i.e., $T_n = P_n^{(1)}$, $n\in\mathbb{N}_0$. For $d\geq 2$ the polynomials $P_n^{(d)}$ are related to the *Gegenbauer polynomials* $C_n^\lambda:[-1,1]\to\mathbb{R}$, $\lambda>0$, cf. [1, Table 22.2], due to

$$C_n^{\frac{d-1}{2}} = C_n^{\frac{d-1}{2}}(1)P_n^{(d)}, \qquad C_n^{\frac{d-1}{2}}(1) = \frac{\Gamma(n+d-1)}{\Gamma(n+1)\Gamma(d-1)}, \quad n\in\mathbb{N}_0. \tag{4.22}$$

We recall that the function space, cf. (4.21),

$$L^2\left([-1,1],(1-t^2)^{\frac{d}{2}-1}\right) := \left\{k:[-1,1]\to\mathbb{R} \;:\; \int_{-1}^{1}|k(t)|^2(1-t^2)^{\frac{d}{2}-1}\mathrm{d}t<\infty\right\} \tag{4.23}$$

can be made into a Hilbert space and that any function $f\in L^2([-1,1],(1-t^2)^{\frac{d}{2}-1})$ can be expanded in a series of Gegenbauer polynomials. The relation between the expansion of k and that of a zonal kernel K, cf. (4.18), in terms of spherical harmonics is presented in the following Theorem 4.2, which allows us to compute the Fourier coefficients of a zonal kernel more easily.

Theorem 4.2. *For $d\in\mathbb{N}$, $d\geq 2$, let the sphere $\mathbb{S}^d$ with an orthonormal basis of spherical harmonics $Y_{n,k}\in L^2(\mathbb{S}^d)$, $n\in\mathbb{N}_0$, $k=1,\dots,D_{d,n}$, be given. Then the zonal kernel, cf.* (4.23)*,*

$$K(\boldsymbol{x},\boldsymbol{y}) := k(\boldsymbol{x}^\top\boldsymbol{y}), \quad \boldsymbol{x},\boldsymbol{y}\in\mathbb{S}^d, \qquad k\in L^2\left([-1,1],(1-t^2)^{\frac{d}{2}-1}\right), \tag{4.24}$$

admits the $\mu_{\mathbb{S}^d\times\mathbb{S}^d}$ almost everywhere convergent Fourier expansion

$$K(\boldsymbol{x},\boldsymbol{y}) = \sum_{n=0}^{\infty}\lambda_n\sum_{k=1}^{D_{d,n}} Y_{n,k}(\boldsymbol{x})\overline{Y}_{n,k}(\boldsymbol{y}), \quad \boldsymbol{x},\boldsymbol{y}\in\mathbb{S}^d, \qquad \lambda_n := \omega_d\frac{d-1}{2n+d-1}a_n, \quad n\in\mathbb{N}_0, \tag{4.25}$$

where $\omega_d := \mu_{\mathbb{S}^d}(\mathbb{S}^d)$, cf. (4.17)*, and*

$$a_n := \frac{1}{C_{d,n}}\int_{-1}^{1} k(t)C_n^{\frac{d-1}{2}}(t)(1-t^2)^{\frac{d}{2}-1}\mathrm{d}t, \quad C_{d,n} := \frac{\pi 2^{3-d}\Gamma(n+d-1)}{\Gamma(n+1)(2n+d-1)\Gamma\left(\frac{d-1}{2}\right)^2}, \quad n\in\mathbb{N}_0. \tag{4.26}$$

Proof. The function $k : [-1,1] \to \mathbb{R}$ can be expanded by (4.24) in terms of Gegenbauer polynomials as

$$k = \sum_{n=0}^{\infty} a_n C_n^{\frac{d-1}{2}},$$

where the Fourier coefficients are determined by (4.26). For the normalization constant $C_{d,n}$ we refer to [1, Table 22.2]. From the relations (4.16) and (4.22) we get

$$\frac{D_{d,n}}{C_n^{\frac{d-1}{2}}(1)} = \frac{2n+d-1}{d-1}, \qquad n \in \mathbb{N}_0, \qquad d \geq 2.$$

Together with the addition theorem (4.20) we arrive for $\boldsymbol{x}, \boldsymbol{y} \in \mathbb{S}^d$ at the formal expansion, cf. (4.25),

$$K(\boldsymbol{x},\boldsymbol{y}) = k(\boldsymbol{x}^\top \boldsymbol{y}) = \frac{1}{\omega_d} \sum_{n=0}^{\infty} \lambda_n \frac{2n+d-1}{d-1} C_n^{\frac{d-1}{2}}(\boldsymbol{x}^\top \boldsymbol{y}) = \sum_{n=0}^{\infty} \lambda_n \sum_{k=1}^{D_{d,n}} Y_{n,k}(\boldsymbol{x}) \overline{Y}_{n,k}(\boldsymbol{y}),$$

which can be shown, by the theory of Hilbert spaces, to converge $\mu_{\mathbb{S}^d \times \mathbb{S}^d}$ almost everywhere. ■

Another useful tool in harmonic analysis is that of convolution. The convolution of two kernels $F, G \in L^2(\mathbb{S}^d \times \mathbb{S}^d)$ on the sphere $\mathbb{S}^d$ is defined by

$$(F * G)(\boldsymbol{x},\boldsymbol{y}) := \int_{\mathbb{S}^d} F(\boldsymbol{x},\boldsymbol{z}) G(\boldsymbol{z},\boldsymbol{y}) \mathrm{d}\mu_{\mathbb{S}^d}(\boldsymbol{z}), \qquad \boldsymbol{x},\boldsymbol{y} \in \mathbb{S}^d, \tag{4.27}$$

and one checks that $F * G \in L^2(\mathbb{S}^d \times \mathbb{S}^d)$. Furthermore, by the rotational invariance of the canonical measure $\mu_{\mathbb{S}^d}$ we find that the convolution of two zonal kernels on the sphere $\mathbb{S}^d$ is again a zonal kernel. We remark, that the following Theorem 4.3 is an easy consequence of the famous Funk-Hecke Theorem, cf. [94, Theorem 6].

Theorem 4.3. *For the sphere $\mathbb{S}^d$, $d \geq 2$, let $F, G \in L^2(\mathbb{S}^d \times \mathbb{S}^d)$ be zonal kernels given by*

$$F(\boldsymbol{x},\boldsymbol{y}) := f(\boldsymbol{x}^\top \boldsymbol{y}),\ G(\boldsymbol{x},\boldsymbol{y}) := g(\boldsymbol{x}^\top \boldsymbol{y}), \quad \boldsymbol{x},\boldsymbol{y} \in \mathbb{S}^d, \quad f := \sum_{n=0}^{\infty} a_n C_n^{\frac{d-1}{2}},\ g := \sum_{n=0}^{\infty} b_n C_n^{\frac{d-1}{2}}.$$

Then the convolution of F and G can be computed by

$$(F * G)(\boldsymbol{x},\boldsymbol{y}) = h(\boldsymbol{x}^\top \boldsymbol{y}), \qquad \boldsymbol{x},\boldsymbol{y} \in \mathbb{S}^d, \qquad h := \omega_d \sum_{n=0}^{\infty} \frac{d-1}{2n+d-1} a_n b_n C_n^{\frac{d-1}{2}}, \tag{4.28}$$

where $\omega_d := \mu_{\mathbb{S}^d}(\mathbb{S}^d)$, cf. (4.17).

Proof. We apply the definition of the convolution, cf. (4.27), to the kernels F, G and obtain after interchange of integration and summation the relation

$$(F * G)(\boldsymbol{x},\boldsymbol{y}) = \sum_{n,m=0}^{\infty} a_n b_m \int_{\mathbb{S}^d} C_n^{\frac{d-1}{2}}(\boldsymbol{x}^\top \boldsymbol{z}) C_m^{\frac{d-1}{2}}(\boldsymbol{z}^\top \boldsymbol{y}) \mathrm{d}\mu_{\mathbb{S}^d}(\boldsymbol{z}), \qquad \boldsymbol{x},\boldsymbol{y} \in \mathbb{S}^d. \tag{4.29}$$

From the addition theorem (4.20) we infer that the reproducing kernel K_n of $\Pi_n(\mathbb{S}^d)$ is related to Gegenbauer polynomials, cf. (4.22), by

$$K_n(\boldsymbol{x},\boldsymbol{y}) := \frac{1}{\omega_d} \frac{2n+d-1}{d-1} C_n^{\frac{d-1}{2}}(\boldsymbol{x}^\top \boldsymbol{y}), \qquad \boldsymbol{x},\boldsymbol{y} \in \mathbb{S}^d, \quad n \in \mathbb{N}_0,\ d \geq 2.$$

Hence, with the reproducing property of the kernel K_n we obtain

$$\begin{aligned}\frac{1}{\omega_d}\frac{2n+d-1}{d-1}C_n^{\frac{d-1}{2}}(\boldsymbol{x}^\top\boldsymbol{y}) &= K_n(\boldsymbol{x},\boldsymbol{y}) = (K_n(\boldsymbol{x},\cdot),K_n(\boldsymbol{y},\cdot))_{L^2(\mathbb{S}^d)}\\ &= \frac{1}{\omega_d^2}\left(\frac{2n+d-1}{d-1}\right)^2\int_{\mathbb{S}^d} C_n^{\frac{d-1}{2}}(\boldsymbol{x}^\top\boldsymbol{z})C_n^{\frac{d-1}{2}}(\boldsymbol{z}^\top\boldsymbol{y})\mathrm{d}\mu_{\mathbb{S}^d}(\boldsymbol{z}).\end{aligned}$$

This yields together with the orthogonality of the spaces $\Pi_n(\mathbb{S}^d)$ and $\Pi_m(\mathbb{S}^d)$ for $n \neq m$ in relation (4.29) the assertion (4.28). ■

4.2.2 Reproducing Kernels

We recall by Remark 2.3 that any zonal kernel of the form, cf. Theorem 4.2,

$$K(\boldsymbol{x},\boldsymbol{y}) = \sum_{n=0}^{\infty}\lambda_n\sum_{k=1}^{D_{d,n}} Y_{n,k}(\boldsymbol{x})\overline{Y}_{n,k}(\boldsymbol{y}), \qquad \boldsymbol{x},\boldsymbol{y}\in\mathbb{S}^d, \tag{4.30}$$

is a positive definite kernel, for any orthonormal basis of spherical harmonics $Y_{n,k}$, $n \in \mathbb{N}_0$, $k = 1,\dots,D_{d,n}$, whenever $\lambda_n \geq 0$, $n \in \mathbb{N}_0$, and $\sum_{n=0}^{\infty} D_{d,n}\lambda_n < \infty$. Thus, K gives rise to a reproducing kernel Hilbert space $H_K(\mathbb{S}^d)$, cf. Theorem 2.4. In what follows we investigate the Fourier expansions (4.30) of certain disrepancy kernels, cf. Section 2.4.

We observe that the Euclidean distance and the geodesic distance on $\mathbb{S}^d$ can be written as, cf. (3.68),

$$\|\boldsymbol{x}-\boldsymbol{y}\|_2 = \sqrt{2-2\boldsymbol{x}^\top\boldsymbol{y}}, \qquad \mathrm{d}_{\mathbb{S}^d}(\boldsymbol{x},\boldsymbol{y}) = \arccos(\boldsymbol{x}^\top\boldsymbol{y}), \qquad \boldsymbol{x},\boldsymbol{y}\in\mathbb{S}^d, \tag{4.31}$$

respectively. Hence, any kernel which depends only on the Euclidean distance between two points $\boldsymbol{x},\boldsymbol{y}\in\mathbb{S}^d$ is zonal and allows for a Fourier expansion (4.30). We note that the Euclidean distance kernel K_{E}, cf. Corollary 2.15, and the kernels $K_{\mathcal{B}_{\mathbb{R}^n},R}$, cf. Theorem 2.16, which correspond to L^2-discrepancies over Euclidean balls $D^2_{\mathcal{B}_{/R^n},R}$, are zonal kernels. The Fourier coefficients of the Euclidean distance kernel K_{E} and other related (conditionally) positive definite kernels may be found in [95]. Another way for computing the Fourier coefficients of zonal kernels is to utilize Theorem 4.2 with known Gegenbauer expansions. A list of Gegenbauer expansions for commonly used zonal kernels in the radial basis function community is given in [11]. However, we aim to make use of convolution and like to present further interesting relations.

We start by remarking that on the sphere $\mathbb{S}^d$ the L^2-discrepancies over halfspaces $D^2_{\mathcal{H}_+}$, cf. (2.69), and the L^2-discrepancies over Euclidean balls $D^2_{\mathcal{B}_{\mathbb{R}^n},R}$, cf. (2.76), can be considered as weighted ball discrepancies $D^2_{\mathcal{B}_{\mathrm{d}_{\mathbb{S}^d}}}$, cf. (2.56). Indeed, by the relations, see the definition of halfspaces (2.59),

$$\mathbb{S}^d \cap h_+(\boldsymbol{x},\cos(r)) = \left\{\boldsymbol{y}\in\mathbb{S}^d \,:\, \boldsymbol{x}^\top\boldsymbol{y}\geq\cos(r)\right\} = B_{\mathbb{S}^d}(\boldsymbol{x},r), \qquad \boldsymbol{x}\in\mathbb{S}^d,\ r\in[0,\pi], \tag{4.32}$$

and

$$\mathbb{S}^d \cap B_{\mathbb{R}^{d+1}}(\boldsymbol{x},r) = \left\{\boldsymbol{y}\in\mathbb{S}^d \,:\, \boldsymbol{x}^\top\boldsymbol{y}\geq\frac{1}{2}\big(\|\boldsymbol{x}\|_2^2+1-r^2\big)\right\}, \qquad \boldsymbol{x}\in\mathbb{R}^{d+1},\ r\geq 0, \tag{4.33}$$

we observe that the balls $B_{\mathbb{S}^d}(\boldsymbol{x},r)\subset\mathbb{S}^d$ (spherical caps) are exactly intersections of the sphere $\mathbb{S}^d$ with halfspaces or Euclidean balls. Hence, measures on the set of halfspaces $\mathcal{H}_+$ or Euclidean balls $\mathcal{B}_{\mathbb{R}^n}$ induce measures on the basis set $\mathcal{B}_{\mathrm{d}_{\mathbb{S}^d}}$, which consists of spherical caps. The remarkable relation between the canonical L^2-discrepancies $D^2_{\mathcal{H}_+}$ over halfspaces and that of the weighted

ball discrepancy $D^2_{\mathcal{B}_{\mathrm{d}_{\mathbb{S}^d}}}$ leads to the following result.

Theorem 4.4. *Let the sphere $\mathbb{S}^d$, $d \in \mathbb{N}$, with geodesic distance $\mathrm{d}_{\mathbb{S}^d}$ and canonical measure $\mu_{\mathbb{S}^d}$ be given. Then the discrepancy kernel $K_{\mathcal{B}_{\mathrm{d}_{\mathbb{S}^d}}}$, which corresponds to the weighted ball discrepancy $D^2_{\mathcal{B}_{\mathrm{d}_{\mathbb{S}^d}}}$ with respect to the density $\mathrm{d}\mu_{\mathbb{R}_+}(r) = \sin(r)\mathrm{d}r$, $r \in [0,\pi]$, reads as*

$$K_{\mathcal{B}_{\mathrm{d}_{\mathbb{S}^d}}}(\boldsymbol{x},\boldsymbol{y}) = \int_0^\pi A_r(\boldsymbol{x},\boldsymbol{y})\sin(r)\mathrm{d}r = \omega_d - \frac{\omega_{d-1}}{d}\|\boldsymbol{x}-\boldsymbol{y}\|_2, \qquad \boldsymbol{x},\boldsymbol{y} \in \mathbb{S}^d, \tag{4.34}$$

where $A_r(\boldsymbol{x},\boldsymbol{y}) := \mu_{\mathbb{S}^d}(B_{\mathbb{S}^d}(\boldsymbol{x},r) \cap B_{\mathbb{S}^d}(\boldsymbol{y},r))$ and $\omega_d := \mu_{\mathbb{S}^d}(\mathbb{S}^d)$, cf. (4.17).

Proof. By relation (4.32) we will apply Theorem 2.14 for the set $\mathbb{S}^d \subset \mathbb{R}^{d+1}$ and the natural measure $\mu_D := \mu_{\mathbb{S}^d} \times \mu_{\mathbb{R}}$, cf. Example 2.13. Since the set of all hyperplanes which intersect the sphere $\mathbb{S}^d$ is given by, cf. (2.63),

$$H_{\mathrm{conv}(\mathbb{S}^d)} = \{h(\boldsymbol{n},s) \ : \ \boldsymbol{n} \in \mathbb{S}^d, \ s \in [-1,1]\}$$

we calculate by definition (2.62) that

$$\mu_{\mathcal{H}}(H_{\mathrm{conv}(\mathbb{S}^d)}) = \frac{1}{2}\mu_D \circ \Phi^{-1}(H_{\mathrm{conv}(\mathbb{S}^d)}) = \frac{1}{2}\int_{-1}^1 \int_{\mathbb{S}^d} \mathrm{d}\mu_{\mathbb{S}^d}(\boldsymbol{n})\mathrm{d}s = \omega_d.$$

Hence, for $\boldsymbol{x},\boldsymbol{y} \in \mathbb{S}^d$ the relation (2.70) of Theorem 2.14 reads after a change of variable $s = \cos(r)$ and the use of (4.32) as

$$\begin{aligned} \omega_d - \mathrm{d}_{\mathbb{S}^d,\mathcal{H}}(\boldsymbol{x},\boldsymbol{y}) &= K_{\mathcal{H}_+}(\boldsymbol{x},\boldsymbol{y}) \\ &= \int_{-1}^1 \int_{\mathbb{S}^d} 1_{h_+(\boldsymbol{n},s)}(\boldsymbol{x}) 1_{h_+(\boldsymbol{n},s)}(\boldsymbol{y}) \mathrm{d}\mu_{\mathbb{S}^d}(\boldsymbol{n})\mathrm{d}s \\ &= \int_0^\pi \int_{\mathbb{S}^d} 1_{B_{\mathbb{S}^d}(\boldsymbol{c},r)}(\boldsymbol{x}) 1_{B_{\mathbb{S}^d}(\boldsymbol{c},r)}(\boldsymbol{y}) \mathrm{d}\mu_{\mathbb{S}^d}(\boldsymbol{c})\mathrm{d}\sin(r)\mathrm{d}r = K_{\mathcal{B}_{\mathrm{d}_{\mathbb{S}^d}}}(\boldsymbol{x},\boldsymbol{y}). \end{aligned} \tag{4.35}$$

From Example 2.13 we know that the distance $\mathrm{d}_{\mathbb{S}^d,\mathcal{H}}$ is a multiple of the Euclidean distance. Using the rotational invariance of the canonical measure $\mu_{\mathbb{S}^d}$ we obtain that the relation (2.68) can be written for $\boldsymbol{e}_{d+1} := (0,\ldots,0,1)^\top \in \mathbb{S}^d$ as

$$\mathrm{d}_{\mathbb{S}^d,\mathcal{H}}(\boldsymbol{x},\boldsymbol{y}) = \frac{1}{2}\|\boldsymbol{x}-\boldsymbol{y}\|_2 \int_{\mathbb{S}^d} |\boldsymbol{n}^\top \boldsymbol{e}_{d+1}| \mathrm{d}\mu_{\mathbb{S}^d}(\boldsymbol{n}) = \frac{\omega_{d-1}}{2}\|\boldsymbol{x}-\boldsymbol{y}\|_2 \int_0^\pi |\cos(\theta_d)| \sin(\theta_d)^{d-1}\mathrm{d}\theta_d. \tag{4.36}$$

By symmetry and a change of variable $t = \sin(\theta_d)$ we get

$$\int_0^\pi |\cos(\theta_d)| \sin(\theta_d)^{d-1}\mathrm{d}\theta_d = 2\int_0^{\frac{\pi}{2}} \cos(\theta_d)\sin(\theta_d)^{d-1}\mathrm{d}\theta_d = 2\int_0^1 t^{d-1}\mathrm{d}t = \frac{2}{d},$$

and arrive together with (4.35) and (4.36) at the assertion (4.34). ∎

We utilize the convolution on the sphere $\mathbb{S}^d$, cf. Theorem 4.3, in order to obtain in Theorem 4.5 closed form expressions for the Fourier coefficients of the weighted ball discrepancy kernels $K_{\mathcal{B}_{\mathrm{d}_{\mathbb{S}^2}}}$. Before we state these results we recall the definition of the gamma function Γ, cf. (2.77), and that of the *normalized incomplete beta function*

$$I_x(a,b) := \frac{B_x(a,b)}{B_1(a,b)}, \quad B_x(a,b) := \int_0^x t^{a-1}(1-t)^{b-1}\mathrm{d}t, \qquad a,b>0, \ x \in \mathbb{R}.$$

Theorem 4.5. *Let the sphere $\mathbb{S}^d$, $d \geq 2$, with canonical measure $\mu_{\mathbb{S}^d}$, cf. (3.72), and geodesic distance $\mathrm{d}_{\mathbb{S}^d}$, cf. (3.68), be given. Then the discrepancy kernel $K_{\mathcal{B}_{\mathrm{d}_{\mathbb{S}^d}}}$, which corresponds to the weighted ball discrepancy $D^2_{\mathcal{B}_{\mathrm{d}_{\mathbb{S}^d}}}$, cf. Theorem 2.11, with respect to some finite Borel measure $\mu_{\mathbb{R}_+}$ supported on the interval $[0, R]$, $0 \leq R \leq \pi$, has the uniformly and absolutely convergent Fourier expansion, cf. (4.30),*

$$K_{\mathcal{B}_{\mathrm{d}_{\mathbb{S}^d}}}(\boldsymbol{x}, \boldsymbol{y}) = \sum_{n=0}^{\infty} \lambda_n \sum_{k=1}^{D_{d,n}} Y_{n,k}(\boldsymbol{x}) \overline{Y}_{n,k}(\boldsymbol{y}), \qquad \boldsymbol{x}, \boldsymbol{y} \in \mathbb{S}^d,$$

where the Fourier coefficients are given by

$$\lambda_n := \left(\frac{2^{d+1} \pi^d \Gamma(n)}{\omega_d \Gamma(n+d)} \right)^2 \int_0^R \left(\sin(r)^d C_{n-1}^{\frac{d+1}{2}}(\cos(r)) \right)^2 \mathrm{d}\mu_{\mathbb{R}_+}(r), \qquad n \in \mathbb{N}, \tag{4.37}$$

and

$$\lambda_0 := \omega_d^2 \int_0^R \left(I_{\frac{1-\cos(r)}{2}} \left(\frac{d}{2}, \frac{d}{2} \right) \right)^2 \mathrm{d}\mu_{\mathbb{R}_+}(r), \qquad \omega_d = \mu_{\mathbb{S}^d}(\mathbb{S}^d). \tag{4.38}$$

Proof. We consider the balls $B_{\mathbb{S}^d}(\boldsymbol{x}, r)$, $\boldsymbol{x} \in \mathbb{S}^d$, $r \in [0, R]$, on the sphere $\mathbb{S}^d$ as intersections of $\mathbb{S}^d$ with halfspaces $h_+(\boldsymbol{x}, s)$, $s := \cos(r)$, cf. (4.32). Furthermore, we observe that the function

$$H_s(\boldsymbol{x}, \boldsymbol{y}) := 1_{h_+(\boldsymbol{x},s)}(\boldsymbol{y}) = 1_{[s,1]}(\boldsymbol{x}^\top \boldsymbol{y}) = \begin{cases} 1, & \boldsymbol{x}^\top \boldsymbol{y} \geq s, \\ 0, & \boldsymbol{x}^\top \boldsymbol{y} < s, \end{cases} \qquad \boldsymbol{x}, \boldsymbol{y} \in \mathbb{S}^d, \quad s \in [-1, 1], \tag{4.39}$$

is a zonal kernel. Hence, from the definition of the convolution (4.27) we obtain for $r \in [0, R]$ the relation

$$A_r(\boldsymbol{x}, \boldsymbol{y}) = \int_{\mathbb{S}^d} 1_{h_+(\boldsymbol{x},s)}(\boldsymbol{z}) 1_{h_+(\boldsymbol{y},s)}(\boldsymbol{z}) \mathrm{d}\mu_{\mathbb{S}^d}(\boldsymbol{z}) = (H_{\cos(r)} * H_{\cos(r)})(\boldsymbol{x}, \boldsymbol{y}), \quad \boldsymbol{x}, \boldsymbol{y} \in \mathbb{S}^d. \tag{4.40}$$

Expanding the rotational invariant function $A_r(\boldsymbol{x}, \boldsymbol{y})$ in terms of Gegenbauer polynomials C_n^λ we obtain, after interchanging integration and summation, the relation

$$K(\boldsymbol{x}, \boldsymbol{y}) = \int_0^R A_r(\boldsymbol{x}, \boldsymbol{y}) \mathrm{d}\mu_{\mathbb{R}_+} = \sum_{n=0}^{\infty} \int_0^R a_{d,n}(r) \mathrm{d}\mu_{\mathbb{R}_+} C_n^{\frac{d-1}{2}}(\boldsymbol{x}^\top \boldsymbol{y}), \qquad \boldsymbol{x}, \boldsymbol{y} \in \mathbb{S}^d, \tag{4.41}$$

where the Fourier coefficients $a_{d,n}(r)$ are computed with help of Theorem 4.3.

Therefore, we consider the Fourier expansion of the characteristic functions $1_{[s,1]}$ in terms of Gegenbauer polynomials

$$1_{[s,1]} = \sum_{n=0}^{\infty} b_{d,n}(s) C_n^{\frac{d-1}{2}}, \qquad s \in [-1, 1], \tag{4.42}$$

where the Fourier coefficients $b_{d,n}(s)$ are computed by, cf. (4.26),

$$b_{d,n}(s) := \frac{1}{C_{d,n}} \int_{-1}^{1} 1_{[s,1]}(t) C_n^{\frac{d-1}{2}}(t) (1 - t^2)^{\frac{d}{2}-1} \mathrm{d}t, \qquad s \in [-1, 1], \quad n \in \mathbb{N}_0. \tag{4.43}$$

Since $C_0^{(d-1)/2} \equiv 1$ we obtain for $n = 0$ after a change of variable $t := 1 - 2\tilde{t}$ the normalized

incomplete beta function

$$b_{d,0}(s) = \frac{\int_s^1 (1-t^2)^{\frac{d}{2}-1}\mathrm{d}t}{\int_{-1}^1 (1-t^2)^{\frac{d}{2}-1}\mathrm{d}t} = I_{\frac{1-s}{2}}\left(\frac{d}{2},\frac{d}{2}\right), \qquad s \in [-1,1]. \tag{4.44}$$

For $n \in \mathbb{N}$ we calculate the integral in (4.43) with help of the Rodrigues Formula of the Gegenbauer polynomials, cf. [1, Table 22.11],

$$(1-t^2)^{\frac{d}{2}-1} C_n^{\frac{d-1}{2}}(t) = \tilde{C}_{d,n} \frac{\mathrm{d}^n}{\mathrm{d}t^n}(1-t^2)^{\frac{d}{2}-1+n}, \qquad t \in [-1,1],$$

where

$$\tilde{C}_{d,n} := (-2)^{-n} \frac{\Gamma(n+d-1)\Gamma\left(\frac{d}{2}\right)}{\Gamma(n+1)\Gamma(d-1)\Gamma\left(n+\frac{d}{2}\right)}.$$

Thus, for $s \in [-1,1]$ and $n \in \mathbb{N}$ we find the relations

$$\begin{aligned} b_{d,n}(s) &= \frac{\tilde{C}_{d,n}}{C_{d,n}} \int_s^1 \frac{\mathrm{d}^n}{\mathrm{d}t^n}(1-t^2)^{\frac{d}{2}-1+n}\mathrm{d}t = \frac{\tilde{C}_{d,n}}{C_{d,n}} \frac{\mathrm{d}^{n-1}}{\mathrm{d}t^{n-1}}(1-t^2)^{\frac{d+2}{2}-1+(n-1)}\Big|_{t=s}^1 \\ &= \frac{\tilde{C}_{d,n}}{C_{d,n}} \frac{1}{\tilde{C}_{d+2,n-1}}(1-t^2)^{\frac{d+2}{2}-1} C_{n-1}^{\frac{d+1}{2}}(t)\Big|_{t=s}^1 = -\frac{\tilde{C}_{d,n}}{\tilde{C}_{d+2,n-1}C_{d,n}}(1-s^2)^{\frac{d}{2}} C_{n-1}^{\frac{d+1}{2}}(s). \end{aligned}$$

We apply now the convolution Theorem 4.3 to the functions H_s defined by (4.39) and infer from relation (4.40) and expansion (4.42) that the Fourier coefficients $a_{d,n}(r)$, $n \in \mathbb{N}$, $d \geq 2$, are determined by

$$\begin{aligned} a_{d,n}(r) &= \omega_d \frac{d-1}{2n+d-1} b_{d,n}(\cos(r))^2 \\ &= \omega_d \frac{d-1}{2n+d-1} \frac{\tilde{C}_{d,n}^2}{\tilde{C}_{d+2,n-1}^2 C_{d,n}^2} \left(\sin(r)^d C_{n-1}^{\frac{d+1}{2}}(\cos(r))\right)^2 \\ &= \frac{1}{\omega_d} \frac{d-1}{2n+d-1} \left(\frac{2^{1+d}\pi^d \Gamma(n)}{\omega_d \Gamma(d+n)}\right)^2 \left(\sin(r)^d C_{n-1}^{\frac{d+1}{2}}(\cos(r))\right)^2, \qquad r \in [0,R]. \end{aligned}$$

This leads with the expansion (4.41) of the kernel $K_{\mathcal{B}_{\mathrm{d}_{\mathbb{S}^d}}}$ and the relation (4.25) between λ_n and $a_{d,n}$ to the assertion (4.37). Similarly, we arrive with (4.44) at the assertion (4.38). ■

Using Theorem 4.5 we can compute for the Euclidean distance kernel K_{E} the corresponding Fourier expansion in spherical harmonics.

Theorem 4.6. *The Euclidean distance kernel K_{E}, cf. Corollary 2.15, restricted to the sphere $\mathbb{S}^d$, $d \in \mathbb{N}$, has the uniformly and absolutely convergent Fourier expansion, cf.* (4.30),

$$K_{\mathrm{E}}(\boldsymbol{x},\boldsymbol{y}) = C - \|\boldsymbol{x}-\boldsymbol{y}\|_2 = \sum_{n=0}^{\infty} \lambda_n \sum_{k=1}^{D_{d,n}} Y_{n,k}(\boldsymbol{x}) \overline{Y}_{n,k}(\boldsymbol{y}), \qquad \boldsymbol{x},\boldsymbol{y} \in \mathbb{S}^d, \quad C \in \mathbb{R},$$

with Fourier coefficients

$$\lambda_n := \delta_{0,n}\omega_d C + \frac{4^{d+1}\pi^d}{\omega_d} \prod_{k=0}^{d} \frac{1}{(2n+2k-1)}, \qquad n \in \mathbb{N}_0, \tag{4.45}$$

where $\omega_d = \mu_{\mathbb{S}^d}(\mathbb{S}^d)$, cf. (3.72), *and δ denotes the Kronecker delta defined by* (2.15).

Proof. The proof is by induction, where we deduce from d to $d+2$ with $d \geq 2$. Therefore, we use the cases $d = 2, 3$ as induction base. The case $d = 1$ is done seperately. Without loss of generality we may assume $C = 0$ since this affects only the Fourier coefficient λ_0 by adding the constant $\omega_d C$.

For $d = 1$ the assertion (4.45) follows immediately from the investigations on the torus $\mathbb{T}^1 = \mathbb{S}^1$, cf. (4.8), where we need to remark that in the setting here the spherical harmonics $Y_{n,k}$ are orthonormal.

For $d = 2$ we make use of Theorem 4.4 where we have shown that the discrepancy kernel $K_{\mathcal{B}_{\mathrm{d}_{\mathbb{S}^2}}}$ of the weighted ball discrepancy $D^2_{\mathcal{B}_{\mathrm{d}_{\mathbb{S}^2}}}$ with respect to the measure $\mu_{\mathbb{R}_+}$ with density $\mathrm{d}\mu_{\mathbb{R}_+}(r) = \sin(r)\mathrm{d}r$, $r \in [0, \pi]$, is related to the Euclidean distance kernel by

$$K_{\mathrm{E}}(\boldsymbol{x}, \boldsymbol{y}) = -\|\boldsymbol{x} - \boldsymbol{y}\|_2 = \frac{1}{\pi}\left(K_{\mathcal{B}_{\mathrm{d}_{\mathbb{S}^2}}}(\boldsymbol{x}, \boldsymbol{y}) - 4\pi\right), \qquad \boldsymbol{x}, \boldsymbol{y} \in \mathbb{S}^d.$$

Hence, if we denote by $\tilde{\lambda}_n$, $n \in \mathbb{N}_0$, the Fourier coefficients of the discrepancy kernel $K_{\mathcal{B}_{\mathrm{d}_{\mathbb{S}^2}}}$ we have the relation

$$\lambda_n = \frac{2}{\omega_1}\tilde{\lambda}_n = \frac{\tilde{\lambda}_n}{\pi}, \quad n \in \mathbb{N}, \qquad \lambda_0 = \frac{1}{\pi}(\tilde{\lambda}_0 - (4\pi)^2) = \frac{\tilde{\lambda}_0}{\pi} - 16\pi. \tag{4.46}$$

We use Theorem 4.5 to calculate the Fourier coefficients $\tilde{\lambda}_n$, where the integrals in (4.37) are computed by a change of variable $s := \cos(r)$ as follows

$$\int_0^\pi \left(\sin(r)^2 C_{n-1}^{\frac{3}{2}}(\cos(r))\right)^2 \sin(r)\mathrm{d}r = \int_{-1}^1 (1-s^2)^2 C_{n-1}^{\frac{3}{2}}(s)^2 \mathrm{d}s, \qquad n \in \mathbb{N}.$$

With help of the recurrence relation of the Gegenbauer polynomials, cf. [1, Eq. 22.7.23],

$$C_n^\lambda = \frac{\lambda}{n+\lambda}(C_n^{\lambda+1} - C_{n-2}^{\lambda+1}), \qquad \lambda > 0,\ n \in \mathbb{N}, \qquad C_k \equiv 0, \quad k < 0, \tag{4.47}$$

and the normalization constant $C_{d,n}$, cf. (4.26), we find that the above integrals simplify by the orthogonality of the Gegenbauer polynomials to

$$\begin{aligned}
\int_{-1}^1 (1-s^2)^2 C_{n-1}^{\frac{3}{2}}(s)^2 \mathrm{d}s &= \int_{-1}^1 (1-s^2)^2 \left(\frac{3}{2n+1}\left(C_{n-1}^{\frac{5}{2}}(s) - C_{n-3}^{\frac{5}{2}}(s)\right)\right)^2 \mathrm{d}s \\
&= \left(\frac{3}{2n+1}\right)^2 (C_{6,n-1} - C_{6,n-3}) \\
&= \frac{4n^2(1+n)^2}{(2n-1)(2n+1)(2n+3)}, \quad n \in \mathbb{N}.
\end{aligned}$$

We remark that for the normalization constants we have $C_{d,-k} = 0$, $k \in \mathbb{N}$, since $1/\Gamma(-k) = 0$. This observation is in agreement with the recurrence relation (4.47). Hence, we arrive for $n \in \mathbb{N}$, cf. (4.37), at

$$\tilde{\lambda}_n = \left(\frac{2^3\pi^2\Gamma(n)}{4\pi\Gamma(n+d)}\right)^2 \frac{4n^2(1+n)^2}{(2n-1)(2n+1)(2n+3)} = \frac{16\pi^2}{(2n-1)(2n+1)(2n+3)}$$

and for $n = 0$ we obtain

$$\tilde{\lambda}_0 = (4\pi)^2 \int_{-1}^1 \left(I_{\frac{1-s}{2}}(1,1)\right)^2 \mathrm{d}s = (4\pi)^2 \int_{-1}^1 \left(\frac{1-s}{2}\right)^2 \mathrm{d}s = 16\pi^2 - \frac{16\pi^2}{3}.$$

This proves together with (4.46) the assertion (4.45) for $d = 2$.

For $d = 3$ we use that the Chebyshev polynomials of the first kind T_n satisfy, cf. [1, Eq. 22.3.15],

$$T_n(\cos(\alpha)) = \cos(n\alpha), \qquad \alpha \in \mathbb{R}, \qquad n \in \mathbb{N}_0.$$

Together with the Fourier series (4.7) and the addition theorem (4.20) we find the Fourier expansion

$$K_{\mathrm{E}}(\boldsymbol{x}, \boldsymbol{y}) = -\sqrt{2 - 2\boldsymbol{x}^\top \boldsymbol{y}} = -2 \sin\left(\frac{\mathrm{d}_{\mathbb{S}^3}(\boldsymbol{x}, \boldsymbol{y})}{2}\right) = \sum_{n=1}^{\infty} c_n T_n(\boldsymbol{x}^\top \boldsymbol{y}), \qquad \boldsymbol{x}, \boldsymbol{y} \in \mathbb{S}^3, \tag{4.48}$$

where

$$c_n := \frac{8}{\pi} \frac{1}{(2n-1)(2n+1)}, \quad n \in \mathbb{N}, \qquad c_0 = -\frac{4}{\pi}. \tag{4.49}$$

Since the Gegenbauer polynomials $C_n^{\frac{d-1}{2}} = C_n^1$ equal the Chebyshev polynomials of the second kind U_n, cf. [1, Table 22.2], we infer from relation [1, Table 22.5.8] that

$$T_n = \frac{1}{2}(C_n^1 - C_{n-2}^1), \quad n \in \mathbb{N}, \qquad T_0 = C_0^1, \quad C_{-1} \equiv 0. \tag{4.50}$$

Hence, substituting the above relation in the expansion (4.48) we get

$$K_{\mathrm{E}}(\boldsymbol{x}, \boldsymbol{y}) = \left(c_0 - \frac{c_2}{2}\right) C_0^1(\boldsymbol{x}^\top \boldsymbol{x}) + \sum_{n=1}^{\infty} \frac{c_n - c_{n+2}}{2} C_n^1(\boldsymbol{x}^\top \boldsymbol{y}) = \sum_{n=0}^{\infty} a_n C_n^1(\boldsymbol{x}^\top \boldsymbol{y}), \qquad \boldsymbol{x}, \boldsymbol{y} \in \mathbb{S}^3,$$

with

$$a_n := \frac{64(n+1)}{\pi(2n-1)(2n+1)(2n+3)(2n+5)}, \qquad n \in \mathbb{N}_0.$$

The assertion (4.45) for $d = 3$ follows from $\omega_3 = 2\pi^2$ thogether with relation between the coefficients a_n and λ_n, cf. (4.25).

The induction step proceeds from d to $d+2$. Hence, we assume that the assertion (4.45) holds for given $d \geq 2$. Then the Euclidean distance kernel K_{E} can be written as

$$K_{\mathrm{E}}(\boldsymbol{x}, \boldsymbol{y}) = k_{\mathbb{R}^n}(\boldsymbol{x}^\top \boldsymbol{y}), \quad \boldsymbol{x}, \boldsymbol{y} \in \mathbb{S}^d, \qquad k_{\mathbb{R}^n}(t) := -\sqrt{2 - 2t}, \quad t \in [-1, 1],$$

where the expansion

$$k_{\mathbb{R}^n}(t) = \sum_{n=0}^{\infty} a_{d,n} C_n^{\frac{d-1}{2}}(t), \qquad t \in [-1, 1],$$

is valid by induction hypothesis with, cf. (4.25),

$$a_{d,n} := \frac{2^{d+1} \pi^d (2n + d - 1) \Gamma\left(n - \frac{1}{2}\right)}{\omega_d^2 (d-1) \Gamma\left(n + d + \frac{1}{2}\right)}, \qquad n \in \mathbb{N}_0.$$

From the recurrence relation (4.47) we obtain

$$k_{\mathbb{R}^n} = \sum_{n=0}^{\infty} b_{d,n} C_n^{\frac{(d+2)-1}{2}}, \quad b_{d,n} := \left(\frac{d-1}{2n+d-1} a_{d,n} - \frac{d-1}{2n+d+1} a_{d,n+2}\right), \qquad n \in \mathbb{N}_0,$$

so that by Theorem 4.2 all we need to show is $b_{d,n} = a_{d+2,n}$, $n \in \mathbb{N}_0$. Simplifying yields

$$\begin{aligned} b_{d,n} &= \frac{2^{d+1}\pi^d}{\omega_d^2}\left(\frac{\Gamma\left(n-\frac{1}{2}\right)}{\Gamma\left(n+d+\frac{1}{2}\right)} - \frac{\Gamma\left(n+\frac{3}{2}\right)}{\Gamma\left(n+d+\frac{5}{2}\right)}\right) \\ &= \frac{2^{d+1}\pi^d\Gamma\left(n-\frac{1}{2}\right)}{\omega_d^2\Gamma\left(n+d+\frac{5}{2}\right)}\left(\left(n+d+\frac{3}{2}\right)\left(n+d+\frac{1}{2}\right) - \left(n-\frac{1}{2}\right)\left(n+\frac{1}{2}\right)\right) \\ &= \frac{2^{d+1}\pi^d(d+1)(2n+d+1)\Gamma\left(n-\frac{1}{2}\right)}{\omega_d^2\Gamma\left(n+d+\frac{5}{2}\right)}, \qquad n \in \mathbb{N}_0, \end{aligned}$$

and from the formula (4.17) of ω_d we infer

$$\frac{\omega_{d+2}^2}{4\pi^2} = \frac{4\pi^{d+3}}{4\pi^2\Gamma\left(\frac{d+3}{2}\right)^2} = \frac{\pi^{d+1}}{\left(\frac{d+1}{2}\right)^2\Gamma\left(\frac{d+1}{2}\right)^2} = \frac{\omega_d^2}{(d+1)^2}, \qquad d \geq 2,$$

and finish the proof by observing

$$b_{d,n} = \frac{2^{(d+2)+1}\pi^{d+2}(2n+(d+2)-1)\Gamma\left(n-\frac{1}{2}\right)}{\omega_{d+2}^2((d+2)-1)\Gamma\left(n+(d+2)+\frac{1}{2}\right)} = a_{d+2,n}, \qquad n \in \mathbb{N}_0. \qquad \blacksquare$$

4.3 The Rotation Group SO(3)

We briefly recapitulate in Section 4.3.1 the basics of harmonic analysis on the rotation group SO(3). In Section 4.3.2 we present thoroughly the well-known connection between the rotation group SO(3) and the sphere $\mathbb{S}^3$ by means of quaternions, as we have done in [53]. The corresponding results are summarized in Theorem 4.7, which enables us to switch between Fourier expansions of kernels on the sphere $\mathbb{S}^3$ and that of kernels on the rotation group SO(3). Therefore, it is reasonable to restrict our attention in Section 4.3.3 to the Euclidean distance kernel K_{E}, for which the Fourier expansion is given in Theorem 4.8.

4.3.1 Harmonic Analysis

Since the rotation group SO(3) is a compact group one can construct an orthonormal basis of the space $L^2(\mathrm{SO}(3))$ by the use of group representations. For a deeper treatment of harmonic analysis on groups we refer to the monographs [47, 41]. We briefly recapitulate that the mapping $D^n : \mathrm{SO}(3) \to \mathcal{L}(\Pi_n(\mathrm{SO}(3)))$, $n \in \mathbb{N}_0$, defined by

$$D^n(\boldsymbol{R})f := f(\boldsymbol{R}^\top \cdot), \qquad f \in \Pi_n(\mathbb{S}^2), \quad \boldsymbol{R} \in \mathrm{SO}(3),$$

is a irreducible group homomorphism from the rotation group into the space of bounded linear operators on the space $\Pi_n(\mathbb{S}^2)$ of spherical harmonics, i.e.,

$$D^n(\boldsymbol{R}_1)D^n(\boldsymbol{R}_2) = D^n(\boldsymbol{R}_1\boldsymbol{R}_2), \qquad \boldsymbol{R}_1, \boldsymbol{R}_2 \in \mathrm{SO}(3).$$

The mapping D^n, $n \in \mathbb{N}_0$, is called the left regular representation of the rotation group SO(3) on the harmonic space $\Pi_n(\mathbb{S}^2)$ of the sphere $\mathbb{S}^2$. Informally speaking, it rotates the coordinate system of a given function $f \in \Pi_n(\mathbb{S}^2)$ by the rotation $\boldsymbol{R}$. Hence, if we fix an orthonormal basis of spherical harmonics $Y_{n,k} \in \Pi_n(\mathbb{S}^2)$, $n \in \mathbb{N}_0$, $k = -n, \ldots, n$, cf. (4.16), we obtain a matrix

representation of the linear operator $D^n(\boldsymbol{R}) : \Pi_n(\mathbb{S}^2) \to \Pi_n(\mathbb{S}^2)$, $\boldsymbol{R} \in \mathrm{SO}(3)$, by

$$\begin{aligned} \boldsymbol{D}^n(\boldsymbol{R}) &:= (D^n_{k,k'}(\boldsymbol{R}))^n_{k,k'=-n} \in \mathbb{C}^{(2n+1)\times(2n+1)}, \\ D^n_{k,k'}(\boldsymbol{R}) &:= (D^n(\boldsymbol{R})Y_{n,k'}, Y_{n,k})_{L^2(\mathbb{S}^2)} = \int_{\mathbb{S}^2} Y_{n,k'}(\boldsymbol{R}^\top \boldsymbol{x})\overline{Y}_{n,k}(\boldsymbol{x})\mathrm{d}\mu_{\mathbb{S}^2}(\boldsymbol{x}), \end{aligned} \tag{4.51}$$

i.e., cf. [135, Eq. (1), p. 141],

$$Y_{n,k'}(\boldsymbol{R}^\top \boldsymbol{x}) = \sum_{k=-n}^{n} D^n_{k,k'}(\boldsymbol{R})Y_{n,k}(\boldsymbol{x}), \qquad \boldsymbol{x} \in \mathbb{S}^2, \quad n \in \mathbb{N}_0, \quad k' = -n, \ldots, n, \quad \boldsymbol{R} \in \mathrm{SO}(3).$$

The matrix elements $D^n_{k,k'} : \mathrm{SO}(3) \to \mathbb{C}$, $n \in \mathbb{N}_0$, $k, k' = -n, \ldots, n$, are smooth functions on the rotation group $\mathrm{SO}(3)$ and known as *Wigner D-functions*. The famous Peter-Weyl Theorem states that the Wigner D-functions form an orthogonal basis of the space $L^2(\mathrm{SO}(3))$ with the orthogonality relations, cf. [135, p. 97],

$$(D^n_{k,k'}, D^m_{l,l'})_{L^2(\mathrm{SO}(3))} = \int_{\mathrm{SO}(3)} D^n_{k,k'}(\boldsymbol{R})\overline{D}^m_{l,l'}(\boldsymbol{R})\mathrm{d}\mu_{\mathrm{SO}(3)} = \frac{8\pi^2}{2n+1}\delta_{n,m}\delta_{k,l}\delta_{k',l'}, \tag{4.52}$$

where $n, m \in \mathbb{N}_0$, $k, k' = -n, \ldots, n$, $l, l' = -m, \ldots, m$. Similar to the harmonic spaces $\Pi_n(\mathbb{S}^2)$ and $\Pi^N(\mathbb{S}^2)$, cf. (4.15), we define the spaces

$$\begin{aligned} \Pi_n(\mathrm{SO}(3)) &:= \mathrm{span}\{D^n_{k,k'} \ : \ k, k' = -n, \ldots, n\}, \qquad n \in \mathbb{N}_0, \\ \Pi^N(\mathrm{SO}(3)) &:= \mathrm{span}\{D^n_{k,k'} \ : \ n = 0, \ldots, N, \ k, k' = -n, \ldots, n\}, \qquad N \in \mathbb{N}_0, \end{aligned} \tag{4.53}$$

which consist of the polynomials on $\mathrm{SO}(3)$ of degree exactly n and at most N, respectively. Furthermore, we recall the addition theorem for Wigner D-functions $D^n_{k,k'}$ of degree $n \in \mathbb{N}_0$, cf. [135, p. 89, 100], which states

$$\sum_{k,k'=-n}^{n} D^n_{k,k'}(\boldsymbol{R}_1)\overline{D}^n_{k,k'}(\boldsymbol{R}_2) = C^1_{2n}\left(\cos\left(\frac{\alpha(\boldsymbol{R}_1, \boldsymbol{R}_2)}{2}\right)\right), \qquad \boldsymbol{R}_1, \boldsymbol{R}_2 \in \mathrm{SO}(3), \tag{4.54}$$

where C^1_n is a Gegenbauer polynomial , cf. (4.22). We observe that this relation is similar to the addition theorem for the sphere $\mathbb{S}^3$, cf. (4.20), which is due to the well-known relation between the sphere $\mathbb{S}^3$ and the rotation group $\mathrm{SO}(3)$ presented in the next section.

4.3.2 Relations to the Sphere $\mathbb{S}^3$

Following the approach we presented in [53], we recall that the sphere $\mathbb{S}^3$ admits a group structure similar to that of the rotation group $\mathrm{SO}(3)$. In order to establish this well-know connection we write points on the sphere $\mathbb{S}^3$ in the form of *unit quaternions*

$$\boldsymbol{q} := \begin{pmatrix} s \\ \boldsymbol{v} \end{pmatrix} \in \mathbb{S}^3, \quad s \in \mathbb{R}, \quad \boldsymbol{v} \in \mathbb{R}^3,$$

with *real part* $s \in \mathbb{R}$ and *vector part* $\boldsymbol{v} \in \mathbb{R}^3$. Then, two unit quaternions $\boldsymbol{q}_1, \boldsymbol{q}_2 \in \mathbb{S}^3$ are multiplied via the formula

$$\boldsymbol{q}_1 \odot \boldsymbol{q}_2 := \begin{pmatrix} s_1 s_2 - \boldsymbol{v}_1^\top \boldsymbol{v}_2 \\ s_1\boldsymbol{v}_2 + s_2\boldsymbol{v}_1 + \boldsymbol{v}_1 \times \boldsymbol{v}_2 \end{pmatrix}, \quad \boldsymbol{q}_1 = \begin{pmatrix} s_1 \\ \boldsymbol{v}_1 \end{pmatrix}, \boldsymbol{q}_2 = \begin{pmatrix} s_2 \\ \boldsymbol{v}_2 \end{pmatrix} \in \mathbb{S}^3, \tag{4.55}$$

where the vector product is defined by

$$\boldsymbol{v} \times \boldsymbol{w} := \begin{pmatrix} v_2 w_3 - v_3 w_2 \\ v_3 w_1 - v_1 w_3 \\ v_1 w_2 - v_2 w_1 \end{pmatrix}, \qquad \boldsymbol{v} := \begin{pmatrix} v_1 \\ v_2 \\ v_3 \end{pmatrix}, \boldsymbol{v} := \begin{pmatrix} v_1 \\ v_2 \\ v_3 \end{pmatrix} \in \mathbb{R}^3.$$

It is seen readily that the sphere $\mathbb{S}^3$ forms a group under the quaternion multiplication (4.55). More precisely, the identity is given by $\boldsymbol{e}_1 = (1,0,0,0)^\top \in \mathbb{S}^3$ and the inverse element is given by *quaternion conjugation*

$$\overline{\boldsymbol{q}} := \begin{pmatrix} s \\ -\boldsymbol{v} \end{pmatrix}, \qquad \boldsymbol{q} = \begin{pmatrix} s \\ \boldsymbol{v} \end{pmatrix} \in \mathbb{S}^3. \tag{4.56}$$

The connection between quaternions and rotations is given by the following operation on the sphere $\mathbb{S}^2$. We define the action of a unit quaternion $\boldsymbol{q} \in \mathbb{S}^3$ on a point $\boldsymbol{p} \in \mathbb{S}^2$ by

$$\boldsymbol{q}[\boldsymbol{p}] := \boldsymbol{q} \odot \begin{pmatrix} 0 \\ \boldsymbol{p} \end{pmatrix} \odot \overline{\boldsymbol{q}} \in \mathbb{S}^3. \tag{4.57}$$

If we parameterize a unit quaternion $\boldsymbol{q}$ by an axis $\boldsymbol{r} \in \mathbb{S}^2$ and an angle $\alpha \in [0, \pi]$ due to

$$\boldsymbol{q}(\boldsymbol{r}, \alpha) := \begin{pmatrix} \cos\left(\frac{\alpha}{2}\right) \\ \sin\left(\frac{\alpha}{2}\right) \boldsymbol{r} \end{pmatrix} \in \mathbb{S}^3 \tag{4.58}$$

we arrive at the identity

$$\boldsymbol{q}(\boldsymbol{r}, \alpha)[\boldsymbol{p}] = \begin{pmatrix} 0 \\ \boldsymbol{R}(\boldsymbol{r}, \alpha)\boldsymbol{p} \end{pmatrix}, \qquad \boldsymbol{p} \in \mathbb{S}^2, \tag{4.59}$$

where $\boldsymbol{R}(\boldsymbol{r}, \alpha) \in \mathrm{SO}(3)$ is the parameterization of a rotation in terms of the rotation axis $\boldsymbol{r}$ and rotation angle α, cf. (3.90). This shows that the actions of rotations and quaternions on points $\boldsymbol{p} \in \mathbb{S}^2$ are identical. We call $\boldsymbol{R} \in \mathrm{SO}(3)$ the *corresponding rotation of the unit quaternion* $\boldsymbol{q} \in \mathbb{S}^3$, if for all points $\boldsymbol{p} \in \mathbb{S}^2$ the relation (4.59) is valid. Since the quaternion multiplication is associative it follows immediately that the quaternion multiplication of two unit quaternions $\boldsymbol{q}_1, \boldsymbol{q}_2 \in \mathbb{S}^3$ is consistent with the composition of the corresponding rotations $\boldsymbol{R}_1, \boldsymbol{R}_2 \in \mathrm{SO}(3)$, i.e.,

$$\begin{pmatrix} 0 \\ \boldsymbol{R}_2 \boldsymbol{R}_1 \boldsymbol{p} \end{pmatrix} = (\boldsymbol{q}_2 \odot \boldsymbol{q}_1)[\boldsymbol{p}], \qquad \boldsymbol{p} \in \mathbb{S}^2. \tag{4.60}$$

By definition (4.58) the quaternion $\boldsymbol{q}(\boldsymbol{r}, \alpha) = (s, \boldsymbol{v}^\top)^\top$ is in the upper hemisphere of $\mathbb{S}^3$, i.e., $s \geq 0$. Since $\boldsymbol{q}$ and $-\boldsymbol{q}$ corresponds by (4.57) and (4.59) to the same rotation $\boldsymbol{R}$ we obtain that $\mathbb{S}^3$ is a double cover of SO(3), cf. [20, Chap. III, Sect. 10]. Hence, the rotation group SO(3) can be identified with the quotient space $\mathbb{S}^3_* := \mathbb{S}^3 / \{-1, 1\}$, which is also known as the three-dimensional real projective space, i.e.,

$$\mathrm{SO}(3) \cong \mathbb{S}^3_* = \{\{\boldsymbol{x}, -\boldsymbol{x}\} \subset \mathbb{S}^3 \ : \ \boldsymbol{x} \in \mathbb{S}^3\}. \tag{4.61}$$

In other words, any rotation $\boldsymbol{R} \in \mathrm{SO}(3)$ corresponds to exactly one *pair of antipodal points* $\boldsymbol{x}_* := \{\boldsymbol{x}, -\boldsymbol{x}\} \in \mathbb{S}^3_*(\mathbb{R})$, $\boldsymbol{x} \in \mathbb{S}^3$. Thus, between the rotation group SO(3) and the quotient space $\mathbb{S}^3_*$ we have the following isomorphism, cf. (3.90) and (4.58),

$$\boldsymbol{q}_* : \mathrm{SO}(3) \to \mathbb{S}^3_*, \qquad \boldsymbol{q}_*(\boldsymbol{R}(\boldsymbol{r}, \alpha)) = \{-\boldsymbol{q}(\boldsymbol{r}, \alpha), \boldsymbol{q}(\boldsymbol{r}, \alpha)\}, \qquad \boldsymbol{r} \in \mathbb{S}^2, \quad \alpha \in [0, \pi], \tag{4.62}$$

which obeys the relation

$$\boldsymbol{q}_*(\boldsymbol{R}_2) \odot \boldsymbol{q}_*(\boldsymbol{R}_1) := \{\pm \boldsymbol{q}_2 \odot \boldsymbol{q}_1\} = \boldsymbol{q}_*(\boldsymbol{R}_2\boldsymbol{R}_1), \qquad \boldsymbol{R}_1, \boldsymbol{R}_2 \in \mathrm{SO}(3), \tag{4.63}$$

where the rotation $\boldsymbol{R}_i$ correspond to the unit quaternion $\boldsymbol{q}_i$, $i = 1, 2$. Furthermore, we obtain by definition (4.61) in a natural way a metric $\mathrm{d}_{\mathbb{S}^3_*}$ and measure $\mu_{\mathbb{S}^3_*}$ on the quotient space $\mathbb{S}^3_*$ induced by the sphere $\mathbb{S}^3$. More precisely, the metric is defined by

$$\mathrm{d}_{\mathbb{S}^3_*}(\boldsymbol{x}_{1*}, \boldsymbol{x}_{2*}) := \min_{\substack{\boldsymbol{y}_1 \in \boldsymbol{x}_{1*}, \\ \boldsymbol{y}_2 \in \boldsymbol{x}_{2*}}} \mathrm{d}_{\mathbb{S}^3}(\boldsymbol{y}_1, \boldsymbol{y}_2) = \arccos |\boldsymbol{x}_1 \boldsymbol{x}_2^\top|, \qquad \boldsymbol{x}_{1*} = \{\pm \boldsymbol{x}_1\}, \boldsymbol{x}_{2*} = \{\pm \boldsymbol{x}_2\} \in \mathbb{S}^3_*, \tag{4.64}$$

and the measure by

$$\mu_{\mathbb{S}^3_*}(O_*) := \mu_{\mathbb{S}^3}(O) + \mu_{\mathbb{S}^3}(-O), \qquad O_* = \{\boldsymbol{x}_* \ : \ \boldsymbol{x} \in O\} \subset \mathbb{S}^3_*, \tag{4.65}$$

for any measurable set $O \subset \mathbb{S}^3$ with $\mu_{\mathbb{S}^3}(O \cap -O) = 0$. Similarly, any even function on the sphere $\mathbb{S}^3$ corresponds to exactly one function on the rotation group $\mathrm{SO}(3)$. More precisely, to any even function $f : \mathbb{S}^3 \to \mathbb{C}$ we associate the unique function $\tilde{f} : \mathbb{S}^3_* \to \mathbb{C}$ satisfying

$$\tilde{f}(\boldsymbol{x}_*) = f(\boldsymbol{x}), \qquad \boldsymbol{x}_* := \{\boldsymbol{x}, -\boldsymbol{x}\} \in \mathbb{S}^3_*, \quad \boldsymbol{x} \in \mathbb{S}^3, \tag{4.66}$$

and obtain so with the isomorphism (4.62) a function $\breve{f} : \mathrm{SO}(3) \to \mathbb{C}$ by $\breve{f}(\boldsymbol{R}) := \tilde{f}(\boldsymbol{q}_*(\boldsymbol{R}))$, $\boldsymbol{R} \in \mathrm{SO}(3)$. Conversely, any function $\breve{f} : \mathrm{SO}(3) \to \mathbb{C}$ can be continued uniquely to an even function $f : \mathbb{S}^3 \to \mathbb{C}$. The following Theorem 4.7, which summarizes our results of [53, Theorem 1 and Lemma 2], states that in a certain sense we can carry over the analysis on the rotation group $\mathrm{SO}(3)$ to the analysis on the sphere $\mathbb{S}^3$ and vice versa.

Theorem 4.7. *Let the rotation group* $\mathrm{SO}(3)$ *with distance* $\mathrm{d}_{\mathrm{SO}(3)}$ *and measure* $\mu_{\mathrm{SO}(3)}$ *defined by* (3.96) *and* (3.97)*, respectively, be given. Then the isomorphism* $\boldsymbol{q}_* : \mathrm{SO}(3) \to \mathbb{S}^3_*$*, cf.* (4.62)*, yields the identities, cf.* (4.64) *and* (4.65)*,*

$$\begin{aligned} \mathrm{d}_{\mathrm{SO}(3)}(\boldsymbol{R}_1, \boldsymbol{R}_2) &= 2\, \mathrm{d}_{\mathbb{S}^3_*}(\boldsymbol{q}_*(\boldsymbol{R}_1), \boldsymbol{q}_*(\boldsymbol{R}_2)), & \boldsymbol{R}_1, \boldsymbol{R}_2 \in \mathrm{SO}(3), \\ \mu_{\mathrm{SO}(3)}(O) &= 4\, \mu_{\mathbb{S}^3_*}(\boldsymbol{q}_*(O)), & \boldsymbol{q}_*(O) := \{\boldsymbol{q}_*(\boldsymbol{R}) \ : \ \boldsymbol{R} \in O\}, \end{aligned} \tag{4.67}$$

for measurable sets $O \subset \mathrm{SO}(3)$*. Moreover, by using* (4.66) *it holds the following equivalence of the harmonic spaces*

$$f(\cdot) \in \Pi_{2n}(\mathbb{S}^3) \qquad \Leftrightarrow \qquad \tilde{f}(\boldsymbol{q}_*(\cdot)) \in \Pi_n(\mathrm{SO}(3)), \qquad n \in \mathbb{N}_0. \tag{4.68}$$

Proof. We obtain the first identity in (4.67) by using for $\boldsymbol{R}_1, \boldsymbol{R}_2 \in \mathrm{SO}(3)$ the parameterization with rotation axes $\boldsymbol{r}_1, \boldsymbol{r}_2 \in \mathbb{S}^2$ and rotation angles $\alpha_1, \alpha_2 \in [0, \pi]$, cf. (3.90). With the relation (4.60) between rotations and quaternions we infer from (4.58) and the quaternion multiplication formula (4.55) that

$$\cos\left(\frac{\alpha(\boldsymbol{R}_1^\top \boldsymbol{R}_2)}{2}\right) = \left|\cos\left(\frac{\alpha_1}{2}\right)\cos\left(\frac{\alpha_2}{2}\right) + \boldsymbol{r}_1^\top \boldsymbol{r}_2 \sin\left(\frac{\alpha_1}{2}\right)\sin\left(\frac{\alpha_2}{2}\right)\right|$$

where we used additionally the relation $\boldsymbol{R}(\alpha, \boldsymbol{r})^\top = \boldsymbol{R}(\alpha, -\boldsymbol{r})$, $\alpha \in [0, \pi]$, $\boldsymbol{r} \in \mathbb{S}^2$, cf. (4.56). This yields with the definitions (3.96) and (4.64) the desired result

$$\begin{aligned} \mathrm{d}_{\mathrm{SO}(3)}(\boldsymbol{R}_1, \boldsymbol{R}_2) &= 2 \arccos\left|\cos\left(\frac{\alpha_1}{2}\right)\cos\left(\frac{\alpha_2}{2}\right) + \boldsymbol{r}_1^\top \boldsymbol{r}_2 \sin\left(\frac{\alpha_1}{2}\right)\sin\left(\frac{\alpha_2}{2}\right)\right| \\ &= 2 \arccos\left|\boldsymbol{q}(\boldsymbol{r}_1, \alpha_1)^\top \boldsymbol{q}(\boldsymbol{r}_2, \alpha_2)\right| = 2\, \mathrm{d}_{\mathbb{S}^3_*}(\boldsymbol{q}_*(\boldsymbol{R}_1), \boldsymbol{q}_*(\boldsymbol{R}_2)). \end{aligned}$$

In order to prove the second identity in (4.67) we make use of the uniqueness of the translation invariant Haar measure, cf. [47, Section 2.2]. Therefore, we let a rotation $\boldsymbol{R} \in \mathrm{SO}(3)$ and a measurable set $O \subset \mathrm{SO}(3)$ be given. Since the quaternionic multiplication $\boldsymbol{q} \odot \boldsymbol{x}$ of a vector $\boldsymbol{x} \in \mathbb{R}^4$ with a unit quaternion $\boldsymbol{q} \in \mathbb{S}^3$ can be considered as a norm preserving linear transformation $\boldsymbol{T}_{\boldsymbol{q}}\boldsymbol{x}$ with determinant $\det \boldsymbol{T}_{\boldsymbol{q}} = 1$, we conclude that the antipodal points $\boldsymbol{q}_*(\boldsymbol{R})$ represent rotations $\pm\boldsymbol{T}_{\boldsymbol{q}} \in \mathrm{SO}(4)$. Hence, we infer from relation (4.63) that

$$\boldsymbol{T}_{\boldsymbol{q}}\boldsymbol{q}_*(O) := \{\{\pm\boldsymbol{T}_{\boldsymbol{q}}\boldsymbol{x}\} \,:\, \boldsymbol{x} \in \boldsymbol{q}_*(\boldsymbol{O}),\, \boldsymbol{O} \in O\} = \{\boldsymbol{q}_*(\boldsymbol{R}) \odot \boldsymbol{q}_*(\boldsymbol{O}) \,:\, \boldsymbol{O} \in O\} = \boldsymbol{q}_*(\boldsymbol{R}O).$$

Together with the rotational invariance of the measure $\mu_{\mathbb{S}^3}$ on the sphere $\mathbb{S}^3$ and the definition (4.65) we obtain the rotational invariance invariance of the induced measure

$$\mu_{\mathbb{S}^3_*}(\boldsymbol{q}_*(\boldsymbol{R}O)) = \mu_{\mathbb{S}^3_*}(\boldsymbol{T}_{\boldsymbol{q}}\boldsymbol{q}_*(O)) = \mu_{\mathbb{S}^3_*}(\boldsymbol{q}_*(O)).$$

With the normalization

$$\mu_{\mathrm{SO}(3)}(\mathrm{SO}(3)) = 8\pi^2 = 4 \cdot 2\pi^2 = 4\mu_{\mathbb{S}^3}(\mathbb{S}^3) = 4\mu_{\mathbb{S}^3_*}(\mathbb{S}^3_*)$$

and the uniqueness of the Haar measure we arrive at the first assertion (4.67).

The equivalence of the polynomial spaces (4.68) is seen as follows. From the addition theorems on the sphere $\mathbb{S}^3$, cf. (4.20), and the rotation group SO(3), cf. (4.54), we conclude that the reproducing kernels of the polynomial spaces $\Pi_{2n}(\mathbb{S}^3)$ and $\Pi_n(\mathrm{SO}(3))$ with respect to the corresponding L^2-inner product are given by the Gegenbauer polynomials C_n^1. Moreover, since the spaces $\Pi_{2n}(\mathbb{S}^3)$ and $\Pi_n(\mathrm{SO}(3))$ have dimension $(2n+1)^2$, it is easily seen that the property (iv) in Theorem 2.4 reads as

$$\begin{aligned}
\Pi_{2n}(\mathbb{S}^3) &= \left\{ \sum_{i=1}^{(2n+1)^2} a_i C_n^1(\cos(\mathrm{d}_{\mathbb{S}^3}(\boldsymbol{x}_i, \boldsymbol{x}))) \,:\, \boldsymbol{x}_i \in \mathrm{SO}(3),\, a_i \in \mathbb{C} \right\}, \\
\Pi_n(\mathrm{SO}(3)) &= \left\{ \sum_{i=1}^{(2n+1)^2} a_i C_n^1\left(\cos\left(\frac{\mathrm{d}_{\mathrm{SO}(3)}(\boldsymbol{R}_i, \boldsymbol{R})}{2}\right)\right) \,:\, \boldsymbol{R}_i \in \mathrm{SO}(3),\, a_i \in \mathbb{C} \right\}.
\end{aligned} \tag{4.69}$$

Now, let $f \in \Pi_{2n}(\mathbb{S}^3)$ be given. Then, there exists points $\boldsymbol{x}_i \in \mathbb{S}^3$ and coefficients $a_i \in \mathbb{C}$, $i = 1, \ldots, (2n+1)^2$, with

$$f(\boldsymbol{x}) = \sum_{i=1}^{(2n+1)^2} a_i C_{2n}^1(\cos \mathrm{d}_{\mathbb{S}^3}(\boldsymbol{x}_i, \boldsymbol{x})), \qquad \boldsymbol{x} \in \mathbb{S}^3,$$

and since f is even we infer from the first identity in (4.67) the relation

$$\begin{aligned}
\tilde{f}(\boldsymbol{x}_*) &= \sum_{i=1}^{(2n+1)^2} a_i C_{2n}^1(\cos(\mathrm{d}_{\mathbb{S}^3_*}(\boldsymbol{x}_{i*}, \boldsymbol{x}_*))) \\
&= \sum_{i=1}^{(2n+1)^2} a_i C_{2n}^1\left(\cos\left(\frac{\mathrm{d}_{\mathrm{SO}(3)}(\boldsymbol{q}_*^{-1}(\boldsymbol{x}_{i*}), \boldsymbol{q}_*^{-1}(\boldsymbol{x}_*))}{2}\right)\right), \qquad \boldsymbol{x}_* = \{\pm\boldsymbol{x}\} \in \mathbb{S}^3.
\end{aligned}$$

Hence, we infer from (4.69) that $\tilde{f}(\boldsymbol{q}_*(\cdot)) \in \Pi_n(\mathrm{SO}(3))$, and the proof is finished, since the dimensions of the polynomial spaces $\Pi_{2n}(\mathbb{S}^3)$ and $\Pi_n(\mathrm{SO}(3)$ are equal. ∎

4.3.3 Reproducing Kernels

From the addition theorem (4.54) and Remark 2.3 we find that any function of the form, cf. (3.92),

$$K(\boldsymbol{R}_1, \boldsymbol{R}_2) = \sum_{n=0}^{\infty} \lambda_n \sum_{k,k'=-n}^{n} D_{k,k'}^n(\boldsymbol{R}_1) \overline{D}_{k,k'}^n(\boldsymbol{R}_2) = \sum_{n=0}^{\infty} \lambda_n C_{2n}^1 \left(\frac{\sqrt{\operatorname{tr}(\boldsymbol{R}_1^\top \boldsymbol{R}_2) + 1}}{2} \right) \tag{4.70}$$

with rotations $\boldsymbol{R}_1, \boldsymbol{R}_2 \in \mathrm{SO}(3)$ is a positive definite kernel on the rotationg group SO(3) if the Fourier coefficients satisfy $\lambda_n \geq 0$, $n \in \mathbb{N}_0$, and $\sum_{n=0}^{\infty}(2n+1)\lambda_n < \infty$. Thus, K gives rise to a reproducing kernel Hilbert space $H_K(\mathrm{SO}(3))$, cf. Theorem 2.4. We restrict our attention to the Euclidean distance kernel K_{E}, cf. Corollary 2.15, and remark that certain other discrepancy kernels can be investigated by Theorem 4.7, which relates the polynomial spaces on the rotation group SO(3) with the harmonic spaces on the sphere $\mathbb{S}^3$, together with Theorem 4.5 for Fourier expansions of weighted ball discrepancy kernels on the sphere $\mathbb{S}^3$.

We recall that a rotation matrix $\boldsymbol{R} \in \mathbb{R}^{n \times n}$ can be considered equivalently as a point in the Euclidean space $\mathbb{R}^{n^2}$. Since the Frobenius norm, cf. (3.80), corresponds to the Euclidean norm we define the Euclidean distance kernel for matrices by

$$K_{\mathrm{E}}(\boldsymbol{X}, \boldsymbol{Y}) := C - \frac{\sqrt{2}}{2} \|\boldsymbol{X} - \boldsymbol{Y}\|_{\mathrm{F}}, \qquad \boldsymbol{X}, \boldsymbol{Y} \in \mathbb{R}^{n \times n}. \tag{4.71}$$

The normalization constant $\sqrt{2}/2$ is chosen for convenience, cf. Remark 3.17.

Theorem 4.8. *The Euclidean distance kernel K_{E}, cf.* (4.71)*, restricted to the rotation group* SO(3) *has the uniformly and absolutely convergent Fourier expansion, cf.* (4.70)*,*

$$K_{\mathrm{E}}(\boldsymbol{R}_1, \boldsymbol{R}_2) = \sum_{n=0}^{\infty} \lambda_n \sum_{k,k'=-n}^{n} D_{k,k'}^n(\boldsymbol{R}_1) \overline{D}_{k,k'}^n(\boldsymbol{R}_2), \qquad \boldsymbol{R}_1, \boldsymbol{R}_2 \in \mathrm{SO}(3),$$

with Fourier coefficients

$$\lambda_n = \delta_{n,0} C - \frac{16}{\pi(2n-1)(2n+1)(2n+3)}, \qquad n \in \mathbb{N}_0, \tag{4.72}$$

where δ denotes the Kronecker delta defined by (2.15)*.*

Proof. Using the orthogonality of the matrices $\boldsymbol{R}_1, \boldsymbol{R}_2 \in \mathrm{SO}(3)$ and the relations (3.91), (3.96) we find that the Euclidean distance kernel, cf. (4.70), reads as

$$\begin{aligned} K_{\mathrm{E}}(\boldsymbol{R}_1, \boldsymbol{R}_2) &= C - \sqrt{\frac{1}{2}\operatorname{tr}\big((\boldsymbol{R}_1 - \boldsymbol{R}_2)^\top (\boldsymbol{R}_1 - \boldsymbol{R}_2)\big)} \\ &= C - \sqrt{3 - \operatorname{tr}(\boldsymbol{R}_1^\top \boldsymbol{R}_2)} = C - 2\sin\left(\frac{\mathrm{d}_{\mathrm{SO}(3)}(\boldsymbol{R}_1, \boldsymbol{R}_2)}{2}\right). \end{aligned} \tag{4.73}$$

We use the same idea as in the proof of Theorem 4.6 for the case $d = 3$. That is, we start from an expansion in terms of Chebyshev polynomials of the first kind T_n given by (4.48). Using the definition of the Chebyshev polynomials we arrive for $s \in [0, \pi]$ at

$$-2\sin\left(\frac{s}{2}\right) = \sum_{n=0}^{\infty} c_n T_n(\cos(s)) = \sum_{n=0}^{\infty} c_n T_{2n}\left(\frac{\cos(s)}{2}\right) = \sum_{n=0}^{\infty} \lambda_n C_{2n}^1\left(\frac{\cos(s)}{2}\right)$$

where the Fourier coefficients c_n are defined in (4.49). With the relation (4.50) between the

Chebyshev polynomials T_n and the Gegenbauer polynomials C_n^1 we obtain, as as in the proof of Theorem 4.6, that

$$\lambda_0 = c_0 - \frac{c_1}{2} = -\frac{16}{3\pi}, \qquad \lambda_n = \frac{c_n - c_{n+1}}{2} = \frac{16}{\pi(2n-1)(2n+1)(2n+3)}, \qquad n \in \mathbb{N}.$$

This leads together with the relation of the Euclidean distance kernel K_{E} ,cf. (4.73), and the Fourier expansion (4.70) to the assertion (4.72). ■

5

Efficient Function Evaluations for the Optimization of Quadrature Errors

We recall from Chapter 2 that for a given compact set $X \subset \mathbb{R}^n$, a positive definite kernel $K : X \times X \to \mathbb{R}$, and a (complex) Borel measure $\nu \in M_{\mathbb{C}}(\mathbb{R}^n)$ we are interested, for a prescribed number of points $M \in \mathbb{N}$, in the computation of an optimal quadrature functional $Q(\boldsymbol{P}, \boldsymbol{w})$, $\boldsymbol{P} \in X^M$, $\boldsymbol{w} \in \mathbb{C}^M$, or an equal weights quadrature functionals $Q_\nu(\boldsymbol{P})$, which minimizes the worst case quadrature error $\mathrm{err}_K(\nu, \boldsymbol{P}, \boldsymbol{w})$, or the equal weights worst case quadrature error $\mathrm{err}_K(\nu, \boldsymbol{P})$, respectively, cf. Section 2.2.2. In the case of a manifold $\mathcal{M} = X \subset \mathbb{R}^n$ we aim to apply the optimization methods on Riemannian manifolds introduced in Section 3.3, where we recall that the nonlinear conjugate gradient method is of particular interest, cf. Remark 3.21 and Section 3.3.3. In order to perform every step of the CG method, cf. Algorithm 3.3, efficiently we propose two evaluation approachs which compute the squared worst case quadrature error $(\mathrm{err}_K(\nu, \boldsymbol{P}, \boldsymbol{w}))^2$, its gradient $\nabla_{\mathcal{M}^M \times \mathbb{R}^M}(\mathrm{err}_K(\nu, \boldsymbol{P}, \boldsymbol{w}))^2$ and matrix-vector multiplications with its Hessian $\mathrm{H}_{\mathcal{M}^M \times \mathbb{R}^M}(\mathrm{err}_K(\nu, \boldsymbol{P}, \boldsymbol{w}))^2$ in a fast way. We will restrict our attention to finite Borel measures ν and real weights $\boldsymbol{w} \in \mathbb{R}^M$, and remark that the general case might be treated similarly, by splitting complex values into real and imaginary parts.

We recall that the worst case quadrature error $\mathrm{err}_K(\nu, \boldsymbol{P}, \boldsymbol{w})$ with quadrature points $\boldsymbol{P} := (\boldsymbol{p}_i)_{i=1}^M \in X^M$ and quadrature weights $\boldsymbol{w} := (w_i)_{i=1}^M \in \mathbb{R}^M$ allows by Theorem 2.7 for two different points of view, which lead us to two different evaluation approaches. The first relation (2.43) in Theorem 2.7 can be written as

$$E_K(\boldsymbol{P}, \boldsymbol{w}) := \sum_{i,j=1}^{M} w_i w_j K(\boldsymbol{p}_i, \boldsymbol{p}_j) + 2 \sum_{i=1}^{M} w_i h_{K,\nu}(\boldsymbol{p}_i) + C = \mathrm{err}_K(\nu, \boldsymbol{P}, \boldsymbol{w})^2, \tag{5.1}$$

where the function $h_{K,\nu} : X \to \mathbb{R}$ and the constant $C \in \mathbb{R}$ depend on the measure ν and the kernel K. In this representation, the worst case quadrature error can be interpreted as a potential energy, cf. Section 2.3. The second relation (2.44) in Theorem 2.7 reads as

$$\hat{E}_K(\boldsymbol{P}, \boldsymbol{w}) := \sum_{l=0}^{\infty} \lambda_l \Big| \hat{\nu}_l - \sum_{i=1}^{M} w_i \overline{\psi}_l(\boldsymbol{p}_i) \Big|^2 = \mathrm{err}_K(\nu, \boldsymbol{P}, \boldsymbol{w})^2, \tag{5.2}$$

where $\psi_l : X \to \mathbb{C}$, $l \in \mathbb{N}_0$, are prescribed basis functions, and where the coefficients $\lambda_l \geq 0$

and $\hat{\nu}_l \in \mathbb{C}$, $l \in \mathbb{N}_0$, depend on the measure ν and the kernel K, respectively. With this relation the worst case quadrature error can be interpreted as a nonlinear least squares problem with an infinite number of equations.

Remark 5.1. Both representations E_K, cf. (5.1), and $\hat{E}_K$, cf. (5.2), have its own advantages and disadvantages for the evaluation of the worst case quadrature error err_K, respectively.

The function E_K allows for a direct evaluation, but only if the kernel K and the function $h_{K,\nu}$ are given by explicit expressions. For example, we have seen in Section 2.5.2 that even for quite simple measures ν the functions $h_{K,\nu}$ might be not easy to compute. Moreover, for M quadrature points one needs in general $\mathcal{O}(M^2)$ function evaluations of K, which might be far to much for big M. However, the arithmetic complexity can be reduced by considering local kernels, as presented in Section 5.1. This leads us to an optimization approach based on local kernels.

On the other hand, the evaluation of the worst case quadrature error err_K by the representation $\hat{E}_K$ is in general inapplicable, since the series might be infinite. That is, $\hat{E}_K$ can be computed exactly only for kernels K with a finite Fourier expansion (2.24). However, we can evaluate, for certain instances, the function $\hat{E}_K$ very efficiently by the use of fast Fourier transforms, cf. Section 5.2. This leads us to an optimization approach based on Fourier approximation.

Both optimization approaches, that of local kernels and that of Fourier approximation, find application for the computation of low-discrepancy points on the sphere $\mathbb{S}^d$, cf. Section 6.4. Moreover, the Fourier based approach leads to an efficient method for halftoning of images, cf. Section 6.5. □

For the optimization of the worst case quadrature errors err_K by the representations E_K, or $\hat{E}_K$ with the optimization methods introduce in Section 3.3, we need to evaluate the gradient and the Hessian of the function E_K and $\hat{E}_K$, respectively.

In Section 5.1, we restrict our attention to the function E_K, and summarize the corresponding formulas in the case of the usual gradient and Hessian in Theorem 5.3, where the necessary modifications to general Riemannian manifolds are given in Remark 5.5. By inspection of the arithmetic complexity of the evaluations, cf. Remark 5.6 and Table 5.1, we are lead to the introduction of local kernels, cf. (5.11). Using ideas from computational physics for the computation of near-fields, cf. [68], we can compute efficiently the function E_K, as well as its gradient and its Hessian matrix, for uniformly distributed points with Algorithm 5.1, cf. Corollary 5.9. An application of local kernels can be found in the efficient computation of low-discrepancy points on the sphere $\mathbb{S}^d$, cf. Section 6.4.2.

In Section 5.2, we consider the function $\hat{E}_{K_N}$, where K_N is a kernel with finite Fourier expansion. Formulas for the evaluation of the function $\hat{E}_{K_N}$, its gradient, and its Hessian matrix, are presented for the Euclidean case in Theorem 5.11, where the necessary modifications to general Riemannian manifolds are given in Remark 5.12. Afterward, we restrict in Section 5.2.1–5.2.3 our attention to polynomial kernels K_N on the torus $\mathbb{T}^d$, the sphere $\mathbb{S}^2$, and the rotation group $\mathrm{SO}(3)$. For these particular manifolds we will show that the recently developed nonequispaced fast Fourier transforms, cf. [110, 80, 73, 106, 74], lead to efficient evaluation algorithms for the function E_{K_N}, its gradient, and the matrix-vector multiplication with its Hessian matrix, cf. Corollary 5.18, 5.22, and 5.26. In conjunction with the nonlinear conjugate gradient method, cf. Algorithm 3.3 in Section 3.3, we arrive at a very efficient optimization method for the computation of optimal quadrature functionals on these manifolds. In particular, we are able to compute classical quadratures of high accuracy on the sphere $\mathbb{S}^2$ and the rotation group $\mathrm{SO}(3)$, cf. Section 6.2 and 6.3, respectively. Moreover, we apply these algorithms for the efficient computation of low-discrepancy points on the sphere $\mathbb{S}^2$, cf. Section 6.4.1, and efficient halftoning of images, cf. Section 6.5.

Remark 5.2. For the comparison of the computational complexity of numerical algorithms one usually uses upper bounds of the elementary operations needed. In what follows, we denote *elementary operations* to be the usual comparison operations "<", "=", ">" between real numbers and logical operations "and", "or", as well as the *arithmetic operations* given by "addition", "multiplication", "division", "modulo", and the evaluation of the elementary functions "sin", "cos", "exp" together with their inverses. □

5.1 Local Kernels

In this section we present an algorithm for efficient evaluations of the function $E_K : X^M \times \mathbb{R}^M \to \mathbb{R}$, cf. (5.1), its gradient, and the vector multiplication with its Hessian matrix representation for local kernels $K : X \times X \to \mathbb{R}$ on a Riemannian manifold $X \subset \mathbb{R}^n$.

We postpone the definition (5.11) of local kernels and start by considering evaluation formulas for general kernels K. We remark that for some instances the symmetric function $K : X \times X \to \mathbb{R}$ might not be differentiable on the diagonal $(\boldsymbol{x}, \boldsymbol{x})$, $\boldsymbol{x} \in X$, so that we write the function E_K, cf. (5.1), for convenience as

$$E_K(\boldsymbol{P}, \boldsymbol{w}) = 2 \sum_{i=1}^{M-1} \sum_{j=i+1}^{M} w_i w_j K(\boldsymbol{p}_i, \boldsymbol{p}_j) + 2 \sum_{i=1}^{M} \big(w_i^2 K_{\mathrm{d}}(\boldsymbol{p}_i) + w_i h_{K,\nu}(\boldsymbol{p}_i) \big) + C, \tag{5.3}$$

where $K_{\mathrm{d}} : X \to \mathbb{R}$ is defined by $K_{\mathrm{d}}(\boldsymbol{x}) := \frac{1}{2} K(\boldsymbol{x}, \boldsymbol{x})$, $\boldsymbol{x} \in X$. Hence, the function E_K is differentiable for pairwise distinct points $\boldsymbol{p}_i \in X$, $1, \ldots, M$, if $K_{\mathrm{d}} : X \to \mathbb{R}$ and $K : (X \times X)_* \to \mathbb{R}$ are differentiable, where

$$(X \times X)_* := \{(\boldsymbol{x}, \boldsymbol{y}) \in X \times X \ : \ \boldsymbol{x} \neq \boldsymbol{y}\}.$$

For open subsets of the Euclidean space $\mathbb{R}^n$ the Theorem 5.3 provides us with evaluation formulas for the gradient ∇E_K and the Hessian matrix $\mathbf{H} E_K$. Using these findings we obtain for an arbitrary Riemannian manifold $X \subset \mathbb{R}^n$ formulas for the gradient $\nabla_{\mathcal{M}} E_K$ and the Hessian matrix $\mathbf{H}_{\mathcal{M}} E_K$ on the product manifold $\mathcal{M} := X^M \times \mathbb{R}^M$ by slight modifications, cf. Remark 5.5. Simplified versions of these formulas are given for radial kernels K in Remark 5.4.

Theorem 5.3. *Let an open set $U \subset \mathbb{R}^n$, a symmetric function $K : U \times U \to \mathbb{R}$, and a function $h_{K,\nu} : U \to \mathbb{R}$ be given. Then for fixed points $\boldsymbol{P} := (\boldsymbol{p}_1, \ldots, \boldsymbol{p}_M) \in U^M$ and weights $\boldsymbol{w} := (w_1, \ldots, w_M)^\top \in \mathbb{R}^M$ the function $E_K : U^M \times \mathbb{R}^M \to \mathbb{R}$ defined by (5.3) can be evaluated by*

$$E_K(\boldsymbol{P}, \boldsymbol{w}) = \boldsymbol{w}^\top \boldsymbol{K} \boldsymbol{w} + 2 \boldsymbol{w}^\top \boldsymbol{h} + C \tag{5.4}$$

where

$$\boldsymbol{K} := \begin{pmatrix} K(\boldsymbol{p}_1, \boldsymbol{p}_1) & \ldots & K(\boldsymbol{p}_1, \boldsymbol{p}_M) \\ \vdots & \ddots & \vdots \\ K(\boldsymbol{p}_M, \boldsymbol{p}_1) & \ldots & K(\boldsymbol{p}_M, \boldsymbol{p}_M) \end{pmatrix} \in \mathbb{R}^{M \times M}, \quad \boldsymbol{h} := \begin{pmatrix} h_{K,\nu}(\boldsymbol{p}_1) \\ \vdots \\ h_{K,\nu}(\boldsymbol{p}_M) \end{pmatrix} \in \mathbb{R}^M. \tag{5.5}$$

If additionally K and $K_d, h_{K,\nu}$ is once differentiable at $(\boldsymbol{p}_i, \boldsymbol{p}_j) \in U \times U$ and $\boldsymbol{p}_i \in U$, $i \neq j$, respectively, then the gradient of E_K can be evaluated by

$$\nabla E_K(\boldsymbol{P}, \boldsymbol{w}) = \Big(\nabla_{\boldsymbol{p}_1} E_K(\boldsymbol{P}, \boldsymbol{w})^\top, \ldots, \nabla_{\boldsymbol{p}_M} E_K(\boldsymbol{P}, \boldsymbol{w})^\top, \nabla_{\boldsymbol{w}} E_K(\boldsymbol{P}, \boldsymbol{w})^\top \Big)^\top \in \mathbb{R}^{M(n+1)}, \tag{5.6}$$

where

$$\nabla_{\boldsymbol{p}_i} E_K(\boldsymbol{P},\boldsymbol{w}) := 2w_i(\mathbf{D}\boldsymbol{K}_i\boldsymbol{w} + w_i\mathbf{D}\boldsymbol{K}_{\mathbf{d}i} + \mathbf{D}\boldsymbol{h}_i) \in \mathbb{R}^n, \qquad i = 1,\dots,M,$$
$$\nabla_{\boldsymbol{w}} E_K(\boldsymbol{P},\boldsymbol{w}) := 2(\boldsymbol{K}\boldsymbol{w} + \boldsymbol{h}) \in \mathbb{R}^M$$

with

$$\begin{aligned}
\mathbf{D}\boldsymbol{K}_i &:= \begin{pmatrix} K_{(1)}(\boldsymbol{p}_i,\boldsymbol{p}_1) & \dots & K_{(1)}(\boldsymbol{p}_i,\boldsymbol{p}_{i-1}) & 0 & K_{(1)}(\boldsymbol{p}_i,\boldsymbol{p}_{i+1}) & \dots & K_{(1)}(\boldsymbol{p}_1,\boldsymbol{p}_M) \\ \vdots & & \vdots & \vdots & \vdots & & \vdots \\ K_{(n)}(\boldsymbol{p}_i,\boldsymbol{p}_1) & \dots & K_{(n)}(\boldsymbol{p}_i,\boldsymbol{p}_{i-1}) & 0 & K_{(n)}(\boldsymbol{p}_i,\boldsymbol{p}_{i+1}) & \dots & K_{(n)}(\boldsymbol{p}_1,\boldsymbol{p}_M) \end{pmatrix} \in \mathbb{R}^{n\times M}, \\
\mathbf{D}\boldsymbol{K}_{\mathbf{d}i} &:= \big(K_{d(1)}(\boldsymbol{p}_i),\dots,K_{d(n)}(\boldsymbol{p}_i)\big)^\top \in \mathbb{R}^n, \\
\mathbf{D}\boldsymbol{h}_i &:= \Big(h_{K,\nu(1)}(\boldsymbol{p}_i),\dots,h_{K,\nu(n)}(\boldsymbol{p}_i)\Big)^\top \in \mathbb{R}^n, \qquad i = 1,\dots,M,
\end{aligned} \tag{5.7}$$

defined by the partial derivatives

$$\begin{aligned}
K_{(k)}(\boldsymbol{x},\boldsymbol{y}) &:= \frac{\partial}{\partial x_k}K(\boldsymbol{x},\boldsymbol{y}), \quad K_{\mathrm{d}(k)}(\boldsymbol{x}) := \frac{\partial}{\partial x_k}K_{\mathrm{d}}(\boldsymbol{x}), \qquad \boldsymbol{x} := (x_i)_{i=1}^n, \boldsymbol{y} \in U, \\
h_{K,\nu(k)}(\boldsymbol{x}) &:= \frac{\partial}{\partial x_k}h_{K,\nu}(\boldsymbol{x}), \qquad\qquad\qquad\qquad\qquad\qquad k = 1,\dots,n.
\end{aligned}$$

If additionally K and $K_d, h_{K,\nu}$ are twice differentiable at $(\boldsymbol{p}_i,\boldsymbol{p}_j) \in U\times U$ and $\boldsymbol{p}_i \in U$, $i \neq j$, respectively, then the Hessian matrix representation of E_K can be evaluated by

$$\mathbf{H}E_K(\boldsymbol{P},\boldsymbol{w}) = \begin{pmatrix} \mathbf{H}_{\boldsymbol{P}}E_K(\boldsymbol{P},\boldsymbol{w}) & \mathbf{H}_{\boldsymbol{P},\boldsymbol{w}}E_K(\boldsymbol{P},\boldsymbol{w}) \\ \mathbf{H}_{\boldsymbol{P},\boldsymbol{w}}E_K(\boldsymbol{P},\boldsymbol{w})^\top & 2\boldsymbol{K} \end{pmatrix} \in \mathbb{R}^{M(n+1)\times M(n+1)}, \tag{5.8}$$

where

$$\mathbf{H}_{\boldsymbol{P}}E_K(\boldsymbol{P},\boldsymbol{w}) := \begin{pmatrix} \mathbf{H}_{\boldsymbol{p}_1,\boldsymbol{p}_1} & \dots & \mathbf{H}_{\boldsymbol{p}_1,\boldsymbol{p}_M} \\ \vdots & \ddots & \vdots \\ \mathbf{H}_{\boldsymbol{p}_M,\boldsymbol{p}_1} & \dots & \mathbf{H}_{\boldsymbol{p}_M,\boldsymbol{p}_M} \end{pmatrix} \in \mathbb{R}^{Mn\times Mn},$$
$$\mathbf{H}_{\boldsymbol{P},\boldsymbol{w}}E_K(\boldsymbol{P},\boldsymbol{w}) := \begin{pmatrix} \mathbf{H}_{\boldsymbol{p}_1,w_1} & \dots & \mathbf{H}_{\boldsymbol{p}_1,w_M} \\ \vdots & \ddots & \vdots \\ \mathbf{H}_{\boldsymbol{p}_M,w_1} & \dots & \mathbf{H}_{\boldsymbol{p}_M,w_M} \end{pmatrix} \in \mathbb{R}^{Mn\times M},$$

with

$$\mathbf{H}_{\boldsymbol{p}_i,\boldsymbol{p}_j} := \begin{cases} 2w_iw_j\mathbf{H}_{\mathbf{2}}\boldsymbol{K}_{i,j}, & i \neq j, \\ 2w_i\Big(\sum\limits_{\substack{k=1,\\ k\neq i}}^{M} w_k\mathbf{H}_{\mathbf{1}}\boldsymbol{K}_{i,k} + w_i\mathbf{H}\boldsymbol{K}_{\mathbf{d}i} + \mathbf{H}\boldsymbol{h}_i\Big), & i = j, \end{cases} \in \mathbb{R}^{n\times n},$$

$$\mathbf{H}_{\boldsymbol{p}_i,w_j} := \begin{cases} 2w_i(\mathbf{D}\boldsymbol{K}_i)_j, & i \neq j, \\ 2(\mathbf{D}\boldsymbol{K}_i\boldsymbol{w} + 2w_i\mathbf{D}\boldsymbol{K}_{\mathbf{d}i} + \mathbf{D}\boldsymbol{h}_i), & i = j, \end{cases} \in \mathbb{R}^n$$

and

$$\begin{aligned}
\mathbf{H_1}\boldsymbol{K}_{i,j} &:= \begin{pmatrix} K_{(1,1)}(\boldsymbol{p}_i,\boldsymbol{p}_j) & \dots & K_{(1,n)}(\boldsymbol{p}_i,\boldsymbol{p}_j) \\ \vdots & \ddots & \vdots \\ K_{(n,1)}(\boldsymbol{p}_i,\boldsymbol{p}_j) & \dots & K_{(n,n)}(\boldsymbol{p}_i,\boldsymbol{p}_j) \end{pmatrix} \in \mathbb{R}^{n\times n}, \qquad i \neq j, \\
\mathbf{H_2}\boldsymbol{K}_{i,j} &:= \begin{pmatrix} K_{(1),(1)}(\boldsymbol{p}_i,\boldsymbol{p}_j) & \dots & K_{(1),(n)}(\boldsymbol{p}_i,\boldsymbol{p}_j) \\ \vdots & \ddots & \vdots \\ K_{(n),(1)}(\boldsymbol{p}_i,\boldsymbol{p}_j) & \dots & K_{(n),(n)}(\boldsymbol{p}_i,\boldsymbol{p}_j) \end{pmatrix} \in \mathbb{R}^{n\times n}, \qquad i \neq j, \\
\mathbf{H}\boldsymbol{h}_i &:= \begin{pmatrix} h_{K,\nu(1,1)}(\boldsymbol{p}_i) & \dots & h_{K,\nu(1,n)}(\boldsymbol{p}_i) \\ \vdots & \ddots & \vdots \\ h_{K,\nu(n,1)}(\boldsymbol{p}_i) & \dots & h_{K,\nu(n,n)}(\boldsymbol{p}_i) \end{pmatrix} \in \mathbb{R}^{n\times n}, \\
\mathbf{H}\boldsymbol{K}_{\mathbf{d}i} &:= \begin{pmatrix} K_{\mathrm{d}(1,1)}(\boldsymbol{p}_i) & \dots & K_{\mathrm{d}(1,n)}(\boldsymbol{p}_i) \\ \vdots & \ddots & \vdots \\ K_{\mathrm{d}(n,1)}(\boldsymbol{p}_i) & \dots & K_{\mathrm{d}(n,n)}(\boldsymbol{p}_i) \end{pmatrix} \in \mathbb{R}^{n\times n}, \qquad i,j = 1,\dots,M,
\end{aligned} \tag{5.9}$$

defined by the partial derivatives

$$\begin{aligned}
K_{(k,k')}(\boldsymbol{x},\boldsymbol{y}) &:= \frac{\partial^2 K(\boldsymbol{x},\boldsymbol{y})}{\partial x_k \partial x_{k'}},\ K_{(k),(k')}(\boldsymbol{x},\boldsymbol{y}) := \frac{\partial^2 K(\boldsymbol{x},\boldsymbol{y})}{\partial x_k \partial y_{k'}}, \qquad \boldsymbol{x} := (x_i)_{i=1}^n, \boldsymbol{y} := (y_i)_{i=1}^n \in U, \\
K_{\mathrm{d}(k,k')}(\boldsymbol{x}) &:= \frac{\partial^2 K_{\mathrm{d}}(\boldsymbol{x})}{\partial x_k \partial x_{k'}},\ h_{K,\nu(k,k')}(\boldsymbol{x}) := \frac{\partial^2 h_{K,\nu}(\boldsymbol{x})}{\partial x_k \partial x_{k'}}, \qquad k,k' = 1,\dots,n.
\end{aligned}$$

Proof. The relation (5.4) is a simple application of the matrix-vector products.

The partial derivatives of E_K at $\boldsymbol{P} := (\boldsymbol{p}_1,\dots,\boldsymbol{p}_M) \in U^M$, $\boldsymbol{p}_i := (p_{i,1},\dots,p_{i,n}) \in U$, $i = 1,\dots,M$, $\boldsymbol{w} := (w_1,\dots,w_M)^\top \in \mathbb{R}^M$, with respect to $p_{i,k}$ and w_i, $i,i' = 1,\dots,M$, $k,k' = 1,\dots,n$, are

$$\begin{aligned}
\frac{\partial}{w_i} E_K(\boldsymbol{P},\boldsymbol{w}) &= 2\sum_{j=1}^M w_j K(\boldsymbol{p}_i,\boldsymbol{p}_j) + 2h_{K,\nu}(\boldsymbol{p}_i), \qquad \frac{\partial^2}{w_i w_{i'}} E_K(\boldsymbol{P},\boldsymbol{w}) = 2K(\boldsymbol{p}_i,\boldsymbol{p}_{i'}), \\
\frac{\partial}{\partial p_{i,k}} E_K(\boldsymbol{P},\boldsymbol{w}) &= 2\sum_{\substack{j=1,\\ j\neq i}}^M w_i w_j K_{(k)}(\boldsymbol{p}_i,\boldsymbol{p}_j) + 2w_i^2 K_{\mathrm{d}(k)}(\boldsymbol{p}_i) + 2w_i h_{K,\nu(k)}(\boldsymbol{p}_i), \\
\frac{\partial^2 E_K(\boldsymbol{P},\boldsymbol{w})}{\partial p_{i,k}\partial p_{i',k'}} &= \begin{cases} 2w_i w_{i'} K_{(k),(k')}(\boldsymbol{p}_i,\boldsymbol{p}_{i'}), & i \neq i', \\ 2\sum\limits_{\substack{j=1,\\ j\neq i}}^M w_i w_j K_{(k,k')}(\boldsymbol{p}_i,\boldsymbol{p}_j) + 2w_i^2 K_{\mathrm{d}(k,k')}(\boldsymbol{p}_i) + 2w_i h_{K,\nu(k,k')}(\boldsymbol{p}_i), & i = i', \end{cases} \\
\frac{\partial^2 E_K(\boldsymbol{P},\boldsymbol{w})}{\partial p_{i,k}\partial w_{i'}} &= \begin{cases} 2w_i K_{(k)}(\boldsymbol{p}_i,\boldsymbol{p}_{i'}), & i \neq i', \\ 2\sum\limits_{\substack{j=1,\\ j\neq i}}^M w_j K_{(k)}(\boldsymbol{p}_i,\boldsymbol{p}_j) + 4w_i K_{\mathrm{d}(k)}(\boldsymbol{p}_i) + 2h_{K,\nu(k)}(\boldsymbol{p}_i), & i = i', \end{cases}
\end{aligned}$$

and the remaining assertions follow. ∎

Remark 5.4. The evaluation formulas for $E_K : U^M \times \mathbb{R}^M \to \mathbb{R}$, its gradient, and its Hessian at $(\boldsymbol{P}, \boldsymbol{w}) \in U^M \times \mathbb{R}^M$ in Theorem 5.3 simplify for radial kernels

$$K(\boldsymbol{x}, \boldsymbol{y}) := \tilde{K}(s), \quad s := \|\boldsymbol{x} - \boldsymbol{y}\|_2, \qquad \tilde{K} : [0, \infty) \to \mathbb{R},$$

and functions

$$h_{K,\nu}(\boldsymbol{x}) := \tilde{h}_{K,\nu}(t), \quad t := \|\boldsymbol{x}\|_2, \qquad \tilde{h}_{K,\nu} : [0, \infty) \to \mathbb{R}.$$

We find with $\boldsymbol{x} := (x_1, \ldots, x_n), \boldsymbol{y} := (y_1, \ldots, y_n) \in U$ and $k, k' = 1, \ldots, n$ for $s \neq 0$, $t \neq 0$ the relations

$$\begin{aligned} K_{(k)}(\boldsymbol{x}, \boldsymbol{y}) &= (x_k - y_k)\frac{\tilde{K}'(s)}{s}, \\ K_{(k,k')}(\boldsymbol{x}, \boldsymbol{y}) &= (x_k - y_k)(x_{k'} - y_{k'})\frac{\tilde{K}''(s)s - \tilde{K}'(s)}{s^3} + \delta_{k,k'}\frac{\tilde{K}'(s)}{s} = -K_{(k),(k')}(\boldsymbol{x}, \boldsymbol{y}), \\ K_{\mathrm{d}}(\boldsymbol{x}) &= K_{\mathrm{d}(k)}(\boldsymbol{x}) = K_{\mathrm{d}(k,k')}(\boldsymbol{x}) = 0 \end{aligned}$$

and

$$h_{K,\nu(k)}(\boldsymbol{x}) = \frac{x_k}{t}\tilde{h}'_{K,\nu}(t), \quad h_{K,\nu(k,k')}(\boldsymbol{x}) = x_k x_{k'}\frac{\tilde{h}''_{K,\nu}(t)t - \tilde{h}'_{K,\nu}(t)}{t^3} + \delta_{k,k'}\frac{\tilde{h}'_{K,\nu}(t)}{t}.$$

Hence, by setting

$$\boldsymbol{d}_{i,j} := \boldsymbol{p}_i - \boldsymbol{p}_j \in \mathbb{R}^n, \quad s_{i,j} := \|\boldsymbol{d}_{i,j}\|_2, \quad i \neq j \qquad t_i := \|\boldsymbol{p}_i\|_2, \qquad i, j = 1, \ldots, M,$$

we obtain, cf. (5.7) in Theorem 5.3,

$$\begin{aligned} \mathbf{D}\boldsymbol{K}_i &= \left(\frac{\tilde{K}'(s_{i,1})}{s_{i,1}}\boldsymbol{d}_{i,1}, \ldots \frac{\tilde{K}'(s_{i,i-1})}{s_{i,i-1}}\boldsymbol{d}_{i,i-1}, \boldsymbol{0}, \frac{\tilde{K}'(s_{i,i+1})}{s_{i,i+1}}\boldsymbol{d}_{i,i+1}, \ldots, \frac{\tilde{K}'(s_{i,M})}{s_{i,M}}\boldsymbol{d}_{i,M}\right) \in \mathbb{R}^{n \times M}, \\ \mathbf{D}\boldsymbol{K}_{\boldsymbol{d}i} &= \boldsymbol{0}, \quad \mathbf{D}\boldsymbol{h}_i = \frac{\tilde{h}'_{K,\nu}(t_i)}{t_i}\boldsymbol{p}_i \in \mathbb{R}^n, \qquad i = 1, \ldots, M, \end{aligned}$$

and, cf. (5.9) in Theorem 5.3,

$$\begin{aligned} \mathbf{H_1}\boldsymbol{K}_{i,j} &= \frac{\tilde{K}''(s_{i,j})s_{i,j} - \tilde{K}'(s_{i,j})}{s_{i,j}^3}\boldsymbol{d}_{i,j}\boldsymbol{d}_{i,j}^\top + \frac{K'(s_{i,j})}{s_{i,j}}\boldsymbol{I} = -\mathbf{H_2}\boldsymbol{K}_{i,j}, \qquad \mathbf{H}\boldsymbol{K}_{\boldsymbol{d}i} = \boldsymbol{0} \in \mathbb{R}^{n \times n}, \\ \mathbf{H}\boldsymbol{h}_i &= \frac{\tilde{h}''_{K,\nu}(t_i)t_i - \tilde{h}'_{K,\nu}(t_i)}{t_i^3}\boldsymbol{p}_i\boldsymbol{p}_i^\top + \frac{h'_{K,\nu}(t_i)}{t_i}\boldsymbol{I} \in \mathbb{R}^{n \times n}, \qquad i \neq j, \quad i, j = 1, \ldots, M. \end{aligned}$$

If we assume that $\tilde{K}$ and $\tilde{h}_{K,\nu}$ can be evaluated in a constant amount of arithmetic operations, independent of the dimension $n \in \mathbb{N}$, then the gradient $\nabla E_K(\boldsymbol{P}, \boldsymbol{w}) \in \mathbb{R}^{M(n+1)}$ and the Hessian matrix representation $\mathbf{H}E_K(\boldsymbol{P}, \boldsymbol{w}) \in \mathbb{R}^{M(n+1) \times M(n+1)}$ can be evaluated in $\mathcal{O}(M^2 n)$ and $\mathcal{O}(M^2 n^2)$ arithmetic operations, respectively. Moreover, a multiplication of the Hessian with a vector $\boldsymbol{v} \in \mathbb{R}^{M(n+1)}$ can be computed in $\mathcal{O}(M^2 n)$ arithmetic operations, cf. Remark 5.2. □

Remark 5.5. For the evaluation of the gradient and Hessian matrix representation of E_K on a manifold $X \subset \mathbb{R}^n$ we can apply the relations in Theorem 5.3 together with the observations of representations on product manifolds, cf. (3.58), (3.59), and Corollary 3.6. More precisely, under the assumptions and notations of Theorem 5.3 with $X \subset U \subset \mathbb{R}^n$ the gradient and Hessian matrix representation of the function E_K at fixed points $\boldsymbol{P} := (\boldsymbol{p}_1, \ldots, \boldsymbol{p}_M) \in X^M$ and weights

$\boldsymbol{w} := (w_1, \ldots, p_M)^\top \in \mathbb{R}^M$ restricted to the product manifold $\mathcal{M} := X^M \times \mathbb{R}^M$ reads as, cf. (5.6),

$$\nabla_{\mathcal{M}} E_K(\boldsymbol{P}, \boldsymbol{w}) = \left(\nabla_{X,\boldsymbol{p}_1} E_K(\boldsymbol{P}, \boldsymbol{w})^\top, \ldots, \nabla_{X,\boldsymbol{p}_M} E_K(\boldsymbol{P}, \boldsymbol{w})^\top, \nabla_{\boldsymbol{w}} E_K(\boldsymbol{P}, \boldsymbol{w})^\top \right)^\top \in \mathrm{T}_{(\boldsymbol{P},\boldsymbol{w})}\mathcal{M},$$

and, cf. (5.8),

$$\mathbf{H}_{\mathcal{M}} E_K(\boldsymbol{P}, \boldsymbol{w}) = \begin{pmatrix} \mathbf{H}_{\mathcal{M},\boldsymbol{P}} E_K(\boldsymbol{P}, \boldsymbol{w}) & \mathbf{H}_{\boldsymbol{P},\boldsymbol{w}} E_K(\boldsymbol{P}, \boldsymbol{w}) \\ \mathbf{H}_{\boldsymbol{P},\boldsymbol{w}} E_K(\boldsymbol{P}, \boldsymbol{w})^\top & 2\boldsymbol{K} \end{pmatrix} \in \mathbb{R}^{M(n+1)\times M(n+1)},$$

respectively, where

$$\nabla_{X,\boldsymbol{p}_i} E_K(\boldsymbol{P}, \boldsymbol{w}) := \mathrm{P}_{\mathrm{T}_{\boldsymbol{p}_i} X} \nabla_{\boldsymbol{p}_i} E_K(\boldsymbol{P}, \boldsymbol{w}) \in \mathrm{T}_{\boldsymbol{p}_i} X \subset \mathbb{R}^n, \qquad i = 1, \ldots, M,$$

$$\mathbf{H}_{\mathcal{M},\boldsymbol{P}} E_K(\boldsymbol{P}, \boldsymbol{w}) := \begin{pmatrix} \mathbf{H}_{\boldsymbol{p}_1,\boldsymbol{p}_1} + \mathbf{N}_{p_1} & \ldots & \mathbf{H}_{\boldsymbol{p}_1,\boldsymbol{p}_M} \\ \vdots & \ddots & \vdots \\ \mathbf{H}_{\boldsymbol{p}_M,\boldsymbol{p}_1} & \ldots & \mathbf{H}_{\boldsymbol{p}_M,\boldsymbol{p}_M} + \mathbf{N}_{p_M} \end{pmatrix} \in \mathbb{R}^{Mn\times Mn}$$

with orthogonal projection operator $\mathrm{P}_{\mathrm{T}_{\boldsymbol{x}} X} : \mathbb{R}^n \to \mathrm{T}_{\boldsymbol{x}} X$, $\boldsymbol{x} \in X$, cf. (3.40), and symmetric matrices $\mathbf{N}_{\boldsymbol{p}_i} \in \mathbb{R}^{n\times n}$ satisfying

$$\boldsymbol{v}^\top \mathbf{N}_{\boldsymbol{p}_i} \boldsymbol{v} = \nabla_{\boldsymbol{p}_i} E_K(\boldsymbol{P}, \boldsymbol{w})^\top \boldsymbol{n}_{\boldsymbol{p}_i,\boldsymbol{v}}, \qquad \boldsymbol{v} \in \mathrm{T}_{\boldsymbol{p}_i} X, \qquad i = 1, \ldots, M, \tag{5.10}$$

for the normal vectors $\boldsymbol{n}_{\boldsymbol{p}_i,\boldsymbol{v}} \in \mathrm{T}_{\boldsymbol{p}_i} X^\perp$, $i = 1, \ldots, M$, associated to $\boldsymbol{p}_i$ and $\boldsymbol{v}$, cf. (3.25). □

Remark 5.6. In what follows, we use the assumptions and notations of Theorem 5.3, respectively Remark 5.5, and assume that the matrices and vectors $\boldsymbol{K} \in \mathbb{R}^{M\times M}$, $\boldsymbol{h} \in \mathbb{R}^M$, cf. (5.5), $\mathbf{D}\boldsymbol{K}_i \in \mathbb{R}^{n\times M}$, $\mathbf{D}\boldsymbol{K}_{\boldsymbol{d}i}, \mathbf{D}\boldsymbol{h}_i \in \mathbb{R}^n$, cf. (5.7), and $\mathbf{H_1}\boldsymbol{K}_{i,j}, \mathbf{H_2}\boldsymbol{K}_{i,j}, \mathbf{H}\boldsymbol{h}_i, \mathbf{H}\boldsymbol{K}_{\boldsymbol{d}i} \in \mathbb{R}^{n\times n}$, cf. (5.9), as well as the matrices $\mathbf{N}_{\boldsymbol{p}_i}$, cf. (5.10), and the matrices of the projection operators $\mathrm{P}_{\mathrm{T}_{\boldsymbol{p}_i} X}$ are already given and evaluated at $\boldsymbol{P} := (\boldsymbol{p}_1, \ldots, \boldsymbol{p}_M) \in X^M$, $\boldsymbol{w} := (w_1, \ldots, w_M)^\top \in \mathbb{R}^M$ for $i, j = 1, \ldots, M$. In other words, we do not care about the complexity of the evaluation of K, $h_{K,\nu}$ and their partial derivatives, which might also depend on the dimension n. □

Under the assumptions given in Remark 5.6 we list in Table 5.1 the most expansive parts in the evaluation of the function E_K, cf. (5.4), its gradient ∇E_K, cf. (5.6), and its Hessian matrix representation $\mathbf{H}E_K$, cf. (5.8), together with the total arithmetic complexity. In particular, for fixed dimension n the overall complexity is $\mathcal{O}(M^2)$, which for a large number of points might be far to much.

For that reason we introduce the concept of local kernels. A kernel K is called *local* if, for some fixed *locality radius* $R > 0$, it satisfies the relation

$$K(\boldsymbol{x}, \boldsymbol{y}) = 0, \quad \|\boldsymbol{x} - \boldsymbol{y}\|_2 \geq R, \qquad \boldsymbol{x}, \boldsymbol{y} \in X. \tag{5.11}$$

For local kernels K we observe that the corresponding matrices $\boldsymbol{K}, \mathbf{D}\boldsymbol{K}_i, \mathbf{H_1}\boldsymbol{K}_{i,j}, \mathbf{H_2}\boldsymbol{K}_{i,j}$, $i \neq j$, $i, j = 1, \ldots, M$, may have a lot of zero-entries, depending on the distribution of the points $\boldsymbol{P} := (\boldsymbol{p}_1, \ldots, \boldsymbol{p}_M) \in U^M$. The aim of this section is to present an evaluation algorithm which makes use of this observation. Of course, if we fix the kernel K with locality radius $R > 0$ and let the number M of points tend to infinity we cannot obtain a better arithmetic complexity than $\mathcal{O}(M^2)$.[1] However, if for a fixed compact set X we allow the kernel K to vary with the number M of points, we can obtain for suitable point distributions a more efficient evaluation algorithm

[1] This is easily seen by covering the compact set X with a fixed number of balls of radius $R/2$ and applying the pigeonhole principle.

Matrix-Vector products:	Total number:	Total complexity:
$\boldsymbol{K}\boldsymbol{w} \in \mathbb{R}^M$		$\mathcal{O}(M^2)$
$\mathbf{D}\boldsymbol{K}_i\boldsymbol{w} \in \mathbb{R}^n$	$i = 1, \dots, M$	$\mathcal{O}(M^2 n)$
$w_i(\mathbf{D}\boldsymbol{K}_i)_j \in \mathbb{R}^n$	$i \neq j, \quad i, j = 1, \dots, M$	$\mathcal{O}(M^2 n)$
$w_i w_j \mathbf{H_2} \boldsymbol{K}_{i,j} \in \mathbb{R}^{n \times n}$	$i \neq j,\ i, j = 1, \dots, M$	$\mathcal{O}(M^2 n^2)$
$\sum_{\substack{j=1,\\ j\neq i}}^{M} w_j \mathbf{H_1} \boldsymbol{K}_{i,j} \in \mathbb{R}^{n \times n}$	$i = 1, \dots, M$	$\mathcal{O}(M^2 n^2)$

Table 5.1: The most expansive parts for the evaluation of E_K, its gradient ∇E_K, and its Hessian matrix $\mathbf{H}E_K$ together with the corresponding arithmetic complexity, cf. Theorem 5.3, and Remark 5.2.

of the function E_K and its derivatives. Thus, we are interested in the efficient computation of the energy E_{K_R} for a family of kernels K_R with locality radius $R > 0$, which depends on the number M of points. An application of this idea can be found in the efficient computation of low-discrepancy points in Section 6.4, where we use the family of local discrepancy kernels $K_{\mathcal{B}_{\mathbb{R}^n},R}$ over Euclidean balls with radius $R > 0$ satisfying $R^{-d} = CM$ on the sphere $\mathbb{S}^d \subset \mathbb{R}^{d+1}$, see Section 2.4.3.

The main difficulty in obtaining a more efficient evaluation algorithm for the function E_{K_R}, as well as its derivatives, for a given kernel K_R with locality radius $R > 0$ is the determination of the nearest neighbors of every point $\boldsymbol{p}_i \in X$ given by the index sets, cf. (2.74),

$$\mathcal{I}_{R,\boldsymbol{p}_i} := \big\{ j = 1, \dots, M \ : \ \boldsymbol{p}_j \in B_{\mathbb{R}^n}(\boldsymbol{p}_i, R) \big\}, \qquad i = 1, \dots, M. \tag{5.12}$$

We perform this task by using algorithmic ideas from computational physics, cf. [68]. A particularly simple approach is based on partitioning the Euclidean space $\mathbb{R}^n$ into equally sized cells $\mathcal{C}_R(\boldsymbol{k})$, $\boldsymbol{k} := (k_1, \dots, k_n) \in \mathbb{Z}^n$, $R > 0$, of side length R defined by

$$\mathcal{C}_R(\boldsymbol{k}) := \big\{ \boldsymbol{y} = (y_1, \dots, y_n) \in \mathbb{R}^n \ : \ k_i \leq y_i/R < (k_i + 1), \quad i = 1, \dots, n \big\} \subset \mathbb{R}^n. \tag{5.13}$$

With help of the notation for the integer part of a vector $\boldsymbol{y} \in \mathbb{R}^n$ given by

$$\lfloor \boldsymbol{y} \rfloor := (m_1, \dots, m_n) \in \mathbb{Z}^n, \qquad m_i := \max_{k \in \mathbb{Z}} \{ k \leq y_i \}, \quad i = 1, \dots, n, \tag{5.14}$$

we summarize some simple but important properties of such a partition.

Theorem 5.7. *For $n \in \mathbb{N}$ and $R > 0$ the cells $\mathcal{C}_R(\boldsymbol{k})$, $\boldsymbol{k} \in \mathbb{Z}^n$, defined by* (5.13) *have the following properties:*

(i) $\bigcup_{\boldsymbol{k} \in \mathbb{Z}^n} \mathcal{C}_R(\boldsymbol{k}) = \mathbb{R}^n, \qquad \mathcal{C}_R(\boldsymbol{k}) \cap \mathcal{C}_R(\boldsymbol{l}) = \emptyset, \quad \boldsymbol{k} \neq \boldsymbol{l},\ \boldsymbol{k}, \boldsymbol{l} \in \mathbb{Z}^n,$

(ii) $\boldsymbol{x} \in \mathcal{C}_R(\boldsymbol{k}) \qquad \Leftrightarrow \qquad \boldsymbol{k} = \lfloor \boldsymbol{x}/R \rfloor, \qquad \boldsymbol{x} \in \mathbb{R}^n,$

(iii) $\bigcup_{\substack{\boldsymbol{k} \in \mathbb{Z}^n,\\ \boldsymbol{k} \in [-1,1]^n}} \mathcal{C}_R(\lfloor \boldsymbol{x}/R \rfloor + \boldsymbol{k}) \supset B_{\mathbb{R}^n}(\boldsymbol{x}, R), \qquad \boldsymbol{x} \in \mathbb{R}^n.$

Proof. The properties are simple consequences of the definition of cells, cf. (5.13), and balls, cf. (2.55), and the relation $0 \leq x - R\lfloor x/R \rfloor < R$, $x \in \mathbb{R}$. ∎

In Algorithm 5.1[2] we utilize the properties of the partitioning by the cells $\mathcal{C}_R(\boldsymbol{k})$, stated in Theorem 5.7, together with the lexicographic ordering defined for $\boldsymbol{x} := (x_1, \dots, x_n), \boldsymbol{y} := (y_1, \dots, y_n) \in$

[2] The "linked-cell-list"-algorithm presented in [68], uses a slightly more efficient data structure for the determination of the nearest neighbors. However, for simplicity we make use Algorithm 5.1.

$\mathbb{R}^n$ by the relations

$$\begin{aligned} \boldsymbol{x} =_R \boldsymbol{y} \quad &:\Leftrightarrow \quad \lfloor \boldsymbol{x}/R \rfloor = \lfloor \boldsymbol{y}/R \rfloor, \\ \boldsymbol{x} <_R \boldsymbol{y} \quad &:\Leftrightarrow \quad \exists m \in \{1,\dots,n\}: \quad \lfloor x_m/R \rfloor < \lfloor y_m/R \rfloor, \quad \lfloor x_k/R \rfloor = \lfloor y_k/R \rfloor,\ k < m, \\ \boldsymbol{x} \leq_R \boldsymbol{y} \quad &:\Leftrightarrow \quad \boldsymbol{x} <_R \boldsymbol{y} \quad \text{or} \quad \boldsymbol{x} =_R \boldsymbol{y}, \end{aligned} \tag{5.15}$$

which allow us to determine efficiently the index sets $\mathcal{I}_{R,\boldsymbol{p}_i}$, $i = 1,\dots,M$, $R > 0$,

Algorithm 5.1 (**Nearest Neighbors Search**)

Input: point distribution $\boldsymbol{p}_i \in \mathbb{R}^n$, $i = 1,\dots,M$, locality radius $R > 0$
Initialization: order the points lexicographically $\boldsymbol{p}_{i_1} \leq_R \boldsymbol{p}_{i_2} \leq_R \cdots \leq_R \boldsymbol{p}_{i_M}$, cf. (5.15),
set first left and last right anchors $s_1 := 1$, $r_M := M$
for $m := 2$ to M **do**
  if $\boldsymbol{p}_{i_m} =_R \boldsymbol{p}_{i_{m-1}}$ **then**
    $s_m := s_{m-1}$
  else
    $s_m := m$
  end if
  if $\boldsymbol{p}_{i_{M-m+1}} =_R \boldsymbol{p}_{i_{M-m+2}}$ **then**
    $r_{M-m+1} := r_{M-m+2}$
  else
    $r_{M-m+1} := M - m + 1$
  end if
end for
for $l := 1$ to M **do**
  $\mathcal{I}_{R,\boldsymbol{p}_{i_l}} := \emptyset$
  for $\boldsymbol{k} \in \mathbb{Z}^n \cap [-1,1]^n$ **do**
    perform a binary search such that $\lfloor \boldsymbol{p}_{i_l} + R\boldsymbol{k} \rfloor =_R \boldsymbol{p}_{i_m}$
    if such a point $\boldsymbol{p}_{i_m}$ exists **then**
      for $j := s_m$ to r_m **do**
        if $\|\boldsymbol{p}_{i_l} - \boldsymbol{p}_{i_j}\|_2 \leq R$ **then**
          $\mathcal{I}_{R,\boldsymbol{p}_{i_l}} := \mathcal{I}_{R,\boldsymbol{p}_{i_l}} \cup \{i_j\}$
        end if
      end for
    end if
  end for
end for
Output: nearest neighbor index sets $\mathcal{I}_{R,\boldsymbol{p}_i}$, $i = 1,\dots,M$

Theorem 5.8. *For a given number $M \in \mathbb{N}$ of points $\boldsymbol{p}_1,\dots,\boldsymbol{p}_M \in \mathbb{R}^n$ and a locality radius $R > 0$ the computation of the index sets $\mathcal{I}_{R,\boldsymbol{p}_i}$, $i = 1,\dots,M$, cf. (5.12), by Algorithm 5.1 needs*

$$\mathcal{O}\big(3^n Mn(\log(Mn) + C(R,M))\big) \tag{5.16}$$

elementary operations, cf. Remark 5.2, where

$$C(R,M) := \max_{\boldsymbol{k} \in \mathbb{Z}^n} \big|\{\boldsymbol{p}_1,\dots,\boldsymbol{p}_M\} \cap \mathcal{C}_R(\boldsymbol{k})\big| \tag{5.17}$$

is the maximum number of the given points contained in some cell $\mathcal{C}_R(\boldsymbol{k})$, $\boldsymbol{k} \in \mathbb{Z}^n$, cf. (5.13).

Proof. The ordering $\boldsymbol{p}_{i_1} \leq_R \cdots \leq \boldsymbol{p}_{i_M}$ in the initialization step of Algorithm 5.1 can be realized in $\mathcal{O}(Mn\log(Mn))$ operations, e.g, by using the heap sort algorithm.

For ordered points it follows that all points $\boldsymbol{p}_{i_l}$, $l = 1, \ldots, M$, which are contained in some cell $\mathcal{C}_R(\boldsymbol{k})$, $\boldsymbol{k} \in \mathbb{Z}^n$, are in consecutive order by definition (5.15) and property (ii) in Theorem 5.7. More precisely, we have

$$\{l = 1, \ldots, M \ : \ \boldsymbol{p}_{i_l} \in \mathcal{C}_R(\lfloor \boldsymbol{p}_{i_m}/R \rfloor)\} = \{s_m, \ldots, r_m\}, \qquad m = 1, \ldots, M,$$

where s_m and r_m denotes the index for the starting point and end point of that section of consecutive ordered points which corresponds to the cell where a given point $\boldsymbol{p}_{i_m}$ lies in, respectively. Since all such sections are determined by

$$\boldsymbol{p}_{i_{s_m}} =_R \boldsymbol{p}_{i_{s_m+1}} =_R \cdots =_R \boldsymbol{p}_{i_m} =_R \cdots =_R \boldsymbol{p}_{i_{r_m}}, \qquad m = 1, \ldots, M, \tag{5.18}$$

we find the indices s_m, r_m by the first for-loop in Algorithm 5.1, which needs $\mathcal{O}(Mn)$ operations.

With the above observations we can compute the index sets $\mathcal{I}_{R,\boldsymbol{p}_{i_l}}$ by running through $l = 1, \ldots, M$ and using property (iii) of Theorem 5.7, which states that we need only to examine the 3^n neighboring boxes of the current point $\boldsymbol{p}_{i_l}$ given by $\mathcal{C}_R(\lfloor \boldsymbol{p}_{i_l}/R \rfloor + \boldsymbol{k})$, $\boldsymbol{k} \in \mathbb{Z}^n \cap [-1, 1]^n$. The corresponding sections, cf. (5.18), of the neighboring boxes, if exist, can be found in $\mathcal{O}(\log(Mn))$ operations by a binary search. What remains is to add all points $\boldsymbol{p}_{i_j}$ of the neighboring boxes to the set $I_{R,\boldsymbol{p}_{i_l}}$ with distance $\|\boldsymbol{p}_{i_l} - \boldsymbol{p}_{i_j}\|_2 \leq R$. It follows that the overall complexity of the Algorithm 5.1 is bounded by (5.16), and proof is finished. ∎

We remark, if in Theorem 5.8 all the points $\boldsymbol{p}_i \in \mathbb{R}^n$, $i = 1, \ldots, M$, are contained in a single cell such that $C(R, M) = M$, cf. (5.17), the Algorithm 5.1 has a worser complexity than the trivial pairwise comparison algorithm without partitioning, in particular for growing dimension n. However, for well distributed points and suitable chosen locality radius R the Algorithm 5.1 becomes more efficient for increasing M. More precisely, for a d-dimensional manifold $X \subset \mathbb{R}^n$ we call the points $\boldsymbol{p}_1, \ldots, \boldsymbol{p}_M \in X$ to be (R, M, d, c)-*quasi-uniformly distributed* if there exists a constants $C > 0$, such that the implication, cf. (5.17),

$$MR^d \leq c \qquad \Rightarrow \qquad C(R, M) \leq C \tag{5.19}$$

is fulfilled for any choices of the locality radius R and the number of points M.[3]

From property (iii) in Theorem 5.7 it follows that for (R, M, d, c)-quasi-uniformly distributed points the number of nearest neighbors of every point $\boldsymbol{p}_i \in \mathcal{M}$, $i = 1, \ldots, M$, is uniformly bounded in M by, cf. (5.19),

$$|\mathcal{I}_{R,\boldsymbol{p}_i}| \leq 3^n C(R, M) \leq 3^n C, \quad i = 1, \ldots, M. \tag{5.20}$$

Hence, the arithmetic complexity of the most expansive parts for the evaluation of the function E_{K_R} with local kernels K_R, as well as its derivatives, reduces for (R, M, d, c)-quasi-uniformly distributed points with large numbers M, cf. Table 5.2.

Corollary 5.9. *Let a d-dimensional manifold $X \subset \mathbb{R}^n$ and a family of local kernels $K_R : X \times X \to \mathbb{R}$ with locality radius $R > 0$ be given. Then, under the assumptions and notations of Theorem 5.3, Remark 5.5, and Remark 5.6, the evaluation of the function E_{K_R}, cf.* (5.3)*, its gradient $\nabla_{\mathcal{M}} E_{K_R}$, and the matrix-vector multiplication with its Hessian matrix representation $\mathbf{H}_{\mathcal{M}} E_{K_R}$ at the point $(\boldsymbol{P}, \boldsymbol{w}) := (\boldsymbol{p}_1, \ldots, \boldsymbol{p}_M, w_1, \ldots, w_M) \in \mathcal{M} := X^M \times \mathbb{R}^M$ can be computed, by using Algorithm 5.1,*

[3] The existence of (R, M, d, c)-quasi-uniformly distributed points is assured. For instance, it is well known that for a d-dimensional manifold $X \subset \mathbb{R}^n$ there exists a constant c_X such that X intersects at least $c_X R^{-d}$ different cells $C_R(\boldsymbol{k})$, $\boldsymbol{k} \in \mathbb{Z}^n$. Hence, for $MR^d \leq c$ we can distribute M points in such a way that every cell contains at most $C(R, M) \leq 1 + \lfloor M/(c_X R^{-d}) \rfloor \leq 1 + c/c_X$ points.

Matrix-Vector products:	Total number:	Total complexity:
$\boldsymbol{K}\boldsymbol{w} \in \mathbb{R}^M$		$\mathcal{O}(3^n M)$
$\mathbf{D}\boldsymbol{K}_i\boldsymbol{w} \in \mathbb{R}^n$	$i = 1, \dots, M$	$\mathcal{O}(3^n Mn)$
$w_i(\mathbf{D}\boldsymbol{K}_i)_j \in \mathbb{R}^n$	$i \neq j, \quad i, j = 1, \dots, M$	$\mathcal{O}(3^n Mn)$
$w_i w_j \mathbf{H_2}\boldsymbol{K}_{i,j} \in \mathbb{R}^{n\times n}$	$i \neq j$, $i, j = 1, \dots, M$	$\mathcal{O}(3^n Mn^2)$
$\sum_{\substack{j=1,\\ j\neq i}}^{M} w_j \mathbf{H_1}\boldsymbol{K}_{i,j} \in \mathbb{R}^{n\times n}$	$i = 1, \dots, M$	$\mathcal{O}(3^n Mn^2)$

Table 5.2: The most expansive parts for the evaluation of E_K, its gradient ∇E_K, and its Hessian matrix $\mathbf{H}E_K$ for (R, M, d, c)-quasi-uniformly distributed points together with the corresponding arithmetic complexity, cf. Theorem 5.3 and Remark 5.2.

in

$$\mathcal{O}(3^n Mn^2 \log(Mn))$$

elementary operations, cf. Remark 5.2, if the points $\boldsymbol{p}_1, \dots, \boldsymbol{p}_M \in X$ *are* (R, M, d, c)*-quasi-uniformly distributed, cf.* (5.19).

Proof. The assertions follow from the representations given in Theorem 5.3 and Remark 5.5 together with the bound given in Theorem 5.8 and the relation (5.20) for (R, M, d, c)-quasi-uniformly distributed points. ■

Remark 5.10. The Algorithm 5.1 and thus the overall evaluation algorithm presented in this section is subject to the curse of dimension, which is reflected by the exponential growth of the number 3^n of neighboring cells. Comparing the numbers of points M with the factor 3^n, we infer from Theorem 5.8 a crude estimate on the range of the dimension n, for which Algorithm 5.1 is more efficient than the trivial pairwise comparison algorithm, namely

$$1 \leq n \leq \big(\log M + \log C(M, R)\big) / \log(3). \qquad \square$$

5.2 Polynomial Kernels

In this section we consider algorithms for efficient evaluations of the function $\hat{E}_{K_N} : X^M \times \mathbb{R}^M \to \mathbb{R}$, cf. (5.2), its gradient, and the vector multiplication with its Hessian matrix representation for polynomial kernels $K_N : X \times X \to \mathbb{R}$ of degree $N \in \mathbb{N}_0$, where X is the torus $\mathbb{T}^d$, $d \in \mathbb{N}$, the sphere $\mathbb{S}^2$, or the rotation group SO(3).

We recall that for compact sets $X \subset \mathbb{R}^n$ and kernels K_N with Fourier coefficients $\lambda_l \geq 0$, $l \in \mathbb{N}_0$, and $\lambda_l = 0$, $l \geq d_N$, we consider the function

$$\hat{E}_{K_N}(\boldsymbol{P}, \boldsymbol{w}) = \sum_{l=0}^{d_N} \lambda_l \Big| \hat{\nu}_l - \sum_{i=1}^{M} w_i \overline{\psi}_l(\boldsymbol{p}_i) \Big|^2, \qquad \boldsymbol{P} := (\boldsymbol{p}_1, \dots, \boldsymbol{p}_M) \in X^M,\ \boldsymbol{w} := (w_i)_{i=1}^M \in \mathbb{R}^M, \tag{5.21}$$

where $\psi_l : X \to \mathbb{C}$ and $\hat{\nu}_l \in \mathbb{C}$, $l \in \mathbb{N}_0$, are fixed basis functions and coefficients, respectively.

For open subsets of the Euclidean space $\mathbb{R}^n$, the Theorem 5.11 provides us with evaluation formulas for the gradient $\nabla \hat{E}_{K_N}$ and the Hessian matrix $\mathbf{H}\hat{E}_{K_N}$. Using these findings we obtain for an arbitrary Riemannian manifold $X \subset \mathbb{R}^n$ formulas for the gradient $\nabla_{\mathcal{M}} \hat{E}_{K_N}$ and the Hessian matrix $\mathbf{H}_{\mathcal{M}} \hat{E}_{K_N}$ on the product manifold $\mathcal{M} := X^M \times \mathbb{R}^M$ by slight modifications, cf. Remark 5.12.

Before we state these results, we introduce for convenience the *nonequispaced Fourier matrix*

$$\boldsymbol{Y}_N := \begin{pmatrix} \psi_0(\boldsymbol{p}_1) & \dots & \psi_{d_N-1}(\boldsymbol{p}_1) \\ \vdots & \ddots & \vdots \\ \psi_0(\boldsymbol{p}_M) & \dots & \psi_{d_N-1}(\boldsymbol{p}_M) \end{pmatrix} \in \mathbb{C}^{M\times d_N} \tag{5.22}$$

associated to given points $\boldsymbol{p}_i \in X$, $i = 1,\dots,M$, and degree $N \in \mathbb{N}_0$. Moreover, for sufficiently smooth basis functions ψ_l, $l \in \mathbb{N}_0$, defined on an open set $U \subset \mathbb{R}^n$ we introduce the matrix

$$\boldsymbol{\nabla Y}_N := \begin{pmatrix} \nabla\psi_0(\boldsymbol{p}_1) & \dots & \nabla\psi_{d_N-1}(\boldsymbol{p}_1) \\ \vdots & \ddots & \vdots \\ \nabla\psi_0(\boldsymbol{p}_M) & \dots & \nabla\psi_{d_N-1}(\boldsymbol{p}_M) \end{pmatrix} \in \mathbb{C}^{Mn\times d_N} \tag{5.23}$$

and the matrix

$$\mathbf{H}\boldsymbol{Y}_N := \begin{pmatrix} \mathbf{H}\psi_0(\boldsymbol{p}_1) & \dots & \mathbf{H}\psi_{d_N-1}(\boldsymbol{p}_1) \\ \vdots & \ddots & \vdots \\ \mathbf{H}\psi_0(\boldsymbol{p}_M) & \dots & \mathbf{H}\psi_{d_N-1}(\boldsymbol{p}_M) \end{pmatrix} \in \mathbb{C}^{Mn\times d_N n} \tag{5.24}$$

where for $l = 0,\dots,d_N-1$ and $\boldsymbol{x} := (x_1,\dots,x_n) \in U$ the gradients and the Hessian matrices of the basis functions are given by

$$\nabla\psi_l(\boldsymbol{x}) := \begin{pmatrix} \frac{\partial}{\partial x_1}\psi_l(\boldsymbol{x}) \\ \vdots \\ \frac{\partial}{\partial x_n}\psi_l(\boldsymbol{x}) \end{pmatrix} \in \mathbb{C}^n, \quad \mathbf{H}\psi_l(\boldsymbol{x}) := \begin{pmatrix} \frac{\partial^2}{\partial x_1\partial x_1}\psi_l(\boldsymbol{x}) & \dots & \frac{\partial^2}{\partial x_1\partial x_n}\psi_l(\boldsymbol{x}) \\ \vdots & \ddots & \vdots \\ \frac{\partial^2}{\partial x_n\partial x_1}\psi_l(\boldsymbol{x}) & \dots & \frac{\partial^2}{\partial x_n\partial x_n}\psi_l(\boldsymbol{x}) \end{pmatrix} \in \mathbb{C}^{n\times n}. \tag{5.25}$$

With help of these matrices we can write the evaluation of a bandlimited function $f \in \Pi^N(X) := \operatorname{span}\{\psi_l : l = 0,\dots,d_N-1\}$, $N \in \mathbb{N}_0$, as well as its derivatives, at the points $\boldsymbol{p}_i \in X$, $i = 1,\dots,M$, in matrix-vector notation. More precisely, if f is given by its Fourier coefficients, i.e.,

$$f(\boldsymbol{x}) := \sum_{l=0}^{d_N-1} \hat{f}_l\psi_l(\boldsymbol{x}), \quad \boldsymbol{x} \in X, \qquad \hat{f}_l \in \mathbb{C}, \quad l = 0,\dots,d_N-1,$$

then the evaluation of f at the points $\boldsymbol{p}_i \in X$, $i = 1,\dots,M$, can be written as a matrix-vector product

$$\boldsymbol{f} := \big(f(\boldsymbol{p}_i)\big)_{i=1}^M = \boldsymbol{Y}_N\hat{\boldsymbol{f}} \in \mathbb{C}^M, \qquad \hat{\boldsymbol{f}} := \big(\hat{f}_l\big)_{l=0}^{d_N} \in \mathbb{C}^{d_N}. \tag{5.26}$$

Similarly, we can write the evaluation of the gradients and the Hessian matrices of f simply by the matrix-vector products

$$\boldsymbol{\nabla f} := \begin{pmatrix} \nabla f(\boldsymbol{p}_1) \\ \vdots \\ \nabla f(\boldsymbol{p}_M) \end{pmatrix} = \boldsymbol{\nabla Y}_N\hat{\boldsymbol{f}} \in \mathbb{C}^{Mn}, \qquad \mathbf{H}\boldsymbol{f} := \begin{pmatrix} \mathbf{H}f(\boldsymbol{p}_1) \\ \vdots \\ \mathbf{H}f(\boldsymbol{p}_M) \end{pmatrix} = \mathbf{H}\boldsymbol{Y}_N(\hat{\boldsymbol{f}} \otimes \boldsymbol{I}_n) \in \mathbb{C}^{Mn\times n},$$

where $\boldsymbol{I}_n \in \mathbb{R}^{n\times n}$ is the identity matrix and

$$\nabla f(\boldsymbol{x}) := \begin{pmatrix} \frac{\partial}{\partial x_1}f(\boldsymbol{x}) \\ \vdots \\ \frac{\partial}{\partial x_n}f(\boldsymbol{x}) \end{pmatrix} \in \mathbb{C}^n, \quad \mathbf{H}f(\boldsymbol{x}) := \begin{pmatrix} \frac{\partial^2}{\partial x_1\partial x_1}f(\boldsymbol{x}) & \dots & \frac{\partial^2}{\partial x_1\partial x_n}f(\boldsymbol{x}) \\ \vdots & \ddots & \vdots \\ \frac{\partial^2}{\partial x_n\partial x_1}f(\boldsymbol{x}) & \dots & \frac{\partial^2}{\partial x_n\partial x_n}f(\boldsymbol{x}) \end{pmatrix} \in \mathbb{C}^{n\times n}, \quad \boldsymbol{x} \in U,$$

We recall that the Kronecker product of two matrices is defined by

$$\boldsymbol{A}\otimes\boldsymbol{B}:=\begin{pmatrix}a_{1,1}\boldsymbol{B} & \dots & a_{1,m}\boldsymbol{B}\\ \vdots & \ddots & \vdots\\ a_{n,1}\boldsymbol{B} & \dots & a_{n,m}\boldsymbol{B}\end{pmatrix}\in\mathbb{C}^{np\times mq},\qquad \boldsymbol{A}:=(a_{i,j})_{i,j=1}^{n,m}\in\mathbb{C}^{n\times m},\quad \boldsymbol{B}\in\mathbb{C}^{p\times q}.$$

Theorem 5.11. *Let an open set $U\subset\mathbb{R}^n$ and twice differentiable functions $\psi_l: U\to\mathbb{C}$ with coefficients $\lambda_l\geq 0$, $l\in\mathbb{N}_0$, satisfying $\lambda_l=0$, $l\geq d_N$, be given. Then, for fixed points $\boldsymbol{P}:=(\boldsymbol{p}_1,\dots,\boldsymbol{p}_M)\in U^M$, and weights $\boldsymbol{w}:=(w_1,\dots,w_M)^\top\in\mathbb{R}^M$, the function $\hat{E}_{K_N}: U^M\times\mathbb{R}^M\to\mathbb{R}$, cf. (5.21), can be evaluated via the nonequispaced Fourier matrix $\boldsymbol{Y}_N$, cf. (5.22), by*

$$\hat{E}_{K_N}(\boldsymbol{P},\boldsymbol{w})=\|\boldsymbol{\Lambda}^{\frac{1}{2}}(\overline{\boldsymbol{Y}}_N^\top\boldsymbol{w}-\hat{\boldsymbol{\nu}})\|_2^2=\overline{\boldsymbol{e}}^\top\boldsymbol{\Lambda}\boldsymbol{e},\qquad \boldsymbol{e}:=(\overline{\boldsymbol{Y}}_N^\top\boldsymbol{w}-\hat{\boldsymbol{\nu}})\in\mathbb{C}^{d_N},\tag{5.27}$$

where

$$\boldsymbol{\Lambda}:=\operatorname{diag}(\lambda_0,\dots,\lambda_{d_N-1})=(\delta_{l,l'}\lambda_l)_{l,l'=0}^{d_N-1}\in\mathbb{C}^{d_N\times d_N},\quad \hat{\boldsymbol{\nu}}:=(\hat{\nu}_0,\dots,\hat{\nu}_{d_N-1})^\top\in\mathbb{C}^{d_N}.\tag{5.28}$$

The gradient can be evaluated by

$$\nabla\hat{E}_{K_N}(\boldsymbol{P},\boldsymbol{w})=2\operatorname{Re}\left(\mathbf{D}\boldsymbol{E}\boldsymbol{\Lambda}\boldsymbol{e}\right)\in\mathbb{R}^{M(n+1)}\tag{5.29}$$

where, cf. (5.23),

$$\mathbf{D}\boldsymbol{E}:=\begin{pmatrix}\boldsymbol{W}\boldsymbol{\nabla}\boldsymbol{Y}_N\\ \boldsymbol{Y}_N\end{pmatrix}\in\mathbb{C}^{M(n+1)\times d_N},\qquad \boldsymbol{W}:=\begin{pmatrix}w_1\boldsymbol{I}_n & \mathbf{0} & \dots & \mathbf{0}\\ \mathbf{0} & w_2\boldsymbol{I}_n & & \vdots\\ \vdots & & \ddots & \mathbf{0}\\ \mathbf{0} & \dots & \mathbf{0} & w_M\boldsymbol{I}_n\end{pmatrix}\in\mathbb{R}^{Mn\times Mn}.$$

The Hessian matrix representation can be written as

$$\mathbf{H}\hat{E}_{K_N}(\boldsymbol{P},\boldsymbol{w})=2\operatorname{Re}\left(\mathbf{D}\boldsymbol{E}\boldsymbol{\Lambda}\overline{\mathbf{D}\boldsymbol{E}}^\top+\begin{pmatrix}\mathbf{H}_{\boldsymbol{P}} & \mathbf{H}_{\boldsymbol{P},\boldsymbol{w}}\\ \mathbf{H}_{\boldsymbol{P},\boldsymbol{w}}^\top & \mathbf{0}\end{pmatrix}\right)\in\mathbb{R}^{M(n+1)\times M(n+1)}\tag{5.30}$$

where

$$\mathbf{H}_{\boldsymbol{P}}:=\begin{pmatrix}w_1\mathbf{H}_{\boldsymbol{p}_1} & \mathbf{0} & \dots & \mathbf{0}\\ \mathbf{0} & w_2\mathbf{H}_{\boldsymbol{p}_2} & & \vdots\\ \vdots & & \ddots & \mathbf{0}\\ \mathbf{0} & \dots & \mathbf{0} & w_M\mathbf{H}_{\boldsymbol{p}_M}\end{pmatrix}\in\mathbb{C}^{Mn\times Mn},$$

$$\mathbf{H}_{\boldsymbol{P},\boldsymbol{w}}:=\begin{pmatrix}\mathbf{H}_{\boldsymbol{p}_1,w_1} & \mathbf{0} & \dots & \mathbf{0}\\ \mathbf{0} & \mathbf{H}_{\boldsymbol{p}_2,w_2} & & \vdots\\ \vdots & & \ddots & \mathbf{0}\\ \mathbf{0} & \dots & \mathbf{0} & \mathbf{H}_{\boldsymbol{p}_M,w_M}\end{pmatrix}\in\mathbb{C}^{Mn\times M}$$

with, cf. (5.25),

$$\mathbf{H}_{\boldsymbol{p}_i}:=\sum_{l=0}^{d_N-1}\lambda_l\boldsymbol{e}_l\mathbf{H}\psi_l(\boldsymbol{p}_i)\in\mathbb{C}^{n\times n},\quad \mathbf{H}_{\boldsymbol{p}_i,\boldsymbol{w}_i}:=\sum_{l=0}^{d_N-1}\lambda_l\boldsymbol{e}_l\nabla\psi_l(\boldsymbol{p}_i)\in\mathbb{C}^{n},\qquad i=1,\dots,M.\tag{5.31}$$

Moreover, the matrices $\mathbf{H}_{\boldsymbol{p}_i}$ *and the vectors* $\mathbf{H}_{\boldsymbol{p}_i,\boldsymbol{w}_i}$, $i = 1,\dots,M$, *defined by* (5.31) *can be computed via the matrices* $\boldsymbol{\nabla Y}_N$, $\mathbf{H}\boldsymbol{Y}_N$, *cf.* (5.23), (5.24), *from the relations, cf.* (5.27), (5.28),

$$\begin{pmatrix} \mathbf{H}_{\boldsymbol{p}_1,\boldsymbol{w}_1} \\ \vdots \\ \mathbf{H}_{\boldsymbol{p}_M,\boldsymbol{w}_M} \end{pmatrix} = \boldsymbol{\nabla Y}_N \boldsymbol{\Lambda e} \in \mathbb{C}^{Mn}, \qquad \begin{pmatrix} \mathbf{H}_{\boldsymbol{p}_1} \\ \vdots \\ \mathbf{H}_{\boldsymbol{p}_M} \end{pmatrix} = \mathbf{H}\boldsymbol{Y}_N((\boldsymbol{\Lambda e}) \otimes \boldsymbol{I}_n) \in \mathbb{C}^{Mn\times n}.$$

Proof. The relation (5.27) is a simple application of the matrix-vector products.

We note that for differentiable complex-valued functions $f : \mathbb{R} \to \mathbb{C}$ the product rule leads to the relation

$$\frac{\mathrm{d}}{\mathrm{d}t}|f(t)|^2 = \frac{\mathrm{d}}{\mathrm{d}t}\big(f(t)\overline{f}(t)\big) = f'(t)\overline{f}(t) + \overline{f}'(t)f(t) = 2\mathrm{Re}\left(f'(t)\overline{f}(t)\right), \quad t \in \mathbb{R}.$$

Hence, with the abbreviations of the partial derivatives of the basis functions

$$\psi_{l(k)}(\boldsymbol{x}) := \frac{\partial}{\partial x_k}\psi_l(\boldsymbol{x}),\ \psi_{l(k,k')}(\boldsymbol{x}) := \frac{\partial^2}{\partial x_k \partial x_{k'}}\psi_l(\boldsymbol{x}), \quad \boldsymbol{x} := (x_i)_{i=1}^n \in U,\ l = 0,\dots,d_N-1,$$

we find that the partial derivatives of $\hat{E}_{K_N}$ at $(\boldsymbol{P},\boldsymbol{w}) \in X^M \times \mathbb{R}^M$ with $\boldsymbol{P} := (\boldsymbol{p}_1,\dots,\boldsymbol{p}_M) \in U^M$, $\boldsymbol{p}_i := (p_{i,1},\dots,p_{i,n}) \in U$, $i = 1,\dots,M$, and, $\boldsymbol{w} := (w_1,\dots,w_M)^\top \in \mathbb{R}^M$, with respect to $p_{i,k}$ and w_i, $i,i' = 1,\dots,M$, $k,k' = 1,\dots,n$, are given by

$$\frac{\partial}{w_i}\hat{E}_{K_N}(\boldsymbol{P},\boldsymbol{w}) = 2\mathrm{Re}\left(\sum_{l=0}^{d_N-1}\lambda_l\left(\sum_{j=1}^{M} w_j\overline{\psi}_l(\boldsymbol{p}_j) - \hat{\nu}_l\right)\psi_l(\boldsymbol{p}_i)\right),$$

$$\frac{\partial^2}{w_i w_{i'}}\hat{E}_{K_N}(\boldsymbol{P},\boldsymbol{w}) = 2\mathrm{Re}\left(\sum_{l=0}^{d_N-1}\lambda_l\psi_l(\boldsymbol{p}_i)\overline{\psi}_l(\boldsymbol{p}_{i'})\right),$$

and

$$\frac{\partial}{\partial p_{i,k}}\hat{E}_{K_N}(\boldsymbol{P},\boldsymbol{w}) = 2\mathrm{Re}\left(\sum_{l=0}^{d_N-1}\lambda_l\left(\sum_{j=1}^{M} w_j\overline{\psi}_l(\boldsymbol{p}_j) - \hat{\nu}_l\right)w_i\psi_{l(k)}(\boldsymbol{p}_i)\right),$$

$$\frac{\partial^2\hat{E}_{K_N}(\boldsymbol{P},\boldsymbol{w})}{\partial p_{i,k}\partial p_{i',k'}} =$$

$$2\mathrm{Re}\left(\sum_{l=0}^{d_N-1}\lambda_l\left(w_i w_{i'}\psi_{l(k)}(\boldsymbol{p}_i)\overline{\psi}_{l(k')}(\boldsymbol{p}_{i'}) + \delta_{i,i'}\left(\sum_{j=1}^{M} w_j\overline{\psi}_l(\boldsymbol{p}_j) - \hat{\nu}_l\right)w_i\psi_{l(k,k')}(\boldsymbol{p}_i)\right)\right),$$

$$\frac{\partial^2\hat{E}_{K_N}(\boldsymbol{P},\boldsymbol{w})}{\partial p_{i,k}\partial w_{i'}} = 2\mathrm{Re}\left(\sum_{l=0}^{d_N-1}\lambda_l\left(w_i\psi_{l(k)}(\boldsymbol{p}_i)\overline{\psi}_l(\boldsymbol{p}_{i'}) + \delta_{i,i'}\left(\sum_{j=1}^{M} w_j\overline{\psi}_l(\boldsymbol{p}_j) - \hat{\nu}_l\right)\psi_{l(k)}(\boldsymbol{p}_i)\right)\right)$$

and the assertions (5.29), (5.30) follow. ∎

Remark 5.12. We will use the given relations in Theorem 5.11 for the evaluation of the gradient and Hessian matrix representation of $\hat{E}_{K_N}$ in local coordinates on a d-dimensional Riemannian manifold $X \subset \mathbb{R}^n$. More precisely, let $h : \Omega \to X$, $\Omega \subset \mathbb{R}^d$ open, be a local parameterization of X around the points $\boldsymbol{p}_i = h(\boldsymbol{y}_i) \in X$, $\boldsymbol{y}_i \in \Omega$, $i = 1,\dots,M$, and consider the coordinate

representation

$$\hat{E}_{K_N} \circ H(\boldsymbol{y}, \boldsymbol{w}), \quad H(\boldsymbol{y}, \boldsymbol{w}) := \Big(h(\boldsymbol{y}_1)^\top, \ldots, h(\boldsymbol{y}_M)^\top, \boldsymbol{w}^\top\Big)^\top, \quad \boldsymbol{y} := (\boldsymbol{y}_i)_{i=1}^M \in \Omega^M,\ \boldsymbol{w} \in \mathbb{R}^M,$$

of the function $\hat{E}_{K_N}$ defined by (5.21) on the product manifold $\mathcal{M} := X^M \times \mathbb{R}^M$. Then we can apply Theorem 5.11 to the open set $U = \Omega \in \mathbb{R}^d$ and the function $\hat{E}_{K_N} \circ H : \Omega^M \times \mathbb{R}^M \to \mathbb{R}$ in order to compute the gradient and the Hessian matrix representation in local coordinates, cf. (3.34) and (3.35),

$$\begin{aligned} \nabla_H(\hat{E}_{K_N} \circ H)(\boldsymbol{y}, \boldsymbol{w}) &= \boldsymbol{G}_H(\boldsymbol{y}, \boldsymbol{w})^{-1} \nabla(\hat{E}_{K_N} \circ H)(\boldsymbol{y}, \boldsymbol{w}) \in \mathbb{R}^{M(d+1)}, \\ \mathbf{H}_H \hat{E}_{K_N}(\boldsymbol{y}, \boldsymbol{w}) &= \mathbf{H}(\hat{E}_{K_N} \circ H)(\boldsymbol{y}, \boldsymbol{w}) - \mathbf{N}_H(\hat{E}_{K_N} \circ H)(\boldsymbol{y}, \boldsymbol{w}) \in \mathbb{R}^{M(d+1) \times M(d+1)}, \end{aligned} \tag{5.32}$$

where $\boldsymbol{G}_H(\boldsymbol{y}, \boldsymbol{w}) \in \mathbb{R}^{M(d+1)}$ is the matrix representation of the Riemannian structure $g_{\mathcal{M}}$ on $\mathcal{M}$ with respect to the local parameterization $H : \Omega^M \times \mathbb{R}^M \to \mathcal{M}$, cf. (3.53), and the matrix entries of $\mathbf{N}_H(\hat{E}_{K_N} \circ H)(\boldsymbol{y}, \boldsymbol{w})$ depend linearly on the gradient $\nabla(\hat{E}_{K_N} \circ H)(\boldsymbol{y}, \boldsymbol{w})$.

More precisely, we recall that the usual gradients corresponding to the coordinate $\boldsymbol{y}_i \in \Omega$ and $\boldsymbol{w} \in \mathbb{R}^M$ are given by, cf. (3.56),

$$\begin{aligned} \nabla_{\boldsymbol{y}_i}(\hat{E}_{K_N} \circ H)(\boldsymbol{y}, \boldsymbol{w}) &= \Big(\delta_{i,1}\boldsymbol{I}_d \quad \ldots \quad \delta_{i,M}\boldsymbol{I}_d \quad \mathbf{0}_M\Big) \nabla(\hat{E}_{K_N} \circ H)(\boldsymbol{y}, \boldsymbol{w}) \in \mathbb{R}^d, \quad i = 1, \ldots, M, \\ \nabla_{\boldsymbol{w}}(\hat{E}_{K_N} \circ H)(\boldsymbol{y}, \boldsymbol{w}) &= \Big(\mathbf{0}_d \quad \ldots \quad \mathbf{0}_d \quad \boldsymbol{I}_M\Big) \nabla(\hat{E}_{K_N} \circ H)(\boldsymbol{y}, \boldsymbol{w}) \in \mathbb{R}^M, \quad (\boldsymbol{y}, \boldsymbol{w}) \in \Omega^M \times \mathbb{R}^M, \end{aligned}$$

respectively, where the matrices $\mathbf{0}_d, \boldsymbol{I}_d \in \mathbb{R}^{d \times d}$, $\mathbf{0}_M, \boldsymbol{I}_M \in \mathbb{R}^{M \times M}$ are zero and identity matrices of appropriate size, and δ is the Kronecker delta, cf. (2.15). Then we infer from relation (3.57) the representation of the gradient

$$\nabla_H(\hat{E}_{K_N} \circ H)(\boldsymbol{y}, \boldsymbol{w}) = \begin{pmatrix} \boldsymbol{G}_h^{-1}(\boldsymbol{y}_1) \nabla_{\boldsymbol{y}_i}(\hat{E}_{K_N} \circ H)(\boldsymbol{y}, \boldsymbol{w}) \\ \vdots \\ \boldsymbol{G}_h^{-1}(\boldsymbol{y}_M) \nabla_{\boldsymbol{y}_i}(\hat{E}_{K_N} \circ H)(\boldsymbol{y}, \boldsymbol{w}) \\ \nabla_{\boldsymbol{w}}(\hat{E}_{K_N} \circ H)(\boldsymbol{y}, \boldsymbol{w}) \end{pmatrix} \in \mathbb{R}^{M(d+1)}.$$

Furthermore, by relation (3.60) we have

$$\mathbf{N}_H(\hat{E}_{K_N} \circ H)(\boldsymbol{y}, \boldsymbol{w}) := \begin{pmatrix} \mathbf{N}_{\boldsymbol{y}_1}(\boldsymbol{y}, \boldsymbol{w}) & \mathbf{0} & \cdots & \mathbf{0} & \mathbf{0} \\ \mathbf{0} & \ddots & \ddots & \vdots & \vdots \\ \vdots & \ddots & \ddots & \mathbf{0} & \mathbf{0} \\ \mathbf{0} & \cdots & \mathbf{0} & \mathbf{N}_{\boldsymbol{y}_M}(\boldsymbol{y}, \boldsymbol{w}) & \mathbf{0} \\ \mathbf{0} & \cdots & \mathbf{0} & \mathbf{0} & \mathbf{0}_M \end{pmatrix} \in \mathbb{R}^{M(d+1) \times M(d+1)}$$

where, cf. (3.61),

$$\mathbf{N}_{\boldsymbol{y}_i}(\boldsymbol{y}, \boldsymbol{w}) = \Big(\boldsymbol{\Gamma}_h^1(\boldsymbol{y}_i) \quad \ldots \quad \boldsymbol{\Gamma}_h^d(\boldsymbol{y}_i)\Big) (\nabla_{\boldsymbol{y}_i}(\hat{E}_{K_N} \circ H)(\boldsymbol{y}, \boldsymbol{w}) \otimes \boldsymbol{I}_d) \in \mathbb{R}^{d \times d}, \quad i = 1, \ldots, M,$$

with the matrices $\boldsymbol{\Gamma}_h^m \in \mathbb{R}^{d \times d}$, $m = 1, \ldots, d$, associated to the Christoffel symbols of the second kind corresponding to the local parameterization h, cf. (3.20).

It follows, for given matrices $\boldsymbol{G}_h^{-1}(\boldsymbol{y}_i), \boldsymbol{\Gamma}_h^m(\boldsymbol{y}_i) \in \mathbb{R}^{d \times d}$, $i = 1, \ldots, M$, $m = 1, \ldots, d$, we can compute with an additional cost of $\mathcal{O}(Md^3)$ arithmetic operations the local coordinate representations of the gradient and the Hessian of $\hat{E}_{K_N}$ on the Riemannian manifold $\mathcal{M}$. □

We observe by Theorem 5.11 that the computationally most expansive parts for the evaluation of the function $\hat{E}_{K_N}$, cf. (5.21), its gradient $\nabla \hat{E}_{K_N}$, and matrix-vector products with is Hessian matrix representation $\mathbf{H}\hat{E}_{K_N}$ are the matrix-vector products with the nonequispaced Fourier matrix $\boldsymbol{Y}_N$, and the matrices $\boldsymbol{\nabla Y}_N$, $\mathbf{H}\boldsymbol{Y}_N$, cf. (5.22)–(5.24), as well as their adjoint matrices. By Remark 5.12 the same statement is true in the case of Riemannian manifolds $X \subset \mathbb{R}^n$ for the corresponding local coordinate representations, cf. (5.32).

For the matrix-vector product with the nonequispaced Fourier matrix $\boldsymbol{Y}_N$, or in other words for the evaluation of a bandlimited function $f \in \Pi_N(X)$, cf. (5.26), more efficient but approximate algorithms have been developed for the torus $\mathbb{T}^d$, $d \in N$, the sphere $\mathbb{S}^2$, and the rotation group $\mathrm{SO}(3)$. For the computation of the matrix vector product $\boldsymbol{f} = \boldsymbol{Y}_N \hat{\boldsymbol{f}}$ one needs usually $\mathcal{O}(d_N M)$ arithmetic operations. However, with nonequispaced fast Fourier transforms this task can be performed in almost $\mathcal{O}(d_N + M)$ arithmetic operations.

In the following Sections 5.2.1–5.2.3 we will see that for $X = \mathbb{T}^d, \mathbb{S}^2, \mathrm{SO}(3)$ with the usual Fourier bases $\psi_l \in L^2(X)$, $l \in \mathbb{N}_0$, the matrices $\mathbf{D}\boldsymbol{Y}_N$, $\mathbf{H}\boldsymbol{Y}_N$ (in local coordinates) can be expressed via the nonequispaced Fourier matrix $\boldsymbol{Y}_N$, cf. Theorem 5.13, 5.19, 5.23, respectively. These properties together with nonequispaced fast Fourier transforms for the computation of the matrix-vector product $\boldsymbol{f} = \boldsymbol{Y}\hat{\boldsymbol{f}}$, cf. (5.26), leads us to efficient evaluation algorithms for the function $\hat{E}_{K_N}$ and its gradient, and the matrix-vector multiplication with its Hessian matrix representation for polynomial kernels K_N on the torus $\mathbb{T}^d$, the sphere $\mathbb{S}^2$, and the rotation group $\mathrm{SO}(3)$, cf. Corollary 5.18, 5.22, and 5.26, respectively.

5.2.1 The Torus $\mathbb{T}^d$

We recall that on the torus $\mathbb{T}^d$ we use the conventions given in Remark 3.14, i.e., we identify functions $f \in L^2(\mathbb{T}^d)$ with 2π-periodic functions in Euclidean space $\mathbb{R}^d$, where the usual definitions of the gradient and Hessian matrix representation apply.

In Section 4.1 we have already introduced the usual Fourier basis functions on the torus $\mathbb{T}^d$ which are given by the exponentials $\psi_{\boldsymbol{n}}(\boldsymbol{\alpha}) = \mathrm{e}^{\mathrm{i}\boldsymbol{n}^\top \boldsymbol{\alpha}}$, $\boldsymbol{\alpha} \in \mathbb{R}^d$, $\boldsymbol{n} \in \mathbb{Z}^d$, cf. (4.1). We recall that the space of trigonometric polynomials with degree at most $N \in \mathbb{N}_0$ is denote by $\Pi^N(\mathbb{T}^d)$ and has dimension $d_N := (2N+1)^d$, cf. (4.2). Thus, for given points $\boldsymbol{\alpha}_i \in \mathbb{R}^d$, $i = 1, \dots, M$, the nonequispaced Fourier matrix reads as, cf. (5.22),

$$\boldsymbol{Y}_N := \big(\psi_{\boldsymbol{n}}(\boldsymbol{\alpha}_i)\big)_{i=1,\dots,M, \boldsymbol{n} \in I_N} \in \mathbb{C}^{M \times d_N}, \qquad I_N := \mathbb{Z}^d \cap [-N, N]^d, \tag{5.33}$$

where the column indices run in a fixed prescribed order over the index set, e.g., in lexicographic order $\boldsymbol{n} = (-N, \dots, -N, -N), (-N, \dots, -N, -N+1), \dots, (N, \dots, N, N-1), (N, \dots, N, N)$. Similarly, the matrices $\boldsymbol{\nabla Y}_N$, $\mathbf{H}\boldsymbol{Y}_N$, cf. (5.23), (5.24), are given by

$$\begin{aligned} \boldsymbol{\nabla Y}_N &= \big(\nabla \psi_{\boldsymbol{n}}(\boldsymbol{\alpha}_i)\big)_{i=1,\dots,M, \boldsymbol{n} \in I_N} \in \mathbb{C}^{dM \times d_N}, \\ \mathbf{H}\boldsymbol{Y}_N &= \big(\mathbf{H}\psi_{\boldsymbol{n}}(\boldsymbol{\alpha}_i)\big)_{i=1,\dots,M, \boldsymbol{n} \in I_N} \in \mathbb{C}^{dM \times d_N d}, \end{aligned} \tag{5.34}$$

where the usual gradients and Hessian matrices for $\boldsymbol{\alpha} := (\alpha_i)_{i=1}^d \in \mathbb{R}^d$, $\boldsymbol{n} := (n_i)_{i=1}^d \in \mathbb{Z}^d$ are

$$\nabla \psi_{\boldsymbol{n}}(\boldsymbol{\alpha}) = \begin{pmatrix} \frac{\partial}{\partial \alpha_1} \psi_{\boldsymbol{n}}(\boldsymbol{\alpha}) \\ \vdots \\ \frac{\partial}{\partial \alpha_d} \psi_{\boldsymbol{n}}(\boldsymbol{\alpha}) \end{pmatrix} \in \mathbb{C}^d, \quad \mathbf{H}\psi_{\boldsymbol{n}}(\boldsymbol{\alpha}) = \begin{pmatrix} \frac{\partial^2}{\partial \alpha_1 \partial \alpha_1} \psi_{\boldsymbol{n}}(\boldsymbol{\alpha}) & \dots & \frac{\partial^2}{\partial \alpha_1 \partial \alpha_d} \psi_{\boldsymbol{n}}(\boldsymbol{\alpha}) \\ \vdots & \ddots & \vdots \\ \frac{\partial^2}{\partial \alpha_d \partial \alpha_1} \psi_{\boldsymbol{n}}(\boldsymbol{\alpha}) & \dots & \frac{\partial^2}{\partial \alpha_d \partial \alpha_d} \psi_{\boldsymbol{n}}(\boldsymbol{\alpha}) \end{pmatrix} \in \mathbb{C}^{d \times d}.$$

Theorem 5.13. *For given points $\boldsymbol{\alpha}_i \in \mathbb{R}^d$, $i = 1, \dots, M$, and polynomial degree $N \in \mathbb{N}_0$ the matrices defined by* (5.34) *can be expressed via the nonequispaced Fourier matrix $\boldsymbol{Y}_N$, cf.* (5.33),

by

$$\mathbf{D}\boldsymbol{Y}_N = (\boldsymbol{Y}_N \otimes \boldsymbol{I}_d)\boldsymbol{D}_N^{\boldsymbol{\alpha}} \in \mathbb{C}^{dM \times d_N}, \qquad \mathbf{H}\boldsymbol{Y}_N = (\boldsymbol{Y}_N \otimes \boldsymbol{I}_d)\boldsymbol{D}_N^{\boldsymbol{\alpha},\boldsymbol{\alpha}} \in \mathbb{C}^{dM \times d_N d}, \tag{5.35}$$

where $\boldsymbol{D}_N^{\boldsymbol{\alpha}}, \boldsymbol{D}_N^{\boldsymbol{\alpha},\boldsymbol{\alpha}}$ *are block-diagonal matrices defined by*

$$\boldsymbol{D}_N^{\boldsymbol{\alpha}} := \big(\mathrm{i}\boldsymbol{n}\delta_{\boldsymbol{n},\boldsymbol{m}}\big)_{\boldsymbol{n},\boldsymbol{m}\in I_N} \in \mathbb{C}^{d_N d \times d_N}, \qquad \boldsymbol{D}_N^{\boldsymbol{\alpha}} := \big(-\boldsymbol{n}\boldsymbol{n}^\top \delta_{\boldsymbol{n},\boldsymbol{m}}\big)_{\boldsymbol{n},\boldsymbol{m}\in I_N} \in \mathbb{C}^{d_n d \times d_n d}$$

with the multivariate Kronecker delta $\delta_{\boldsymbol{n},\boldsymbol{m}} := \prod_{i=1}^d \delta_{n_i,m_i}$, $\boldsymbol{n} := (n_i)_{i=1}^d, \boldsymbol{m} := (m_i)_{i=1}^d \in \mathbb{Z}^d$, *cf.* (2.15).

Proof. The assertion (5.35) is a simple consequence of the differential relations of the exponentials $\psi_{\boldsymbol{n}}$, $\boldsymbol{n} \in \mathbb{Z}^d$. More precisely, from

$$\frac{\partial}{\partial \alpha_i}\psi_{\boldsymbol{n}}(\boldsymbol{\alpha}) = \mathrm{i}n_i\psi_{\boldsymbol{n}}(\boldsymbol{\alpha}), \qquad \boldsymbol{\alpha} := (\alpha_1, \ldots, \alpha_d) \in \mathbb{R}^d, \quad \boldsymbol{n} := (n_1, \ldots, n_d) \in \mathbb{Z}^d, \quad i = 1, \ldots, d,$$

we infer for the gradient and the Hessian matrix representation the relations

$$\nabla\psi_{\boldsymbol{n}}(\boldsymbol{\alpha}) = \mathrm{i}\boldsymbol{n}\psi_{\boldsymbol{n}}(\boldsymbol{\alpha}) \in \mathbb{C}^d, \qquad \mathbf{H}\psi_{\boldsymbol{n}}(\boldsymbol{\alpha}) = -\boldsymbol{n}\boldsymbol{n}^\top\psi_{\boldsymbol{n}}(\boldsymbol{\alpha}) \in \mathbb{C}^{d\times d}, \qquad \boldsymbol{\alpha} \in \mathbb{R}^d, \quad \boldsymbol{n} \in \mathbb{Z}^d.$$

Hence, with the definitions of the matrices $\mathbf{D}\boldsymbol{Y}_N, \mathbf{H}\boldsymbol{Y}_N$, cf. (5.34), and the relation

$$\boldsymbol{Y}_N \otimes \boldsymbol{I}_d = \big(\psi_{\boldsymbol{n}}(\boldsymbol{\alpha}_i)\boldsymbol{I}_d\big)_{i=1,\ldots,M,\boldsymbol{n}\in I_N} \in \mathbb{C}^{dM\times d_N d}$$

the proof is finished. ∎

Remark 5.14. It is convenient to introduce for $d, D \in \mathbb{N}$ the permutation matrix

$$\boldsymbol{P}_{d,D} := \begin{pmatrix} I_d \otimes \boldsymbol{e}_1^\top \\ \vdots \\ I_d \otimes \boldsymbol{e}_D^\top \end{pmatrix} = \begin{pmatrix} \boldsymbol{e}_1 & \mathbf{0} & \ldots & \mathbf{0} & \boldsymbol{e}_2 & \ldots & \mathbf{0} \\ \mathbf{0} & \boldsymbol{e}_1 & \ddots & \vdots & \mathbf{0} & \ldots & \vdots \\ \vdots & \ddots & \ddots & \mathbf{0} & \vdots & \ldots & \mathbf{0} \\ \mathbf{0} & \ldots & \mathbf{0} & \boldsymbol{e}_1 & \mathbf{0} & \ldots & \boldsymbol{e}_D \end{pmatrix}^\top \in \mathbb{R}^{dD\times dD} \tag{5.36}$$

where $\boldsymbol{I}_d \in \mathbb{R}^{d\times d}$ is the identity matrix and $\boldsymbol{e}_1, \ldots, \boldsymbol{e}_D \in \mathbb{R}^D$ are the standard basis vectors. With these matrices the Kronecker product $\boldsymbol{Y}_N \otimes \boldsymbol{I}_d$ in relation (5.35) of Theorem 5.13 can be brought in block diagonal form

$$\boldsymbol{I}_d \otimes \boldsymbol{Y}_N = \begin{pmatrix} \boldsymbol{Y}_N & \mathbf{0} & \ldots & \mathbf{0} \\ \mathbf{0} & \boldsymbol{Y}_N & \ddots & \vdots \\ \vdots & \ddots & \ddots & \mathbf{0} \\ \mathbf{0} & \ldots & \mathbf{0} & \boldsymbol{Y}_N \end{pmatrix} \in \mathbb{C}^{dM\times d_N d}, \tag{5.37}$$

with the nonequispaced Fourier matrix $\boldsymbol{Y}_N \in C^{M\times d_N}$ on the diagonal, by using the relation

$$\boldsymbol{Y}_N \otimes \boldsymbol{I}_d = \boldsymbol{P}_{d,M}(\boldsymbol{I}_d \otimes \boldsymbol{Y}_N)\boldsymbol{P}_{d_N,d} \in \mathbb{C}^{dM\times d_N d}.$$

Hence, due to the permutation matrices $\boldsymbol{P}_{d,D}$ defined by (5.36) and relation (5.37), we can compute the matrix-vector products with the matrices $\mathbf{D}\boldsymbol{Y}_N$, $\mathbf{H}\boldsymbol{Y}_N$, cf. (5.34) via matrix-vector products of the nonequispaced Fourier matrix $\boldsymbol{Y}_N$, cf (5.33). □

Nonequispaced fast Fourier Transforms on the Torus $\mathbb{T}^d$

For equally distributed points the *fast Fourier transform (FFT)*, cf. [27], is known to be the most efficient algorithm for the computation of matrix-vector multiplications with the Fourier matrix $\boldsymbol{Y}_N$.[4] In the case of arbitrarily distributed points several efficient but approximate algorithms have been proposed, cf. [36, 37, 14, 43]. In this thesis we make use of the algorithms presented in [110], which are implemented in the NFFT-library [72]. The idea of these algorithms is to approximate the nonequispaced Fourier matrix $\boldsymbol{Y}_N$ by a matrix $\tilde{\boldsymbol{Y}}_N$ for which a fast matrix-vector multiplication is available. The precise result is stated in Theorem 5.15, for which we need to recall the definition of the L^1- and L^∞-norm given by

$$\|\boldsymbol{v}\|_1 := \sum_{i=1}^{n} |v_i|, \qquad \|\boldsymbol{v}\|_\infty := \max_{i=1,\dots,n} |v_i|, \qquad \boldsymbol{v} := (v_1, \dots, v_n)^\top \in \mathbb{C}^n. \tag{5.38}$$

Theorem 5.15. *For given points $\boldsymbol{\alpha}_i \in \mathbb{R}^d$, $i = 1, \dots, M$, polynomial degree $N \in \mathbb{N}_0$, and prescribed accuracy $\epsilon > 0$, the nonequispaced Fourier matrix $\boldsymbol{Y}_N \in \mathbb{C}^{M \times d_N}$, cf.* (5.33)*, can be approximated by a matrix $\tilde{\boldsymbol{Y}}_N \in \mathbb{C}^{M \times d_N}$ which obeys the following error bounds, cf.* (5.38)*,*

$$\max_{\hat{\boldsymbol{f}} \in \mathbb{C}^{d_N}, \|\hat{\boldsymbol{f}}\|_1 \le 1} \|(\boldsymbol{Y}_N - \tilde{\boldsymbol{Y}}_N)\hat{\boldsymbol{f}}\|_\infty < \epsilon, \qquad \max_{\boldsymbol{f} \in \mathbb{C}^M, \|\boldsymbol{f}\|_1 \le 1} \|(\overline{\boldsymbol{Y}}_N^\top - \overline{\tilde{\boldsymbol{Y}}}_N^\top)\boldsymbol{f}\|_\infty < \epsilon$$

and where the matrix vector products $\tilde{\boldsymbol{Y}}_N \hat{\boldsymbol{f}}$, $\hat{\boldsymbol{f}} \in \mathbb{C}^{d_N}$, and $\overline{\tilde{\boldsymbol{Y}}}_N^\top \boldsymbol{f}$, $\boldsymbol{f} \in \mathbb{C}^M$, can be computed in

$$\mathcal{O}\big(dN^d \log(N) + M|\log(\epsilon)|^d\big)$$

arithmetic operations.

Proof. We refer to [110]. ∎

Remark 5.16. In numerical computations with finite precision arithmetic one is inevitably confronted with the problem of rounding errors. Hence, it might be reasonable to replace in numerical computations the nonequispaced Fourier matrix $\boldsymbol{Y}_N$ by the approximation $\tilde{\boldsymbol{Y}}_N$ where the prescribed accuracy ϵ in Theorem 5.15 is fixed, say $\epsilon \approx 10^{-16}$ for double precision. We denote such a replacement as *performing a nonequispaced fast Fourier transform (NFFT) with fixed accuracy.*

In that respect we pass on a precise error analysis and refer to the numerical examples given in Chapter 6, especially, to the very precise computations of classical quadratures on the sphere $\mathbb{S}^2$ and the rotation group SO(3) presented in Section 6.2.3 and Section 6.3.3, respectively. □

Corollary 5.17. *For given points $\boldsymbol{\alpha}_i \in \mathbb{R}^d$, $i = 1, \dots, M$, and polynomial degree $N \in \mathbb{N}_0$ the numerical computation of the matrix-vector multiplications with the matrices $\mathbf{D}\boldsymbol{Y}_N \in \mathbb{C}^{dM \times d_N}$, $\mathbf{H}\boldsymbol{Y}_N \in \mathbb{C}^{dM \times d_N d}$, cf.* (5.34)*, can be performed by d NFFTs with fixed accuracy, cf. Remark 5.16, in*

$$\mathcal{O}\big(dN^d \log(N) + dM\big)$$

arithmetic operations.

Proof. The assertions follow from Theorem 5.13, Remark 5.14 and Theorem 5.15. ∎

[4] In [65] it has been discovered that the FFT-algorithm was already known to Gauß.

Corollary 5.18. *On the torus $\mathbb{T}^d$ let a polynomial kernel, cf.* (4.1),

$$K_N(\boldsymbol{x},\boldsymbol{y}) := \sum_{\substack{\boldsymbol{n}\in\mathbb{Z}^d,\\ \boldsymbol{n}\in[-N,N]^d}} \lambda_{\boldsymbol{n}}\psi_{\boldsymbol{n}}(\boldsymbol{x})\overline{\psi}_{\boldsymbol{n}}(\boldsymbol{y}), \qquad \boldsymbol{x},\boldsymbol{y}\in\mathbb{T}^d, \qquad I_N := \mathbb{Z}^d\cap[-N,N]^d,$$

with coefficients $\lambda_{\boldsymbol{n}} \geq 0$ and $\hat{\nu}_{\boldsymbol{n}} \in \mathbb{C}$, $\boldsymbol{n}\in I_N$, be given. Then, for fixed points $\boldsymbol{P} := (\boldsymbol{p}_1,\dots,\boldsymbol{p}_M) \in (\mathbb{T}^d)^M$, and weights $\boldsymbol{w} := (w_1,\dots,w_M)\in\mathbb{R}^M$, the numerical computation of the function, cf. (5.21),

$$\hat{E}_{K_N}(\boldsymbol{P},\boldsymbol{w}) = \sum_{\boldsymbol{n}\in I_N}\lambda_{\boldsymbol{n}}\Big|\hat{\nu}_{\boldsymbol{n}} - \sum_{i=1}^{M} w_i\overline{\psi}_{\boldsymbol{n}}(\boldsymbol{p}_i)\Big|^2,$$

its gradient $\nabla_{\mathcal{M}}\hat{E}_{K_N}(\boldsymbol{P},\boldsymbol{w})$, and the matrix-vector multiplications with the matrix representation of the Hessian $\mathrm{H}_{\mathcal{M}}\hat{E}_{K_N}(\boldsymbol{P},\boldsymbol{w})$ on the product manifold $\mathcal{M} := (\mathbb{T}^d)^M\times\mathbb{R}^M$ can be performed by NFFTs with fixed accuracy, cf. Remark 5.16, in

$$\mathcal{O}\big(dN^d\log(N) + dM\big)$$

arithmetic operations.

Proof. Using Corollary 5.17 the assertions follow from the representations given in Theorem 5.11 together with the Remark 5.12, where we note that on the torus $\mathbb{T}^d$ the Christoffel symbols vanish, see Section 3.1.4. ∎

5.2.2 The Sphere $\mathbb{S}^2$

We recall that the sphere $\mathbb{S}^2$ is usually parameterized in spherical coordinates $(\theta,\varphi)\in[0,\pi]\times[0,2\pi)$, cf. (3.71), and that the canonical measure $\mu_{\mathbb{S}^2}$ is given in this parameterization by the density $\mathrm{d}\mu_{\mathbb{S}^2}(\boldsymbol{x}) = \sin(\theta)\mathrm{d}\theta\mathrm{d}\varphi$, $\boldsymbol{x} = h(\theta,\varphi)$, cf. (3.72).

By abuse of notation we will omit in the following the subscript h in the local coordinate representations of functions $f:\mathbb{S}^2\to\mathbb{C}$, cf. (3.33),

$$f(\theta,\varphi) := f_h(\theta,\varphi) = f(\boldsymbol{x}), \qquad \boldsymbol{x} = h(\theta,\varphi), \quad (\theta,\varphi)\in[0,\pi]\times[0,2\pi).$$

With this convention an orthonormal system of spherical harmonics $Y_{n,k}:\mathbb{S}^2\to\mathbb{C}$ of degree $n\in\mathbb{N}_0$ and order $k=-n,\dots,n$, see Section 4.2, is given by, cf. [135, Eq. (1), p. 133],

$$Y_{n,k}(\theta,\varphi) = \mathrm{e}^{\mathrm{i}k\varphi}\sqrt{\frac{2n+1}{4\pi}\frac{(n-k)!}{(n+k)!}}P_n^k(\cos(\theta)), \qquad (\theta,\varphi)\in[0,\pi]\times[0,2\pi), \tag{5.39}$$

where the *associated Legendre functions*[5] P_n^k, $|k|\leq n$, of degree n and order k are defined by

$$P_n^k(t) := (-1)^k(1-t^2)^{\frac{k}{2}}\frac{\mathrm{d}^k}{\mathrm{d}t^k}P_n(t), \qquad t\in[-1,1], \qquad k=0,\dots,n,$$
$$P_n^k(t) := (-1)^k\frac{(n+k)!}{(n-k)!}P_n^{-k}(t), \qquad t\in[-1,1], \qquad k=-n,\dots,-1,$$

[5] There are several definitions of the associated Legendre functions and the spherical harmonics found in the literature, which depend only on the use of the factors $(-1)^k$.

and P_n are the *Legendre polynomials*[6] given by

$$P_n(t) := \frac{1}{2^n n!}\frac{\mathrm{d}^n}{\mathrm{d}t^n}(t^2-1)^n, \qquad n \in \mathbb{N}_0.$$

By the above choice of the associated Legendre functions with negative order k we have that $\overline{Y}_{n,k} = (-1)^k Y_{n,-k}$, $k = -n, \dots, n$, $n \in \mathbb{N}_0$.

For convenience we introduce the index set $I_N := \{(n,k) \,:\, n = 0, \dots, N,\ k = -n, \dots, n\}$ and recall that $\Pi^N(\mathbb{S}^2) = \operatorname{span}\{Y_{n,k} \,:\, (n,k) \in I_N\}$ denotes the space of spherical polynomials with degree at most $N \in \mathbb{N}_0$, cf. (4.15). The dimension of $\Pi^N(\mathbb{S}^2)$ is denoted by $d_N := (N+1)^2$. Thus, for given points $\boldsymbol{p}_i := h(\theta_i, \varphi_i) \in \mathbb{S}^2$, $(\theta_i, \varphi_i) \in [0,\pi] \times [0, 2\pi)$, $i = 1, \dots, M$, the nonequispaced Fourier matrix, cf. (5.22), reads as

$$\boldsymbol{Y}_N := \big(Y_{n,k}(\theta_i, \varphi_i)\big)_{i=1,\dots,M,(n,k)\in I_N} \in \mathbb{C}^{M \times d_N}, \tag{5.40}$$

where the column indices run in a fixed prescribed order over the index set, e.g., in the lexicographic ordering $(n,k) = (0,0), (1,-1), (1,0), \dots, (N, N-1), (N,N)$. Similarly, the matrices $\boldsymbol{\nabla Y}_N$, $\mathbf{H}\boldsymbol{Y}_N$, cf. (5.23), (5.24), read in local coordinates as

$$\begin{aligned} \boldsymbol{\nabla Y}_N &= \big(\nabla Y_{n,k}(\theta_i, \varphi_i)\big)_{i=1,\dots,M,(n,k)\in I_N} \in \mathbb{C}^{2M \times d_N}, \\ \mathbf{H}\boldsymbol{Y}_N &= \big(\mathbf{H} Y_{n,k}(\theta_i, \varphi_i)\big)_{i=1,\dots,M,(n,k)\in I_N} \in \mathbb{C}^{2M \times 2d_N} \end{aligned} \tag{5.41}$$

where for $(n,k) \in I_N$, $(\theta, \varphi) \in [0,\pi] \times [0, 2\pi)$ the usual gradients and Hessian matrices are given by

$$\nabla Y_{n,k}(\theta,\varphi) = \begin{pmatrix} \frac{\partial}{\partial\theta} Y_{n,k}(\theta,\varphi) \\ \frac{\partial}{\partial\varphi} Y_{n,k}(\theta,\varphi) \end{pmatrix}, \quad \mathbf{H} Y_{n,k}(\theta,\varphi) = \begin{pmatrix} \frac{\partial^2}{\partial\theta^2} Y_{n,k}(\theta,\varphi) & \frac{\partial^2}{\partial\theta\partial\varphi} Y_{n,k}(\theta,\varphi) \\ \frac{\partial^2}{\partial\varphi\partial\theta} Y_{n,k}(\theta,\varphi) & \frac{\partial^2}{\partial\varphi^2} Y_{n,k}(\theta,\varphi) \end{pmatrix}.$$

Theorem 5.19. *For given points $\boldsymbol{p}_i := h(\theta_i, \varphi_i) \in \mathbb{S}^2 \setminus \{\pm(0,0,1)^\top\}$, $(\theta_i, \varphi_i) \in (0,\pi) \times [0, 2\pi)$, $i = 1, \dots, M$, cf.* (3.71)*, and polynomial degree $N \in \mathbb{N}_0$ the matrices $\mathbf{D}\boldsymbol{Y}_N, \mathbf{H}\boldsymbol{Y}_N$ defined by* (5.41) *can be expressed via the nonequispaced Fourier matrix $\boldsymbol{Y}_N$, cf.* (5.40)*, by*

$$\boldsymbol{\nabla Y}_N = \boldsymbol{P}_{2,M} \begin{pmatrix} \boldsymbol{Y}_N^\theta \\ \boldsymbol{Y}_N^\varphi \end{pmatrix} \in \mathbb{C}^{2M \times d_N}, \qquad \mathbf{H}\boldsymbol{Y}_N = \boldsymbol{P}_{2,M} \begin{pmatrix} \boldsymbol{Y}_N^{\theta,\theta} & \boldsymbol{Y}_N^{\theta,\varphi} \\ \boldsymbol{Y}_N^{\varphi,\theta} & \boldsymbol{Y}_N^{\varphi,\varphi} \end{pmatrix} \boldsymbol{P}_{d_N,2} \quad \in \mathbb{C}^{2M \times 2d_N} \tag{5.42}$$

where $\boldsymbol{P}_{2,M}, \boldsymbol{P}_{d_N,2}$ are permutation matrices defined by (5.36) *and the matrices*

$$\begin{aligned} \boldsymbol{Y}_N^\theta &:= \boldsymbol{S}^{-1} \boldsymbol{Y}_{N+1} \boldsymbol{D}_N^\theta \in \mathbb{C}^{M \times d_N}, \\ \boldsymbol{Y}_N^\varphi &:= \boldsymbol{Y}_N \boldsymbol{D}_N^\varphi \in \mathbb{C}^{M \times d_N}, \\ \boldsymbol{Y}_N^{\theta,\theta} &:= \boldsymbol{S}^{-2} (\boldsymbol{Y}_{N+2} \boldsymbol{D}_{N+1}^\theta \boldsymbol{D}_N^\theta - \boldsymbol{C} \boldsymbol{Y}_{N+1} \boldsymbol{D}_N^\theta) \in \mathbb{C}^{M \times d_N}, \\ \boldsymbol{Y}_N^{\theta,\varphi} &:= \boldsymbol{Y}_N^{\varphi,\theta} := \boldsymbol{S}^{-1} \boldsymbol{Y}_{N+1} \boldsymbol{D}_N^\theta \boldsymbol{D}_N^\varphi \in \mathbb{C}^{M \times d_N}, \\ \boldsymbol{Y}_N^{\varphi,\varphi} &:= \boldsymbol{Y}_N \boldsymbol{D}_N^\varphi \boldsymbol{D}_N^\varphi \in \mathbb{C}^{M \times d_N} \end{aligned} \tag{5.43}$$

[6] The Legendre polynomials P_n are exactly the Gegenbauer polynomials $C_n^{\frac{1}{2}}$, cf. [1, Eq. 22.5.36].

are given by the diagonal matrices $\boldsymbol{S}$, $\boldsymbol{C}$, $\boldsymbol{D}_N^{\varphi}$, *and the bidiagonal-like matrix* $\boldsymbol{D}_N^{\theta}$ *defined by*

$$\begin{aligned}
\boldsymbol{S} &:= \operatorname{diag}(\sin(\theta_1),\ldots,\sin(\theta_M)) = (\delta_{i,i'}\sin(\theta_i))_{i,i'=0}^{M} \in \mathbb{R}^{M\times M},\\
\boldsymbol{C} &:= \operatorname{diag}(\cos(\theta_1),\ldots,\cos(\theta_M)) = (\delta_{i,i'}\cos(\theta_i))_{i,i'=0}^{M} \in \mathbb{R}^{M\times M},\\
\boldsymbol{D}_N^{\varphi} &:= \big(\delta_{k',k}\delta_{n',n}\mathrm{i}k\big)_{(n',k')\in I_N,(n,k)\in I_N} \in \mathbb{C}^{d_N\times d_N},\\
\boldsymbol{D}_N^{\theta} &:= \big(\delta_{k',k}(\delta_{n',n+1}a_{n,k} - \delta_{n',n-1}b_{n,k})\big)_{(n',k')\in I_{N+1},(n,k)\in I_N} \in \mathbb{R}^{d_{N+1}\times d_N}
\end{aligned} \tag{5.44}$$

where

$$a_{n,k} := n\sqrt{\frac{(n+1)^2-k^2}{(2n+1)(2n+3)}}, \quad b_{n,k} := (n+1)\sqrt{\frac{n^2-k^2}{(2n-1)(2n+1)}}, \qquad (n,k)\in I_N,$$

and δ *denotes the Kronecker delta, cf.* (2.15).

Proof. The proof is mainly based on the following recurrence relations for spherical harmonics $Y_{n,k}$, $(n,k)\in I_N$, cf. [135, Eq. (4) and (6), p. 147],

$$\begin{aligned}
\frac{\partial}{\partial\varphi}Y_{n,k}(\theta,\varphi) &= \mathrm{i}kY_{n,k}(\theta,\varphi)\\
\sin(\theta)\frac{\partial}{\partial\theta}Y_{n,k}(\theta,\varphi) &= a_{n,k}Y_{n+1,k}(\theta,\varphi) - b_{n,k}Y_{n-1,k}(\theta,\varphi), \qquad (\theta,\varphi)\in[0,\pi]\times[0,2\pi).
\end{aligned} \tag{5.45}$$

The first relation is trivial by definition of the spherical harmonics, cf. (5.39), and the second one is an easy consequence of recurrence relations of the associated Legendre functions, cf. [1, Eq. 8.5.3 and 8.5.4]. Furthermore, we remark that the second relation is well defined since $b_{n,|n|}=0$, $n\in\mathbb{N}_0$.

The relations (5.45) can be written in matrix form. More precisely, by definition of the matrices $\boldsymbol{Y}_N^{\theta}$, $\boldsymbol{Y}_N^{\varphi}$, cf. (5.43) and (5.44) , we obtain

$$\boldsymbol{Y}_N^{\theta} = \left(\frac{\partial}{\partial\theta}Y_{n,k}(\theta_i,\varphi_i)\right)_{i=1,\ldots,M,(n,k)\in I_N}, \ \boldsymbol{Y}_N^{\varphi} = \left(\frac{\partial}{\partial\varphi}Y_{n,k}(\theta_i,\varphi_i)\right)_{i=1,\ldots,M,(n,k)\in I_N} \in \mathbb{C}^{M\times d_N}.$$

In order to obtain the right ordering of the rows in the definition of $\boldsymbol{\nabla Y}_N$ we need in equation (5.41) to multiply from the left with the permutation matrix $\boldsymbol{P}_{2,M}$, cf. (5.36), and arrive at the first relation in (5.42).

The derivation for the representation of the Hessian matrix $\mathbf{H}\boldsymbol{Y}_N$ in equation (5.42) follows similarly from repeated application of (5.45) and the relations

$$\begin{aligned}
\sin(\theta)\frac{\partial}{\partial\theta}\left(\sin(\theta)\frac{\partial}{\partial\theta}Y_{n,k}(\theta,\varphi)\right) &= \sin(\theta)^2\frac{\partial^2}{\partial^2\theta}Y_{n,k}(\theta,\varphi) + \cos(\theta)\sin(\theta)\frac{\partial}{\partial\theta}Y_{n,k}(\theta,\varphi),\\
\frac{\partial}{\partial\varphi}\left(\sin(\theta)\frac{\partial}{\partial\theta}Y_{n,k}(\theta,\varphi)\right) &= \sin(\theta)\frac{\partial}{\partial\theta}\frac{\partial}{\partial\varphi}Y_{n,k}(\theta,\varphi), \qquad (\theta,\varphi)\in[0,\pi]\times[0,2\pi),
\end{aligned}$$

where we additionally need to permute the columns by multiplication from the right with the permutation matrix $\boldsymbol{P}_{d_N,2}$, cf. (5.36). ∎

Nonequispaced fast Fourier Transforms on the Sphere $\mathbb{S}^2$

The first algorithms for the efficient computation of matrix-vector multiplications with a Fourier matrix $\boldsymbol{Y}_N$ on the sphere $\mathbb{S}^2$ were presented in [34, 111, 64] for special grids of points. Later, several approximate algorithms for such multiplications have been proposed in [91, 127], and

more recently for the computations at arbitrary points in [80, 73]. In this thesis we make use of the algorithms presented in [80, 73], which are implemented in the NFFT-library [72]. The idea of these algorithms is to factorize[7] the nonequispaced Fourier matrix $\boldsymbol{Y}_N$ on the sphere $\mathbb{S}^2$, cf. (5.40), into a product of sparse matrices and a nonequispaced Fourier matrix on the torus $\mathbb{T}^2$, cf. (5.33), and performing an NFFT.

Theorem 5.20. *For given points $\boldsymbol{p}_i := h(\theta_i, \varphi_i) \in \mathbb{S}^2 \setminus \{\pm(0,0,1)^\top\}$, $(\theta_i, \varphi_i) \in (0,\pi) \times [0, 2\pi)$, $i = 1, \dots, M$, cf. (3.71), and polynomial degree $N \in \mathbb{N}_0$ the numerical computation of the matrix-vector multiplications with the nonequispaced Fourier matrix $\boldsymbol{Y}_N$ and $\overline{\boldsymbol{Y}}_N^\top$, cf. (5.40), can be performed by an NFFT with fixed accuracy, cf. Remark 5.16, in*

$$\mathcal{O}\big(N^2 \log^2(N) + M\big)$$

arithmetic operations.

Proof. We refer to [80, 73]. ∎

Corollary 5.21. *For given points $\boldsymbol{p}_i := h(\theta_i, \varphi_i) \in \mathbb{S}^2 \setminus \{\pm(0,0,1)^\top\}$, $(\theta_i, \varphi_i) \in (0,\pi) \times [0, 2\pi)$, $i = 1, \dots, M$, cf. (3.71), and polynomial degree $N \in \mathbb{N}_0$ the numerical computation of the matrix-vector multiplications with the matrices $\mathbf{D}\boldsymbol{Y}_N \in \mathbb{C}^{dM \times d_N}$, $\mathbf{H}\boldsymbol{Y}_N \in \mathbb{C}^{dM \times d_N d}$, cf. (5.41), can be performed by at most four NFFTs with fixed accuracy, cf. Remark 5.16, in*

$$\mathcal{O}\big(N^2 \log^2(N) + M\big)$$

arithmetic operations.

Proof. The assertions follow from Theorem 5.19 and Theorem 5.20. ∎

Corollary 5.22. *On the sphere $\mathbb{S}^2$ let a polynomial kernel, cf. (5.39),*

$$K_N(\boldsymbol{x}, \boldsymbol{y}) := \sum_{n=0}^{N} \sum_{k=-n}^{n} \lambda_n Y_{n,k}(\boldsymbol{x}) \overline{Y}_{n,k}(\boldsymbol{y}), \qquad \boldsymbol{x}, \boldsymbol{y} \in \mathbb{S}^d, \qquad \lambda_n \geq 0, \quad n = 0, \dots, N,$$

and coefficients $\hat{\nu}_{n,k} \in \mathbb{C}$, $n = 0, \dots, N$, $k = -n, \dots, n$, be given. Then, for fixed points $\boldsymbol{P} := (\boldsymbol{p}_1, \dots, \boldsymbol{p}_M) \in (\mathbb{S}^2 \setminus \{\pm(0,0,1)^\top\})^M$, and weights $\boldsymbol{w} := (w_1, \dots, w_M) \in \mathbb{R}^M$, the numerical computation of the function, cf. (5.21),

$$\hat{E}_{K_N}(\boldsymbol{P}, \boldsymbol{w}) := \sum_{n=0}^{N} \sum_{k=-n}^{n} \lambda_n \Big| \hat{\nu}_{n,k} - \sum_{i=1}^{M} w_i \overline{Y}_{n,k}(\boldsymbol{p}_i) \Big|^2$$

its gradient $\nabla_{\mathcal{M}} \hat{E}_{K_N}(\boldsymbol{P}, \boldsymbol{w})$, and the matrix-vector multiplications with the matrix representation of the Hessian $\mathrm{H}_{\mathcal{M}} \hat{E}_{K_N}(\boldsymbol{P}, \boldsymbol{w})$ on the product manifold $\mathcal{M} := (\mathbb{S}^2)^M \times \mathbb{R}^M$ can be performed by NFFTs with fixed accuracy, cf. Remark 5.16, in

$$\mathcal{O}\big(N^2 \log^2(N) + M\big)$$

arithmetic operations.

Proof. Using Corollary 5.21 the assertions follow from the representations given in Theorem 5.11 together with Remark 5.12. ∎

[7] The factorization can be realized by fast polynomial transforms, cf. [109, 108].

5.2.3 The Rotation Group SO(3)

We recall for the rotation group SO(3) the parameterization in Euler angles $(\varphi_1, \theta, \varphi_2) \in [0, 2\pi) \times [0, \pi] \times [0, 2\pi)$, cf. (3.94), and that we use in this parameterization the (normalized) canonical measure $\mu_{\mathrm{SO}(3)}$, which is given by the density $\mathrm{d}\mu_{\mathrm{SO}(3)}(\boldsymbol{R}) = \sin(\theta)\mathrm{d}\varphi_1\mathrm{d}\theta\mathrm{d}\varphi_2$, $\boldsymbol{R} = h(\varphi_1, \theta, \varphi_2)$, cf. Remark 3.17. By abuse of notation we will omit in the following the subscript h in the local coordinate representation of functions $f : \mathrm{SO}(3) \to \mathbb{C}$, cf. (3.33),

$$f(\varphi_1, \theta, \varphi_2) := f_h(\varphi_1, \theta, \varphi_2) = f(\boldsymbol{x}), \quad \boldsymbol{x} = h(\varphi_1, \theta, \varphi_2),\ (\varphi_1, \theta, \varphi_2) \in [0, 2\pi) \times [0, \pi] \times [0, 2\pi).$$

With this convention the Wigner D-functions, cf. (4.51), read as, cf. [135, Eq. (1), p. 76],

$$D^n_{k,k'}(\varphi_1, \theta, \varphi_2) = \mathrm{e}^{-\mathrm{i}k\varphi_1} d^n_{k,k'}(\cos(\theta))\mathrm{e}^{-\mathrm{i}k'\varphi_2}, \qquad (\varphi_1, \theta, \varphi_2) \in [0, 2\pi) \times [0, \pi] \times [0, 2\pi), \tag{5.46}$$

where the *Wigner d-functions* $d^n_{k,k'}$, of degree $n \in \mathbb{N}_0$ and order $k, k' = -n, \ldots, n$ are defined for $t \in [-1, 1]$ by, cf. [135, Eq. (7), p. 77],

$$d^n_{k,k'}(t) := (-1)^{n-k'} \frac{1}{2^n} \sqrt{\frac{(n+k)!}{(n-k)!(n+k')!(n-k')!}} \frac{(1-t)^{k'-k}}{(1+t)^{k'+k}} \frac{\mathrm{d}^{n-k}}{\mathrm{d}t^{n-k}} (1-t)^{n-k'}(1+t)^{n+k'}. \tag{5.47}$$

We note further the relation to the spherical harmonics $Y_{n,k}$, $n \in \mathbb{N}$, $k = -n, \ldots, n$, defined by (5.39), cf. [135, Eq. (1), p. 113],

$$D^n_{k,0}(\varphi_1, \theta, \varphi_2) = (-1)\sqrt{\frac{4\pi}{2n+1}} Y_{n,-k}(\theta, \varphi_1), \qquad (\varphi_1, \theta, \varphi_2) \in [0, 2\pi) \times [0, \pi] \times [0, 2\pi).$$

For convenience we introduce the index set $I_N := \{(n, k, k') \ : \ n = 0, \ldots, N,\ k, k' = -n, \ldots, n\}$ and recall that $\Pi^N(\mathrm{SO}(3)) := \mathrm{span}\{D^n_{k,k'} \ : \ (n, k, k') \in I_N\}$ is the space of polynomials with degree at most $N \in \mathbb{N}_0$, cf. (4.53). The dimension of $\Pi^N(\mathrm{SO}(3))$ is given by $d_N := \frac{1}{6}(2N + 1)(2N + 2)(2N + 3)$. Thus, for given points $\boldsymbol{p}_i := h(\varphi_{1i}, \theta_i, \varphi_{2i}) \in \mathrm{SO}(3)$, $(\varphi_{1i}, \theta_i, \varphi_{2i}) \in [0, 2\pi) \times [0, \pi] \times [0, 2\pi)$, $i = 1, \ldots, M$, the nonequispaced Fourier matrix, cf. (5.22), reads as

$$\boldsymbol{Y}_N := \big(D^n_{k,k'}(\varphi_{1i}, \theta_i, \varphi_{2i})\big)_{i=1,\ldots,M,(n,k,k')\in I_N} \in \mathbb{C}^{M \times d_N}, \tag{5.48}$$

where the column indices run in a fixed prescribed order over the index set, e.g., in the lexicographic ordering $(n, k, k') = (0, 0, 0), (1, -1, -1), (1, -1, 0), \ldots, (N, N, N-1), (N, N, N)$. Similarly, the matrices $\boldsymbol{\nabla Y}_N$, $\mathbf{H}\boldsymbol{Y}_N$, cf. (5.23), (5.24), read in local coordinates as

$$\begin{aligned} \boldsymbol{\nabla Y}_N &= \big(\nabla D^n_{k,k'}(\varphi_{1i}, \theta_i, \varphi_{2i})\big)_{i=1,\ldots,M,(n,k,k')\in I_N} \in \mathbb{C}^{3M \times d_N}, \\ \mathbf{H}\boldsymbol{Y}_N &= \big(\mathbf{H}D^n_{k,k'}(\varphi_{1i}, \theta_i, \varphi_{2i})\big)_{i=1,\ldots,M,(n,k,k')\in I_N} \in \mathbb{C}^{3M \times 3d_N}, \end{aligned} \tag{5.49}$$

where for $(n, k, k') \in I_N$, $(\varphi_1, \theta, \varphi_2) \in [0, 2\pi) \times [0, \pi] \times [0, 2\pi)$ the usual gradients and Hessian matrices are given by

$$\nabla D^n_{k,k'}(\varphi_1, \theta, \varphi_2) = \begin{pmatrix} \frac{\partial}{\partial\varphi_1} D^n_{k,k'}(\varphi_1, \theta, \varphi_2) \\ \frac{\partial}{\partial\theta} D^n_{k,k'}(\varphi_1, \theta, \varphi_2) \\ \frac{\partial}{\partial\varphi_2} D^n_{k,k'}(\varphi_1, \theta, \varphi_2) \end{pmatrix},$$

$$\mathbf{H}D^n_{k,k'}(\varphi_1, \theta, \varphi_2) = \begin{pmatrix} \frac{\partial^2}{\partial\varphi_1^2} D^n_{k,k'}(\varphi_1, \theta, \varphi_2) & \frac{\partial^2}{\partial\varphi_1\partial\theta} D^n_{k,k'}(\varphi_1, \theta, \varphi_2) & \frac{\partial^2}{\partial\varphi_1\partial\varphi_2} D^n_{k,k'}(\varphi_1, \theta, \varphi_2) \\ \frac{\partial^2}{\partial\theta\partial\varphi_1} D^n_{k,k'}(\varphi_1, \theta, \varphi_2) & \frac{\partial^2}{\partial\theta^2} D^n_{k,k'}(\varphi_1, \theta, \varphi_2) & \frac{\partial^2}{\partial\theta\partial\varphi_2} D^n_{k,k'}(\varphi_1, \theta, \varphi_2) \\ \frac{\partial^2}{\partial\varphi_2\partial\varphi_1} D^n_{k,k'}(\varphi_1, \theta, \varphi_2) & \frac{\partial^2}{\partial\varphi_2\partial\theta} D^n_{k,k'}(\varphi_1, \theta, \varphi_2) & \frac{\partial^2}{\partial\varphi_2^2} D^n_{k,k'}(\varphi_1, \theta, \varphi_2). \end{pmatrix},$$

Theorem 5.23. *For given points* $\boldsymbol{p}_i := h(\varphi_{1i}, \theta_i, \varphi_{2i}) \in \mathrm{SO}(3)\backslash\{(R_{i,j})_{i,j=1}^3 \in \mathbb{R}^{3\times 3} : R_{3,3} = \pm 1\}$, $(\varphi_{1i}, \theta_i, \varphi_{2i}) \in [0, 2\pi)\times(0,\pi)\times[0,2\pi)$, $i = 1, \ldots, M$, *cf.* (3.94), *and polynomial degree* $N \in \mathbb{N}_0$ *the matrices* $\mathbf{D}\boldsymbol{Y}_N, \mathbf{H}\boldsymbol{Y}_N$ *defined by* (5.49) *can be expressed via the nonequispaced Fourier matrix* $\boldsymbol{Y}_N$, *cf.* (5.48), *by*

$$\boldsymbol{\nabla}\boldsymbol{Y}_N = \boldsymbol{P}_{3,M}\begin{pmatrix}\boldsymbol{Y}_N^{\varphi_1}\\ \boldsymbol{Y}_N^{\theta}\\ \boldsymbol{Y}_N^{\varphi_2}\end{pmatrix} \in \mathbb{C}^{3M\times d_N}, \mathbf{H}\boldsymbol{Y}_N = \boldsymbol{P}_{3,M}\begin{pmatrix}\boldsymbol{Y}_N^{\varphi_1,\varphi_1} & \boldsymbol{Y}_N^{\varphi_1,\theta} & \boldsymbol{Y}_N^{\varphi_1,\varphi_2}\\ \boldsymbol{Y}_N^{\theta,\varphi_1} & \boldsymbol{Y}_N^{\theta,\theta} & \boldsymbol{Y}_N^{\theta,\varphi_2}\\ \boldsymbol{Y}_N^{\varphi_2,\varphi_1} & \boldsymbol{Y}_N^{\varphi_2,\theta} & \boldsymbol{Y}_N^{\varphi_2,\varphi_2}\end{pmatrix}\boldsymbol{P}_{d_N,3} \in \mathbb{C}^{3M\times 3d_N}$$

where $\boldsymbol{P}_{3,M}, \boldsymbol{P}_{d_N,3}$ *are permutation matrices defined by* (5.36) *and the matrices*

$$\begin{aligned}
\boldsymbol{Y}_N^{\varphi_i} &:= \boldsymbol{Y}_N\boldsymbol{D}_N^{\varphi_i} \in \mathbb{C}^{M\times d_N},\\
\boldsymbol{Y}_N^{\theta} &:= \boldsymbol{S}^{-1}\boldsymbol{Y}_{N+1}\boldsymbol{D}_N^{\theta} \in \mathbb{C}^{M\times d_N},\\
\boldsymbol{Y}_N^{\theta,\theta} &:= \boldsymbol{S}^{-2}(\boldsymbol{Y}_{N+2}\boldsymbol{D}_{N+1}^{\theta}\boldsymbol{D}_N^{\theta} - \boldsymbol{C}\boldsymbol{Y}_{N+1}\boldsymbol{D}_N^{\theta}) \in \mathbb{C}^{M\times d_N},\\
\boldsymbol{Y}_N^{\theta,\varphi_i} &:= \boldsymbol{Y}_N^{\varphi_i,\theta} := \boldsymbol{S}^{-1}\boldsymbol{Y}_{N+1}\boldsymbol{D}_N^{\theta}\boldsymbol{D}_N^{\varphi_i} \in \mathbb{C}^{M\times d_N},\\
\boldsymbol{Y}_N^{\varphi_i,\varphi_j} &:= \boldsymbol{Y}_N\boldsymbol{D}_N^{\varphi_i}\boldsymbol{D}_N^{\varphi_j} \in \mathbb{C}^{M\times d_N}, \qquad i,j = 1,2,
\end{aligned}$$

are given by the diagonal matrices $\boldsymbol{S}$, $\boldsymbol{C}$, $\boldsymbol{D}_N^{\varphi_1}$, $\boldsymbol{D}_N^{\varphi_2}$, *and the tridiagonal-like matrix* $\boldsymbol{D}_N^{\theta}$ *defined by*

$$\begin{aligned}
\boldsymbol{S} &:= \mathrm{diag}(\sin(\theta_1), \ldots, \sin(\theta_M)) = (\delta_{i,i'}\sin(\theta_i))_{i,i'=0}^{M} \in \mathbb{R}^{M\times M},\\
\boldsymbol{C} &:= \mathrm{diag}(\cos(\theta_1), \ldots, \cos(\theta_M)) = (\delta_{i,i'}\cos(\theta_i))_{i,i'=0}^{M} \in \mathbb{R}^{M\times M},\\
\boldsymbol{D}_N^{\varphi_1} &:= \big(-\delta_{\tilde{k},k}\delta_{\tilde{k}',k'}\delta_{\tilde{n},n}\mathrm{i}k\big)_{(\tilde{n},\tilde{k},\tilde{k}')\in I_N,(n,k,k')\in I_N} \in \mathbb{C}^{d_N\times d_N},\\
\boldsymbol{D}_N^{\theta} &:= \big(\delta_{\tilde{k},k}\delta_{\tilde{k}',k'}(\delta_{\tilde{n},n+1}a_{n,k,k'} - \delta_{\tilde{n},n}b_{n,k,k'} - \delta_{\tilde{n},n-1}c_{n,k,k'})\big)_{(\tilde{n},\tilde{k},\tilde{k}')\in I_{N+1},(n,k,k')\in I_N} \in \mathbb{R}^{d_{N+1}\times d_N},\\
\boldsymbol{D}_N^{\varphi_2} &:= \big(-\delta_{\tilde{k},k}\delta_{\tilde{k}',k'}\delta_{\tilde{n},n}\mathrm{i}k'\big)_{(\tilde{n},\tilde{k},\tilde{k}')\in I_N,(n,k,k')\in I_N} \in \mathbb{C}^{d_N\times d_N},
\end{aligned}$$

with

$$\begin{aligned}
a_{n,k,k'} &:= \frac{n}{(n+1)(2n+1)}\sqrt{\big((n+1)^2-k^2\big)\big((n+1)^2-k'^2\big)}, \qquad (n,k,k') \in I_N,\\
b_{n,k,k'} &:= \frac{kk'}{n(n+1)}, \quad c_{n,k,k'} := \frac{n+1}{n(2n+1)}\sqrt{(n^2-k^2)(n^2-k'^2)}, \qquad (n,k,k') \in I_N\setminus(0,0,0),
\end{aligned}$$

and $b_{0,0,0} = c_{0,0,0} = 0$, *where* δ *denotes the Kronecker delta, cf.* (2.15).

Proof. The assertions follow as in the proof of Theorem 5.19 by using the recurrence relation for Wigner D-functions $D_{k,k'}^n$, $(n,k,k') \in I_N$, cf. [135, Eq. (1), (8) and (9), p. 94],

$$\begin{aligned}
\frac{\partial}{\partial\varphi_1}D_{k,k'}^n(\varphi_1,\theta,\varphi_2) &= -\mathrm{i}kD_{k,k'}^n(\varphi_1,\theta,\varphi_2),\\
\sin(\theta)\frac{\partial}{\partial\theta}D_{k,k'}^n(\varphi_1,\theta,\varphi_2) &= a_{n,k,k'}D_{k,k'}^{n+1}(\varphi_1,\theta,\varphi_2) - b_{n,k,k'}D_{k,k'}^n(\varphi_1,\theta,\varphi_2) - c_{n,k,k'}D_{k,k'}^{n-1}(\varphi_1,\theta,\varphi_2),\\
\frac{\partial}{\partial\varphi_1}D_{k,k'}^n(\varphi_1,\theta,\varphi_2) &= -\mathrm{i}k'D_{k,k'}^n(\varphi_1,\theta,\varphi_2), \qquad (\varphi_1,\theta,\varphi_2) \in [0,2\pi)\times[0,\pi]\times[0,2\pi). \quad \blacksquare
\end{aligned}$$

Nonequispaced fast Fourier transforms on the Rotation Group $\mathrm{SO}(3)$

Evaluation schemes for Wigner D-functions have been investigated and frequently used in quantum- and geophysics. First efficient algorithms for the matrix-vector multiplication with a Fourier

matrix $\boldsymbol{Y}_N$ on the rotation sphere SO(3) have been proposed in [111, 77] for special grids of points. Similarly to the sphere $\mathbb{S}^2$, more efficient but approximate evaluation algorithms for such matrix-vector multiplications have been derived for arbitrary points in [106, 74]. In this thesis we make use of the algorithms presented in [106], which are implemented in the NFFT-library [72]. The idea of these algorithms, as for the sphere $\mathbb{S}^2$, is to factorize the nonequispaced Fourier matrix $\boldsymbol{Y}_N$ on the rotation group SO(3), cf. (5.48), into a product of sparse matrices and a nonequispaced Fourier matrix on the torus $\mathbb{T}^3$, cf. (5.33), and performing an NFFT.

Theorem 5.24. *For given points $\boldsymbol{p}_i := h(\varphi_{1i}, \theta_i, \varphi_{2i}) \in \mathrm{SO}(3) \setminus \{(R_{i,j})_{i,j=1}^3 \in \mathbb{R}^{3\times 3} \ : \ R_{3,3} = \pm 1\}$, $(\varphi_{1i}, \theta_i, \varphi_{2i}) \in [0, 2\pi) \times (0, \pi) \times [0, 2\pi)$, $i = 1, \ldots, M$, cf. (3.94), and polynomial degree $N \in \mathbb{N}_0$ the numerical computation of the matrix-vector multiplications with the nonequispaced Fourier matrix $\boldsymbol{Y}_N$ and $\overline{\boldsymbol{Y}}_N$, cf. (5.48), can be performed by an NFFT with fixed accuracy, cf. Remark 5.16, in*

$$\mathcal{O}\big(N^3 \log^2(N) + M\big)$$

arithmetic operations.

Proof. We refer to [106]. ∎

Corollary 5.25. *For given points $\boldsymbol{p}_i := h(\varphi_{1i}, \theta_i, \varphi_{2i}) \in \mathrm{SO}(3) \setminus \{(R_{i,j})_{i,j=1}^3 \in \mathbb{R}^{3\times 3} \ : \ R_{3,3} = \pm 1\}$, $(\varphi_{1i}, \theta_i, \varphi_{2i}) \in [0, 2\pi) \times (0, \pi) \times [0, 2\pi)$, $i = 1, \ldots, M$, cf. (3.94), and polynomial degree $N \in \mathbb{N}_0$ the numerical computation of the matrix-vector multiplications with the matrices $\mathbf{D}\boldsymbol{Y}_N \in \mathbb{C}^{dM\times d_N}$, $\mathbf{H}\boldsymbol{Y}_N \in \mathbb{C}^{dM\times d_N d}$, cf. (5.49), can be performed by at most nine NFFTs with fixed accuracy, cf. Remark 5.16, in*

$$\mathcal{O}\big(N^3 \log^2(N) + M\big)$$

arithmetic operations.

Proof. The assertions follow from Theorem 5.23 and Theorem 5.24. ∎

Corollary 5.26. *On the rotation group* SO(3) *let a polynomial kernel*

$$K_N(\boldsymbol{R}_1, \boldsymbol{R}_2) = \sum_{n=0}^{N} \sum_{k,k'=-n}^{n} \lambda_n D_{k,k'}^n(\boldsymbol{R}_1) \overline{D}_{k,k'}^n(\boldsymbol{R}_2), \qquad \boldsymbol{R}_1, \boldsymbol{R}_2 \in \mathrm{SO}(3), \qquad \lambda_n \geq 0,$$

and coefficients $\hat{\nu}_{k,k'}^n \in \mathbb{C}$, $n = 0, \ldots, N$, $k, k' = -n, \ldots, n$, be given. Then, for fixed points $\boldsymbol{P} := (\boldsymbol{R}_1, \ldots, \boldsymbol{R}_M) \in \mathrm{SO}(3) \setminus \{(R_{i,j})_{i,j=1}^3 \in \mathbb{R}^{3\times 3} \ : \ R_{3,3} = \pm 1\}$, and weights $\boldsymbol{w} := (w_1, \ldots, w_M) \in \mathbb{R}^M$, the numerical computation of the function, cf. (5.21),

$$\hat{E}_{K_N}(\boldsymbol{P}, \boldsymbol{w}) = \sum_{n=0}^{N} \sum_{k,k'=-n}^{n} \lambda_n \Big| \hat{\nu}_{k,k'}^n - \sum_{i=1}^{M} w_i \overline{D}_{k,k'}^n(\boldsymbol{R}_i) \Big|^2,$$

its gradient $\nabla_{\mathcal{M}} \hat{E}_{K_N}(\boldsymbol{P}, \boldsymbol{w})$, and the matrix-vector multiplications with the matrix representation of the Hessian $\mathrm{H}_{\mathcal{M}} \hat{E}_{K_N}(\boldsymbol{P}, \boldsymbol{w})$ on the product manifold $\mathcal{M} := (\mathrm{SO}(3))^M \times \mathbb{R}^M$ can be performed by NFFTs with fixed accuracy, cf. Remark 5.16, in

$$\mathcal{O}\big(N^3 \log^2(N) + M\big)$$

arithmetic operations.

Proof. Using Corollary 5.25 the assertions follow from the representations given in Theorem 5.11 together with Remark 5.12. ∎

6

Applications and Numerical Examples

In this chapter we show that the general framework for optimizing the worst case quadrature errors in reproducing kernel Hilbert spaces introduced in Chapter 2 allows for many applications in several fields of mathematics. Moreover, we will see that the optimization methods on Riemannian manifolds presented in Chapter 3 lead in conjunction with the efficient evaluation methods proposed in Chapter 5 to an efficient optimization approach for the worst case quadrature errors on the torus $\mathbb{T}^d$, the sphere $\mathbb{S}^d$, and the rotation group $\mathrm{SO}(3)$. In particular, we present several interesting results, with new contributions to classical quadrature problems on the sphere $\mathbb{S}^2$, and the rotation group $\mathrm{SO}(3)$, cf. Section 6.2 and 6.3, which includes the numerical computation of new quadrature rules, and numerical t-designs up to degree $t = 1000$. Further applications are given by the efficient computation of low-discrepancy points on the sphere $\mathbb{S}^d$, cf. Section 6.4, and efficient halftoning, cf. Section 6.5, which is of particular use in computer graphics and image processing.

In Section 6.1 we describe the relation of the worst case quadrature error in reproducing kernel Hilbert spaces to what we call classical quadrature problems. In the classical setting of quadrature rules, one is interested in the computation of quadrature points and weights such that all functions of a given finite dimensional space are integrated exactly. It turns out that we have to solve in general a system of nonlinear equations, for which the worst case quadrature error can be considered as an associated least squares functional. In Theorem 6.1 we show that such classical quadrature functionals do exists. Examples which fit into this setting are the classical Gauß or Chebyshev quadrature rules for polynomials on the interval, or constructions of quadrature rules which integrate polynomials up to certain degree on the sphere $\mathbb{S}^d$, and the rotation group $\mathrm{SO}(3)$.

In Section 6.2 we consider classical quadrature problems for the sphere $\mathbb{S}^d$, where the focus is on the efficient computation of classical quadrature rules on the sphere $\mathbb{S}^2$. Of particular interest are quadrature functionals of minimal size M, such that all polynomials with prescribed degree at most N are integrated exactly. For that reason we make use of the heuristic concept given by the efficiency of a quadrature functional, which has been originally introduced by McLaren [89] for the sphere $\mathbb{S}^2$. As a rule of thumb, quadrature functionals with efficiency about one are particular efficient and can be considered as Gauß-type quadrature rules, cf. Remark 6.3. The construction of such highly efficient quadrature rules has been considered by many authors after the seminal papers of Sobolev [122] and McLaren [89]. For the sphere $\mathbb{S}^2$, the main contributions of algebraic constructions are due to Lebedev et al. [83, 84, 85] and the recent papers of Popov [103, 104, 105], whereas numerical constructions are given by Fliege and Maier [45], Sloan and Womersley [117], and Ahrens and Beylkin [2], to name but a few. All algebraic constructions,

and the numerical construction given in [2], are based on the idea of Sobolev presented in [122], who introduced the concept of quadratures invariant under orthogonal groups, which leads to a substantial reduction of the size of the nonlinear equation systems to be solved. We recapitulate this idea thoroughly in Section 6.2.1, with emphasis on the sphere $\mathbb{S}^2$. For constructions on higher dimensional spheres $\mathbb{S}^d$ we refer to the work of Goethals and Seidel [52] and de la Harpe et al. [63]. In Section 6.2.2 we recapitulate the concept of a spherical t-design introduced by Delsarte et al. [32], which corresponds in our terminology to an equal weights quadrature functional on the sphere $\mathbb{S}^d$. For the sphere $\mathbb{S}^2$, Hardin and Sloane [62] investigated spherical t-designs with degree up to $t = 21$. Further numerical computations up to degree $t = 100$ have been performed by Sloan and Womersley [118], and very recently Chen et al. [22, 21] have verified the existence of spherical t-designs of size $M = (t+1)^2$ by interval arithmetic up to degree $t = 100$. The numerical results in Section 6.2.3 show that we are able to compute numerically spherical t-designs of size $M \approx \frac{1}{2}(t+1)^2$ up to degree $t = 1000$, which has been published for the first time in our paper [57]. Moreover, we present a list of new and highly efficient quadrature functionals (with nonequal weights) up to degree $N = 44$ and a list of new and highly efficient spherical t-designs up to degree $t = 124$, which are invariant under orthogonal groups and apparently optimal with respect to the number of quadrature points M, cf. Table 6.1 and Table 6.2, respectively.

In Section 6.3 we consider classical quadrature problems on the rotation group SO(3), similar to those on the sphere $\mathbb{S}^d$, cf. Section 6.2. That is, we are mostly interested in highly efficient quadrature functionals. Surprisingly, we can construct very efficient quadrature functionals on the rotation group SO(3) by a simple tensor product construction from efficient quadrature functionals on the sphere $\mathbb{S}^2$, cf. Theorem 6.22, which has been originally established in our paper [56]. However, as in the case of the sphere $\mathbb{S}^d$, we can construct more efficient quadrature functionals on the rotation group SO(3) by the use of groups actions. Therefore, we recapitulate in Section 6.3.1 the necessary ideas. Similarly, we recapitulate in Section 6.3.2 the concept of t-designs on the rotation group SO(3), which is by Theorem 6.21 strongly related to spherical t-designs on the sphere $\mathbb{S}^3$. Using this relation with some other results we are able to present in Theorem 6.26 an explicit construction of an apperantly new spherical 15-designs with 336 points on the sphere $\mathbb{S}^3$, which seems to be optimal with respect to the number of points. In Section 6.3.3 we present a list of new and highly efficient quadrature functionals (with nonequal weights) up to degree $N = 14$ and t-designs up to degree $t = 23$, which are invariant under orthogonal groups and might be optimal with respect to the number of quadrature points, cf. Table 6.5 and 6.6.

In Section 6.4 we consider the computation of uniformly distributed points on the sphere $\mathbb{S}^d$. Therefore, we aim to minimize the L^2-discrepancy over halfspaces $D^2_{\mathcal{H}_+}$ introduced in Section 2.4.2, which has been extensively studied, as seen in the monographs of Drmota and Tichy [35] and Matoušek [88]. However, the direct optimization of the L^2-discrepancy over halfspaces $D^2_{\mathcal{H}_+}$ is for large numbers of points M too expansive, so that we propose in Section 6.4.1 and 6.4.2 two optimization approaches which are more efficient. The first approach presented in Section 6.4.1 is restricted to the sphere $\mathbb{S}^2$ and makes use of the nonequispaced fast Fourier transforms described in Section 5.2.2, where we truncate the Fourier expansion of the corresponding discrepancy kernel. The second approach presented in Section 6.4.1 applies for higher dimensional spheres $\mathbb{S}^d$ and makes use of local discrepancy kernels, such that the efficient evaluation algorithm of Section 5.1 can be used. The numerical Examples 6.33 and 6.36 illustrate the suitability of both optimization approaches, where we observe that the computed point distributions follow the well-know asymptotic of optimal point distributions with respect to the L^2-discrepancy over halfspaces $D^2_{\mathcal{H}_+}$, cf. Theorem 6.29.

In Section 6.5 we consider a problem arising in image processing, where one asks for a distribution of black dots which mimics the gray values of a given image. We will refer to such a process as halftoning, see the monograph of Ulichney [132]. Recently, a new halftoning approach has been proposed by Schmaltz et al. [114], where an electrostatic has to be minimized. This

optimization approach has been generalized and analyzed by Teuber et al. [129]. We will recapitulate the relations to L^2-discrepancies and worst case quadrature errors, which enables us to consider halftoning on the torus $\mathbb{T}^2$ and the sphere $\mathbb{S}^2$ in Section 6.5.1 and 6.5.2, respectively. Moreover, we demonstrate the use of the nonequispaced fast Fourier transforms on the torus $\mathbb{T}^2$ and the sphere $\mathbb{S}^2$, cf. Section 5.2.1 and 5.2.2, respectively, by several numerical examples.

6.1 Classical Quadrature Problems

For finite dimensional spaces $H(X) \subset C(X)$, $X \subset \mathbb{R}^n$, the general quadrature problem discussed in Section 2.1 might be considered in a more restricted sense, which follows in some way the classical approach of quadrature rules. More precisely, given an integral functional I_ν, $\nu \in M_{\mathbb{C}}(\mathbb{R}^n)$, cf. (2.4), we are now interested in quadrature functionals $Q(\boldsymbol{P}, \boldsymbol{w})$, cf. (2.5), of size M with quadrature points $\boldsymbol{P} := (\boldsymbol{p}_1, \dots, \boldsymbol{p}_M) \in X^M$ and quadrature weights $\boldsymbol{w} := (w_1, \dots, w_M) \in \mathbb{C}^M$ which satisfy

$$I_\nu f = \int_X f(\boldsymbol{x}) \mathrm{d}\nu(\boldsymbol{x}) = \sum_{i=1}^{M} w_i f(\boldsymbol{p}_i) = Q(\boldsymbol{P}, \boldsymbol{w}) f, \qquad f \in H(X). \tag{6.1}$$

In other words, the integral functional I_ν and the quadrature functional $Q(\boldsymbol{P}, \boldsymbol{w})$ coincide on the function space $H(X)$. In other words, functions of $H(X)$ are integrated exactly by simple function evaluations. We recall that in infinite dimensional spaces equality might not be attained. However, as stated in Theorem 6.1, the classical quadrature condition (6.1) can be always fulfilled in finite dimensional spaces $H(X)$.

Theorem 6.1. *Let a finite dimensional space $H(X) \subset C(X)$, $X \subset \mathbb{R}^n$, of dimension $L \in \mathbb{N}$ and a complex Borel measure $\nu \in M_{\mathbb{C}}(\mathbb{R}^n)$ be given. Then for $M \geq L$ there exist quadrature points $\boldsymbol{P} := (\boldsymbol{p}_1, \dots, \boldsymbol{p}_M) \in X^M$ and quadrature weights $\boldsymbol{w} := (w_1, \dots, w_M) \in \mathbb{C}^M$ such that the classical quadrature condition* (6.1) *is satisfied.*

Proof. We fix a basis of $H(X)$, given by the functions $\psi_l \in H(X)$, $l = 0, \dots, L-1$. Then the quadrature condition (6.1) is equivalent to the following system of equations

$$\sum_{i=1}^{M} w_i \psi_l(\boldsymbol{p}_i) = \tilde{\nu}_l, \qquad \tilde{\nu}_l := \int_X \psi_l(x) \mathrm{d}\nu(x), \quad l = 0, \dots, L-1.$$

We note that for fixed points $\boldsymbol{P}$ this is a linear equation system in the weights $\boldsymbol{w} \in \mathbb{C}^M$. Without loss of generality we consider only the case $M = L$, since we might assign to any additional quadrature point a zero weight. Hence, for proving the theorem it is sufficient to show the existence of quadrature points $\boldsymbol{P}$ for which the quadratic matrix $\boldsymbol{A} := \big(\psi_l(\boldsymbol{p}_i)\big)_{l=0,\dots,L-1,i=1,\dots,L} \in \mathbb{C}^{L \times L}$ is non-singular.

The proof, which follows the ideas for the sphere $\mathbb{S}^d$ given in [94, Theorem 3], is by induction over the quadratic submatrices $\boldsymbol{A}_k := \big(\psi_l(\boldsymbol{p}_i)\big)_{l=0,\dots,k-1,i=1,\dots,k} \in \mathbb{C}^{k \times k}$, $k = 1, \dots, L$, of $\boldsymbol{A}$. The induction base for $k = 1$ is satisfied for any point $\boldsymbol{p}_1$ with $\psi_0(\boldsymbol{p}_1) \neq 0$, which exists by the linear independence of the basis functions ψ_l, $l = 0, \dots, L-1$. By a similar argument, we can carry out the induction step from $k-1$ to $k \leq L$. Therefore, we write the determinant of $\boldsymbol{A}_k$ via Laplace's formula

$$\det(\boldsymbol{A}_k) = \sum_{l=0}^{k-1} a_l \psi_l(\boldsymbol{p}_k), \qquad a_l := (-1)^{l+k-1} \det(\boldsymbol{A}_k^{l,k}), \quad l = 0, \dots, k-1,$$

where the matrices $\boldsymbol{A}_k^{l,k} \in \mathbb{C}^{(k-1)\times(k-1)}$ are determined by deleting the lth row and the kth column of $\boldsymbol{A}_k$, and thus are independent of the point $\boldsymbol{p}_k \in X$. By the induction hypothesis there exist points $\boldsymbol{p}_i$, $i = 1, \dots, k-1$, such that $\det(\boldsymbol{A}_{k-1}) \neq 0$. Hence, with $a_{k-1} = \det(\boldsymbol{A}_{k-1})$ the determinant of $\boldsymbol{A}_k$ can be written as a nonzero linear combination of $k \leq L$ linearly independent functions ψ_l, $l = 0, \dots, k-1$, which cannot vanish identically. In other words, $\boldsymbol{A}_k$ is non-singular for some point $\boldsymbol{p}_k \in X$ and the proof is finished. ■

We note that in general the lower bound L on the number M of quadrature points in Theorem 6.1 is optimal. However, it is remarkable that for certain non-trivial instances this bound can be improved. Indeed, the search for quadrature functionals of minimal size M which satisfy (6.1) turns out to be an interesting and challenging problem, cf. Section 6.2 and Section 6.3.

Example 6.2. We consider the classical quadrature problem for polynomials on the interval $X = [-1, 1]$. That is, given an integrable weight function $w : [-1, 1] \to (0, \infty)$ we ask for quadrature functionals $Q(\boldsymbol{P}, \boldsymbol{w})$ with quadrature points $\boldsymbol{P} := (p_1, \dots, p_M) \in [-1, 1]^M$ and quadrature weights $\boldsymbol{w} := (w_1, \dots, w_M) \in \mathbb{R}^M$ which satisfy for some prescribed degree $N \in \mathbb{N}_0$ the relation

$$\int_{-1}^{1} f(x)w(x)\mathrm{d}x = \sum_{i=1}^{M} w_i f(p_i), \qquad f \in \Pi^N([-1, 1]), \tag{6.2}$$

where $\Pi^N([-1, 1])$ denotes the space of polynomials $f : \mathbb{R} \to \mathbb{C}$ with degree at most N. From the theory of orthogonal polynomials it is well know that there exist quadrature functionals $Q(\boldsymbol{P}, \boldsymbol{w})$ which satisfy for $N = 2M - 1$ the relation (6.2), cf. [50, Sec. 1.4]. Such quadrature functionals are know as *Gauß quadrature rules*. Since the dimension of the space $\Pi^N([-1, 1])$ is $L = N + 1$ we find that Gauß quadrature rules need for even dimension L only $M = L/2$ quadrature points. Hence, in that case, the lower bound in Theorem 6.1 is improved by a factor of two. In fact, Gauß quadrature rules are optimal with respect to the number of quadrature points. □

For the numerical computation of quadrature functionals which satisfy the classical quadrature condition (6.1) for compact $X \subset \mathbb{R}^n$ one can pass to the worst case quadrature error in reproducing kernel Hilbert spaces. For that reason, we recall that any finite dimensional space $H(X) \subset C(X)$ on $X \subset \mathbb{R}^n$, which is spanned by $L \in \mathbb{N}$ real-valued functions, admits a reproducing kernel $K_L : X \times X \to \mathbb{R}$, which may be chosen somehow arbitrary, cf. Remark 2.5. For simplicity, we fix an L^2-product on $H(X)$, induced by a finite Borel measure μ_X, cf. (2.12), and denote by $\psi_l \in H(X)$, $l = 0, \dots, L-1$, a basis of orthonormal real-valued functions. From Remark 2.3 and definition (2.26) we know that any function of the form

$$K_L(\boldsymbol{x}, \boldsymbol{y}) := \sum_{l=0}^{L-1} \lambda_l \psi_l(\boldsymbol{x})\overline{\psi}_l(\boldsymbol{y}), \qquad \boldsymbol{x}, \boldsymbol{y} \in X, \qquad \lambda_l > 0, \quad l = 0, \dots, L-1, \tag{6.3}$$

can be considered as a reproducing kernel of $H(X) = H_{K_L}(X)$ with respect to a certain inner-product. Then by definition of the worst case quadrature error in $H_{K_L}(X)$, cf. (2.32), it is obvious that the classical quadrature condition (6.1) is equivalent to, cf. Theorem 2.7,

$$\mathrm{err}_{K_L}(\nu, \boldsymbol{P}, \boldsymbol{w})^2 = \sum_{l=0}^{L-1} \lambda_l \Big| \int_X \overline{\psi}_l(\boldsymbol{x})\mathrm{d}\overline{\nu}(\boldsymbol{x}) - \sum_{i=1}^{M} \overline{w_i \psi_l(\boldsymbol{p}_i)} \Big|^2 = 0. \tag{6.4}$$

Hence, the computation of quadrature functionals $Q(\boldsymbol{P}, \boldsymbol{w})$ satisfying the classical quadrature condition (6.1) can be performed by minimizing the worst case quadrature in the reproducing kernel Hilbert space $H_{K_L}(X)$ with an arbitrary reproducing kernel K_L of the form (6.3).

For instance, if we consider the polynomial space $\Pi^N([-1,1])$ in Example 6.2 with respect to the inner-product induced by the weight function $w : [-1,1] \to (0,\infty)$, we find that the Christoffel-Darboux kernel associated to the corresponding orthonormal polynomials, cf. (2.31) in Remark 2.5, is a reproducing kernel. However, we note that the interval $[-1,1]$ is not a Riemannian manifold in the sense given by (3.4), such that the optimization methods presented in Section 3.3 cannot be applied without modification for the computation of Gauß quadratures rules. Nevertheless, it is in principle possible to compute Gauß quadrature rules by the minimization of the squared worst case quadrature error, even if there are more appropriate algorithms based on the QR algorithm, cf. [50, Ch. 3].

The minimization of the worst case quadrature error in (6.4) can also be interpreted as a least squares problem associated to the following system of nonlinear equations in the quadrature points $\boldsymbol{P} := (\boldsymbol{p}_1, \dots, \boldsymbol{p}_M) \in X^M$ and the quadrature weights $\boldsymbol{w} := (w_1, \dots, w_M) \in \mathbb{C}^M$ given by[1]

$$\sum_{i=1}^{M} \overline{w_i \psi_l(\boldsymbol{p}_i)} = \hat{\overline{\nu}}_l, \qquad \hat{\overline{\nu}}_l := \int_X \overline{\psi}_l(x) \mathrm{d}\overline{\nu}(x), \quad l = 0, \dots, L-1, \tag{6.5}$$

which is equivalent to the condition (6.1), see the proof of Theorem 6.1. This point of view allows for a rough estimate for the size of a quadrature functional satisfying (6.1), where we simply compare in equation system (6.5) the degrees of freedom, determined by the number M of points, with the number of equations, determined by the dimension of the space $H(X)$.

For instance, in the case of Gauß quadrature rules, cf. Example 6.2, the degree of freedom results from M point coordinates and M weights. Thus, the degree of freedom matches exactly the dimension $2M$ of the space $\Pi_{2M-1}([-1,1])$. This observation explains heuristically that M quadrature points might suffice for the exact integration of all polynomials up to degree $2M-1$ on the interval $[-1,1]$ by a Gauß quadrature rule. For the computation of classical quadrature functionals on the sphere $\mathbb{S}^2$ and the rotation group $\mathrm{SO}(3)$, which are intended to have particular small size M, we will make frequently use of this idea, i.e., we try to match the degrees of freedom with the number of equations in equation systems of the form (6.5).

6.2 Classical Quadrature Problems on the Sphere $\mathbb{S}^d$

For the sphere $X := \mathbb{S}^d$, the classical quadrature condition (6.1) with respect to the normalized canonical measure $\nu := \frac{1}{\omega_d}\mu_{\mathbb{S}^d}$, $\omega_d := \mu_{\mathbb{S}^d}(\mathbb{S}^d)$, and the harmonic spaces $\Pi^N(\mathbb{S}^d)$, $N \in \mathbb{N}_0$, reads as

$$\frac{1}{\omega_d} \int_{\mathbb{S}^d} f(\boldsymbol{x}) \mathrm{d}\mu_{\mathbb{S}^d}(\boldsymbol{x}) = \sum_{i=1}^{M} w_i f(\boldsymbol{p}_i), \qquad f \in \Pi^N(\mathbb{S}^d), \tag{6.6}$$

where $\boldsymbol{p}_i \in \mathbb{S}^d$ and $w_i \in \mathbb{R}$, $i = 1, \dots, M$. Following the classical terminology, we will say that any quadrature functional $Q(\boldsymbol{P}, \boldsymbol{w})$ which satisfies the condition (6.6) has *degree of exactness* N.

For convenience we fix an orthonormal basis of spherical harmonics $Y_{n,k} \in \Pi_n(\mathbb{S}^d)$ of degree $n \in \mathbb{N}_0$ and order $k = 1, \dots, D_{d,n}$, cf. (4.16), with respect to the L^2-product induced by the measure $\mu_{\mathbb{S}^d}$. Then the quadrature functionals $Q(\boldsymbol{P}, \boldsymbol{w})$ which satisfy the condition (6.6) on the sphere $\mathbb{S}^d$, $d \in \mathbb{N}$, are exactly determined by the solutions $\boldsymbol{p}_i \in \mathbb{S}^d$, $w_i \in \mathbb{R}$, $i = 1, \dots, M$, of the system of nonlinear equations, cf. (6.4),

$$\sum_{i=1}^{M} w_i Y_{n,k}(\boldsymbol{p}_i) = \frac{1}{\sqrt{\omega_d}} \delta_{n,0}, \qquad n = 0, \dots, N, \quad k = 1, \dots, D_{d,n}. \tag{6.7}$$

[1] Conversely, a common approach for solving numerically a system of nonlinear equations is to pass to the corresponding nonlinear least squares problem, cf. [96, Ch. 11].

The objective function of the associated nonlinear least squares problem reads as, cf. (5.2),

$$E_N(\boldsymbol{P},\boldsymbol{w}) := \sum_{n=0}^{N}\sum_{k=1}^{D_{d,n}} \Big| \frac{1}{\sqrt{\omega_d}}\delta_{0,n} - \sum_{i=1}^{M} w_i \overline{Y}_{n,k}(\boldsymbol{p}_i)\Big|^2 = \mathrm{err}_{K_N}(\nu,\boldsymbol{P},\boldsymbol{w})^2, \tag{6.8}$$

which is exactly the squared worst case quadrature error between the integral functional I_ν and the quadrature functional $Q(\boldsymbol{P},\boldsymbol{w})$ in the reproducing kernel Hilbert space $\Pi^N(\mathbb{S}^d)$, $N \in \mathbb{N}_0$, equipped with the usual L^2-product induced by the canonical measure $\mu_{\mathbb{S}^d}$, cf. Theorem 2.7. The corresponding reproducing kernel is the Christoffel–Darboux kernel $K_N : \mathbb{S}^d \times \mathbb{S}^d \to \mathbb{R}$, cf. (2.31), and can be written via the addition theorem, cf. (4.20), as

$$K_N(\boldsymbol{x},\boldsymbol{y}) := \sum_{n=0}^{N}\sum_{k=1}^{D_{d,n}} Y_{n,k}(\boldsymbol{x})\overline{Y}_{n,k}(\boldsymbol{y}) = \sum_{n=0}^{N} \frac{D_{d,n}}{\omega_d} P_n^{(d)}(\boldsymbol{x}^\top \boldsymbol{y}), \qquad \boldsymbol{x},\boldsymbol{y} \in \mathbb{S}^d,$$

where $P_n^{(d)} : [-1,1] \to \mathbb{R}$, $n \in \mathbb{N}_0$, are the orthogonal polynomials which satisfy $P(1) = 1$ and the relation (4.21).

Since the kernel K_N is rotational invariant, cf. (4.19), we find that the worst case quadrature error is rotational invariant in the sense

$$\mathrm{err}_{K_N}(\nu,\boldsymbol{P},\boldsymbol{w}) = \mathrm{err}_{K_N}(\nu,\boldsymbol{R}\bullet\boldsymbol{P},\boldsymbol{w}), \qquad \boldsymbol{R}\bullet\boldsymbol{P} := (\boldsymbol{R}\boldsymbol{p}_1,\dots,\boldsymbol{R}\boldsymbol{p}_M), \quad \boldsymbol{R} \in \mathrm{SO}(d+1). \tag{6.9}$$

In words, if a quadrature functional $Q(\boldsymbol{P},\boldsymbol{w})$ satisfies the classical quadrature problem (6.6), then the rotated version with the quadrature points $\boldsymbol{R}\bullet\boldsymbol{P}$ satisfies it as well.

Before we can try to compute quadrature functionals with a prescribed degree of exactness N, by solving the associated equation system (6.7), we need to estimate the required size M. We do so by comparing the degrees of freedom with the number of conditions imposed by the equation system (6.7). At first glance, we have $(d+1)M$ degrees of freedom, dM for the quadrature points $\boldsymbol{p}_i \in \mathbb{S}^d$, since the sphere $\mathbb{S}^d$ is an d-dimensional manifold, cf. Theorem 3.9, and M for the weights w_i, $i = 1,\dots,M$, in order to satisfy the $D_d^N := \sum_{n=0}^{N} D_{d,n}$ equations in (6.7). However, by the above observed rotational invariance of the worst case quadrature error, cf. (6.9), we 'loose' $d(d+1)/2$ degrees of freedom for $M \geq d$, given by the dimension of the rotation group $\mathrm{SO}(d+1)$, cf. Theorem 3.9. These observations motivate the definition of the *efficiency* of a quadrature functional $Q(\boldsymbol{P},\boldsymbol{w})$, $\boldsymbol{P} \in (\mathbb{S}^d)^M$, $\boldsymbol{w} \in \mathbb{R}^M$, of size M and degree of exactness $N \in \mathbb{N}$ on the sphere $\mathbb{S}^d$ given by

$$\mathrm{eff}_{\mathbb{S}^d}(Q(\boldsymbol{P},\boldsymbol{w})) := \frac{\lceil D_d^N + d(d+1)/2 \rceil_{d+1}}{(d+1)M}, \qquad D_d^N := \sum_{n=0}^{N} D_{d,n}, \qquad M \geq d, \tag{6.10}$$

where we define for convenience the function

$$\lceil x \rceil_k := k \left\lceil \frac{x}{k} \right\rceil, \qquad \lceil y \rceil := \min_{l \in \mathbb{Z}} \{ l \geq y \}, \qquad x,y \in \mathbb{R}, \qquad k \in \mathbb{N}, \tag{6.11}$$

which denotes the smallest integer that is greater or equal than x and divisible by k. With definition (6.10), we call, for a fixed degree of exactness N, a quadrature functional more efficient than an other if it has a higher efficiency. In other words, any quadrature functional of smaller size which achieves the same degree of exactness N is called more efficient.

From the above discussion one might expect that for any degree of exactness $N \in \mathbb{N}$ there exist quadrature functionals $Q(\boldsymbol{P},\boldsymbol{w})$ with efficiency $\mathrm{eff}_{\mathbb{S}^d}(Q(\boldsymbol{P},\boldsymbol{w})) = 1$. Surprisingly, it is possible to construct quadrature functionals with efficiency $\mathrm{eff}_{\mathbb{S}^d}(Q(\boldsymbol{P},\boldsymbol{w})) > 1$ by the use of group actions

and the idea of matching the degrees of freedom with the number of conditions imposed by the classical quadrature condition (6.6), cf. Theorem 6.13 for the sphere $\mathbb{S}^2$.

Remark 6.3. We emphasize that the efficiency defined by (6.10) is just a yard stick to estimate the size M of a quadrature functional $Q(\boldsymbol{P}, \boldsymbol{w})$ with prescribed degree of exactness N. Nevertheless, we know from Theorem 6.1 that an efficiency $\operatorname{eff}_{\mathbb{S}^d}(Q(\boldsymbol{P}, \boldsymbol{w})) \geq 1/(d+1)$ can be achieved for any degree $N \in \mathbb{N}_0$, by considering quadrature functionals of size $M = D_d^N$.

In the case of quadrature functionals $Q(\boldsymbol{P}, \boldsymbol{w})$, $\boldsymbol{P} \in (\mathbb{S}^1)^M$, $\boldsymbol{w} \in \mathbb{R}^M$, with degree of exactness $N \in \mathbb{N}_0$ on the circle $\mathbb{S}^1$ the efficiency simplifies to

$$\operatorname{eff}_{\mathbb{S}^1}(Q(\boldsymbol{P}, \boldsymbol{w})) = \frac{(2N+1)+1}{2M} = \frac{N+1}{M}.$$

It is known that the most efficient quadrature functionals with degree of exactness N on $\mathbb{S}^1$ consists of $M = N+1$ evenly spaced quadrature points, in which case we have $\operatorname{eff}_{\mathbb{S}^1}(Q(\boldsymbol{P}, \boldsymbol{w})) = 1$. Hence, the definition of the efficiency by (6.10) might be reasonable, so that such Gauß-type quadrature rules have efficiency at least one.

For quadrature functionals $Q(\boldsymbol{P}, \boldsymbol{w})$, $\boldsymbol{P} \in (\mathbb{S}^2)^M$, $\boldsymbol{w} \in \mathbb{R}^M$, with degree of exactness $N \in \mathbb{N}_0$ on the sphere $\mathbb{S}^2$, which is of particular interest to us, the efficiency reads as[2]

$$\operatorname{eff}_{\mathbb{S}^2}(Q(\boldsymbol{P}, \boldsymbol{w})) = \begin{cases} \frac{(N+1)^2+3}{3M}, & N \equiv 2 \mod 3, \\ \frac{(N+1)^2+5}{3M}, & N \not\equiv 2 \mod 3, \end{cases} \qquad M \geq 2. \tag{6.12}$$

Furthermore, we recall that the Gauß–Legendre quadrature rules on the sphere $\mathbb{S}^2$ with degree of exactness N are constructed by a tensor product of Gauß quadrature rules on the interval $[-1, 1]$ with respect to the Legendre polynomials, cf. Example 6.2, and the above mentioned Gauß-type quadrature rule on the circle $\mathbb{S}^1$. Hence, the corresponding quadrature functionals have size $M \approx (N+1)^2/2$ which leads to an asymptotic efficiency of $2/3$ for $N \to \infty$. That is Gauß–Legendre quadrature rules are not as efficient as a general quadrature functional might be, cf. Table 6.1. We note further that such tensor product rules tend to cluster at the poles, due to the singularities of the parameterization in spherical coordinates. However, the computation of such tensor product rules is much easier. □

For the numerical computation of quadrature points $\boldsymbol{P} := (\boldsymbol{p}_1, \dots, \boldsymbol{p}_M) \in (\mathbb{S}^d)^M$ and quadrature weights $\boldsymbol{w} := (w_1, \dots, w_M) \in \mathbb{R}^M$ satisfying the classical quadrature condition (6.6), it is practical to minimize the squared worst quadrature error $\operatorname{err}_{K_N}(\boldsymbol{\nu}, \boldsymbol{P}, \boldsymbol{w})^2$ given by (6.8), over the product manifold $\mathcal{M} = (\mathbb{S}^d)^M \times \mathbb{R}^M$. For that reason we can apply the optimization procedures on manifolds presented in Section 3.3. In particular for the sphere $\mathbb{S}^2$, the nonlinear conjugate gradient method, cf. Algorithm 3.3 and Theorem 3.27, leads in conjunction with the nonequispaced fast Fourier transforms on the sphere $\mathbb{S}^2$, cf. Corollary 5.22, to a very efficient optimization approach for the determination of classical quadrature functionals with high degree of exactness. In spite of the following Remark 6.4, the numerical results presented in Section 6.2.3 will illustrate the use of these algorithms.

Remark 6.4. The determination of classical quadrature functionals $Q(\boldsymbol{P}, \boldsymbol{w})$ on the sphere $\mathbb{S}^d$ for a prescribed degree of exactness N, cf. (6.6), of minimal size M or with a high efficiency $\operatorname{eff}_{\mathbb{S}^d}(Q(\boldsymbol{P}, \boldsymbol{w})) \approx 1$, cf. (6.10), turns out to be a challenging task, in particular for high degrees of exactness N, or high dimensions d. The main problem is that we do not know in advance if the equation system (6.7) possess a solution with $M < D_d^N$ quadrature points, and in case

[2] This definition differs slightly from that defined in [89] given by the ratio $(N+1)^2/(3M)$, since we incorporate the rotational invariance of the quadrature error and the divisibility of N by 3.

the determination of the minimal number of quadrature points. Moreover, from a computational point of view the complexity of the equation system (6.7) is $\mathcal{O}(N^d)$, which shows the rapid increase in N and d, such that efficient solvers are necessary. Furthermore, since we aim to apply the optimization algorithms presented in Section 3.3 we are confronted with the problem that the worst case quadrature error (6.8) has, even for moderate degrees of exactness N, many local minimizers, which are not necessarily global minimizers. We also remind that the use of numerical algorithms based on floating point arithmetic makes it practically impossible to compute the exact value of the worst case quadrature error, so that the presented numerical examples in Section 6.2.3 do at most indicate the existence of classical quadrature functionals $Q(\boldsymbol{P}, \boldsymbol{w})$ of size M which satisfy the quadrature condition (6.6) for degree of exactness N. □

In the following Sections 6.2.1 and 6.2.2 we restrict our attention to particular interesting quadrature functionals. In Section 6.2.1 we consider quadrature functionals which are invariant under the actions of finite orthogonal groups. The restriction to such invariant quadrature functionals reduces significantly the number of local minimizers which are not global minimizers, and thus increases the likelihood of finding a global minimizers by the proposed optimization methods. We note that the number of unknowns is approximately reduced by the size of the group. Moreover, invariant quadrature functionals seem to be particular efficient candidates, cf. Theorem 6.13 and Remark 6.14. In Section 6.2.2 we consider spherical-t designs, which correspond in our notation to equal weights quadrature functionals. We note that for such quadrature functionals the number of unknowns is reduced by a factor of 2/3, and that the additional uniformity of the quadrature weights seem to make the optimization easier. Especially, in conjunction with the concept of invariant quadrature functionals we find particular efficient candidates of equal weights quadrature functionals, cf. Theorem 6.16 and Remark 6.17. For the numerical evidence of the results presented in Sections 6.2.1 and 6.2.2 we refer to the Tables 6.1 and 6.2 in Section 6.2.3. Moreover, we will see that our numerical optimization approach is capable to construct numerically quadrature functionals with degree of exactness up to $N = 1000$.

6.2.1 Quadratures Invariant under Finite Orthogonal Groups

Sobolev introduced in [122] the idea to make use of orthogonal groups acting on the sphere $\mathbb{S}^2$, in order to reduce the size of the equation system (6.7). This approach has been successfully adopted by several authors, who constructed quadrature functionals on the sphere $\mathbb{S}^2$ of high efficiency and degree of exactness, e.g., up to $N = 131$ algebraically, cf. [89, 83, 84, 105], and up to $N = 210$ numerically, cf. [2]. In particular, for higher dimensional spheres $\mathbb{S}^d$ the use of group actions turns out to be an important tool, cf. [52, 63], since the dimensions of the harmonic spaces increase exponentially in d. For later reference in Section 6.3.1, we introduce the general notion of an invariant quadrature functional and recapitulate the fundamental Theorems 6.5 and 6.6 of this section, which are attributed to Sobolev [122] and Molien [92], respectively. Afterward, we restrict our attention to the sphere $\mathbb{S}^2$, where we introduce the rotational symmetry groups of the platonic solids, for which we present in Theorem 6.11 explicit formulas corresponding to Theorem 6.6. Using this result we arrive at Theorem 6.13, which shows that it might be possible to construct quadrature functionals with efficiency greater than one, as already pointed out by McLaren in [89]. The numerical results in Section 6.2.3 confirm these results in the most cases, cf. Remark 6.4.

We recall that a set of matrices $\mathcal{G} \subset \mathbb{R}^{n \times n}$ is called a *group* if for any two elements $\boldsymbol{G}, \boldsymbol{H} \in \mathcal{G}$ it holds $\boldsymbol{G}^{-1}, \boldsymbol{GH} \in \mathcal{G}$. A quadrature functional $Q(\boldsymbol{P}, \boldsymbol{w})$, $\boldsymbol{P} := (\boldsymbol{p}_1, \dots, \boldsymbol{p}_M) \in (\mathbb{S}^d)^M$, $\boldsymbol{w} := (w_1, \dots, w_M) \in \mathbb{R}^M$, on the sphere $\mathbb{S}^d$ is called *invariant under the group* $\mathcal{G} \subset \mathrm{O}(d+1)$ if it satisfies, cf. (6.9),

$$Q(\boldsymbol{P}, \boldsymbol{w}) f = Q(\boldsymbol{G}^{-1} \bullet \boldsymbol{P}, \boldsymbol{w}) f = Q(\boldsymbol{P}, \boldsymbol{w}) f(\boldsymbol{G}^{-1} \cdot), \qquad f \in C(\mathbb{S}^d), \quad \boldsymbol{G} \in \mathcal{G}. \tag{6.13}$$

Similarly, a function $f : \mathbb{S}^d \to \mathbb{C}$ is called invariant under $\mathcal{G}$ if $f(\boldsymbol{x}) = f(\boldsymbol{G}^{-1}\boldsymbol{x})$, $\boldsymbol{x} \in \mathbb{S}^d$, $\boldsymbol{G} \in \mathcal{G}$. We denote the invariant subspaces of the harmonic spaces $\Pi_n(\mathbb{S}^d)$, $\Pi^N(\mathbb{S}^d)$, $n, N \in \mathbb{N}_0$, cf. (4.15), by

$$\begin{aligned} \Pi_{n,\mathcal{G}}(\mathbb{S}^d) &:= \{f \in \Pi_n(\mathbb{S}^d) \ : \ f = f(\boldsymbol{G}^{-1}\cdot),\ \boldsymbol{G} \in \mathcal{G}\}, \\ \Pi^N_{\mathcal{G}}(\mathbb{S}^d) &:= \{f \in \Pi^N(\mathbb{S}^d) \ : \ f = f(\boldsymbol{G}^{-1}\cdot),\ \boldsymbol{G} \in \mathcal{G}\}, \end{aligned} \tag{6.14}$$

which consist of the spherical harmonics invariant under $\mathcal{G}$ of degree exactly n and at most N, respectively.

Using the property

$$\mathcal{G} = \mathcal{G}\boldsymbol{H} := \{\boldsymbol{G}\boldsymbol{H} \ : \ \boldsymbol{G} \in \mathcal{G}\} = \{\boldsymbol{H}\boldsymbol{G} \ : \ \boldsymbol{G} \in \mathcal{G}\} =: \boldsymbol{H}\mathcal{G}, \qquad \boldsymbol{H} \in \mathcal{G},$$

we find that invariant quadrature functionals and functions may be simply constructed by averaging. More precisely, for any arbitrary quadrature functional $Q(\boldsymbol{P}, \boldsymbol{w})$ and function $f \in C(\mathbb{S}^d)$ the average over a finite group $\mathcal{G}$, i.e., $|\mathcal{G}| < \infty$, defined by

$$Q_{\mathcal{G}}(\boldsymbol{P}, \boldsymbol{w}) := \frac{1}{|\mathcal{G}|} \sum_{\boldsymbol{G} \in \mathcal{G}} Q(\boldsymbol{G} \bullet \boldsymbol{P}, \boldsymbol{w}), \qquad \boldsymbol{P} \in (\mathbb{S}^d)^M, \quad \boldsymbol{w} \in \mathbb{R}^M, \tag{6.15}$$

and

$$f_{\mathcal{G}}(\boldsymbol{x}) = \frac{1}{|\mathcal{G}|} \sum_{\boldsymbol{G} \in \mathcal{G}} f(\boldsymbol{G}\boldsymbol{x}), \qquad \boldsymbol{x} \in \mathbb{S}^d, \tag{6.16}$$

is invariant under $\mathcal{G}$, respectively.

We recall that for a fixed point $\boldsymbol{x} \in \mathbb{S}^d$ the *orbit of* $\boldsymbol{x}$ generated by $\mathcal{G}$ and the *stabilizer of* $\boldsymbol{x}$ in $\mathcal{G}$ is defined by

$$\mathcal{G}\boldsymbol{x} := \{\boldsymbol{G}\boldsymbol{x} \ : \ \boldsymbol{G} \in \mathcal{G}\} \subset \mathbb{S}^d, \qquad \boldsymbol{x}_{\mathcal{G}} := \{\boldsymbol{G} \in \mathcal{G} \ : \ \boldsymbol{x} = \boldsymbol{G}\boldsymbol{x}\} \subset \mathcal{G}, \tag{6.17}$$

respectively. These two sets are related for finite groups $\mathcal{G}$ by the relation $|\mathcal{G}\boldsymbol{x}||\boldsymbol{x}_{\mathcal{G}}| = |\mathcal{G}|$, known as the orbit stabilizer theorem, which means that any point in the orbit $\mathcal{G}\boldsymbol{x}$ is generated by exactly $|\mathcal{G}|/|\boldsymbol{x}_{\mathcal{G}}|$ different group elements. Hence, the averaged quadrature functional $Q_{\mathcal{G}}(\boldsymbol{P}, \boldsymbol{w})$ can by rewritten as

$$Q_{\mathcal{G}}(\boldsymbol{P}, \boldsymbol{w}) = \frac{1}{|\mathcal{G}|} \sum_{i=1}^{M} w_i \sum_{\boldsymbol{G} \in \mathcal{G}} I_{\delta_{\boldsymbol{G}\boldsymbol{p}_i}} = \sum_{i=1}^{M} \frac{w_i}{|\mathcal{G}\boldsymbol{p}_i|} \sum_{\boldsymbol{p} \in \mathcal{G}\boldsymbol{p}_i} I_{\delta_{\boldsymbol{p}}} = \sum_{i=1}^{M} \tilde{w}_i \sum_{\boldsymbol{p} \in \mathcal{G}\boldsymbol{p}_i} I_{\delta_{\boldsymbol{p}}}, \tag{6.18}$$

where $\tilde{w}_i := w_i/|\mathcal{G}\boldsymbol{p}_i|$ is the weight associated to each orbit $\mathcal{G}\boldsymbol{p}_i$, $i = 1, \dots, M$, and $I_{\delta\boldsymbol{x}}$, $\boldsymbol{x} \in \mathbb{S}^d$, denotes the point evaluation functional, cf. (2.30). In words, the averaged quadrature functional $Q_{\mathcal{G}}(\boldsymbol{P}, \boldsymbol{w})$ is composed by the orbits $\mathcal{G}\boldsymbol{p}_i$ of the quadrature points $\boldsymbol{p}_i$, where every point of the orbit $\mathcal{G}\boldsymbol{p}_i$ has the same weight $\tilde{w}_i$, $i = 1, \dots, M$. We note that some of the orbits may coincide or may have cardinality less than $|\mathcal{G}|$. In such cases one might discard some quadrature points and adjust the corresponding quadrature weights, such that the averaged quadrature functional $Q_{\mathcal{G}}(\boldsymbol{P}, \boldsymbol{w})$ can be composed by distinct orbits with distinct quadrature points. Conversely, any invariant quadrature functional is composed by distinct group orbits, where the weights are constant on each orbit. The above observations lead to the following result, cf. [122, Theorem 1].

Theorem 6.5. *For $d \in \mathbb{N}$, let the sphere $\mathbb{S}^d$, a finite orthogonal group $\mathcal{G} \subset \mathrm{O}(d+1)$, and an $N \in \mathbb{N}_0$ be given. Then any quadrature functional $Q(\boldsymbol{P}, \boldsymbol{w})$, $\boldsymbol{P} := (\boldsymbol{p}_1, \dots, \boldsymbol{p}_M) \in (\mathbb{S}^d)^M$, $\boldsymbol{w} := (w_1, \dots, w_M) \in \mathbb{R}^M$, invariant under the group $\mathcal{G}$, cf.* (6.13), *satisfies the classical quadrature condition* (6.6) *for all spherical harmonics $f \in \Pi^N(\mathbb{S}^d)$ if and only if it satisfies the condition for all spherical harmonics $f \in \Pi^N_{\mathcal{G}}(\mathbb{S}^d)$, cf.* (6.14).

Proof. By the invariance of the quadrature functional $Q(\boldsymbol{P},\boldsymbol{w})$ we have $Q(\boldsymbol{P},\boldsymbol{w}) = Q_{\mathcal{G}}(\boldsymbol{P},\boldsymbol{w})$, cf. (6.15), and arrive together with the rotational invariance of the canonical measure $\mu_{\mathbb{S}^d}$ at

$$\big(I_{\mu_{\mathbb{S}^d}} - Q(\boldsymbol{P},\boldsymbol{w})\big)f = \big(I_{\mu_{\mathbb{S}^d}} - Q_{\mathcal{G}}(\boldsymbol{P},\boldsymbol{w})\big)f = \big(I_{\mu_{\mathbb{S}^d}} - Q(\boldsymbol{P},\boldsymbol{w})\big)f_{\mathcal{G}}, \qquad f \in \Pi^N(\mathbb{S}^d).$$

Hence, the assertion follows, since any function f which is invariant under $\mathcal{G}$ satisfies $f = f_{\mathcal{G}}$, cf. (6.16). ∎

The use of groups $\mathcal{G}$ for the computation of quadrature functionals is that the subspace $\Pi^N_{\mathcal{G}}(\mathbb{S}^d)$, cf. (6.14), of spherical harmonics invariant under the group $\mathcal{G}$ is much smaller than $\Pi^N(\mathbb{S}^d)$. Hence, the number of conditions to satisfy the classical quadrature condition (6.6) of an invariant quadrature functional is effectively reduced by Theorem 6.5. Moreover, it turns out that for certain instances of invariant quadrature functionals the efficiency is greater than one. From invariant theory it is know that the exact dimension of the invariant subspace $\Pi^N_{\mathcal{G}}(\mathbb{S}^d)$ can be computed by the use of the Molien series associated to the group $\mathcal{G}$, cf. [52, Theorem (4.6)].

Theorem 6.6. *For $d \in \mathbb{N}$, let the sphere $\mathbb{S}^d$ and a finite orthogonal group $\mathcal{G} \subset \mathrm{O}(d+1)$ be given. Then the dimension $h^n_{\mathcal{G}}$, $d^N_{\mathcal{G}}$ of the harmonic spaces $\Pi_{n,\mathcal{G}}(\mathbb{S}^d)$, $n \in \mathbb{N}_0$, and $\Pi^N_{\mathcal{G}}(\mathbb{S}^d)$, $N \in \mathbb{N}_0$, cf. (6.14), are determined by the generating function*

$$M_{\mathcal{G}}(t) := \frac{1}{|\mathcal{G}|}\sum_{\boldsymbol{G}\in\mathcal{G}} \frac{1-t^2}{\det(\boldsymbol{I}_{d+1} - t\boldsymbol{G})}, \qquad \boldsymbol{I}_{d+1} := \begin{pmatrix} 1 & 0 & \boldsymbol{0} \\ 0 & \ddots & 0 \\ \boldsymbol{0} & 0 & 1 \end{pmatrix} \in \mathbb{R}^{(d+1)\times(d+1)}, \tag{6.19}$$

due to the relations

$$d^N_{\mathcal{G}} := \sum_{n=0}^{N} h^n_{\mathcal{G}}, \qquad M_{\mathcal{G}}(t) = \sum_{n=0}^{\infty} h^n_{\mathcal{G}} t^n. \tag{6.20}$$

Proof. We refer to the proof of [52, Theorem (4.6)]. ∎

Example 6.7. For the *trivial group* $\mathrm{C}_1 := \{\boldsymbol{I}_{d+1} \in \mathbb{R}^{(d+1)\times(d+1)}\} \subset \mathrm{SO}(d+1)$ in $(d+1)$-dimensional space $\mathbb{R}^{d+1}$, the generating function is simply $M_{\mathrm{C}_1}(t) = \frac{1+t}{(1-t)^d}$, cf. (6.19), and we may recover with Theorem 6.6 the dimension formula (4.16) of the harmonic spaces $\Pi_n(\mathbb{S}^d) = \Pi_{n,\mathrm{C}_1}(\mathbb{S}^d)$.

For the *inversion group* $\overline{\mathrm{C}}_1 := \{\pm\boldsymbol{I}_{d+1} \in \mathbb{R}^{(d+1)\times(d+1)}\} \subset \mathrm{O}(d+1)$ it is obvious that only the even polynomials are invariant under $\overline{\mathrm{C}}_1$, i.e., $\Pi_{n,\overline{\mathrm{C}}_1}(\mathbb{S}^d) = \Pi_n(\mathbb{S}^d)$ for $n = 2k$ and $\Pi_{n,\overline{\mathrm{C}}_1}(\mathbb{S}^d) = \{0\}$ for $n = 2k+1$, $k \in \mathbb{N}_0$. We remark that the same result could be obtained by Theorem 6.6 and the generating function $M_{\overline{\mathrm{C}}_1}(t) = \frac{(1-t)^{1+d}+(1+t)^{1+d}}{(1-t^2)^d}$. □

We recall that we aim to compute quadrature functionals $Q(\boldsymbol{P},\boldsymbol{w})$ with degree of exactness $N \in \mathbb{N}_0$ by minimizing the squared worst case quadrature error $E_N(\boldsymbol{P},\boldsymbol{w})$, cf. (6.8), with help of the optimization algorithms on manifolds presented in Section 3.3.1. By the following Theorem 6.8 we will see that for this optimization approach we can easily incorporate the structure of group invariant quadrature functionals on the sphere $\mathbb{S}^d$. In particular, Corollary 6.9 states that the conjugate gradient method on Riemannian manifolds, cf. Algorithm 3.3, respects naturally the constraints imposed by the group invariance. This enables us to use the efficient evaluation methods presented in Chapter 5 without serious modifications, cf. Remark 6.10, for the computation of classical quadrature functionals $Q(\boldsymbol{P},\boldsymbol{w})$ which are invariant under orthogonal groups $\mathcal{G} \subset \mathrm{O}(d+1)$.

Theorem 6.8. *For $d \in \mathbb{N}$, let the sphere $\mathbb{S}^d$, a finite orthogonal group $\mathcal{G} := \{\boldsymbol{G}_1, \dots, \boldsymbol{G}_{M_\mathcal{G}} = \boldsymbol{I}\} \subset \mathrm{O}(d+1)$, quadrature points $\boldsymbol{P} := (\boldsymbol{p}_1, \dots, \boldsymbol{p}_M) \in (\mathbb{S}^d)^M$, and quadrature weights $\boldsymbol{w} := (w_1, \dots, w_M)^\top \in \mathbb{R}^M$ with $M := M_{\mathrm{gen}} M_\mathcal{G}$ be given. Then the gradient of the squared worst case quadrature error $E_N : \mathcal{M} \to \mathbb{R}$, $N \in \mathbb{N}_0$, cf. (6.8), on the product manifold $\mathcal{M} := (\mathbb{S}^d)^M \times \mathbb{R}^M$ given by, cf. (3.58),*

$$\nabla_\mathcal{M} E_N(\boldsymbol{P}, \boldsymbol{w}) = (\nabla_{\mathbb{S}^d, \boldsymbol{p}_1} E_N(\boldsymbol{P}, \boldsymbol{w})^\top, \dots, \nabla_{\mathbb{S}^d, \boldsymbol{p}_M} E_N(\boldsymbol{P}, \boldsymbol{w})^\top, \nabla_{\boldsymbol{w}} E_N(\boldsymbol{P}, \boldsymbol{w})^\top)^\top \in \mathrm{T}_{(\boldsymbol{P}, \boldsymbol{w})} \mathcal{M},$$

satisfies the relations

$$\begin{aligned} \nabla_{\mathbb{S}^d, \boldsymbol{p}_{m+(l-1)M_\mathcal{G}}} E_N(\boldsymbol{P}, \boldsymbol{w}) &= \boldsymbol{G}_m \nabla_{\mathbb{S}^d, \boldsymbol{p}_{lM_\mathcal{G}}} E_N(\boldsymbol{P}, \boldsymbol{w}), \\ \frac{\partial}{\partial w_{m+(l-1)M_\mathcal{G}}} E_N(\boldsymbol{P}, \boldsymbol{w}) &= \frac{\partial}{\partial w_{lM_\mathcal{G}}} E_N(\boldsymbol{P}, \boldsymbol{w}), \qquad m = 1, \dots, M_\mathcal{G}, \quad l = 1, \dots, M_{\mathrm{gen}}, \end{aligned} \tag{6.21}$$

whenever the quadrature points $\boldsymbol{p}_1, \dots, \boldsymbol{p}_M \in \mathbb{S}^d$ and quadrature weights $w_1, \dots, w_M \in \mathbb{R}$ satisfy the relations

$$\boldsymbol{p}_{m+(l-1)M_\mathcal{G}} = \boldsymbol{G}_m \boldsymbol{p}_{lM_\mathcal{G}}, \quad w_{m+(l-1)M_\mathcal{G}} = w_{lM_\mathcal{G}}, \qquad m = 1, \dots, M_\mathcal{G}, \quad l = 1, \dots, M_{\mathrm{gen}}. \tag{6.22}$$

Proof. Let the points $\boldsymbol{p}_1, \dots, \boldsymbol{p}_M \in \mathbb{S}^d$ and quadrature weights $w_1, \dots, w_M \in \mathbb{R}$ satisfy the relations (6.22). For fixed index $n := m + (l-1)M_\mathcal{G}$, with $m = 1, \dots, M_\mathcal{G}$, $l = 1, \dots, M_{\mathrm{gen}}$ we consider the gradient $\nabla_{\mathbb{S}^d, \boldsymbol{p}_n} E_N(\boldsymbol{P}, \boldsymbol{w})$, for which we recall from Theorem 3.5 the relations

$$\nabla_{\mathbb{S}^d, \boldsymbol{p}_n} E_N(\boldsymbol{P}, \boldsymbol{w})^\top \boldsymbol{v} = \frac{\mathrm{d}}{\mathrm{d}t} E_N(\boldsymbol{p}_1, \dots, \boldsymbol{p}_{n-1}, \gamma_{\boldsymbol{p}_n, \boldsymbol{v}}(t), \boldsymbol{p}_{n+1}, \dots, \boldsymbol{p}_M, \boldsymbol{w}), \quad \boldsymbol{v} \in \mathrm{T}_{\boldsymbol{p}_n} \mathbb{S}^d,$$

where $\gamma_{\boldsymbol{p}_n, \boldsymbol{w}} : \mathbb{R} \to \mathbb{S}^d$ is a maximal geodesic curve with $\gamma_{\boldsymbol{p}_n, \boldsymbol{v}}(0) = \boldsymbol{p}_n$, $\dot{\gamma}_{\boldsymbol{p}_n, \boldsymbol{v}}(0) = \boldsymbol{v}$. By the rotational invariance of the worst case quadrature error, cf. (6.9), we infer the relation

$$\begin{aligned} \nabla_{\mathbb{S}^d, \boldsymbol{p}_n} E_N(\boldsymbol{P}, \boldsymbol{w})^\top \boldsymbol{v} &= \frac{\mathrm{d}}{\mathrm{d}t} E_N(\boldsymbol{p}_1, \dots, \boldsymbol{p}_{n-1}, \gamma_{\boldsymbol{p}_n, \boldsymbol{v}}(t), \boldsymbol{p}_{n+1}, \dots, \boldsymbol{p}_M, \boldsymbol{w}) \\ &= \frac{\mathrm{d}}{\mathrm{d}t} E_N(\boldsymbol{G}_m^\top \boldsymbol{p}_1, \dots, \boldsymbol{G}_m^\top \boldsymbol{p}_{n-1}, \gamma_{\boldsymbol{G}_m^\top \boldsymbol{p}_n, \boldsymbol{G}_m^\top \boldsymbol{v}}(t), \boldsymbol{G}_m^\top \boldsymbol{p}_{n+1}, \dots, \boldsymbol{G}_m^\top \boldsymbol{p}_M, \boldsymbol{w}) \\ &= \frac{\mathrm{d}}{\mathrm{d}t} E_N(\boldsymbol{G}_m^\top \boldsymbol{p}_1, \dots, \boldsymbol{G}_m^\top \boldsymbol{p}_{n-1}, \gamma_{\boldsymbol{p}_{lM_\mathcal{G}}, \boldsymbol{G}_m^\top \boldsymbol{v}}(t), \boldsymbol{G}_m^\top \boldsymbol{p}_{n+1}, \dots, \boldsymbol{G}_m^\top \boldsymbol{p}_M, \boldsymbol{w}) \\ &= \nabla_{\mathbb{S}^d, \boldsymbol{p}_{lM_\mathcal{G}}} E_N(\boldsymbol{G}_m^\top \bullet \boldsymbol{P}, \boldsymbol{w})^\top \boldsymbol{G}_m^\top \boldsymbol{v}, \qquad \boldsymbol{v} \in \mathrm{T}_{\boldsymbol{p}_n} \mathbb{S}^d. \end{aligned}$$

Moreover, since the order of the points $\boldsymbol{p}_1, \dots, \boldsymbol{p}_M$ does not alter the value of the function E_N we arrive by the group invariance of the quadrature points at

$$\nabla_{\mathbb{S}^d, \boldsymbol{p}_{m+(l-1)M_\mathcal{G}}} E_N(\boldsymbol{P}, \boldsymbol{w})^\top \boldsymbol{v} = \nabla_{\mathbb{S}^d, \boldsymbol{p}_{lM_\mathcal{G}}} E_N(\boldsymbol{P}, \boldsymbol{w})^\top \boldsymbol{G}_m^\top \boldsymbol{v}, \qquad \boldsymbol{v} \in \mathrm{T}_{\boldsymbol{p}_{m+(l-1)M_\mathcal{G}}} \mathbb{S}^d.$$

Since the above relation holds for every tangent vector $\boldsymbol{v} \in \mathrm{T}_{\boldsymbol{p}_{m+(l-1)M_\mathcal{G}}} \mathbb{S}^d$ we arrive at the assertion (6.21), for the points $\boldsymbol{p}_1, \dots, \boldsymbol{p}_M$. The assertion for the weights follows similarly. ∎

Corollary 6.9. *For $d \in \mathbb{N}$, let the sphere $\mathbb{S}^d$, a finite orthogonal group $\mathcal{G} \subset \mathrm{O}(d+1)$, and a quadrature functional $Q(\boldsymbol{P}, \boldsymbol{w})$, $\boldsymbol{P} := (\boldsymbol{p}_1, \dots, \boldsymbol{p}_M) \in (\mathbb{S}^d)^M$, $\boldsymbol{w} := (w_1, \dots, w_M)^\top \in \mathbb{R}^M$, which is invariant under the group $\mathcal{G}$ be given, cf. (6.13). If Algorithm 3.3 is applied to the squared worst case quadrature error $E_N : \mathcal{M} \to \mathbb{R}$ defined by (6.8) on the product manifold $\mathcal{M} := (\mathbb{S}^d)^M \times \mathbb{R}^M$, with initial point $(\boldsymbol{P}^{(0)}, \boldsymbol{w}^{(0)}) := (\boldsymbol{P}, \boldsymbol{w}) \in \mathcal{M}$, then for every iteration point $(\boldsymbol{P}^{(k)}, \boldsymbol{w}^{(k)}) \in \mathcal{M}$, $k = 0, 1, 2, \dots$, the corresponding quadrature functional $Q(\boldsymbol{P}^{(k)}, \boldsymbol{w}^{(k)})$ is invariant under $\mathcal{G}$.*

Proof. Without loss of generality we may assume that the points $\boldsymbol{p}_1, \dots, \boldsymbol{p}_M \in \mathbb{S}^d$ and the quadrature weights $w_1, \dots, w_M \in \mathbb{R}$ satisfy the assumption (6.22) with $\mathcal{G} = \{\boldsymbol{G}_1 = 1, \dots, \boldsymbol{G}_{M_\mathcal{G}}\} \subset \mathrm{O}(d+1)$, such that we have in particular $M = M_{\mathrm{gen}} M_\mathcal{G}$.

The proof is by induction over the iterations $k \in \mathbb{N}_0$, where we show that the iteration points

$$(\boldsymbol{P}^{(k)}, \boldsymbol{w}^{(k)}) := (\boldsymbol{p}_1^{(k)}, \dots, \boldsymbol{p}_M^{(k)}, w_1^{(k)}, \dots, w_M^{(k)}) \in \mathcal{M}$$

and the direction vectors, cf. line 12 in Algorithm 3.3,

$$\boldsymbol{d}^{(k)} := (\boldsymbol{d}_{\boldsymbol{p}_1}^{(k)}, \dots \boldsymbol{d}_{\boldsymbol{p}_M}^{(k)}, \mathrm{d}_{w_1}^{(k)}, \dots, d_{w_M}^{(k)}) \in \mathrm{T}_{\boldsymbol{p}_1^{(k)}}\mathbb{S}^d \times \dots \times \mathrm{T}_{\boldsymbol{p}_M^{(k)}}\mathbb{S}^d \times \mathrm{T}_{\boldsymbol{w}^{(k)}}\mathbb{R}^M = \mathrm{T}_{(\boldsymbol{P}^{(k)}, \boldsymbol{w}^{(k)})}\mathcal{M},$$

which determine for the iteration point $(\boldsymbol{P}^{(k)}, \boldsymbol{w}^{(k)})$ the next search direction, satisfy the relations

$$\boldsymbol{p}_{m+(l-1)M_\mathcal{G}}^{(k)} = \boldsymbol{G}_m \boldsymbol{p}_{lM_\mathcal{G}}^{(k)}, \qquad w_{m+(l-1)M_\mathcal{G}}^{(k)} = w_{lM_\mathcal{G}}^{(k)} \tag{6.23}$$

and

$$\boldsymbol{d}_{\boldsymbol{p}_{m+(l-1)M_\mathcal{G}}}^{(k)} = \boldsymbol{G}_m \boldsymbol{d}_{\boldsymbol{p}_{lM_\mathcal{G}}}^{(k)}, \qquad d_{w_{m+(l-1)M_\mathcal{G}}}^{(k)} = d_{w_{lM_\mathcal{G}}}^{(k)} \tag{6.24}$$

for $m = 1, \dots, M_\mathcal{G}, \quad l = 1, \dots, M_{\mathrm{gen}}$, respectively.

The induction base for $k = 0$ is fulfilled by assumption and Theorem 6.8, since the initial direction vector is $\boldsymbol{d}^{(0)} := -\nabla_\mathcal{M} E(\boldsymbol{P}^{(0)}, \boldsymbol{w}^{(0)})$.

The induction step proceeds from k to $k+1$ as follows. We consider the geodesics given for some $\alpha^{(k)}$ by, cf. (3.55),

$$\gamma_{(\boldsymbol{P}^{(k)}, \boldsymbol{w}^{(k)}), \boldsymbol{d}^{(k)}}(\alpha^{(k)}) = \big(\gamma_{\boldsymbol{p}_1^{(k)}, \boldsymbol{d}_{\boldsymbol{p}_1}^{(k)}}(\alpha^{(k)}), \dots, \gamma_{\boldsymbol{p}_M^{(k)}, \boldsymbol{d}_{\boldsymbol{p}_M}^{(k)}}(\alpha^{(k)}), w_1 + \alpha^{(k)} d_{w_1}^{(k)}, \dots, w_M + \alpha^{(k)} d_{w_M}^{(k)}\big).$$

Hence, by construction, cf. line 8 in Algorithm 3.3, and induction hypothesis we arrive at the relations

$$\begin{aligned}
\boldsymbol{p}_{m+(l-1)M_\mathcal{G}}^{(k+1)} &= \gamma_{\boldsymbol{p}_{m+(l-1)M_\mathcal{G}}^{(k)}, \boldsymbol{d}_{\boldsymbol{p}_{m+(l-1)M_\mathcal{G}}}^{(k)}}(\alpha^{(k)}) = \boldsymbol{G}_m \gamma_{\boldsymbol{p}_{lM_\mathcal{G}}^{(k)}, \boldsymbol{d}_l^{(k)}}(\alpha) = \boldsymbol{G}_m \boldsymbol{p}_{lM_\mathcal{G}}^{(k+1)}, \\
w_{m+(l-1)M_\mathcal{G}}^{(k+1)} &= w_{m+(l-1)M_\mathcal{G}}^{(k)} + \alpha^{(k)} d_{w_{m+(l-1)M_\mathcal{G}}}^{(k)} = w_{lM_\mathcal{G}}^{(k)} + \alpha^{(k)} d_{w_{lM_\mathcal{G}}}^{(k)} = w_{lM_\mathcal{G}}^{(k+1)},
\end{aligned}$$

for $m = 1, \dots, M_\mathcal{G}, \quad l = 1, \dots, M_{\mathrm{gen}}$, which proofs the assertions (6.23) for the iteration points $(\boldsymbol{P}^{(k+1)}, \boldsymbol{w}^{(k+1)})$. The assertion (6.23) follows again from Theorem 6.8 by the construction $\boldsymbol{d}^{(k+1)} := -\nabla_\mathcal{M} E(\boldsymbol{P}^{(k+1)}, \boldsymbol{w}^{(k+1)}) + \beta^{(k)} \tilde{\boldsymbol{d}}^{(k)}$, cf. line 12 of Algorithm 3.3, since the tangent vector $\tilde{\boldsymbol{d}}^{(k)} := \dot{\gamma}_{(\boldsymbol{P}^{(k)}, \boldsymbol{w}^{(k)})}(\alpha^{(k)})$, satisfies by induction hypothesis (6.24) the relations, cf. (3.66),

$$\tilde{\boldsymbol{d}}_{\boldsymbol{p}_{m+(l-1)M_\mathcal{G}}}^{(k)} = \dot{\gamma}_{\boldsymbol{G}_m \boldsymbol{p}_{lM_\mathcal{G}}^{(k)}, \boldsymbol{G}_m d_{\boldsymbol{p}_l}^{(k)}}(\alpha^{(k)}) = \boldsymbol{G}_m \dot{\gamma}_{\boldsymbol{p}_{lM_\mathcal{G}}^{(k)}, d_{\boldsymbol{p}_{lM_\mathcal{G}}}^{(k)}}(\alpha^{(k)}) = \tilde{\boldsymbol{d}}^{(k)}, \qquad \tilde{d}_{w_{m+(l-1)M_\mathcal{G}}} = \tilde{d}_{w_{lM_\mathcal{G}}}$$

for $m = 1, \dots, M_\mathcal{G}, \quad l = 1, \dots, M_{\mathrm{gen}}$.

Thus, we proved the relations (6.23) for all iteration points $(\boldsymbol{P}^{(k)}, \boldsymbol{w}^{(k)}) \in \mathcal{M}$, $k \in \mathbb{N}_0$, which correspond by relation (6.18) to quadrature functionals $Q(\boldsymbol{P}^{(k)}, \boldsymbol{w}^{(k)})$, which are invariant under the group $\mathcal{G}$. ∎

Remark 6.10. For the computation of optimal quadrature functional on the sphere $\mathbb{S}^d$ which are invariant under a certain finite orthogonal group $\mathcal{G} \subset O(d+1)$, it is sufficient by Corollary 6.9 to initialize the CG method on Riemannian manifolds, cf. Algorithm 3.3, with invariant quadrature points and weights, since the following iterations will maintain this symmetry. This remarkable property of optimization methods on Riemannian manifolds makes the implementation particular

easy, since we can simply use the evaluation algorithms presented in Chapter 5 without serious modifications.

The only problem we are confronted with is that in numerical computations rounding errors might break the symmetries. Therefore, we use the simple relations (6.21) of Theorem 6.8 in order to force the symmetry in our implementations. To be more precise, with the notations of Theorem 6.8 and the proof of Corollary 6.9 we choose the representatives $\boldsymbol{p}_{lM_\mathcal{G}}$ of the orbits, cf. (6.17),

$$\mathcal{G}\boldsymbol{p}_{lM_\mathcal{G}} = \{\boldsymbol{G}_m \boldsymbol{p}_{lM_\mathcal{G}} \ : \ m = 1, \dots, M_\mathcal{G}\} = \{\boldsymbol{p}_{1+(l-1)M_\mathcal{G}}, \dots, \boldsymbol{p}_{lM_\mathcal{G}}\} \subset \mathbb{S}^d, \qquad l = 1, \dots, M_{\text{gen}},$$

and replace at each iteration step of the proposed optimization methods the numerical values of all points $\boldsymbol{p}_{m+(l-1)M_\mathcal{G}} \in \mathcal{G}\boldsymbol{p}_{lM_\mathcal{G}}$ and the corresponding gradients $\nabla_{\boldsymbol{p}_{m+(l-1)M_\mathcal{G}}} E_N(\boldsymbol{P}, \boldsymbol{w})$ by

$$\boldsymbol{p}_{m+(l-1)M_\mathcal{G}} := \boldsymbol{G}_m \boldsymbol{p}_{lM_\mathcal{G}}, \quad \nabla_{\boldsymbol{p}_{m+(l-1)M_\mathcal{G}}} E_N(\boldsymbol{P}, \boldsymbol{w}) := \boldsymbol{G}_m \nabla_{\boldsymbol{p}_{lM_\mathcal{G}}} E_N(\boldsymbol{P}, \boldsymbol{w}), \qquad m = 1, \dots, M_\mathcal{G},$$

respectively.

We mention that the above results are also valid for other rotational invariant energies, such as the electrostatic energy restricted to the sphere, cf. Section 2.3. □

Invariant Quadrature Functionals on the Sphere $\mathbb{S}^2$

For the rest of this section we restrict our attention to the sphere $\mathbb{S}^2$ and consider some particular finite orthogonal groups,[3] which seem to lead to sequences of quadrature functionals $Q(\boldsymbol{P}, \boldsymbol{w})$ with efficiency $\text{eff}_{\mathbb{S}^2}(Q(\boldsymbol{P}, \boldsymbol{w})) \geq 1$, for all degrees $N \in \mathbb{N}$. We begin with introducing the three dimensional rotation groups $\mathrm{T}, \mathrm{O}, \mathrm{I} \subset \mathrm{SO}(3)$, which are representations of the rotational symmetry groups of the tetrahedron, octahedron (or cube), and icosahedron (or dodecahedron), respectively. Particular nice representations are found if we align the tetrahedron, the octahedron, and icosahedron such that the projections of the vertices, face centers, and edge centers on the unit sphere $\mathbb{S}^2$ are given by

$$\begin{aligned}
\mathrm{T}_\mathrm{v} &:= \left\{(a,a,a)^\top, (-a,-a,a)^\top, (-a,a,-a)^\top, (a,-a,-a)^\top\right\},\\
\mathrm{T}_\mathrm{f} &:= \left\{(-a,-a,-a)^\top, (a,a,-a)^\top, (a,-a,a)^\top, (-a,a,a)^\top\right\},\\
\mathrm{T}_\mathrm{e} &:= \left\{(\pm 1,0,0)^\top, (0,\pm 1,0)^\top, (0,0,\pm 1)^\top, \right\},\\
\mathrm{O}_\mathrm{v} &:= \left\{(\pm 1,0,0)^\top, (0,\pm 1,0)^\top, (0,0,\pm 1)^\top\right\},\\
\mathrm{O}_\mathrm{f} &:= \left\{(\pm a,\pm a,\pm a)^\top\right\},\\
\mathrm{O}_\mathrm{e} &:= \left\{(\pm b,\pm b,0)^\top, (0,\pm b,\pm b)^\top, (\pm b,0,\pm b)^\top\right\},\\
\mathrm{I}_\mathrm{v} &:= \left\{(\pm c,\pm d,0)^\top, (0,\pm c,\pm d)^\top, (\pm d,0,\pm c)^\top\right\},\\
\mathrm{I}_\mathrm{f} &:= \left\{(\pm e,\pm f,0)^\top, (0,\pm e,\pm f)^\top, (\pm e,0,\pm f)^\top, (\pm a,\pm a,\pm a)^\top\right\},\\
\mathrm{I}_\mathrm{e} &:= \left\{(\pm r,\pm s,\pm t)^\top, (\pm t,\pm r,\pm s)^\top, (\pm s,\pm t,\pm r)^\top, (\pm 1,0,0)^\top, (0,\pm 1,0)^\top, (0,0,\pm 1)^\top\right\} \subset \mathbb{S}^2,
\end{aligned} \tag{6.25}$$

[3] A complete list of all finite subgroups of the orthogonal group O(3) can be found in the monograph [26].

respectively, where

$$a := 1/\sqrt{3}, \quad b := 1/\sqrt{2}, \quad c := \sqrt{(5+\sqrt{5})/10}, \quad d := \sqrt{(5-\sqrt{5})/10},$$
$$e := \sqrt{(3-\sqrt{5})/6}, \quad f := \sqrt{(3+\sqrt{5})/6}, \quad r := (\sqrt{5}+1)/4, \quad s := (\sqrt{5}-1)/4, \quad t := 1/2.$$

For an illustration of these point sets see Figure 6.1.

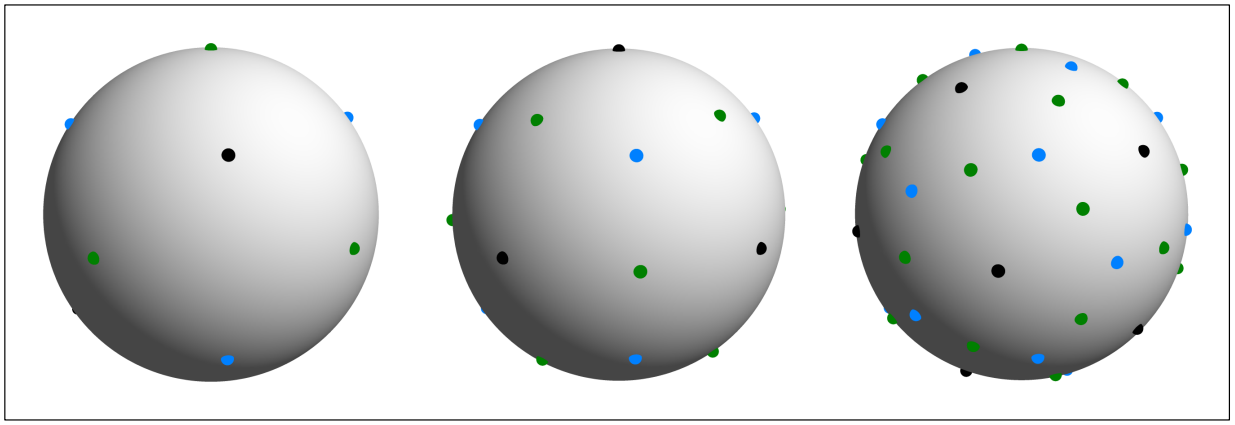

Figure 6.1: Illustration of the projections of the vertices $\mathrm{T_v}$, $\mathrm{O_v}$, $\mathrm{I_v}$ (black), the face centers $\mathrm{T_f}$, $\mathrm{O_f}$, $\mathrm{I_f}$ (blue), and the edge centers $\mathrm{T_e}$, $\mathrm{O_e}$, $\mathrm{I_e}$ (green) of the tetrahedron (left), the octahedron (middle), and the icosahedron (right) on the unit sphere $\mathbb{S}^2$, respectively.

After this preparation we define the *tetrahedral group, octahedral group, and icosahedral group* by

$$\begin{aligned}
\mathrm{T} &:= \left\{ \boldsymbol{R}\left(\boldsymbol{r}_\mathrm{v}, \frac{2}{3}\pi\right), \boldsymbol{R}\left(\boldsymbol{r}_\mathrm{f}, \frac{2}{3}\pi\right), \boldsymbol{R}\left(\boldsymbol{r}_\mathrm{e}, \pi\right) \;:\; \boldsymbol{r}_\mathrm{v} \in \mathrm{T_v}, \boldsymbol{r}_\mathrm{f} \in \mathrm{T_f}, \boldsymbol{r}_\mathrm{e} \in \mathrm{T_e} \right\}, \\
\mathrm{O} &:= \left\{ \boldsymbol{R}\left(\boldsymbol{r}_\mathrm{v}, \frac{1}{2}l\pi\right), \boldsymbol{R}\left(\boldsymbol{r}_\mathrm{f}, \frac{2}{3}\pi\right), \boldsymbol{R}\left(\boldsymbol{r}_\mathrm{e}, \pi\right) \;:\; \boldsymbol{r}_\mathrm{v} \in \mathrm{O_v},\ \boldsymbol{r}_\mathrm{f} \in \mathrm{O_f},\ \boldsymbol{r}_\mathrm{e} \in \mathrm{O_e},\ l = 1,2 \right\}, \\
\mathrm{I} &:= \left\{ \boldsymbol{R}\left(\boldsymbol{r}_\mathrm{v}, \frac{2}{5}l\pi\right), \boldsymbol{R}\left(\boldsymbol{r}_\mathrm{f}, \frac{2}{3}\pi\right), \boldsymbol{R}\left(\boldsymbol{r}_\mathrm{e}, \pi\right) \;:\; \boldsymbol{r}_\mathrm{v} \in \mathrm{I_v},\ \boldsymbol{r}_\mathrm{f} \in \mathrm{I_f},\ \boldsymbol{r}_\mathrm{e} \in \mathrm{I_e},\ l = 1,2 \right\} \subset \mathrm{SO}(3),
\end{aligned} \tag{6.26}$$

respectively, where we recall that the rotation matrix $\boldsymbol{R}(\boldsymbol{r}, \alpha) \in \mathrm{SO}(3)$ with rotation axis $\boldsymbol{r} \in \mathbb{S}^2$ and rotation angle $\alpha \in \mathbb{R}$ is defined by (3.90). We note further, the rotations with rotation angle of π are counted twice in (6.26), so that the tetrahedral group T, the octahedral group O, and the icosahedral group I have a total number of 12, 24, and 60 group elements, respectively. The other groups of consideration are only generated by one rotational axis and given by the *cyclic groups*

$$\mathrm{C}_k := \left\{ \boldsymbol{R}\left(\boldsymbol{r}, \frac{2}{k}l\pi\right) \in \mathrm{SO}(3) \;:\; \boldsymbol{r} := (0,0,1)^\top,\ l = 0, \dots, k-1 \right\}, \qquad k \in \mathbb{N}. \tag{6.27}$$

We note that the group C_4 seems to be of particular importance for efficient invariant quadrature functionals on the sphere $\mathbb{S}^2$. Finally, any rotation group $\mathcal{G} \subset \mathrm{SO}(3)$ can be extended by including the inversion group $\overline{\mathrm{C}}_1$, cf. Example 6.7, by setting

$$\overline{\mathcal{G}} := \{ \pm \boldsymbol{G} \in \mathrm{O}(3) \;:\; \boldsymbol{G} \in \mathcal{G} \}, \qquad \mathcal{G} \subset \mathrm{SO}(3). \tag{6.28}$$

We recall that any quadrature functional $Q_{\mathcal{G}}(\boldsymbol{P},\boldsymbol{w})$ invariant under a group $\mathcal{G}$ is determined by the orbits $\mathcal{G}\boldsymbol{p}_i \subset \mathbb{S}^2$ of given quadrature points $\boldsymbol{p}_i \in \mathbb{S}^2$ and corresponding quadrature weights $w_i \in \mathbb{R}$, $i = 1,\dots,\tilde{M}$, where the size of the quadrature functional $Q_{\mathcal{G}}(\boldsymbol{P},\boldsymbol{w})$ is $M = \sum_{i=1}^{\tilde{M}} |\mathcal{G}\boldsymbol{p}_i|$, cf. (6.17) and (6.18). In the case of subgroups $\mathcal{G} \subset \mathrm{SO}(3)$ the only orbits with cardinality less than $|\mathcal{G}|$ are given by the orbits of the rotational axes of the group elements. In particular, for the rotation groups $\mathrm{T},\mathrm{O},\mathrm{I}$ these exceptional orbits are given by the special sets $\mathcal{G}_{\mathrm{v}},\mathcal{G}_{\mathrm{f}},\mathcal{G}_{\mathrm{e}}$ for $\mathcal{G} \in \{\mathrm{T},\mathrm{O},\mathrm{I}\}$, cf. (6.25), and we may write any invariant quadrature functional as

$$Q_{\mathcal{G}}(\boldsymbol{P},\boldsymbol{w}) = \sum_{i=1}^{M_{\mathrm{gen}}} w_i \sum_{\boldsymbol{G}\in\mathcal{G}} I_{\delta_{\boldsymbol{G}\boldsymbol{p}_i}} + w_{\mathrm{v}} \sum_{\boldsymbol{p}_{\mathrm{v}}\in\mathcal{G}_{\mathrm{v}}} I_{\delta_{\boldsymbol{p}_{\mathrm{v}}}} + w_{\mathrm{f}} \sum_{\boldsymbol{p}_{\mathrm{f}}\in\mathcal{G}_{\mathrm{f}}} I_{\delta_{\boldsymbol{p}_{\mathrm{f}}}} + w_{\mathrm{e}} \sum_{\boldsymbol{p}_e\in\mathcal{G}_{\mathrm{e}}} I_{\delta_{\boldsymbol{p}_{\mathrm{e}}}}, \quad w_i, w_{\mathrm{v}}, w_{\mathrm{f}}, w_{\mathrm{e}} \in \mathbb{R}, \tag{6.29}$$

where the generating quadrature points $\boldsymbol{p}_i, \in \mathbb{S}^2 \setminus (\mathcal{G}_{\mathrm{v}},\mathcal{G}_{\mathrm{f}},\mathcal{G}_{\mathrm{e}})$ satisfy $\boldsymbol{p}_i \notin \mathcal{G}\boldsymbol{p}_j$, $i \neq j$, $i,j = 1,\dots,M_{\mathrm{gen}}$. Thus, the size of the invariant quadrature functional is $M = |\mathcal{G}|M_{\mathrm{gen}} + M_{\mathrm{fix}}$, where the number $M_{\mathrm{fix}} \in \{0, |\mathcal{G}_{\mathrm{v}}|, |\mathcal{G}_{\mathrm{f}}|, |\mathcal{G}_{\mathrm{e}}|, |\mathcal{G}_{\mathrm{v}}| + |\mathcal{G}_{\mathrm{f}}|, |\mathcal{G}_{\mathrm{v}}| + |\mathcal{G}_{\mathrm{e}}|, |\mathcal{G}_{\mathrm{f}}| + |\mathcal{G}_{\mathrm{e}}|, |\mathcal{G}_{\mathrm{v}}| + |\mathcal{G}_{\mathrm{f}}| + |\mathcal{G}_{\mathrm{e}}|\}$ depends on the special sets used in $Q_{\mathcal{G}}(\boldsymbol{P},\boldsymbol{w})$, $\mathcal{G} \in \{\mathrm{T},\mathrm{O},\mathrm{I}\}$. For the cyclic group C_k, $k \in \mathbb{N}$, the general invariant quadrature functional reads as

$$Q_{\mathrm{C}_k}(\boldsymbol{P},\boldsymbol{w}) = \sum_{i=1}^{M_{\mathrm{gen}}} w_i \sum_{\boldsymbol{G}\in\mathrm{C}_k} I_{\delta_{\boldsymbol{G}\boldsymbol{p}_i}} + w_+ I_{\delta_{(0,0,1)^\top}} + w_- I_{\delta_{(0,0,-1)^\top}}, \qquad w_i, w_+, w_- \in \mathbb{R}, \tag{6.30}$$

where $\boldsymbol{p}_i \in \mathbb{S}^2 \setminus \{(0,0,\pm 1)^\top\}$ with $\boldsymbol{p}_i \notin \mathrm{C}_k\boldsymbol{p}_j$ for $i \neq j$, $i,j = 1,\dots,M_{\mathrm{gen}}$. In that case the size of the invariant quadrature functional $Q_{\mathrm{C}_k}(\boldsymbol{P},\boldsymbol{w})$ is given by $M = kM_{\mathrm{gen}} + M_{\mathrm{fix}}$, where $M_{\mathrm{fix}} \in \{0,1,2\}$. For the inversion group $\overline{\mathrm{C}}_1$ all orbits have the same cardinality and the general invariant quadrature is of the form

$$Q_{\overline{\mathrm{C}}_1}(\boldsymbol{P},\boldsymbol{w}) = \sum_{i=1}^{M_{\mathrm{gen}}} w_i (I_{\delta_{\boldsymbol{p}_i}} + I_{\delta_{-\boldsymbol{p}_i}}), \qquad \boldsymbol{p}_i \in \mathbb{S}^2, \quad w_i \in \mathbb{R}, \quad i = 1,\dots,M_{\mathrm{gen}}, \tag{6.31}$$

where $\boldsymbol{p}_i \notin \{\pm\boldsymbol{p}_j\}$ for $i \neq j$, $i,j = 1,\dots,M_{\mathrm{gen}}$. Thus, the size of the quadrature functional $Q_{\overline{\mathrm{C}}_1}(\boldsymbol{P},\boldsymbol{w})$ is $M = 2M_{\mathrm{gen}}$.

As in the noninvariant case we make the assumption that the number of the conditions imposed by (6.6) should match the degrees of freedom provided by an invariant quadrature functional. Therefore, we calculate the dimension of certain group invariant subspaces of $\Pi^N(\mathbb{S}^2)$, which is approximately reduced by a factor of the size of the group.

Theorem 6.11. *Let the sphere* $\mathbb{S}^2$ *with the inversion group* $\overline{\mathrm{C}}_1$, *cf.* (6.28), *the cyclic group* C_4 *cf.* (6.27), *the tetrahedral group* T, *the octahedral group* O, *and the icosahedral group* I, *cf.* (6.26), *be given. Then the dimension* $d^N_{\overline{\mathrm{C}}_1}$, $d^N_{\mathrm{C}_4}$, d^N_{T}, d^N_{O}, d^N_{I} *of the harmonic space* $\Pi^N_{\overline{\mathrm{C}}_1}(\mathbb{S}^2)$, $\Pi^N_{\mathrm{C}_4}(\mathbb{S}^2)$, $\Pi^N_{\mathrm{T}}(\mathbb{S}^2)$, $\Pi^N_{\mathrm{O}}(\mathbb{S}^2)$, $\Pi^N_{\mathrm{I}}(\mathbb{S}^2)$, *respectively, is given by, cf.* (5.14) *and* (6.11),

$$\begin{aligned} d^N_{\overline{\mathrm{C}}_1} &= \left(\left\lfloor \frac{N}{2} \right\rfloor + 1\right)\left(2\left\lfloor \frac{N}{2} \right\rfloor + 1\right), \quad d^N_{\mathrm{C}_4} = \left\lceil \frac{(N+1)^2}{4} \right\rceil + r^N_{\mathrm{C}_4}, \\ d^N_{\mathrm{T}} &= \left\lceil \frac{(N+1)^2}{12} \right\rceil, \quad d^N_{\mathrm{O}} = \left\lceil \frac{(N+1)^2}{24} \right\rceil, \quad d^N_{\mathrm{I}} = \left\lceil \frac{(N+1)^2}{60} \right\rceil + r^N_{\mathrm{I}}, \end{aligned} \tag{6.32}$$

where

$$r^N_{\mathrm{C}_4} = \begin{cases} 1, & N \equiv 1 \mod 4, \\ 0, & \textit{else}, \end{cases} \qquad r^N_{\mathrm{I}} = \begin{cases} 1, & N \equiv 6,12,16,22 \mod 30, \\ 0, & \textit{else}. \end{cases}$$

Proof. From Example 6.7 we know that the dimension of $\Pi_{\overline{\mathrm{C}}_1}^N(\mathbb{S}^2)$ is given by the sum over the dimensions of $\Pi_n(\mathbb{S}^2)$ for even n, i.e.,

$$d_{\overline{\mathrm{C}}_1}^N = \sum_{k=0}^{\lfloor \frac{N}{2} \rfloor} (4k+1) = \left(\left\lfloor \frac{N}{2} \right\rfloor + 1 \right) \left(2 \left\lfloor \frac{N}{2} \right\rfloor + 1 \right), \qquad N \in \mathbb{N}_0.$$

For the other groups C_4, T, O, I we compute the associated generating functions defined in Theorem 6.6 and obtain

$$M_{\mathrm{C}_4}(t) = \frac{1+t^4}{(1-t)(1-t^4)}, \qquad M_{\mathrm{T}}(t) = \frac{1+t^6}{(1-t^3)(1-t^4)},$$
$$M_{\mathrm{O}}(t) = \frac{1+t^9}{(1-t^4)(1-t^6)}, \qquad M_{\mathrm{I}}(t) = \frac{1+t^{15}}{(1-t^6)(1-t^{10})}.$$

For the groups T, O, I the corresponding power series coefficients, cf. (6.20), are found in [122, Theorem 2] to satisfy

$$h_{\mathrm{T}}^n = 2\left\lfloor \frac{n}{3} \right\rfloor + \left\lfloor \frac{n}{2} \right\rfloor - n + 1, \quad h_{\mathrm{O}}^n = \left\lfloor \frac{n}{4} \right\rfloor + \left\lfloor \frac{n}{3} \right\rfloor + \left\lfloor \frac{n}{2} \right\rfloor - n + 1, \quad h_{\mathrm{I}}^n = \left\lfloor \frac{n}{5} \right\rfloor + \left\lfloor \frac{n}{3} \right\rfloor + \left\lfloor \frac{n}{2} \right\rfloor - n + 1,$$

for $n \in \mathbb{N}_0$. In the case of the group C_4 one checks the relation $h_{\mathrm{C}_4}^n = 2\left\lfloor \frac{n}{4} \right\rfloor + 1$. By summation over n the assertion (6.32) can be proved as in [89, Section 3]. ∎

From Theorem 6.11 and Theorem 6.5 we arrive immediately at the well known result that the exceptional orbits of the rotation groups $\mathrm{T}, \mathrm{O}, \mathrm{I}$, given by the vertices of the platonic solids $\mathrm{T_v}, \mathrm{O_v}, \mathrm{I_v}$, provide quadrature functionals of degree $N = 2, 3, 5$, respectively, which are particular efficient, cf. Table 6.1.

Theorem 6.12. *Let the sphere $\mathbb{S}^2$, the tetrahedral group T, the octahedral group O, and the icosahedral group I, cf. (6.26), be given. Then the invariant quadrature functionals $Q_{\mathcal{G}}(\boldsymbol{P}, \boldsymbol{w})$, $\boldsymbol{P} \in (\mathbb{S}^2)^M$, $\boldsymbol{w} \in \mathbb{R}^M$, determined by (6.29) with $M_{\mathrm{gen}} := 0$, $w_{\mathrm{f}} := w_{\mathrm{e}} := 0$, and $w_{\mathrm{v}} := 1/|\mathcal{G}_{\mathrm{v}}|$ have degree of exactness $N = 2, 3, 5$, for $\mathcal{G} = \mathrm{T}, \mathrm{O}, \mathrm{I}$, respectively.*

Proof. By Theorem 6.11 we find that the polynomial $f \equiv 1 \in \Pi_{\mathcal{G}}^N(\mathbb{S}^2)$ is the only spherical harmonic of degree at most $N = 2, 3, 5$ which is invariant the group $\mathcal{G} = \mathrm{T}, \mathrm{O}, \mathrm{I}$, respectively. Since f is integrate exactly by the given quadrature functionals $Q_{\mathcal{G}}(\boldsymbol{P}, \boldsymbol{w})$ we arrive at the assertion by Theorem 6.5. ∎

From the proof of Theorem 6.12 we observe that, depending on the orbits of the group $\mathcal{G} \subset \mathrm{O}(3)$, the degrees of freedom of an invariant quadrature functional need not to be a multiple of three. That means, for particular instances of quadrature functionals invariant under the group $\mathcal{G}$, we can match exactly the degrees of freedom with the number of conditions given by the dimension $d_{\mathcal{G}}^N$ of the invariant subspace $\Pi_{\mathcal{G}}^N(\mathbb{S}^2)$, $N \in \mathbb{N}_0$, cf. Theorem 6.11. For the finite rotation groups C_4, T, O, I there is only one degree of freedom for the exceptional orbits, namely the value of the associated weights, cf. (6.29), (6.30). We note further that for the rotation groups T, O, I we have no loss of degrees of freedom by rotational invariance, since no other rotations than the group elements of T, O, I will keep the special sets $\mathrm{T_v}$, $\mathrm{O_v}$, $\mathrm{I_v}$ fix, respectively. Hence, the degrees of freedom of an invariant quadrature functional of the form (6.29) is given by $3M_{\mathrm{gen}}$, $3M_{\mathrm{gen}} + 1$, $3M_{\mathrm{gen}} + 2$, or $3M_{\mathrm{gen}} + 3$, depending on the choice of the special sets $\mathcal{G}_{\mathrm{v}}, \mathcal{G}_{\mathrm{f}}, \mathcal{G}_{\mathrm{e}}$. Since we are particular interested in the most efficient quadrature functionals we will consider for the

rotation group $\mathcal{G} \in \{\mathrm{T}, \mathrm{O}, \mathrm{I}\}$ only the quadrature functionals determined by, cf. (6.29),

$$M_{\text{gen}} := \left\lfloor \frac{d_{\mathcal{G}}^N}{3} \right\rfloor, \qquad M_{\text{fix}} := \begin{cases} 0, & d_{\mathcal{G}}^N \equiv 0 \mod 3, \\ |\mathcal{G}_{\mathrm{v}}|, & d_{\mathcal{G}}^N \equiv 1 \mod 3, \\ |\mathcal{G}_{\mathrm{v}}| + |\mathcal{G}_{\mathrm{f}}|, & d_{\mathcal{G}}^N \equiv 2 \mod 3, \end{cases} \qquad N \in \mathbb{N}, \tag{6.33}$$

i.e., we will use only the sets $\mathcal{G}_{\mathrm{v}}, \mathcal{G}_{\mathrm{f}}$, which have the smallest cardinality among the exceptional orbits $\mathcal{G}_{\mathrm{v}}, \mathcal{G}_{\mathrm{f}}, \mathcal{G}_{\mathrm{e}}$.

In the case of the cyclic group C_4 the two orbits $\{(0,0,1)^\top\}$, $\{(0,0,-1)^\top\}$ add in each case one degree of freedom, cf. (6.27). Moreover, since the group C_4 keeps only the points $(0,0,\pm 1)^\top \in \mathbb{S}^2$ fix, we 'loose' one degree of freedom for $M_{\text{gen}} \geq 1$, which corresponds to the one dimensional subgroup keeping the same points fix. In total we obtain $3M_{\text{gen}} - 1$, $3M_{\text{gen}}$, or $3M_{\text{gen}} + 1$ degrees of freedom for a quadrature functional of the form (6.27). Hence, we will consider only the quadrature functionals invariant under C_4 determined by

$$M_{\text{gen}} := \left\lfloor \frac{d_{\mathrm{C}_4}^N + 1}{3} \right\rfloor, \qquad M_{\text{fix}} := d_{\mathrm{C}_4}^N + 1 \mod 3, \qquad N \in \mathbb{N}. \tag{6.34}$$

For the group of central inversion $\overline{\mathrm{C}}_1$ there are no special sets, and thus the degrees of freedom cannot always match the number of conditions, (6.31). Moreover, as in the noninvariant case we 'loose' for $M_{\text{gen}} \geq 2$ three degrees of freedom, which results in $3M_{\text{gen}} - 3$ degrees of freedom. Hence, we will consider only quadrature functional invariant under $\overline{\mathrm{C}}_1$ determined by

$$M_{\text{gen}} := \begin{cases} 1, & N = 1, \\ \left\lceil \frac{d_{\overline{\mathrm{C}}_1}^N + 3}{3} \right\rceil, & N \geq 2, \end{cases} \qquad M_{\text{fix}} := 0, \qquad N \in \mathbb{N}. \tag{6.35}$$

We recapitulate that the relations (6.33), (6.34), (6.35) provide use with a precise number of quadrature points in a quadrature functional invariant under the rotation groups $\mathrm{T}, \mathrm{O}, \mathrm{I}, \mathrm{C}_4$, and the group $\overline{\mathrm{C}}_1$, respectively, such that the degrees of freedom match the number of conditions imposed by the classical quadrature condition (6.6) for the invariant spherical harmonics. In order to determine the most efficient ones among the invariant quadrature functionals $Q_{\mathcal{G}}(\boldsymbol{P}, \boldsymbol{w})$, $\mathcal{G} \in \{\mathrm{T}, \mathrm{O}, \mathrm{I}, \mathrm{C}_4, \overline{\mathrm{C}}_1\}$, we need to compute the corresponding efficiencies defined by (6.10), provided the degree of exactness N can be achieved. Surprisingly, for certain instances these invariant quadrature functionals would have an efficiency greater than one. We note that this observation was already made by McLaren in [89] for the cases $\mathcal{G} \in \{\mathrm{T}, \mathrm{O}, \mathrm{I}\}$.

Theorem 6.13. *Let the sphere $\mathbb{S}^2$ and $N \in \mathbb{N}$ with $N \geq 2$ be given. If there exists a quadrature functional $Q_{\mathcal{G}}(\boldsymbol{P}, \boldsymbol{w})$, $\boldsymbol{P} \in (\mathbb{S}^2)^M$, $\boldsymbol{w} \in \mathbb{R}^M$, with degree of exactness N, which is invariant under the group $\mathcal{G} \in \{\overline{\mathrm{C}}_1, \mathrm{C}_4, \mathrm{T}, \mathrm{O}, \mathrm{I}\}$, and has size $M = |\mathcal{G}| M_{\text{gen}} + M_{\text{fix}}$ determined by* (6.35), (6.34), (6.33), *respectively, then the efficiency is, cf.* (6.12),

$$\begin{aligned} \operatorname{eff}_{\mathbb{S}^2}(Q_{\overline{\mathrm{C}}_1}(\boldsymbol{P}, \boldsymbol{w})) &\begin{cases} = 1 + \frac{3+6\lfloor (N-2)/6 \rfloor}{\lceil (N+1)^2 \rceil_3 - 6\lfloor (N-2)/6 \rfloor}, & N \equiv 1 \mod 2, \\ < 1, & \textit{else}, \end{cases} \\ \operatorname{eff}_{\mathbb{S}^2}(Q_{\mathrm{C}_4}(\boldsymbol{P}, \boldsymbol{w})) &\begin{cases} = 1 + \frac{3}{\lceil (N+1)^2 \rceil_3}, & N \equiv 3, 7 \mod 12, \\ = 1, & N \equiv 0, 4, 6, 10, 11 \mod 12, \\ < 1, & \textit{else}, \end{cases} \end{aligned} \tag{6.36}$$

$$
\begin{aligned}
\operatorname{eff}_{\mathbb{S}^2}(Q_{\mathrm{T}}(\boldsymbol{P},\boldsymbol{w}))&\begin{cases} = 1+\frac{3}{(N+1)^2}, & N \equiv 5 \mod 6,\\ = 1, & N \equiv 2 \mod 6,\\ < 1, & \textit{else},\end{cases}\\
\operatorname{eff}_{\mathbb{S}^2}(Q_{\mathrm{O}}(\boldsymbol{P},\boldsymbol{w}))&\begin{cases} = 1+\frac{3}{\lceil (N+1)^2 \rceil_3}, & N \equiv 3,11,15,19,23,31,35 \mod 36,\\ < 1, & \textit{else},\end{cases}\\
\operatorname{eff}_{\mathbb{S}^2}(Q_{\mathrm{I}}(\boldsymbol{P},\boldsymbol{w}))&\begin{cases} = 1+\frac{12}{\lceil (N+1)^2 \rceil_3 - 9}, & N \equiv 14 \mod 30,\\ = 1+\frac{9}{\lceil (N+1)^2 \rceil_3 - 6}, & N \equiv 9,19 \mod 60,\\ = 1+\frac{3}{\lceil (N+1)^2 \rceil_3}, & N \equiv 5,23,29 \mod 30,\\ < 1, & \textit{else},\end{cases}
\end{aligned}
\tag{6.37}
$$

respectively.

Proof. Before we proof the assertions (6.36) and (6.37), we recall two useful relations from modular arithmetic. The first one states that

$$
a \equiv b \mod m \quad \Rightarrow \quad p(a) \equiv p(b) \mod m, \qquad a,b \in \mathbb{Z}, \quad m \in \mathbb{N}, \tag{6.38}
$$

for any polynomial $p : \mathbb{R} \to \mathbb{R}$ with coefficient in $\mathbb{Z}$. The second is

$$
a \equiv b \mod lm \quad \Rightarrow \quad \left\lceil \frac{a}{l} \right\rceil \equiv \left\lceil \frac{b}{l} \right\rceil \mod m, \qquad a,b \in \mathbb{Z}, \quad m,l \in \mathbb{N}, \tag{6.39}
$$

which is also valid for the floor function $\lfloor \cdot \rfloor$.

From the relations (6.38), (6.39) we conclude that

$$
\left\lceil \frac{(N+1)^2+3}{3} \right\rceil = \frac{1}{3}(N+1)^2 + r(N), \qquad N \in \mathbb{N}, \tag{6.40}
$$

where $r : \mathbb{N} \to \mathbb{R}$ is a three periodic function, i.e., $r(N) = r(N+3)$, $N \in \mathbb{N}$. Similarly, we find for the rotation groups $\mathcal{G} = \mathrm{C}_4, \mathrm{T}, \mathrm{O}, \mathrm{I}$ by the definitions of M_{gen}, M_{fix}, cf. (6.33), (6.34), and Theorem 6.11 that

$$
M = |\mathcal{G}| M_{\mathrm{gen}} + M_{\mathrm{fix}} = \frac{1}{3}(N+1)^2 + r_{\mathcal{G}}(N), \qquad N \in \mathbb{N}, \tag{6.41}
$$

where $r_{\mathcal{G}} : \mathbb{N} \to \mathbb{R}$ is a $3|\mathcal{G}|$ periodic function, i.e., $r_{\mathcal{G}}(N) = r_{\mathcal{G}}(N + 3|\mathcal{G}|)$, $N \in \mathbb{N}$. Hence, the difference of the equations (6.40) and (6.41) is a $3|\mathcal{G}|$ periodic function

$$
\left\lceil \frac{(N+1)^2+3}{3} \right\rceil - M = r(N) - r_{\mathcal{G}}(N), \qquad N \in \mathbb{N}. \tag{6.42}
$$

In order to determine the degrees N for which the efficiency is greater or equal to one, cf. (6.12), it is sufficient to consider only the positive values of the difference (6.42) for $N = 2, \ldots, 3|\mathcal{G}| + 1$, and the assertions (6.36), (6.37) can be easily checked for the rotation groups $\mathcal{G} = \mathrm{C}_4, \mathrm{T}, \mathrm{O}, \mathrm{I}$.

For the inversion group $\overline{\mathrm{C}}_1$ we consider only the case for odd degrees of exactness N. In that case we find with the relations (6.38), (6.39), the definition (6.35), and Theorem (6.11) that

$$
M = 2M_{\mathrm{gen}} = \frac{1}{3}(4k^2+6k+2) + r_{\overline{\mathrm{C}}_1}(k), \qquad N := 2k+1, \quad k \in \mathbb{N},
$$

where $r_{\overline{\mathrm{C}}_1} : \mathbb{N} \to \mathbb{R}$ is three periodic, i.e., $r_{\overline{\mathrm{C}}_1}(k) = r_{\overline{\mathrm{C}}_1}(k+3)$, $k \in \mathbb{N}$. Hence, we obtain together

with (6.40) the relation

$$\left\lceil \frac{(N+1)^2+3}{3} \right\rceil - M = \frac{2}{3}(k+1) + r(2k+1) - r_{\overline{\mathrm{C}}_1}(k), \qquad k \in \mathbb{N},$$

which equals $1 + 2\lfloor (2k-1)/6 \rfloor$, $k \in \mathbb{N}$, and the remaining assertion in (6.36) follows. ■

Remark 6.14. Under the assumption that the size M of the invariant quadrature functionals described in Theorem 6.13 is sufficient and necessary, then the most efficient quadrature functionals we find by inspection of (6.36), (6.37) are given for odd degrees of exactness $N = 2k+1$, $k \in \mathbb{N}_0$, by quadrature functionals invariant under the inversion group $\overline{\mathrm{C}}_1$. For even degrees of exactness $N = 2k$, $k \in \mathbb{N}$, the most efficient quadrature functional are invariant under the cyclic group C_4 for $N \equiv 0, 4 \mod 6$, and under the tetrahedral group T for $N \equiv 2 \mod 6$. Moreover, for $N \equiv 14 \mod 30$ the most efficient quadrature functionals are invariant under the icosahedral group I.

Numerical results indicate that the given assumptions may be true in the most cases, cf. Table 6.1. We found only one exception for the degree of exactness $N = 11$, where we are not able to present a quadrature functional of size $M = 46$, cf. (6.35). However, we found a quadrature functional of size $M = 48$ which is invariant under the octahedral group O, cf. (6.33), which has by Theorem 6.13 an efficiency greater than one. Indeed, that particular quadrature functional has been already constructed in [102]. □

6.2.2 Spherical t-Designs

Delsarte, Goethals, and Seidel [32] introduced the concept of a spherical design, which in our notation corresponds to the set of quadrature points of an equal weights quadrature functional on the sphere $\mathbb{S}^d$. The study of spherical designs has been attracted a lot attention in several fields of mathematics. For a nice survey on spherical designs and related topics we refer to [10].

A point set $\mathcal{X}_M = \{\boldsymbol{p}_1, \ldots, \boldsymbol{p}_M\} \subset \mathbb{S}^d$, $M \in \mathbb{N}$, is called a *spherical t-design*, $t \in \mathbb{N}_0$, if it satisfies

$$\frac{1}{\omega_d} \int_{\mathbb{S}^d} f(\boldsymbol{x}) \mathrm{d}\mu_{\mathbb{S}^d}(\boldsymbol{x}) = \frac{1}{M} \sum_{i=1}^{M} f(\boldsymbol{p}_i), \qquad f \in \Pi^t(\mathbb{S}^d), \tag{6.43}$$

where $\mu_{\mathbb{S}^d}$ is the canonical measure of the sphere $\mathbb{S}^d$ and $\omega_d := \mu_{\mathbb{S}^d}(\mathbb{S}^d)$. Hence, by comparing the condition (6.43) with the classical quadrature condition (6.6), a spherical t-design $\mathcal{X}_M = \{\boldsymbol{p}_1, \ldots, \boldsymbol{p}_M\} \subset \mathbb{S}^d$ can be considered as an equal weights quadrature functional $Q_\nu(\boldsymbol{P})$, $\boldsymbol{P} := (\boldsymbol{p}_1, \ldots, \boldsymbol{p}_M) \in (\mathbb{S}^d)^M$, cf. (2.33), with degree of exactness $N = t$, where $\nu := \frac{1}{\omega_d}\mu_{\mathbb{S}^d}$. In this section we write for convenience $Q(\boldsymbol{P}) = Q_\nu(\boldsymbol{P})$ since the measure ν is fixed.

Remark 6.15. In contrast to quadrature functionals with general weights and degree of exactness $N = t$, it is not obvious that spherical t-designs do exist for every $t \in \mathbb{N}_0$, cf. Theorem 6.1. The first proof for the existence of spherical t-designs for every $t \in \mathbb{N}_0$ was presented in [116]. However, this proof is nonconstructive and gives no bound on the number of points needed. Later on, several authors presented upper bounds, cf. [136, 8, 76], which culminated in the recently proved optimal asymptotic of the minimal number M of points of a spherical t-designs. More precisely, it is shown in [15] that for fixed dimension $d \in \mathbb{N}$ there exists a constants $C_d > 0$ such that for $M \leq C_d t^d$ there is a spherical t-design $\mathcal{X}_M$ of cardinality M. Indeed, this bound is asymptotically optimal since a spherical t-design must have cardinality at least $M \geq c_d t^d$ for some constant $c_d > 0$, cf. [32]. Moreover, the numerical results of [62] and Table 6.2 provide us with evidence that on the sphere $\mathbb{S}^2$ numerical t-designs might exist for $M = \frac{1}{2}t^2 + o(1)$ for $t \to \infty$. □

In what follows, we restrict our attention to the sphere $\mathbb{S}^2$ and stick to the notation of equal weights quadrature functionals $Q(\boldsymbol{P})$ with degree of exactness N, where we keep in mind that these are equivalent to spherical t-designs with $t = N$. By Remark 6.15 we have theoretical foundation that equal weights quadrature functionals $Q(\boldsymbol{P})$ with degree of exactness N do exists for any $N \in \mathbb{N}_0$. For the numerical computation of such quadrature functionals we proceed as in the case of quadrature functionals with general weights, cf. (6.6). That is, we aim to minimize the squared worst case quadrature error, cf. (6.8), which simplifies to[4]

$$E_N(\boldsymbol{P}) := \frac{1}{M^2} \sum_{n=1}^{N} \sum_{k=-n}^{n} \Big| \sum_{i=1}^{M} \overline{Y}_{n,k}(\boldsymbol{p}_i) \Big|^2 = \operatorname{err}_{K_N}(\nu, \boldsymbol{P})^2, \qquad \boldsymbol{P} := (\boldsymbol{p}_1, \dots, \boldsymbol{p}_M) \in (\mathbb{S}^2)^M. \tag{6.44}$$

In order to estimate the number M of quadrature points needed for a polynomial degree of exactness $N \in \mathbb{N}_0$, we introduce the efficiency for equal weights quadrature functionals $Q(\boldsymbol{P})$ on the sphere $\mathbb{S}^2$ as, cf. (6.11),

$$\operatorname{eff}_{\mathbb{S}^2}(Q(\boldsymbol{P})) := \frac{\lceil (N+1)^2 + 2 \rceil_2}{2M} = \begin{cases} \frac{(N+1)^2+2}{2M}, & N \equiv 1 \mod 2, \\ \frac{(N+1)^2+3}{2M}, & N \equiv 0 \mod 2, \end{cases} \qquad N \in \mathbb{N}, \quad M \geq 2, \tag{6.45}$$

which is motivated like the efficiency defined by (6.10), i.e., we try to match the $2M$ degrees of freedom with the $(N+1)^2 - 1$ conditions imposed by (6.43). That means, there might exist equal weights quadrature functionals $Q(\boldsymbol{P})$ with efficiency $\operatorname{eff}_{\mathbb{S}^2}(Q(\boldsymbol{P})) = 1$. Moreover, by the use of groups acting on the sphere $\mathbb{S}^2$ one might construct for any $N \in \mathbb{N}$ equal weights quadrature functionals with $\operatorname{eff}_{\mathbb{S}^2}(Q(\boldsymbol{P})) > 1$, cf. Theorem 6.16. From Remark 6.15 we know that there exists a lower bound $c > 0$ such that $\operatorname{eff}_{\mathbb{S}^2}(Q(\boldsymbol{P})) \geq c$ can be achieved for any degree $N \in \mathbb{N}$.

The numerical results given in [62] provide evidence that equal weights quadrature functionals with a minimal number of points are likely to be invariant under certain orthogonal groups. Therefore, we will apply the same ideas from the previous section, and look for the most efficient equal weights quadrature functionals invariant under the groups $\overline{\mathrm{C}}_1, \mathrm{C}_4, \mathrm{T}, \mathrm{O}, \mathrm{I}$, cf. (6.28), (6.27), and (6.26). We recall that for a rotation group $\mathcal{G} \in \{\mathrm{T}, \mathrm{O}, \mathrm{I}\}$ the invariant quadrature functionals can be written as, cf. (6.29),

$$Q_{\mathcal{G}}(\boldsymbol{P}) := \frac{1}{M} \left(\sum_{i=1}^{M_{\mathrm{gen}}} \sum_{\boldsymbol{G} \in \mathcal{G}} I_{\delta_{\boldsymbol{G}\boldsymbol{p}_i}} + \sum_{\boldsymbol{p}_{\mathrm{v}} \in \mathcal{G}_{\mathrm{v}}} I_{\delta_{\boldsymbol{p}_{\mathrm{v}}}} + \sum_{\boldsymbol{p}_{\mathrm{f}} \in \mathcal{G}_{\mathrm{f}}} I_{\delta_{\boldsymbol{p}_{\mathrm{f}}}} + \sum_{\boldsymbol{p}_{\mathrm{e}} \in \mathcal{G}_{\mathrm{e}}} I_{\delta_{\boldsymbol{p}_{\mathrm{e}}}} \right), \qquad \boldsymbol{p}_i \in \mathbb{S}^2 \setminus (\mathcal{G}_{\mathrm{v}} \cup \mathcal{G}_{\mathrm{f}} \cup \mathcal{G}_{\mathrm{e}}), \tag{6.46}$$

with $\boldsymbol{p}_i \notin \mathcal{G}\boldsymbol{p}_j$, $i \neq j$, $i, j = 1, \dots, M_{\mathrm{gen}}$, where $M := |\mathcal{G}| M_{\mathrm{gen}} + M_{\mathrm{fix}}$ is the size of the quadrature functional. For the cyclic group C_k we find, cf. (6.30),

$$Q_{\mathrm{C}_k}(\boldsymbol{P}) := \frac{1}{M} \left(\sum_{i=1}^{M_{\mathrm{gen}}} \sum_{\boldsymbol{G} \in \mathrm{C}_k} I_{\delta_{\boldsymbol{G}\boldsymbol{p}_i}} + I_{\delta_{(0,0,1)^\top}} + \delta_{(0,0,-1)^\top} \right), \qquad \boldsymbol{p}_i \in \mathbb{S}^2 \setminus \{(0,0,\pm 1)^\top\}, \tag{6.47}$$

with $\boldsymbol{p}_i \notin \mathrm{C}_k \boldsymbol{p}_j$ for $i \neq j$, $i, j = 1, \dots, M_{\mathrm{gen}}$, and $M := k M_{\mathrm{gen}} + M_{\mathrm{fix}}$. Whereas for the inversion group $\overline{\mathrm{C}}_1$ it is, cf. (6.31),

$$Q_{\overline{\mathrm{C}}_1}(\boldsymbol{P}) := \frac{1}{M} \sum_{i=1}^{M_{\mathrm{gen}}} (I_{\delta_{\boldsymbol{p}_i}} + I_{\delta_{-\boldsymbol{p}_i}}), \qquad \boldsymbol{p}_i \in \mathbb{S}^2, \tag{6.48}$$

[4] In [118] the function E_N is also used for a variational characterization of spherical t-designs.

with $\boldsymbol{p}_i \notin \{\pm \boldsymbol{p}_j\}$ for $i \neq j$, $i, j = 1, \ldots, M_{\text{gen}}$, and $M := 2M_{\text{gen}}$.

In contrast to general quadrature functionals, we observe that for the equal weights quadrature functionals (6.46) and (6.30) the special sets determined by M_{fix} provide no additional degree of freedom since the weights have been already chosen. Therefore, we try to omit the special sets, since we are particular interested in the most efficient quadrature functionals. However, numerical investigation indicates that for quadrature functionals invariant under the icosahedral group I the special set I_{v} is apparently needed.

From these observations we consider for the rotation group $\mathcal{G} \in \{\mathrm{T}, \mathrm{O}, \mathrm{I}\}$ only equal weights quadrature functionals of the form (6.46) which are determined by

$$M_{\text{gen}} := \left\lceil \frac{d_{\mathcal{G}}^N - 1}{2} \right\rceil, \qquad M_{\text{fix}} := \begin{cases} 12, & \mathcal{G} = \mathrm{I}, \\ 0, & \text{else}, \end{cases} \qquad N \in \mathbb{N}, \quad N \geq 4. \tag{6.49}$$

We note that for $N = t = 2, 3$ the special point sets T_{v}, O_{v}, are spherical t-designs by Theorem 6.12, respectively, which are exceptional in the sense that they do not fit into the classes of equal weight quadrature functionals determined by (6.49). For the groups C_4, $\overline{\mathrm{C}}_1$ we will consider only the equal weights quadrature functionals (6.47), (6.48) which are determined by

$$M_{\text{gen}} := \left\lceil \frac{d_{\mathrm{C}_4}^N}{2} \right\rceil, \qquad M_{\text{fix}} := 0, \qquad N \in \mathbb{N}, \tag{6.50}$$

and

$$M_{\text{gen}} := \begin{cases} 1, & N = 1, \\ \left\lceil \frac{d_{\overline{\mathrm{C}}_1}^N + 2}{2} \right\rceil, & N \geq 2, \end{cases} \qquad M_{\text{fix}} := 0, \qquad N \in \mathbb{N}, \tag{6.51}$$

respectively.

Theorem 6.16. *Let the sphere* $\mathbb{S}^2$ *and* $N \in \mathbb{N}$ *with* $N \geq 4$ *be given. If there exists an equal weights quadrature functional* $Q_{\mathcal{G}}(\boldsymbol{P})$, $\boldsymbol{P} \in (\mathbb{S}^2)^M$, *with degree of exactness* N, *which is invariant under the group* $\mathcal{G} \in \{\overline{\mathrm{C}}_1, \mathrm{C}_4, \mathrm{T}, \mathrm{O}, \mathrm{I}\}$, *and has size* $M = |\mathcal{G}| M_{\text{gen}} + M_{\text{fix}}$ *determined by* (6.51), (6.50), (6.49), *respectively, then the efficiency is, cf.* (6.45),

$$\begin{aligned}
\operatorname{eff}_{\mathbb{S}^2}(Q_{\overline{\mathrm{C}}_1}(\boldsymbol{P})) &\begin{cases} = 1 + \frac{2+4\lfloor (N-2)/4 \rfloor}{(N+1)^2 - 4\lfloor (N-2)/4 \rfloor}, & N \equiv 1 \mod 2, \\ < 1, & \textit{else}, \end{cases} \\
\operatorname{eff}_{\mathbb{S}^2}(Q_{\mathrm{C}_4}(\boldsymbol{P})) &\begin{cases} = 1 + \frac{2}{(N+1)^2}, & N \equiv 3 \mod 4, \\ < 1, & \textit{else}, \end{cases} \\
\operatorname{eff}_{\mathbb{S}^2}(Q_{\mathrm{T}}(\boldsymbol{P})) &\begin{cases} = 1 + \frac{14}{(N+1)^2 - 12}, & N \equiv 5 \mod 12, \\ = 1 + \frac{12}{(N+1)^2 - 9}, & N \equiv 2, 8 \mod 12, \\ = 1 + \frac{6}{(N+1)^2 - 4}, & N \equiv 1, 9 \mod 12, \\ = 1 + \frac{4}{(N+1)^2 - 1}, & N \equiv 0, 4, 6, 10 \mod 12, \\ = 1 + \frac{2}{(N+1)^2}, & N \equiv 11 \mod 12, \\ < 1, & \textit{else}, \end{cases}
\end{aligned} \tag{6.52}$$

$$\begin{aligned}
\operatorname{eff}_{\mathbb{S}^2}(Q_{\mathrm{O}}(\boldsymbol{P}))\begin{cases} = 1 + \frac{18}{(N+1)^2-16}, & N \equiv 3,7 \mod 12, \\ = 1 + \frac{12}{(N+1)^2-9}, & N \equiv 2,20 \mod 24, \\ = 1 + \frac{6}{(N+1)^2-4}, & N \equiv 1,9 \mod 12, \\ = 1 + \frac{4}{(N+1)^2-1}, & N \equiv 0,6,16,22 \mod 24, \\ = 1 + \frac{2}{(N+1)^2}, & N \equiv 11,23 \mod 24, \\ < 1, & \text{else}, \end{cases} \\
\operatorname{eff}_{\mathbb{S}^2}(Q_{\mathrm{I}}(\boldsymbol{P}))\begin{cases} = 1 + \frac{38}{(N+1)^2-36}, & N \equiv 29 \mod 60, \\ = 1 + \frac{18}{(N+1)^2-16}, & N \equiv 19,39 \mod 60, \\ = 1 + \frac{14}{(N+1)^2-12}, & N \equiv 5,53 \mod 60, \\ = 1 + \frac{4}{(N+1)^2-1}, & N \equiv 4,24 \mod 30, \\ = 1 + \frac{2}{(N+1)^2}, & N \equiv 11,47 \mod 60, \\ < 1, & \text{else}, \end{cases}
\end{aligned} \tag{6.53}$$

respectively.

Proof. The assertions (6.52) and (6.53) can be proved as those of Theorem 6.13. ■

Remark 6.17. Under the assumption that the size M of the invariant equal weights quadrature functionals described in Theorem 6.16 is sufficient and necessary, then the most efficient equal weights quadrature functionals we find by inspection of (6.52), (6.53) are given for odd degrees of exactness $N = 2k+1$, $k \in \mathbb{N}_0$, by quadrature functionals invariant under the group $\overline{\mathrm{C}}_1$ with some exceptions for small N. More precisely, for $N = 7, 9, 15$ and for $N = 29$ the equal weights quadrature functionals invariant under the octahedral group O and the icosahedral group I are more efficient, respectively. For even degrees of exactness $N = 2k$, $k \in \mathbb{N}$, the most efficient equal weights quadrature functionals are all invariant under the tetrahedral group T. In particular, for $N \equiv 0, 2, 6, 16, 20, 22 \mod 24$ and $N \equiv 4, 24 \mod 30$ these quadratures are also invariant under the octahedral group O and the icosahedral group I, respectively.

Numerical results indicate that these assumptions may be true in the most cases, cf. Table 6.2. For the odd degrees of exactness we found only one exception for $N = 11$, where we are not able to present an equal weights quadrature functional of size $M = 68$, cf. (6.51). However, we found an equal weights quadrature functional invariant under the cyclic group C_5 of size $M = 70$. The corresponding spherical 11-design is also listed in [62]. For even degrees the only exceptional cases we encountered are for equal weights quadratures invariant under the octahedral group O and the icosahedral group I with degree of exactness $N = 16, 20$ and $N = 24$, respectively. All the other cases listed in Table 6.2 are found to satisfy the above given assumptions. □

6.2.3 Numerical Examples

In this section we present several numerical examples for the computation of classical quadrature functionals $Q(\boldsymbol{P}, \boldsymbol{w})$ of size $M \in \mathbb{N}$ with quadrature points $\boldsymbol{P} := (\boldsymbol{p}_1, \dots, \boldsymbol{p}_M) \in (\mathbb{S}^2)^M$ and quadrature weights $\boldsymbol{w} := (w_1, \dots, w_M)^\top \in \mathbb{R}^M$, and prescribed degree of exactness $N \in \mathbb{N}_0$ on the sphere $\mathbb{S}^2$, cf. (6.6). We recall that for a quadrature functional $Q(\boldsymbol{P}, \boldsymbol{w})$ and an equal weights quadrature functional $Q(\boldsymbol{P})$ with degree of exactness N the squared worst case quadrature error, cf. (6.8),

$$E_N(\boldsymbol{P}, \boldsymbol{w}) := \sum_{n=0}^{N} \sum_{k=-n}^{n} \left| \frac{1}{\sqrt{4\pi}} \delta_{0,n} - \sum_{i=1}^{M} w_i \overline{Y}_{n,k}(\boldsymbol{p}_i) \right|^2 \tag{6.54}$$

and the squared equal weights worst case quadrature error, cf. (6.44),

$$E_N(\boldsymbol{P}) := E_N(\boldsymbol{P}, (M^{-1}, \dots, M^{-1})) = \frac{1}{M^2} \sum_{n=1}^{N} \sum_{k=-n}^{n} \Big| \sum_{i=1}^{M} \overline{Y}_{n,k}(\boldsymbol{p}_i) \Big|^2 \tag{6.55}$$

vanishes, respectively. Note that the orthonormal spherical harmonics $Y_{n,k} : \mathbb{S}^2 \to \mathbb{C}$, $n \in \mathbb{N}_0$, $k = -n, \dots, n$, are defined in Section 5.2.2 by (5.39).

Hence, for the numerical computation of classical quadrature functionals $Q(\boldsymbol{P}, \boldsymbol{w})$ and $Q(\boldsymbol{P})$ we aim to minimize the functions $E_N(\boldsymbol{P}, \boldsymbol{w})$ and $E_N(\boldsymbol{P})$, respectively. For that reason we apply the nonlinear conjugate gradient method on Riemannian manifolds introduced in Section 3.3.1, since it is particular efficient in conjunction with fast matrix-vector multiplications with the Hessian and leads to very accurate results, which are needed for the computation of classical quadrature functionals. More precisely, we apply the Algorithm 3.3 and use the nonequispaced fast Fourier transforms on the sphere $\mathbb{S}^2$ for the evaluation of $E_N(\boldsymbol{P}, \boldsymbol{w})$, or $E_N(\boldsymbol{P})$, as well as its derivatives, cf. Section 5.2.2. In particular, we are able to compute by Corollary 5.22 every step in the CG method, cf. Algorithm 3.3, in $\mathcal{O}(N^2 \log^2(N) + M)$ arithmetic operations, which is much more efficient, especially for $M \approx N^2$, than the naive evaluation of the sole functions $E_N(\boldsymbol{P}, \boldsymbol{w})$, or $E_N(\boldsymbol{P})$, cf. (6.54), (6.55), with arithmetic complexity $\mathcal{O}(N^2 M)$. Moreover, we recall that quadrature functionals invariant under orthogonal groups are naturally incorporated by the proposed optimization method on Riemannian manifolds, cf. Corollary 6.9 and Remark 6.10. In addition to the default parameters of Algorithm 3.3 given in Remark 3.29 we use after the kth iteration the termination conditions

$$\frac{E_N(\boldsymbol{P}^{(k)}, \boldsymbol{w}^{(k)}) - E_N(\boldsymbol{P}^{(k+1)}, \boldsymbol{w}^{(k+1)})}{|E_N(\boldsymbol{P}^{(k)}, \boldsymbol{w}^{(k)})|} < 10^{-6}, \qquad \|\nabla_{(\mathbb{S}^2)^M \times \mathbb{R}^M} E_N(\boldsymbol{P}^{(k+1)}, \boldsymbol{w})\|_2 < 10^{-13},$$

and

$$\frac{E_N(\boldsymbol{P}^{(k)}) - E_N(\boldsymbol{P}^{(k+1)})}{|E_N(\boldsymbol{P}^{(k)})|} < 10^{-6}, \qquad \|\nabla_{(\mathbb{S}^2)^M} E_N(\boldsymbol{P}^{(k+1)})\|_2 < 10^{-13},$$

respectively.

The corresponding algorithms are implemented in C++ and utilize the Eigen template library [39], and the NFFT library [72]. For the NFSFT routines of the NFFT library we set the cutoff parameter $m = 7$ and the threshold parameter $\kappa = 1000$. The computations are performed on an Intel® Core™ i7 CPU 920 with 12 GB RAM.

The Example 6.18 and 6.19 shows that with the proposed optimization approach we are able to compute for moderate polynomial degrees of exactness $N \in \mathbb{N}_0$ very precise and highly efficient quadrature functionals $Q(\boldsymbol{P}, \boldsymbol{w})$ and $Q(\boldsymbol{P})$, respectively. As discussed in Remark 6.4 we are confronted with the problem that the functions $E_N(\boldsymbol{P}, \boldsymbol{w})$, $E_N(\boldsymbol{P})$ possess even for moderate numbers of points M and polynomial degrees N many local minimizers for which the functions do not vanish. Therefore, we propose in Example 6.18 and 6.19 a naive restart strategy in order to determine numerically a global minimum $(\boldsymbol{P}^*, \boldsymbol{w}^*) \in (\mathbb{S}^2)^M \times \mathbb{R}^M$ and $\boldsymbol{P}^{**} \in (\mathbb{S}^2)^M$ of the squared worst case quadrature error which satisfies

$$E_N(\boldsymbol{P}^*, \boldsymbol{w}^*) < 10^{-20} \qquad \text{and} \qquad E_N(\boldsymbol{P}^{**}) < 10^{-20}, \tag{6.56}$$

respectively. We just remark that the above bound on the squared worst case quadrature error E_N seems sufficient for the determination of a global minimum, at least for moderate polynomial degrees N. Finally, we observe in Example 6.20 that for the computation of equal weights quadrature functionals $Q(\boldsymbol{P})$ with efficiency $\mathrm{eff}_{\mathbb{S}^2}(Q(\boldsymbol{P}))$ slightly smaller than one, the convergence is much faster and there is no restart strategy needed for randomly distributed initial points, which

enables us to compute very efficient equal weights quadrature functionals with polynomial degree up to $N = 1000$, cf. Table 6.3.

Example 6.18. For selected polynomial degrees $N \leq 44$ we aim to compute the most efficient invariant quadrature functionals $Q_{\mathcal{G}}(\boldsymbol{P}, \boldsymbol{w})$, $\boldsymbol{P} \in (\mathbb{S}^2)^M$, $\boldsymbol{w} \in \mathbb{R}^M$, on the sphere $\mathbb{S}^2$ suggested by Theorem 6.13, where the group $\mathcal{G}$ is among the inversion group $\overline{\mathrm{C}}_1$, the tetrahedral group T, the octahedral group O, the icosahedral group I, and the cyclic groups C_k, $k = 3, 4, 5$, cf. (6.28), (6.26), (6.27). For that reason we consider only the configurations for the degree N, the size M and the group $\mathcal{G}$ given in Remark 6.14. We recall that is sufficient to initialize Algorithm 3.3 with quadrature points $\boldsymbol{P}^{(0)} \in (\mathbb{S}^2)^M$ and quadrature weights $\boldsymbol{w}^{(0)} \in \mathbb{R}^M$ which are invariant under the corresponding group $\mathcal{G}$, cf. Remark 6.10.

The task is now to compute, for such configurations, on the manifold $\mathcal{M} := (\mathbb{S}^2)^M \times \mathbb{R}^M$ a global minimizer $(\boldsymbol{P}^*, \boldsymbol{w}^*) \in \mathcal{M}$ of the squared worst case quadrature error $E_N : \mathcal{M} \to [0, \infty)$. Since, our computations are performed in double precision we are satisfied if the squared worst case quadrature error passes the test (6.56).

The search strategy is as follows. For prescribed polynomial degree N, size M, and group $\mathcal{G}$ we perform at most 100 runs of the following procedure. In order to start with almost uniformly distributed points, we begin to perform 10 CG iterations for randomly distributed initial points invariant under the group $\mathcal{G}$ with respect to the electrostatic energy

$$E(\boldsymbol{P}) := \sum_{\substack{i,j=1 \\ i \neq j}}^{M} \frac{1}{\|\boldsymbol{p}_i - \boldsymbol{p}_j\|_2}, \qquad \boldsymbol{P} := (\boldsymbol{p}_1, \ldots, \boldsymbol{p}_M) \in (\mathbb{S}^d)^M,$$

by using naive evaluation methods, which is reasonable for the given problem sizes. Afterward, the resulting point distribution is used for minimizing the squared equal weights worst case quadrature error $E_N(\boldsymbol{P})$, where we use at most 250 CG iterations. Finally, we optimize the obtained point distribution together with initial equal weights over the squared worst case quadrature error $E_N(\boldsymbol{P}, \boldsymbol{w})$, where the maximal number of CG iterations is 10000. For some computed local minimizers which have not passed the test (6.56), by too slow convergence, we tried another run of the CG method.

In Table 6.1 we present the summarized results, where we observed for several quadrature functionals higher symmetry groups. We like to mention that we recomputed several quadrature functionals constructed by Popov and McLaren with precision of at least 11 digits in the Cartesian coordinates of the quadrature points and weights. More precisely, besides the well-know equal weights quadrature functional with polynomial degree of exactness $N = 1, 2, 3, 5$ we find in [100] those for $N = 4, 6, 7, 17$, in [101] that for $N = 8$, in [102] that for $N = 11$, and in [89] those for polynomial degree $N = 9, 14$. All the remaining computed quadrature functionals seem to be new and improve the size of some other known constructions. The computed quadrature rules are publicly available at http://www.tu-chemnitz.de/~potts/workgroup/graef/quadrature/.

□

Example 6.19. For selected polynomial degrees $N \leq 124$ we aim to compute the most efficient invariant equal weights quadrature functionals $Q_{\mathcal{G}}(\boldsymbol{P})$, $\boldsymbol{P} \in (\mathbb{S}^2)^M$, on the sphere $\mathbb{S}^2$ suggested by Theorem 6.16, where the group $\mathcal{G}$ is among the inversion group $\overline{\mathrm{C}}_1$, the tetrahedral group T, the octahedral group O, the icosahedral group I, and the cyclic groups C_k, $k = 3, 4, 5$, cf. (6.28), (6.26), (6.27). For that reason we consider only the configurations for the degree N, the size M and the group $\mathcal{G}$ given in Remark 6.17. We recall that is sufficient to initialize Algorithm 3.3 with quadrature points $\boldsymbol{P}^{(0)} \in (\mathbb{S}^2)^M$ which are invariant under the corresponding group $\mathcal{G}$, cf. Remark 6.10.

N	M	$\mathcal{E}$	$\mathcal{G}$	N	M	$\mathcal{E}$	$\mathcal{G}$	N	M	$\mathcal{E}$	$\mathcal{G}$
1	2	$1+\frac{1}{2}$	$\overline{\mathrm{C}}_1$	14	72	$1+\frac{4}{72}$	I	27	254	$1+\frac{9}{254}$	$\overline{\mathrm{C}}_3$
2	4	1	$\overline{\mathrm{T}}$	15	82	$1+\frac{5}{82}$	$\overline{\mathrm{C}}_5$	28	282	1	C_4
3	6	$1+\frac{1}{6}$	$\overline{\mathrm{O}}$	16	98	1	C_4	29	292	$1+\frac{9}{292}$	$\overline{\mathrm{C}}_5$
4	10	1	C_4	17	104	$1+\frac{5}{104}$	$\overline{\mathrm{C}}_3$	30	322	1	C_4
5	12	$1+\frac{1}{12}$	$\bar{\mathrm{I}}$	18	122	1	C_4	32	364	1	T
6	18	1	C_4	19	130	$1+\frac{5}{130}$	$\overline{\mathrm{C}}_1$	34	410	1	C_4
7	22	$1+\frac{1}{22}$	$\overline{\mathrm{C}}_4$	20	148	1	T	35	422	$1+\frac{11}{422}$	$\overline{\mathrm{C}}_5$
8	28	1	T	21	156	$1+\frac{7}{156}$	$\overline{\mathrm{C}}_3$	36	458	1	C_4
9	32	$1+\frac{3}{32}$	$\bar{\mathrm{I}}$	22	178	1	C_4	37	472	$1+\frac{11}{472}$	$\overline{\mathrm{C}}_5$
10	42	1	C_4	23	186	$1+\frac{7}{186}$	$\overline{\mathrm{C}}_3$	38	508	1	T
11	48	$1+\frac{1}{48}$	O	24	210	1	C_4	39	522	$1+\frac{13}{522}$	$\overline{\mathrm{C}}_5$
12	58	1	C_4	25	220	$1+\frac{7}{220}$	$\overline{\mathrm{C}}_1$	44	672	$1+\frac{4}{672}$	I
13	64	$1+\frac{3}{64}$	$\overline{\mathrm{C}}_1$	26	244	1	T				

Table 6.1: The putatively most efficient quadrature functionals $Q(\boldsymbol{P},\boldsymbol{w})$, $\boldsymbol{P}\in(\mathbb{S}^2)^M$, $\boldsymbol{w}\in\mathbb{R}^M$, invariant under the inversion group $\overline{\mathrm{C}}_1$, the tetrahedral group T, the octahedral group O, the icosahedral group I, and the cyclic groups C_k, $k=3,4,5$, with prescribed degree of exactness N are listed. M denotes the size of the quadrature functional $Q(\boldsymbol{P},\boldsymbol{w})$ and $\mathcal{E}:=\mathrm{eff}_{\mathbb{S}^2}(Q(\boldsymbol{P},\boldsymbol{w}))$ its efficiency defined by (6.12). $\mathcal{G}$ denotes the group under which the computed quadrature functionals are invariant, cf. (6.18). The quadrature functionals are found numerically and have a squared worst case quadrature error of $E_N(\boldsymbol{P},\boldsymbol{w})<$ 1e-20, cf. (6.54). For details see Example 6.18.

The task is now to compute, for such configurations, on the manifold $\mathcal{M}:=(\mathbb{S}^2)^M$ a global minimizer $\boldsymbol{P}^{**}\in\mathcal{M}$ of the squared worst case quadrature error $E_N:\mathcal{M}\to[0,\infty)$. Since, our computations are performed in double precision we are satisfied if the squared worst case quadrature error passes the test (6.56).

The search strategy is as follows. For prescribed polynomial degree N, size M, and group $\mathcal{G}$ we perform at most 150 runs of the CG method applied to the squared equal weights worst case quadrature error $E_N(\boldsymbol{P})$ of uniformly distributed initial points invariant under the group $\mathcal{G}$. For some computed local minimizers which have not passed the test (6.56), by too slow convergence, we tried another run of the CG method.

In Table 6.2 we present the summarized results, where we observed for several quadrature functionals higher symmetry groups. We like to mention that Hardin and Sloane [62] computed numerically spherical t-designs up to degree $t\le 24$, and proved the existence of the 9-design, for which we are able to compute the Cartesian coordinates of the points with precision of at least 11 digits. Moreover, we improved the size of the 15-,19-,21-, and 23-designs. The remaining equal weights quadrature functionals seem to be new and improve the size of some other known constructions. The computed quadrature rules are publicly available at http://www.tu-chemnitz.de/~potts/workgroup/graef/quadrature/. □

Example 6.20. We aim to illustrate that the proposed optimization approach is also applicable for the computation of equal weights quadrature functionals $Q(\boldsymbol{P})$, $\boldsymbol{P}\in(\mathbb{S}^2)^M$, on the sphere $\mathbb{S}^2$ with polynomial degree of exactness up to $N=1000$. In contrast to the previous examples, where we tried to compute quadrature functionals $Q(\boldsymbol{P})$ with efficiency $\mathrm{eff}_{\mathbb{S}^2}(Q(\boldsymbol{P}))\ge 1$, we consider slightly less efficient quadrature functionals. Since we allow the quadrature functionals to have more quadrature points than assumed to be needed, we might increase the chance of finding a

N	M	$\mathcal{E}$	$\mathcal{G}$	N	M	$\mathcal{E}$	$\mathcal{G}$	N	M	$\mathcal{E}$	$\mathcal{G}$
1	2	$1+\frac{1}{2}$	$\overline{\mathrm{C}}_1$	26	360	$1+\frac{6}{360}$	O	56	1620	$1+\frac{6}{1620}$	T
2	4	$1+\frac{2}{4}$	$\overline{\mathrm{T}}$	27	380	$1+\frac{13}{380}$	$\overline{\mathrm{C}}_3$	58	1740	$1+\frac{2}{1740}$	T
3	6	$1+\frac{3}{6}$	$\overline{\mathrm{O}}$	28	420	$1+\frac{2}{420}$	T	60	1860	$1+\frac{2}{1860}$	T
5	12	$1+\frac{7}{12}$	$\bar{\mathrm{I}}$	29	432	$1+\frac{19}{432}$	I	62	1980	$1+\frac{6}{1980}$	T
7	24	$1+\frac{9}{24}$	O	30	480	$1+\frac{2}{480}$	O	64	2112	$1+\frac{2}{2112}$	I
8	36	$1+\frac{6}{36}$	T	31	498	$1+\frac{15}{498}$	$\overline{\mathrm{C}}_3$	66	2244	$1+\frac{2}{2244}$	T
9	48	$1+\frac{3}{48}$	O	32	540	$1+\frac{6}{540}$	T	68	2376	$1+\frac{6}{2376}$	O
10	60	$1+\frac{2}{60}$	T	33	564	$1+\frac{15}{564}$	$\overline{\mathrm{C}}_3$	70	2520	$1+\frac{2}{2520}$	O
11	70	$1+\frac{3}{70}$	C_5	34	612	$1+\frac{2}{612}$	I	72	2664	$1+\frac{2}{2664}$	O
12	84	$1+\frac{2}{84}$	T	35	632	$1+\frac{17}{632}$	$\overline{\mathrm{C}}_3$	74	2808	$1+\frac{6}{2808}$	O
13	94	$1+\frac{5}{94}$	$\overline{\mathrm{C}}_1$	36	684	$1+\frac{2}{684}$	T	76	2964	$1+\frac{2}{2964}$	T
14	108	$1+\frac{6}{108}$	T	37	706	$1+\frac{17}{706}$	$\overline{\mathrm{C}}_1$	78	3120	$1+\frac{2}{3120}$	O
15	120	$1+\frac{9}{120}$	O	38	756	$1+\frac{6}{756}$	T	82	3444	$1+\frac{2}{3444}$	T
16	144	$1+\frac{2}{144}$	T	39	782	$1+\frac{19}{782}$	$\overline{\mathrm{C}}_3$	84	3612	$1+\frac{2}{3612}$	I
17	156	$1+\frac{7}{156}$	T	40	840	$1+\frac{2}{840}$	O	86	3780	$1+\frac{6}{3780}$	T
18	180	$1+\frac{2}{180}$	T	41	864	$1+\frac{19}{864}$	$\overline{\mathrm{C}}_3$	88	3960	$1+\frac{2}{3960}$	O
19	192	$1+\frac{9}{192}$	$\overline{\mathrm{C}}_3$	42	924	$1+\frac{2}{924}$	T	90	4140	$1+\frac{2}{4140}$	T
20	216	$1+\frac{6}{216}$	T	44	1008	$1+\frac{6}{1008}$	O	94	4512	$1+\frac{2}{4512}$	I
21	234	$1+\frac{9}{234}$	$\overline{\mathrm{C}}_3$	46	1104	$1+\frac{2}{1104}$	O	98	4896	$1+\frac{6}{4896}$	O
22	264	$1+\frac{2}{264}$	O	48	1200	$1+\frac{2}{1200}$	O	100	5100	$1+\frac{2}{5100}$	T
23	278	$1+\frac{11}{278}$	$\overline{\mathrm{C}}_3$	50	1296	$1+\frac{6}{1296}$	O	114	6612	$1+\frac{2}{6612}$	I
24	312	$1+\frac{2}{312}$	O	52	1404	$1+\frac{2}{1404}$	T	124	7812	$1+\frac{2}{7812}$	I
25	328	$1+\frac{11}{328}$	$\overline{\mathrm{C}}_1$	54	1512	$1+\frac{2}{1512}$	I				

Table 6.2: The putatively most efficient equal weights quadrature functionals $Q(\boldsymbol{P})$, $\boldsymbol{P} \in (\mathbb{S}^2)^M$, invariant under the inversion group $\overline{\mathrm{C}}_1$, the tetrahedral group T, the octahedral group O, the icosahedral group I, and the cyclic groups C_k, $k = 3, 4, 5$, with prescribed degree of exactness N are listed. M denotes the size of the equal weights quadrature functional $Q(\boldsymbol{P})$ and $\mathcal{E} := \mathrm{eff}_{\mathbb{S}^2}(Q(\boldsymbol{P}))$ its efficiency defined by (6.45). $\mathcal{G}$ denotes the group under which the computed quadrature functionals are invariant, cf. (6.18). The quadrature functionals are found numerically and have a squared worst case quadrature error of $E_N(\boldsymbol{P}) <$ 1e-20, cf. (6.55). For details see Example 6.19.

N	M	$\mathcal{E}$	$E_N(\boldsymbol{P}^{(k)})$	$\left\|\nabla_{(\mathbb{S}^2)^M} E_N(\boldsymbol{P}^{(k)})\right\|_2$	iteration k	time
100	5200	0.98	9.8e-23	9.8e-14	4211	27 minutes
200	21000	0.96	1.7e-23	9.9e-14	2597	1 hour
500	130000	0.97	9.9e-23	9.9e-14	5394	21 hours
500	260000	0.48	5.6e-23	9.9e-14	2985	14 hours
1000	520000	0.96	9.6e-22	1.8e-13	10600	10 days
1000	1002000	0.50	9.4e-23	9.8e-14	4286	5 days

Table 6.3: Performance results of the CG method, cf. Algorithm 3.3, in conjunction with the nonequispaced fast Fourier transforms on the sphere $\mathbb{S}^2$, cf. Section 5.2.2, for the computation of equal weights quadrature functionals $Q(\boldsymbol{P})$, $\boldsymbol{P} \in (\mathbb{S}^2)^M$, with high polynomial degrees of exactness N, by minimizing the squared worst case quadrature error $E_N(\boldsymbol{P})$, cf. (6.55), for randomly distributed initial points $\boldsymbol{P}^{(0)} \in (\mathbb{S}^2)^M$, where the efficiency is denoted by $\mathcal{E} := \mathrm{eff}_{\mathbb{S}^2}(Q(\boldsymbol{P}))$.

global minimum. Indeed, the numerical results indicate that it is much easier to find numerically equal weights quadrature functionals with an efficiency less than one, such that we do not need any restart strategy as proposed in Example 6.19.

We apply the CG method to the squared equal weights quadrature error $E_N(\boldsymbol{P})$, cf. (6.55), with randomly distributed initial points $\boldsymbol{P}^{(0)} \in (\mathbb{S}^2)^M$, for polynomial degrees $N = 100, 200, 500, 10000$ and selected numbers of quadrature points $M \in \mathbb{N}$. The results are illustrated in Table 6.3 and have been already published in [57]. There we observe faster convergence of the CG method for a prescribed polynomial degree N if the size M of the quadrature functional is increased.

Finally, we emphasize that in view of the classical quadrature problem (6.6) we should keep in mind that we have to solve for polynomial degree $N = 1000$ and size $M = 520000$ a linear system with about one million equations and unknowns, cf. (6.7). The computed quadrature rules are publicly available at http://www.tu-chemnitz.de/~potts/workgroup/graef/quadrature/. □

6.3 Classical Quadrature Problems on the Rotation Group SO(3)

For the rotation group $X := \mathrm{SO}(3)$ we consider the classical quadrature condition (6.1) with respect to the normalized canonical measure $\nu := \frac{8\pi^2}{\mu_{\mathrm{SO}(3)}}$ and the harmonic spaces $\Pi^N(\mathrm{SO}(3))$, $N \in \mathbb{N}_0$, cf. Section 4.3, i.e.,

$$\frac{1}{8\pi^2} \int_{\mathrm{SO}(3)} f(\boldsymbol{R}) \mathrm{d}\mu_{\mathrm{SO}(3)}(\boldsymbol{R}) = \sum_{i=1}^{M} w_i f(\boldsymbol{R}_i), \qquad f \in \Pi^N(\mathrm{SO}(3)), \tag{6.57}$$

where $\boldsymbol{R}_i \in \mathrm{SO}(3)$ and $w_i \in \mathbb{R}$, $i = 1, \ldots, M$. As in the case of the sphere $\mathbb{S}^d$, we will call N the degree of exactness of a quadrature functional $Q(\boldsymbol{P}, \boldsymbol{w})$, $\boldsymbol{P} := (\boldsymbol{R}_1, \ldots, \boldsymbol{R}_M) \in (\mathrm{SO}(3))^M$ if the condition (6.57) is satisfied. Since the Wigner D-functions $D^n_{k,k'}$, $n = 0, \ldots, N$, $k, k' = -n, \ldots, n$, cf. (4.51), form an orthogonal basis of $\Pi^N(\mathrm{SO}(3))$ with respect to the L^2-product induced by the measure $\mu_{\mathrm{SO}(3)}$, we find that quadrature functionals satisfying (6.57) are exactly determined by the solutions $\boldsymbol{R}_i \in \mathrm{SO}(3)$, $w_i \in \mathbb{R}$, $i = 1, \ldots, M$, of the system of nonlinear equations

$$\sum_{i=1}^{M} w_i D^n_{k,k'}(\boldsymbol{R}_i) = \delta_{n,0}, \qquad n = 0, \ldots, N, \quad k, k' = -n, \ldots, n. \tag{6.58}$$

We recall that the Wigner D-functions are normalized by $\|D^n_{k,k'}\|^2_{L^2(\mathrm{SO}(3))} = 8\pi^2/(2n+1)$, cf. (4.52). Hence, the objective function of the associated weighted least squares problem reads as, cf. (5.2),

$$E_N(\boldsymbol{P},\boldsymbol{w}) := \sum_{n=0}^{N} \frac{2n+1}{8\pi^2} \sum_{k,k'=-n}^{n} \left| \delta_{n,0} - \sum_{i=1}^{M} w_i \overline{D}^n_{k,k'}(\boldsymbol{R}_i) \right|^2 = \mathrm{err}_{K_N}(\nu,\boldsymbol{P},\boldsymbol{w})^2, \tag{6.59}$$

which is exactly the squared worst case quadrature error between the integral functional I_ν and the quadrature functional $Q(\boldsymbol{P},\boldsymbol{w})$ in the reproducing kernel Hilbert space $\Pi^N(\mathrm{SO}(3))$, $N \in \mathbb{N}_0$, equipped with the usual L^2-product induced by the canonical measure $\mu_{\mathrm{SO}(3)}$, cf. Theorem 2.7. As in the case of the sphere $\mathbb{S}^d$, we aim to minimize the squared worst case quadrature error $E_N(\boldsymbol{P},\boldsymbol{w})$ for the numerical computation of quadrature points $\boldsymbol{P} \in (\mathrm{SO}(3))^M$ and quadrature weights $\boldsymbol{w} \in \mathbb{R}^M$ satisfying the classical quadrature condition (6.57). For details we refer to the numerical examples of Section 6.3.3.

We recall from Section 4.3.2 that it is useful to identify the rotation group $\mathrm{SO}(3)$ with the quotient space $\mathbb{S}^3_* = \mathbb{S}^3/\{-1,1\}$, cf. (4.61), via the isomorphism $\boldsymbol{q}_* : \mathrm{SO}(3) \to \mathbb{S}^3_*$ defined by (4.62), where a rotation $\boldsymbol{R} \in \mathrm{SO}(3)$ corresponds to a set of antipodal points $\boldsymbol{q}_*(\boldsymbol{R}) = \{\pm\boldsymbol{x}\} \in \mathbb{S}^3_*$, $\boldsymbol{x} \in \mathbb{S}^3$. Moreover, for $n \in \mathbb{N}_0$ the harmonic spaces $\Pi_n(\mathrm{SO}(3))$ on the rotation group $\mathrm{SO}(3)$ are in one-to-one correspondence with the harmonic spaces $\Pi_{2n}(\mathbb{S}^3)$ on the sphere $\mathbb{S}^3$, cf. Theorem 4.7. Together with the correspondence between the canonical measure $\mu_{\mathrm{SO}(3)}$ and $\mu_{\mathbb{S}^3}$, cf. (4.67), we find the following result, which relates classical quadrature functionals on the rotation group $\mathrm{SO}(3)$ with classical quadrature functionals on the sphere $\mathbb{S}^3$.

Theorem 6.21. *Let the rotation group* $\mathrm{SO}(3)$*, the sphere* $\mathbb{S}^3$*, and* $N \in \mathbb{N}_0$ *be given. Then, for every quadrature functional* $Q(\boldsymbol{P},\boldsymbol{w})$*,* $\boldsymbol{P} := (\boldsymbol{R}_1,\dots,\boldsymbol{R}_M) \in (\mathrm{SO}(3))^M$*,* $\boldsymbol{w} := (w_1,\dots,w_M) \in \mathbb{R}^M$*, of size* $M \in \mathbb{N}$ *and degree of exactness* N*, cf.* (6.57)*, the isomorphism* $\boldsymbol{q}_* : \mathrm{SO}(3) \to \mathbb{S}^3_*$*, cf.* (4.62)*, provides a quadrature functional* $Q_{\overline{\mathrm{C}}_1}(\tilde{\boldsymbol{P}},\tilde{\boldsymbol{w}})$*,* $\tilde{\boldsymbol{P}} := (\tilde{\boldsymbol{p}}_1,\dots,\tilde{\boldsymbol{p}}_{2M}) \in (\mathbb{S}^3)^{2M}$*,* $\tilde{\boldsymbol{w}} := (\tilde{w}_1,\dots,\tilde{w}_{2M}) \in \mathbb{R}^{2M}$ *of size* $2M$ *and degree of exactness* $2N+1$*, cf.* (6.6)*, which is invariant under the inversion group* $\overline{\mathrm{C}}_1 := \{\pm\boldsymbol{I} \in \mathbb{R}^{4\times4}\} \in \mathrm{SO}(4)$ *and determined by the relations, cf.* (6.31)*,*

$$\boldsymbol{q}_*(\boldsymbol{R}_i) = \{\tilde{\boldsymbol{p}}_i, \tilde{\boldsymbol{p}}_{i+M}\} \subset \mathbb{S}^3, \qquad \frac{1}{2} w_i = \tilde{w}_i = \tilde{w}_{i+M}, \qquad i = 1,\dots,M. \tag{6.60}$$

Conversely, any such quadrature functional $Q_{\overline{\mathrm{C}}_1}(\tilde{\boldsymbol{P}},\tilde{\boldsymbol{w}})$ *invariant under the inversion group* $\overline{\mathrm{C}}_1$ *with degree of exactness* $2N+1$ *on the sphere* $\mathbb{S}^3$*, provides by the relations* (6.60) *a quadrature functional* $Q(\boldsymbol{P},\boldsymbol{w})$ *on the rotation group* $\mathrm{SO}(3)$ *with degree of exactness* N*.*

Proof. The assertion follows immediately from Theorem 4.7, where we note that on the sphere $\mathbb{S}^3$ the odd spherical harmonics $f \in \Pi_{2n+1}(\mathbb{S}^3)$, $n \in \mathbb{N}_0$, are exactly integrated by the invariance of the quadrature functional $Q_{\overline{\mathrm{C}}_1}(\tilde{\boldsymbol{P}},\tilde{\boldsymbol{w}})$ under the inversion group $\overline{\mathrm{C}}_1$. We remark further that the relation for the weights $\boldsymbol{w}$, $\tilde{\boldsymbol{w}}$, cf. (6.60), is imposed by the condition $\sum_{i=1}^M w_i = 1 = \sum_{i=1}^{2M} \tilde{w}_i$, which is due to the normalization of the canonical measures $\mu_{\mathrm{SO}(3)}$, $\mu_{\mathbb{S}^3}$, in the classical quadrature conditions (6.57), (6.6), respectively. ∎

By Theorem 6.21 we can simply identify quadrature functionals on the rotation group $\mathrm{SO}(3)$ with degree of exactness N by quadrature functionals on the sphere $\mathbb{S}^3$ with degree of exactness $2N+1$ which are invariant under the inversion group $\overline{\mathrm{C}}_1 \in \mathrm{SO}(4)$. Hence, we define the efficiency of a quadrature functional $Q(\boldsymbol{P},\boldsymbol{w})$, $\boldsymbol{P} \in (\mathrm{SO}(3))^M$, $\boldsymbol{w} \in \mathbb{R}^M$, of size M and degree of exactness $N \in \mathbb{N}_0$ by

$$\mathrm{eff}_{\mathrm{SO}(3)}(Q(\boldsymbol{P},\boldsymbol{w})) := \frac{\left\lceil \frac{1}{6}(2N+1)(2N+2)(2N+3)+6 \right\rceil_4}{4M}, \qquad M \geq 4, \tag{6.61}$$

where we note that the additional 6 degrees of freedom in the numerator come from the dimension of the rotation group SO(4), which acts on the sphere $\mathbb{S}^3$, cf. (3.62). Similarly, to the sphere it seems that quadrature functionals $Q(\boldsymbol{P}, \boldsymbol{w})$ with efficiency $\mathrm{eff}_{\mathrm{SO}(3)} Q(\boldsymbol{P}, \boldsymbol{w}) = 1$ do exist, and that by the use of group actions one might construct quadrature functionals with efficiency $\mathrm{eff}_{\mathrm{SO}(3)} Q(\boldsymbol{P}, \boldsymbol{w}) > 1$.

As in the case of the sphere $\mathbb{S}^2$ it is possible to construct quadrature functionals on the rotation group SO(3) by a kind of tensor product, cf. [56]. However, in contrast to the Gauß–Legendre quadrature rules on the sphere $\mathbb{S}^2$ with asymptotic efficiency of 2/3 for $N \to \infty$, cf. Remark 6.3, such a construction leads on the rotation group SO(3) to quadrature functionals with asymptotic efficiency of 1 for $N \to \infty$, whenever quadrature functionals on the sphere $\mathbb{S}^2$ with asymptotic efficiency of 1 for $N \to \infty$ do exist.

Theorem 6.22. *Let the rotation group* SO(3)*, the sphere* $\mathbb{S}^2$*, and* $N \in \mathbb{N}_0$ *be given. Then, for every quadrature functional* $Q(\boldsymbol{P}, \boldsymbol{w})$*,* $\boldsymbol{P} := (\boldsymbol{p}_1, \ldots, \boldsymbol{p}_M) \in (\mathbb{S}^2)^M$*,* $\boldsymbol{w} := (w_1, \ldots, w_M) \in \mathbb{R}^M$*, of size* $M \in \mathbb{N}$ *and degree of exactness* N*, cf.* (6.6)*, the quadrature functional* $Q(\tilde{\boldsymbol{P}}, \tilde{\boldsymbol{w}})$*,* $\tilde{\boldsymbol{P}} := (\boldsymbol{R}_1, \ldots, \boldsymbol{R}_{\tilde{M}}) \in (\mathrm{SO}(3))^{\tilde{M}}$*,* $\tilde{\boldsymbol{w}} := (\tilde{w}_1, \ldots, \tilde{w}_{\tilde{M}}) \in \mathbb{R}^{\tilde{M}}$*, of size* $\tilde{M} := M(N+1)$ *determined by the relations*

$$\boldsymbol{R}_i \boldsymbol{e}_3 = \boldsymbol{p}_i \in \mathbb{S}^2, \qquad \tilde{w}_i = \frac{w_i}{N+1}, \qquad i = 1, \ldots, M, \qquad \boldsymbol{e}_3 := (0,0,1)^\top \in \mathbb{S}^2, \tag{6.62}$$

together with, cf. (3.90)*,*

$$\boldsymbol{R}_{i+jM} := \boldsymbol{R}_i \boldsymbol{R}\left(\boldsymbol{e}_3, \frac{2\pi j}{N+1}\right) \in \mathrm{SO}(3), \qquad \tilde{w}_{i+jM} := \tilde{w}_i, \qquad i = 1, \ldots, M, \quad j = 1, \ldots, N, \tag{6.63}$$

has degree of exactness N*, cf.* (6.57)*. In particular, for quadrature functionals* $Q(\boldsymbol{P}, \boldsymbol{w})$ *with efficiency* $\mathrm{eff}_{\mathbb{S}^2}(Q(\boldsymbol{P}, \boldsymbol{w})) \geq 1$*, cf.* (6.12)*, the quadrature functional* $Q(\tilde{\boldsymbol{P}}, \tilde{\boldsymbol{w}})$ *has efficiency, cf.* (6.61)*,*

$$\mathrm{eff}_{\mathrm{SO}(3)}(Q(\tilde{\boldsymbol{P}}, \tilde{\boldsymbol{w}})) \geq 1 - \frac{3(1+7N)}{4\,(6+8N+3N^2+N^3)}, \qquad N \in \mathbb{N}. \tag{6.64}$$

Proof. We follow the lines of the proof given for [56, Lemma 3.1]. Therefore, we consider the spherical coordinates of the quadrature points, i.e., $\boldsymbol{p}_i = h(\theta_i, \varphi_i) \in \mathbb{S}^2$, $(\theta_i, \varphi_i) \in [0, \pi] \times [0, 2\pi)$, $i = 1, \ldots, M$, cf. (3.71). Any rotation matrix $\boldsymbol{R}_i \in \mathrm{SO}(3)$ which maps the vector $\boldsymbol{e}_3 = (0,0,1)^\top \in \mathbb{S}^2$ to the vector $\boldsymbol{p}_i$, cf. (6.62), can be represented by Euler angles due to, cf. (3.94),

$$\boldsymbol{R}_i = \boldsymbol{R}(\boldsymbol{e}_3, \varphi_i) \boldsymbol{R}(\boldsymbol{e}_2, \theta_i) \boldsymbol{R}(\boldsymbol{e}_3, \psi_i), \qquad i = 1, \ldots, M,$$

where $\psi_i \in [0, 2\pi)$, $i = 1, \ldots, M$, can be chosen arbitrary. From that relation we infer from the addition theorems of the sine and cosine that the Euler angles representation of the quadrature points on the rotation group SO(3) determined by (6.62) and (6.63) is

$$\boldsymbol{R}_{i+jM} = \boldsymbol{R}(\boldsymbol{e}_3, \varphi_i) \boldsymbol{R}(\boldsymbol{e}_2, \theta_i) \boldsymbol{R}\left(\boldsymbol{e}_3, \psi_i + \frac{2\pi j}{N+1}\right), \qquad i = 1, \ldots, M, \quad j = 0, \ldots, N.$$

In order to show that the quadrature functional $Q(\tilde{\boldsymbol{P}}, \tilde{\boldsymbol{w}})$ has degree of exactness N we need to confirm the equations of the system (6.58). We recall the representation (5.46) of the Wigner D-functions in Euler angles so that the equation system (6.58) reads for the quadrature functional

$Q(\tilde{\boldsymbol{P}}, \tilde{\boldsymbol{w}})$ as

$$\sum_{i=1}^{M}\sum_{j=0}^{N} \tilde{w}_{i+Mj} D_{k,k'}^{n}(\boldsymbol{R}_{i+Mj}) = \sum_{i=1}^{M} w_i \mathrm{e}^{-\mathrm{i}k\varphi_i} d_{k,k'}^{n}(\cos(\theta_i)) \mathrm{e}^{-\mathrm{i}k'\psi_i} \frac{1}{N+1} \sum_{j=0}^{N} \mathrm{e}^{-2\pi\mathrm{i}\frac{kj}{N+1}} = \delta_{n,0}, \tag{6.65}$$

for $n = 0, \ldots, N$, and $k, k' = -n, \ldots, n$. By the identity

$$\frac{1}{N+1} \sum_{j=0}^{N} \mathrm{e}^{-2\pi\mathrm{i}\frac{kj}{N+1}} = \begin{cases} 1, & k \equiv 0 \mod N+1, \\ 0, & \text{else}, \end{cases}$$

we observe that the conditions (6.65) are fulfilled for $1 \leq |k'| \leq N$, $k = -N, \ldots, N$, $n = \max\{|k|, |k'|\}, \ldots, N$. For $k' = 0$, $k = -N, \ldots, N$, $n = \max\{|k|, |k'|\}, \ldots, N$ the remaining conditions are fulfilled by the relation

$$\sum_{i=1}^{M} w_i \mathrm{e}^{-\mathrm{i}k\varphi_i} d_{k,k'}^{n}(\cos(\theta_i)) = \sum_{i=1}^{M} w_i (-1) \sqrt{\frac{4\pi}{2n+1}} Y_{n,-k}(\boldsymbol{p}_i) = \delta_{n,0},$$

where we use the relation (5.47) and that the quadrature functional $Q(\boldsymbol{P}, \boldsymbol{w})$ has degree of exactness N, cf. (6.7).

Finally, the bound for the efficiency (6.64) is obtained by the simple estimates of the numerator

$$\begin{aligned} \left\lceil \frac{1}{6}(2N+1)(2N+2)(2N+3) + 6 \right\rceil_4 &\geq \frac{1}{6}(2N+1)(2N+2)(2N+3) + 6 \\ &= \frac{1}{3}(21 + 11N + 12N^2 + 4N^3) \end{aligned}$$

and the denominator

$$4M(N+1) \leq \frac{4}{3}((N+1)^2 + 5)(N+1) = \frac{4}{3}(6 + 8N + 3N^2 + N^3)$$

of the efficiency (6.61), where we use for the bound on the denominator that $\mathrm{eff}(Q(\boldsymbol{P}, \boldsymbol{w})) \geq 1$, cf. (6.12), ■

Remark 6.23. The construction of quadrature functionals on the rotation group SO(3) provided by Theorem 6.22 is motivated from the one-to-one correspondence between the product manifold $\mathbb{S}^2 \times \mathbb{S}^1$ and the rotation group SO(3), cf. [56], which results from the famous Hopf fibration of the sphere $\mathbb{S}^3$, cf. [86]. Moreover, we showed in [56, Theorem 2.4] that the quadrature points constructed in this way are uniformly distributed over the entire rotation group SO(3), which might explain the high efficiency of such quadrature functionals. However, we note that these quadrature functionals are not uniquely determined, since for every quadrature point on the sphere we have the freedom to choose a single rotation from a one-parameter family of rotations that satisfy the relation (6.62). This might explain that the efficiency of such quadrature functionals is in the most cases slightly smaller than one. □

Similarly to the consideration on the sphere $\mathbb{S}^d$ in Section 6.2, we will restrict our attention in the following Sections 6.3.1 and 6.3.2 to particular interesting quadrature functionals. In Section 6.3.1 we consider quadrature functionals invariant under certain orthogonal groups which act on the rotation group SO(3). However, for brevity we consider only groups which seem to be particular promising for the construction of highly efficient quadrature functionals, cf. Theorem 6.24 and Table 6.4. In Section 6.3.2 we generalize the notion of spherical t-designs on the sphere $\mathbb{S}^d$

to the notion of t-designs on the rotation group SO(3), and recapitulate the well-know result that the rotational symmetry groups of the platonic solids are particular efficient t-designs, cf. Theorem 6.25. Moreover, we are able to present in Theorem 6.26 an explicit construction for a new 7-design on the rotation group SO(3) with $M = 168$ quadrature points. Finally, the numerical results of Section 6.3.3 provide us with evidence that on the rotation group SO(3) quadrature functionals and t-designs with efficiency at least one do exist for selected polynomial degrees of exactness up to $N = t = 23$, respectively, cf. Table 6.5 and 6.6.

6.3.1 Quadratures Invariant under Finite Orthogonal Groups

The notion of invariant quadrature functionals on the sphere $\mathbb{S}^d$, $d \in \mathbb{N}$, given in Section 6.2.1 generalizes straightforward to the notion of invariant quadrature functionals on the rotation group SO(3). Moreover, the special relationship between the rotation group SO(3) and the sphere $\mathbb{S}^3$, given by Theorem 6.21, enables us to apply the definitions and relations for the sphere $\mathbb{S}^d$, such as Theorem 6.5 and Theorem 6.6.

On the rotation group SO(3) we restrict our attention to selected groups.[5] That is, we consider only the tetrahedral group T, the octahedral group O, the icosahedral group I, the cyclic group C_k, $k \in \mathbb{N}$, cf. (6.26), (6.27), and the *product group* $\mathcal{G} \times \mathcal{H}$ with $\mathcal{G}, \mathcal{H} \in \{\mathrm{T}, \mathrm{O}, \mathrm{I}, \mathrm{C}_k \ : \ k \in \mathbb{N}\}$ with the canonical group multiplication defined by

$$(\boldsymbol{G}_1, \boldsymbol{H}_1)(\boldsymbol{G}_2, \boldsymbol{H}_2) := (\boldsymbol{G}_1\boldsymbol{G}_2, \boldsymbol{H}_1\boldsymbol{H}_2), \qquad (\boldsymbol{G}_1, \boldsymbol{H}_1), (\boldsymbol{G}_2, \boldsymbol{H}_2) \in \mathcal{G} \times \mathcal{H}.$$

For a group $\mathcal{G} \in \{\mathrm{T}, \mathrm{O}, \mathrm{I}, \mathrm{C}_k \ : \ k \in \mathbb{N}\}$, which is not a product group, we define its action on the rotation group $\mathcal{G} \subset \mathrm{SO}(3)$ by *conjugation*, i.e.,

$$\boldsymbol{G} \cdot \boldsymbol{R} := \boldsymbol{G}\boldsymbol{R}\boldsymbol{G}^\top, \qquad \boldsymbol{R} \in \mathrm{SO}(3), \qquad \boldsymbol{G} \in \mathcal{G}. \tag{6.66}$$

Whereas, for a product group $\mathcal{G} \times \mathcal{H}$ with $\mathcal{G}, \mathcal{H} \in \{\mathrm{T}, \mathrm{O}, \mathrm{I}, \mathrm{C}_k \ : \ k \in \mathbb{N}\}$ we define its action by the *left-right multiplication*, which is defined by

$$(\boldsymbol{G}, \boldsymbol{H}) \cdot \boldsymbol{R} := \boldsymbol{G}\boldsymbol{R}\boldsymbol{H}^\top, \qquad \boldsymbol{R} \in \mathrm{SO}(3), \qquad (\boldsymbol{G}, \boldsymbol{H}) \in \mathcal{G} \times \mathcal{H}. \tag{6.67}$$

The corresponding orbits of a rotation $\boldsymbol{R} \in \mathrm{SO}(3)$ are given by, cf. (6.17),

$$\mathcal{G} \cdot \boldsymbol{R} := \{\boldsymbol{G}\boldsymbol{R}\boldsymbol{G}^\top \ : \ \boldsymbol{G} \in \mathcal{G}\}, \quad \mathcal{G} \times \mathcal{H} \cdot \boldsymbol{R} := \{\boldsymbol{G}\boldsymbol{R}\boldsymbol{H}^\top \ : \ (\boldsymbol{G}, \boldsymbol{H}) \in \mathcal{G} \times \mathcal{H}\} \subset \mathrm{SO}(3), \tag{6.68}$$

respectively.

We note that, by the above definitions, the rotation groups $\mathrm{T}, \mathrm{O}, \mathrm{I}, \mathrm{C}_k$, $k \in \mathbb{N}$, allow for two essentially different group actions, since any group $\mathcal{G} \in \{\mathrm{T}, \mathrm{O}, \mathrm{I}, \mathrm{C}_k \ : \ k \in \mathbb{N}\}$ is isomorphic to the product group $\mathcal{G} \times \mathrm{C}_1$, which by definition (6.67) and (6.66) has a different group action than $\mathcal{G}$. In the case $\mathcal{G} \times \mathrm{C}_1$, the left-right multiplication (6.67) simplifies to left-multiplication

$$(\boldsymbol{G}, \boldsymbol{I}) \cdot \boldsymbol{R} = \boldsymbol{G}\boldsymbol{R}, \qquad \boldsymbol{R} \in \mathrm{SO}(3), \qquad \boldsymbol{G} \in \mathcal{G}, \tag{6.69}$$

where $\boldsymbol{I} \in \mathbb{R}^{3\times 3}$ denotes the identity matrix. In particular, the orbit of the identity matrix $\boldsymbol{I} \in \mathbb{R}^{3\times 3}$ generated by $\mathcal{G}$ is $\mathcal{G} \cdot \boldsymbol{I} = \{\boldsymbol{I}\}$, whereas the isomorphic product group $\mathcal{G} \times \mathrm{C}_1$ generates the orbit $\mathcal{G} \times \mathrm{C}_1 \cdot \boldsymbol{I} = \mathcal{G}$. Moreover, every orbit of the product group $\mathcal{G} \times \mathrm{C}_1$ has the same cardinality as the group $\mathcal{G}$.

Keeping these different group actions in mind, we define the corresponding invariant harmonic

[5] A complete list of all finite subgroups of the orthogonal group $SO(4)$ can be found in the monograph [26].

spaces of degree at most $N \in \mathbb{N}_0$ by, cf. (6.14),

$$\begin{aligned}\Pi^N_{\mathcal{G}}(\mathrm{SO}(3)) &:= \{f \in \Pi^N(\mathrm{SO}(3)) \ : \ f(\boldsymbol{G}\boldsymbol{R}\boldsymbol{G}^\top) = f(\boldsymbol{R}), \quad \boldsymbol{G} \in \mathcal{G},\ \boldsymbol{R} \in \mathrm{SO}(3)\},\\ \Pi^N_{\mathcal{G}\times\mathcal{H}}(\mathrm{SO}(3)) &:= \{f \in \Pi^N(\mathrm{SO}(3)) \ : \ f(\boldsymbol{G}\boldsymbol{R}\boldsymbol{H}^\top) = f(\boldsymbol{R}), \quad (\boldsymbol{G},\boldsymbol{H}) \in \mathcal{G}\times\mathcal{H},\ \boldsymbol{R} \in \mathrm{SO}(3)\}.\end{aligned} \tag{6.70}$$

Similarly to the sphere $\mathbb{S}^d$, every quadrature functional on the rotation group $\mathrm{SO}(3)$ which is invariant under the group $\mathcal{G}$ or $\mathcal{G}\times\mathcal{H}$ can be composed by disjoint orbits of given quadrature points $\boldsymbol{R}_i \in \mathrm{SO}(3)$, and corresponding quadrature weights $w_i \in \mathbb{R}$, $i = 1,\dots,M_{\mathrm{gen}}$, by setting, cf. (6.18),

$$Q_{\mathcal{G}}(\boldsymbol{P},\boldsymbol{w}) := \sum_{i=1}^{M_{\mathrm{gen}}} w_i \sum_{\boldsymbol{R}\in\mathcal{G}\cdot\boldsymbol{R}_i} I_{\delta_{\boldsymbol{R}}}, \qquad Q_{\mathcal{G}\times\mathcal{H}}(\boldsymbol{P},\boldsymbol{w}) := \sum_{i=1}^{M_{\mathrm{gen}}} w_i \sum_{\boldsymbol{R}\in\mathcal{G}\times\mathcal{H}\cdot\boldsymbol{R}_i} I_{\delta_{\boldsymbol{R}}}, \tag{6.71}$$

respectively.

In order to determine for an invariant quadrature functional the number of conditions imposed by the classical quadrature condition (6.57) we can apply directly the Theorem 6.5 for the sphere $\mathbb{S}^3$ in conjunction with Theorem 6.21. In other words, we need to determine the dimensions of the invariant subspaces $\Pi^N_{\mathcal{G}}(\mathrm{SO}(3))$, $\Pi^N_{\mathcal{G}\times\mathcal{H}}(\mathrm{SO}(3))$, $\mathcal{G},\mathcal{H} \in \{\mathrm{T},\mathrm{O},\mathrm{I},\mathrm{C}_k \ : \ k \in \mathbb{N}\}$, which can be achieved by the use of Molien series via Theorem 6.6. We will restrict our attention to the rotation groups of the platonic solids which are associated to conjugation, cf. (6.66) and left multiplication, cf. (6.69). That is we consider only the groups $\mathrm{T},\mathrm{O},\mathrm{I}$ and the product groups $\mathrm{T}\times\mathrm{C}_1$, $\mathrm{O}\times\mathrm{C}_1$, $\mathrm{I}\times\mathrm{C}_1$. For example, we list in Table 6.4 the dimensions of the corresponding invariant harmonic spaces up to degree $N = 21$.

Theorem 6.24. *Let the rotation group* $\mathrm{SO}(3)$*, the tetrahedral group* T*, the octahedral group* O*, the icosahedral group* I*, cf.* (6.26)*, and* $N \in \mathbb{N}_0$ *be given. Then the dimensions* $d^N_{\mathcal{G}}$*,* $d^N_{\mathcal{G}\times\mathrm{C}_1}$ *of the harmonic spaces* $\Pi^N_{\mathcal{G}}(\mathrm{SO}(3))$*,* $\Pi^N_{\mathcal{G}\times\mathrm{C}_1}(\mathrm{SO}(3))$*,* $\mathcal{G} \in \{\mathrm{T},\mathrm{O},\mathrm{I}\}$*, cf.* (6.70)*, are determined by the generating functions*

$$\begin{aligned}M_{\mathrm{T}}(t) &:= \frac{(1+t^2)(1+t^3)}{(1-t)(1-t^2)(1-t^3)}, \qquad M_{\mathrm{O}}(t) := \frac{1+t^5}{(1-t)(1-t^2)(1-t^3)},\\ M_{\mathrm{I}}(t) &:= \frac{1+t^8}{(1-t^3)(1-t^5)}, \qquad M_{\mathrm{T}\times\mathrm{C}_1}(t) := \frac{1-2t^2+5t^3+10t^4-10t^5-5t^6+2t^7-t^9}{(1-t^2)^2(1-t^3)^2},\\ M_{\mathrm{O}\times\mathrm{C}_1}(t) &:= \frac{1-2t^3+7t^4+14t^6-14t^7-7t^9+2t^{10}-t^{13}}{(1-t^3)^2(1-t^4)^2},\\ M_{\mathrm{I}\times\mathrm{C}_1}(t) &:= \big(1-2t^2-2t^3+t^4+2t^5+14t^6+2t^7-24t^8-28t^9+28t^{10}+24t^{11}-\\ &\qquad 2t^{12}-14t^{13}-2t^{14}-t^{15}+2t^{16}+2t^{17}-t^{19}\big)/\big((1-t^2)^2(1-t^3)^2(1-t^5)^2\big),\end{aligned}$$

due to the relations

$$d^N_{\mathcal{G}} := \sum_{n=0}^{N} h^n_{\mathcal{G}}, \quad M_{\mathcal{G}}(t) = \sum_{n=0}^{\infty} h^n_{\mathcal{G}} t^n, \qquad d^N_{\mathcal{G}\times\mathrm{C}_1} := \sum_{n=0}^{N} h^n_{\mathcal{G}\times\mathrm{C}_1}, \quad M_{\mathcal{G}\times\mathrm{C}_1}(t) = \sum_{n=0}^{\infty} h^n_{\mathcal{G}\times\mathrm{C}_1} t^n,$$

respectively.

Proof. We aim to apply Theorem 6.6. Therefore, we translate the group actions of the groups $\mathcal{G}$, $\mathcal{G}\times\mathrm{C}_1$ for $\mathcal{G} \in \{\mathrm{T},\mathrm{O},\mathrm{I}\}$ into the corresponding group actions on the sphere $\mathbb{S}^3$, by the isomorphism $\boldsymbol{q}_* : \mathrm{SO}(3) \to \mathbb{S}^3_*$, cf. (4.62). More precisely, we define explicitly group representations $T_{\mathcal{G}}, T_{\mathcal{G}\times\mathrm{C}_1} \subset$

N	0	1	2	3	4	5	6	7	8	9	10
d^N	1	10	35	84	165	286	455	680	969	1330	1771
d^N_{T}	1	2	5	10	17	28	43	62	87	118	155
$d^N_{\mathrm{T}\times\mathrm{C}_1}$	1	1	1	8	17	17	43	58	75	113	155
d^N_{O}	1	2	4	7	11	17	25	35	48	64	83
$d^N_{\mathrm{O}\times\mathrm{C}_1}$	1	1	1	1	10	10	23	23	40	59	80
d^N_{I}	1	2	3	5	7	10	14	18	24	31	39
$d^N_{\mathrm{I}\times\mathrm{C}_1}$	1	1	1	1	1	1	14	14	14	14	35
N	11	12	13	14	15	16	17	18	19	20	21
d^N	2300	2925	3654	4495	5456	6545	7770	9139	10660	12341	14190
d^N_{T}	200	253	314	385	466	557	660	775	902	1043	1198
$d^N_{\mathrm{T}\times\mathrm{C}_1}$	178	253	307	365	458	557	627	775	892	1015	1187
d^N_{O}	106	133	164	200	241	287	339	397	461	532	610
$d^N_{\mathrm{O}\times\mathrm{C}_1}$	80	130	157	186	217	283	318	392	431	513	599
d^N_{I}	49	60	73	88	105	124	145	169	195	224	256
$d^N_{\mathrm{I}\times\mathrm{C}_1}$	35	60	60	60	91	124	124	161	161	202	245

Table 6.4: The dimensions $d^N_{\mathcal{G}}$, $d^N_{\mathcal{G}\times\mathrm{C}_1}$ of the invariant subspaces $\Pi^N_{\mathcal{G}}(\mathrm{SO}(3))$, $\Pi^N_{\mathcal{G}\times\mathrm{C}_1}(\mathrm{SO}(3))$, $\mathcal{G}\in\{\mathrm{T},\mathrm{O},\mathrm{I}\}$, respectively, in comparison with the dimension d^N of the harmonic space $\Pi^N(\mathrm{SO}(3))$ for degree $N=0,\dots,21$, cf. Theorem 6.24.

SO(4), so that the invariant harmonic space $\Pi^{2N}_{T_{\mathcal{G}}}(\mathbb{S}^3)$, $\Pi^{2N}_{T_{\mathcal{G}\times\mathrm{C}_1}}(\mathbb{S}^3)$ is in one-to-one correspondence with the harmonic space $\Pi^N_{\mathcal{G}}(\mathrm{SO}(3))$, $\Pi^N_{\mathcal{G}\times\mathrm{C}_1}(\mathrm{SO}(3))$, respectively.

For unit quaternions $\boldsymbol{q}:=(a,b,c,d)\in\mathbb{S}^3$ we define the matrices

$$\boldsymbol{S}_{\boldsymbol{q}}:=\begin{pmatrix}1&0&0&0\\0&1-2(c^2+d^2)&2(bc-ad)&2(ac+bd)\\0&2(bc+ad)&1-2(b^2+d^2)&2(cd-ab)\\0&2(bd-ac)&2(ab+cd)&1-2(b^2+c^2)\end{pmatrix},\quad \boldsymbol{T}_{\boldsymbol{q}}:=\begin{pmatrix}a&-b&-c&-d\\b&a&-d&c\\c&d&a&-b\\d&-c&b&a\end{pmatrix}$$

which are in fact rotation matrices, i.e., $\boldsymbol{S}_{\boldsymbol{q}},\boldsymbol{T}_{\boldsymbol{q}}\in\mathrm{SO}(4)$. The canonical action of these rotation matrices can be written in terms of quaternion multiplication, cf. (4.55), and conjugation, cf. (4.56), as

$$\boldsymbol{S}_{\boldsymbol{q}}\boldsymbol{x}=\boldsymbol{q}\odot\boldsymbol{x}\odot\overline{\boldsymbol{q}},\qquad \boldsymbol{T}_{\boldsymbol{q}}\boldsymbol{x}=\boldsymbol{q}\odot\boldsymbol{x},\qquad \boldsymbol{x}\in\mathbb{S}^3,\quad \boldsymbol{q}\in\mathbb{S}^3. \tag{6.72}$$

We observe the similarity between the actions (6.66), (6.67) on the rotation group SO(3) and the above actions (6.72) on the sphere $\mathbb{S}^3$, and define the finite sets

$$T_{\mathcal{G}}:=\{\boldsymbol{S}_{\boldsymbol{q}}\in\mathrm{SO}(4)\ :\ \boldsymbol{q}\in\boldsymbol{q}_*(\boldsymbol{G}),\,\boldsymbol{G}\in\mathcal{G}\},\quad T_{\mathcal{G}\times\mathrm{C}_1}:=\{\boldsymbol{T}_{\boldsymbol{g}}\in\mathrm{SO}(4)\ :\ \boldsymbol{q}\in\boldsymbol{q}_*(\boldsymbol{G}),\,\boldsymbol{G}\in\mathcal{G}\}.$$

Since the isomorphism $\boldsymbol{q}_*:\mathrm{SO}(3)\to\mathbb{S}^3_*$ respects the matrix multiplication in the sense, cf. (4.63),

$$\boldsymbol{q}_*(\boldsymbol{R}_1)\odot\boldsymbol{q}_*(\boldsymbol{R}_2)\odot\boldsymbol{q}_*(\boldsymbol{R}_3)=\boldsymbol{q}_*(\boldsymbol{R}_1\boldsymbol{R}_2\boldsymbol{R}_3),\qquad \boldsymbol{R}_1,\boldsymbol{R}_2,\boldsymbol{R}_3\in\mathrm{SO}(3),$$

we conclude that the sets $T_{\mathcal{G}}$, $T_{\mathcal{G}\times\mathrm{C}_1}$ are actually subgroups of the rotation group SO(4). Moreover, by the relation (4.68) of Theorem 4.7 we obtain for $N\in\mathbb{N}_0$ the following correspondences between

the invariant harmonic spaces on the sphere $\mathbb{S}^3$ and the rotation group SO(3), cf. (4.66),

$$\begin{aligned} f \in \Pi^{2N}_{T_\mathcal{G}}(\mathbb{S}^3) \quad &\Leftrightarrow \quad \tilde{f} \circ q_* \in \Pi^N_\mathcal{G}(\mathrm{SO}(3)), \\ f \in \Pi^{2N}_{T_{\mathcal{G}\times \mathrm{C}_1}}(\mathbb{S}^3) \quad &\Leftrightarrow \quad \tilde{f} \circ q_* \in \Pi^N_{\mathcal{G}\times \mathrm{C}_1}(\mathrm{SO}(3)). \end{aligned} \tag{6.73}$$

Hence, by Theorem 6.6 it is sufficient to determine the generating functions $M_{T_\mathcal{G}}(t)$, $M_{T_{\mathcal{G}\times \mathrm{C}_1}}(t)$, cf. (6.19), associated to the the groups $T_\mathcal{G}$, $T_{\mathcal{G}\times \mathrm{C}_1}$, respectively. The proof is finished by using the the relations

$$M_{T_\mathcal{G}}(t) = M_\mathcal{G}(t^2), \qquad M_{T_{\mathcal{G}\times \mathrm{C}_1}}(t) = M_{\mathcal{G}\times \mathrm{C}_1}(t^2),$$

which incorporates the correspondences (6.73), respectively. ■

We utilize Theorem 6.24 for the determination of candidates of highly efficient quadrature functionals on the rotation group SO(3), as illustrated in Example 6.27 and 6.28 of Section 6.3.3.

6.3.2 t-Designs on the Rotation Group SO(3)

The notion of spherical t-designs, cf. Section 6.2.2, generalizes straightforward to the notion of t-designs on the rotation group SO(3). We call a point set $\mathcal{X}_M = \{\boldsymbol{R}_1, \ldots, \boldsymbol{R}_M\} \subset \mathrm{SO}(3)$ a *t-design on the rotation group* SO(3), $t \in \mathbb{N}_0$, if it satisfies

$$\frac{1}{8\pi^2} \int_{\mathrm{SO}(3)} f(\boldsymbol{R}) \mathrm{d}\mu_{\mathrm{SO}(3)}(\boldsymbol{R}) = \frac{1}{M} \sum_{i=1}^{M} f(\boldsymbol{R}_i), \qquad f \in \Pi^t(\mathrm{SO}(3)), \tag{6.74}$$

where $\mu_{\mathrm{SO}(3)}$ is the canonical measure on the rotation group SO(3). Hence, by comparing the condition (6.74) with the classical quadrature condition (6.57), a t-design $\mathcal{X}_M = \{\boldsymbol{R}_1, \ldots, \boldsymbol{R}_M\} \subset \mathrm{SO}(3)$ on the rotation group can be considered as an equal weights quadrature functional $Q_\nu(\boldsymbol{P})$, $\boldsymbol{P} := (\boldsymbol{R}_1, \ldots, \boldsymbol{R}_M) \in (\mathrm{SO}(3))^M$, cf. (2.33), with degree of exactness $N = t$, where $\nu := \frac{1}{8\pi^2}\mu_{\mathrm{SO}(3)}$. In this section we write for convenience $Q(\boldsymbol{P}) = Q_\nu(\boldsymbol{P})$ since the measure ν is fixed.

We note that the Remark 6.15 applies by Theorem 6.21 also to t-designs on the rotation group SO(3). That is, t-designs of size $M < Ct^3$ do exist for any degree $t \in \mathbb{N}_0$, where $C > 0$ is some constant. Moreover, we can construct by Theorem 6.22 t-designs on the rotation group SO(3) from spherical t-designs on the sphere $\mathbb{S}^2$.

In the numerical examples, cf. Section 6.3.3, we aim to compute equal weights quadrature functionals $Q(\boldsymbol{P})$, $\boldsymbol{P} := (\boldsymbol{R}_1, \ldots, \boldsymbol{R}_M) \in (\mathrm{SO}(3))^M$, with degree of exactness $N \in \mathbb{N}_0$ by minimizing the squared worst case quadrature error, cf. (6.59),

$$E_N(\boldsymbol{P}) := \frac{1}{M^2} \sum_{n=1}^{N} \frac{2n+1}{8\pi^2} \sum_{k,k'=-n}^{n} \Big| \sum_{i=1}^{M} \overline{D}^n_{k,k'}(\boldsymbol{R}_i) \Big|^2 = \mathrm{err}_{K_N}(\nu, \boldsymbol{P})^2. \tag{6.75}$$

In order to estimate the number M of quadrature points needed for such a quadrature functional $Q(\boldsymbol{P})$, we introduce the efficiency, cf. (6.11),

$$\mathrm{eff}_{\mathrm{SO}(3)}(Q(\boldsymbol{P})) := \frac{\left\lceil \frac{1}{6}(2N+1)(2N+2)(2N+3) + 5 \right\rceil_3}{3M}, \qquad M \geq 4, \tag{6.76}$$

which is motivated like the efficiency defined by (6.61), i.e., we try to match the $3M$ degrees of freedom with the number of conditions imposed by (6.57). That means, there might exist equal weight quadrature functionals $Q(\boldsymbol{P})$ with efficiency $\mathrm{eff}_{\mathrm{SO}(3)}(Q(\boldsymbol{P})) = 1$. Moreover, one can construct equal weights quadrature functionals with $\mathrm{eff}_{\mathrm{SO}(3)}(Q(\boldsymbol{P})) > 1$, by the use of groups,

cf. Table 6.6. From Remark 6.15 for spherical t-designs we know that there exists a lower bound $c > 0$ such that $\mathrm{eff}_{\mathrm{SO}(3)}(Q(\boldsymbol{P})) \geq c$ can be achieved for any degree $N \in \mathbb{N}_0$.

Finally, from Theorem 6.24 we arrive at the well-known fact that the finite rotation groups $\mathrm{T}, \mathrm{O}, \mathrm{I} \subset \mathrm{SO}(3)$, cf. (6.26), are 2,3, and 5-designs on the rotation group SO(3), respectively, which are particular efficient, cf. Table 6.6. Moreover, together with Theorem 6.22 we are able to prove the existence of the numerically found 7-design of size $M = 168$ on the rotation group which is invariant under the group $\mathrm{O} \times \mathrm{C}_7$ acting on the rotation group SO(3). The corresponding polytope on the sphere $\mathbb{S}^3$ seems to be new and provides by Theorem 6.21 a spherical 15-design of size $M = 336$.

Theorem 6.25. *The tetrahedral group* T*, the octahedral group* O*, and the icosahedral group* I*, cf.* (6.26)*, are* 2,3*, and* 5*-designs on the rotation group* SO(3)*, cf.* (6.74)*, respectively.*

Proof. For any finite rotation group $\mathcal{G} \subset \mathrm{SO}(3)$, the set $\mathcal{G}$ is itself a orbit generated by the group $\mathcal{G} \times \mathrm{C}_1$, i.e., $\mathcal{G} \times \mathrm{C}_1 \cdot \boldsymbol{I} = \mathcal{G}$, where $\boldsymbol{I} \in \mathbb{R}^{3\times 3}$ is the identity matrix, cf. (6.67). By Theorem 6.24, cf. Table 6.4, we find that the polynomial $f \equiv 1$ in $\Pi^N_{\mathcal{G}\times \mathrm{C}_1}(\mathrm{SO}(3))$ is the only harmonic of degree at most $N = 2, 3, 5$ which is invariant under the group $\mathcal{G} \times \mathrm{C}_1 = \mathcal{T} \times \mathrm{C}_1, \mathcal{O} \times \mathrm{C}_1, \mathcal{I} \times \mathrm{C}_1$, respectively. Since f is integrated exactly by the corresponding equal weights quadrature functionals we arrive at the assertion by Theorem 6.5 in conjunction with Theorem 6.21. ∎

Theorem 6.26. *Let the rotation group* SO(3)*, the octahedral group* O*, cf.* (6.26)*, and the cyclic group* C_7*, cf.* (6.27)*, be given. Then every rotation* $\boldsymbol{R} \in \mathrm{SO}(3)$ *which satisfies the relation*

$$\boldsymbol{R}\boldsymbol{e}_3 = \boldsymbol{p}, \qquad \boldsymbol{e}_3 := (0,0,1)^\top \in \mathbb{S}^2, \qquad \boldsymbol{p} := (p_1, p_2, p_3)^\top \in \mathbb{S}^2, \tag{6.77}$$

provides a 7*-design* $\mathcal{X}$ *on the rotation group* SO(3) *by setting*

$$\mathcal{X} := \{\boldsymbol{O}\boldsymbol{R}\boldsymbol{C} \in \mathrm{SO}(3) \ : \ \boldsymbol{O} \in \mathrm{O}, \quad \boldsymbol{C} \in \mathrm{C}_7\} \subset \mathrm{SO}(3), \tag{6.78}$$

where $p_1 = 0.866246\ldots$, $p_2 = 0.422518\ldots$, $p_3 = 0.266635\ldots$ *are the positive roots of the polynomial*

$$105p^6 - 105p^4 + 21p^2 - 1.$$

Proof. We know from [89, Sec. 6.2] that the orbit $\mathrm{O}\boldsymbol{p} \subset \mathbb{S}^2$, cf. (6.17), of the point $\boldsymbol{p} := (p_1, p_2, p_3) \in \mathbb{S}^2$ given by (6.77) is a spherical 7-design, cf. (6.43). Hence, by Theorem 6.22 we conclude that the set $\mathcal{X}$ defined by (6.78) is a 6-design on the rotation group SO(3), cf. (6.74). Moreover, since the dimensions of the harmonic spaces $\Pi^6_{\mathrm{O}}(\mathrm{SO}(3))$ and $\Pi^7_{\mathrm{O}}(\mathrm{SO}(3))$ are equal, cf. Table 6.4, we find that the set $\mathcal{X}$ is in fact a 7-design on the rotation group SO(3) and the proof is finished. ∎

6.3.3 Numerical Examples

In this section we present several numerical examples for the computation of classical quadrature functionals $Q(\boldsymbol{P}, \boldsymbol{w})$ of size $M \in \mathbb{N}$ with quadrature points $\boldsymbol{P} := (\boldsymbol{R}_1, \ldots, \boldsymbol{R}_M) \in (\mathrm{SO}(3))^M$ and quadrature weights $\boldsymbol{w} := (w_1, \ldots, w_M)^\top \in \mathbb{R}^M$, and prescribed degree of exactness $N \in \mathbb{N}_0$ on the rotation group SO(3), cf. (6.57). We recall that for a quadrature functional $Q(\boldsymbol{P}, \boldsymbol{w})$ and an equal weights quadrature functional $Q(\boldsymbol{P})$ with degree of exactness N the squared worst case quadrature error, cf. (6.59),

$$E_N(\boldsymbol{P}, \boldsymbol{w}) := \sum_{n=0}^{N} \frac{2n+1}{8\pi^2} \sum_{k,k'=-n}^{n} \left| \delta_{0,n} - \sum_{i=1}^{M} w_i \overline{D}^n_{k,k'}(\boldsymbol{R}_i) \right|^2 \tag{6.79}$$

and the squared equal weights worst case quadrature error, cf. (6.75),

$$E_N(\boldsymbol{P}) := E_N(\boldsymbol{P}, (M^{-1}, \ldots, M^{-1})) = \frac{1}{M^2} \sum_{n=1}^{N} \frac{2n+1}{8\pi^2} \sum_{k,k'=-n}^{n} \Big| \sum_{i=1}^{M} w_i \overline{D}^n_{k,k'}(\boldsymbol{R}_i) \Big|^2 \tag{6.80}$$

vanishes, respectively. Note that the Wigner D-functions $D^n_{k,k'} : \mathrm{SO}(3) \to \mathbb{C}$, $n \in \mathbb{N}_0$, $k, k' = -n, \ldots, n$, are defined in Section 5.2.3 by (5.46).

Hence, for the numerical computation of classical quadrature functionals $Q(\boldsymbol{P}, \boldsymbol{w})$ and $Q(\boldsymbol{P})$ we aim to minimize the functions $E_N(\boldsymbol{P}, \boldsymbol{w})$ and $E_N(\boldsymbol{P})$, respectively. For that reason we apply the nonlinear conjugate gradient method on Riemannian manifolds introduced in Section 3.3.1, since it is particular efficient in conjunction with fast matrix-vector multiplications with the Hessian and leads to very accurate results, which are needed for the computation of classical quadrature functionals. More precisely, we apply the Algorithm 3.3 and use the nonequispaced fast Fourier transforms on the rotation group SO(3) for the evaluation of $E_N(\boldsymbol{P}, \boldsymbol{w})$, or $E_N(\boldsymbol{P})$, as well as its derivatives, cf. Section 5.2.3. In particular, we are able to compute by Corollary 5.26 every step in the CG method, cf. Algorithm 3.3, in $\mathcal{O}(N^3 \log^2(N) + M)$ arithmetic operations, which is much more efficient, especially for $M \approx N^3$, than the naive evaluation of the sole functions $E_N(\boldsymbol{P}, \boldsymbol{w})$, or $E_N(\boldsymbol{P})$, cf. (6.54), (6.55), with arithmetic complexity $\mathcal{O}(N^3 M)$. Moreover, we note that quadrature functionals on the rotation group SO(3) which are invariant under orthogonal groups are naturally incorporated by the proposed optimization method on Riemannian manifolds, since Corollary 6.9 and Remark 6.10 for the sphere $\mathbb{S}^d$ can be stated similarly for the rotation group SO(3). In addition to the default parameters of Algorithm 3.3 given in Remark 3.29 we use after the kth iteration the termination conditions

$$\frac{E_N(\boldsymbol{P}^{(k)}, \boldsymbol{w}^{(k)}) - E_N(\boldsymbol{P}^{(k+1)}, \boldsymbol{w}^{(k+1)})}{|E_N(\boldsymbol{P}^{(k)}, \boldsymbol{w}^{(k)})|} < 10^{-6}, \qquad \|\nabla_{(\mathrm{SO}(3))^M \times \mathbb{R}^M} E_N(\boldsymbol{P}^{(k+1)}, \boldsymbol{w})\|_2 < 10^{-13},$$

and

$$\frac{E_N(\boldsymbol{P}^{(k)}) - E_N(\boldsymbol{P}^{(k+1)})}{|E_N(\boldsymbol{P}^{(k)})|} < 10^{-6}, \qquad \|\nabla_{(\mathrm{SO}(3))^M} E_N(\boldsymbol{P}^{(k+1)})\|_2 < 10^{-13},$$

respectively.

The corresponding algorithms are implemented in C++ and utilize the NFFT library [72] and the Eigen template library [39], which includes a matrix exponentiation algorithm for the computation of geodesics on the rotation group SO(3), cf. Theorem 3.15. For the NFSOFT routines of the NFFT library we set the cutoff parameter $m = 7$ and the threshold parameter $\kappa = 1000$. The computations are performed on an Intel® Core™ i7 CPU 920 with 12 GB RAM.

The Example 6.27 and 6.28 shows that with the proposed optimization approach we are able to compute for small polynomial degrees of exactness $N \in \mathbb{N}_0$ very precise and highly efficient quadrature functionals $Q(\boldsymbol{P}, \boldsymbol{w})$ and $Q(\boldsymbol{P})$, respectively. As discussed in Remark 6.4 for the sphere $\mathbb{S}^d$, we are confronted with the problem that the functions $E_N(\boldsymbol{P}, \boldsymbol{w})$, $E_N(\boldsymbol{P})$ possess even for moderate numbers of points M and polynomial degrees N many local minimizers for which the functions do not vanish. Therefore, we use a similar restart strategy to determine numerically a global minimum $(\boldsymbol{P}^*, \boldsymbol{w}^*) \in (\mathrm{SO}(3))^M \times \mathbb{R}^M$ and $\boldsymbol{P}^{**} \in (\mathrm{SO}(3))^M$ of the squared worst case quadrature error which satisfies

$$E_N(\boldsymbol{P}^*, \boldsymbol{w}^*) < 10^{-20} \qquad \text{and} \qquad E_N(\boldsymbol{P}^{**}) < 10^{-20}, \tag{6.81}$$

respectively. As in the case of the sphere $\mathbb{S}^2$ it seems that the above bound on the squared worst case quadrature error E_N might be sufficient for the determination of a global minimum, at least for moderate polynomial degrees N.

For the construction of high polynomial degrees we refer to the tensor-like construction given in Theorem 6.22, which leads in conjunction with our findings for quadrature functionals on the sphere $\mathbb{S}^2$ in Section 6.2.3 to very efficient quadrature functionals on the rotation group SO(3).

Example 6.27. For selected polynomial degrees $N \leq 14$ we aim to compute the most efficient quadrature functionals $Q(\boldsymbol{P}, \boldsymbol{w})$, $\boldsymbol{P} \in (\mathrm{SO}(3))^M$, $\boldsymbol{w} \in \mathbb{R}^M$, on the rotation group SO(3). Therefore, as on the sphere $\mathbb{S}^2$, we consider candidates of quadrature functionals $Q(\boldsymbol{P}, \boldsymbol{w})$ invariant under orthogonal groups, cf. Section 6.3.1, for which the efficiency $\mathrm{eff}_{\mathrm{SO}(3)}(Q(\boldsymbol{P}, \boldsymbol{w}))$ defined by (6.61) is greater than one.

We restrict our attention to the product group $\mathcal{G} \times \mathrm{C}_1$, where the group $\mathcal{G}$ is among the tetrahedral group T, the octahedral group O, the icosahedral group I, cf. (6.26), since for these groups the dimension $d^N_{\mathcal{G}\times\mathrm{C}_1}$ of the invariant polynomial space $\Pi^N_{\mathcal{G}\times\mathrm{C}_1}(\mathrm{SO}(3))$, cf. (6.70), is particular small with respect to the group size $|\mathcal{G} \times \mathrm{C}_1| = |\mathcal{G}|$, cf. Table 6.4 of Theorem 6.24. We recall that for these groups the invariant quadrature functional can be written as, cf. (6.71),

$$Q_{\mathcal{G}\times\mathrm{C}_1}(\boldsymbol{P}, \boldsymbol{w}) = \sum_{i=1}^{M_{\mathrm{gen}}} w_i \sum_{\boldsymbol{G}\in\mathcal{G}} I_{\delta_{\boldsymbol{G}\boldsymbol{R}_i}}, \qquad \boldsymbol{P} := (\boldsymbol{R}_1, \ldots, \boldsymbol{R}_M), \quad \boldsymbol{w} := (w_1, \ldots, w_M)^\top \in \mathbb{R}^M, \tag{6.82}$$

with $\boldsymbol{R}_i \notin \mathcal{G} \times \mathrm{C}_1 \cdot \boldsymbol{R}_j$ for $i \neq j$, $i, j = 1, \ldots, M_{\mathrm{gen}}$, where $M := |\mathcal{G}| M_{\mathrm{gen}}$, since all orbits have size $|\mathcal{G}|$, cf. (6.68). Now, we aim to match the degrees of freedom provided by an invariant quadrature functionals $Q_{\mathcal{G}\times\mathrm{C}_1}(\boldsymbol{P}, \boldsymbol{w})$ of the form (6.82) with the number of conditions imposed by the classical quadrature condition (6.57). We note, if we keep one orbit fixed, than there is no loss of degrees of freedom by rotational invariance, so that the the degrees of freedom are determined by $4(M_{\mathrm{gen}} - 1) + 1$. Hence, we consider only quadrature functionals $Q_{\mathcal{G}\times\mathrm{C}_1}(\boldsymbol{P}, \boldsymbol{w})$ of size

$$M := |\mathcal{G}| M_{\mathrm{gen}}, \quad M_{\mathrm{gen}} := \left\lceil \frac{d_{\mathcal{G}\times\mathrm{C}_1} + 3}{4} \right\rceil, \qquad N \in \mathbb{N}, \quad \mathcal{G} \in \{\mathrm{T}, \mathrm{O}, \mathrm{I}\},$$

in order to determine the most efficient candidates of quadrature functional invariant under the groups $\mathrm{T} \times \mathrm{C}_1$, $\mathrm{O} \times \mathrm{C}_1$, $\mathrm{I} \times \mathrm{C}_1$. By inspection of Table 6.4 we find under the above assumptions that the candidates for quadrature functionals $Q_{\mathcal{G}\times\mathrm{C}_1}(\boldsymbol{P}, \boldsymbol{w})$ with polynomial degree of exactness $N \leq 14$ and efficiency $\mathrm{eff}_{\mathrm{SO}(3)}(Q(\boldsymbol{P}, \boldsymbol{w})) \geq 1$ are invariant under the icosahedral group $\mathrm{I} \times \mathrm{C}_1$ for $N = 5, 9, 14$, the octahedral group $\mathrm{O} \times \mathrm{C}_1$ for $N = 7, 11$, and the tetrahedral group $\mathrm{T} \times \mathrm{C}_1$ for $N = 8$. For the remaining degrees $N \leq 14$ the efficiency turns out to be smaller than one. Therefore, we consider additionally to these particularly efficient cases noninvariant quadrature functionals $Q(\boldsymbol{P}, \boldsymbol{w})$ with efficiency one for polynomial degree $N \leq 6$, cf. Table 6.5.

The task is now to compute, for the above described configurations of the polynomial degree N, the size M, and the group $\mathcal{G}$, on the manifold $\mathcal{M} := (\mathrm{SO}(3))^M \times \mathbb{R}^M$ a global minimizer $(\boldsymbol{P}^*, \boldsymbol{w}^*) \in \mathcal{M}$ of the squared worst case quadrature error $E_N : \mathcal{M} \to [0, \infty)$, cf. (6.79). Since, our computations are performed in double precision we are satisfied if the squared worst case quadrature error passes the test (6.81).

The search strategy is the same as for the computation of optimal quadrature functionals on the sphere $\mathbb{S}^2$, cf. Example 6.18. For prescribed polynomial degree N, size M, and group $\mathcal{G}$ we perform at most 100 runs of the following procedure. In order to start with almost uniformly distributed points, we begin to perform 10 CG iterations for randomly distributed initial points invariant under the group $\mathcal{G}$ with respect to the electrostatic energy, generalized to the rotation group SO(3), defined by, cf. (3.80),

$$E(\boldsymbol{P}) := \sum_{\substack{i,j=1 \\ i\neq j}}^{M} \frac{1}{\|\boldsymbol{R}_i - \boldsymbol{R}_j\|_{\mathrm{F}}}, \qquad \boldsymbol{P} := (\boldsymbol{R}_1, \ldots, \boldsymbol{R}_M) \in (\mathrm{SO}(3))^M,$$

N	M	$\mathcal{E}$	$\mathcal{G}$	N	M	$\mathcal{E}$	$\mathcal{G}$
1	4	1	O	7	168	$1+\frac{4}{168}$	$\mathrm{O}\times\mathrm{C}_7$
2	11	1	T	8	240	$1+\frac{4}{240}$	$\mathrm{T}\times\mathrm{C}_1$
3	23	1	C_1	9	300	$1+\frac{34}{300}$	$\mathrm{I}\times\mathrm{C}_1$
4	43	1	C_1	11	504	$1+\frac{73}{504}$	$\mathrm{O}\times\mathrm{C}_1$
5	60	$1+\frac{13}{60}$	$\mathrm{I}\times\mathrm{I}$	14	960	$1+\frac{166}{960}$	$\mathrm{I}\times\mathrm{C}_1$
6	116	1	C_1				

Table 6.5: The putatively most efficient quadrature functionals $Q(\boldsymbol{P},\boldsymbol{w})$, $\boldsymbol{P}\in(\mathrm{SO}(3))^M$, $\boldsymbol{w}\in\mathbb{R}^M$, invariant under the tetrahedral group $\mathrm{T}\times\mathrm{C}_1$, the octahedral group $\mathrm{O}\times\mathrm{C}_1$, and the icosahedral group $\mathrm{I}\times\mathrm{C}_1$, with prescribed degree of exactness N are listed. M denotes the size of the quadrature functional $Q(\boldsymbol{P},\boldsymbol{w})$ and $\mathcal{E}:=\mathrm{eff}_{\mathrm{SO}(3)}(Q(\boldsymbol{P},\boldsymbol{w}))$ its efficiency defined by (6.61). $\mathcal{G}$ denotes the group under which the computed quadrature functionals are invariant, cf. (6.71). The quadrature functionals are found numerically and have a squared worst case quadrature error of $E_N(\boldsymbol{P},\boldsymbol{w})<$ 1e-20, cf. (6.79). For details see Example 6.27.

by using naive evaluation methods, which is reasonable for the given problem sizes. Afterward, the resulting point distribution is used for minimizing the squared equal weights worst case quadrature error $E_N(\boldsymbol{P})$, where we use at most 250 CG iterations. Finally, we optimize the obtained point distribution together with initial equal weights over the squared worst case quadrature error $E_N(\boldsymbol{P},\boldsymbol{w})$, where the maximal number of CG iterations is 10000. For some computed local minimizers which have not passed the test (6.81), by too slow convergence, we tried another run of the CG method.

In Table 6.5 we present the summarized results, where we observed for several quadrature functionals higher symmetry groups. We like to mention that on the sphere $\mathbb{S}^3$ the corresponding quadrature functionals with polynomial degree of exactness $2N+1$ for $N=1,3,4,5$ are already known, cf. [63], the remaining quadrature functionals seem to be new and improve the size of some other known constructions. Surprisingly, the quadrature functional with degree $N=2$ of size $M=11$ has not been established previously. The computed quadrature rules are publicly available at http://www.tu-chemnitz.de/~potts/workgroup/graef/quadrature/. □

Example 6.28. For selected polynomial degrees $N\le 23$ we aim to compute the most efficient equal weights quadrature functionals $Q(\boldsymbol{P})$, $\boldsymbol{P}\in(\mathrm{SO}(3))^M$, on the rotation group $\mathrm{SO}(3)$.

Therefore, as in Example 6.27, we consider candidates of quadrature functionals $Q(\boldsymbol{P})$ invariant under the product group $\mathcal{G}\times\mathrm{C}_1$, where the group $\mathcal{G}$ is among the tetrahedral group T, the octahedral group O, the icosahedral group I, cf. (6.26). We recall that for these groups the invariant quadrature functional can be written as, cf. (6.71),

$$Q_{\mathcal{G}\times\mathrm{C}_1}(\boldsymbol{P})=\frac{1}{M}\sum_{i=1}^{M_{\mathrm{gen}}}\sum_{\boldsymbol{G}\in\mathcal{G}}I_{\delta_{\boldsymbol{G}\boldsymbol{R}_i}},\qquad \boldsymbol{P}:=(\boldsymbol{R}_1,\ldots,\boldsymbol{R}_M),\tag{6.83}$$

with $\boldsymbol{R}_i\notin\mathcal{G}\times\mathrm{C}_1\cdot\boldsymbol{R}_j$ for $i\ne j$, $i,j=1,\ldots,M_{\mathrm{gen}}$, and $M:=|\mathcal{G}|M_{\mathrm{gen}}$. Again, we aim to match the degrees of freedom provided by an invariant quadrature functionals $Q_{\mathcal{G}\times\mathrm{C}_1}(\boldsymbol{P})$ of the form (6.83) with the number of conditions imposed by the classical quadrature condition (6.57), given by the dimension $d^N_{\mathcal{G}\times\mathrm{C}_1}$ of the invariant polynomial space $\Pi^N_{\mathcal{G}\times\mathrm{C}_1}(\mathrm{SO}(3))$, cf. (6.70). We note, if we keep one orbit fixed, than there is no loss of degrees of freedom by rotational invariance, so that the the degrees of freedom are determined by $3(M_{\mathrm{gen}}-1)$ where in contrast to general quadrature functionals only $d^N_{\mathcal{G}\times\mathrm{C}_1}-1$ conditions need to be satisfied . Hence, we consider only

N	M	$\mathcal{E}$	$\mathcal{G}$	N	M	$\mathcal{E}$	$\mathcal{G}$
1	4	$1+\frac{1}{4}$	O	9	360	$1+\frac{85}{360}$	$\mathrm{I}\times\mathrm{C}_3$
2	12	$1+\frac{2}{12}$	$\mathrm{T}\times\mathrm{T}$	11	672	$1+\frac{97}{672}$	$\mathrm{O}\times\mathrm{C}_2$
3	24	$1+\frac{6}{24}$	$\mathrm{O}\times\mathrm{O}$	13	1176	$1+\frac{44}{1176}$	$\mathrm{O}\times\mathrm{C}_7$
4	57	1	C_1	14	1260	$1+\frac{240}{1260}$	$\mathrm{I}\times\mathrm{C}_7$
5	60	$1+\frac{37}{60}$	$\mathrm{I}\times\mathrm{I}$	15	1776	$1+\frac{45}{1776}$	$\mathrm{O}\times\mathrm{C}_1$
6	154	1	C_1	17	2520	$1+\frac{72}{2520}$	$\mathrm{I}\times\mathrm{C}_1$
7	168	$1+\frac{61}{168}$	$\mathrm{O}\times\mathrm{C}_7$	19	3300	$1+\frac{255}{3300}$	$\mathrm{I}\times\mathrm{C}_1$
8	312	$1+\frac{13}{312}$	$\mathrm{T}\times\mathrm{C}_2$	23	5880	$1+\frac{263}{5880}$	$\mathrm{I}\times\mathrm{C}_7$

Table 6.6: The putatively most efficient equal weights quadrature functionals $Q(\boldsymbol{P})$, $\boldsymbol{P}\in(\mathrm{SO}(3))^M$, invariant under the tetrahedral group $\mathrm{T}\times\mathrm{C}_1$, the octahedral group $\mathrm{O}\times\mathrm{C}_1$, and the icosahedral group $\mathrm{I}\times\mathrm{C}_1$, with prescribed degree of exactness N are listed. M denotes the size of the quadrature functional $Q(\boldsymbol{P})$ and $\mathcal{E}:=\mathrm{eff}_{\mathrm{SO}(3)}(Q(\boldsymbol{P}))$ its efficiency defined by (6.76). $\mathcal{G}$ denotes the group under which the computed quadrature functionals are invariant, cf. (6.71). The quadrature functionals are found numerically and have a squared worst case quadrature error of $E_N(\boldsymbol{P})<$ 1e-20, cf. (6.80). For details see Example 6.28.

quadrature functionals $Q_{\mathcal{G}\times\mathrm{C}_1}(\boldsymbol{P},\boldsymbol{w})$ of size

$$M:=|\mathcal{G}|M_{\mathrm{gen}},\quad M_{\mathrm{gen}}:=\left\lceil\frac{d_{\mathcal{G}\times\mathrm{C}_1}+2}{3}\right\rceil,\qquad N\in\mathbb{N},\quad \mathcal{G}\in\{\mathrm{T},\mathrm{O},\mathrm{I}\},$$

in order to determine the most efficient candidates of quadrature functional invariant under the groups $\mathrm{T}\times\mathrm{C}_1$, $\mathrm{O}\times\mathrm{C}_1$, $\mathrm{I}\times\mathrm{C}_1$. By inspection of Table 6.4 we find under the above assumptions that the candidates for quadrature functionals $Q_{\mathcal{G}\times\mathrm{C}_1}(\boldsymbol{P})$ with polynomial degree of exactness $N\le 19$ and efficiency $\mathrm{eff}_{\mathrm{SO}(3)}(Q(\boldsymbol{P}))\ge 1$ are invariant under the tetrahedral group $\mathrm{T}\times\mathrm{C}_1$ for $N=2,8$, the octahedral group $\mathrm{O}\times\mathrm{C}_1$ for $N=3,7,11,13,15$, and icosahedral group $\mathrm{I}\times\mathrm{C}_1$ for $N=5,9,14,17,19$. For the remaining degrees $N\le 19$ the efficiency turns out to be smaller than one. Therefore, we consider additionally to these particularly efficient cases noninvarint quadrature functionals $Q(\boldsymbol{P},\boldsymbol{w})$ with efficiency one for polynomial degree $N\le 6$, cf. Table 6.5.

The task is now to compute, for the above described configurations of the polynomial degree N, the size M, and the group $\mathcal{G}$, on the manifold $\mathcal{M}:=(\mathrm{SO}(3))^M$ a global minimizer $(\boldsymbol{P}^*)\in\mathcal{M}$ of the squared worst case quadrature error $E_N:\mathcal{M}\to[0,\infty)$, cf. (6.80). Since, our computations are performed in double precision we are satisfied if the squared worst case quadrature error passes the test (6.81).

The search strategy is the same as for the computation of optimal equal weights quadrature functionals on the sphere $\mathbb{S}^2$, cf. Example 6.19. For prescribed polynomial degree N, size M, and group $\mathcal{G}$ we perform at most 150 runs of the CG method applied to the squared equal weights worst case quadrature error $E_N(\boldsymbol{P})$ of uniformly distributed initial points invariant under the group $\mathcal{G}$. For some computed local minimizers which have not passed the test (6.81), by too slow convergence, we tried another run of the CG method.

In Table 6.6 we present the summarized results, where we observed for several quadrature functionals higher symmetry groups. We like to mention that on the sphere $\mathbb{S}^3$ the corresponding t-designs with degree $t=2N+1$ for $N=1,2,3,5$ are well-know cf. [52]. The remaining equal weight quadrature functionals seem to be new and improve the size of some other known constructions. The computed quadrature rules are publicly available at http://www.tu-chemnitz.de/~potts/workgroup/graef/quadrature/. □

6.4 Low-Discrepancy Points on the Sphere $\mathbb{S}^d$

An important and interesting problem in several applications of mathematics is the computation of uniformly distributed points on the sphere $\mathbb{S}^2$, cf. [112], or more generally on the sphere $\mathbb{S}^d$, $d \in \mathbb{N}$. In that respect, the L^2-discrepancy introduced in Section 2.4 seems to be an appropriate optimality criterion. In particular, the case of the L^2-discrepancy over halfspaces $D^2_{\mathcal{H}_+}(\nu, \boldsymbol{P}, \boldsymbol{w})$, $\boldsymbol{P} \in (\mathbb{S}^d)^M$, $\boldsymbol{w} \in \mathbb{R}^M$, cf. (2.69), with respect to the natural product measure $\mu_D := \mu_{\mathbb{S}^d} \times \mu_{\mathbb{R}}$, cf. (2.66), has been extensively studied for the normalized canonical measure $\nu := \frac{1}{\omega_d}\mu_{\mathbb{S}^d}$, $\omega_d := \mu_{\mathbb{S}^d}(\mathbb{S}^d)$, and equal weights $\boldsymbol{w} := \frac{1}{M}(1, \dots, 1)^\top \in \mathbb{R}^M$, see the monographs [13, 35] and the references therein. For that reason, we will restrict our attention to that particular case and write for convenience $D^2_{\mathcal{H}_+}(\boldsymbol{P}) = D^2_{\mathcal{H}_+}(\nu, \boldsymbol{P}, \boldsymbol{w})$ since the measure ν and the weights $\boldsymbol{w}$ are fixed.

We recall that the so defined L^2-discrepancy $D^2_{\mathcal{H}_+}(\boldsymbol{P})$ has by Theorem 2.14 and Theorem 4.4, cf. (4.32), the discrepancy kernel

$$K_{\mathcal{H}_+}(\boldsymbol{x}, \boldsymbol{y}) = \omega_d - \frac{\omega_{d-1}}{d}\|\boldsymbol{x} - \boldsymbol{y}\|_2, \qquad \boldsymbol{x}, \boldsymbol{y} \in \mathbb{S}^d, \tag{6.84}$$

where $\omega_d := \mu_{\mathbb{S}^d}(\mathbb{S}^d)$, cf. (4.17). Hence, by Theorem 2.10, the L^2-discrepancy over halfspaces $D^2_{\mathcal{H}_+}(\boldsymbol{P})$ coincides with the worst case quadrature error $\mathrm{err}_{K_{\mathcal{H}_+}}(\nu, \boldsymbol{P})$, which by Theorem 2.7 can be written as

$$\begin{aligned}(D^2_{\mathcal{H}_+}(\boldsymbol{P}))^2 = \mathrm{err}_{K_{\mathcal{H}_+}}(\nu, \boldsymbol{P})^2 &= \frac{1}{M^2}\sum_{i,j=1}^{M} K_{\mathcal{H}_+}(\boldsymbol{p}_i, \boldsymbol{p}_j) - C_d \\ &= \frac{\omega_{d-1}}{d}\left(\frac{2\omega_{2d}\omega_{d-1}}{\omega_{2d-1}\omega_d} - \frac{1}{M^2}\sum_{i,j=1}^{M}\|\boldsymbol{p}_i - \boldsymbol{p}_j\|_2\right), \qquad \boldsymbol{P} := (\boldsymbol{p}_1, \dots, \boldsymbol{p}_M) \in (\mathbb{S}^d)^M,\end{aligned} \tag{6.85}$$

where the constant

$$C_d := \int_{\mathbb{S}^d}\int_{S^d} K_{\mathcal{H}_+}(\boldsymbol{x}, \boldsymbol{y})\mathrm{d}\nu(\boldsymbol{x})\mathrm{d}\nu(\boldsymbol{y}) = \omega_d - \frac{2\omega_{2d}\omega_{d-1}^2}{d\omega_{2d-1}\omega_d}, \qquad d \in \mathbb{N}, \tag{6.86}$$

is obtained from the Fourier coefficient λ_0 in the Fourier expansion of the Euclidean distance kernel $K_{\mathrm{E}}(\boldsymbol{x}, \boldsymbol{y}) = C - \|\boldsymbol{x} - \boldsymbol{y}\|_2$ given in Theorem 4.6. We remark that the relation (6.85) is known as Stolarsky's Invariant Principle, cf. [126], which states that the suitably normalized sum of the pairwise Euclidean distances between the points $\boldsymbol{p}_1, \dots, \boldsymbol{p}_M \in \mathbb{S}^d$ adds with the squared L^2-discrepancy $D^2_{\mathcal{H}_+}(\boldsymbol{P})$ to a constant.

The asymptotic of the optimal (lowest) L^2-discrepancy over halfspaces $D^2_{\mathcal{H}_+}(\boldsymbol{P}^*)$ for increasing $M \in \mathbb{N}$ has been established after a series of papers in [12]. In Theorem 6.29 we state this remarkable result equivalently for the minimal worst case quadrature error $\mathrm{err}^{**}_{K_{H_+},\nu}(M)$, cf. (2.42), and we remark that it improves the upper bound, cf. (6.86),

$$\mathrm{err}^{**}_{K_{\mathcal{H}_+},\nu}(M) \le \sqrt{\omega_d - C_d}M^{-\frac{1}{2}}, \qquad M \in \mathbb{N}, \tag{6.87}$$

obtained from Corollary 2.8. We note that the upper bound in (6.87) is the expectation value of the discrepancy for randomly distributed points, see the proof of Corollary 2.8.

Theorem 6.29. *Let the sphere $\mathbb{S}^d$ with normalized canonical measure $\nu := \frac{1}{\omega_d}\mu_{\mathbb{S}^d}$, $\omega_d := \mu_{\mathbb{S}^d}(\mathbb{S}^d)$, cf. (3.72), be given. Then the minimal equal weights worst case quadrature error $\mathrm{err}^{**}_{K_{H_+},\nu}(M)$, $M \in \mathbb{N}$, cf. (2.42), with respect to the discrepancy kernel $K_{\mathcal{H}_+} : \mathbb{S}^d \times \mathbb{S}^d \to \mathbb{R}$, cf. (6.84), which corresponds to the L^2-discrepancy over halfspaces $D^2_{\mathcal{H}_+}(\nu, \boldsymbol{P}, \boldsymbol{w})$, $\boldsymbol{P} \in (\mathbb{S}^d)^M$, $\boldsymbol{w} := \frac{1}{M}(1, \dots, 1) \in$*

$\mathbb{R}^M$, *cf.* (2.69), *obeys the bounds*

$$c_d M^{-\frac{1}{2}-\frac{1}{2d}} \leq \mathrm{err}^{**}_{\mathcal{H}_+,\nu}(M) \leq C_d M^{-\frac{1}{2}-\frac{1}{2d}}, \qquad M \in \mathbb{N}, \tag{6.88}$$

for some fixed constants $c_d, C_d > 0$, $d \in \mathbb{N}$.

Proof. The lower bound in (6.88) follows from the correspondence $D^2_{\mathcal{H}_+}(\boldsymbol{P}) = \mathrm{err}_{K_{\mathcal{H}_+}}(\nu, \boldsymbol{P})$, cf. (6.85), and the proof of the lower bound provided by [35, Theorem 2.24], cf. [35, Proposition 2.26]. As note in [35, p. 248], the lower bound in (6.88) can be proved to be sharp by a probability argument, which finishes the proof. ∎

Accordingly to Theorem 6.29 we call points $\boldsymbol{P}_M \in (\mathbb{S}^d)^M$, $d \in \mathbb{N}$, of a sequence $\{\boldsymbol{P}_M\}_{M\in\mathbb{N}}$, *low-discrepancy points on the sphere* $\mathbb{S}^d$ if they obey the bounds (6.88), i.e., there exists a fixed constant $\tilde{C} \geq 1$ such that

$$D^2_{\mathcal{H}_+}(\boldsymbol{P}_M) \leq \tilde{C}\mathrm{err}^{**}_{\mathcal{H}_+,\nu}(M) \leq \tilde{C} C_d M^{-\frac{1}{2}-\frac{1}{2d}}, \qquad M \in \mathbb{N}. \tag{6.89}$$

Since the computation of the L^2-discrepancy over halfspaces $D^2_{\mathcal{H}+}$ is with an arithmetic complexity of $\mathcal{O}(M^2)$ too expansive for large numbers of points M, we propose in Section 6.4.1 and 6.4.2 two alternative optimization approaches for the efficient computation of low-discrepancy points on the sphere $\mathbb{S}^d$ for moderate dimensions $d \in \mathbb{N}$. Both are based on the conjugate gradient method on Riemannian manifolds, where the efficient function evaluation algorithms of Chapter 5 are used. In Section 6.4.1 we restrict our attention to the sphere $\mathbb{S}^2$, and like to mention that the computation of low-discrepancy points on the sphere $\mathbb{S}^2$ is of particular interest in geoscience, see the monograph [48, Ch. 7] and Remark 6.30. We aim to approximate the discrepancy kernel $K_{\mathcal{H}_+}$, cf. (6.84), by polynomial kernels K_N, such that we are able to apply the nonequispaced fast Fourier transforms for the sphere $\mathbb{S}^2$ for efficient function evaluations, cf. Section 5.2.2. In Section 6.4.2 we consider a family of local kernels for the efficient computation of low-discrepancy points on the sphere $\mathbb{S}^d$. The kernels of consideration are discrepancy kernels $K_{\mathcal{B}_{\mathbb{R}^n},R}$, which correspond to the L^2-discrepancy over Euclidean balls $D^2_{\mathcal{B}_{\mathbb{R}^n},R}$, $R > 0$, cf. Section 2.4.3. The numerical results illustrated in Figure 6.3, 6.5, and 6.6 confirm the suitability of both optimization approaches.

6.4.1 Optimization by Fourier Approximation on the Sphere $\mathbb{S}^2$

For the sphere $\mathbb{S}^2$ the squared L^2-discrepancy over halfspaces $D^2_{\mathcal{H}_+}$ takes the form, cf. (6.85),

$$(D^2_{\mathcal{H}_+}(\boldsymbol{P}))^2 = \pi\left(\frac{4}{3} - \sum_{i,j=1}^{M} \|\boldsymbol{p}_i - \boldsymbol{p}_j\|_2\right), \qquad \boldsymbol{P} := (\boldsymbol{p}_1, \ldots, \boldsymbol{p}_M) \in (\mathbb{S}^2)^M. \tag{6.90}$$

Hence, from Theorem 4.6 in Section 4.2.2 the Fourier expansion of the discrepancy kernel $K_{\mathcal{H}_+} : \mathbb{S}^2 \times \mathbb{S}^2 \to \mathbb{R}$, cf. (6.84), in orthonormal spherical harmonics $Y_{n,k} \in L^2(\mathbb{S}^2)$ is given by

$$\begin{aligned} K_{\mathcal{H}_+}(\boldsymbol{x}, \boldsymbol{y}) &= 4\pi - \pi\|\boldsymbol{x} - \boldsymbol{y}\|_2 \\ &= 16\pi^2 + \sum_{n=1}^{\infty}\sum_{k=-n}^{n} \frac{16\pi^2}{(2n-1)(2n+1)(2n+3)} Y_{n,k}(\boldsymbol{x})\overline{Y}_{n,k}(\boldsymbol{y}), \qquad \boldsymbol{x}, \boldsymbol{y} \in \mathbb{S}^2. \end{aligned} \tag{6.91}$$

Remark 6.30. Cui and Freeden [29] introduced the notion of a generalized discrepancy as a quality criterion for the uniformity of point distributions on the sphere $\mathbb{S}^2$. It is readily seen that the generalized discrepancy, cf. [29, Definition 3.1], coincides with an equal weights worst case

quadrature error $\mathrm{err}_K(\mu_{\mathbb{S}^2}, \boldsymbol{P})$, $\boldsymbol{P} \in (\mathbb{S}^2)^M$, in a certain reproducing kernel Hilbert space $H_K(\mathbb{S}^2)$. In particular, the positive definite kernel

$$\begin{aligned} K_{\mathrm{CF}}(\boldsymbol{x}, \boldsymbol{y}) &:= 1 - 2\ln\left(1 + \sqrt{\frac{1 - \boldsymbol{x}^\top \boldsymbol{y}}{2}}\right) \\ &= 1 + \sum_{n=1}^{\infty} \sum_{k=-n}^{n} \frac{4\pi}{(2n+1)n(n+1)} Y_{n,k}(\boldsymbol{x}) \overline{Y}_{n,k}(\boldsymbol{y}), \qquad \boldsymbol{x}, \boldsymbol{y} \in \mathbb{S}^2, \end{aligned} \tag{6.92}$$

has been considered in [29], in order to compare several constructions of uniformly distributed points on the sphere $\mathbb{S}^2$ with respect to the equal weights quadrature error $\mathrm{err}_{K_{\mathrm{CF}}}(\mu_{\mathbb{S}^2}, \boldsymbol{P})$.

It is interesting to note that the discrepancy kernel $K_{\mathcal{H}_+}$, cf. (6.91), and the kernel K_{CF}, cf. (6.92), span the same Sobolev space

$$H^{\frac{3}{2}}(\mathbb{S}^2) := \left\{ f = \sum_{n=0}^{\infty} \sum_{k=-n}^{n} \hat{f}_{n,k} Y_{n,k} \in L^2(\mathbb{S}^2) \ : \ \sum_{n=0}^{\infty} \sum_{k=-n}^{n} (n+1)^3 |\hat{f}_{n,k}|^2 < \infty \right\} \subset L^2(\mathbb{S}^2),$$

such that low-discrepancy points, cf. (6.89), are almost optimally distributed with respect to the generalized discrepancy associated to the kernel K_{CF}. Especially, low-discrepancy points are equidistributed in $H^{\frac{3}{2}}(\mathbb{S}^2)$, cf. [29, Definition 3.2]. □

For the computation of low-discrepancy points $\boldsymbol{P} \in (\mathbb{S}^2)^M$, cf. (6.89), we apply the conjugate gradient method on Riemannian manifolds, cf. Section 3.3.1, to an approximate version of the squared L^2-discrepancy over halfspaces $(D^2_{\mathcal{H}_+}(\boldsymbol{P}))^2$. More precisely, we approximate the kernel $K_{\mathcal{H}_+}$, for some polynomial degree $N \in \mathbb{N}_0$, by the kernel

$$K_N(\boldsymbol{x}, \boldsymbol{y}) := 16\pi^2 + \sum_{n=1}^{N} \sum_{k=-n}^{n} \frac{16\pi^2}{(2n-1)(2n+1)(2n+3)} Y_{n,k}(\boldsymbol{x}) \overline{Y}_{n,k}(\boldsymbol{y}), \qquad \boldsymbol{x}, \boldsymbol{y} \in \mathbb{S}^2,$$

and optimize numerically the associated squared equal weights worst case quadrature error, cf. Theorem 2.7,

$$(\mathrm{err}_{K_N}(\nu, \boldsymbol{P}))^2 = \sum_{n=1}^{N} \sum_{k=-n}^{n} \frac{16\pi^2}{(2n-1)(2n+1)(2n+3)} \Big| \frac{1}{M} \sum_{i=1}^{M} \overline{Y}_{n,k}(\boldsymbol{p}_i) \Big|^2 \approx D^2_{\mathcal{H}_+}(\boldsymbol{P})^2, \ \nu := \frac{\mu_{\mathbb{S}^2}}{4\pi}, \tag{6.93}$$

instead of the L^2-discrepancy $D^2_{\mathcal{H}_+}$. In conjunction with the efficient evaluation algorithms for polynomial kernels on the sphere $\mathbb{S}^2$, cf. Section 5.2.2, we are able to compute, for the function err_{K_N}, every step of the nonlinear conjugate gradient method, cf. Algorithm 3.3, by Corollary 5.22 in $\mathcal{O}(N^2 \log^2(N) + M)$ arithmetic operations. Furthermore, we relate the number of points M and the polynomial degree N for some fixed constant $C > 0$ by

$$N := \lfloor C M^{\frac{1}{2}} \rfloor \tag{6.94}$$

and evaluate the function err_{K_N}, as well as its derivatives, in $\mathcal{O}(M \log^2(M))$ arithmetic operations, which is for large M much more efficient than the naive evaluation of the L^2-discrepancy $D^2_{\mathcal{H}_+}$ with $\mathcal{O}(M^2)$ arithmetic operations, cf. (6.90). For a comparison between the actual time consumption of a complete CG-iteration, cf. Algorithm 3.3, applied to the squared L^2-discrepancy $(D^2_{\mathcal{H}_+})^2$ and the squared equal weights worst case quadrature error $(\mathrm{err}_{K_N})^2$ we refer to the final Example 6.37 in Section 6.4.2. In spite of Remark 6.31 we show in Example 6.32 and 6.33 the suitability of this approximation approach.

Remark 6.31. We pass on a precise error analysis between the L^2-discrepancy over halfspaces $D^2_{\mathcal{H}_+}$, cf. (6.90), and the equal weights worst case quadrature error err_{K_N}, cf. (6.93), in dependence on the polynomial degree N and the number of points M. However, we note that, for a suitable approximation of $D^2_{\mathcal{H}^+}$ by err_{K_N}, the constant C in (6.94) should be sufficiently large, say greater than 2, as explained as follows.

From Remark 6.15 we know that equal weights quadrature functionals of size M with degree of exactness N do exist for $cN^2 \leq M$ for some constant $c > 0$. In other words, the equal weights worst case quadrature error err_{K_N} vanishes at a global minimizer for polynomial degrees N up to $c^{-\frac{1}{2}} M^{\frac{1}{2}}$. In contrast, the L^2-discrepancy over halfspaces $D^2_{\mathcal{H}_+}$ does not vanish at all, by the lower bound given in Theorem 6.29. □

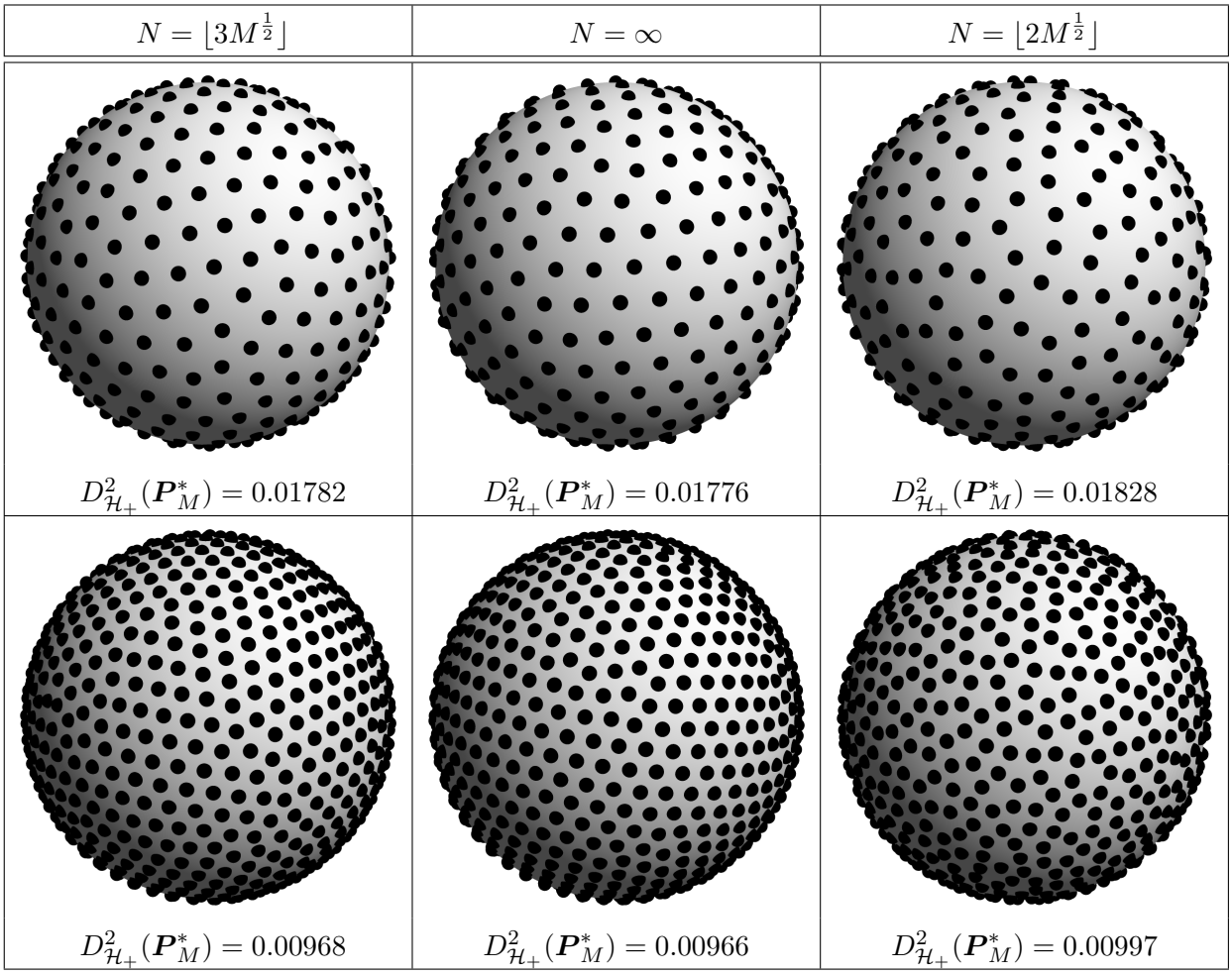

Figure 6.2: Illustrations of local minimizers $\boldsymbol{P}^*_M \in (\mathbb{S}^2)^M$, for $M = 400$ (top row) and $M = 900$ (bottom row), of the equal weights worst case quadrature error err_{K_N}, cf. (6.93), with polynomial degree $N = \lfloor 3M^{\frac{1}{2}} \rfloor$ (left column) and $N = \lfloor 2M^{\frac{1}{2}} \rfloor$ (right column), and of the L^2-discrepancy over halfspaces $D^2_{\mathcal{H}_+}$, cf. (6.90), (middle column) indicated by $N = \infty$. The corresponding values of the L^2-discrepancies over halfspaces $D^2_{\mathcal{H}_+}(\boldsymbol{P}^*_M)$ are given below the illustrations. For details see Example 6.32.

Example 6.32. We compute local minimizers $\boldsymbol{P}^*_M \in (\mathbb{S}^2)^M$ of the L^2-discrepancy over halfspaces $D^2_{\mathcal{H}_+}$, cf. (6.90), and the equal weights worst case quadrature error err_{K_N}, cf. (6.93), with $M = 400$ and $M = 900$ points, where the polynomial degree N is given by $N = \lfloor 3M^{\frac{1}{2}} \rfloor$ and

$N = \lfloor 2M^{\frac{1}{2}} \rfloor$, cf. (6.94). For that reason we apply Algorithm 3.3 with default parameters given in Remark 3.29 to the squared functions $(D^2_{\mathcal{H}_+})^2$, $(\mathrm{err}_{K_N})^2$, where we use the same randomly distributed initial points $\boldsymbol{P}^{(0)} \in (\mathbb{S}^2)^M$.

The algorithms are implemented in C++ and utilize the Eigen template library [39], and the NFFT library [72]. For the evaluation of the squared L^2-discrepancy $D^2_{\mathcal{H}_+}$ we use a naive summation algorithm, whereas for the squared worst case quadrature error $(\mathrm{err}_{K_N})^2$ we use the NFSFT routines of the NFFT library for the fast evaluation algorithms described in Section 5.2.2. In particular, we set the NFFT cutoff parameter $m = 7$ and the threshold parameter $\kappa = 1000$. We remark that the only termination condition is given by the maximal number of 50 line search iterations, cf. Remark 3.29.

As illustrated in Figure 6.2, it seems that the point distribution of the local minimizers with respect to $N = \lfloor 3M^{\frac{1}{2}} \rfloor$ mimics the point distribution of the local minimizers of the L^2-discrepancy $D^2_{\mathcal{H}_+}$ in a better way than that with respect to $N = \lfloor 2M^{\frac{1}{2}} \rfloor$, which is indicated by the slightly smaller values of the corresponding L^2-discrepancies $D^2_{\mathcal{H}_+}$. However, the latter choice of the polynomial degree N is computationally less expansive and seems to be sufficient for the computation of low-discrepancy points, as illustrated in Example 6.33. □

Example 6.33. For $M = 2^k$, $k = 3, \dots, 16$, we compute local minimizers $\boldsymbol{P}^*_M \in (\mathbb{S}^2)^M$ of the equal weights worst case quadrature error err_{K_N}, cf. (6.93), with polynomial degree $N = \lfloor 2M^{\frac{1}{2}} \rfloor$. We apply the same algorithm as described in Example 6.33 with an additional termination condition, in order to reduce the running time. More precisely, we terminate the CG method if the conditions, cf. Algorithm 3.3,

$$\frac{(\mathrm{err}_{K_N}(\nu, \boldsymbol{P}^{(k)}))^2 - (\mathrm{err}_{K_N}(\nu, \boldsymbol{P}^{(k+1)}))^2}{(\mathrm{err}_{K_N}(\nu, \boldsymbol{P}^{(k)}))^2} < 10^{-4}, \qquad \mathrm{d}_{(\mathbb{S}^2)^M}(\boldsymbol{P}^{(k+1)}, \boldsymbol{P}^{(k)}) < 10^{-4}$$

are fulfilled after the kth CG iteration.

Afterward, we compute for the local minimizers $\boldsymbol{P}^*_M$ the exact L^2-discrepancy over halfspaces $D^2_{\mathcal{H}_+}$, cf. (6.90), by a naive summation algorithm. As illustrated in Figure 6.3, it seems that these points follow the asymptotic behavior of low-discrepancy points, cf. (6.89). Moreover, it is remarkable that the L^2-discrepancies $D^2_{\mathcal{H}_+}(\boldsymbol{P}^*_M)$ are almost on the optimal asymptotic line $c_{\mathrm{opt}} M^{-\frac{3}{4}}$ conjectured by Brauchart, Hardin, and Saff [19, Conjecture 3], where the constant

$$c_{\mathrm{opt}} := 3^{5/8}(2\pi)^{1/4} \left(\zeta\left(\frac{3}{2}, 0\right) \left(\zeta\left(-\frac{1}{2}, \frac{1}{3}\right) - \zeta\left(-\frac{1}{2}, \frac{2}{3}\right) \right) \right)^{\frac{1}{2}} = -1.583855.. \quad , \tag{6.95}$$

can be computed by the use of the *Hurwitz zeta function* $\zeta(s, a)$, which is defined for $s \in \mathbb{C} \setminus \{1\}$ by analytic continuation of the series

$$\zeta(s, a) := \sum_{k=0}^{\infty} \frac{1}{(k + a)^s}, \qquad \mathrm{Re}(s) > 1, \quad \mathrm{Re}(a) > 0.$$

Finally, we compute the exact L^2-discrepancy over halfspaces $D^2_{\mathcal{H}_+}(\boldsymbol{P}_M)$ for 20 trials of randomly distributed points $\boldsymbol{P}_M \in (\mathbb{S}^2)^M$ and compare it in Figure 6.3 with the expectation value $\sqrt{\frac{4}{3}\pi} M^{-\frac{1}{2}}$ given by the upper bound in (6.87). Figure 6.3 illustrates that the numerical results are in perfect accordance with the theoretical result for low-discrepancy points and random points, cf. Theorem 6.29 and the proof of Corollary 2.8, respectively. □

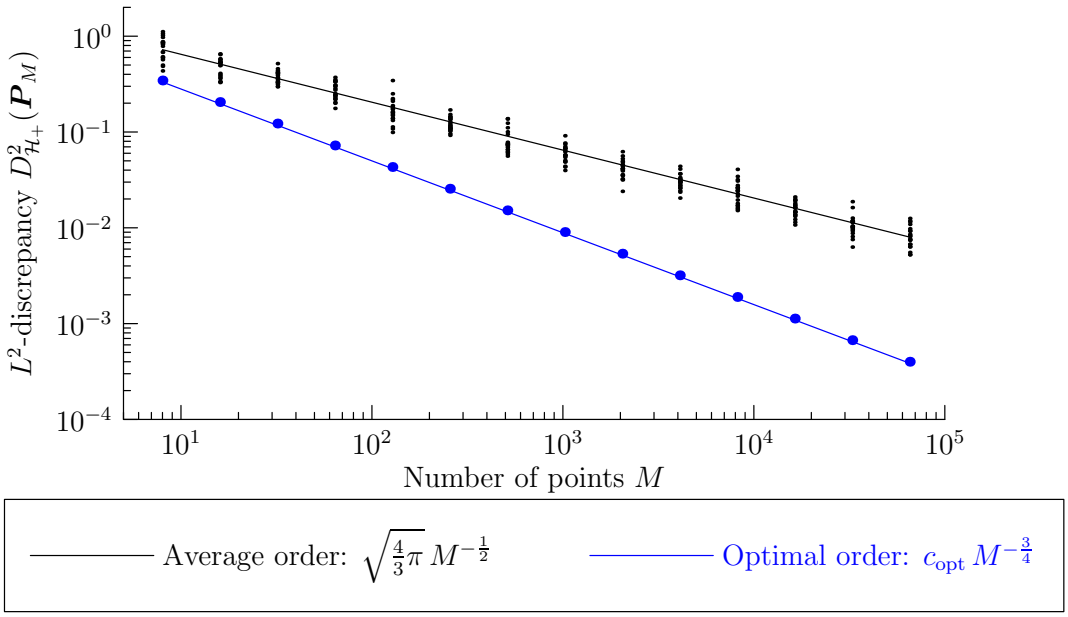

Figure 6.3: The L^2-discrepancy over halfspaces $D^2_{\mathcal{H}_+}(\boldsymbol{P}_M)$, cf. (6.90), of points $\boldsymbol{P}_M \in (\mathbb{S}^2)^M$, $M = 2^k$, $k = 3, \dots, 16$, are plotted for 20 trials of randomly distributed points (black dots) and for local minimizers (blue dots) of the equal weights worst case quadrature error err_{K_N}, cf. (6.93), with polynomial degree $N = \lfloor 2M^{\frac{1}{2}} \rfloor$. For details see Example 6.33, where the constant c_{opt} is defined by (6.95).

6.4.2 Optimization by Local Kernels on the sphere $\mathbb{S}^d$

We recall that the L^2-discrepancy over halfspaces $D^2_{\mathcal{H}_+}$ reads as, cf. (6.85),

$$(D^2_{\mathcal{H}_+}(\boldsymbol{P}))^2 = \frac{\omega_{d-1}}{d}\left(\frac{2\omega_{2d}\omega_{d-1}}{\omega_{2d-1}\omega_d} - \frac{1}{M^2}\sum_{i,j=1}^{M}\|\boldsymbol{p}_i - \boldsymbol{p}_j\|_2\right), \qquad \boldsymbol{P} := (\boldsymbol{p}_1, \dots, \boldsymbol{p}_M) \in (\mathbb{S}^d)^M, \tag{6.96}$$

where $\omega_d := \mu_{\mathbb{S}^d}(\mathbb{S}^d)$. Moreover, from the original definition (2.69) of the L^2-discrepancy over halfspaces $D^2_{\mathcal{H}_+}(\nu, \boldsymbol{P}, \boldsymbol{w})$, $\boldsymbol{P} \in (\mathbb{S}^d)^M$, $\boldsymbol{w} := \frac{1}{M}(1, \dots, 1)^\top \in \mathbb{R}^M$, we can, by the relation (4.32) between halfspaces and spherical caps

$$B_{\mathbb{S}^d}(\boldsymbol{c}, r) = \{\boldsymbol{y} \in \mathbb{S}^d \ : \ \boldsymbol{c}^\top \boldsymbol{y} \geq \cos(r)\}, \qquad \boldsymbol{c} \in \mathbb{S}^d, \quad r \in [0, \pi],$$

write equivalently

$$(D^2_{\mathcal{H}_+}(\boldsymbol{P}))^2 = \int_D \left|\nu(B_{\mathbb{S}^d}(\boldsymbol{c}, r)) - \frac{1}{M}\sum_{i=1}^{M}\delta_{\boldsymbol{p}_i}(B_{\mathbb{S}^d}(\boldsymbol{c}, r))\right|^2 \mathrm{d}\mu_D(\boldsymbol{c}, r), \qquad \nu := \frac{\mu_{\mathbb{S}^d}}{\omega_d}, \tag{6.97}$$

where the Borel measure μ_D is given by the density $\mathrm{d}\mu_D(\boldsymbol{c}, r) := \mathrm{d}\mu_{\mathbb{S}^d}(\boldsymbol{c})\sin(r)\mathrm{d}r$, $(\boldsymbol{c}, r) \in D := \mathbb{S}^d \times [0, \pi]$. In words, the L^2-discrepancy over halfspaces $D^2_{\mathcal{H}_+}$ can be considered by (6.97) as a weighted root mean square error of the differences between the measure $\nu(B_{\mathbb{S}^d}(\boldsymbol{c}, r))$ and the relative number of points $\boldsymbol{p}_1, \dots, \boldsymbol{p}_M \in \mathbb{S}^d$ contained in a spherical cap $B_{\mathbb{S}^d}(\boldsymbol{c}, r)$ with center $\boldsymbol{c} \in \mathbb{S}^d$ and radius $r \in [0, \pi]$. This geometric interpretation motivates us to consider the L^2-discrepancy over Euclidean balls $D^2_{\mathcal{B}_{\mathbb{R}^{d+1},R}}(\boldsymbol{P}) := D^2_{\mathcal{B}_{\mathbb{R}^{d+1},R}}(\nu, \boldsymbol{P}, \boldsymbol{w})$ with radius $R > 0$, cf. Section 2.4.3, which can be considered similarly as a weighted root mean squared error over spherical caps. More precisely, the L^2-discrepancy over Euclidean balls $D^2_{\mathcal{B}_{\mathbb{R}^{d+1},R}}$ can be written as, cf. (2.76),

(4.33),

$$\begin{aligned}(D^2_{\mathcal{B}_{\mathbb{R}^{d+1}},R}(\boldsymbol{P}))^2 &= \int_{\mathbb{R}^{d+1}} \left|\nu(B_{\mathbb{R}^{d+1}}(\boldsymbol{c},R)) - \frac{1}{M}\sum_{i=1}^{M}\delta_{\boldsymbol{p}_i}(B_{\mathbb{R}^{d+1}}(\boldsymbol{c},R))\right|^2 \mathrm{d}\boldsymbol{c} \\ &= \int_{D_R} \left|\nu(B_{\mathbb{S}^d}(\boldsymbol{c},r)) - \frac{1}{M}\sum_{i=1}^{M}\delta_{\boldsymbol{p}_i}(B_{\mathbb{S}^d}(\boldsymbol{c},r))\right|^2 \mathrm{d}\mu_{D_R}(\boldsymbol{c},r), \qquad R>0,\end{aligned} \tag{6.98}$$

where μ_{D_R} is some suitable finite Borel measure which is supported on a compact set $D_R \subset \mathbb{S}^d \times [0,\pi] \subset \mathbb{R}^{d+2}$ depending on the radius R. By comparing the right hand sides of the identities (6.97) and (6.98) we observe that the L^2-discrepancy over halfspaces $D^2_{\mathcal{H}_+}$ and the L^2-discrepancy over Euclidean balls $D^2_{\mathcal{B}_{\mathbb{R}^{d+1}},R}$ differ only in the choice of the weighting measure μ_D and μ_{D_R}. Due to this relation, we aim to compute local minimizers for the L^2-discrepancy over Euclidean balls $D^2_{\mathcal{B}_{\mathbb{R}^{d+1}},R}$ in order to approximate local minimizers of the L^2-discrepancy over halfspaces $D^2_{\mathcal{H}_+}$.

The advantage of considering the L^2-discrepancy over Euclidean balls $D^2_{\mathcal{B}_{\mathbb{R}^{d+1}},R}$ is that the corresponding discrepancy kernels $K_{\mathcal{B}_{\mathbb{R}^{d+1}},R}$ are local kernels, cf. (6.101), and thus allow for the efficient evaluation algorithm proposed in Section 5.1. We recall that the essence of the efficient evaluation for local kernels lies in the determination of the nearest neighbors of every point $\boldsymbol{p}_i \in \mathbb{S}^d$, $i = 1,\dots,M$, by Algorithm 5.1. Hence, the arithmetic complexity $\mathcal{O}(M^2)$ of the naive evaluation approach can only be beaten if we allow the locality radius R of the discrepancy kernel $K_{\mathcal{B}_{\mathbb{R}^{d+1}},R}$ to vary with the number of points M, cf. Theorem 5.8.

For the computation of low-discrepancy points $\boldsymbol{P} := (\boldsymbol{p}_1,\dots,\boldsymbol{p}_M) \in (\mathbb{S}^d)^M$, cf. (6.89), we compute with the conjugate gradient method on Riemannian manifolds, cf. Section 3.3.1, local minimizers of the L^2-discrepancy over Euclidean balls $D^2_{\mathcal{B}_{\mathbb{R}^{d+1}},R}$, where we relate the number of points M with the radius R for some fixed constant $C_d > 0$ by

$$R := C_d M^{-\frac{1}{d}}. \tag{6.99}$$

We recall that the L^2-discrepancy over Euclidean balls $D^2_{\mathcal{B}_{\mathbb{R}^{d+1}},R}$ can be written by Theorem 2.7 for some constant $C_{d,R} > 0$ as

$$(D^2_{\mathcal{B}_{\mathbb{R}^{d+1}},R}(\boldsymbol{P}))^2 = E_{d,R}(\boldsymbol{P}) - C_{d,R}, \qquad E_{d,R}(\boldsymbol{P}) := \frac{1}{M^2}\sum_{\substack{i,j=1,\\ i\neq j}}^{M} K_{\mathcal{B}_{\mathbb{R}^{d+1}},R}(\boldsymbol{p}_i,\boldsymbol{p}_j), \tag{6.100}$$

where the discrepancy kernel $K_{\mathcal{B}_{\mathbb{R}^{d+1}},R}$ reads by Theorem 2.10 and Theorem 2.16 with $s := \|\boldsymbol{x}-\boldsymbol{y}\|_2$, $\boldsymbol{x},\boldsymbol{y} \in \mathbb{S}^2$, as

$$K_{\mathcal{B}_{\mathbb{R}^{d+1}},R}(\boldsymbol{x},\boldsymbol{y}) = \begin{cases} \pi^{\frac{d+1}{2}} R^{d+1}\left(\frac{1}{\Gamma\left(\frac{d+3}{2}\right)} - \frac{s\,{}_2F_1\left(-\frac{d}{2},\frac{1}{2};\frac{3}{2};\frac{s^2}{4R^2}\right)}{\sqrt{\pi}R\Gamma\left(\frac{d}{2}+1\right)}\right), & 0 \le s \le 2R \\ 0, & s \ge 2R. \end{cases} \tag{6.101}$$

Hence, the L^2-discrepancy over Euclidean balls $D^2_{\mathcal{B}_{\mathbb{R}^{d+1}},R}$ can be computed explicitly (up to the constant $C_{d,R}$), and we will apply the evaluation algorithm described in Section 5.1 to the energy $E_{d,R}$, which has obviously the same local minimizers as $D^2_{\mathcal{B}_{\mathbb{R}^{d+1}},R}$, cf. (6.100). We remark that for (R,M,d,c)-quasi-uniformly distributed points, cf. (5.19), the evaluation of the energy $E_{d,R}$, as well as its derivatives, can be performed by Corollary 5.9 in $\mathcal{O}(3^{d+1}(d+1)^2 M\log((d+1)M))$ arithmetic operations, which is for large M much more efficient than the naive evaluation of the L^2-discrepancy $D^2_{\mathcal{H}_+}$ with $\mathcal{O}(M^2)$ arithmetic operations, cf. (6.96). For a comparison between the

actual time consumption of a complete CG-iteration, cf. Algorithm 3.3, applied to the squared L^2-discrepancy $(D^2_{\mathcal{H}_+})^2$ on the sphere $\mathbb{S}^2$ and the energy $E_{2,R}$, we refer to the final Example 6.37. Furthermore, after an appropriate choice of the constant C_d in (6.99) given in Remark 6.34, we show by the numerical Examples 6.35 and 6.36 the suitability of this optimization approach.

Remark 6.34. In order to ensure that the points of all local minimizers of the energy $E_{d,R}$, cf. (6.100), are uniformly distributed, we aim to avoid that the energy $E_{d,R}$ vanishes for any choices of the points $\boldsymbol{P} := (\boldsymbol{p}_1, \dots, \boldsymbol{p}_M) \in (\mathbb{S}^d)^M$. For $d \geq 2$, it is readily seen by a simple volume argument and the relation $R = \sqrt{2 - 2\cos(r)}$ between the Euclidean distance $R \in (0, 2]$ and the geodesic distance $r \in (0, \pi]$ on the sphere $\mathbb{S}^d$, cf. (4.31), that whenever M satisfies

$$M > \frac{\mu_{\mathbb{S}^d}(\mathbb{S}^d)}{\mu_{\mathbb{S}^d}(B_{\mathbb{S}^d}(\boldsymbol{c}, r))} \geq d\frac{\omega_d}{\omega_{d-1}R^d}, \qquad \boldsymbol{c} \in \mathbb{S}^d, \qquad \omega_d := \mu_{\mathbb{S}^d}(\mathbb{S}^d),$$

there exists two distinct points $\boldsymbol{x}, \boldsymbol{y} \in \{\boldsymbol{p}_1, \dots, \boldsymbol{p}_M\}$ such that the Euclidean distance $\|\boldsymbol{x} - \boldsymbol{y}\|_2$ is smaller than $2R$, so that $E_{d,R}(\boldsymbol{P}) > 0$, cf. (6.101). Hence, by comparing the left and right term in the above inequality we find that the constant C_d in (6.99) should satisfy

$$C_d \geq \left(d\frac{\omega_d}{\omega_{d-1}}\right)^{\frac{1}{d}}, \qquad d \geq 2. \qquad \square$$

Example 6.35. For the sphere $\mathbb{S}^2$, we compute local minimizers $\boldsymbol{P}^*_M \in (\mathbb{S}^2)^M$ of the L^2-discrepancy over halfspaces $D^2_{\mathcal{H}_+}$, cf. (6.96), and the L^2-discrepancy over Euclidean balls $D^2_{\mathcal{B}_{\mathbb{R}^3},R}$, cf. (6.100), with $M = 400$ and $M = 900$ points, where the radius R is given by $R = 2.4M^{-\frac{1}{2}}$ and $R = 2.9M^{-\frac{1}{2}}$, cf. (6.99). For that reason we apply Algorithm 3.3 with default parameters given in Remark 3.29 to the squared functions $(D^2_{\mathcal{H}_+})^2$, $(\mathrm{err}_{K_N})^2$, where we use the same randomly distributed initial points $\boldsymbol{P}^{(0)} \in (\mathbb{S}^2)^M$.

The algorithms are implemented in C++ and utilize the Eigen template library [39]. For the evaluation of the squared L^2-discrepancy over halfspaces $D^2_{\mathcal{H}_+}$ we use a naive summation algorithm, whereas for the squared L^2-discrepancy over Euclidean balls $D^2_{\mathcal{B}_{\mathbb{R}^3},R}$ we use the fast evaluation algorithms described in Section 5.1. We remark that the only termination condition is given by the maximal number of 50 line search iterations, cf. Remark 3.29.

As illustrated in Figure 6.4, it seems that the point distribution of the local minimizers with respect to $R = 2.4M^{-\frac{1}{2}}$ mimics the point distribution of the local minimizers of the L^2-discrepancy $D^2_{\mathcal{H}_+}$ in a better way than that with respect to $R = 2.9M^{-\frac{1}{2}}$, which is indicated by the slightly smaller values of the corresponding L^2-discrepancies $D^2_{\mathcal{H}_+}$. $\square$

Example 6.36. For $d = 2, 3, 4, 5$ and $M = 2^k$, $k = 3, \dots, 16$, we compute local minimizers $\boldsymbol{P}^*_M \in (\mathbb{S}^2)^M$ of the L^2-discrepancy over Euclidean balls $D^2_{\mathcal{B}_{\mathbb{R}^{d+1}},R}$, cf. (6.100), with $R := C_d M^{-\frac{1}{d}}$ and $C_2 := 2.4$, $C_3 := 1.8$, $C_4 := 1.7$, $C_5 := 1.6$. We note that the kernels $K_{\mathcal{B}_{\mathbb{R}^{d+1}},R}$, cf. (6.101), have for $s := \|\boldsymbol{x} - \boldsymbol{y}\|_2 \leq 2R$, $\boldsymbol{x}, \boldsymbol{y} \in \mathbb{S}^d$, the special form

$$\begin{aligned}
K_{\mathcal{B}_{\mathbb{R}^3},R}(\boldsymbol{x}, \boldsymbol{y}) &= \frac{1}{12}\pi(2R - s)^2(4R + s), \\
K_{\mathcal{B}_{\mathbb{R}^4},R}(\boldsymbol{x}, \boldsymbol{y}) &= \frac{1}{24}\pi R\left(24R^3 \arccos\left(\frac{s}{2R}\right) - s\sqrt{4 - \frac{s^2}{R^2}}\left(10R^2 - s^2\right)\right), \\
K_{\mathcal{B}_{\mathbb{R}^5},R}(\boldsymbol{x}, \boldsymbol{y}) &= \frac{1}{480}\pi^2(2R - s)^3\left(32R^2 + 18Rs + 3s^2\right),
\end{aligned}$$

$$K_{\mathcal{B}_{\mathbb{R}^6,R}}(\boldsymbol{x},\boldsymbol{y}) = \frac{1}{360}\pi^2 R\left(120R^5 \arccos\left(\frac{s}{2R}\right) - s\sqrt{4-\frac{s^2}{R^2}}\left(66R^4 - 13R^2s^2 + s^4\right)\right).$$

We apply the same algorithm as described in Example 6.35 with an additional termination condition, in order to reduce the running time. More precisely, we terminate the CG method if the conditions, cf. Algorithm 3.3,

$$\frac{(D^2_{\mathcal{B}_{\mathbb{R}^{d+1},R}}(\boldsymbol{P}^{(k)}))^2 - (D^2_{\mathcal{B}_{\mathbb{R}^{d+1},R}}(\boldsymbol{P}^{(k+1)}))^2}{(D^2_{\mathcal{B}_{\mathbb{R}^{d+1},R}}(\boldsymbol{P}^{(k)}))^2} < 10^{-4}, \qquad \mathrm{d}_{(\mathbb{S}^d)^M}(\boldsymbol{P}^{(k+1)},\boldsymbol{P}^{(k)}) < 10^{-4}$$

are fulfilled after the kth CG iteration.

Afterward, we compute for the points $\boldsymbol{P}^*_M$ the exact L^2-discrepancy over halfspaces $D^2_{\mathcal{H}_+}$, cf. (6.96), by a naive summation algorithm. As illustrated in Figure 6.5, it seems that these points have the asymptotic behavior of low-discrepancy points, cf. (6.89), so that the numerical results are in perfect accordance with the theoretical results provided by Theorem 6.29. □

Example 6.37. For $M = 200k$, $k = 1,\dots,25$, we compare the two optimization approaches given in Section 6.4.1 and 6.4.2 for the efficient computation of low-discrepancy points $\boldsymbol{P}_M \in (\mathbb{S}^2)^M$ on the sphere $\mathbb{S}^2$, cf. (6.89), with the naive optimization approach of minimizing the L^2-discrepancy over halfspace $D^2_{\mathcal{H}_+}$ directly. For that reason we measure, for randomly distributed initial points, the average time consumptions over the first 100 CG iterations of the conjugate gradient method on Riemannian manifolds, cf. Algorithm 3.3, applied to the squared L^2-discrepancy over halfspaces $(D^2_{\mathcal{H}_+})^2$, cf. (6.90), the squared equal weights worst case quadrature error $(\mathrm{err}_{K_N})^2$, cf. (6.93), and the energy $E_{2,R}$, cf. (6.100), where the polynomial degree and the radius is given by $N := \lfloor 2M^{\frac{1}{2}} \rfloor$ and $R := 2.4M^{-\frac{1}{2}}$, respectively.

For the evaluation of the squared L^2-discrepancy $(D^2_{\mathcal{H}_+})^2$, as well as its derivatives, we use the naive summation with arithmetic complexity $\mathcal{O}(M^2)$, whereas for the energy $E_{2,R}$ and the squared quadrature error $(\mathrm{err}_{K_N})^2$ we use the algorithms described in Section 5.1 and Section 5.2, respectively, for which the arithmetic complexity is almost linear in M. We implemented the algorithms in C++ by utilizing the Eigen template library [39], and the NFFT library [72], as in Example 6.32 and 6.35. The time measurements are performed on a single core of an AMD Phenom™ II X4 910e CPU with 8 GB RAM.

The numerical results are illustrated in Figure 6.6 and confirm the theoretical results given in Corollary 5.9 and Corollary 5.22. Especially, the optimization approach with local kernels is particular promising for the efficient computation of low-discrepancy points. □

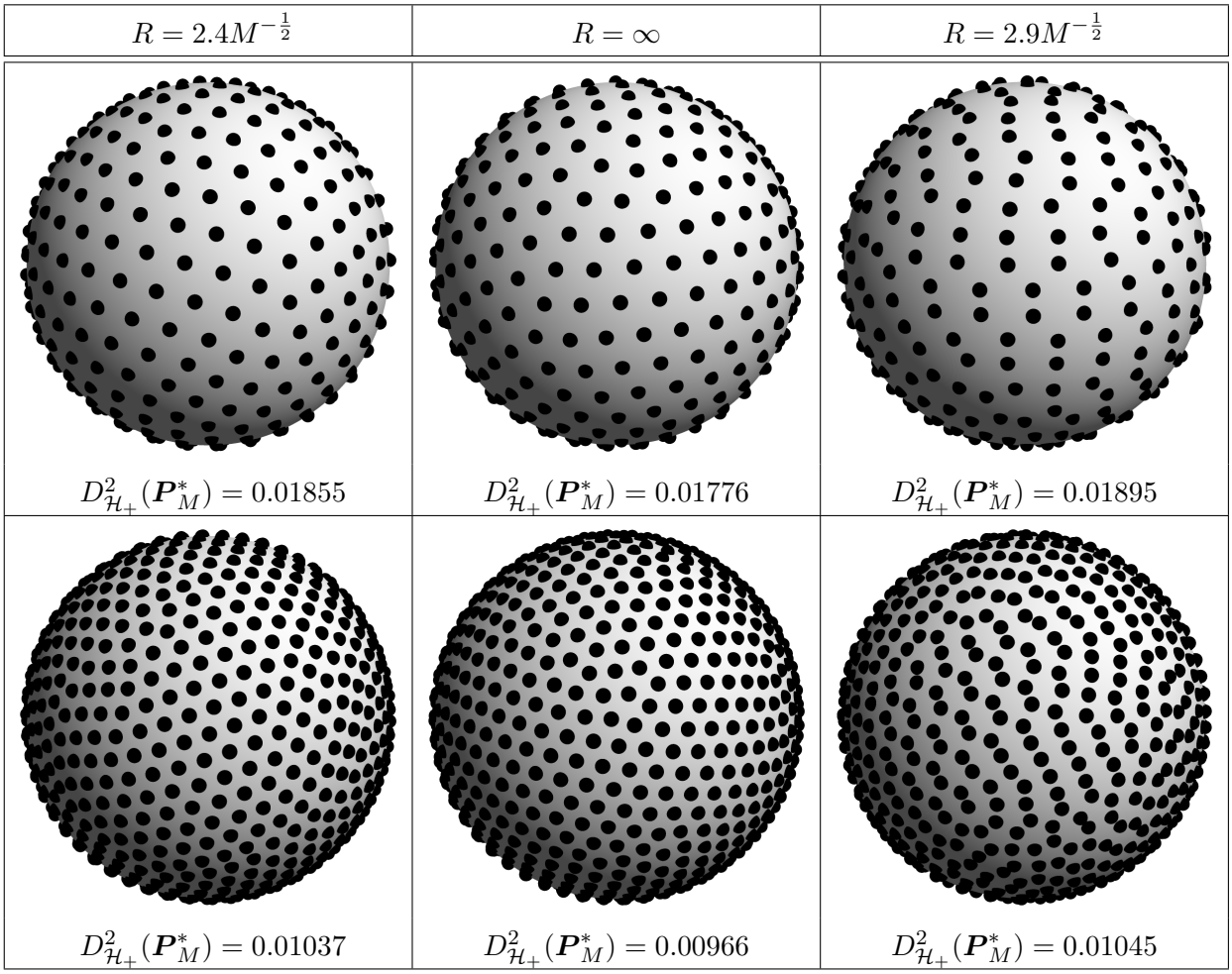

Figure 6.4: Illustrations of local minimizers $\boldsymbol{P}^*_M \in (\mathbb{S}^2)^M$, for $M = 400$ (top row) and $M = 900$ (bottom row), of the L^2-discrepancy over Euclidean Balls $D^2_{\mathcal{B}_{\mathbb{R}^3},R}$, cf. (6.100), with radius $R = 2.4M^{-\frac{1}{2}}$ (left column) and $R = 2.9M^{-\frac{1}{2}}$ (right column), and of the L^2-discrepancy over halfspaces $D^2_{\mathcal{H}_+}$, cf. (6.96), (middle column) indicated by $R = \infty$. The corresponding values of the L^2-discrepancies over halfspaces $D^2_{\mathcal{H}_+}(\boldsymbol{P}^*_M)$ are given below the illustrations. For details see Example 6.35.

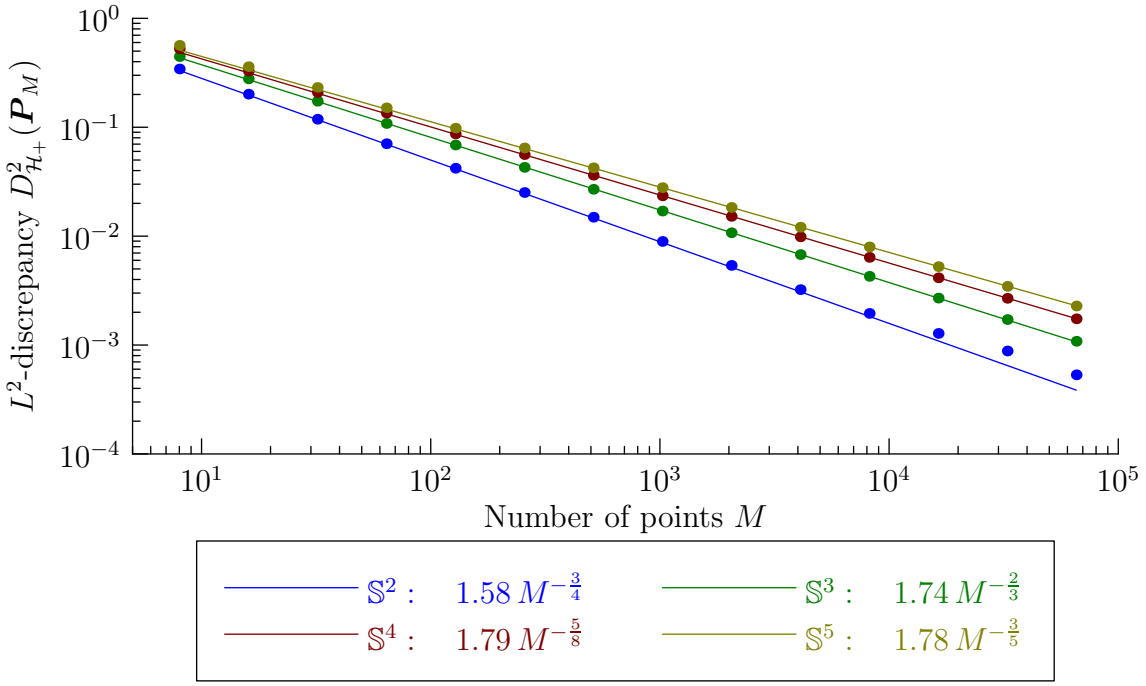

Figure 6.5: The L^2-discrepancy over halfspaces $D^2_{\mathcal{H}_+}(\boldsymbol{P}_M)$, cf. (6.96), of points $\boldsymbol{P}_M \in (\mathbb{S}^d)^M$, $M = 2^k$, $k = 3, \dots, 16$, is plotted for local minimizers of the L^2-discrepancy over Euclidean balls $D^2_{\mathcal{B}_{\mathbb{R}^{d+1},R}}$, cf. (6.100), for $d = 2$ (blue dots), $d = 3$ (green dots), $d = 4$ (red dots), and $d = 5$ (orange dots), with radius $R := C_d M^{-\frac{1}{d}}$ and $C_2 := 2.4$, $C_3 := 1.8$, $C_4 := 1.7$, $C_5 := 1.6$. For details see Example 6.36.

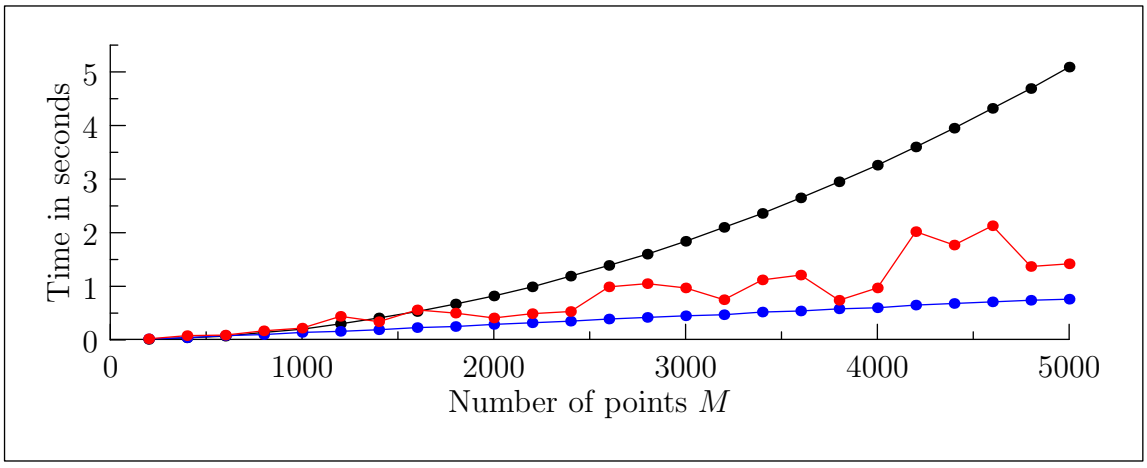

Figure 6.6: Time consumption of one CG iteration (averaged over the first 100 CG iterations), cf. Algorithm 3.3, for randomly distributed initial points $\boldsymbol{P}_M \in (\mathbb{S}^2)^M$, applied to the squared L^2-discrepancy over halfspaces $(D^2_{\mathcal{H}_+})^2$, cf. (6.90), (black dots), the squared equal weights worst case quadrature error $(\mathrm{err}_{K_N})^2$, cf. (6.93), (red dots), and the energy $E_{2,R}$, cf. (6.100), (blue dots), where the polynomial degree and the radius is given by $N := \lfloor 2M^{\frac{1}{2}} \rfloor$ and $R := 2.4M^{-\frac{1}{2}}$, respectively. For details see Example 6.37.

6.5 Halftoning

Halftoning is a method for creating the illusion of a continuous tone image having only a small number of tones available, see the monograph [132]. In what follows, we focus on two tones (black and white) and ask for the appropriate distribution of black dots. In contrast to *dithering*, where the dots are placed on a prescribed grid, we allow the dots to be distributed over a continuous domain. Such a particular halftoning process is also known as *stippling* or *continuous-domain quantization*. For an illustration of an image processed by halftoning see Figure 6.7. We remark that halftoning has been an active field of research for many years with many applications including printing and geometry processing [128] as well as sampling problems occurring in rendering [134], re-lighting [75], and artistic non-photorealistic image visualization [9, 115]. For a further and more detailed discussion we refer to our paper [58].

Figure 6.7: Left: Original 256×256 image 'Trui.png' provided by MATLAB® [87]. Right: Halftoning result by minimizing the energy (6.103) for the Euclidean distance kernel $K_{\mathrm{E}}(\boldsymbol{x}, \boldsymbol{y}) := \|\boldsymbol{x} - \boldsymbol{y}\|_2$, $\boldsymbol{x}, \boldsymbol{y} \in \mathbb{R}^2$, with $M = 30150$ points using the technique from [129].

Recently, a new approach for halftoning of images, which is based on electrostatic repulsion, has been proposed in [114]. More precisely, the positions $\boldsymbol{P} := (\boldsymbol{p}_1, \ldots, \boldsymbol{p}_M) \in \Omega^M$ of the black dots over a rectangular image domain $\Omega := [0, a] \times [0, b] \in \mathbb{R}^2$, $a, b > 0$, are determined by minimizing the electrostatic energy cf. (2.47),

$$E_\nu(\boldsymbol{P}) = \frac{1}{2} \sum_{i,j=1}^{M} \frac{q}{\|\boldsymbol{p}_i - \boldsymbol{p}_j\|_2} - \sum_{i=1}^{M} \int_\Omega \frac{1}{\|\boldsymbol{p}_i - \boldsymbol{x}\|_2} \mathrm{d}\nu(\boldsymbol{x}), \qquad q := \frac{1}{M}\nu(\Omega), \tag{6.102}$$

where the Borel measure ν is a continuous measure determined by the density $\mathrm{d}\nu(\boldsymbol{x}) = (1 - f(\boldsymbol{x}))\mathrm{d}\boldsymbol{x}$, $\boldsymbol{x} \in \Omega$, with a continuous function $f : \Omega \to [0, 1]$, which represents the gray values (0 is black, 1 is white) of the image. We recall that the particle positions $\boldsymbol{p}_i \in \Omega$, $i = 1, \ldots, M$, of the black dots are governed by electrostatic forces, and thus will arrange in an equilibrium state which mimics the gray distribution of the image, cf. Figure 6.7.

The algorithm described in [114] approximates the measure ν by a discrete measure $\tilde{\nu}$, which is obtained by sampling the density function f at an equispaced grid, and then aims to minimize the corresponding electrostatic energy by simulating the evolution of such a dynamic system. We note

that the evaluation of the energy E_ν and the electrostatic forces has an arithmetic complexity of $\mathcal{O}(M^2)$, such that in a following paper [129] a fast summation method, based on nonequispaced fast Fourier transforms, cf. [42, 107], has been applied for the evaluation in order to reduce this complexity.

Moreover, in [129] the electrostatic energy (6.102) has been generalized to energies of the form

$$E_{K,\nu}(\boldsymbol{P}) := \frac{\lambda}{2}\sum_{i,j=1}^{M} K(\boldsymbol{p}_i,\boldsymbol{p}_j) - \sum_{i=1}^{M}\int_\Omega K(\boldsymbol{p}_i,\boldsymbol{x})\mathrm{d}\nu(\boldsymbol{x}), \qquad \lambda := \frac{\nu(\Omega)}{M}, \tag{6.103}$$

where $K : \Omega\times\Omega \to \mathbb{R}$ is a radial kernel $K(\boldsymbol{x},\boldsymbol{y}) = \varphi(\|\boldsymbol{x}-\boldsymbol{y}\|_2)$ with $\varphi : [0,\infty) \to \mathbb{R}$. In particular, the Euclidean distance kernel $K_{\mathrm{E}}(\boldsymbol{x},\boldsymbol{y}) := -\|\boldsymbol{x}-\boldsymbol{y}\|_2$, $\boldsymbol{x},\boldsymbol{y}\in\mathbb{R}^2$, has been analyzed in [129]. We note that the relations, presented in Chapter 2, between the energy $E_{K,\nu}$ used for halftoning, and L^2-discrepancies, as well as the worst case quadrature error in reproducing kernel Hilbert spaces, has been established in our paper [58], where we introduced a more general approach of halftoning on compact domains like the torus $\mathbb{T}^2$ or the sphere $\mathbb{S}^2$. Especially, the relation to L^2-discrepancies leads to a geometric point of view, which is strongly related to the capacity constrained methods used in [6, 9].

For instance, we recall that the Euclidean distance kernel $K_{\mathrm{E}}(\boldsymbol{x},\boldsymbol{y}) = -\|\boldsymbol{x}-\boldsymbol{y}\|_2$ can be considered up to an additive constant as a discrepancy kernel of the L^2-discrepancy over halfspaces $D^2_{\mathcal{H}_+}$, cf. the proof of Corollary 2.15. Hence, the energy $E_{K_{\mathrm{E}},\nu}(\boldsymbol{P})$, cf. (6.103), can be considered, for equal weights $\boldsymbol{w} := (\lambda,\ldots,\lambda)\in\mathbb{R}^M$, as a squared L^2-discrepancy over halfspaces, cf. (2.69),

$$(D^2_{\mathcal{H}_+}(\nu,\boldsymbol{P},\boldsymbol{w}))^2 = \int_{D_\Omega}\left|\nu(h_+(\boldsymbol{n},d)\cap\Omega) - \lambda\sum_{i=1}^{M}\delta_{\boldsymbol{p}_i}(h_+(\boldsymbol{n},d)\cap\Omega)\right|^2\mathrm{d}\mu_D(\boldsymbol{n},d), \tag{6.104}$$

where $D_\Omega := \Phi^{-1}(H_\Omega)\subset D := \mathbb{S}^1\times\mathbb{R}$ is the set of all intersections of halfspaces $h_+(\boldsymbol{n},d)$ with Ω, cf. (2.61), and where the measure μ_D is determined by the density $\mathrm{d}\mu_D(\boldsymbol{n},d) := \mathrm{d}\mu_{\mathbb{S}^1}(\boldsymbol{n})\mathrm{d}d$, $(\boldsymbol{n},d)\in D$, cf. Example 2.13.

We recall that the geometric interpretation of the L^2-discrepancy $D^2_{\mathcal{H}_+}(\nu,\boldsymbol{P},\boldsymbol{w})$ is given as a weighted root mean square error of the differences between the measure $\nu(h_+(\boldsymbol{n},d)\cap\Omega)$ and the relative number of points $\boldsymbol{p}_1,\ldots,\boldsymbol{p}_M\in\Omega$ contained in the intersection $h_+(\boldsymbol{n},d)\cap\Omega$, see Figure 6.8 for an illustration. Using this point of view are able to generalize straightforwardly the setting of halftoning to arbitrary domains $X\subset\mathbb{R}^n$, by minimizing certain types of L^2-discrepancies for prescribed Borel measures ν. Moreover, our evaluation approach is based on Fourier approximation rather than spatial discretization, where we approximate the kernel K by a polynomial kernel K_N and not the measure ν by a discrete measure $\tilde{\nu}$ as done in [114, 129]. We emphasize on this difference, since the exact evaluation of the potential function, cf. (6.103), $h_{K,\nu}(\boldsymbol{y}) := \int_\Omega K(\boldsymbol{x},\boldsymbol{y})\mathrm{d}\nu(\boldsymbol{x})$, $\boldsymbol{y}\in\Omega$, is in general a very tough problem for continuous measures ν, cf. the examples in Section 2.5.2.

In the following Section 6.5.1 and 6.5.2 we consider halftoning on the torus $\mathbb{T}^2$ and the sphere $\mathbb{S}^2$, respectively, where we aim to approximate a given finite Borel measure ν by an appropriate distribution of points $\boldsymbol{P}\in X^M$, $X = \mathbb{T}^2,\mathbb{S}^2$. Therefore, we aim to minimize a weighted ball L^2-discrepancy $D^2_{\mathcal{B}_{\mathrm{d}_X}}$, cf. Section 2.4.1. In order to obtain efficient halftoning procedures we approximate the corresponding discrepancy kernel $K_{\mathcal{B}_{\mathrm{d}_X}}$ by polynomial kernels K_N and apply the conjugate gradient method on Riemannian manifolds, cf. Section 3.3.1, to the associated squared equal weights worst case quadrature error $(\mathrm{err}_{K_N}(\nu,\boldsymbol{P}))^2$, where we make use of the fast nonequispaced fast Fourier transforms, cf. Section 5.2. The numerical results presented in Example 6.39 and 6.41 show the suitability of our halftoning approach.

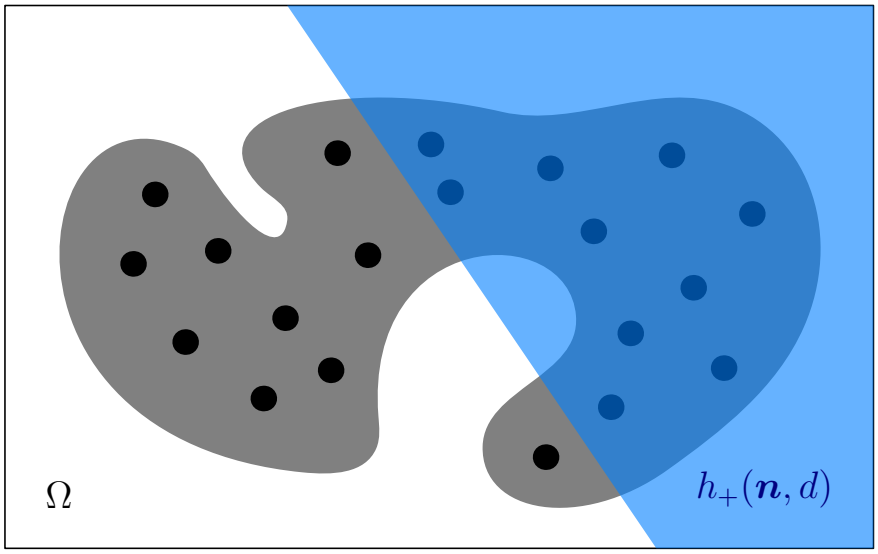

Figure 6.8: Illustration of a halfspace $h_+(\boldsymbol{n}, d)$ (blue) which intersects the image domain $\Omega \in \mathbb{R}^2$. The black dots are uniformly distributed over the support of the measure ν (gray), such that the L^2-discrepancy over halfspaces $D^2_{\mathcal{H}_+}$, cf. (6.104), becomes small.

6.5.1 The Torus $\mathbb{T}^2$

For halftoning on the torus $\mathbb{T}^2$, we consider, for a prescribed finite Borel measure ν supported on the torus $\mathbb{T}^2$, points $\boldsymbol{P} := (\boldsymbol{p}_1, \dots, \boldsymbol{p}_M) \in (\mathbb{T}^2)^M$, and equals weights $\boldsymbol{w} := (\lambda, \dots, \lambda) \in \mathbb{R}^M$, $\lambda := \frac{\nu(\mathbb{T}^2)}{M}$, the weighted ball L^2-discrepancy $D^2_{\mathcal{B}_{\mathrm{d}_{\mathbb{T}^2}}}(\nu, \boldsymbol{P}, \boldsymbol{w})$, which is defined in Section 2.4.1 by (2.56). For convenience we write $D^2_{\mathcal{B}_{\mathrm{d}_{\mathbb{T}^2}}}(\nu, \boldsymbol{P}) := D^2_{\mathcal{B}_{\mathrm{d}_{\mathbb{T}^2}}}(\nu, \boldsymbol{P}, \boldsymbol{w})$, since the weights $\boldsymbol{w}$ are uniquely determined by the measure ν. We recall that the basis set $\mathcal{B}_{\mathrm{d}_{\mathbb{T}^2}}$ of the weighted ball L^2-discrepancy $D^2_{\mathcal{B}_{\mathrm{d}_{\mathbb{T}^2}}}$ consists of balls

$$B_{\mathbb{T}^2}(\boldsymbol{c}, r) = \{\boldsymbol{x} \in \mathbb{T}^2 \ : \ \mathrm{d}_{\mathbb{T}^2}(\boldsymbol{x}, \boldsymbol{c}) < r\}, \qquad \boldsymbol{c} \in \mathbb{T}^2, \quad r > 0,$$

with respect to the geodesic distance, cf. (3.78),

$$\mathrm{d}_{\mathbb{T}^2}(\boldsymbol{x}, \boldsymbol{y}) = \min_{\boldsymbol{k} \in \mathbb{Z}^2} \|\boldsymbol{\alpha} - \boldsymbol{\beta} + 2\pi \boldsymbol{k}\|_2, \qquad \boldsymbol{x} = h(\boldsymbol{\alpha}), \quad \boldsymbol{y} = h(\boldsymbol{\beta}), \quad \boldsymbol{\alpha}, \boldsymbol{\beta} \in \mathbb{R}^2,$$

where we use the parameterization

$$h(\boldsymbol{\alpha}) := (\cos(\alpha_1), \sin(\alpha_1), \cos(\alpha_2), \sin(\alpha_2))^\top \in \mathbb{T}^2, \qquad \boldsymbol{\alpha} := (\alpha_1, \alpha_2)^\top \in \mathbb{R}^2. \tag{6.105}$$

For simplicity we restrict our attention to the weighted ball L^2-discrepancy $D^2_{\mathcal{B}_{\mathrm{d}_{\mathbb{T}^2}}}(\nu, \boldsymbol{P})$ with Lebesgue measure $\mu_{\mathbb{R}_+} := \mu_{[0,\pi]}$ on the interval $[0, \pi]$, which reads as, cf. (2.56),

$$(D^2_{\mathcal{B}_{\mathrm{d}_{\mathbb{T}^2}}}(\nu, \boldsymbol{P}))^2 = \int_0^\pi \int_{\mathbb{T}^2} \left| \nu(B_{\mathbb{T}^2}(\boldsymbol{c}, r)) - \lambda \sum_{i=1}^M \delta_{\boldsymbol{p}_i}(B_{\mathbb{T}^2}(\boldsymbol{c}, r)) \right|^2 \mathrm{d}\mu_{\mathbb{T}^2}(\boldsymbol{c}) \mathrm{d}r, \quad \lambda := \frac{\nu(\mathbb{T}^2)}{M}. \tag{6.106}$$

For that particular case we can use the explicit formula of the corresponding discrepancy kernel

$K_{\mathcal{B}_{\mathrm{d}_{\mathbb{T}^2}}}$ given in Theorem 4.1, which simplifies to

$$K_{\mathcal{B}_{\mathrm{d}_{\mathbb{T}^2}}}(\boldsymbol{x},\boldsymbol{y}) = \int_0^\pi \mu_{\mathbb{T}^2}(B_{\mathbb{T}^2}(\boldsymbol{x},r)\cap B_{\mathbb{T}^2}(\boldsymbol{y},r))\mathrm{d}r = \sum_{i=1}^4 A(s_i), \qquad \boldsymbol{x},\boldsymbol{y}\in\mathbb{T}^2, \tag{6.107}$$

where the function

$$\begin{aligned} A(s) &:= \int_0^\pi a(r,s)\mathrm{d}r \\ &= \begin{cases} \frac{\pi}{3}(2\pi^2\arccos(s/(2\pi)) - s\sqrt{4\pi^2-s^2}) - \frac{s^3}{12}\log(s/(2\pi+\sqrt{4\pi^2-s^2}))), & 0\le s\le 2\pi, \\ 0, & 2\pi\le s, \end{cases} \end{aligned}$$

is obtained by integration over the area of intersection of two Euclidean balls $B_{\mathbb{R}^2}(\boldsymbol{\alpha},r), B_{\mathbb{R}^2}(\boldsymbol{\beta},r)$ in the plane $\mathbb{R}^2$ with distance $s := \|\boldsymbol{\alpha}-\boldsymbol{\beta}\|_2$, $\boldsymbol{\alpha},\boldsymbol{\beta}\in\mathbb{R}^2$, and radius $r\in[0,\pi]$ given by

$$a(r,s) := \begin{cases} 2r^2\arccos(s/(2r)) - s\sqrt{r^2-s^2/4}, & r\ge s/2, \\ 0, & \text{else.} \end{cases}$$

The four distances s_i, $i=1,\dots,4$, of (6.107) are given by

$$\begin{aligned} s_1 &:= \|\boldsymbol{d}(\boldsymbol{x},\boldsymbol{y}) + (0,0)^\top\|_2, & s_2 &:= \|\boldsymbol{d}(\boldsymbol{x},\boldsymbol{y}) + (2\pi,0)^\top\|_2, \\ s_3 &:= \|\boldsymbol{d}(\boldsymbol{x},\boldsymbol{y}) + (0,2\pi)^\top\|_2, & s_4 &:= \|\boldsymbol{d}(\boldsymbol{x},\boldsymbol{y}) + (2\pi,2\pi)^\top\|_2, \end{aligned} \tag{6.108}$$

where the minimal distance vector $\boldsymbol{d}(\boldsymbol{x},\boldsymbol{y})\in\mathbb{R}^2$ is determined by, cf. (6.105),

$$\|\boldsymbol{d}(\boldsymbol{x},\boldsymbol{y})\|_2 = \min_{\substack{\boldsymbol{\alpha}\in h^{-1}(\boldsymbol{x}),\\ \boldsymbol{\beta}\in h^{-1}(\boldsymbol{y})}} \|\boldsymbol{\alpha}-\boldsymbol{\beta}\|_2.$$

For an illustration of the above relations we refer to the left of Figure 6.9, where we can easily observe that the discrepancy kernel $K_{\mathcal{B}_{\mathrm{d}_{\mathbb{T}^2}}}$ can be considered as a 2π-periodization of the radial kernel associated to function A, cf. (6.107). Furthermore, we recall that its Fourier expansion is given by, cf. Theorem 4.1,

$$K_{\mathcal{B}_{\mathrm{d}_{\mathbb{T}^2}}}(\boldsymbol{x},\boldsymbol{y}) = \sum_{\boldsymbol{n}\in\mathbb{Z}^2} \frac{\pi^5}{20}\,{}_2F_3\left(\frac{3}{2},\frac{5}{2};2,3,\frac{7}{2};-\pi^2\|\boldsymbol{n}\|_2^2\right)\mathrm{e}^{\mathrm{i}\boldsymbol{n}^\top(\boldsymbol{\alpha}-\boldsymbol{\beta})}, \qquad \boldsymbol{x}=h(\boldsymbol{\alpha}),\boldsymbol{y}=h(\boldsymbol{\beta})\in\mathbb{T}^2, \tag{6.109}$$

where the hypergeometric function ${}_2F_3$ is defined in (2.78).

For the efficient computation of points $\boldsymbol{P} := (\boldsymbol{p}_1,\dots\boldsymbol{p}_M)\in(\mathbb{T}^2)^M$, which approximate a prescribed finite Borel measure ν in an almost optimal way, we apply the nonlinear conjugate gradient method on Riemannian manifolds[6], cf. Section 3.3.1, to an approximate version of the squared weighted ball L^2-discrepancy $(D^2_{\mathcal{B}_{\mathrm{d}_{\mathbb{T}^2}}}(\nu,\boldsymbol{P}))^2$, cf. (6.106). More precisely, we approximate the discrepancy kernel $K_{\mathcal{B}_{\mathrm{d}_{\mathbb{T}^2}}}$, for some degree $N\in\mathbb{N}_0$ with index set $I_N := \mathbb{Z}^2\cap[-N,N]^2$, by

[6]The nonlinear conjugate gradient method on the torus $\mathbb{T}^2$ simplifies to the usual nonlinear conjugate gradient method in Euclidean space $\mathbb{R}^2$, cf. Remark 3.14 in Section 3.2.2.

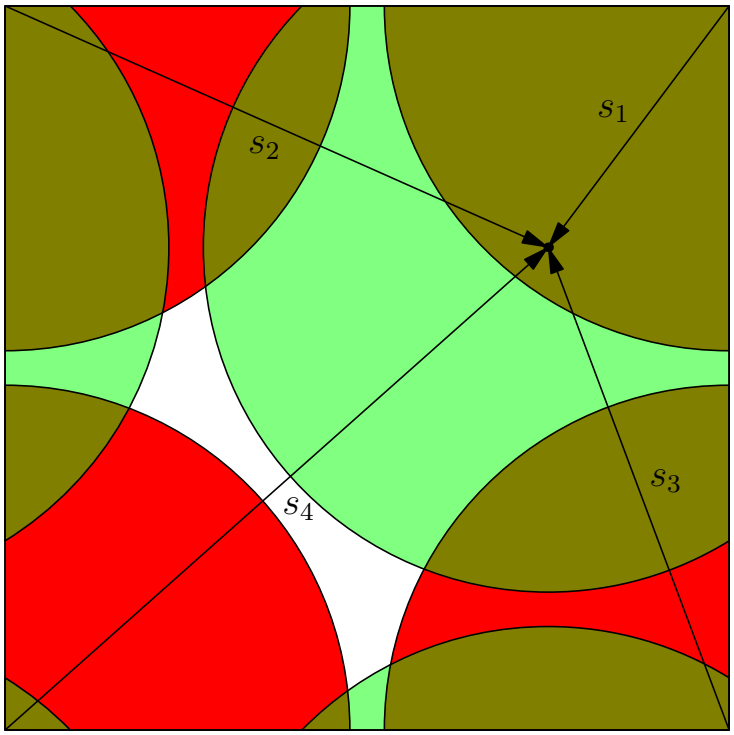

Figure 6.9: Visualization of the intersection of two distinct balls on the torus $\mathbb{T}^2$, where s_i, $i = 1, \ldots, 4$, are the four shortest distances between the two centers, cf. (6.108).

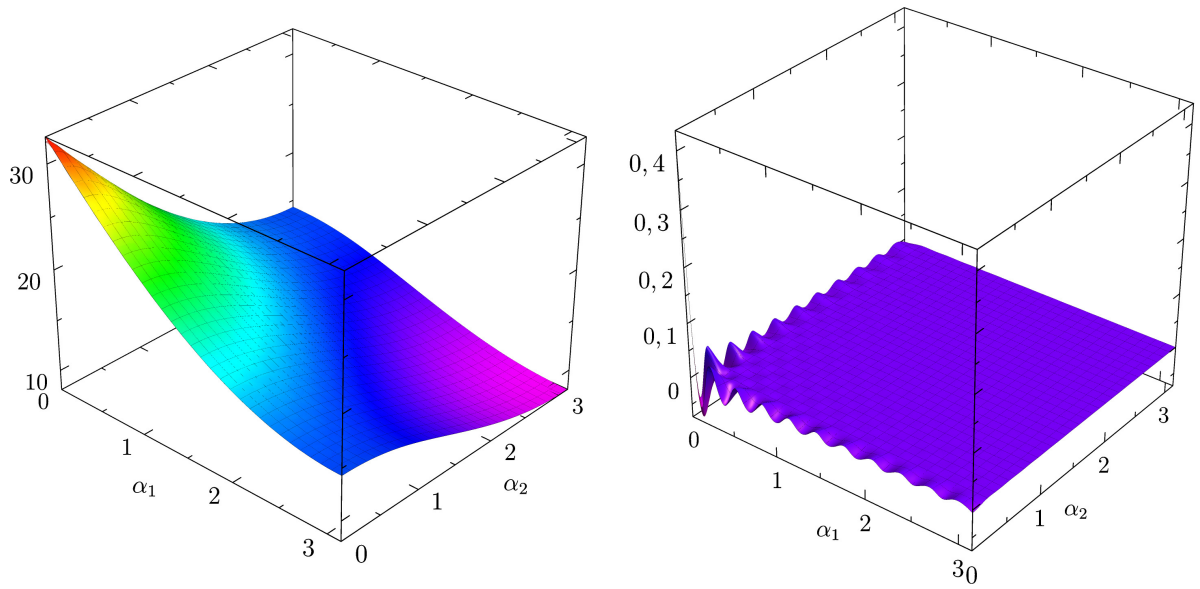

Figure 6.10: Illustration of the discrepancy kernel $K_{\mathcal{B}_{\mathrm{d}_{\mathbb{T}^2}}}$, cf. (6.107), and its polynomial approximation K_N, $N = 20$, cf. (6.110), by the function $k(\boldsymbol{\alpha}) := K_{\mathcal{B}_{\mathrm{d}_{\mathbb{T}^2}}}(h(\mathbf{0}), h(\boldsymbol{\alpha}))$ and $k_N(\boldsymbol{\alpha}) := K_N(h(\mathbf{0}), h(\boldsymbol{\alpha}))$ of $\boldsymbol{\alpha} = (\alpha_1, \alpha_2) \in [0, \pi]^2$, cf. (6.105), respectively. Left: Plot of k and k_N. Right: Plot of the difference $k - k_N$.

the kernel, cf. (6.109),

$$K_N(\boldsymbol{x},\boldsymbol{y}) := \sum_{\boldsymbol{n}\in I_N} \frac{\pi^5}{20}\, {}_2F_3\left(\frac{3}{2},\frac{5}{2};2,3,\frac{7}{2};-\pi^2\|\boldsymbol{n}\|_2^2\right) \mathrm{e}^{\mathrm{i}\boldsymbol{n}^\top(\boldsymbol{\alpha}-\boldsymbol{\beta})}, \qquad \boldsymbol{x}=h(\boldsymbol{\alpha}),\boldsymbol{y}=h(\boldsymbol{\beta})\in\mathbb{T}^2, \tag{6.110}$$

and optimize numerically the associated squared equal weights worst case quadrature error, cf. Theorem 2.7,

$$(\mathrm{err}_{K_N}(\nu,\boldsymbol{P}))^2 = \sum_{\boldsymbol{n}\in I_N} \frac{\pi^5}{20}\, {}_2F_3\left(\frac{3}{2},\frac{5}{2};2,3,\frac{7}{2};-\pi^2\|\boldsymbol{n}\|_2^2\right) \left|\hat{\nu}_{\boldsymbol{n}} - \lambda\sum_{i=1}^{M}\mathrm{e}^{-\mathrm{i}\boldsymbol{n}^\top\boldsymbol{p}_i}\right|^2 \approx (D^2_{\mathcal{B}_{\mathrm{d}_{\mathbb{T}^2}}}(\nu,\boldsymbol{P}))^2, \tag{6.111}$$

where $\lambda := \frac{4\pi^2}{M}\hat{\nu}_{\boldsymbol{0}}$ and where the Fourier coefficients of the measure ν are given by

$$\hat{\nu}_{\boldsymbol{n}} := \int_{\mathbb{T}^2} \mathrm{e}^{-\mathrm{i}\boldsymbol{n}^\top\boldsymbol{x}}\mathrm{d}\nu(\boldsymbol{x}), \qquad \boldsymbol{n}\in\mathbb{Z}^2. \tag{6.112}$$

For an illustration of the approximation of the discrepancy kernel $K_{\mathcal{B}_{\mathrm{d}_{\mathbb{T}^2}}}$ by the polynomial kernel K_N we refer to Figure 6.10.

In spite of Remark 6.38 we show in Example 6.39 the suitability of the proposed halftoning approach. For a comparison of our results with other halftoning methods we refer to the extensive experiments provided in [129], which show that the related method of energy minimizing achieves unsurpassed quality. Hence, our approach can keep up with the state-of-the-art techniques for halftoning of images. However, we note that in contrast to [129] the periodic boundary conditions on the torus $\mathbb{T}^2$ lead to some boundary artifacts, cf. Figure 6.7 and Figure 6.12.

Remark 6.38. For halftoning on the torus $\mathbb{T}^2$ we are only interested in visual appealing distributions of points $\boldsymbol{P}\in(\mathbb{T}^2)^M$ which approximate a prescribed finite Borel measure ν. Hence, we pass on a precise error analysis between the weighted ball L^2-discrepancy $D^2_{\mathcal{B}_{\mathrm{d}_{\mathbb{T}^2}}}$, cf. (6.106), and the equal weights worst case quadrature error err_{K_N}, cf. (6.111), in dependence on the measure ν, the polynomial degree N and the number of points M. However, it might be reasonable to relate the polynomial degree N and the number of points M, by some suitable large constant $C_\nu>0$ depending on the measure ν, due to the relation $N := \lfloor C_\nu M^{\frac{1}{2}}\rfloor$, as for the computation of low-discrepancy points on the sphere $\mathbb{S}^2$, cf. Section 6.4.1. In such a case we are able to evaluate every step of the nonlinear conjugate gradient method, cf. Algorithm 3.3, with help of the nonequispaced fast Fourier transforms in $\mathcal{O}(M\log(M))$ arithmetic operations, cf. Corollary 5.18. □

Example 6.39. We consider two Borel measures ν_1 and ν_2 supported on the torus $\mathbb{T}^2$ induced by functions $u_i:[0,2\pi)^2\to[0,1]$, $i=1,2$, of gray values (0 is black, 1 is white), which describe the densities $\mathrm{d}\nu_i(\boldsymbol{x}) = (1-u_i(\boldsymbol{\alpha}))\mathrm{d}\boldsymbol{\alpha}$, $\boldsymbol{x}=h(\boldsymbol{\alpha})$, $i=1,2$, cf. (6.105). The first function u_1 corresponds to the left image of Figure 6.7 and the second function u_2 to the Gaussian peak given by the left image of Figure 6.11. For the evaluation of the squared equal weights quadrature error $\mathrm{err}_{K_N}(\nu_i,\boldsymbol{P})$, $\boldsymbol{P}\in(\mathbb{T}^2)^M$, cf. (6.111), we need to determine the Fourier coefficients $(\hat{\nu}_i)_{\boldsymbol{n}}$, cf. (6.112), of the measures ν_i, $i=1,2$, for the index set $I_N := \mathbb{Z}^2\cap[-N,N]^2$. We perform this task by the use of two-dimensional FFTs in $\mathcal{O}(N^2\log(N))$ arithmetic operations.

After these preliminary steps we apply the Algorithm 3.3 with default parameters given in Remark 3.29 to the squared equal weights quadrature error $(\mathrm{err}_{K_N})^2$ in order to compute approximate local minimizers $\boldsymbol{P}^*\in(\mathbb{T}^2)^M$ of the weighted ball L^2-discrepancy $D^2_{\mathcal{B}_{\mathrm{d}_{\mathbb{T}^2}}}$, cf. (6.106). For efficient function evaluations we use the nonequispaced fast Fourier transforms on the torus $\mathbb{T}^2$ discussed in Section 5.2.1. The algorithm has been implemented in MATLAB® [87], where the

mex-interface to the NFFT library [72] is used. For the NFFT routine on the torus $\mathbb{T}^2$ we set the cutoff parameter $m = 9$. The computations are performed on an Intel® Core™ i7 CPU 920 with 12 GB RAM.

In Figure 6.12 we illustrate two halftoning results for the measure ν_1 with $M = 30150$ points. For comparison reasons, we terminate the CG method, applied to randomly distributed initial points $\boldsymbol{P}^{(0)}$, if the condition

$$\left\|\nabla_{\mathbb{T}^2}\left(\mathrm{err}_{K_N}\left(\nu_1, \boldsymbol{P}^{(k+1)}\right)\right)^2\right\|_2 \Big/ \left\|\nabla_{\mathbb{T}^2}\left(\mathrm{err}_{K_N}\left(\nu_1, \boldsymbol{P}^{(0)}\right)\right)^2\right\|_2 \leq \varepsilon$$

is fulfilled after the kth iteration, cf. Algorithm 3.3, for some prescribed accuracy $\varepsilon > 0$. The top image in Figure 6.12 shows the result for polynomial degree $N = 650$, where the accuracy $\varepsilon =$ 1e-3 is achieved after $k = 744$ CG iterations. The point distribution seems to be quite far from being a local minimizer of the equal weights quadrature error err_{K_N}. However, the halftoning result is reasonable and the computation takes about 15 minutes. In contrast, the bottom image of Figure 6.12 shows the result for polynomial degree $N = 1300$ and prescribed accuracy $\varepsilon =$ 1e-10 obtained after $k = 21157$ CG iterations. In that case the point distribution shows more regular 'hexagonal' patterns which is besides the low norm of the gradient a further indication to be very close to a local minimum, where such 'regularity artifacts' seem to occur, cf. [129]. However, the computation takes about 1 day, which illustrates the difficulty of finding highly accurate minimizers of such a high dimensional, nonlinear and nonconvex optimization problem. However, as seen in the top image of Figure 6.12, quite appealing point distributions are obtained after relatively few iterations, compared to the dimension of the problem.

In Figure 6.11 we illustrate on the right-hand side the halftoning result with respect to the measure ν_2 of a Gaussian peak for $M = 10023$ points and polynomial degree $N = 1300$. □

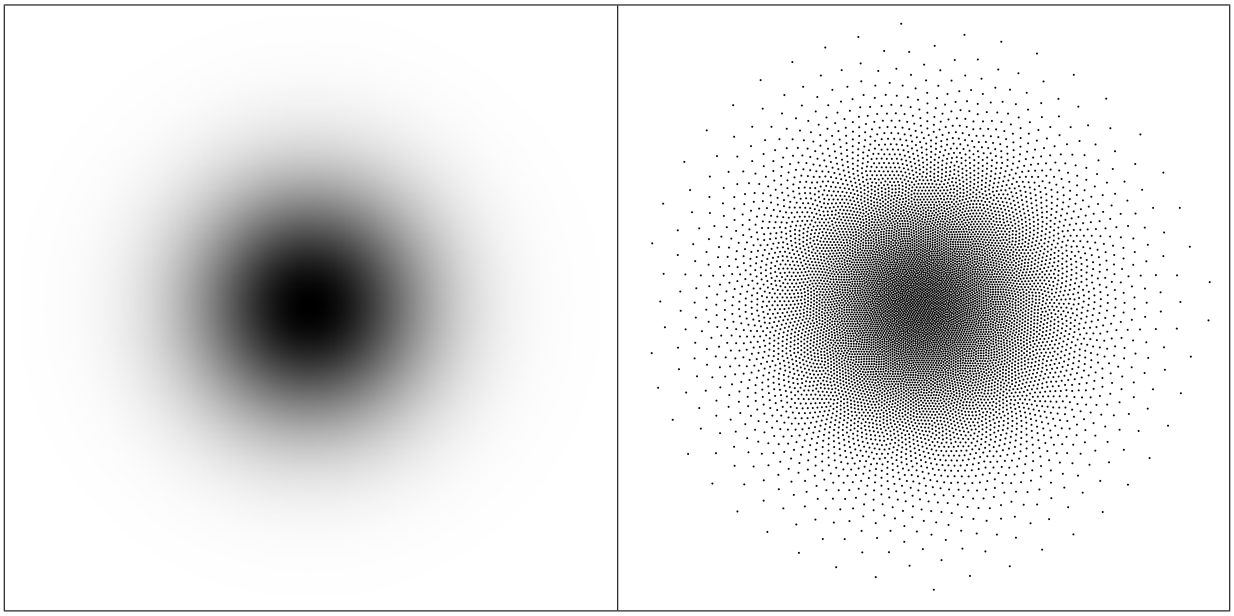

Figure 6.11: Halftoning result (right) on the torus $\mathbb{T}^2$ for an image of a Gaussian peak (left), which is obtained by minimizing the squared equal weights worst case quadrature error $(\mathrm{err}_{K_N})^2$, cf. (6.111), for $M = 10023$ randomly distributed initial points by the nonlinear conjugate gradient method, cf. Algorithm 3.3, for a polynomial degree $N = 1300$ after $k = 20000$ CG iterations. For details see Example 6.39.

Figure 6.12: Halftoning results on the torus $\mathbb{T}^2$ for the left image in Figure 6.7 with $M = 30150$ points, which are obtained by minimizing the squared equal weights worst case quadrature error $(\mathrm{err}_{K_N})^2$, cf. (6.111), for randomly distributed initial points by the nonlinear conjugate gradient method, cf. Algorithm 3.3, for polynomial degree $N = 650$ after $k = 744$ CG iterations (top) and for polynomial degree $N = 1300$ after $k = 21157$ CG iterations (bottom). For details see Example 6.39.

6.5.2 The Sphere $\mathbb{S}^2$

For halftoning on the sphere $\mathbb{S}^2$, we consider, for a prescribed finite Borel measure ν supported on the sphere $\mathbb{S}^2$, points $\boldsymbol{P} := (\boldsymbol{p}_1, \ldots, \boldsymbol{p}_M) \in (\mathbb{S}^2)^M$, and equal weights $\boldsymbol{w} := (\lambda, \ldots, \lambda) \in \mathbb{R}^M$, $\lambda := \frac{\nu(\mathbb{S}^2)}{M}$, the weighted ball L^2-discrepancy $D^2_{\mathcal{B}_{\mathrm{d}_{\mathbb{S}^2}}}(\nu, \boldsymbol{P}, \boldsymbol{w})$, which is defined in Section 2.4.1 by (2.56). For convenience we write $D^2_{\mathcal{B}_{\mathrm{d}_{\mathbb{S}^2}}}(\nu, \boldsymbol{P}) := D^2_{\mathcal{B}_{\mathrm{d}_{\mathbb{S}^2}}}(\nu, \boldsymbol{P}, \boldsymbol{w})$, since the weights $\boldsymbol{w}$ are uniquely determined by the measure ν. We recall that the basis set $\mathcal{B}_{\mathrm{d}_{\mathbb{S}^2}}$ of the weighted ball L^2-discrepancy $D^2_{\mathcal{B}_{\mathrm{d}_{\mathbb{S}^2}}}$ consists of spherical caps

$$B_{\mathbb{S}^2}(\boldsymbol{c}, r) = \{\boldsymbol{x} \in \mathbb{S}^2 \ : \ \mathrm{d}_{\mathbb{S}^2}(\boldsymbol{x}, \boldsymbol{c}) < r\}, \qquad \boldsymbol{c} \in \mathbb{S}^2, \quad r > 0,$$

with respect to the geodesic distance, cf. (3.68),

$$\mathrm{d}_{\mathbb{S}^2}(\boldsymbol{x}, \boldsymbol{y}) = \arccos(\boldsymbol{x}^\top \boldsymbol{y}), \qquad \boldsymbol{x}, \boldsymbol{y} \in \mathbb{S}^2.$$

For simplicity we restrict our attention to the weighted ball L^2-discrepancy $D^2_{\mathcal{B}_{\mathrm{d}_{\mathbb{S}^2}}}(\nu, \boldsymbol{P})$ with Lebesgue measure $\mu_{\mathbb{R}_+}$ given by the density $\mathrm{d}\mu_{\mathbb{R}_+}(r) = \frac{1}{\pi}\sin(r)\mathrm{d}r$ on the interval $[0, \pi]$, which reads as, cf. (2.56),

$$(D^2_{\mathcal{B}_{\mathrm{d}_{\mathbb{S}^2}}}(\nu, \boldsymbol{P}))^2 = \frac{1}{\pi}\int_0^\pi \int_{\mathbb{S}^2} \left|\nu(B_{\mathbb{S}^2}(\boldsymbol{c}, r)) - \lambda \sum_{i=1}^M \delta_{\boldsymbol{p}_i}(B_{\mathbb{S}^2}(\boldsymbol{c}, r))\right|^2 \mathrm{d}\mu_{\mathbb{S}^2}(\boldsymbol{c}) \sin(r)\mathrm{d}r, \ \lambda := \frac{\nu(\mathbb{S}^2)}{M}. \tag{6.113}$$

For that particular case we recall the explicit formula of the corresponding discrepancy kernel $K_{\mathcal{B}_{\mathrm{d}_{\mathbb{S}^2}}}$ given in Theorem 4.4, which simplifies to the Euclidean distance kernel, cf. Corollary 2.15,

$$K_{\mathcal{B}_{\mathrm{d}_{\mathbb{S}^2}}}(\boldsymbol{x}, \boldsymbol{y}) = \int_0^\pi \mu_{\mathbb{S}^2}(B_{\mathbb{S}^2}(\boldsymbol{x}, r) \cap B_{\mathbb{S}^2}(\boldsymbol{y}, r)) \sin(r)\mathrm{d}r = 4 - \|\boldsymbol{x} - \boldsymbol{y}\|_2, \qquad \boldsymbol{x}, \boldsymbol{y} \in \mathbb{S}^2,$$

with Fourier expansion in orthonormal spherical harmonics $Y_{n,k} \in L^2(\mathbb{S}^2)$, Theorem 4.6,

$$K_{\mathcal{B}_{\mathrm{d}_{\mathbb{S}^2}}}(\boldsymbol{x}, \boldsymbol{y}) = 16\pi + \sum_{n=1}^\infty \sum_{k=-n}^n \frac{16\pi}{(2n-1)(2n+1)(2n+3)} Y_{n,k}(\boldsymbol{x})\overline{Y}_{n,k}(\boldsymbol{y}), \qquad \boldsymbol{x}, \boldsymbol{y} \in \mathbb{S}^2. \tag{6.114}$$

We remark that this type of kernel has been already successfully applied for halftoning of images in Euclidean space $\mathbb{R}^2$, cf. [129].

For the efficient computation of points $\boldsymbol{P} := (\boldsymbol{p}_1, \ldots, \boldsymbol{p}_M) \in (\mathbb{S}^2)^M$, which approximate a prescribed finite Borel measure ν in an almost optimal way, we apply the conjugate gradient method on Riemannian manifolds, cf. Section 3.3.1, to an approximate version of the squared weighted ball L^2-discrepancy $(D^2_{\mathcal{B}_{\mathrm{d}_{\mathbb{S}^2}}}(\nu, \boldsymbol{P}))^2$, cf. (6.113). More precisely, we approximate the discrepancy kernel $K_{\mathcal{B}_{\mathrm{d}_{\mathbb{S}^2}}}$, for some polynomial degree $N \in \mathbb{N}_0$, by the kernel, cf. (6.114),

$$K_N(\boldsymbol{x}, \boldsymbol{y}) := 16\pi + \sum_{n=1}^N \sum_{k=-n}^n \frac{16\pi}{(2n-1)(2n+1)(2n+3)} Y_{n,k}(\boldsymbol{x})\overline{Y}_{n,k}(\boldsymbol{y}), \qquad \boldsymbol{x}, \boldsymbol{y} \in \mathbb{S}^2,$$

and optimize numerically the associated squared equal weights worst case quadrature error, cf.

Theorem 2.7,

$$(\mathrm{err}_{K_N}(\nu,\boldsymbol{P}))^2 = \sum_{n=1}^{N}\sum_{k=-n}^{n}\frac{16\pi}{(2n-1)(2n+1)(2n+3)}\Big|\nu_{n,k}-\lambda\sum_{i=1}^{M}\overline{Y}_{n,k}(\boldsymbol{p}_i)\Big|^2 \approx (D^2_{\mathcal{B}_{\mathrm{d}_{\mathbb{S}^2}}}(\nu,\boldsymbol{P}))^2, \tag{6.115}$$

where $\lambda := \frac{\sqrt{4\pi}}{M}\hat{\nu}_{0,0}$ and where the Fourier coefficients of the measure ν are given by

$$\hat{\nu}_{n,k} := \int_{\mathbb{S}^2}\overline{Y}_{n,k}(\boldsymbol{x})\mathrm{d}\nu(\boldsymbol{x}), \qquad n\in\mathbb{N}_0, \quad k=-n,\ldots,n. \tag{6.116}$$

In spite of Remark 6.40 we show in Example 6.41 the suitability of the proposed halftoning approach.

Remark 6.40. For halftoning on the sphere $\mathbb{S}^2$ we are only interested in visual appealing distributions of points $\boldsymbol{P}\in(\mathbb{S}^2)^M$ which approximate a prescribed finite Borel measure ν. Hence, we pass on a precise error analysis between the weighted ball L^2-discrepancy $D^2_{\mathcal{B}_{\mathrm{d}_{\mathbb{S}^2}}}$, cf. (6.113), and the equal weights worst case quadrature error err_{K_N}, cf. (6.115), in dependence on the measure ν, the polynomial degree N, and the number of points M. However, it might be reasonable to relate the polynomial degree N and the number of points M, by some suitable large constant $C_\nu>0$ depending on the measure ν, due to the relation $N := \lfloor C_\nu M^{\frac{1}{2}}\rfloor$, see also the Remark 6.31 given in Section 6.4.1 for the computation of low-discrepancy points on the sphere $\mathbb{S}^2$. In that case we are able to evaluate every step of the nonlinear conjugate gradient method, cf. Algorithm 3.3, with help of the nonequispaced fast Fourier transforms in $\mathcal{O}(M\log(M))$ arithmetic operations, cf. Corollary 5.22. □

Example 6.41. We consider two Borel measures ν_1 and ν_2 supported on the sphere $\mathbb{S}^2$ induced by the weight functions $v_i:\mathbb{S}^2\to[0,1]$, $i=1,2$, which describe the densities $\mathrm{d}\nu_i(\boldsymbol{x}) = v_i(\boldsymbol{x})\mathrm{d}\mu_{\mathbb{S}^2}(\boldsymbol{x})$. The first function v_1 is obtain from the topography map of the earth provided by MATLAB® [87], cf. Figure 6.14, where we scale the earth's elevation data to the range of gray values $[0,1]$. We remark that the data is only available on the grid

$$\mathcal{G} := \Big\{\boldsymbol{x}_{i,j} := h\Big(i\frac{\pi}{180}, j\frac{\pi}{180}\Big)\in\mathbb{R}^3 \ :\ i=1,\ldots,180,\ j=1,\ldots,360\Big\}\subset\mathbb{S}^2, \tag{6.117}$$

where $h:[0,\pi]\times(0,2\pi]\to\mathbb{S}^2$ is the standard parameterization in spherical coordinate, cf. (3.71). The second function v_2 is given by

$$v_2(\boldsymbol{x}) := \begin{cases}\frac{1}{3\sqrt{1-x_3^2}}\mathrm{sech}\left(3\sqrt{1-x_3^2}\right)^2\tanh\left(3\sqrt{1-x_3^2}\right), & -1<x_3<1,\\ 1, & \text{else},\end{cases} \quad \boldsymbol{x} := \begin{pmatrix}x_1\\x_2\\x_3\end{pmatrix}\in\mathbb{S}^2, \tag{6.118}$$

which is taken from a test case given in [46], in which the authors used a similar approach for distributing points accordingly to a given weighting measure.

For the evaluation of the squared equal weights quadrature error $\mathrm{err}_{K_N}(\nu_i,\boldsymbol{P})$, $\boldsymbol{P}\in(\mathbb{S}^2)^M$, cf. (6.115), we need to determine the Fourier coefficients $(\hat{\nu}_i)_{n,k}$, cf. (6.116), of the measures ν_i, $i=1,2$, for $n\in\mathbb{N}_0$, $k=-n,\ldots,n$. We perform this task by the use of a quadrature rule for the grid $\mathcal{G}$, cf. (6.117), by setting

$$(\hat{\nu}_l)_{n,k} := \begin{cases}\sum_{i=1}^{180}\sum_{j=1}^{360} w_{i,j}v(\boldsymbol{x}_{i,j})\overline{Y}_{n,k}(\boldsymbol{x}_{i,j}), & n=0,\ldots,179, \quad k=-n,\ldots,n,\\ 0, & \text{else},\end{cases} \qquad l=1,2, \tag{6.119}$$

where the weights $w_{i,j} \geq 0$, $i = 1, \ldots, 180$, $j = 1, \ldots, 360$, are computed by the simple CG method proposed in our paper [55], such that the corresponding quadrature functional has polynomial degree of exactness $N = 179$. We remark that the evaluation of sums of the form given in (6.119) can be performed efficiently by an adjoint nonequispaced fast Fourier transform on the sphere $\mathbb{S}^2$, cf. Theorem 5.20.

After these preliminary steps we apply the Algorithm 3.3 with default parameters given in Remark 3.29 to the squared equal weights quadrature error $(\mathrm{err}_{K_N})^2$ in order to compute approximate local minimizers $\boldsymbol{P}^* \in (\mathbb{S}^2)^M$ of the weighted ball L^2-discrepancy $D^2_{\mathcal{B}_{\mathbb{S}^2}}$, cf. (6.113). For efficient function evaluations we use the nonequispaced fast Fourier transforms on the sphere $\mathbb{S}^2$ discussed in Section 5.2.2. The algorithm has been implemented in MATLAB® [87], where the mex-interface to the NFFT library [72] is used. For the NFSFT routine on the sphere $\mathbb{S}^2$ we set the cutoff parameter $m = 9$, the threshold $\kappa = 1000$, and use the flags PRE_PSI and PRE_PHI_HUT. The computations are performed on an Intel® Core™ i7 CPU 920 with 12 GB RAM.

In Figure 6.14 we illustrate on the bottom the halftoning result with respect to the measure ν_1 of the earth's topographic map for $M = 200000$ points and polynomial degree $N = 1000$, which is obtained after $k = 3600$ CG iterations for randomly distributed initial points. We note that an iteration takes about 1.5min. In Figure 6.13 we illustrate on the right-hand side the halftoning result with respect to the measure ν_2, cf. (6.118), for $M = 1849$ points and polynomial degree $N = 400$, which is obtained after $k = 1000$ CG iterations for randomly distributed initial points. We note that the point distribution is similar to that obtained in [46]. □

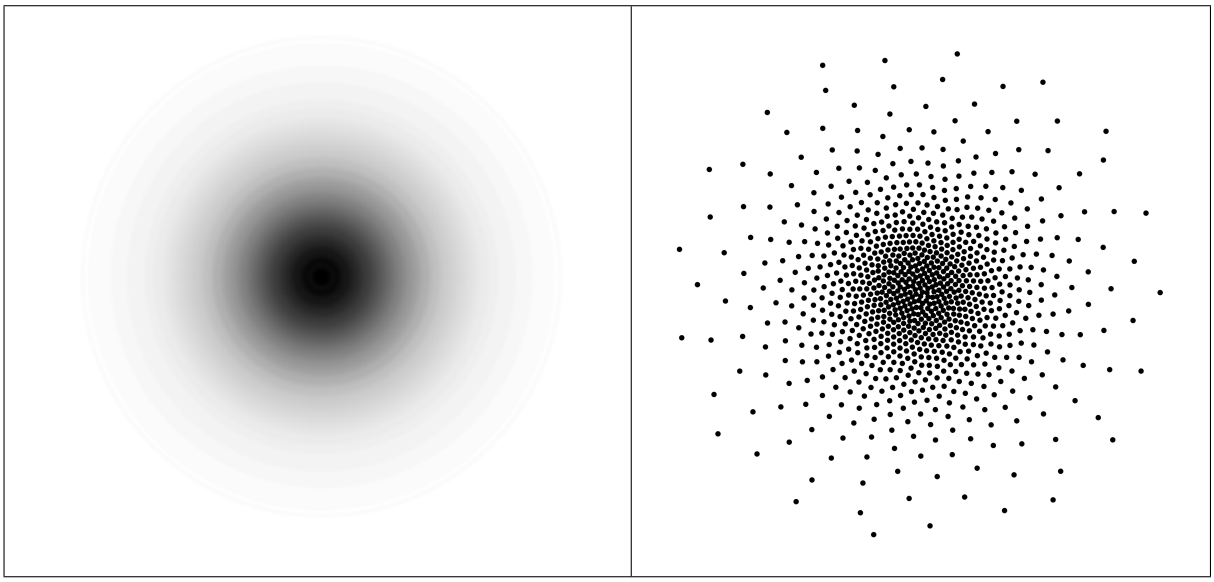

Figure 6.13: Halftoning result (right) on the sphere $\mathbb{S}^2$ with respect to the weight function v_2, cf. (6.118), Which is obtained by minimizing the squared equal weights worst case quadrature error $(\mathrm{err}_{K_N})^2$, cf. (6.115), for $M = 1849$ randomly distributed initial points by the nonlinear conjugate gradient method, cf. Algorithm 3.3, for a polynomial degree $N = 400$ after $k = 1000$ CG iterations. For details see Example 6.41.

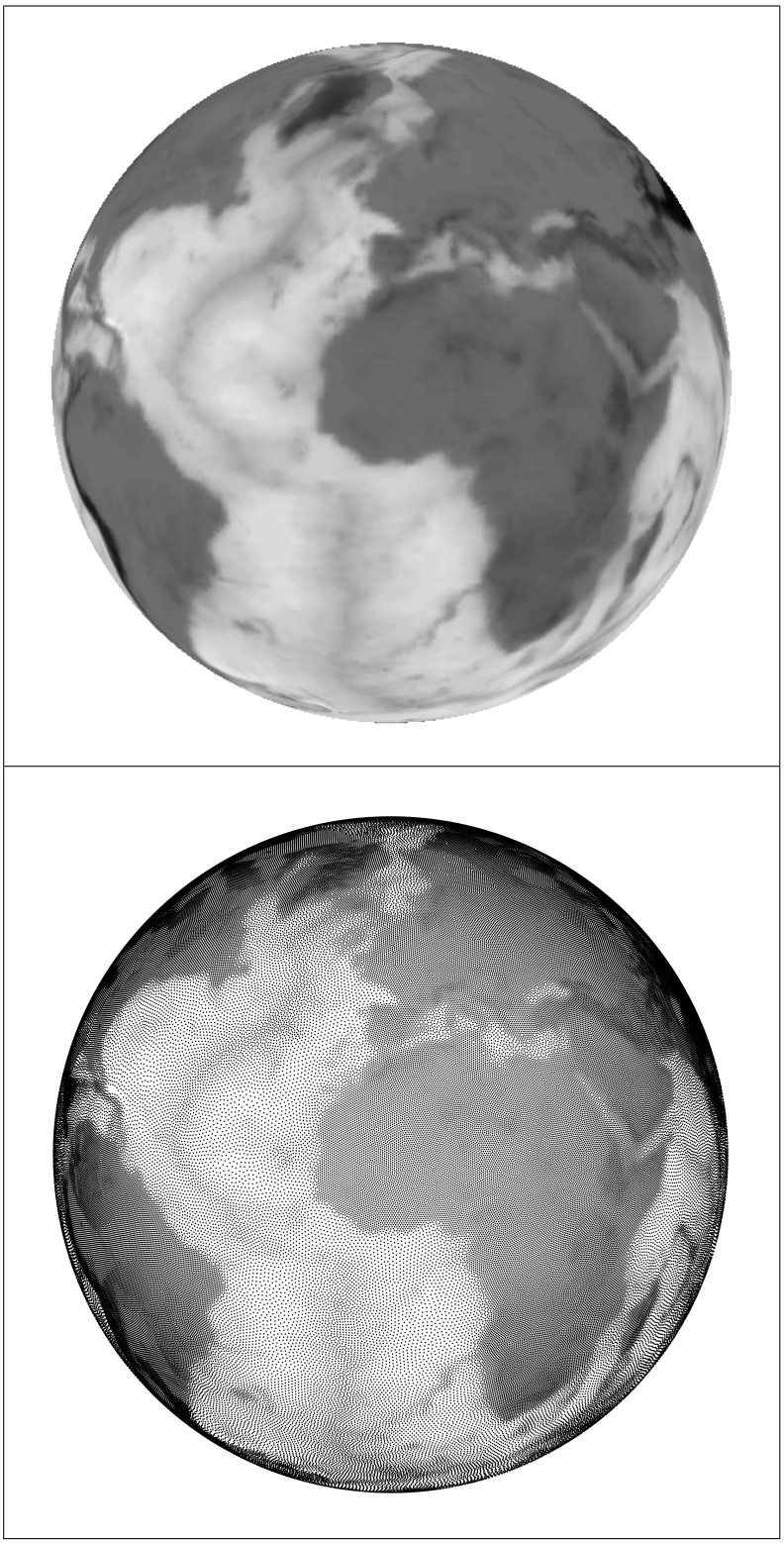

Figure 6.14: Halftoning result (bottom) on the sphere $\mathbb{S}^2$ of the earth's topography data provided by MATLAB® [87] (top), which is obtained by minimizing the squared equal weights worst case quadrature error $(\mathrm{err}_{K_N})^2$, cf. (6.115), for $M = 200000$ randomly distributed initial points by the nonlinear conjugate gradient method, cf. Algorithm 3.3, for a polynomial degree $N = 1000$ after $k = 3600$ CG iterations. For details see Example 6.41.

Bibliography

[1] M. Abramowitz and I. A. Stegun (eds.). *Handbook of Mathematical Functions*. National Bureau of Standards, Washington, 10th edn., 1972.
URL http://eric.ed.gov/ERICWebPortal/detail?accno=ED250164 (Cited on Page 38, 39, 43, 46, 101, 102, 106, 107, 108, 136, and 137)

[2] C. Ahrens and G. Beylkin. *Rotationally invariant quadratures for the sphere*. Proc. R. Soc. Lond. Ser. A Math. Phys. Eng. Sci., 465: pp. 3103–3125, 2009.
URL http://dx.doi.org/10.1098/rspa.2009.0104 (Cited on Page 7, 143, 144, and 150)

[3] M. Al-Baali and R. Fletcher. *An efficient line search for nonlinear least squares*. J. Optim. Theory Appl., 48: pp. 359–377, 1986.
URL http://dx.doi.org/10.1007/BF00940566 (Cited on Page 83 and 84)

[4] R. Alexander. *Generalized sums of distances*. Pacific J. Math., 56: pp. 297–304, 1975.
URL http://projecteuclid.org/euclid.pjm/1102906360 (Cited on Page 9, 33, and 34)

[5] N. Aronszajn. *Theory of reproducing kernels*. Trans. Amer. Math. Soc., 68: pp. 337–404, 1950.
URL http://www.jstor.org/stable/1990404 (Cited on Page 17)

[6] F. Aurehammer, F. Hoffmann, and B. Aronov. *Minkowski-type theorems and least-squares clustering*. Algorithmica, 20: pp. 61–76, 1998.
URL http://dx.doi.org/10.1007/PL00009187 (Cited on Page 194)

[7] R. Backofen, M. Gräf, D. Potts, S. Praetorius, A. Voigt, and T. Witkowski. *A continuous approach to discrete ordering on* $\mathbb{S}^2$. Multiscale Model. Simul., 9: pp. 314–334, 2011.
URL http://dx.doi.org/10.1137/100787532 (Cited on Page 28)

[8] B. Bajnok. *Construction of spherical t-designs*. Geom. Dedicata, 43: pp. 167–179, 1992.
URL http://dx.doi.org/10.1007/BF00147866 (Cited on Page 161)

[9] M. Balzer, T. Schlömer, and O. Deussen. *Capacity-constrained point distributions: A variant of Lloyd's method*. ACM Transactions on Graphics, 28: p. Article 86, 2009.
URL http://dx.doi.org/10.1145/1531326.1531392 (Cited on Page 193 and 194)

[10] E. Bannai and E. Bannai. *A survey on spherical designs and algebraic combinatorics on spheres*. European J. Combin., 30: pp. 1392–1425, 2009.
URL http://dx.doi.org/10.1016/j.ejc.2008.11.007 (Cited on Page 161)

[11] B. Baxter and S. Hubbert. *Radial basis functions for the sphere*. In *Recent Progress in Multivariate Approximation*, vol. 137 of *International Series of Numerical Mathematics*, pp. 33–47. Birkhäuser, Basel, 2001. (Cited on Page 103)

[12] J. Beck. *Sums of distances between points on a sphere — an application of the theory of irregularities of distribution to discrete geometry.* Mathematika, 31: pp. 33–41, 1984.
URL http://dx.doi.org/10.1112/S0025579300010639 (Cited on Page 8 and 182)

[13] J. Beck and W. W. L. Chen. *Irregularities of Distribution*, vol. 89 of *Cambridge Tracts in Mathematics*. Cambridge University Press, New York, 1987. (Cited on Page 29 and 182)

[14] G. Beylkin. *On the fast Fourier transform of functions with singularities.* Appl. Comput. Harmon. Anal., 2: pp. 363–381, 1995.
URL http://dx.doi.org/10.1006/acha.1995.1026 (Cited on Page 134)

[15] A. Bondarenko, D. Radchenko, and M. Viazovska. *Optimal asymptotic bounds for spherical designs.* arXiv:1009.4407v3 [math.MG], 2011. (Cited on Page 161)

[16] M. Bowick, C. Cecka, L. Giomi, A. Middleton, and K. Zielnicki. *Thomson applet.*
URL http://thomson.phy.syr.edu (Cited on Page 28 and 91)

[17] J. P. Boyd. *Chebyshev and Fourier Spectral Methods.* Dover Books on Mathematics. Dover Press, New York, NY, USA, 2nd edn., 2000. (Cited on Page 7)

[18] J. Brauchart and J. Dick. *Quasi–monte carlo rules for numerical integration over the unit sphere.* Numer. Math., 121: pp. 473–502, 2012.
URL http://dx.doi.org/10.1007/s00211-011-0444-6 (Cited on Page 8)

[19] J. Brauchart, D. Hardin, and E. B. Saff. *The next-order term for minimal Riesz and logarithmic energy asymptotics on the sphere.* Contemp. Math., 578: pp. 31–61, 2012. (Cited on Page 186)

[20] G. E. Bredon. *Topology and Geometry*, vol. 139 of *Graduate Texts in Mathematics*. Springer, New York, 1993. (Cited on Page 111)

[21] X. Chen, A. Frommer, and B. Lang. *Computational existence proofs for spherical t-designs.* Numer. Math., 117: pp. 289–305, 2011.
URL http://dx.doi.org/10.1007/s00211-010-0332-5 (Cited on Page 144)

[22] X. Chen and R. S. Womersley. *Existence of solutions to systems of underdetermined equations and spherical designs.* SIAM J. Numer. Anal., 44: pp. 2326–2341, 2006.
URL http://dx.doi.org/10.1137/050626636 (Cited on Page 7 and 144)

[23] G. S. Chirikjian and A. B. Kyatkin. *Engineering Applications of Noncommutative Harmonic Analysis: with Emphasis on Rotation and Motion Groups.* CRC Press, Boca Raton, FL, USA, 2001. (Cited on Page 7)

[24] A. I. Cohen. *Rate of convergence of several conjugate gradient algorithms.* SIAM J. Numer. Anal., 9: pp. 248–259, 1972.
URL http://dx.doi.org/http://www.jstor.org/stable/2156398 (Cited on Page 10 and 90)

[25] D. L. Cohn. *Measure Theory.* Birkhäuser, Boston, 1993. (Cited on Page 14, 15, 17, 18, and 30)

[26] J. H. Conway and D. A. Smith. *On Quaternions and Octanions.* A K Peters, Natick, 2003. (Cited on Page 155 and 173)

[27] J. W. Cooley and J. W. Tukey. *An algorithm for machine calculation of complex Fourier series.* Math. Comput., 19: pp. 297–301, 1965.
URL http://www.jstor.org/stable/2003354 (Cited on Page 134)

[28] F. Cucker and S. Smale. *On the mathematical foundations of learning.* Bull. Amer. Math. Soc. (N.S.), 39: pp. 1–49, 2002.
URL http://dx.doi.org/10.1090/S0273-0979-01-00923-5 (Cited on Page 18, 19, and 21)

[29] J. Cui and W. Freeden. *Equidistribution on the sphere.* SIAM J. Sci. Comput., 18: pp. 595–609, 1997.
URL http://dx.doi.org/10.1137/S1064827595281344 (Cited on Page 183 and 184)

[30] S. Damelin. *A walk through energy, discrepancy, numerical integration and group invariant measures on measurable subsets of euclidean space.* Numer. Algorithms, 48: pp. 213–235, 2008.
URL http://dx.doi.org/10.1007/s11075-008-9187-6 (Cited on Page 8 and 13)

[31] J. W. Daniel. *The conjugate gradient method for linear and nonlinear operator equations.* SIAM J. Numer. Anal., 4: pp. 10–26, 1967.
URL http://dx.doi.org/http://www.jstor.org/stable/2949731 (Cited on Page 9, 80, and 81)

[32] P. Delsarte, J. Goethals, and J. Seidel. *Spherical codes and designs.* Geom. Dedicata, 6: pp. 363–388, 1977.
URL http://dx.doi.org/10.1007/BF03187604 (Cited on Page 144 and 161)

[33] J. E. Dennis and R. B. Schnabel. *Numerical Methods for Unconstrained Optimization and Nonlinear Equations*, vol. 16 of *Classics in applied mathematics.* SIAM, Philadelphia, 1996.
URL http://dx.doi.org/10.1137/1.9781611971200 (Cited on Page 79 and 84)

[34] J. Driscoll and D. Healy. *Computing Fourier transforms and convolutions on the 2-sphere.* Adv. in Appl. Math., 15: pp. 202–250, 1994.
URL http://dx.doi.org/10.1006/aama.1994.1008 (Cited on Page 137)

[35] M. Drmota and R. F. Tichy. *Sequences, Discrepancies and Applications*, vol. 1651 of *Lecture Notes in Mathematics.* Springer, Berlin, 1997. (Cited on Page 8, 29, 30, 144, 182, and 183)

[36] A. Dutt and V. Rokhlin. *Fast Fourier transforms for nonequispaced data.* SIAM J. Sci. Comput., 14: pp. 1368–1393, 1993.
URL http://dx.doi.org/10.1137/0914081 (Cited on Page 134)

[37] A. Dutt and V. Rokhlin. *Fast Fourier transforms for nonequispaced data II.* Appl. Comput. Harmon. Anal., 2: pp. 85–100, 1995.
URL http://dx.doi.org/10.1006/acha.1995.1007 (Cited on Page 134)

[38] A. Edelman, T. A. Arias, and S. T. Smith. *The geometry of algorithms with orthogonality constraints.* SIAM J. Matrix Anal. Appl., 20: pp. 303–353, 1999.
URL http://dx.doi.org/10.1137/S0895479895290954 (Cited on Page 81 and 94)

[39] Eigen. *A C++ template library for linear algebra.* Version 3.1.1.
URL http://eigen.tuxfamily.org (Cited on Page 91, 165, 178, 186, 189, and 190)

[40] P. Erdős and P. Turán. *On interpolation III.* Ann. of Math., 41: pp. 510–553, 1940.
URL http://www.jstor.org/stable/1968733 (Cited on Page 41)

[41] J. Faraut. *Analysis on Lie Groups*, vol. 110 of *Cambridge Studies in Advanced Mathematics.* Cambridge University Press, Cambridge, 2008. (Cited on Page 101 and 109)

[42] M. Fenn and G. Steidl. *Fast NFFT based summation of radial functions.* Sampl. Theory Signal Image Process., 3: pp. 1–28, 2004. (Cited on Page 194)

[43] J. A. Fessler and B. P. Sutton. *Nonuniform fast Fourier transforms using min-max interpolation.* IEEE Trans. Signal Process., 51: pp. 560–574, 2003.
URL http://dx.doi.org/10.1109/TSP.2002.807005 (Cited on Page 134)

[44] R. Fletcher and C. M. Reeves. *Function minimization by conjugate gradients.* Comput. J., 7: pp. 149–154, 1964.
URL http://dx.doi.org/10.1093/comjnl/7.2.149 (Cited on Page 81)

[45] J. Fliege and U. Maier. *The distribution of points on the sphere and corresponding cubature formulae.* IMA J. Numer. Anal., 19: pp. 317–334, 1999.
URL http://dx.doi.org/10.1093/imanum/19.2.317 (Cited on Page 143)

[46] N. Flyer and E. Lehto. *Rotational transport on a sphere: Local node refinement with radial basis functions.* J. Comput. Phys., 229: pp. 1954–1969, 2010.
URL http://dx.doi.org/10.1016/j.jcp.2009.11.016 (Cited on Page 202 and 203)

[47] G. B. Folland. *A Course in Abstract Harmonic Analysis.* Studies in Advanced Mathematics. CRC Press, Boca Raton, 1995. (Cited on Page 77, 109, and 113)

[48] W. Freeden, T. Gervens, and M. Schreiner. *Constructive Approximation on the Sphere.* Oxford University Press, New York, 1998. (Cited on Page 7 and 183)

[49] S. Gallot, D. Hulin, and J. Lafontaine. *Riemannian Geometry.* Universitext. Springer, Berlin, 3rd edn., 2004. (Cited on Page 51 and 64)

[50] W. Gautschi. *Orthogonal polynomials.* Numerical Mathematics and Scientific. Oxford Univ. Press, Oxford, 2004. (Cited on Page 146 and 147)

[51] T. Gneiting. *Radial positive definite functions generated by Euclid's hat.* J. Multivariate Anal., 69: pp. 88–119, 1999.
URL http://dx.doi.org/10.1006/jmva.1998.1800 (Cited on Page 37)

[52] J. Goethals and J. Seidel. *Cubature formulae, polytopes, and spherical designs.* In *The Geometric Vein: The Coxeter Festschrift*, edited by C. Davis, B. Grünbaum, and F. Sherk, pp. 203–218. Springer, New York, 1981. (Cited on Page 7, 144, 150, 152, and 181)

[53] M. Gräf. *A unified approach to scattered data approximation on $\mathbb{S}^3$ and SO(3).* Adv. Comput. Math., 37: pp. 379–392, 2012.
URL http://dx.doi.org/10.1007/s10444-011-9214-3 (Cited on Page 8, 10, 109, 110, and 112)

[54] M. Gräf and S. Kunis. *Stability results for scattered data interpolation on the rotation group.* Electron. Trans. Numer. Anal., 31: pp. 30–39, 2008. (Cited on Page 8)

[55] M. Gräf, S. Kunis, and D. Potts. *On the computation of nonnegative quadrature weights on the sphere.* Appl. Comput. Harmon. Anal., 27: pp. 124–132, 2009.
URL http://dx.doi.org/10.1016/j.acha.2008.12.003 (Cited on Page 203)

[56] M. Gräf and D. Potts. *Sampling sets and quadrature formulae on the rotation group.* Numer. Funct. Anal. Optim., 30: pp. 665–688, 2009.
URL http://dx.doi.org/10.1080/01630560903163508 (Cited on Page 8, 144, 171, and 172)

[57] M. Gräf and D. Potts. *On the computation of spherical designs by a new optimization approach based on fast spherical Fourier transforms.* Numer. Math., 119: pp. 699–724, 2011.
URL http://dx.doi.org/10.1007/s00211-011-0399-7 (Cited on Page 8, 144, and 169)

[58] M. Gräf, D. Potts, and G. Steidl. *Quadrature erros, discrepancies and their relations to halftoning on the torus and the sphere.* SIAM J. Sci. Comput., 34: pp. A2760–A2791, 2012.
URL http://dx.doi.org/10.1137/100814731 (Cited on Page 8, 193, and 194)

[59] M. Gräf, D. Potts, and G. Steidl. *Quadrature nodes meet stippling dots.* In *Lecture Notes in Computer Science 6667*, edited by A. M. Bruckstein, B. M. ter Haar Romeny, A. M. Bronstein, and M. M. Bronstein, Scale Space and Variational Methods in Computer Vision, pp. 568–579. Springer, 2012. (Cited on Page 8)

[60] L. Grafakos. *Classical and Modern Fourier Analysis.* Pearson, Upper Saddle River, N.J., 2004. (Cited on Page 99)

[61] W. W. Hager and H. Zhang. *A survey of nonlinear conjugate gradient methods.* Pac. J. Optim., 2: pp. 35–58, 2006. (Cited on Page 80)

[62] R. H. Hardin and N. J. A. Sloane. *McLaren's improved snub cube and other new spherical designs in three dimensions.* Discrete Comput. Geom., 15: pp. 429–441, 1996.
URL http://dx.doi.org/DOI:10.1007/BF02711518 (Cited on Page 7, 144, 161, 162, 164, and 167)

[63] P. de la Harpe, C. Pache, and B. Venkov. *Construction of spherical cubature formulas using lattices.* St. Petersburg Math. J., 18: pp. 119–139, 2007. (Cited on Page 7, 144, 150, and 180)

[64] D. Healy, D. Rockmore, P. Kostelec, and S. Moore. *FFTs for the 2-sphere - improvements and variations.* J. Fourier Anal. Appl., 9: pp. 341–385, 2003.
URL http://dx.doi.org/10.1007/s00041-003-0018-9 (Cited on Page 137)

[65] M. T. Heideman, D. H. Johnson, and C. S. Burrus. *Gauss and the history of the fast Fourier transform.* Arch. Hist. Exact Sci., 34: pp. 265–277, 1985.
URL http://dx.doi.org/10.1007/BF00348431 (Cited on Page 134)

[66] S. Helgason. *Differential Geometry, Lie Groups, and Symmetric Spaces*, vol. 80 of *Pure and Applied Mathematics.* Academic Press, Boston, 6th edn., 1993. (Cited on Page 51, 56, 59, and 81)

[67] M. R. Hestenes and E. L. Stiefel. *Methods of conjugate gradients for solving linear systems.* J. Research Nat. Bur. Standards, 49: pp. 409–436, 1952. (Cited on Page 81)

[68] R. W. Hockney and J. W. Eastwood. *Computer Simulation using Particles.* Hilger, Bristol, 1992. (Cited on Page 7, 10, 118, and 124)

[69] R. Horst and P. Pardalos (eds.). *Handbook of Global Optimization*, vol. 2 of *Nonconvex Optimization and Its Applications.* Kluwer Academic Publishers, Dodrecht, 1995. (Cited on Page 78)

[70] J. Jost. *Riemannian Geometry and Geometric Analysis.* Universitext. Springer, Berlin, 6th edn., 2011.
URL http://dx.doi.org/10.1007/978-3-642-21298-7 (Cited on Page 51)

[71] J. Keiner, S. Kunis, and D. Potts. *Efficient reconstruction of functions on the sphere from scattered data.* J. Fourier Anal. Appl., 13: pp. 435–458, 2007.
URL http://dx.doi.org/10.1007/s00041-006-6915-y (Cited on Page 8)

[72] J. Keiner, S. Kunis, and D. Potts. *Using NFFT3—a software library for various nonequispaced fast Fourier transforms.* ACM Trans. Math. Software, 36: pp. 1–30, 2009.
URL http://dx.doi.org/10.1145/1555386.1555388 (Cited on Page 8, 10, 134, 138, 141, 165, 178, 186, 190, 199, and 203)

[73] J. Keiner and D. Potts. *Fast evaluation of quadrature formulae on the sphere.* Math. Comput., 77: pp. 397–419, 2008.
URL http://dx.doi.org/10.1090/S0025-5718-07-02029-7 (Cited on Page 118 and 138)

[74] J. Keiner and A. Vollrath. *A new algorithm for the nonequispaced fast Fourier transform on the rotation group.* SIAM J. Sci. Comput., 34: pp. A2599—A2624, 2012.
URL http://dx.doi.org/10.1137/110835232 (Cited on Page 118 and 141)

[75] T. Kolling and A. Keller. *Efficient illumination by high dynamic range images.* In *Proceedings of the 14th Eurographics Workshop on Rendering*, vol. 44 of *ACM International Conference Proceeding Series*, pp. 45–50. 2003. (Cited on Page 193)

[76] J. Korevaar and J. Meyers. *Spherical Faraday cage for the case of equal point charges and Chebyshev-type quadrature on the sphere.* Integral Transform. Spec. Funct., 1: pp. 105–117, 1993.
URL http://dx.doi.org/10.1080/10652469308819013 (Cited on Page 161)

[77] P. J. Kostelec and D. N. Rockmore. *FFTs on the rotation group.* J. Fourier Anal. Appl., 14: pp. 145–179, 2008.
URL http://dx.doi.org/10.1007/s00041-008-9013-5 (Cited on Page 141)

[78] L. Kuipers and H. Niederreiter. *Uniform Distribution of Sequences.* Wiley, New York, 1974. (Cited on Page 29 and 30)

[79] S. Kunis. *Nonequispaced FFT - Generalisation and Inversion.* Dissertation, Institut für Mathematik, Universität zu Lübeck, 2006. (Cited on Page 8)

[80] S. Kunis and D. Potts. *Fast spherical Fourier algorithms.* J. Comput. Appl. Math., 161: pp. 75–98, 2003.
URL http://dx.doi.org/10.1016/S0377-0427(03)00546-6 (Cited on Page 118 and 138)

[81] S. Kunis and D. Potts. *Stability results for scattered data interpolation by trigonometric polynomials.* SIAM J. Sci. Comput., 29: pp. 1403–1419, 2007.
URL http://dx.doi.org/10.1137/060665075 (Cited on Page 8)

[82] N. S. Landkof. *Foundations of Modern Potential Theory*, vol. 180 of *Die Grundlehren der mathematischen Wissenschaften in Einzeldarstellungen.* Springer, Berlin, 1972. (Cited on Page 27 and 28)

[83] V. I. Lebedev. *Quadratures on the sphere.* USSR Comp. Math. and Phys., 16: p. 10–24, 1976.
URL http://dx.doi.org/10.1016/0041-5553(76)90100-2 (Cited on Page 143 and 150)

[84] V. I. Lebedev and D. N. Laikov. *A quadrature formula for the sphere of the 131st algebraic order of accuracy.* Dokl. Math., 59: pp. 477–481, 1999. (Cited on Page 7, 143, and 150)

[85] V. I. Lebedev and A. L. Skorokhodov. *Quadrature formulas for a sphere of orders* 41, 47 *and* 53. Dokl. Akad. Nauk, 324: pp. 519–524, 1992. (Cited on Page 143)

[86] D. W. Lyons. *An elementary introduction to the Hopf fibration.* Math. Mag., 76: pp. 87–98, 2003.
URL http://dx.doi.org/10.2307/3219300 (Cited on Page 172)

[87] MATLAB®. Version R2010a. The MathWorks Inc., Natick, Massachusetts.
URL http://www.mathworks.com/products/matlab/ (Cited on Page 193, 198, 202, 203, and 204)

[88] J. Matoušek. *Geometric Discrepancy*, vol. 18 of *Algorithms and Combinatorics.* Springer, Berlin, 2010.
URL http://dx.doi.org/10.1007/978-3-642-03942-3 (Cited on Page 29 and 144)

[89] A. D. McLaren. *Optimal numerical integration on a sphere.* Math. Comput., 17: pp. 361–383, 1963.
URL http://www.jstor.org/stable/2003998 (Cited on Page 7, 10, 143, 149, 150, 158, 159, 166, and 177)

[90] J. Mercer. *Functions of positive and negative type and their connection with the theory of integral equations.* Philos. Trans. Roy. Soc. London Ser. A, 209: pp. 415–446, 1909.
URL http://dx.doi.org/10.1098/rsta.1909.0016 (Cited on Page 18)

[91] M. J. Mohlenkamp. *A fast transform for spherical harmonics.* J. Fourier Anal. Appl., 5: pp. 159–184, 1999.
URL http://dx.doi.org/10.1007/BF01261607 (Cited on Page 137)

[92] T. Molien. *Über die invarianten der linearen substitutionsgruppen.* S. B. K. Preuss. Akad. Wiss., Berlin, 52: pp. 1152–1156, 1897. (Cited on Page 150)

[93] J. J. Moré and D. J. Thuente. *Line search algorithms with guaranteed sufficient decrease.* ACM Trans. Math. Software, 20: pp. 286–307, 1994.
URL http://dx.doi.org/10.1145/192115.192132 (Cited on Page 83 and 84)

[94] C. Müller. *Spherical Harmonics*, vol. 17 of *Lecture Notes in Mathematics.* Springer, Berlin, 1966.
URL http://dx.doi.org/10.1007/BFb0094775 (Cited on Page 100, 101, 102, and 145)

[95] F. Narcowich, X. Sun, J. Ward, and Z. Wu. *Leveque type inequalities and discrepancy estimates for minimal energy configurations on spheres.* J. Approx. Theory, 162: pp. 1256–1278, 2010.
URL http://dx.doi.org/10.1016/j.jat.2010.01.003 (Cited on Page 103)

[96] J. Nocedal and S. J. Wright. *Numerical Optimization.* Springer Series in Operations Research and Financial Engineering. Springer, New York, 2nd edn., 2006.
URL http://dx.doi.org/10.1007/978-0-387-40065-5 (Cited on Page 77, 79, 82, 83, 84, 86, and 147)

[97] E. Novak and H. Woźniakowski. *Tractability of Multivariate Problems. Volume II: Standard Information for Functionals*, vol. 12 of *EMS Tracts in Mathematics.* EMS, Zürich, 2010. (Cited on Page 8, 13, 17, 29, 32, and 40)

[98] P. Pardalos and H. Romeijn (eds.). *Handbook of Global Optimization Volume 2*, vol. 62 of *Nonconvex Optimization and Its Applications.* Springer, Berlin, 2002. (Cited on Page 78)

[99] E. Polak. *Optimization*, vol. 124 of *Applied Mathematical Sciences*. Springer, New York, 1997. (Cited on Page 42 and 79)

[100] A. S. Popov. *Cubature formulae for a sphere invariant under cyclic rotation groups*. Russian J. Numer. Anal. Math. Modelling, 9: pp. 535–546, 1994.
URL http://dx.doi.org/10.1515/rnam.1994.9.6.535 (Cited on Page 166)

[101] A. S. Popov. *Cubature formulae for a sphere which are invariant with respect to the tetrahedral group*. Comput. Math. Math. Phys., 35: pp. 369–374, 1995. (Cited on Page 166)

[102] A. S. Popov. *Cubature formulas on a sphere that are invariant with respect to octahedron rotation groups*. Comput. Math. Math. Phys., 38: pp. 30–37, 1998. (Cited on Page 161 and 166)

[103] A. S. Popov. *The search for the sphere of the best cubature formulae invariant under octahedral group of rotations*. Sib. Zh. Vychisl. Mat., 5: pp. 367–372, 2002. (Cited on Page 143)

[104] A. S. Popov. *The search for the best cubature formulae invariant under the octahedral group of rotations with inversion for a sphere*. Sib. Zh. Vychisl. Mat., 8: pp. 143–148, 2005. (Cited on Page 143)

[105] A. S. Popov. *Cubature formulas on a sphere invariant under the icosahedral rotation group*. Numer. Anal. Appl., 1: pp. 355–361, 2008.
URL http://dx.doi.org/10.1134/S199542390804006X (Cited on Page 7, 143, and 150)

[106] D. Potts, J. Prestin, and A. Vollrath. *A fast algorithm for nonequispaced Fourier transforms on the rotation group*. Numer. Algorithms, 52: pp. 355–384, 2009.
URL http://dx.doi.org/10.1007/s11075-009-9277-0 (Cited on Page 8, 118, and 141)

[107] D. Potts, G. Steidl, and A. Nieslony. *Fast convolution with radial kernels at nonequispaced knots*. Numerische Mathematik, 98: pp. 329–351, 2004.
URL http://dx.doi.org/10.1007/s00211-004-0538-5 (Cited on Page 194)

[108] D. Potts, G. Steidl, and M. Tasche. *Fast algorithms for discrete polynomial transforms*. Math. Comput., 67: pp. 1577–1590, 1998.
URL http://dx.doi.org/10.1090/S0025-5718-98-00975-2 (Cited on Page 138)

[109] D. Potts, G. Steidl, and M. Tasche. *Fast and stable algorithms for discrete spherical Fourier transforms*. Linear Algebra Appl., 275–276: pp. 433–450, 1998.
URL http://dx.doi.org/10.1016/S0024-3795(97)10013-1 (Cited on Page 138)

[110] D. Potts, G. Steidl, and M. Tasche. *Fast Fourier transforms for nonequispaced data: A tutorial*. In *Modern Sampling Theory: Mathematics and Applications*, edited by J. J. Benedetto and P. J. S. G. Ferreira, pp. 247–270. Birkhäuser, Boston, MA, USA, 2001. (Cited on Page 118 and 134)

[111] T. Risbo. *Fourier transform summation of Legendre series and D-Functions*. J. Geod., 70: pp. 383–396, 1996.
URL http://dx.doi.org/10.1007/BF01090814 (Cited on Page 137 and 141)

[112] E. B. Saff and A. B. J. Kuijlaars. *Distributing many points on a sphere*. Math. Intelligencer, 19: pp. 5–11, 1997.
URL http://dx.doi.org/10.1007/BF03024331 (Cited on Page 182)

[113] E. B. Saff and V. Totik. *Logarithmic Potentials with External Fields*, vol. 316 of *Die Grundlehren der mathematischen Wissenschaften in Einzeldarstellungen*. Springer, Berlin, 1997. (Cited on Page 27 and 28)

[114] C. Schmaltz, P. Gwosdek, A. Bruhn, and J. Weickert. *Electrostatic halftoning*. Computer Graphics Forum, 29: pp. 2313 — 2327, 2010.
URL http://dx.doi.org/10.1111/j.1467-8659.2010.01716.x (Cited on Page 11, 27, 144, 193, and 194)

[115] A. Secord. *Weighted Voronoi stippling*. In *Proceedings of the 2nd International Symposium on Non-Photorealistic Animation and Rendering*, pp. 37–43. ACM Press, 2002. (Cited on Page 193)

[116] P. Seymour and T. Zaslavsky. *Averaging sets: A generalization of mean values and spherical designs*. Adv. in Math., 52: pp. 213–240, 1984.
URL http://dx.doi.org/10.1016/0001-8708(84)90022-7 (Cited on Page 161)

[117] I. H. Sloan and R. S. Womersley. *Extremal systems of points and numerical integration on the sphere*. Adv. Comput. Math., 21: pp. 107–125, 2004.
URL http://dx.doi.org/10.1023/B:ACOM.0000016428.25905.da (Cited on Page 7 and 143)

[118] I. H. Sloan and R. S. Womersley. *A variational characterisation of spherical designs*. J. Approx. Theory, 159: pp. 308–318, 2009.
URL http://dx.doi.org/10.1016/j.jat.2009.02.014 (Cited on Page 7, 144, and 162)

[119] N. Sloane, R. Hardin, and P. Cara. *Spherical designs in four dimensions*. In *Information Theory Workshop*, pp. 253–258. IEEE, Paris, 2003.
URL http://dx.doi.org/10.1109/ITW.2003.1216742 (Cited on Page 8)

[120] S. Smale. *Mathematical problems for the next century*. Math. Intelligencer, 20: pp. 7–15, 1998.
URL http://dx.doi.org/10.1007/BF03025291 (Cited on Page 28 and 79)

[121] S. T. Smith. *Optimization techniques on Riemannian manifolds*. In *Hamiltonian and gradient flows, algorithms and control*, vol. 3 of *Fields Inst. Commun.*, pp. 113–136. AMS, Providence, 1994. (Cited on Page 7, 9, 51, 81, 89, and 90)

[122] S. L. Sobolev. *Cubature formulas on the sphere invariant under finite groups of rotations*. Dokl. Akad. Nauk SSSR, 146: pp. 310–313, 1962.
URL http://dx.doi.org/10.1007/978-0-387-34149-1_21 (Cited on Page 7, 10, 143, 144, 150, 151, and 158)

[123] M. Spivak. *Calculus on Manifolds: A Modern Aproach to Classical Theorems of Advanced Calculus*. Mathematics Monograph Series. Addison–Wesley, 1965. (Cited on Page 53 and 54)

[124] M. Spivak. *Comprehensive Introduction to Differential Geometry. Volume 1–5*. Publish or Perish, Berkely, 3rd edn., 1999. (Cited on Page 51 and 81)

[125] I. Steinwart and C. Scovel. *Mercer's theorem on general domains: on the interaction between measures, kernels, and RKHSs*. Constr. Approx., 35: pp. 363–417, 2011.
URL http://dx.doi.org/10.1007/s00365-012-9153-3 (Cited on Page 18)

[126] K. B. Stolarsky. *Sums of distances between points on a sphere. ii*. Proc. Amer. Math. Soc., 41: pp. 575–82, 1973.
URL http://www.jstor.org/stable/2039137 (Cited on Page 182)

[127] R. Suda and M. Takami. *A fast spherical harmonics transform algorithm.* Math. Comput., 71: pp. 703–715, 2002.
URL http://dx.doi.org/10.1090/S0025-5718-01-01386-2 (Cited on Page 137)

[128] V. Surazhsky, P. Alliez, and C. Gotsman. *Isotropic remeshing of surfaces: A local parameterization approach.* In *Proceedings of the 12th International Meshing Roundtable*, pp. 215–224. 2003. (Cited on Page 193)

[129] T. Teuber, G. Steidl, P. Gwosdek, C. Schmaltz, and J. Weickert. *Dithering by differences of convex functions.* SIAM J. on Imaging Science, 4: pp. 79–108, 2011.
URL http://dx.doi.org/10.1137/100790197 (Cited on Page 8, 145, 193, 194, 198, 199, and 201)

[130] J. J. Thomson. *On the structure of the atom: an investigation of the stability and periods of oscillation of a number of corpuscles arranged at equal intervals around the circumference of a circle; with application of the results to the theory of atomic structure.* Philos. Mag., 7: pp. 237–265, 1904. (Cited on Page 28)

[131] C. Udrişte. *Convex Functions and Optimization Methods on Riemannian Manifolds*, vol. 297 of *Mathematics and Its Applications*. Kluwer Academic Publishers, Dordrecht, 1994. (Cited on Page 7, 51, and 79)

[132] R. Ulichney. *Digital Halftoning.* The MIT Press, Cambridge, 1987. (Cited on Page 8, 144, and 193)

[133] J. L. Ullman. *On the regular behavior of orthogonal polynomials.* Proc. London Math. Soc., 24: pp. 119–148, 1972.
URL http://dx.doi.org/10.1112/plms/s3-24.1.119 (Cited on Page 41)

[134] D. Vanderhaeghe and V. Ostromoukhov. *Polyomino-based digital halftoning.* In *IADIS International Conference on Computer Graphics and Visualization*, edited by P. Isaías, pp. 11–18. 2008. (Cited on Page 193)

[135] D. Varshalovich, A. Moskalev, and V. Khersonskii. *Quantum Theory of Angular Momentum.* World Scientific, Singapore, 1988. (Cited on Page 75, 110, 135, 137, 139, and 140)

[136] G. Wagner. *On averaging sets.* Monatsh. Math., 111: pp. 69–78, 1991.
URL http://dx.doi.org/10.1007/BF01299278 (Cited on Page 161)

[137] D. J. Wales, H. McKay, and E. L. Altschuler. *Defect motifs for spherical topologies.* Phys. Rev. B, 79: p. 224115, 2009.
URL http://dx.doi.org/10.1103/PhysRevB.79.224115 (Cited on Page 28)

[138] D. J. Wales and S. Ulker. *Structure and dynamics of spherical crystals characterized for the Thomson problem.* Phys. Rev. B, 74: p. 212101, 2006.
URL http://dx.doi.org/10.1103/PhysRevB.74.212101 (Cited on Page 28)